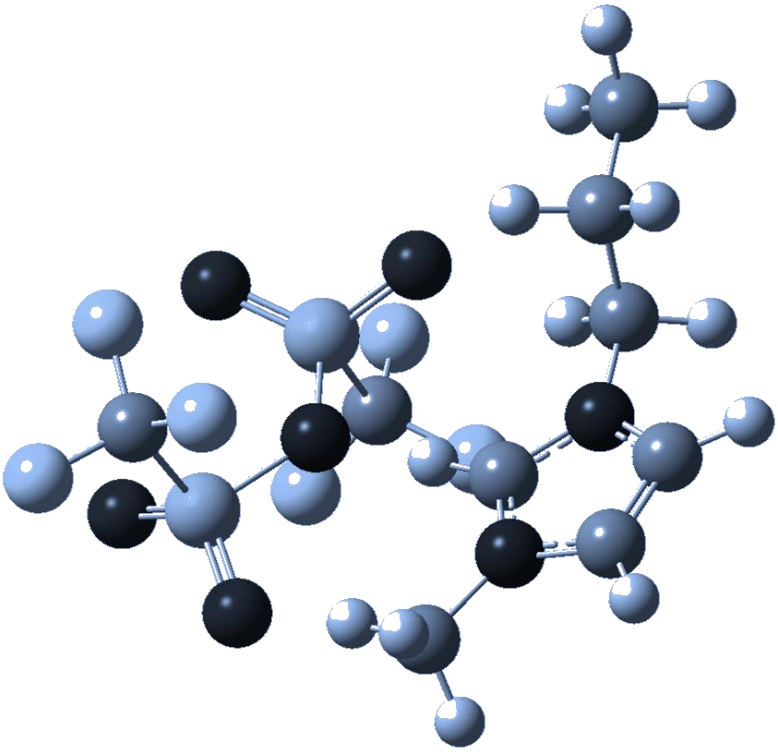

Thermophysical Properties of Ionic Liquids

Marisa Alexandra Alves da Rocha
Doutoramento em Química
Departamento de Química e Bioquímica
2013

Luís Manuel das Neves Belchior Faia dos Santos
Professor Associado
Faculdade de Ciências da Universidade do Porto

Centro de Investigação em Química
Universidade do Porto

Thermophysical Properties of Ionic Liquids

Marisa Alexandra Alves da Rocha
Doutoramento em Química
Departamento de Química e Bioquímica
2013

Orientador
Luís Manuel das Neves Belchior Faia dos Santos
Professor Associado
Faculdade de Ciências da Universidade do Porto

"I am among those who think that science has great beauty. A scientist in his laboratory is not only a technician: he is also a child placed before natural phenomena which impress him like a fairy tale."

Maria Skłodowska-Curie

Nobel Prize in Physics (1903) and in Chemistry (1911)

"I am turned into a sort of machine for observing facts and grinding out conclusions."

Charles Robert Darwin

English Naturalist

Aos Meus Pais

RESUMO

Este trabalho teve como principal objectivo, avaliar o efeito da estrutura e nano-estruturação dos líquidos iónicos nas suas propriedades termofísicas. Para tal, realizou-se o estudo de algumas propriedades termofísicas em 41 líquidos iónicos apróticos, explorando diferentes séries representativas destes sistemas constituídos por diferentes catiões (imidazólios e piridínios), e aniões, (hexafluorofosfato e o bis(trifluorometilsulfonil)imida), de forma a explorar o efeito do aumento da cadeia alquílica, simetria do catião, topologia do catião e do anião. No decorrer neste projecto de doutoramento foi ainda, desenhada, construída e testada uma nova instalação para medições de pressões de vapor pelo método de efusão de Knudsen acoplada a uma microbalança de cristal de quartzo e reconstruído, modernizado e testado um calorímetro de alta precisão para medição de capacidades caloríficas do tipo *Drop*.

O estudo termofísico foi restrito ao estudo do equilíbrio líquido-vapor, capacidades caloríficas, densidades, viscosidades e índices de refracção. Com base na dependência das propriedades termofísicas estudadas com a temperatura foram derivadas propriedades termodinâmicas tais como, entalpias vaporização, entropias de vaporização e coeficientes de expansão isobárica. O estudo da dependência da viscosidade com a temperatura permitiu avaliar para alguns líquidos iónicos a energia de barreira de fluxo viscoso a partir do ajuste da equação de Vogel-Tamman-Fulcher (VTF).

Com base nos resultados obtidos, em especial, na análise da dependência das propriedades termodinâmicas com o tamanho da cadeia alquílica, foram estabelecidas relações entre a estrutura e a nano-estruturação dos líquidos iónicos e adicionalmente foram analisadas as tendências do regime das propriedades termofísicas em séries homólogas. Os resultados de equilíbrio líquido-vapor (entalpias e entropias de vaporização) vieram mostrar a existência de um tamanho de cadeia alquílica a partir do qual se observa um menor aumento das entalpias e entropias de vaporização, tendo sido relacionado e interpretado com a intensificação da nano-estruturação nos líquidos iónicos de cadeia longa. Alterações de tendências na evolução das propriedades ao longo da cadeia alquílica, tais como, viscosidade, capacidade caloríficas e índices de refracção vieram dar suporte adicional às evidências anteriores. O trabalho realizado nesta tese veio dar um forte suporte experimental e termodinâmico à existência de uma significativa nano-estruturação nos líquidos iónicos, resultante da formação de uma rede iónica e à nano-segregação de regiões de carácter predominantemente apolar em especial nos líquidos iónicos com cadeia alquílica longa.

ABSTRACT

The main goal of this study was to evaluate the structural and nanostructural effect on the thermophysical properties of ionic liquids. For that propose, the thermophysical study of 41 aprotic ionic liquids was carried out, and the effect of the alkyl chain length, cation symmetry, cation and anion topologies were evaluated, based on the study of different extended ionic liquids series composed by imidazolium and pyridinium cations and hexafluorophosphate and bis(trifluoromethylsulfonyl)imide anions.

Along this Ph.D. project, a new Knudsen effusion method combined with a quartz crystal microbalance installation, for the vapor pressures measurement of ionic liquids was designed, assembled and tested. A calorimeter based on the drop method for the measurement of high precision heat capacities was also reassembled, modernized and tested.

The thermophysical study was restricted to the equilibrium vapor-liquid, heat capacities, densities, viscosities, and refractive indices. Based on the thermophysical properties and their dependence with temperature, the thermodynamic properties of vaporization and isobaric thermal expansion coefficients were derived. The temperature dependence of viscosity was correlated using the Vogel-Tammann-Fulcher (VTF) model and the energy barrier related to the fluid shear stress was derived.

The effect of nanostructuration of ionic liquids on the thermophysical properties was evaluated and relationships between the nanostructuration of ionic liquids and their thermophysical properties were established. A trend shift on the thermodynamic properties of vaporization along the alkyl chain length has been detected from the equilibrium vapor - liquid study. Starting from a critical alkyl length size, a decrease on the contribution of the methylene group, $-CH_2-$, to the enthalpies and entropies of vaporization was observed, which was related to a change in the structuration of the liquid phase. These findings are supported by the trends shifts along the alkyl chain length of the other studied properties, such as, heat capacities, viscosities and refractive indices.

The work presented in this thesis has given a strong experimental support and a thermodynamic insight concerning the nanostructuration of ionic liquids, which results from the formation of medium-range nano-scale domains with polar and non-polar regions for the ionic liquids with a longer alkyl chain length.

ACKNOWLEDGMENTS

Ao longo do Doutoramento é percorrido um caminho individual, porém, como em todas as alturas da vida, surgem sempre pessoas que nos acompanham e apoiam. Este trabalho de Doutoramento resultou do meu intenso trabalho e perseverança, mas também e em muito, da ajuda, acompanhamento e esforço do meu orientador. Esta tese de Doutoramento é dedicada a todas essas pessoas.

Ao meu orientador, Professor Luís Belchior Santos, agradeço o apoio, confiança, amizade, compreensão e boa disposição. Agradeço, o dinamismo, grau de exigência e conhecimentos transmitidos ao longo de todos estes anos de colaboração. Desejo um dia atingir o teu nível científico. Obrigada por acreditares em mim!

Ao Professor João Coutinho pela colaboração, apoio e discussões sempre cativantes/motivadoras sobre o grande mundo dos líquidos iónicos.

Ao Sr. Manuel Carlos Torres pelo apoio incondicional, ajuda no desenho e construção do novo Knudsen, sistema de secagem e muitos outros obstáculos que me ajudou a ultrapassar. Agradeço em especial a disponibilidade que sempre teve para satisfazer a minha curiosidade relativamente a detalhes do equipamento da oficina e sistemas de vácuo.

À Professora Margarida Bastos pela simpatia, apoio e incentivo sempre demonstrados desde a minha chegada ao grupo.

À Professora Emilia Tojo agradeço a simpatia e confiança, e a forma como me recebeu no seu laboratório, no Departamento de Química Orgânica da Faculdade de Química da Universidade de Vigo.

Dr. Bernd Rathke und Frau Ulrike Wegener danke ich für die mir entgegengebrachte Sympathie, für Enthusiasmus und Vertrauen, und nicht zuletzt für die Art und Weise, wie ich im Fachgebiet Technische Thermodynamik der Universität Bremen aufgenommen wurde.

Agradeço as todos os membros do grupo de Química–Física em especial à Dra. Ana Paula Carvalho, pela amabilidade e ajuda durante todos estes anos.

Aos meus amigos de laboratório, em especial, Nana, Sandra ("Química-Física convertida"), Isabel, Inês, Ricardo e Piotr, agradeço a amizade, o apoio e a boa disposição.

À Ana ("Lobinho"), Filipe, Rodrigo e Bernd, agradeço a amizade e o grande apoio. Muito Obrigada!

Aos meus pais, Isaura e Ilídio, ao meu irmão Nuno e cunhadinha Annet pelo amor, apoio incondicional, compreensão e paciência. Em especial ao pequeno Lucas que foi uma fonte de alegria para mim e para todos.

Por fim, agradeço a minha Bolsa de Doutoramento (SFRH/BD/60513/2009) às seguintes entidades: European Regional Development Fund (ERDF); Fundação Fundação para a Ciência e Tecnologia pelo apoio financeiro no âmbito do COMPETE - Competitiveness Programme e European Social Fund; Centro de Investigação em Química, Universidade do Porto (projecto estratégico PEst-C/QUI/UI0081/2011).

TABLE OF CONTENTS

Figure Index

Table Index

CHAPTER 1

Introduction

1.1 General Introduction

Room temperature ionic liquids, RTILs, have gained popularity, mainly due to their particular properties, such as, low vapor pressure, stable liquid phase over a wide temperature range, low-flammability and thermal stability at high temperatures, as well as, due to their wide range of applications in chemistry and industry.[1–3] Intense research in these systems were performed both in fundamental and applied fields, contributing to the progress in the understanding of the ionic liquids at a molecular level, and consequently, to the advance in the applied field.[1,4,5]

1.1.1. Ionic Liquids

The discovery of ionic liquids can be dated back to the work of S. Gabriel and J. Weiner published in 1888.[6] The melting point for ethanolammonium nitrate, a protic ionic liquid, was found to lie between 52 - 55ºC.[6] The first ionic liquid with a low melting point of (13 - 14)ºC, ethylammonium nitrate, was synthesized by Walden in 1914.[7] Despite the work published by Gabriel and Weiner, it is commonly accepted in the literature that the beginning of the history of ionic liquids began with the work reported by Walden. In 1951, Hurley and Wler [8] developed low melting salts with chloroaluminate ions for electrodeposition of aluminum in the form of white or shiny adherent plates. The 1980s decade was the period were the low melting ionic liquids were proposed as solvents for organic synthesis.[9–11] The breakthrough of dialkylimidazolium chloroaluminate ionic liquids by Wilkes and co-workers [9], led to a steady increase in findings of new ionic liquids based on organic cations. The chloroaluminate based ionic liquids presented the disadvantage of being reactive with water. In 1992, for the first time, Wilkes and Zaworotko [12] reported the synthesis of air and water stable ionic liquids composed of imidazolium or pyridinium cations and acetate or tetrafluoroborate anions. This was the starting point for the intense search of new classes of ionic liquids as well as exploring their unique properties, which has prompted a fast growing number of publications per year in several research areas.

Nowadays, room temperature ionic liquids, RTILs, are considered as salts composed of an organic cation and an inorganic or organic anion that are liquids at or near room temperature with melting points below 100ºC. The adopted temperature of 100 ºC has no special fundament; it is just an indicative value and was probably chosen considering the normal boiling point of water. Compared to conventional organic solvents, the unique properties of ionic liquids favor their application in diverse fields, such as synthesis, extraction, catalysis, and electrochemistry. [1,4,13,14] These liquids present desirable properties for such uses, including low vapor pressure, thermal stability up to high temperatures, wide electrochemical windows, good thermal conductivity, high miscibility with substances having a wide range of polarities and a capability of dissolving organic and inorganic substances. These are some general physicochemical properties of ionic liquids which can vary considerably depending on the combination of cations and anions. Figure 1.1 presents some of the common cations and anions found in the literature, as well as, their common abbreviations.

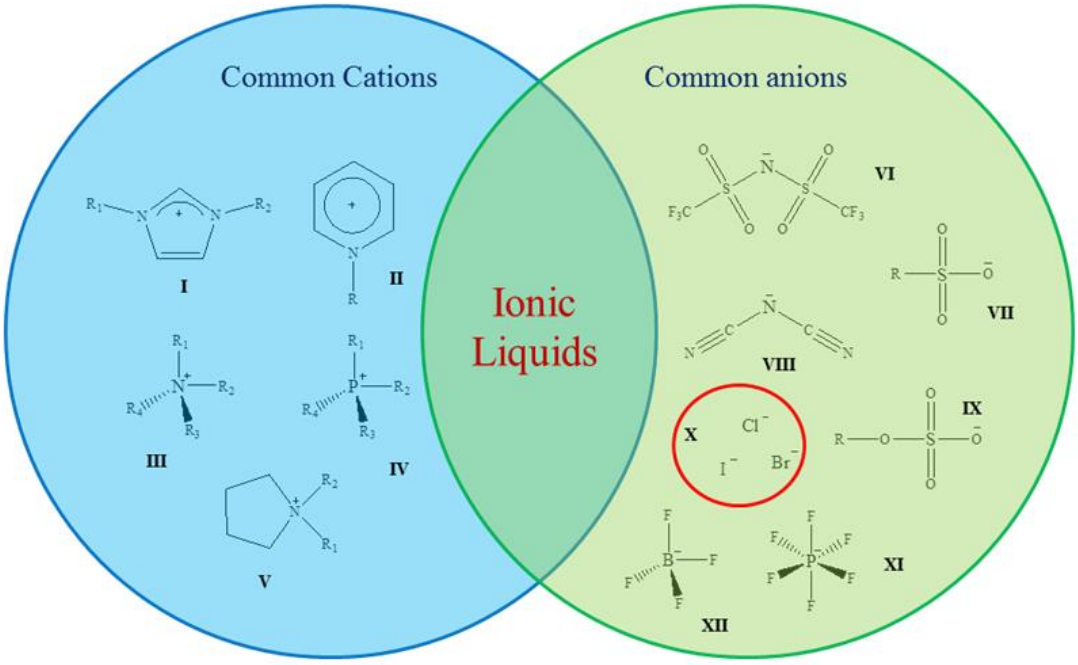

Figure 1.1. Common cations and anions of RTILs. **I**: 1,3-dialkylimidazolium ($[C_{N/2}C_{N/2}im]^+$); **II**: N-alkylpyridinium ($[C_NPy]^+$); **III**: tetraalkylammonium ($[N_{ijkl}]^+$); **IV**: tetraalkylphosphonium ($[P_{ijkl}]^+$)v; **V**: N,N-dialkylpyrrolidinium ($[C_{N/2}C_{N/2}pyr]^+$); **VI**: bis(trifluoromethanesulfonyl)imide ($[NTf_2]^-$); **VII**: alkylsulfonate ($([C_NSO_3]^-$); **VIII**: dicyanimide ($[N(CN)_2]^-$); **IX**: alkylsulfates ($[C_NOSO_3]^-$); **X**: chloride, bromide, iodide; **XI**: hexafluorophosphate ($[PF_6]^-$); **XII**: tetrafluoroborate ($[BF_4]^-$). (adapted from source [15])

Among the anions presented in figure 1.1, much work was done on $[BF_4]^-$ and $[PF_6]^-$. However, in the presence of moisture, these anions hydrolyze and form HF, being the least acceptable media for electrochemistry. The anions based on halides have the disadvantage of being extremely hygroscopic, and in some conditions, they can hydrolyze. Less hygroscopic, less water-soluble, and water-resistant ionic liquids based on trifluoromethanesulfonate (triflate; $[TfO]^-$), bis(trifluoromethanesulfonyl)imide (bistriflamide; $[NTf_2]^-$), and tri{(trifluoromethyl)sulfonyl}methanide ($[CTf_3]^-$) anions, were synthesized by Grätzel and coworkers.[16,17] Usually, for the preparation of ionic liquids with low viscosity, most of the anions include a halogen, particularly fluorine. The electron-withdrawing effect of the fluorine atom on the anionic structure is useful for delocalizing the anionic charge.[18] These ionic liquids have received much attention not only because of their low reactivity with water, but also due to their low viscosity, thermal and electrochemical stability.[14,19] In general, the ionic liquids exhibit a relatively weak coulombic interactions, which causes an inefficient arrangement of the crystal lattice, and consequently, lower melting points; in many cases leading to glass formation with marked inhibition of crystallization.

The distinctive properties of the ionic liquids are governed by the structure and interaction between the ions. The typical ionic liquid cations have aromatic rings with high delocalized charge. For quaternary ammonium cations, the charge density delocalization is also achieved. In this case, the charge is relatively localized at the central nitrogen atom, but is not accessible from the molecular surface. As a result, the charge densities are delocalized over the large the alkyl surface. Usually, the ionic liquid anions have high symmetry, and as a consequence, the charge density is delocalized over the substituting groups, as can be seen for the cases of $[BF_4]^-$, $[PF_6]^-$ or $[ClO_4]^-$. In bis(trifluoromethanesulfonyl)imide (bistriflamide, $[NTf_2]^-$), the negative charge is delocalized over several atoms.[20] Figure 1.2 presents the σ-surfaces (charge density) of common ionic liquid cations and anions.

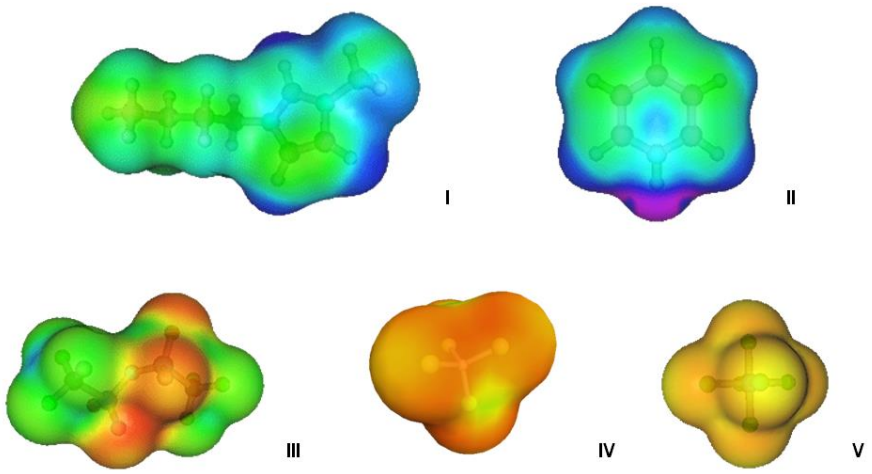

Figure 1.2. σ-Surfaces of common ionic liquids cations and anions. In the upper row the 1-butyl-3-methylimidazolium, **I**, and pyridinium, **II**, and in the row below, bis(trifluoromethanesulfonyl)imide, **III**, tetrafluoroborate, **IV**, and hexafluorophosphate, **V**, are represented. (source of the figures [21])

1.1.2. Structure of Ionic Liquids

The electronic structure of gas-phase ion pairs was explored mainly by quantum-chemical calculations, through electronic wavefunction or density methods.[1,4,22] Nevertheless, different methods can produce very different charge distributions and as a consequence, there is an uncertainty about how to best describe the nature of the cation-anion interactions.[1,23,24] Quantum chemical methods reproduce the detailed electronic interactions within and between molecules, but only few ions or ion pairs can be computed. The typical methods employed to ionic liquid ions are Hartree-Fock (HF), density functional theory (DFT), and second-order Møller-Plesset Perturbation Theory (MP2). The MP2 method includes part of the electron correlation of the system, which is important for describing aromatic systems, such as the imidazolium cation, for recovering dispersion effects with accuracy and describing the hydrogen bonds. The DFT methods are capable of recovering some of the correlation for approximately the cost of a HF computation. However, the lack of a dispersion term is problematic because of the importance of the van der Waals interactions between the alkyl chains of the ions, $\pi\cdots\pi$ interactions and charge dispersion terms.

One of the most widely used and studied ionic liquid family is the one based on the imidazolium cation (figure 1.3).

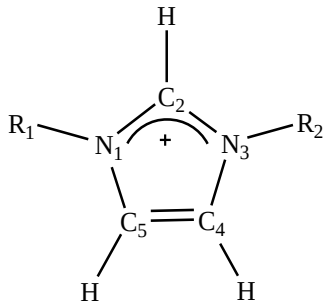

Figure 1.3. Structural formula and electronic structure of the 1,3-dialkylimidazolium cation.

The electronic structures of the $[C_4C_1im]^+$ cation and the ion pair $[C_4C_1im]Cl$ in the gas phase were analyzed at the B3LYP and MP2/6-31++G(d,p) levels of theory by Hunt and coworkers.[22] The $[C_4C_1im]^+$ cation can be described by a double bond between C4 and C5, a delocalized three centre 4 electron configuration across the front of the imidazolium ring (N1-C2-N3), and a weak delocalization in the central region.[22] The hydrogen atoms in the C2, C4, and C5 positions bear almost the same charge (natural bond orbitals, NBO), the carbons C4 and C5 are practically neutral, whereas the carbon C2 is positively charged due to the electron deficit on the C=N bond.[22] As a result, the hydrogen atom in the C2 position presents a higher acidity. Additionally, this characteristic enhances the formation of hydrogen bonds as already verified in the literature, where the C2-H was shown to bind specifically with a solute molecule [25] or its counter ion [26] as a good hydrogen bond donor.

The main problem when studying loosely bound ion pairs is the large number of possible conformations and other structural features which have to be taken into account, e.g. in the case of alkylimidazolium halide ILs, the position of the halide around the imidazolium ring (figure 1.4), and the rotation of the alkyl chain of the cation. The halide preferentially occurs at seven possible positions around the imidazolium cation, where the in-plane positions (and out-of-plane) near to C2 are energetically preferred, and the positions near to C4 and C5 are less stable. Earlier studies only consider one possible ion pair structure, with the halide hydrogen bonding the hydrogen atom in C2.[1] Nowadays, a variety of strategies are applied in order to obtain the energetically most stable geometries.[22,27–29]

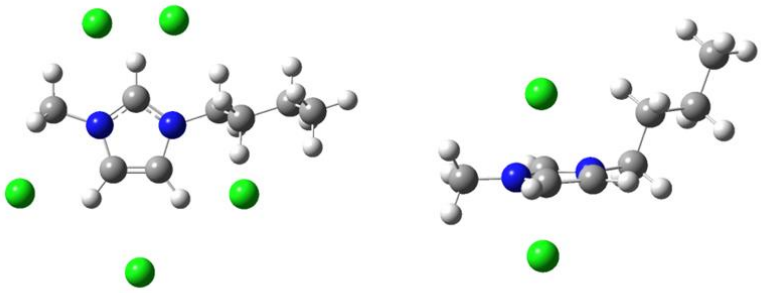

Figure 1.4. Positions of local energy minima for a Cl^- anion around an imidazolium cation.

In the case of fluorine, Turner *et al.* [28] found that this halide prefers to covalently bond at C2, C4 and C5 positions of the imidazolium cation or remove a hydrogen atom from one of the considered positions and form HF. For the ionic liquids, $[C_3C_1im]X$ and $[C_4C_1im]X$, with the bromide and iodine anions, the most stable structure were found to lie above the imidazolium ring.[28] Recently, Kempter and Kirchner [30] explored the role of hydrogen atoms in interactions involving imidazolium based ionic liquids. The theoretical work has shown that the existence of hydrogen bonding in the context of imidazolium-based ionic liquids is possible.

The increase of length of the substituents of the cations enhances the conformational flexibility due to the many rotational degrees of freedom, which can give rise to conformational equilibria. *trans-trans* and *trans-gauche* conformers were found in the cation $[C_4C_1im]^+$, resulting from the rotational modes of the alkyl groups (and hydrogen bond interactions).[31,32] Turner *et al.* [28] also explored rotational barriers of the alkyl chain of the imidazolium cation and found that the rotation of C-C bonds cost very little energy, except where the steric interactions with hydrogen atoms of the alkyl chain dominate. Hunt and Gould [29] investigated the effect of the halide on the alkyl chain rotational barriers in $[C_4C_1im]Cl$. Based on this work, it was found that the presence of the anion deepens and flattens the torsional potential energy wells. Additionally, the hydrogen atoms of the alkyl chains participate in H-bonding with the anion. When the hydrogen atoms of the alkyl chains of the cation are not involved in H-bonding with the anion, the presence of the anion augments low energy rotational movements in the alkyl chains.[29]

The structure of the ionic liquid $[C_4C_1im][PF_6]$ was studied using semi-empirical methods by Meng *et al.*. [33] In this work, seven stable ion pairs were identified. Watanabe and coworkers [34] calculated the most stable ion pair structure for $[C_2C_1im][PF_6]$, where the anion $[PF_6]^-$ is placed over the imidazolium ring, with three fluorine atoms forming a triangle with short contacts to the hydrogen of C2 position and to the hydrogen atoms of the alkyl chain groups (figure 1.5).

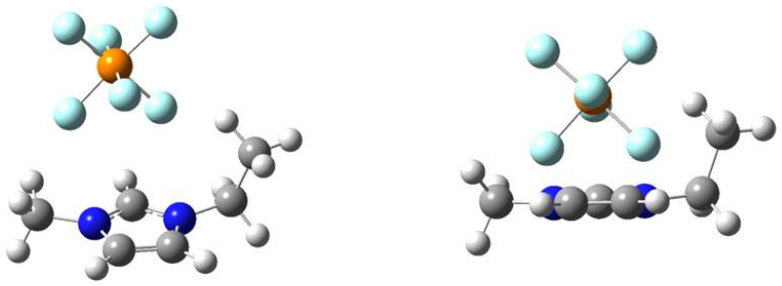

Figure 1.5. Most stable cation-anion structure in $[C_2C_1im][PF_6]$. Geometry obtained using a B3LYP/6-31+G(d) level of theory.

Similar out-of-plane positions are observed for other large anions, such as $[BF_4]^-$. In 2004, Gozzo *et al.* [35] explored the hydrogen bonding ability of the anions $[BF_4]^-$, $[PF_6]^-$, trifluoroacetate ($[CF_3CO_2]^-$) and tetraphenylborate ($[B(C_6H_5)_4]^-$) with the $[C_4C_1im]^+$ cation, based on calculations carried out at the B3LYP/6-311+G(d,p) level of theory. The distances of the hydrogen bond between the anion and the hydrogen atom of C2 position were found to be 1.88, 2.01, 1.95 and 2.43 Å, respectively. The H-bonding strength of this series of anions was determined using both computational and experimental data, and the following order was found; $[CF_3CO_2]^-$ > $[BF_4]^-$ > $[PF_6]^-$ > $[B(C_6H_5)_4]^-$, indicating that the distances of the H-bonding do not correlate well with the order of strength found.

The structure of $[NTf_2]^-$ in the gaseous state was studied by Kabo and coworkers [36], by means of quantum chemical methods. Internal rotation of the CF_3O_2S- and F_3C- tops occurs, two conformers are formed, *cis* and *trans*, as shown in figure 1.6. As it can be seen, in the *cis* conformer, both the F_3C- groups lie on the same side with respect to the S-N-S plane, and in the *trans* conformer the groups lie on the opposite sides.

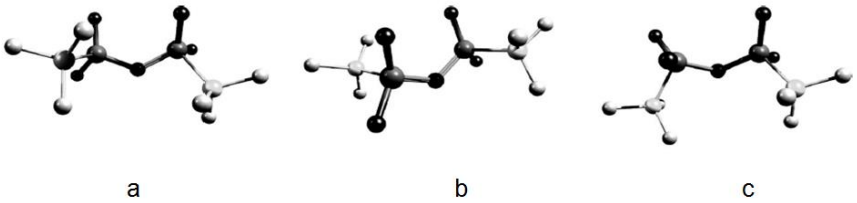

Figure 1.6. Conformers of the $[NTf_2]^-$ anion, (a) cis; (b) trans; (c) cis*. (adapted from the source [36])

The structure of the ionic liquids $[C_4C_1im][NTf_2]$ and $[C_4C_1C_1im][NTf_2]$ were explored based on calculations carried out at the B3LYP/6-31+G(d) level of theory.[37] Despite of the two stable *cis* and *trans* conformers of the $[NTf_2]^-$ anion, the *trans* conformer is energetically preferred in the cation-anion structure (figure 1.7). As it can be seen, the methylation of the C2 position of imidazolium based ionic liquids disrupts the predominant hydrogen bonding interaction between the cation and anion, leading to changes not only at structural level but also of the physicochemical properties.

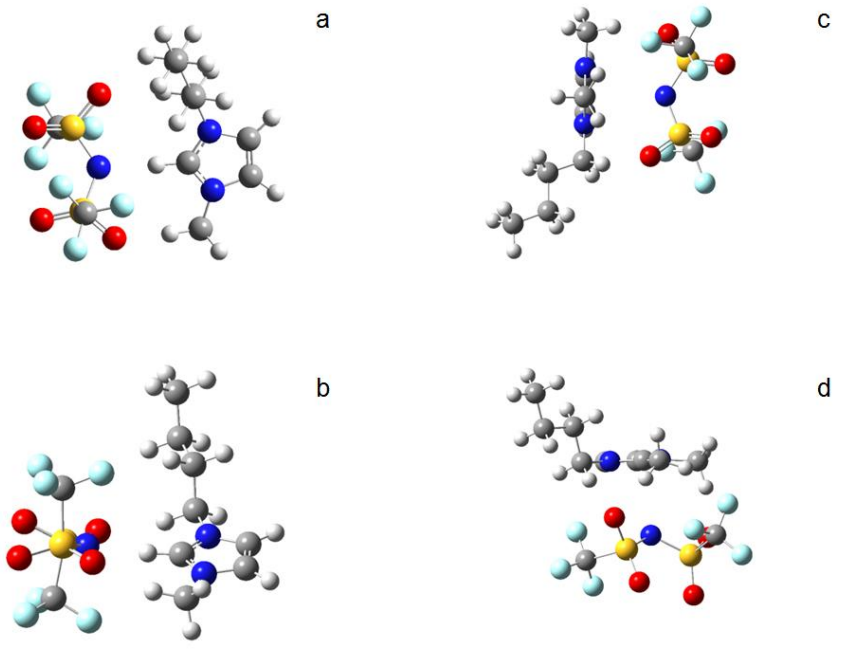

Figure 1.7. Most stable cation-anion structure in $[C_4C_1im][NTf_2]$ (a, b) and in $[C_4C_1C_1im][NTf_2]$ (c, d). Geometries obtained using the B3LYP/6-31+G(d) level of theory.

Depending on the combination of anion and cation, there are other interactions that play an important role in the condensed phases of the ionic liquids. If the molecular interactions present in the liquid and solid phases were fully understood, it will be a breakthrough in the design of ionic liquids to a certain application.

1.1.3. Structural Organization of Ionic Liquids

In condensed phases, the arrangement of molecules into bulk materials are highly dependent of their intra- and intermolecular interactions, pressure and temperature. Even in so-called isotropic liquids, intra- and intermolecular interactions could play an important role to create some local order in the structural and nanostructural organization. In order to obtain a better understanding about the stability, physico-chemical properties and reactivity of the systems, the knowledge of the structural/ nanostructural and supramolecular organization is of fundamental importance.

In ionic liquids, the molecular interactions between the ions results from their configurational arrangement and charge distribution, which involves not only coulombic interactions[38–41], but also van der Waals interactions [41–45] and hydrogen bonding[44–52], leading to a complex structural/nanostructural organization. Considering the enormous number of publications concerning this topic, this thesis will focus on some representative studies, which contributed for the better understanding of the structural/nanostructural organization of ionic liquids.

A first assumption regarding the nature of the liquid structure of ionic liquids considered them as networks of cations and anions interacting via electrostatic interactions and hydrogen bonds. [50,53] As discussed above, ionic liquids result from the combination of an organic cation and an inorganic or organic anion. Usually, the cations are composed of a polar headgroup where most of the electrostatic charge is concentrated, and a nonpolar group. In order to satisfy the electroneutrality condition and to enhance the electrostatic interactions between the cation and anion, ionic liquids must have some short range organization. [50,53]

The long-range structure of ionic liquids was studied by Urahata and Ribeiro[54], using computer simulation. The purpose of this work was to provide a perspective view of the ionic motions and the onset of distinct dynamical processes in ionic liquids. [54] Static structure factors, obtained using a united-atom model of the imidazolium based ionic liquids, showed low wave-vector peaks that are not characteristic of simple molten salts and with the increase of the alkyl side chain length, the peaks became more evident which indicates long-range ordering.

Wang and Voth[55] explored the effect of the alkyl side chain length of the cation in ionic liquids, using a multiscale coarse-graining (MS-CG) method. [55,56] Based on this work, it was found that, for sufficient lengths of the alkyl chains of the cation, the tail groups (alkyl chains) of the cations aggregates to form spatially heterogeneous tail domains, where the headgroups and the anions distributes reasonably homogeneously in order to maintain the electroneutrality as well as to maximize the electrostatic interactions, while the tail groups tend to segregate elsewhere.[55] In 2006, for the first time, Lopes and Pádua[57], used atomistic simulation to focus on the nanostructuration of 1-alkyl-3-methylimidazolium based ionic liquids, $[C_{N-1}C_1im]^+$ (N = 3 up to 13), in the liquid phase, and to investigate the effect of the alkyl side length in the cations on the long-range structures. Based on the computer simulation using an all-atom force field, it was possible to predict that the structure of the liquid phase of the studied ionic liquids exhibits microphase separation between polar and nonpolar regions. Additionally, it was observed that the polar regions has the structure of a tridimensional network of ionic channels, while the nonpolar regions are arranged as dispersed microphases, for the $[C_2C_1im]^+$ based ILs, and as a continuous phase for higher alkyl chains lengths (figures 1.8 and 1.9) .[57]

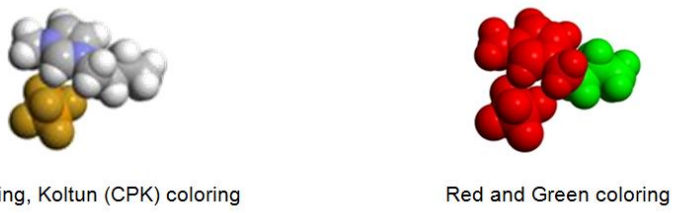

Figure 1.8. Coloring code proposed by Lopes and Pádua[57], in order to distinguish the "polar" and "nonpolar" domains of the ions. (adapted from source [57])

These three studies[54,55,57] have provided a more refined view of the structural organization of the liquid phase of ionic liquids, where the polar regions (high charge density) organized themselves in order to satisfy the electroneutrality conditions and to enhance the electrostatic interactions between the cation and anion, and the alkyl chains of the cation (low charge density) segregate elsewhere. The interaction between these two types of regions (polar and non-polar) led to the recognition of ionic liquids as high-charge density (polar) network permeated by low-charge density (non-polar) regions. [4,57]

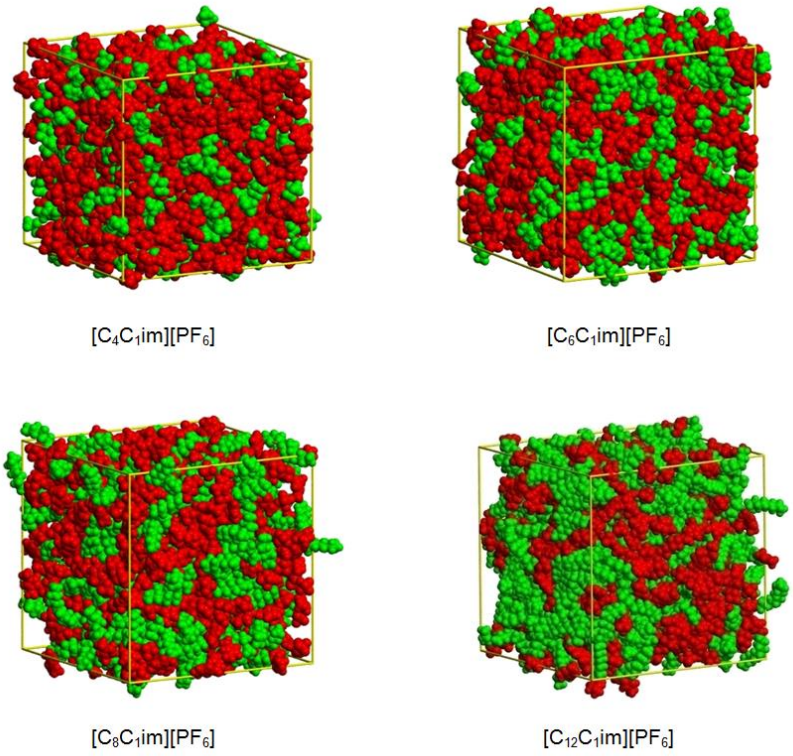

Figure 1.9. Snapshots of simulation boxes of $[C_{N-1}C_1im][PF_6]$. The code coloring, figure 1.8, enables a clear identification of the polar and nonpolar domains that form in ionic liquids. (adapted from source [57])

This characteristic of the structural organization in ionic liquids was first supported experimentally by X-ray diffraction[58] and later by small-wide angle X-ray scattering (SWAXS). [59,60]

Neutron diffraction was used to study the structures of 1,3-dimethylimidazolium chloride[61], $[C_1C_1im][Cl]$, and hexafluorophosphate[62], $[C_1C_1im][PF_6]$, ionic liquids. The comparison of diffraction patterns of deuterated and protiated liquids enables a detailed picture of the anion-cation and cation-cation

interactions. Based on this work, a strong charge ordering with similar anion-cation interactions for both anions was found. In both works, a strong correlation between the solid and liquid phases was detected. Later on, the liquid structure of 1,3-dimethylimidazolium bis{(trifluoromethane)sulfonyl}amide ionic liquid, $[C_1C_1im][NTf_2]$, was also explored.[63] In this ionic liquid, a significantly smaller charge ordering was observed, when compared with the analogous chloride [61] and hexafluorophosphate [62] based ionic liquids. This is related with the increase of the diffuse nature of the negative charge and the size of the $[NTf_2]^-$ anion. A comparative analysis concerning the similarities between the solid and liquid phases of $[C_1C_1im][Cl]$, $[C_1C_1im][PF_6]$, and $[C_1C_1im][NTf_2]$ was also performed. [63] Unlike the analogous chloride [61,64] and hexafluorophosphate[62,65] based ionic liquids, the liquid structure indicates little correlation with the solid state structure of $[C_1C_1im][NTf_2]$, as reported by Holbrey *et al.*.[66] The main reason for this is the fact that the $[NTf_2]^-$ anion presents a conformational flexibility (*trans* and *cis* conformers), with the *trans* conformation prevailing mainly in the liquid phase [63,67], while in the solid phase, the *cis* conformation is dominant.[66] Figure 1.10 presents the packing diagram for $[C_1C_1im][NTf_2]$, exhibiting two-dimensional layered structures.[66]

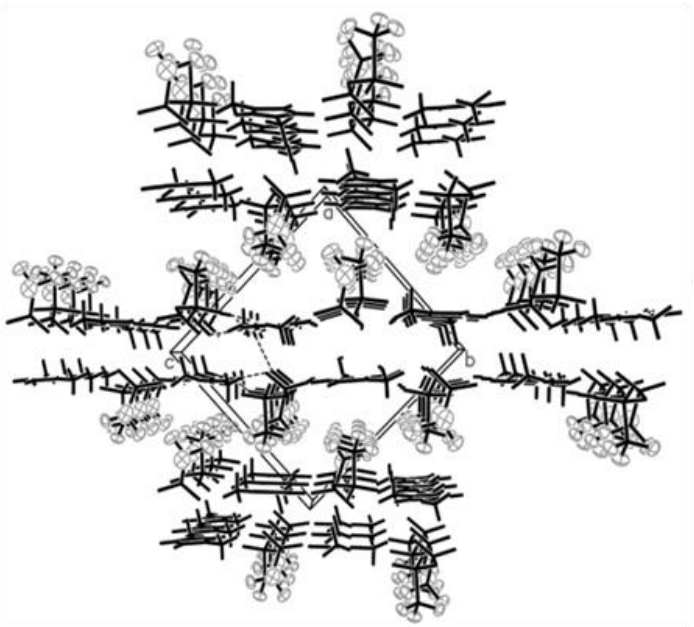

Figure 1.10. Packing diagram for $[C_1C_1im][NTf_2]$, revealing a two-dimensional layered structuring. (adapted from source [66])

In the high charge density region, the $[NTf_2]^-$ anion of the $[C_1C_1im][NTf_2]$ is hydrogen bonded to three in-plane $[C_1C_1im]^+$ cations, through C−H···O and C−H···N contacts with an additional imidazolium cation below each anion, from the nest layer of the double layer (figure 1.11).[66] Each anion is constrained by seven hydrogen-bonding interactions from hydrogen atoms of the cations to either oxygen or nitrogen atoms of the anions.

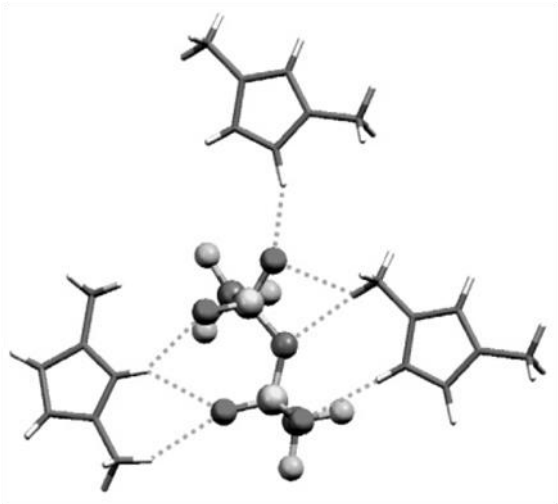

Figure 1.11. Cation anion hydrogen bonding in $[C_1C_1im][NTf_2]$, showing the three in-plane cations surrounding each anion. (adapted from source [66])

Bodo and coworkers [68] performed the first combined experimental and theoretical study of X-ray diffraction structure factors and the relative radial functions for a series of 1-alkyl-3-methylimidazolium bis(trifluoromethanesulfonyl)imide ionic liquids ($[C_{N-1}C_1im][NTf_2]$, *N* = 2, 5, 7, and 9). Using the obtained data, the geometric conformations of the anion and of the alkyl chains attached to the imidazolium ring were analyzed. It was found that, in the liquid, the alkyl side chains are characterized by a sequence of dihedral angles in the *anti* conformation and that the $[NTf_2]^-$ anion prefers the *trans* conformation, in agreement with previous works. [63,67] The authors also analyzed the behavior of the hydrogen bonds that are formed between the hydrogen of C2 position of the imidazolium cation and the anion. The detected hydrogen bonding is slightly directional and stronger with the hydrogen of the C2 position.

The methylation of the C2 position of imidazolium based ionic liquids inhibits the predominant hydrogen bonding interaction between the cation and anion, leading to changes not only at structural level but also of the physicochemical properties. Despite expectations, the C2-methylated ionic liquids present higher melting points and viscosities than their C2-protonated counterparts. [69,70] Ludwig and coworkers [46,52] hypothesized that, in the C2-methylated ionic liquids, the ions form a coulombic network and stabilize the whole system. In the C2-protonated ionic liquids, the formation of H-bonds between the anion and the H-C2 of the imidazolium ring weakens the coulombic network, hence destabilizing the system and resulting in lower melting points and viscosities.

Depending on the combination of anion and cation, there are other interactions that play an important role in the condensed phases of the ionic liquids. For example, in 1-ethyl-3-methylimidazolium bis(trifluoromethanesulfonyl)imide, $[C_2C_1im][NTf_2]$, the existence of interactions such as C-F$\cdots\pi$ and C-H$\cdots\pi$ were identified. [71]

1.1.4. Characteristics and Applications of Ionic Liquids

In the last decade, the interest in RTILs has increased gradually, mainly due their wide range of applications in chemistry and industry.[1,2,72] The possibility of concisely tuning the physical chemical properties by changing the anion-cation combination is one of the biggest advantages of these systems. The ionic liquids share common characteristics, such as:

- The ionic liquids were designated as "green solvents" due to their **low volatility**, which prevents their spread into the atmosphere. This characteristic limits the range of techniques available for their separation and purification, reducing the options for recycling after a manufacturing process as well as their recovery. However, due to this characteristic, the ionic liquids have the potential to replace many volatile organic solvents.
- The **wide liquidus ranges** exhibited by ionic liquids, together with low melting points, low volatility and the high number of possible anion-cation

possible combinations, offer opportunities for better reactivity control, which, to such an extent, was not feasible to achieve with common molecular solvents.

- The **high thermal stability** and low volatility allows carrying out reactions well beyond 100 ºC in non-pressurized reactors.
- Ionic liquids have **high thermal conductivities** which, combined with their wide liquidus temperature ranges and relatively high volumic heat capacities, make them excellent materials for thermal fluid applications.
- The solubility of water in ionic liquids can vary from complete miscibility to almost total immiscibility, simply by changing the anion from, e.g. Cl^- to $[PF_6]^-$. The ionic liquid's **polarity** is the driving force between water and chlorinated organic solvents and will vary depending on the nature of the ionic liquid constituents.
- **High capacity of dissolving gases**, due to the possibility of many types of interactions such as C−F···π, C−H···π, hydrogen bonding, charge dispersion, non-polar and polar interactions, as well as acid/ base equilibria. Ionic liquids can be tuned to act as gas carriers and to play a role in the development of gas membranes.
- Ionic liquids have a wide and stable **electrochemical window** and very high **ionic conductivities**, and together with the **nonflammability**, they are practical materials for use in electrochemistry. [73,74]

Due to these characteristics and some others not mentioned, the application of ionic liquids goes beyond their use as solvents. Over the years, a growing number of applications for these fluids were developed and nowadays they can be used in:

- **Organic reactions**, as ionic liquids may have a significant role in controlling reactions as **solvent** or **catalysts**. [1,3] It was found that ionic liquids are able to increase the reactivity and/or selectivity of a number of processes. The microenvironment generated by a solvent can change the outcome of a reaction, in terms of equilibria as well as rates.[75,76]
- Wood fractionation is usually attained by the Kraft process, which is not an environmental friendly process. The main challenge of designing these processes becoming environmentally more benign lies in the recovery and, in extension, reuse of applied solvents. Ionic liquids were widely investigated

as solvents for dissolution and **processing of biomass** because of some of the unique properties that they possess.[72,77,78]

- **Liquid-liquid separation** based on the immiscibility between two liquid phases at room temperature is an advantageous alternative to separate the components of an azeotropic mixture as well as to reduce energy consumption and the environmental impact. Taking into account the characteristics of ionic liquids, these systems are considered good candidates to be used as extracting solvents in the separation of azeotropic mixtures. [77,79–81]
- Ammonium based ionic liquids are being used as **metal extraction agents**, **phase transfer catalysts, surfactants** and **anti-static agents**. [82]
- Due to the wide and stable electrochemical window, ionic liquids were used in the fields of **electrosynthesis**, **electrocatalysis** and energy storage and conversion applications, especially, **lithium batteries and fuel cells**.[83]

1.1.5. Thermophysical Properties of Ionic Liquids

As mentioned above, the possible tuning of the physical-chemical properties by varying the nature of the anions and cations is one of the many advantages of these systems, which contributes to a design of "greener" ionic liquids for a specific application. In order to benefit from this characteristic of ionic liquids, highly accurate data regarding their physical-chemical properties is needed and essential to a deep understanding of ionic liquids on a molecular level, as well as for the application support and process optimization involving ionic liquids.

Thermal Phase Behavior of Ionic Liquids

The ionic liquids exhibit a wide liquidus range, which can be much greater than those found in common molecular solvents. This is dependent of the lower temperature limit (crystallization or glass formation) and of the upper temperature limit (usually the thermal decomposition temperature instead of the boiling temperature). The utility of the ionic liquids largely depends on its solid - liquid transition temperature and on the thermal decomposition temperature. [1,84]

The solid - liquid phase behavior of many ionic liquids is somewhat complex. They display low fusion temperatures due to the lower lattice energies compared with the traditional organic salts[1,31,85], which results from the asymmetric ions that have a shielded or delocalized charge, disturbing the anion - cation interaction. [85–87] For many ionic liquids, the cooling of the liquid phase tends to pass to a state of a metastable equilibrium (supercooling), and later to glass formation. In these cases, the kinetics of the transition, mainly governed by the liquid cooling rate (rapid or slow cooling), plays an important role. As a result, in order to obtain reliable thermal phase behavior data, long equilibration times and small samples are needed. [88,89]

The thermal phase behavior of ionic liquids was studied using mainly differential scanning calorimetry (DSC). The obtained data for these systems have revealed multiple solid-solid transitions, e.g. crystal-crystal polymorphism, as detected for $[C_4C_1im]Cl$ [31], and in some cases the ionic liquid exhibit plastic-crystal transitions, which consumes a fraction of the energy of fusion leading to crystal - liquid transition with a lower enthalpy of fusion. [90] The liquid, amorphous, and polymorphous crystalline phases of $[C_4C_1im][PF_6]$ were studied by Triolo *et al.*.[91] In this work, thermodynamic, structural, and dynamical information were obtained using quasi-adiabatic, continuous calorimetry, X-ray and neutron scattering. The obtained results show that conformational equilibria, solid polymorphism, or high viscosities, as well as experimental conditions may be relevant for supercooling behavior. The most widely studied ionic liquids are based on the bis(trifluoromethanesulfonyl)imide anion. The delocalized negative charge along the S−N−S atoms of the anion, and the steric features of the sulfonyl oxygen's and trifluoromethane groups reduces the ability for ion - ion interactions. Triolo *et al.*[60] reported the thermal phase behavior of *N*-alkyl-*N*-methylpiperidinium bis(trifluoromethanesulfonyl)imide, $[^1C_n{}^1C_1Pip][NTf_2]$, ionic liquids using differential scanning calorimetry. The studied series of $[^1C_n{}^1C_1Pip][NTf_2]$ (where n = 1 - 8), presented a complex thermal behavior, where some of the ionic liquids did not crystallize ($[^1C_4{}^1C_1Pip][NTf_2]$ and $[^1C_8{}^1C_1Pip][NTf_2]$), while the others have shown a variable number of crystalline phases ($[^1C_1{}^1C_1Pip][NTf_2]$ and $[^1C_2{}^1C_1Pip][NTf_2]$). $[^1C_1{}^1C_1Pip][NTf_2]$ presented two solid-solid transitions prior to the fusion transition at 398 K, while for $[^1C_2{}^1C_1Pip][NTf_2]$ was reported at least four solid-solid transitions previous to the fusion transition at 360 K, in agreement with a previous work.[92] Forsyth *el al.* [93] reported the thermal phase behavior of ionic liquids based on the tricyanomethanide anion. The temperatures of fusion of several pyrrolidinium and

imidazolium based ionic liquids, with different anions, were compared. The substitution of the cation from an imidazolium to a pyrrolidinium in the studied ionic liquids significantly affects the temperature of fusion. [93] The methylation of the C2 position of imidazolium based ionic liquids disrupts the predominant hydrogen bonding interaction between the cation and anion, and it would be expected a decrease of the temperature of fusion. However, the substitution of the C2 position leads to an increase of the temperature of fusion, which implies that the formation of H-bonding between the anion and the H-C2 of the imidazolium ring weakens the Coulombic network, destabilizing the system.[68,69,94]

In general, the thermal phase behavior of ionic liquids, particularly the temperature of fusion, depends on a number of features:

- Typically, the increase of the **cation or anion sizes** leads to a decrease of the temperature of fusion, which is related with the weaker electrostatic interactions in the crystal lattice.[1,85,94,95]
- The **symmetry** increase of the ions enhances a more efficient packing in the crystal, leading to higher temperatures of fusion.[1,85]
- The asymmetry increases due to the elongation **of the alkyl chains** of the ions, causing a disruption of the electrostatic interactions between the cation - anion and consequently results in the inhibition of the crystal formation and a pronounced tendency to supercool.[66,96] For the 1-alkyl-3-methylimidazolium based ionic liquids, the temperature of fusion decreases with the increase of the alkyl chain length, up to $[C_5C_1im]^+$ - $[C_6C_1im]^+$, and around $[C_8C_1im]^+$ - $[C_{10}C_1im]^+$, the temperature of fusion starts to increase.[1] This increase of the temperature of fusion for longer alkyl chain imidazolium ionic liquids is related with the contribution of the van der Waals interactions to the efficient packing.[1,85]
- The type and extend of the **hydrogen bonding** in ionic liquids.[46,52,85] However, the influence of hydrogen bonds in ionic liquids is still widely discussed. [22,44,97,98]
- The greater the **charge delocalization**, the lower the temperature of fusion. [1,14,85]
- The **branching** of the alkyl group results in temperature of fusion higher than the linear analogs.[1,99] The $[i\text{-}C_3C_1im][PF_6]$ presents a temperature of fusion about 60 K higher than the isomer $[C_3C_1im][PF_6]$.[94]

Thermal Stability of Ionic Liquids

The thermal stability and the short/long-term performance of ionic liquids are of great importance for engineering applications of ionic liquids. The upper temperature limit is usually related with the thermal decomposition temperature, due to the low volatility of ionic liquids. Thermal decomposition strongly depends on the structure of the ionic liquid. Usually, most of the ionic liquids can be kept in the liquid phase up to 600 K, with the thermal decomposition temperature around 600 to 700 K. [95,99] Thermal decomposition temperature are similar between different cations, nevertheless the imidazolium cations tend to be thermally more stable that the tetra-alkyl ammonium cations. [95,99] Unlike the observed effect of the cation, the anion can change dramatically the thermal stability of the ionic liquids.[1,94,95,99,100] The following order of the relative anion stabilities was found [94,99,101]:

$$[NTf_2]^- > [PF_6]^- \approx [BF_4]^- > \text{halides}$$

The thermal stability of an ionic liquid can also depend on the sample pan composition used in the thermal analysis experiments.[94] Ngo *et al.* [94] found that for $[C_2C_1im][PF_6]$ ionic liquid, the thermal stability is strongly affected by the pan composition, displaying 373 K lower thermal stability in the presence of aluminum compared to alumina.

Vaporization of Ionic Liquids

Until recently, ionic liquids were regarded as non-volatile, and thus did not exhibit measurable vapor pressure, even at higher temperatures. In fact, at room temperature, the vapor pressures of ionic liquids are too low to be detected. However, Earle *et al.*[102] have shown that some ionic liquids can be distilled at low pressure without decomposition. In this work, the distillation under different experimental conditions (time, pressure, temperature) of a range of ionic liquids was reported; some of the selected families did not show signs of degradation in the distilled samples.[102] Additionally, the authors presented a mechanism of mass transfer that could explain the obtained results, ignoring the possibility that ionic liquids could vaporize as ionic species. The vaporization mechanism was proposed to be via cluster formation in the gaseous phase (figure 1.12).[102]

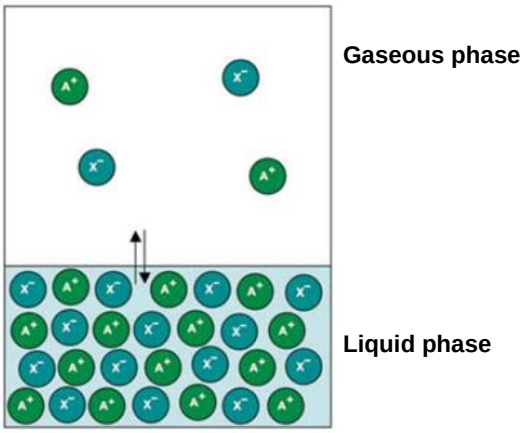

Figure 1.12. Schematic representation of the vaporization mechanism of an aprotic ionic liquid, in both liquid and gaseous phases, where the ionic liquid vaporizes as separated ionic species. (adapted from source [102])

This work was followed by that of Paulechka *et al.*[103] who determined the thermal stability of 1-butyl-3-methylimidazolium bis(trifluoromethylsulfonyl)amide, $[C_4C_1im][NTf_2]$, in vacuum, and evaluated the possibility of the measurement of vapor pressure and enthalpy of vaporization of this ionic liquid. Kabo and collaborators[104] reported the first experimental determinations of vapor pressures for a series of 1-alkyl-3-methylimidazolium bis(trifluoromethylsulfonyl)imide, $[C_{N-1}C_1im][NTf_2]$ (N = 3, 5, 7, and 9), ionic liquids, \ Based on this work, it was possible to prove that the balance of the thermal stability and volatility for $[C_{N-1}C_1im][NTf_2]$ allowed measurements of vapor pressures in a temperature range suitable for a proper evaluation of the thermodynamic properties of vaporization.[104] In the same year, Santos *et al.*[105] presented the first proof that the vaporization of ionic liquids occurs as a direct liquid to gas transfer of the intact ionic pair (figure 1.13), opposing the first proposed hypothesis[102].

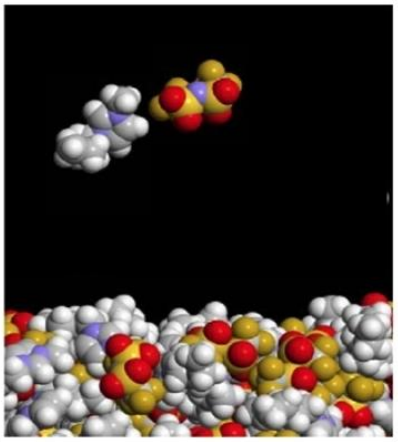

Figure 1.13. Current schematic representation of the vaporization mechanism of an aprotic ionic liquid, in both liquid and gaseous phases, where the ionic liquid vaporizes as neutral ion pairs. (adapted from source [105])

In this work, the enthalpies of vaporization, $\Delta_l^g H_m^o$, for 1-alkyl-3-methylimidazolium bis(trifluoromethylsulfonyl)imide, $[C_{N-1}C_1im][NTf_2]$ (N = 3 - 9), were directly determined using a Calvet drop microcalorimeter. [105–107] The $\Delta_l^g H_m^o$ obtained re-enforced the view of ionic liquids as structured media, and with the increase of alkyl side chains length, the nonpolar domains increase in size but the ionic network remains intact. Additionally, the experimental $\Delta_l^g H_m^o$ data, in the range of (130 to 160) kJ·mol^{-1}, where much higher than those of common organic solvents but lower than the predicted value of 300 kJ·mol^{-1}. [101–103,108] The reasonable agreement with the simulation results suggested that the gaseous phase is most likely to be composed of neutral ion pairs.[105] The proposed vaporization mechanism (vaporization of the ionic liquids via neutral ion pairs) where supported by studies using photoionization[109], line of sight mass spectrometry [110–112], Fourier transform ion cyclotron resonance[113,114], and by tunable vacuum ultraviolet photoionization [115]. Recently, Chaban and Prezhdo[116] reported equilibrium and real time non-equilibrium molecular dynamics simulations in order to get insights on the boiling and critical behavior of *N*-butylpyridinium tetrafluoroborate, $[C_4Py][BF_4]$, and 1-ethyl-3-methylimidazolium bis(trifluoromethylsulfonyl)imide, $[C_2C_1im][NTf_2]$. It was found, that in contrast to traditional gases, the saturated vapor of ionic liquids consists of neutral and charged species, where the species distribution depends on the ionic liquid chemical nature as well as the experimental conditions (temperature and pressure).[116]

For most of the ionic liquids, the determination of vapor pressures is extremely difficulty due to the competition between the vaporization and decomposition mechanisms as well as the effect of the presence of impurities.[117] Therefore, for many of the ionic liquid families, the vaporization does not occur due to the limit imposed by the decomposition temperature, as reported for $[C_4C_1im][PF_6]$ [118,119]. In fact, it was found that $[C_4C_1im][PF_6]$ was stable at 430 K under vacuum conditions, however the vapor pressure was too low to be determined with the available apparatus. Nevertheless, the authors estimated the vapor pressure of $[C_4C_1im][PF_6]$, at 298.15 K, to be (10^{-11})Pa, based on a combination of thermodynamic properties of the gaseous and liquid phases.[118–121]

These pioneering works[102–105] contributed to the knowledge of a window of opportunity[117] for the vaporization of some ionic liquids without decomposition. Moreover, it was possible to conclude that some ionic liquids can be vaporized under moderate temperatures and vacuum conditions, and that the gaseous phase is most likely to be composed of neutral ion pairs. Since then, different approaches were used to predict or / and to measure the properties related to the vapor-liquid equilibrium: vapor pressures, enthalpies of vaporization and boiling temperature.[117] In addition to the already cited works concerning the vapor pressure measurements by the integral Knudsen effusion method[104], and the determination of enthalpies of vaporization by Calvet drop calorimetry[105], several other techniques and strategies were used to determine the enthalpies of vaporization. Nowadays, there are a number of publications reporting enthalpies of vaporization, at a reference temperature, for a wide range of ionic liquids determined using both experimental[111,112,115,122–127] and theoretical methods[128,129]. Wang *et al.*[125] calculated enthalpies of vaporization based on the UV absorption spectra for a group of imidazolium and pyrrolidinium based ionic liquids over a range of temperature, while Chambreau *et al.*[115] measured $\Delta_l^g H_m^o$ of several ionic liquids using a heated effusive vapor source in conjunction with single photon ionization by a tunable vacuum ultraviolet synchrotron source. Jones and collaborators[111,112,122,126,130,131] determined the enthalpies of vaporization by temperature programmed desorption using line of sight mass spectrometry. In the first work[111], the authors developed a theory for rationalising and predicting the enthalpies of vaporization of ionic liquids. Recently, the extension of the work for more ionic liquids[112,122,131], allowed the refinement of the theory [122], and thereby the application to more ionic liquids. The

considered method comprises the decomposition of the enthalpy of vaporization into a coulombic contribution (which is a function of the molar volume of the ionic liquid) and a van der Waals contribution (which is the non-coulombic contribution to the enthalpy of vaporization). [111,112,122,126,130,131]

Despite all of these efforts, the experimental results gathered until now, mainly for the series $[C_{N-1}C_1im][NTf_2]$ [104,105], exhibit a controversial discrepancy between the enthalpies of vaporization with regard to the cation's alkyl chain length effect. It must be stressed that the data published are concerned with vapor - liquid equilibria, consisting mainly of repetitions using in some cases inappropriate techniques/ methodologies, extrapolations and predictions for essentially the same ionic liquid family and for a relatively small set of experiments, which leads, sometimes, to inaccurate conclusions. Accurate thermodynamic properties of vaporization equilibrium of ionic liquids are scarce and yet crucial for a better understanding of the liquid phase of ionic liquids, the evaluation of cohesive energy, as well as the nature of the gaseous phase. Furthermore, these data are required for validation and parameterization of the models (force fields) used to describe ionic liquids in different simulation techniques.[57,117,132] Despite of the importance of the vapor pressures of ionic liquids and the related thermodynamic properties of vaporization, $\Delta_l^g H_m^o$, $\Delta_l^g S_m^o$, and $\Delta_l^g G_m^o$, respectively, most of the works performed until now are focused on estimation and determination of enthalpies of vaporization.[117]

Heat Capacities of Ionic Liquids

Heat capacity is widely used in several areas such as: thermodynamics for obtaining entropy and enthalpy values, thermochemistry for calculating changes in reaction enthalpies and in chemical engineering for establishing energy balances.[133–136] The possible use of ionic liquids as heat transfer fluids for heat exchange in chemical plants and solar thermal power generation was discussed, and it was found that the imidazolium based ionic liquids present higher heat capacities per unit of volume that two high performance commercial thermal fluids. [136–138] Therefore, this knowledge of the heat capacity is required for the evaluation of the applicability of the ionic liquid as heat transfer fluids.[136–138]

In most works, the heat capacity of ionic liquids were determined using calorimetric methods, mainly differential scanning calorimetry, DSC, and modulated DSC, however their uncertainty is in the order of 5%.[136,139] The most exhaustive compilations of heat capacities of ionic liquids are presented in the IL Thermo database[140], and in the well-known reviews on heat capacities of ionic liquids by Y. Paulechka[136] and liquids by Zábranský *et al.*[134], where experimental data on heat capacities of 50 ionic liquids were presented. Shimizu *et al.*[141–143] reported the alkyl chain length dependency of the heat capacities of imidazolium based ionic liquids, $[C_{N-1}C_1im][NTf_2]$, n-alkanes, 1-alkanols and 1-chloroalkanes. The heat capacities of the studied ionic liquids were measured by adiabatic calorimetry, and are in agreement with the data obtained by Paulechka *et al.*[118,144–146]. It was found that the heat capacity values increase linearly along the alkyl side chain, which indicates that the methylene group, $-CH_2-$, equally contributes to the heat capacity in each series of substances. Additionally, it was found that the thermal motion of the alkyl chain of $[C_{N-1}C_1im][NTf_2]$ in the liquid phase is nearly identical to those of typical molecular liquids, despite of the different intermolecular interactions subsisting between constituent particles.[141] Coutinho and collaborator[147], explored the effect of the anion on several thermophysical properties of 1-ethyl-3-methylimidazolium based ionic liquids, $[C_2C_1im]^+$. The heat capacities of the studied ionic liquids were measured using a high-precision heat capacity drop calorimeter, and it was found that, at 298.15 K, the molar heat capacities decrease with the following anion sequence: $[(CH_3O)_2PO_2]^-$ > $[CF_3SO_3]^-$ > $[CH_3OHPO_2]^-$ > $[CH_3SO_3]^-$ > $[CH_3CO_2]^-$ > $[N(CN)_2]^-$ > $[SCN]^-$, a finding which is related with the size of the anion. The effect of the cation on the heat capacities is less pronounced than the effect of the anion.[148–150] Paulechka *et al.* [151] reported heat capacity data for nine ionic liquids with different cations and anions, measured by adiabatic calorimetry. Based on the obtained results and reliable literature data, the molar heat capacity data were correlated with the molar volume over a wide temperature range. It was found that, at a given temperature, the volumic heat capacity of ILs remains constant within ±5% and that the volumic heat capacity of ionic liquids linearly changes with temperature in the range of (258 to 370)K.[151]

Viscosities of Ionic Liquids

An important property which characterizes the behavior of liquids is the viscosity, due to fact that it relates the shear stress in a moving fluid to the strain rate of the fluid, which is caused by intermolecular interactions present in the fluid. The flow characteristics of the liquids are essentially dependent on the viscosity and are divided into two broad categories: Newtonian and non-Newtonian. A fluid for which the viscosity does not change with the shear rate is defined as Newtonian fluid. Fluids in which the viscosity varies with the shear rate are termed non-Newtonian fluids.[152,153]

Usually the viscosities of ionic liquids were measured using the falling or rolling ball, capillary, and rotational methods.[1] Ionic liquids present a higher viscosity (around 10 mPa·s to 726 mPa·s)[1,154] than typical molecular liquids (around 0.2 mPa·s and 10 mPa·s) [1,154,155], and widely depends on the type of the combination of cation and anion. Compilations of thermophysical properties, including viscosity data, were published, describing the main aspects of the effect of the cation or anion, impurities and used methods on the thermophysical properties.[1,13,100,140,154,156] The viscosity of imidazolium based ionic liquids increases with growing alkyl side chain and is more pronounced in ionic liquids which contains the chloride anion.[1,148,154] The viscosity decreases with the following anion sequence[1,154]: Cl^- > $[CH_3COO]^-$ > $[PF_6]^-$ > $[BF_4]^-$ > $[OTf]^-$ > $[NTf_2]^-$, which seems to be related with the size, symmetry and sphericity of the anion. For the cases considering the same anion, the viscosity decreases with the following cation sequence[154]: pyrrolidinium > pyridinium > imidazolium, in agreement with the findings with the results reported by Crosthwaite *et al.*.[148] Besides of the effect of the cation and anion on the viscosities of ionic liquids, the effect of water content and chloride impurities was also evaluated in the literature[156–160], and it was pointed out that the presence of very low concentrations of chloride in the ionic liquid sample drastically increases the viscosity, whereas the presence of water reduces the viscosity. In general, in a viscous liquid, such as an ionic liquid, the viscosity decreases more markedly with the increase of temperature than in a molecular liquid, such as dodecanol (figure 1.14).[13,154,161,162]

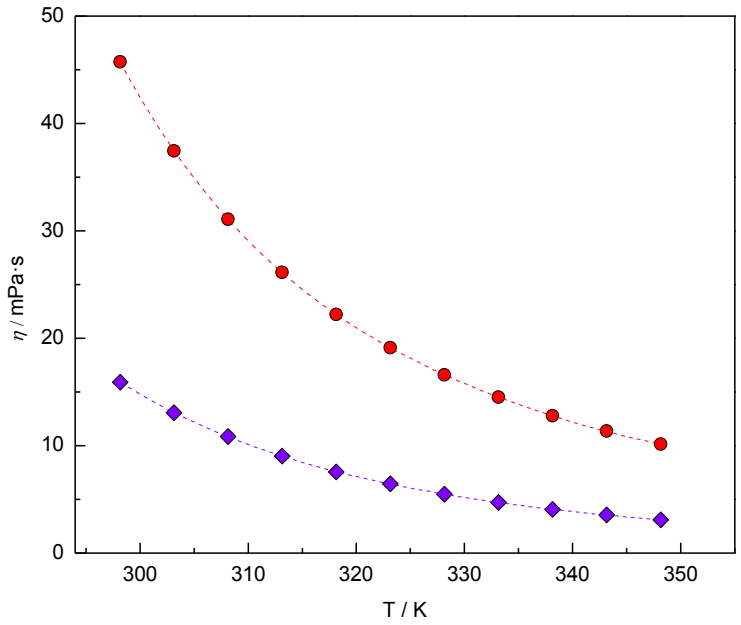

Figure 1.14. Viscosity of $[C_3C_1im][NTf_2]$[162] (filled circles, ●) and dodecanol[161] (filled diamonds, ◆).

Densities of Ionic Liquids

Density is a property required for industrial process design and implementation as well as for the development of equations of state.[1,85,154,163] Most of the ionic liquids are denser than water, with values ranging between (1000 to 1600) kg m^{-3}. [1,13,154,164–166] Usually the density of ionic liquids is measured using the vibrating-tube densimeter[163,166–168] and pycnometric [118,164,166] methods. In some cases, the density of ionic liquids are obtained by calculation through speed of sound measurements.[154,169]

Compilations of thermophysical properties, including density data, were published, describing the main aspects of the effect of the cation or anion, impurities and used methods on the thermophysical properties. [1,13,140,154,163–168,170,171] Densities are related with the molar masses and, in general, ionic liquids containing heavy atoms are denser. A qualitative analysis of the evolution of density and viscosity with cation and anion was performed by Jacquemin *et al.*.[160] In this work, the authors studied six ionic liquids with different anions and cations, and as expected the densities of the studied ionic liquids decrease with the following anion sequence: $[NTf_2]^-$ > $[PF_6]^-$ > $[BF_4]^-$.[160] Considering the same anion, the density decreases with

increasing length of the alkyl chain on the imidazolium cation. [13,160] Additionally to the study of the pure ionic liquids, the same properties were measured for water-saturated ionic liquids, and it was observed that the obtained results differ from the dried samples of about 1 to 2%, which is almost negligible. The effect of chloride impurities was evaluated in the literature[172], and was shown that increasing chloride contamination leads to a decrease in the density over a wide range of values. In general, the densities of ionic liquids do not shown a marked dependency with the temperature and the density decreases almost linear with increasing temperature.

Refractive Indices of Ionic Liquids

The refractive index is a fundamental property which is widely used for identification and assessment of purity of a compound, to estimate the boiling point and the liquid viscosity. It is most commonly used in the characterization of hydrocarbons and petroleum samples[173], and to measure the concentration of a solute in an aqueous solution (e.g. determination of sugar content in a solution of sugar, Brix).[174] The refractive index is itself an important optical property of a substance that describes how radiation propagates through the medium.

Despite of the intensive research on ionic liquid properties, the refractive index is one of the least studied.[147,175–184] Tariq *et al.* [179] reported a systematic study of densities and refractive indices of several ionic liquids. In this work, different empirical models for the density calculation of ionic liquids were tested; the molar refractions were calculated from the volumetric and refractive index data, as well.
The main goal of this work was to systematically study the effect of the alkyl chain length increase of the 1-alkyl-3-methylimidazolium cation, the nature of the anion or cation, and temperature. It was found that the refractive index of the studied ionic liquids increases when enlarging the alkyl side chain length of the cation. Furthermore, the refractive index is ordered in the following sequence of anions, for the same cation in the respective ionic liquid's composition:

$$[PF_6]^- < [BF_4]^- < [NTf_2]^- < [OTf]^- < [MeSO_4]^- < [OAc]^-$$

Later on, the previous work[179] was complemented by the calculated density and cohesive molar internal energy using molecular dynamic simulations for the same

ionic liquids.[185] Based on this work, the relationship between the molecular refractive indices and the cohesive molecular internal energies was established.

Recently, Schröder and collaborators [175] published the molar polarizabilities and molar volume for 71 ionic liquids, which were extracted from the refractive index and density data. Based on this work, the authors developed a "Designed Regression analysis" model that can be used to predict the molar polarizability, the density, and the refractive index of any chosen imidazolium-based ionic liquid in reasonable agreement with experimental data. However, this model only applies to imidazolium based ionic liquids.

1.2 Aim of the Work and Organization of the Thesis

The initial working plan proposed for this Ph.D. project was related with the thermodynamic study of some representative pure ionic liquids and their mixtures with molecular solvents. However, the first thermodynamic results obtained for the extended series of 1-alkyl-3-methylimidazolium bis(trifluoromethylsulfonyl)imide, $[C_{N-1}C_1im][NTf_2]$ ionic liquids, showed that the so-called nanostructuration of ionic liquids could be detected based on the trend change of the thermodynamic properties along the series. Therefore, the aim of this work was focused in study of the effect of nanostructuration of pure ionic liquids on their thermophysical properties.

This work was planned and performed with the main goal to provide new insights in the nanostructuration of ionic liquids, as well as, to contribute to a better understanding of the cohesive interaction in the ionic liquids in the liquid phase. In order to achieve this molecular view of the thermophysical properties obtained in this work, several representative pure ionic liquids were studied, exploring the effect of the alkyl side chain length, symmetry of the cation and the cation/anion topology.

After a brief introduction to the central themes and the aim of this Ph.D. project in the present chapter, the thermophysical characterization of some ionic liquid families performed in this project is organized as follow:

Chapter 2 presents the ionic liquid families that were used to evaluate the effects of structural changes (length of the alkyl side chain, symmetry, nature of anion and cation) on the thermophysical properties. It also describes the purification

process and characterization of the studied ionic liquids, as well as additional materials used for the calibration and test of experimental techniques.

In Chapter 3, the description of the methodologies and strategies used for the measurement of the ionic liquids is described in detail. This chapter includes the description of the construction and test of a new Knudsen/Quartz Crystal Effusion (KEQCM II) and the reassembling and test of a high precision heat capacity drop calorimeter. The description of the Knudsen/Quartz Crystal Effusion installation I (KEQCM I) was also briefly described. A comparison between the two Knudsen/ Quartz Crystal Effusion installations, underlining the advantages and disadvantages inherent to each one of them, is presented. A brief description of the commercial apparatus used for viscosity and density measurements, as well as, refractive indices, is also provided.

Chapter 4 is dedicated to the presentation of the experimental results obtained during this Ph.D. project and the discussion. The experimental results and discussion are presented in article format, and a brief summary of each work is given. Each article is presented as sub-chapter in the following order:

I. Reassembling and testing of a high-precision heat capacity drop calorimeter. Heat capacity of some polyphenyls at T = 298.15 K.
II. High-Accuracy Vapor Pressure Data of the Extended $[C_nC_1im][Ntf_2]$ Ionic Liquid Series: Trend Changes and Structural Shifts.
III. Heat Capacities at 298.15 K of the Extended $[C_nC_1im][Ntf_2]$ Ionic Liquid Series.
IV. Cation Symmetry Effect on the Volatility of Ionic Liquids.
V. Evidence of Nanostructuration from the Heat Capacities of the $[C_{N/2}C_{N/2}im][NTf_2]$ Ionic Liquid Series.
VI. Volatility Study of $[C_1C_1im][NTf_2]$ and $[C_2C_3im][NTf_2]$ Ionic Liquids.
VII. Alkylimidazolium Based Ionic Liquids: Impact of Cation Symmetry on their Nanoscale Structural Organization.
VIII. Vapor Pressures of 1,3-Dialkylimidazolium Bis(trifluoromethylsulfonyl)imide Ionic Liquid Series with Long Alkyl Chain Length.
IX. Thermophysical Properties of $[C_{N-1}C_1im][PF_6]$ Ionic Liquids.
X. Heat Capacities of $[C_{N-1}C_1im][PF_6]$ Ionic Liquids.
XI. First Volatility Study of the 1-Alkylpyridinium based Ionic Liquids by Knudsen Effusion.
XII. Novel 1-Ethyl-2-Alkylpyridinium based Ionic Liquids: Synthesis and Volatility.
XIII. Thermophysical Properties of a Novel Pyridinium Based Ionic Liquids Family.

The description of the reassembling and testing of a twin heat conduction and high-precision drop microcalorimeter for the measurement of heat capacities of small samples, which was used in the heat capacities measurements of the ionic liquids, is presented in Paper I.

Papers II and III explore the effect of nanostructuration of ionic liquids on the thermodynamic properties of vaporization and heat capacity data. The results presented are an important contribution to the thermodynamic view of the nanostructuration of ionic liquids that was only detected due to the experimental strategy of exploring the extended series of $[C_{N-1}C_1im][NTf_2]$ ionic liquids.

Papers IV - VIII deal with the effect of symmetry of the imidazolium cation on the thermophysical properties explored in this project. The effect of symmetry and the dependence of the thermophysical properties with growing alkyl chain length was explored on the $[C_{N/2}C_{N/2}im][NTf_2]$ ionic liquid series.

Papers IX and X explore the effect of the anion on the thermophysical properties of $[C_{N-1}C_1im][PF_6]$. Vapor pressures were not measured for this ionic liquid family, mainly due to the early decomposition occurring at temperatures before a measurable vapor pressure.

The effect of the cation and the dependence of the thermophysical properties with growing alkyl chain length on $[C_NPy][NTf_2]$ and $[^1C_2{}^2C_NPy][NTf_2]$ were explored in Papers XI to XIII. The obtained results were rationalized based on a comparative analysis with the thermophysical properties obtained for $[C_{N-1}C_1im][NTf_2]$ ionic liquid series.

Finally, in Chapter 5, general conclusions are drawn concerning the accomplishments of the presented work and some considerations concerning the future perspectives are outlined.

References

(1) Wasserscheid, P.; Welton, T., Eds.; *Ionic Liquids in Synthesis*, Wiley-VCH Verlag GmbH Weinheim, Germany, **2007**.

(2) Wang, C.; Cui, G.; Luo, X.; Xu, Y.; Li, H.; Dai, S., *J. Am. Chem. Soc.* 133 (**2011**) 11916–11919.

(3) Clare, B.; Sirwardana, A.; MacFarlane, D. R., *Top. Curr. Chem.* 290 (**2010**) 1–40.

(4) Kirchner, B., Ed.; *Ionic Liquids*; Springer Berlin Heidelberg, Berlin, Heidelberg, **2010**.

(5) Kadokawa, J.-I., Ed.; *Ionic Liquids - New Aspects for the Future*; InTech, **2013**.

(6) Gabriel S.; Weiner, J., *Ber. Dtsch. Chem. Ges.* 21 (**1888**) 2669 – 2679.

(7) Walden, P., *Bull. Acad. Imp. Sci.* 8 (**1914**) 405 – 422.

(8) Hurley; F. H.; Wler, Jr.; T. P., *J. Electrochem. Soc.* 98 (**1951**) 207–212.

(9) Wilkes, J. S.; Levisky, J. A.; Wilson, R. A.; Hussey, C. L., *Inorg. Chem.* 21 (**1982**) 1263–1264.

(10) Boon, J. A.; Levisky, J. A.; Pflug, J. L.; Wilkes, J. S., *J. Org. Chem.* 51 (**1986**) 480–483.

(11) Fry, S. E.; Pienta, N. J., *J. Am. Chem. Soc.* 107 (**1985**) 6399–6400.

(12) Wilkes, J. S.; Zaworotko, M. J., *J. Chem. Soc., Chem. Commun.* (**1992**) 965–967.

(13) Marsh, K. N.; Boxall, J. A.; Lichtenthaler, R., *Fluid Phase Equilib.* 219 (**2004**) 93–98.

(14) Weingärtner, H., *Angew. Chem. Int. Ed.* 47 (**2008**) 654–670.

(15) Joshi, M. D.; Anderson, J. L., *RSC Adv.* 2 (**2012**) 5470–5484.

(16) Grätzel, M., *J. Photoch. Photobio. C: Photochem. Rev.* 4 (**2003**) 145–153.

(17) Bonhôte, P.; Dias, A.-P.; Papageorgiou, N.; Kalyanasundaram, K.; Grätzel, M., *Inorg. Chem.* 35 (**1996**) 1168–1178.

(18) Ohno, H., *Bull. Chem. Soc. Jpn.* 79 (**2006**) 1665–1680.

(19) Plechkova, N. V; Seddon, K. R., *Chem. Soc. Rev.* 37 (**2008**) 123–150.

(20) Klamt, A. *COSMO-RS: From Quantum Chemistry to Fluid Phase Thermodynamics and Drug Design*; Elsevier Science, **2005**.

(21) COSMOtherm property prediction for Ionic Liquid Solutions. Basics & Visualization http://www.cosmologic.de/index.php?cosId=4205&crId=4 (accessed May 15, 2013).

(22) Hunt, P. A.; Kirchner, B.; Welton, T., *Chem. Eur. J.* 12 (**2006**) 6762–6775.

(23) Hanke, C. G.; Price, S. L.; Lynden-Bell, R. M., *Mol. Phys.* 99 (**2001**) 801–809.

(24) Canongia Lopes, J. N.; Deschamps, J.; Pádua, A. A. H., *J. Phys. Chem. B* 108 (**2004**) 2038–2047.

(25) Aggarwal, A.; Lancaster, N. L.; Sethi, A. R.; Welton, T., *Green Chem.* 4 (**2002**) 517–520.

(26) Dieter, K. M.; Dymek, C. J.; Heimer, N. E.; Rovang, J. W.; Wilkes, J. S., *J. Am. Chem. Soc.* 110 (1988) 2722–2726.

(27) Bühl, M.; Chaumont, A.; Schurhammer, R.; Wipff, G., *J. Phys. Chem. B* 109 (**2005**) 18591–18599.

(28) Turner, E. A.; Pye, C. C.; Singer, R. D., *J. Phys. Chem. A* 107 (**2003**) 2277–2288.

(29) Hunt, P. A.; Gould, I. R., *J. Phys. Chem. A* 110 (**2006**) 2269–2282.

(30) Kempter, V.; Kirchner, B., *J. Mol. Struct.* 972 (**2010**) 22–34.

(31) Holbrey, J. D.; Reichert, W. M.; Nieuwenhuyzen, M.; Johnson, S.; Seddon, K. R.; Rogers, R. D., *Chem. Commun.* (**2003**) 1636–1637.

(32) Saha, S.; Hayashi, S.; Kobayashi, A.; Hamaguchi, H., *Chem. Lett.* 32 (**2003**) 740–741.

(33) Meng, Z.; Dölle, A.; Robert Carper, W., *J. Mol. Struct.: THEOCHEM* 585 (**2002**) 119–128.

(34) Tsuzuki, S.; Tokuda, H.; Hayamizu, K.; Watanabe, M., *J. Phys. Chem. B* 109 (**2005**) 16474–16481.

(35) Gozzo, F. C.; Santos, L. S.; Augusti, R.; Consorti, C. S.; Dupont, J.; Eberlin, M. N., *Chem. Eur. J.* 10 (**2004**) 6187–6193.

(36) Paulechka, Y. U.; Kabo, G. J.; Emel'yanenko, V. N., *J. Phys. Chem. B* 112 (**2008**) 15708–15717.

(37) Fernandes, A. M.; Rocha, M. A. A.; Freire, M. G.; Marrucho, I. M.; Coutinho, J. A. P.; Santos, L. M. N. B. F., *J. Phys. Chem. B* 115 (**2011**) 4033–4041.

(38) Spohr, H. V; Patey, G. N., *J. Chem. Phys.* 132 (**2010**) 234510.

(39) Spohr, H. V; Patey, G. N., *J. Chem. Phys.* 132 (**2010**) 154504.

(40) Spohr, H. V; Patey, G. N., *J. Chem. Phys.* 130 (**2009**) 104506.

(41) Ballone, P.; Pinilla, C.; Kohanoff, J.; Del Pópolo, M. G., *J. Phys. Chem. B* 111 (**2007**) 4938–4950.

(42) Zahn, S.; Bruns, G.; Thar, J.; Kirchner, B., *Phys. Chem. Chem. Phys.* 10 (**2008**) 6921–6924.

(43) Zahn, S.; Uhlig, F.; Thar, J.; Spickermann, C.; Kirchner, B., *Angew. Chem. Int. Ed.* 47 (**2008**) 3639–3641.

(44) Lehmann, S. B. C.; Roatsch, M.; Schöppke, M.; Kirchner, B., *Phys. Chem. Chem. Phys.* 12 (**2010**) 7473–7486.

(45) Zahn, S.; Thar, J.; Kirchner, B., *J. Chem. Phys.* 132 (**2010**) 124506.

(46) Fumino, K.; Wulf, A.; Ludwig, R., *Phys. Chem. Chem. Phys.* 11 (**2009**) 8790–8794.

(47) Qiao, B.; Krekeler, C.; Berger, R.; Delle Site, L.; Holm, C., *J. Phys. Chem. B* 112 (**2008**) 1743–1751.

(48) Thar, J.; Brehm, M.; Seitsonen, A. P.; Kirchner, B., *J. Phys. Chem. B* 113 (**2009**) 15129–15132.

(49) Dommert, F.; Schmidt, J.; Krekeler, C.; Zhao, Y. Y.; Berger, R.; Delle Site, L.; Holm, C., *J. Mol. Liq.* 152 (**2010**) 2–8.

(50) Gomes, M. F. C.; Lopes, J. N. C.; Padua, A. A. H. *Top. Curr. Chem.* 290 (**2010**) 161–183.

(51) Stark, A. *Top. Curr. Chem.* 290 (**2010**) 41–81.

(52) Roth, C.; Peppel, T.; Fumino, K.; Köckerling, M.; Ludwig, R., *Angew. Chem. Int. Ed.* 49 (**2010**) 10221–10224.

(53) Hansen J.-P.; McDonald, I. R.; *Theory of Simple Liquids*; Academic Press, Elsevier, London, UK, **2006**.

(54) Urahata, S. M.; Ribeiro, M. C. C., *J. Chem. Phys.* 122 (**2005**) 024511.

(55) Wang, Y.; Voth, G. A., *J. Am. Chem. Soc.* 127 (**2005**) 12192–12193.

(56) Izvekov, S.; Voth, G. A., *J. Chem. Phys.* 123 (**2005**) 123, 134105.

(57) Canongia Lopes, J. N. A.; Pádua, A. A. H., *J. Phys. Chem. B* 110 (**2006**) 110, 3330–3335.

(58) Triolo, A.; Russina, O.; Bleif, H.-J.; Di Cola, E., *J. Phys. Chem. B* 111 (**2007**) 4641–4644.

(59) Russina, O.; Triolo, A.; Gontrani, L.; Caminiti, R.; Xiao, D.; Hines Jr, L. G.; Bartsch, R. A.; Quitevis, E. L.; Pleckhova, N.; Seddon, K. R., *J. Phys.: Condens. Matter* 21 (**2009**) 424121.

(60) Triolo, A.; Russina, O.; Fazio, B.; Appetecchi, G. B.; Carewska, M.; Passerini, S., *J. Chem. Phys.* 130 (**2009**) 164521.

(61) Hardacre, C.; Holbrey, J. D.; McMath, S. E. J.; Bowron, D. T.; Soper, A. K., *J. Chem. Phys.* 118 (2003) 118, 273–279.

(62) Hardacre, C.; McMath, S. E. J.; Nieuwenhuyzen, M.; Bowron, D. T.; Soper, A. K., *J. Phys.: Condens. Matter* 15 (**2003**) S159–S166.

(63) Deetlefs, M.; Hardacre, C.; Nieuwenhuyzen, M.; Padua, A. A. H.; Sheppard, O.; Soper, A. K., *J. Phys. Chem. B* 110 (**2006**) 12055–12061.

(64) Arduengo, A. J.; Dias, H. V. R.; Harlow, R. L.; Kline, M., *J. Am. Chem. Soc.* 114 (1992) 5530–5534.

(65) Holbrey, J. D.; Reichert, W. M.; Nieuwenhuyzen, M.; Sheppard, O.; Hardacre, C.; Rogers, R. D. *Chem. Commun.* (**2003**) 476–477.

(66) Holbrey, J. D.; Reichert, W. M.; Rogers, R. D., *Dalton Trans.* (**2004**) 2267–2271.

(67) Fujii, K.; Fujimori, T.; Takamuku, T.; Kanzaki, R.; Umebayashi, Y.; Ishiguro, S.-I., *J. Phys. Chem. B* 110 (**2006**) 8179–8183.

(68) Bodo, E.; Gontrani, L.; Caminiti, R.; Plechkova, N. V; Seddon, K. R.; Triolo, A., *J. Phys. Chem. B* 114 (**2010**) 16398–16407.

(69) Zhang, Y.; Maginn, E. J., *Phys. Chem. Chem. Phys.* 14 (**2012**) 12157–12164.

(70) Noack, K.; Schulz, P. S.; Paape, N.; Kiefer, J.; Wasserscheid, P.; Leipertz, A., Phys. Chem. Chem. Phys. 12 (**2010**) 14153–14161.

(71) Dean, P. M.; Pringle, J. M.; Forsyth, C. M.; Scott, J. L.; MacFarlane, D. R. *New J. Chem.* 32 (**2008**) 2121–2126.

(72) Tan, S. S. Y.; MacFarlane, D. R., *Top. Curr. Chem.* 290 (**2010**) 311–339.

(73) Ohno, H., Ed.; *Electrochemical Aspects of Ionic Liquids*; John Wiley & Sons, Inc., Hoboken, New Jersey, **2005**.

(74) Angell, C. A.; Xu, W.; Yoshizawa, M.; Hayashi, A.; Belieres, J.-P.; Lucas, P.; Videa, M., in *Electrochemical Aspects of Ionic Liquids*; Ohno, H., Ed.; John Wiley & Sons, Inc., Hoboken, New Jersey, **2005**, 5–23.

(75) Pârvulescu, V. I.; Hardacre, C., *Chem. Rev.* 107 (**2007**) 2615–2665.

(76) Zhang, Q.; Zhang, S.; Deng, Y., *Green Chem.* 13 (**2011**) 2619–2637.

(77) Kokorin, A., Ed.; *Ionic Liquids: Applications and Perspectives*; InTech, **2011**.

(78) Pinkert, A.; Marsh, K. N.; Pang, S.; Staiger, M. P. *Chem. Rev.* 109 (**2009**) 6712–6728.

(79) Kroon, M. C.; Peters, C. J., in *Applied Thermodynamics of Fluids*; Goodwin, A. R., Sengers, J.; Peters, C. J., Eds.; Royal Society of Chemistry, **2010**; 368–393.

(80) Cláudio, A. F. M.; Ferreira, A. M.; Freire, M. G.; Coutinho, J. A. P., *Green Chem.* 15 (**2013**) 2002–2010.

(81) Neves, C. M. S. S.; Ventura, S. P. M.; Freire, M. G.; Marrucho, I. M.; Coutinho, J. A. P., *J. Phys. Chem. B* 113 (**2009**) 5194–5199.

(82) Stojanovic, A.; Morgenbesser, C.; Kogelnig, D.; Krachler, R.; Keppler, B. K., in *Ionic Liquids: Theory, Properties, New Approaches*; Kokorin, A., Ed.; InTech, **2011**; 657–680.

(83) Liu, Y.-S.; Pan, G.-B., in *Ionic Liquids: Applications and Perspectives*; Kokorin, A., Ed.; Intech, **2011**; 627–642.

(84) Castner, E. W.; Wishart, J. F., *J. Chem. Phys.* 132 (**2010**) 120901.

(85) Dean, P. M.; Pringle, J. M.; MacFarlane, D. R., *Phys. Chem. Chem. Phys.* 12 (**2010**) 9144–9153.

(86) Reichert, W. M.; Holbrey, J. D.; Vigour, K. B.; Morgan, T. D.; Broker, G. A.; Rogers, R. D., *Chem. Commun.* **2006**, 4767–4779.

(87) Forsyth, C. M.; MacFarlane, D. R.; Golding, J. J.; Huang, J.; Sun, J.; Forsyth, M., *Chem. Mater.* 14 (**2002**) 2103–2108.

(88) Donth, E.-J.; Zunger, A.; Hull, R.; Osgood, Jr., R. M.; Sakaki, H. Eds.; *The Glass Transition: Relaxation Dynamics in Liquids and Disordered Materials*; Springer Series in Materials Science, V. 48, Springer, Berlin, Heidelberg, **2001**.

(89) Papon, P.; Leblond, J.; Meijer, P. H. E., Eds.; *The Physics of Phase Transitions: Concepts and Applications*, Springer, Berlin, Heidelberg, **2006**.

(90) Hardacre, C.; Holbrey, J. D.; McCormac, P. B.; McMath, S. E. J.; Nieuwenhuyzen, M.; Seddon, K. R., *J. Mater. Chem.* 11 (**2001**) 346–350.

(91) Triolo, A.; Mandanici, A.; Russina, O.; Rodriguez-Mora, V.; Cutroni, M.; Hardacre, C.; Nieuwenhuyzen, M.; Bleif, H.-J.; Keller, L.; Ramos, M. A., *J. Phys. Chem. B* 110 (**2006**) 21357–21364.

(92) Henderson, W. A.; Young Jr., V. G.; Pearson, W.; Passerini, S.; De Long, H. C.; Trulove, P. C., *J. Phys.: Condens. Matter* 18 (**2006**) 10377–10390.

(93) Forsyth, S. A.; Batten, S. R.; Dai, Q.; MacFarlane, D. R., *Aust. J. Chem.* 57 (**2004**) 121–124.

(94) Ngo, H. L.; LeCompte, K.; Hargens, L.; McEwen, A. B., *Thermochim. Acta* 357–358 (**2000**) 97–102.

(95) Zhang, S.; Sun, N.; He, X.; Lu, X.; Zhang, X. *J. Phys. Chem. Ref. Data* 35 (**2006**) 1475–1517.

(96) Bradley, A. E.; Hardacre, C.; Holbrey, J. D.; Johnston, S.; McMath, S. E. J.; Nieuwenhuyzen, M., *Chem. Mater.* 14 (**2002**) 629–635.

(97) Tsuzuki, S.; Tokuda, H.; Mikami, M., *Phys. Chem. Chem. Phys.* 9 (**2007**) 4780–4784.

(98) Fumino, K.; Wulf, A.; Ludwig, R., *Angew. Chem. Int. Ed.* 47 (**2008**) 8731–8734.

(99) Huddleston, J. G.; Visser, A. E.; Reichert, W. M.; Willauer, H. D.; Broker, G. A.; Rogers, R. D., *Green Chem.* 3 (**2001**) 156–164.

(100) Aparicio, S.; Atilhan, M.; Karadas, F. *Ind. Eng. Chem. Res.* 49 (**2010**) 9580–9595.

(101) Rebelo, L. P. N.; Lopes, J. N. C.; Esperança, J. M. S. S.; Filipe, E., *J. Phys. Chem. B* 109 (**2005**) 6040–6043.

(102) Earle, M. J.; Esperança, J. M. S. S.; Gilea, M. A.; Lopes, J. N. C.; Rebelo, L. P. N.; Magee, J. W.; Seddon, K. R.; Widegren, J. A., *Nature* 439 (**2006**) 831–834.

(103) Paulechka, Y. U.; Zaitsau, D. H.; Kabo, G. J.; Strechan, A. A., *Thermochim. Acta* 439 (**2005**) 158–160.

(104) Zaitsau, D. H.; Kabo, G. J.; Strechan, A. A.; Paulechka, Y. U.; Tschersich, A.; Verevkin, S. P.; Heintz, A., *J. Phys. Chem. A* 110 (**2006**) 7303–7306.

(105) Santos, L. M. N. B. F.; Lopes, J. N. C.; Coutinho, J. A. P.; Esperança, J. M. S. S.; Gomes, L. R.; Marrucho, I. M.; Rebelo, L. P. N., *J. Am. Chem. Soc.* 129 (**2007**) 284–285.

(106) Adedeji, F. A.; Lalage, D.; Brown, S.; Connor, J. A.; Leung, M. L.; Paz-Andrade, I. M.; Skinner, H. A., *J. Organomet. Chem.* 97 (**1975**) 221–228.

(107) Santos, L. M. N. B. F.; Schröder, B.; Fernandes, O. O. P.; Ribeiro da Silva, M. A. V., *Thermochim. Acta* 415 (**2004**) 15–20.

(108) Rebelo, L. P. N.; Lopes, J. N. C.; Esperança, J. M. S. S.; Guedes, H. J. R.; Łachwa, J.; Najdanovic-Visak, V.; Visak, Z. P., *Acc. Chem. Res.* 40 (**2007**) 1114–1121.

(109) Strasser, D.; Goulay, F.; Kelkar, M. S.; Maginn, E. J.; Leone, S. R., *J. Phys. Chem. A* 111 (**2007**) 3191–3195.

(110) Emel'yanenko, V. N.; Verevkin, S. P.; Heintz, A.; Corfield, J.-A.; Deyko, A.; Lovelock, K. R. J.; Licence, P.; Jones, R. G., *J. Phys. Chem. B* 112 (**2008**) 11734–11742.

(111) Armstrong, J. P.; Hurst, C.; Jones, R. G.; Licence, P.; Lovelock, K. R. J.; Satterley, C. J.; Villar-Garcia, I. J., *Phys. Chem. Chem. Phys.* 9 (**2007**) 982–990.

(112) Lovelock, K. R. J.; Deyko, A.; Corfield, J.-A.; Gooden, P. N.; Licence, P.; Jones, R. G. *ChemPhysChem* 10 (**2009**) 337–340.

(113) Leal, J. P.; Piedade, M. E. M.; Lopes, J. N. C.; Tomaszowska, A. A.; Esperança, J. M. S. S.; Rebelo, L. P. N.; Seddon, K. R. *J. Phys. Chem. B* 113 (**2009**) 3491–3498.

(114) Leal, J. P.; Esperança, J. M. S. S.; Piedade, M. E. M.; Lopes, J. N. C.; Rebelo, L. P. N.; Seddon, K. R., *J. Phys. Chem. A* 111 (**2007**) 6176–6182.

(115) Chambreau, S. D.; Vaghjiani, G. L.; To, A.; Koh, C.; Strasser, D.; Kostko, O.; Leone, S. R., *J. Phys. Chem. B* 114 (**2010**) 1361–1367.

(116) Chaban, V. V.; Prezhdo, O. V. *J. Phys. Chem. Lett.* 3 (**2012**) 1657–1662.

(117) Esperança, J. M. S. S.; Lopes, J. N. C.; Tariq, M.; Santos, L. M. N. B. F.; Magee, J. W.; Rebelo, L. P. N., *J. Chem. Eng. Data* 55 (**2010**) 3–12.

(118) Kabo, G. J.; Blokhin, A. V.; Paulechka, Y. U.; Kabo, A. G.; Shymanovich, M. P.; Magee, J. W., *J. Chem. Eng. Data* 49 (**2004**) 453–461.

(119) Paulechka, Y. U.; Kabo, G. J.; Blokhin, A. V.; Vydrov, O. A.; Magee, J. W.; Frenkel, M., *J. Chem. Eng. Data* 48 (**2003**) 457–462.

(120) Morrow, T. I.; Maginn, E. J., *J. Phys. Chem. B* 106 (**2002**) 12807–12813.

(121) Shah, J. K.; Brennecke, J. F.; Maginn, E. J., *Green Chem.* 4 (**2002**) 112–118.

(122) Deyko, A.; Lovelock, K. R. J.; Corfield, J.-A.; Taylor, A. W.; Gooden, P. N.; Villar-Garcia, I. J.; Licence, P.; Jones, R. G.; Krasovskiy, V. G.; Chernikova, E. A.; Kustov, L. M., *Phys. Chem. Chem. Phys.* 11 (**2009**) 8544–8555.

(123) Verevkin, S. P.; Zaitsau, D. H.; Emel'yanenko, V. N.; Ralys, R. V.; Yermalayeu, A. V.; Schick, C., *J. Chem. Thermodyn.* 54 (**2012**) 433–437.

(124) Fumino, K.; Wulf, A.; Verevkin, S. P.; Heintz, A.; Ludwig, R., *ChemPhysChem* 11 (**2010**) 1623–1626.

(125) Wang, C.; Luo, H.; Li, H.; Dai, S., *Phys. Chem. Chem. Phys.* 12 (**2010**) 7246–7250.

(126) Deyko, A.; Hessey, S. G.; Licence, P.; Chernikova, E. A.; Krasovskiy, V. G.; Kustov, L. M.; Jones, R. G., *Phys. Chem. Chem. Phys.* 14 (**2012**) 3181–3193.

(127) Verevkin, S. P.; Ralys, R. V.; Zaitsau, D. H.; Emel'yanenko, V. N.; Schick, C., *Thermochim. Acta* 538 (**2012**) 55–62.

(128) Köddermann, T.; Paschek, D.; Ludwig, R., *ChemPhysChem* 9 (**2008**) 549–555.

(129) Ludwig, R., *Phys. Chem. Chem. Phys.* 10 (**2008**) 4333–4339.

(130) Deyko, A.; Lovelock, K. R. J.; Licence, P.; Jones, R. G. *Phys. Chem. Chem. Phys.* 13 (**2011**) 16841–16850.

(131) Lovelock, K. R. J.; Deyko, A.; Licence, P.; Jones, R. G., *Phys. Chem. Chem. Phys.* 12 (**2010**) 8893–8901.

(132) Dommert, F.; Wendler, K.; Berger, R.; Delle Site, L.; Holm, C., *ChemPhysChem* 13 (**2012**) 1625–1637.

(133) Zábranský, M.; Růžička, V.; Domalski, E. S., *J. Phys. Chem. Ref. Data* 30 (**2001**) 1199–1689.

(134) Zábranský, M.; Kolská, Z.; Růžička, V.; Domalski, E. S., *J. Phys. Chem. Ref. Data* 39 (**2010**) 013103.

(135) Wilhelm, E.; Letcher, T.; Eds.; *Heat Capacities: Liquids, Solutions and Vapours*; Royal Society of Chemistry, Cambridge, UK, **2010**.

(136) Paulechka, Y. U., *J. Phys. Chem. Ref. Data* 39 (**2010**) 033108.

(137) França, J. M. P.; Nieto de Castro, C. A.; Lopes, M. M.; Nunes, V. M. B., *J. Chem. Eng. Data* 54 (**2009**) 2569–2575.

(138) Chaban, V. V.; Prezhdo, O. V., *J. Phys. Chem. Lett.* 4 (2013) 1423–1431.

(139) Chirico, R. D.; Diky, V.; Magee, J. W.; Frenkel, M.; Marsh, K. N., *Pure and Appl. Chem.* 81 (**2009**) 791–828.

(140) IL Thermo database, http://ilthermo.boulder.nist.gov/ILThermo/mainmenu.uix. NIST Standard Reference Database Number 147 (National Institute of Standards and Technology, Gaithersburg, MD) (accessed 02 July, 2013).

(141) Shimizu, Y.; Ohte, Y.; Yamamura, Y.; Saito, K., *Chem. Phys. Lett.* 470 (**2009**) 295–299.

(142) Shimizu, Y.; Ohte, Y.; Yamamura, Y.; Saito, K.; Atake, T., *J. Phys. Chem. B* 110 (**2006**) 13970–13975.

(143) Shimizu, Y.; Ohte, Y.; Yamamura, Y.; Saito, K., *Chem. Lett.* 36 (**2007**) 1484–1485.

(144) Blokhin, A. V.; Paulechka, Y. U.; Kabo, G. J., *J. Chem. Eng. Data* 51 (**2006**) 1377–1388.

(145) Blokhin, A. V; Paulechka, Y. U.; Strechan, A. A.; Kabo, G. J., *J. Phys. Chem. B* 112 (**2008**) 4357–4364.

(146) Paulechka, Y. U.; Blokhin, A. V.; Kabo, G. J.; Strechan, A. A., *J. Chem. Thermodyn.* 39 (**2007**) 866–877.

(147) Freire, M. G.; Teles, A. R. R.; Rocha, M. A. A.; Schröder, B.; Neves, C. M. S. S.; Carvalho, P. J.; Evtuguin, D. V.; Santos, L. M. N. B. F.; Coutinho, J. A. P., *J. Chem. Eng. Data* 56 (**2011**) 4813–4822.

(148) Crosthwaite, J. M.; Muldoon, M. J.; Dixon, J. K.; Anderson, J. L.; Brennecke, J. F., *J. Chem. Thermodyn.* 37 (**2005**) 559–568.

(149) Ge, R.; Hardacre, C.; Jacquemin, J.; Nancarrow, P.; Rooney, D. W., *J. Chem. Eng. Data* 53 (**2008**) 2148–2153.

(150) Brigouleix, C.; Anouti, M.; Jacquemin, J.; Caillon-Caravanier, M.; Galiano, H.; Lemordant, D., *J. Phys. Chem. B* 114 (**2010**) 1757–1766.

(151) Paulechka, Y. U.; Kabo, A. G.; Blokhin, A. V.; Kabo, G. J.; Shevelyova, M. P., *J. Chem. Eng. Data* 55 (**2010**) 2719–2724.

(152) Brujan, E.-A.; *Non-Newtonian Fluids With Biomedical and Bioengineering Applications*, Springer-Verlag, Berlin, Heidelberg, **2011**.

(153) Viswanath, D. S., Ghosh, T. K., Prasad, D. H. L., Dutt, N. V. K., Rani, K. Y.; V*iscosity of Liquids: Theory, Estimation, Experiment, and Data*; Springer, **2007**.

(154) Rooney, D.; Jacquemin, J.; Gardas, R., *Top. Curr. Chem.* 290 (**2010**) 185–212.

(155) Lide, D. R., Ed.; *CRC Handbook of Chemistry and Physics*, 84th ed., CRC Press, **2003**.

(156) Seddon, K. R.; Stark, A.; Torres, M.-J., in *Clean Solvents*; Abraham, M. A.; Moens, L., Eds.; ACS Symposium Series, **2002**.

(157) Baker, S. N.; Baker, G. A.; Bright, F. V., *Green Chem.* 4 (**2002**) 165–169.

(158) Widegren, J. A.; Laesecke, A.; Magee, J. W., *Chem. Commun.* (**2005**) 1610–1612.

(159) Saha, S.; Hamaguchi, H., *J. Phys. Chem. B* 110 (**2006**) 2777–2781.

(160) Jacquemin, J.; Husson, P.; Padua, A. A. H.; Majer, V., *Green Chem.* 8 (**2006**) 172–180.

(161) Matsuo, S.; Makita, T., *Int. J. Thermophys.* 10 (**1989**) 833–843.

(162) Tariq, M.; Carvalho, P. J.; Coutinho, J. A. P.; Marrucho, I. M.; Lopes, J. N. C.; Rebelo, L. P. N., *Fluid Phase Equilib.* 301 (**2011**) 22–32.

(163) Goodwin, A. R. H.; Marsh, K. N.; Wakeham, W. A., Eds.; *Measurement of the Thermodynamic Properties of Single Phases, Experimental Thermodynamics*, Vol. VI; Elsevier Science B. V., Amsterdam, The Netherlands, **2003**.

(164) Fredlake, C. P.; Crosthwaite, J. M.; Hert, D. G.; Aki, S. N. V. K.; Brennecke, J. F., *J. Chem. Eng. Data* 49 (**2004**) 954–964.

(165) Almeida, H. F. D.; Passos, H.; Lopes-da-Silva, J. A.; Fernandes, A. M.; Freire, M. G.; Coutinho, J. A. P., *J. Chem. Eng. Data* 57 (**2012**) 3005–3013.

(166) Machanová, K.; Boisset, A.; Sedláková, Z.; Anouti, M.; Bendová, M.; Jacquemin, J., *J. Chem. Eng. Data* 57 (**2012**) 2227–2235.

(167) Tariq, M.; Esperança, J. M. S. S.; Soromenho, M. R. C.; Rebelo, L. P. N.; Lopes, J. N. C., *Phys. Chem. Chem. Phys.* 15 (**2013**) 10960–10970.

(168) Harris, K. R.; Woolf, L. A.; Kanakubo, M., *J. Chem. Eng. Data* 50 (**2005**) 1777–1782.

(169) Dzida, M.; Chorążewski, M.; Geppert-Rybczyńska, M.; Zorębski, E.; Zorębski, M.; Żarska, M.; Czech, B., *J. Chem. Eng. Data* 58 (**2013**) 1571–1576.

(170) Esperança, J. M. S. S.; Visak, Z. P.; Plechkova, N. V.; Seddon, K. R.; Guedes, H. J. R.; Rebelo, L. P. N., *J. Chem. Eng. Data* 51 (**2006**) 2009–2015.

(171) Gardas, R. L.; Freire, M. G.; Carvalho, P. J.; Marrucho, I. M.; Fonseca, I. M. A.; Ferreira, A. G. M.; Coutinho, J. A. P., *J. Chem. Eng. Data* 52 (**2007**) 1881–1888.

(172) Troncoso, J.; Cerdeiriña, C. A.; Sanmamed, Y. A.; Romaní, L.; Rebelo, L. P. N., *J. Chem. Eng. Data* 51 (**2006**) 1856–1859.

(173) Speight, J. G. *The Chemistry and Technology of Petroleum*; 4th Ed.; CRC Press, **2006**.

(174) Cantor, J. M., Ed.; *Progress in Food Engineering Research and Development*; Nova Science Pub. Inc., **2008**.

(175) Bica, K.; Deetlefs, M.; Schröder, C.; Seddon, K. R., *Phys. Chem. Chem. Phys.* 15 (**2013**) 2703–2711.

(176) Seki, S.; Tsuzuki, S.; Hayamizu, K.; Umebayashi, Y.; Serizawa, N.; Takei, K.; Miyashiro, H., *J. Chem. Eng. Data* 57 (**2012**) 2211–2216.

(177) Xu, W.-G.; Li, L.; Ma, X.-X.; Wei, J.; Duan, W.-B.; Guan, W.; Yang, J.-Z., *J. Chem. Eng. Data* 57(**2012**) 2177–2184.

(178) Iglesias-Otero, M. A.; Troncoso, J.; Carballo, E.; Romaní, L., *J. Chem. Thermodyn.* 40 (**2008**) 949–956.

(179) Tariq, M.; Forte, P. A. S.; Gomes, M. F. C.; Lopes, J. N. C.; Rebelo, L. P. N., *J. Chem. Thermodyn.* 41 (**2009**) 790–798.

(180) Deetlefs, M.; Seddon, K. R.; Shara, M., *Phys. Chem. Chem. Phys.* 8 (**2006**) 642–649.

(181) Gómez, E.; González, B.; Calvar, N.; Tojo, E.; Domínguez, Á., *J. Chem. Eng. Data* 51 (**2006**) 2096–2102.

(182) Kim, K.-S.; Shin, B.-K.; Lee, H.; Ziegler, F., *Fluid Phase Equilib.* 218 (**2004**) 215–220.

(183) Pereiro, A. B.; Rodríguez, A., *J. Chem. Eng. Data* 52 (**2007**) 600–608.

(184) Fröba, A. P.; Kremer, H.; Leipertz, A., *J. Phys. Chem. B* 112 (**2008**) 12420–12430.

(185) Shimizu, K.; Tariq, M.; Costa Gomes, M. F.; Rebelo, L. P. N.; Canongia Lopes, J. N., *J. Phys. Chem. B* 114 (**2010**) 5831–5834.

CHAPTER 2

Sample Preparation and Purification

2.1 Studied Ionic Liquids

The studied ionic liquids covered some representative ionic liquid families that were used to evaluate the effects of structural changes (length of the alkyl side chain, symmetry, impact of chosen anion and cation) on the thermophysical properties. The following ionic liquid families were explored:

- 1-alkyl-3-methylimidazolium bis(trifluoromethylsulfonyl)imide, $[C_{N-1}C_1im][NTf_2]$;
- 1,3- dialkylimidazolium bis(trifluoromethylsulfonyl)imide, $[C_{N/2}C_{N/2}im][NTf_2]$;
- 1-alkyl-3-methylimidazolium hexafluorophosphate, $[C_{N-1}C_1im][PF_6]$;
- 1-alkylpyridinium bis(trifluoromethylsulfonyl)imide, $[C_NPy][NTf_2]$;
- 1-ethyl-2-alkylpyridinium bis(trifluoromethylsulfonyl)imide, $[^1C_2{}^2C_{N-2}Py][NTf_2]$.

The majority of the studied ionic liquids were purchased from IoLiTec with a stated purity better than 98%. Some of the samples of 1-alkyl-3-methylimidazolium bis(trifluoromethylsulfonyl)imide used in the volatility study were synthesized and purified in the Queen's University Ionic Liquid Laboratories (QUILL), following the reported procedure.[1] The 1-ethyl-2-alkylpyridinium bis(trifluoromethylsulfonyl)imide ionic liquid family were synthesized, characterized and purified by a researcher from the group of Emilia Tojo at the Faculty of Chemistry of the University of Vigo. The information regarding the ionic liquids under study is compiled in table 2.1.

Table 2.1. Summary of the ionic liquids studied in this work.

Name of Ionic liquid	Abbreviation Molecular formula	Schematic Structural formula	Molar Mass / g·mol^{-1}	Purity / %	Supplier
1,3-dimethylimidazolium bis(trifluoromethylsulfonyl)imide	$[C_1C_1im][NTf_2]$ $C_7H_9F_6N_3O_4S_2$	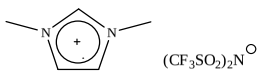	377.286	99 / 99	Synthesized U. Aveiro / IoLiTec
1-ethyl-3-methylimidazolium bis(trifluoromethylsulfonyl)imide	$[C_2C_1im][NTf_2]$ $C_8H_{11}F_6N_3O_4S_2$	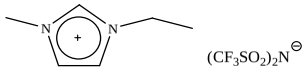	391.313	99 / 99.5	Synthesized QUILL / IoLiTec
1-methyl-3-propylimidazolium bis(trifluoromethylsulfonyl)imide	$[C_3C_1im][NTf_2]$ $C_9H_{13}F_6N_3O_4S_2$	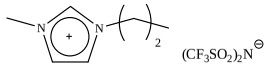	405.340	99 / 99	Synthesized QUILL / IoLiTec
1-butyl-3-methylimidazolium bis(trifluoromethylsulfonyl)imide	$[C_4C_1im][NTf_2]$ $C_{10}H_{15}F_6N_3O_4S_2$	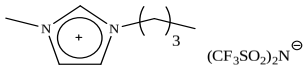	419.366	99 / 99.5	Synthesized QUILL / IoLiTec
1-methyl-3-pentylimidazolium bis(trifluoromethylsulfonyl)imide	$[C_5C_1im][NTf_2]$ $C_{11}H_{17}F_6N_3O_4S_2$	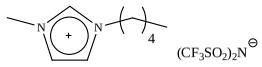	433.393	99 / > 99	Synthesized QUILL / IoLiTec

Table 2.1. Summary of the ionic liquids studied in this work. Continuation.

Name of Ionic liquid	Abbreviation Molecular formula	Schematic Structural formula	Molar Mass / g·mol^{-1}	Purity / %	Supplier
1-hexyl-3-methylimidazolium bis(trifluoromethylsulfonyl)imide	$[C_6C_1im][NTf_2]$ $C_{12}H_{19}F_6N_3O_4S_2$	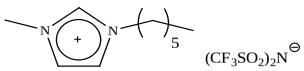	447.420	99 / 99	Synthesized QUILL / IoLiTec
1-heptyl-3-methylimidazolium bis(trifluoromethylsulfonyl)imide	$[C_7C_1im][NTf_2]$ $C_{13}H_{21}F_6N_3O_4S_2$	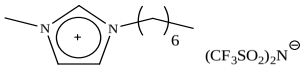	461.446	99 / > 99	Synthesized QUILL / IoLiTec
1-methyl-3-octylimidazolium bis(trifluoromethylsulfonyl)imide	$[C_8C_1im][NTf_2]$ $C_{14}H_{23}F_6N_3O_4S_2$	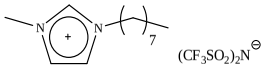	475.473	99 / 99	Synthesized QUILL / IoLiTec
1- methyl-3-nonylimidazolium bis(trifluoromethylsulfonyl)imide	$[C_9C_1im][NTf_2]$ $C_{15}H_{25}F_6N_3O_4S_2$	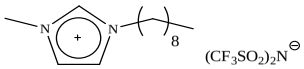	489.500	> 99	IoLiTec
1-decyl-3-methylimidazolium bis(trifluoromethylsulfonyl)imide	$[C_{10}C_1im][NTf_2]$ $C_{16}H_{27}F_6N_3O_4S_2$	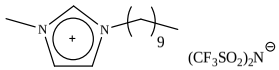	503.526	99 / > 98	Synthesized QUILL / IoLiTec

Table 2.1. Summary of the ionic liquids studied in this work. Continuation.

Name of Ionic liquid	Abbreviation Molecular formula	Schematic Structural formula	Molar Mass / g·mol^{-1}	Purity / %	Supplier
1-methyl-3-undecylimidazolium bis(trifluoromethylsulfonyl)imide	$[C_{11}C_1im][NTf_2]$ $C_{17}H_{29}F_6N_3O_4S_2$	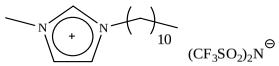	517.553	97	IoLiTec
1-dodecyl-3-methylimidazolium bis(trifluoromethylsulfonyl)imide	$[C_{12}C_1im][NTf_2]$ $C_{18}H_{31}F_6N_3O_4S_2$	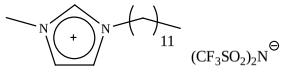	531.580	99 / > 98	Synthesized QUILL / IoLiTec
1-tetradecyl-3-methylimidazolium bis(trifluoromethylsulfonyl)imide	$[C_{14}C_1im][NTf_2]$ $C_{20}H_{35}F_6N_3O_4S_2$	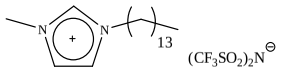	559.633	> 98	IoLiTec
1-hexadecyl-3-methylimidazolium bis(trifluoromethylsulfonyl)imide	$[C_{16}C_1im][NTf_2]$ $C_{22}H_{39}F_6N_3O_4S_2$	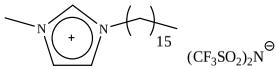	587.686	> 98	IoLiTec
1-butyl-3-methylimidazolium hexafluorophosphate	$[C_4C_1im][PF_6]$ $C_8H_{15}F_6N_2P$	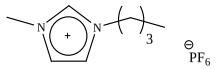	284.183	99	IoLiTec

Table 2.1. Summary of the ionic liquids studied in this work. Continuation.

Name Ionic liquid	Abbreviation Molecular formula	Schematic Structural formula	Molar Mass / g·mol^{-1}	Purity / %	Supplier
1-methyl-3-pentylimidazolium hexafluorophosphate	$[C_5C_1im][PF_6]$ $C_9H_{17}F_6N_2P$	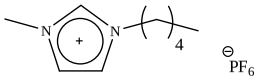	298.210	> 99	IoLiTec
1-hexyl-3-methylimidazolium hexafluorophosphate	$[C_6C_1im][PF_6]$ $C_{10}H_{19}F_6N_2P$	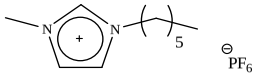	312.236	99	IoLiTec
1-heptyl-3-methylimidazolium hexafluorophosphate	$[C_7C_1im][PF_6]$ $C_{11}H_{21}F_6N_2P$	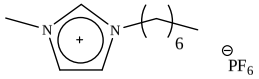	326.263	> 99	IoLiTec
1-methyl-3-octylimidazolium hexafluorophosphate	$[C_8C_1im][PF_6]$ $C_{12}H_{23}F_6N_2P$	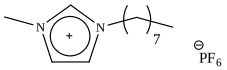	340.290	99	IoLiTec
1- methyl-3-nonylimidazolium hexafluorophosphate	$[C_9C_1im][PF_6]$ $C_{13}H_{25}F_6N_2P$	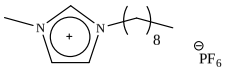	354.316	> 99	IoLiTec

Table 2.1. Summary of the ionic liquids studied in this work. Continuation.

Name Ionic liquid	Abbreviation Molecular formula	Schematic Structural formula	Molar Mass / g·mol^{-1}	Purity / %	Supplier
1,3-diethylimidazolium bis(trifluoromethylsulfonyl)imide	$[C_2C_2im][NTf_2]$ $C_9H_{13}F_6N_3O_4S_2$	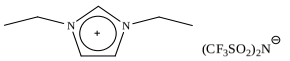	405.340	> 99	IoLiTec
1-ethyl-3-propylimidazolium bis(trifluoromethylsulfonyl)imide	$[C_2C_3im][NTf_2]$ $C_{10}H_{15}F_6N_3O_4S_2$	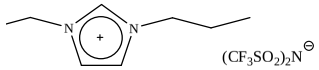	419.366	> 99.5	IoLiTec
1,3-dipropylimidazolium bis(trifluoromethylsulfonyl)imide	$[C_3C_3im][NTf_2]$ $C_{11}H_{17}F_6N_3O_4S_2$	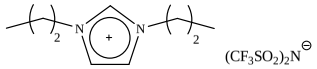	433.393	99	IoLiTec
1,3-dibutylimidazolium bis(trifluoromethylsulfonyl)imide	$[C_4C_4im][NTf_2]$ $C_{13}H_{21}F_6N_3O_4S_2$	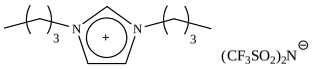	461.446	99	IoLiTec
1,3-dipentylimidazolium bis(trifluoromethylsulfonyl)imide	$[C_5C_5im][NTf_2]$ $C_{15}H_{25}F_6N_3O_4S_2$	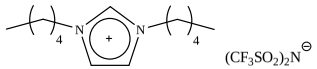	489.500	98.5	IoLiTec

Table 2.1. Summary of the ionic liquids studied in this work. Continuation.

Name Ionic liquid	Abbreviation Molecular formula	Schematic Structural formula	Molar Mass / g·mol^{-1}	Purity / %	Supplier
1,3-dihexylimidazolium bis(trifluoromethylsulfonyl)imide	$[C_6C_6im][NTf_2]$ $C_{17}H_{29}F_6N_3O_4S_2$	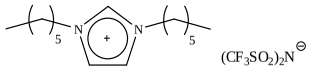	517.553	> 99	IoLiTec
1,3-diheptylimidazolium bis(trifluoromethylsulfonyl)imide	$[C_7C_7im][NTf_2]$ $C_{19}H_{33}F_6N_3O_4S_2$	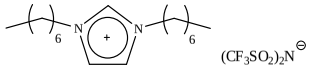	545.606	> 98	IoLiTec
1,3-dioctylimidazolium bis(trifluoromethylsulfonyl)imide	$[C_8C_8im][NTf_2]$ $C_{21}H_{37}F_6N_3O_4S_2$	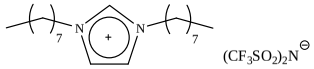	573.66	> 98	IoLiTec
1,3-dinonylimidazolium bis(trifluoromethylsulfonyl)imide	$[C_9C_9im][NTf_2]$ $C_{23}H_{41}F_6N_3O_4S_2$	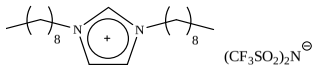	601.713	98	IoLiTec
1,3-didecylimidazolium bis(trifluoromethylsulfonyl)imide	$[C_{10}C_{10}im][NTf_2]$ $C_{25}H_{45}F_6N_3O_4S_2$	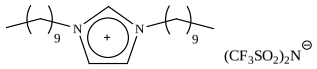	629.766	> 98	IoLiTec

Table 2.1. Summary of the ionic liquids studied in this work. Continuation.

Name Ionic liquid	Abbreviation Molecular formula	Schematic Structural formula	Molar Mass / g·mol^{-1}	Purity / %	Supplier
1,3-didodecylimidazolium bis(trifluoromethylsulfonyl)imide	$[C_{12}C_{12}im][NTf_2]$ $C_{29}H_{53}F_6N_3O_4S_2$	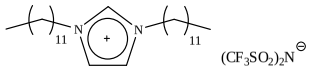	685.873	> 98	IoLiTec
1-ethylpyridinium bis(trifluoromethylsulfonyl)imide	$[C_2Py][NTf_2]$ $C_9H_{10}F_6N_2O_4S_2$	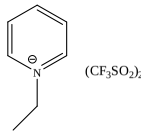	388.309	99	IoLiTec
1-propylpyridinium bis(trifluoromethylsulfonyl)imide	$[C_3Py][NTf_2]$ $C_{10}H_{12}F_6N_2O_4S_2$	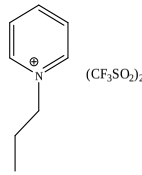	402.336	99	IoLiTec
1-butylpyridinium bis(trifluoromethylsulfonyl)imide	$[C_4Py][NTf_2]$ $C_{11}H_{14}F_6N_2O_4S_2$	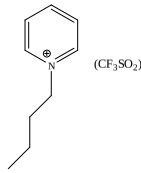	416.362	99	IoLiTec
1,2-diethylpyridinium bis(trifluoromethylsulfonyl)imide	$[^2C_2{}^1C_2Py][NTf_2]$ $C_{11}H_{14}F_6N_2O_4S_2$	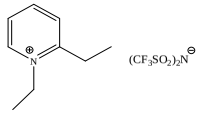	416.362	> 99	Synthesized U. Vigo

Table 2.1. Summary of the ionic liquids studied in this work. Continuation.

Name Ionic liquid	Abbreviation Molecular formula	Schematic Structural formula	Molar Mass / g·mol^{-1}	Purity / %	Supplier
1-ethyl-2-propylpyridinium bis(trifluoromethylsulfonyl)imide	$[^2C_3{}^1C_2Py][NTf_2]$ $C_{12}H_{16}F_6N_2O_4S_2$	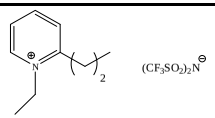	430.389	> 99	Synthesized U. Vigo
1-ethyl-2-butylpyridinium bis(trifluoromethylsulfonyl)imide	$[^2C_4{}^1C_2Py][NTf_2]$ $C_{13}H_{18}F_6N_2O_4S_2$	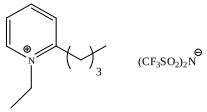	444.416	> 99	Synthesized U. Vigo
1-ethyl-2-pentylpyridinium bis(trifluoromethylsulfonyl)imide	$[^2C_5{}^1C_2Py][NTf_2]$ $C_{14}H_{20}F_6N_2O_4S_2$	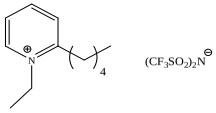	458.442	> 99	Synthesized U. Vigo
1-ethyl-2-hexylpyridinium bis(trifluoromethylsulfonyl)imide	$[^2C_6{}^1C_2Py][NTf_2]$ $C_{15}H_{22}F_6N_2O_4S_2$	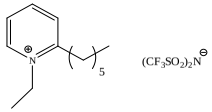	472.469	> 99	Synthesized U. Vigo
1-ethyl-2-heptylpyridinium bis(trifluoromethylsulfonyl)imide	$[^2C_7{}^1C_2Py][NTf_2]$ $C_{16}H_{24}F_6N_2O_4S_2$	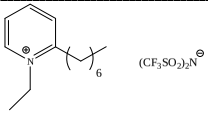	486.496	> 99	Synthesized U. Vigo
1-ethyl-2-octylpyridinium bis(trifluoromethylsulfonyl)imide	$[^2C_8{}^1C_2Py][NTf_2]$ $C_{17}H_{26}F_6N_2O_4S_2$	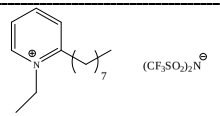	500.522	> 99	Synthesized U. Vigo

2.2 Purification and Characterization

The laboratory was not equipped with a drying installation suitable to be used in small-scale routine purification of ionic liquids samples. Therefore, a prototype of an apparatus with the possibility of simultaneous drying of four different ionic liquid samples was developed. The prototype was after replicate. The system consists of a customized *schlenk* and a temperature controlled aluminum block. The customized drying *Schlenk* flask was based on a tube shape (external diameter 17 mm, internal diameter 13 mm) fitted with a vacuum greaseless valve (J. Young Right Angel Taps) and a male joint (B 19/26, diameter = 19 mm and height = 26 mm), allowing to simplify the sample manipulation and avoiding contamination with grease. The *Schlenk* flask is covered with a female glass cap and was designed for small-scale purification/drying of samples (3 cm^3), with sufficient free space which avoids bumping of the sample to the glass cap and the vacuum valve. The image and the schematic representation of the *Schlenk* flask is presented in figure 2.1.

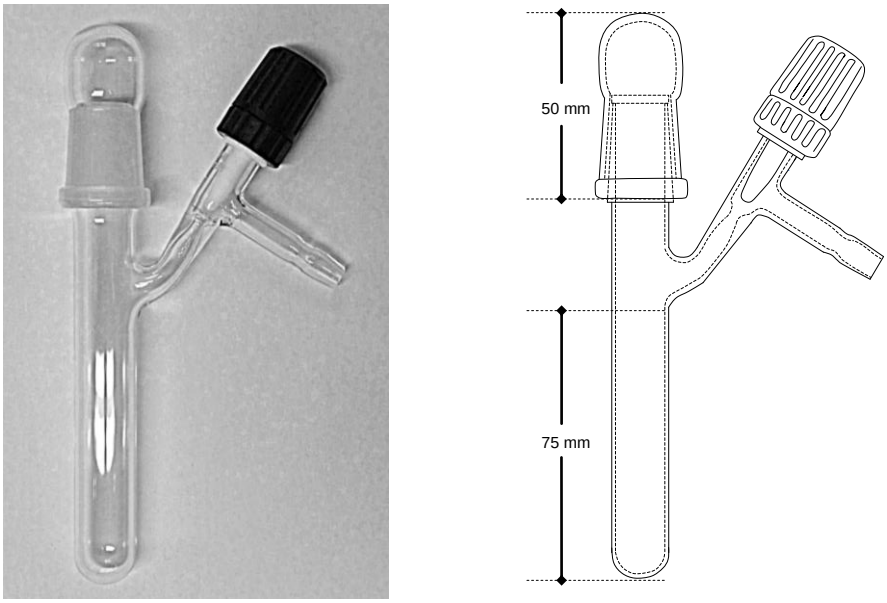

Figure 2.1. Image and schematic representation of the *Schlenk* flask.

The cylindrical aluminum block (diameter = 100 mm and height = 100 mm) is heated by a customized electrical heater (100 watts at 230 VAC, "Resisterma", 8 mm external diameter, 50 mm heating length), placed in the center of the block. The

temperature of the block is kept constant by a ON/OFF temperature controller which receives information of a thermistor, located near to the electrical heater, as presented schematically in figure 2.2.

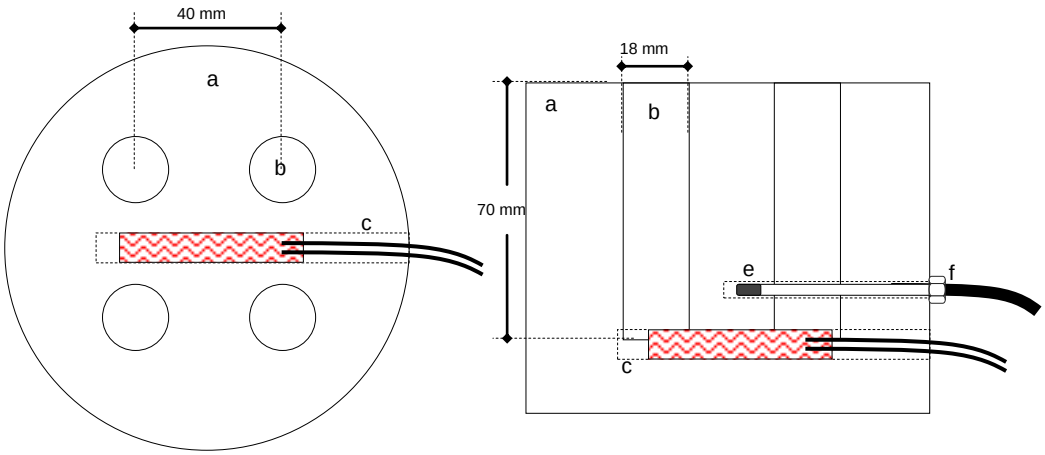

Figure 2.2. Schematic representation of the temperature controlled aluminum block of the drying apparatus. a - aluminum block; b - *Schlenk* flask cavity; c - electrical heater cavity; d - electrical heater; e - temperature sensor cavity; f - thermistor for temperature monitoring and control.

The aluminum block is on top of a magnetic stirring plate, which enables constant stirring (Teflon coated spherical magnetic stirring ball, diameter of 8 mm) of the ionic liquid during the drying process (figure 2.3). The system is connected to a glass/aluminum vacuum line already assembled in our laboratory. The vacuum pumping system is based on a dual stage rotary vane vacuum pump (Edwards model E2M8), reaching a final pressure of purification better than 1 Pa.

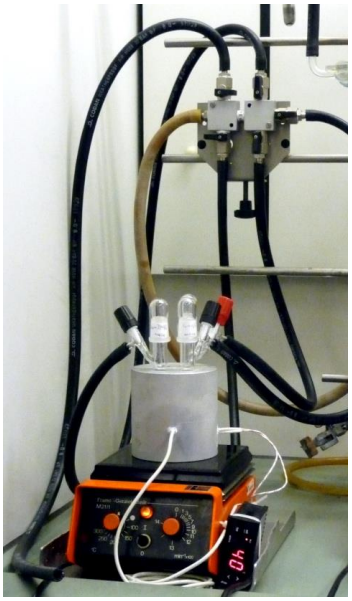

Figure 2.3. Overall picture of the purification/drying system.

All ionic liquids were dried under vacuum at moderate temperature (313 K - 373 K) and constant stirring, in order to reduce the presence of water, gases or other volatile components. This process was performed systematically before and during the thermophysical property measurements. For ionic liquids with low viscosity, the water contents of the degassed samples were determined with a Metrohm 737 Karl Fischer coulometer, using the Hydranal® - Coulomat AG from Riedel-de Haën.

The purity of each ionic liquid after drying was further evaluated by ^{1}H, ^{13}C, and ^{19}F NMR spectra, and for all ionic liquids, the mass fraction was found to be >0.99.

2.3 Additional Materials

The experimental measurement techniques used in this work were calibrated and tested against recommended standards. The summary of the standards and test compounds, as well as, the applied techniques and purposes of applied materials are listed in table 2.2.

Table 2.2. Standards and test compounds, apparatus and purpose.

Compound	Supplier	Technique	Purpose
1,3,5 - triphenylbenzene	Sigma-Aldrich	KEQCM II [a]	Test
Water	---	Drop Calorimeter / Refractometer	Calibration
Sapphire (α-aluminum oxide)	NBS standard sample, SRM 720	Drop Calorimeter	Calibration
Hexafluorobenzene	Sigma-Aldrich	Drop Calorimeter	Test
Benzoic Acid	NIST Standard Reference Material 39j	Drop Calorimeter	Test
p-Terphenyl	Sigma-Aldrich	Drop Calorimeter	Test
Toluene	Spectranal	Refractometer	Calibration
APN7.5	Paragon Scientific, Ltd	Anton Paar viscometer-densimeter	Calibration
APN26	Paragon Scientific, Ltd	Anton Paar viscometer-densimeter	Calibration
APN415	Paragon Scientific, Ltd	Anton Paar viscometer-densimeter	Calibration

[a] KEQCM - Knudsen effusion quartz crystal microbalance.

The new Knudsen effusion method combined with a quartz microbalance apparatus was tested using a tertiary reference material [2], 1,3,5 - triphenylbenzene (Sigma–Aldrich). The compound was purified by vacuum sublimation by another researcher.

The heat capacity drop calorimeter was calibrated with the reference materials [2], water and α-aluminum oxide. The sample of water (Millipore quality) was degassed under vacuum in order to remove dissolved air, and the sample of α-aluminum oxide was dried at T = 423 K. The calorimeter was tested with benzoic acid, a primary reference material (NIST Standard Reference Material 39j), and was used after previous drying under reduced pressure (at 300 K; p < 10 Pa; 24 h), and

hexafluorobenzene, a secondary reference material (Aldrich, with a mass fraction purity of 0.998), that was used without further purification. The *p*-terphenyl (Sigma–Aldrich) was purified by vacuum sublimation.

The purity of 1,3,5 - triphenylbenzene, benzoic acid, hexafluorobenzene and *p*-terphenyl was checked by gas chromatography, using an HP 4890 apparatus equipped with an HP-5 column, cross-linked, 5% diphenyl and 95% dimethylpolysiloxane. All compounds showed a mass fraction purity greater than 0.998.

The refractometer was calibrated using degassed water (Millipore quality) and Toluene (Sigma-Alrich**,** Spectranal, mass fraction purity 0.999).

The SVM 3000 Anton Paar rotational Stabinger viscometer - densimeter was calibrated using viscosity and density reference standards, APN7.5, APN26 and APN415 and were used without further purification.

References

(1) Bonhôte, P.; Dias, A.-P.; Papageorgiou, N.; Kalyanasundaram, K.; Grätzel, M. *Inorg. Chem.* 35 (**1996**) 1168–1178.

(2) Sabbah, R.; Xu-wu, A.; Chickos, J. S.; Leitão, M. L. P.; Roux, M. V.; Torres, L. A. *Thermochim. Acta* 331 (**1999**) 93–204.

CHAPTER 3

Experimental Strategies and Methodologies

3.1 Vapor Pressure Measurements

3.1.1. General Introduction

The vapor pressures of the studied ionic liquids were measured as a function of temperature using a Knudsen effusion apparatus combined with a quartz crystal microbalance, KEQCM. Based on the previous results, the standard molar enthalpies, $\Delta_{\mathrm{l}}^{\mathrm{g}} H_{\mathrm{m}}^{\mathrm{o}}$, entropies, $\Delta_{\mathrm{l}}^{\mathrm{g}} S_{\mathrm{m}}^{\mathrm{o}}$, and Gibbs energies, $\Delta_{\mathrm{l}}^{\mathrm{g}} G_{\mathrm{m}}^{\mathrm{o}}$ of vaporization were derived.

Basically, this installation is a combination of the Knudsen effusion technique and an in-vacuum quartz crystal microbalance for the real time mass loss detection. In a typical KEQCM experiment, the measurement of the equilibrium vapor pressure at a given temperature, T, is achieved by the vapor effusion trough the orifice of an effusion cell and condensation of a fraction of the vapor on the surface of the cooled quartz crystal microbalance, placed above the effusion cell, as depicted in figure 3.1. This apparatus comprises two mass loss detection techniques, gravimetric and quartz crystal microbalance: the weighed mass of the effusion cell before and after the respective experiment, and the change of the crystal's resonant frequency as the vapor condense on its surface. The combination of these two mass loss detection techniques presents several advantages:

- short effusion times;
- small sample sizes;
- real-time monitoring of the effusion experiment.

In this work, the vapor pressures were measured using two installations, KEQCM I and KEQCM II. The first Knudsen/Quartz crystal effusion technique, constructed and tested in our group, is already described in detail in the literature.[1,2] KEQCM II was designed, constructed and tested during this Ph.D. project, therefore it will be described in detail, focusing on the main differences to the KEQCM I installation.

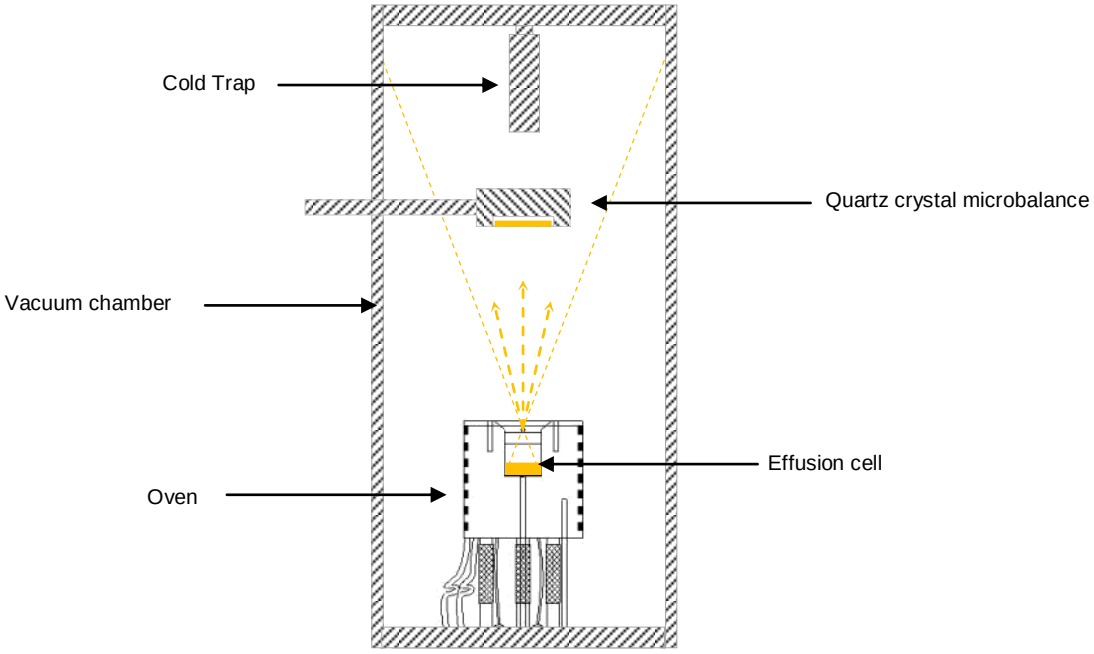

Figure 3.1. Schematic representation of the mass flow gradient during a typical KEQCM experiment.

3.1.2. Vaporization Thermodynamics

Clausius-Clapeyron Equation

During the vaporization process of a pure substance, on can consider that an infinitesimal quantity of substance is transferred from the liquid phase to the vapor phase, dn, maintaining T and p constant. Considering G^{l} and G^{g} are the Gibbs energies of the liquid and the gas phases, respectively, the infinitesimal change in Gibbs energy for this process is:

$$dG = \left(\frac{\partial G^{g}}{\partial n^{g}}\right)_{p,T} \cdot dn^{g} + \left(\frac{\partial G^{l}}{\partial n^{l}}\right)_{p,T} \cdot dn^{l} \qquad (3.1)$$

Taking into account that $dn^{l} = -dn^{g}$ for the transfer of dn moles from the liquid to the vapor phase, equation 3.1 becomes:

$$dG = \left[\left(\frac{\partial G^{g}}{\partial n} \right)_{p,T} - \left(\frac{\partial G^{l}}{\partial n} \right)_{p,T} \right] \cdot dn \tag{3.2}$$

The partial derivatives in equation 3.2 are the chemical potentials of the liquid phase, μ^{l}, and the gas phase, μ^{g}, respectively:

$$\mu^{g} = \left(\frac{\partial G^{g}}{\partial n} \right)_{p,T} \text{ and } \mu^{l} = \left(\frac{\partial G^{l}}{\partial n} \right)_{p,T} \tag{3.3}$$

Therefore, in terms of chemical potentials, equation 3.2 becomes:

$$dG = \left(\mu^{g} - \mu^{l} \right) \cdot dn \quad \text{(constant } T \text{ and } p\text{)} \tag{3.4}$$

If the two phases of a pure substance are in equilibrium (dG = 0), then the chemical potentials in the two phases are equal:

$$\mu^{l}(p,T) = \mu^{g}(p,T) \tag{3.5}$$

The total derivative of both sides of equation 3.5 is:

$$\left(\frac{\partial \mu^{l}}{\partial p} \right)_{T} \cdot dp + \left(\frac{\partial \mu^{l}}{\partial T} \right)_{p} \cdot dT = \left(\frac{\partial \mu^{g}}{\partial p} \right)_{T} \cdot dp + \left(\frac{\partial \mu^{g}}{\partial T} \right)_{p} \cdot dT \tag{3.6}$$

For a single, pure substance, the chemical potential corresponds to the molar Gibbs energy. Considering that, the following is obtained:

$$\left(\frac{\partial \mu}{\partial p} \right)_{T} = \left(\frac{\partial G_{m}}{\partial p} \right)_{T} = V_{m}(T,p) \text{ and } \left(\frac{\partial \mu}{\partial T} \right)_{p} = \left(\frac{\partial G_{m}}{\partial T} \right)_{p} = -S_{m}(T,p) \tag{3.7}$$

Where V_m (T, p) and S_m (T, p) are the molar volume and the molar absolute entropy (at temperature T and pressure p), respectively. The notation V_m (T, p) and S_m (T, p) will be used in a simplified form where the dependence on pressure and temperature will be omitted and will be only shown when necessary. Substituting the expressions in equation 3.6 yields:

$$V_m^l \cdot dp - S_m^l \cdot dT = V_m^g \cdot dp - S_m^g \cdot dT \tag{3.8}$$

Rearranging the above equation gives:

$$\frac{dp}{dT} = \frac{S_m^g(T) - S_m^l(T)}{V_m^g(T) - V_m^l(T)} = \frac{\Delta_l^g S_m(T)}{\Delta_l^g V_m(T)} \tag{3.9}$$

Where $\Delta_l^g S_m$ is the molar entropy of vaporization, and $\Delta_l^g V_m$ is the change in the molar volume between the gas and liquid phases. For a system in equilibrium and at constant pressure, the molar entropy of vaporization is related with the molar enthalpy of vaporization by the following equation:

$$\Delta_l^g S_m(T) = \frac{\Delta_l^g H_m(T)}{T} \tag{3.10}$$

Given the above equation, equation 3.9 becomes:

$$\frac{dp}{dT} = = \frac{\Delta_l^g H_m(T)}{T \cdot \Delta_l^g V_m(T)} \tag{3.11}$$

which is called the Clapeyron equation. For low vapor pressures it can be assumed that $V_m^g(T) >> V_m^l(T)$, and as a result it can be considered that $\Delta_l^g V_m(T) \cong V_m^g(T)$. Additionally, considering the ideal gas behavior and replacing V_m^g by RT / p, equation 3.11 becomes:

$$\frac{1}{p} \cdot \frac{dp}{dT} = \frac{d\ln(p/p^o)}{dT} = \frac{\Delta_l^g H_m(T)}{R \cdot T^2} \tag{3.12}$$

which is the so-called Clausius-Clapeyron equation. Assuming that $\Delta_{\mathrm{l}}^{\mathrm{g}} H_{\mathrm{m}}(T)$ is independent of T, the indefinite integral of equation 3.12, becomes:

$$\ln\left(\frac{p}{p^{\mathrm{o}}}\right) = -\frac{\Delta_{\mathrm{l}}^{\mathrm{g}} H_{\mathrm{m}}}{R \cdot T} + C \qquad (3.13)$$

where p^{o} is a reference pressure and C is a constant. The representation of $\ln p = f(1/T)$ should be linear with a slope of $-\Delta_{\mathrm{l}}^{\mathrm{g}} H_{\mathrm{m}}(T)/R$ and the intercept C, if the temperature dependence of the enthalpy of vaporization is negligible, that is usually true over a short temperature interval.

Clarke and Glew Equation

In 1966, Clarke and Glew developed a new general equilibrium equation, in order to represent the temperature dependence of equilibrium constants for a process in terms of the standard thermodynamic function changes at a chosen reference temperature.[3,4] The Clarke and Glew equation is deduced considering the assumption that the vapor pressure is a function of the temperature which is regular regarding continuity and derivability, so that the standard thermodynamic properties, $\Delta_{\mathrm{l}}^{\mathrm{g}} G_{\mathrm{m}}^{\mathrm{o}}$, $\Delta_{\mathrm{l}}^{\mathrm{g}} H_{\mathrm{m}}^{\mathrm{o}}$, and $\Delta_{\mathrm{l}}^{\mathrm{g}} C_{p,\mathrm{m}}^{\mathrm{o}}$ are similarly functions of temperature. Given the fundamental thermodynamic relation for the liquid - vapor (and solid - vapor) equilibrium:

$$R \cdot \ln\left(\frac{p}{p^{\mathrm{o}}}\right) = -\frac{\Delta_{\mathrm{l}}^{\mathrm{g}} G_{\mathrm{m}}^{\mathrm{o}}(T)}{T} = \Delta_{\mathrm{l}}^{\mathrm{g}} S_{\mathrm{m}}^{\mathrm{o}}(T) - \frac{\Delta_{\mathrm{l}}^{\mathrm{g}} H_{\mathrm{m}}^{\mathrm{o}}(T)}{T} \qquad (3.14)$$

and considering a reference temperature, θ, to determine the values of the standard thermodynamic properties, $\Delta_{\mathrm{l}}^{\mathrm{g}} G_{\mathrm{m}}^{\mathrm{o}}(\theta)$, $\Delta_{\mathrm{l}}^{\mathrm{g}} H_{\mathrm{m}}^{\mathrm{o}}(\theta)$, $\Delta_{\mathrm{l}}^{\mathrm{g}} S_{\mathrm{m}}^{\mathrm{o}}(\theta)$ and $\Delta_{\mathrm{l}}^{\mathrm{g}} C_{p,\mathrm{m}}^{\mathrm{o}}(\theta)$,

$\Delta_l^g C_{p,m}^o(T)$ can be expressed as a perturbation on the value $\Delta_l^g C_{p,m}^o(\theta)$ using the Taylor's series expansion, equation 3.15,

$$\Delta_l^g C_{p,m}^o(T) = \Delta_l^g C_{p,m}^o(\theta) + \left(\frac{d\,\Delta_l^g C_{p,m}^o}{dT}\right)_\theta \cdot (T-\theta) + \frac{1}{2}\cdot\left(\frac{d^2\,\Delta_l^g C_{p,m}^o}{dT^2}\right)_\theta \cdot (T-\theta)^2 + \ldots \quad (3.15)$$

The value $\Delta_l^g H_m^o(T)$ can be expressed as a perturbation on the value $\Delta_l^g H_m^o(\theta)$ using the Taylor's series expansion [3]:

$$\Delta_l^g H_m^o(T) = \Delta_l^g H_m^o(\theta) + \Delta_l^g C_{p,m}^o(\theta)\cdot(T-\theta) + \frac{1}{2}\cdot\left(\frac{d\,\Delta_l^g C_{p,m}^o}{dT}\right)_\theta \cdot (T-\theta)^2 + \ldots \quad (3.16)$$

where the series is arbitrarily terminated at the first derivative of $\Delta_l^g C_{p,m}^o$.[3] Similarly, $\Delta_l^g S_m^o(T)$ can be defined as:

$$\Delta_l^g S_m^o(T) = \Delta_l^g S_m^o(\theta) + \int_\theta^T \frac{\Delta_l^g C_{p,m}^o(T)}{T}\cdot dT \quad (3.17)$$

Considering the equations 3.15, 3.16 and 3.17, equation 3.14 becomes:

$$R\cdot\ln\left(\frac{p}{p^o}\right) = -\frac{\Delta_l^g G_m^o(\theta)}{\theta} + \Delta_l^g H_m^o(\theta)\cdot\left(\frac{1}{\theta}-\frac{1}{T}\right) + \Delta_l^g C_{p,m}^o(\theta)\cdot\left[\left(\frac{\theta}{T}\right)-1+\ln\left(\frac{T}{\theta}\right)\right] + \frac{\theta}{2}\cdot\left(\frac{d\,\Delta_l^g C_{p,m}^o}{dT}\right)_\theta \cdot\left[\left(\frac{T}{\theta}\right)-\left(\frac{\theta}{T}\right)-2\cdot\ln\left(\frac{T}{\theta}\right)\right]+\ldots \quad (3.18)$$

which is an equation (arbitrarily terminated at the second derivative of $\Delta_l^g C_{p,m}^o$) with four constants defining the values for the standard thermodynamic properties. In the application of the Clarke and Glew equation to the experimental values of vapor pressures, the $\left(\frac{d^2\,\Delta_l^g C_{p,m}^o}{dT^2}\right)$ term can be neglected, when it is observed that it

does not differ significantly from zero, within the experimental temperature interval. Nevertheless, when neglecting a term of a given order derivative, all the other terms of higher order derivatives must be also neglected, otherwise this invalidates the use of the Taylor's series expansion. Oonk and co-workers [5,6] have shown that there is no advantage of using the Clarke and Glew equation with more than three parameters, for temperature intervals lower than 60 K. For the working temperature interval around 20 K, usually the Clarke and Glew equation is used with only two parameters, which corresponds using the Clausius-Clapeyron equation.

Standard Molar Thermodynamic Properties of Vaporization

The standard molar enthalpy of vaporization at a given temperature, T_1, $\Delta_l^g H_m^o(T_1)$, represents the enthalpic change of the isothermal process, described by:

Liquid (standard state) ⟶ Gas (standard state)

where the standard state of a liquid at a reference temperature, T_1, is the state which corresponds to the pure liquid at the standard pressure of 10^5 Pa. For a gas, it corresponds to the hypothetic state of the ideal gas, at T_1 and standard pressure of 10^5 Pa. The standard molar enthalpy of vaporization at a reference temperature, T_1, $\Delta_l^g H_m^o(T_1)$, can be related with the molar enthalpy of vaporization measured at a pressure, p_1, and temperature, T_1, $\Delta_l^g H_m^o(T_1)$, as depicted in figure 3.2.

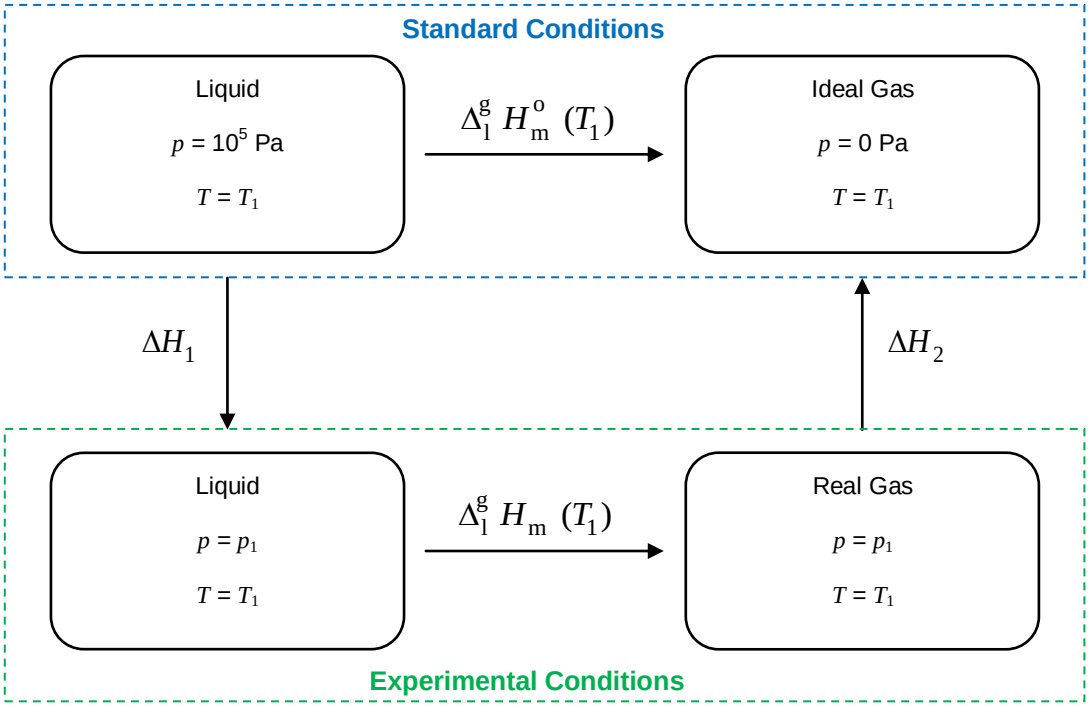

Figure 3.2. Thermodynamic hypothetical cycle for the calculation of the standard molar enthalpy of vaporization at T_1.

Considering the first law of thermodynamics and the thermodynamic cycle represented in figure 3.2, the following relation can be established:

$$\Delta_l^g H_m^o (T_1) = \Delta H_1 + \Delta_l^g H_m (T_1) + \Delta H_2 \tag{3.19}$$

where ΔH_1 and ΔH_2 are defined as:

$$\Delta H_1 = \int_{10^5\,\text{Pa}}^{p_1} \left[-T \cdot \left(\frac{\partial V_m^l}{\partial T} \right)_p + V_m^l \right] \cdot dp \tag{3.20}$$

$$\Delta H_2 = \int_{p_1}^{0} \left[-T \cdot \left(\frac{\partial V_m^g}{\partial T} \right)_p + V_m^g \right] \cdot dp \tag{3.21}$$

Where, T corresponds to the temperature T_1, $V_m^l(T)$ and $V_m^g(T)$ are the molar volume of the liquid and gas phases, respectively. The enthalpic change, ΔH_1

and ΔH_2, related with the pressure change, are negligible when compared with the value of $\Delta_l^g H_m^o(T_1)$. Therefore, it is usual to neglect the contribution of the pressure to the enthalpy correction, and it is assumed that $\Delta_l^g H_m^o(T_1) \cong \Delta_l^g H_m(T_1)$. The standard molar enthalpy of vaporization at temperature T_1, $\Delta_l^g H_m^o(T_1)$, can be converted into the standard molar enthalpy of vaporization at temperature T_2, $\Delta_l^g H_m^o(T_2)$, by the following equation:

$$\Delta_l^g H_m^o(T_2) = \Delta_l^g H_m^o(T_1) + \int_{T_1}^{T_2} \Delta_l^g C_{p,m}^o(T) \cdot dT \qquad (3.22)$$

where $\Delta_l^g C_{p,m}^o(T)$ is the change between the standard molar heat capacities of the gas, $C_{p,m}^o(\mathrm{g})$, and the liquid, $C_{p,m}^o(\mathrm{l})$, at constant pressure. Assuming that $\Delta_l^g C_{p,m}^o(T)$ is constant in the considered temperature interval, equation 3.22 becomes:

$$\Delta_l^g H_m^o(T_2) = \Delta_l^g H_m^o(T_1) + (T_2 - T_1) \cdot \Delta_l^g C_{p,m}^o \qquad (3.23)$$

The standard molar entropy of vaporization at temperature T_2, and standard pressure, p^o = 10^5 Pa, $\Delta_l^g S_m^o(T_2)$, is calculated using the following equation:

$$\Delta_l^g S_m^o(T_2) = \Delta_l^g S_m(T_1, p_1) + \Delta_l^g C_{p,m}^o \cdot \ln\left(\frac{T_2}{T_1}\right) - R \cdot \ln\left(\frac{p^o}{p_1}\right), \qquad (3.24)$$

where $\Delta_l^g S_m(T_1, p_1)$ is the molar entropy of vaporization at temperature T_1, and pressure, p_1, and R is the gas constant (R = 8.3144621 J·K^{-1}·mol^{-1})[7].

The standard molar Gibbs energy at temperature T_2, $\Delta_l^g G_m^o(T_2)$, is calculated taking into account the thermodynamic properties at temperature T_2, referred above, using the following equation:

$$\Delta_l^g G_m^o(T_2) = \Delta_l^g H_m^o(T_2) - T_2 \cdot \Delta_l^g S_m^o(T_2) \qquad (3.25)$$

3.1.3. Knudsen Effusion Methodology

In 1909, M. Knudsen published the development of a vapor pressure measurements method based on the experimental observation of some effects of the Kinetic Theory of Gases on the analysis of the gas behavior at low pressures.[4,8–10] This was the first study designed to test the consequences of the Kinetic Theory of Gases, where two cylindrical tubes and low pressures were used, in order to consider a molecular flow, in which the molecules can move freely, without mutual interference. Under these conditions, Knudsen concluded that the direction in which a molecule rebounds from a solid wall is independent of the direction in which it approaches the wall and is ruled by the Lambert's cosine law. [4,8–10]

The Knudsen effusion method is one of the most widely used methods for measuring vapor pressures. This method is based on the measurements of the effusion rate, v_{eff}, of the vapor inside the effusion cell, in thermal equilibrium, through a small orifice of known area, A_{o}, into a vacuum. [4,8–11] According to the Kinetic Theory of Gases, and considering the collision frequency of the gaseous molecules with the wall, Z_{wall}, with an orifice of known area, A_{o}, the effusion rate of the vapor inside the effusion cell can be calculated by the following equation:

$$v_{\text{eff}} = \frac{dN}{dt} = w_{\text{o}} \cdot Z_{\text{wall}} \cdot A_{\text{o}} = w_{\text{o}} \cdot \frac{p \cdot N_A}{\sqrt{(2 \cdot \pi \cdot R \cdot T \cdot M)}} \cdot A_{\text{o}} \qquad (3.26)$$

Where, (dN / dt) is the number of molecules, N, effusing from the cell in a time interval, dt, w_{o} represents the transmission probability factor, and p is the pressure inside the effusion cell. Considering that (N / N_A)= n and (m / M)= n, and solving for p, the equation 3.26 becomes the Knudsen equation:

$$p = \frac{\Delta m}{w_{\text{o}} \cdot A_{\text{o}} \cdot \Delta t} \cdot \sqrt{\frac{2 \cdot \pi \cdot R \cdot T}{M}} \qquad (3.27)$$

Since the effusing orifice has a finite thickness, l, there is a possibility of a small fraction of the effusing molecules shock into the orifice walls, in which they can continue their path in order to leave the cell or go back inside the cell. In order to evaluate the fraction of gaseous molecules which effuses through the cell orifice, in this work the w_o value was calculated using the Dushman equation [4]:

$$w_o = \left\{ 1 + \left(\frac{3 \cdot l}{8 \cdot r} \right) \right\}^{-1} \tag{3.28}$$

where r is the orifice radius. The characteristics of the effusion orifices used in the effusion cells of the two KEQCM installations are listed in table 3.1.

Table 3.1. Areas and transmission probability factors of the effusion orifices.

Effusion cell	l / mm	r / mm	A_o / mm^2	w_o
KEQCM I	0.0125	0.5000	0.7854	0.9907
KEQCM II	0.0500	0.5925	1.103	0.9693

3.1.4. Quartz Crystal Microbalance

The effusing vapor that condenses on the surface of the quartz crystal forms a thin film of compound in which the thickness increases as the vapor continues effusing from the effusion cell. During this process, the characteristic resonant frequency of the crystal decreases, and taking into account the Sauerbrey equation[12], the change of the resonant frequency with time is related to the mass condensed on the quartz crystal:

$$\Delta f = -\left(\frac{2 \cdot f^2}{\rho_q \cdot \upsilon_q \cdot A_q} \right) \cdot \Delta m_q , \tag{3.29}$$

Where, Δf is the change in the resonant frequency of the quartz crystal due to the deposited mass condensed on the surface of the quartz crystal, Δm_q; f is the resonant frequency of the crystal, ρ_q is the density of the quartz, υ_q the propagating acoustic wave speed, and A_q is the quartz crystal effective area. For a given quartz crystal, f, ρ_q, and υ_q could be considered as constants, and the equation 3.29 can be rewritten as:

$$\Delta f = S_q \cdot \frac{\Delta m_q}{A_q}, \tag{3.30}$$

Where, S_q is the mass sensitivity for a given quartz crystal. In both installations, KEQCM I and KEQCM II, a 6 MHz AT-cut quartz crystal (diameter = 14.0 mm) commercially acquired from Inficon - Maxtek, was used, with a sensitivity typically of S_q = - 81.5 Hz·μg^{-1}·cm^2, at T = 298 K.

3.1.5. KEQCM Data Analysis

As it was already elucidated above, during a typical KEQCM experiment, at a given temperature, a change of the resonant frequency of the quartz crystal with time, $(df / dt)_{obs,T}$, is observed as the mass of compound condenses on the crystal surface. This is essentially a sum of two main contributions:

- the mass of the compound effuses from the effusion cell, at a given temperature, T, with a massic effusion rate of $(dm_{eff} / dt)_T$. As it can be observed from figure 3.1, only a fraction of the effused vapor condenses in the crystal, the remaining spreads into the vacuum chamber walls. Considering equation 3.30, this contribution can be interpreted as:

$$\left(\frac{df}{dt}\right)_{cell,T} = \frac{S_q}{A_q} \cdot \left[\frac{dm_q\ (cell)}{dt}\right]_T = \frac{S_q}{A_q} \cdot g \cdot \left(\frac{dm_{eff}}{dt}\right)_T, \tag{3.31}$$

where dm_q (cell) is the mass of the effused compound which condenses on the crystal surface, and *g* is a geometric factor which defines the fraction of the effused vapor that effectively condenses on the crystal surface. This factor will depend on the shape of the mass flow, the distance between the effusion cell and the quartz crystal microbalance, as well as on the compound under study.

- volatile impurities deposited on walls of the vacuum chamber that eventually condenses on the quartz crystal surface, and background noise, $(df / dt)_{drift}$.

The observed change in the resonant frequency of the quartz crystal with time is given by the following equation (3.32):

$$\left(\frac{df}{dt}\right)_{obs,T} = \left(\frac{df}{dt}\right)_{cell,T} + \left(\frac{df}{dt}\right)_{drift} \qquad (3.32)$$

In order to obtain the direct relation between the signal measured by the quartz crystal microbalance and the mass loss from effusion cell, the contribution $(df / dt)_{drift}$ must be considered (equation 3.33):

$$\left(\frac{df}{dt}\right)_{cell,T} = \left(\frac{df}{dt}\right)_{obs,T} - \left(\frac{df}{dt}\right)_{drift} \equiv \left(\frac{df}{dt}\right)_{corr,T} = \frac{S_q}{A_q} \cdot g \cdot \left(\frac{dm_{eff}}{dt}\right)_T \qquad (3.33)$$

The notation "corr" was used to specify the corrected value. Since S_q depends only on the type of the crystal used, this factor is a constant for all the experiments carried out in KEQCM. Similarly, A_q is also a constant due to the fact that the accessible surface of the quartz crystal, for receiving the effused vapor, is fixed. Hence, an effective mass sensitivity coefficient, W, was defined as:

$$W = -\frac{S_q \cdot g}{A_q} \qquad (3.34)$$

Despite of these two factors being constant during the experiment, is was found that W may change from experiment to experiment and also presents a small dependence on the identity of the studied compound. In this way, equation 3.33 can be rewritten as:

$$\left(\frac{df}{dt}\right)_{\text{corr},T} = -W \cdot \left(\frac{dm_{\text{eff}}}{dt}\right)_T \tag{3.35}$$

Considering that W is constant during an experiment and integrating for a specific time interval, equation 3.35 can be rewritten as:

$$W = -\frac{\Delta f_{\text{corr}}}{\Delta m_{\text{eff}}}, \tag{3.36}$$

where Δf_{corr} represents the total change observed in the resonant frequency of the quartz crystal, taking into account the background noise contribution, during the KEQCM experiment, and Δm_{eff} is the total mass loss from the effusion cell, which is measured gravimetrically by weighing the cell before and after the experiment. W is reported in Hz·mg^{-1}.

Therefore, during a typical KEQCM experiment, the change of the resonant frequency of the quartz crystal with time, $(df / dt)_{\text{obs},T}$, is measured at different temperatures for a specified time. The obtained raw data of a KEQCM experiment are the resonant frequency of the quartz crystal, the temperature set point, the temperature of the effusion cell, and the time. The resonant frequency of the quartz crystal is recorded at regular time intervals (20 s), and $(df / dt)_{\text{obs},T}$ is the slope of the linear representation of the resonant frequency as a function of time, for each temperature. Figure 3.3 presents the graphic representation of a typical KEQCM result. As it can be clearly observed in the representation, when the temperature increases, $(df / dt)_{\text{obs},T}$ becomes more steep, due to the increase of the rate of mass condensed on the surface of the crystal.

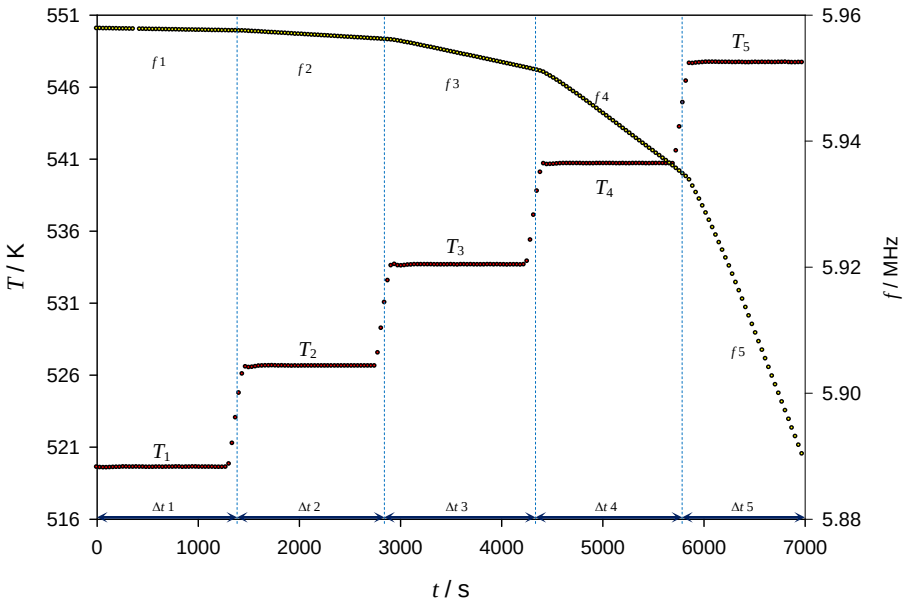

Figure 3.3. Schematic representation of the results obtained in a typical KEQCM experiment. (filled yellow circles, ●) - resonant frequency of the quartz crystal; (filled red circles, ●) - temperature of the effusion cell. (adapted from source [2]).

The same procedure and temperature step profile is repeated with an empty effusion cell, in order to determine $(df / dt)_{\text{drift}}$. Thereby, the obtained values of $(df / dt)_{\text{obs},T}$, for each temperature, are corrected according to equation 3.33. Considering the determined sensitivity coefficient W, the massic effusion ratio, $(dm_{\text{eff}} / dt)_T$, can be calculated for each temperature step taking into account equation 3.35.

The vapor pressure at different temperatures, T, can be calculated using the equation 3.27, expressed as:

$$p = -\left(\frac{df}{dt}\right)_{\text{corr},T} \cdot \frac{1}{w_o \cdot A_o \cdot W} \cdot \left(\frac{2 \cdot \pi \cdot R \cdot T}{M}\right)^{1/2} \qquad (3.37)$$

3.1.6. Knudsen Effusion Quartz Crystal Microbalance

Knudsen Effusion Apparatus I - KEQCM I

The Knudsen effusion apparatus combined with a quartz crystal microbalance, KEQCM I, was constructed and tested in our laboratory, and was previously described in detail.[1,2]

Basically, KEQCM I consist in four main parts:

3.1.6.1. Vacuum pumping system and vacuum chamber;
3.1.6.2. Temperature measurement and control;
3.1.6.3. Quartz crystal microbalance;
3.1.6.4. Data acquisition and control.

The schematic representation of the Knudsen effusion apparatus combined with a quartz crystal microbalance is schematically represented in figure 3.4.

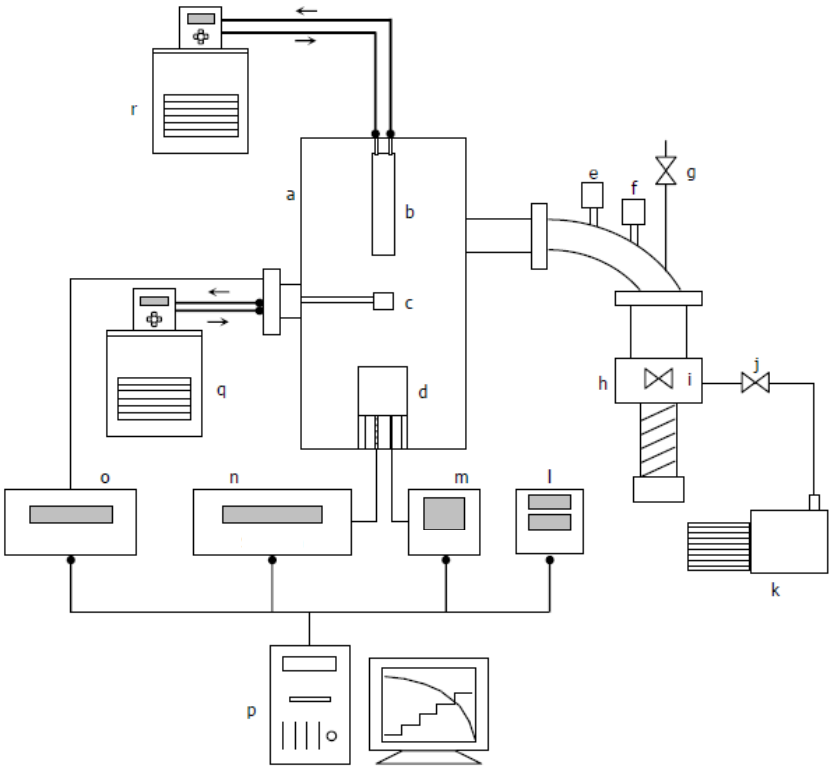

Figure 3.4. Schematic representation of the Knudsen effusion apparatus combined with a quartz crystal microbalance. a - vacuum chamber; b – cold trap; c - quartz crystal microbalance; d – aluminum block (oven); e - Varian high vacuum gauge model Cold cathode; f - Varian vacuum gauge model ConvetTorr; g - gas admittance valve; h - oil diffusion pump (Ilmvac model PDH100); i - butterfly valve; j – two-ways valve; k - rotary pump (Alcatel model Pascal 2010SD); l - CC2C SenTorr reader and vacuum controller; m - PID temperature controller (Omron model E5AR); n - Digital Multimeter (Keithley model 2010, 7½ digit resolution) ; o - high accurate crystal impedance meter (Agilent model E4915A); p - computer; q - quartz crystal microbalance refrigeration; r - trap refrigeration. (source of the figure [2]).

3.1.6.1. Vacuum pumping system and vacuum chamber

The vacuum pumping system consists of a rotary vane pump (Alcatel model Pascal 2010SD), which is used to pre-evacuating the system and to support an oil diffusion pump (Ilmvac model PDH100). The chamber pressure is monitored using two pressure sensors, a Varian vacuum gauge model ConvetTorr for pressures above (1×10^{-1}) Pa and a Varian high vacuum gauge model Cold cathode in the high vacuum stage. Connected to the vacuum pumping system is the vacuum chamber, which is basically a cylindrical chamber, containing a quartz crystal microbalance positioned above the aluminum block (oven), where the effusion cell is placed.

3.1.6.2. Temperature measurement and control

The temperature of the aluminum block (oven) is measured using a platinum resistance thermometer, Pt100 class 1/10. The temperature sensor, which is used to measure the temperature during the experiment, is positioned at the center of the block, in close proximity to the base of the cavity containing the effusion cell. The temperature is controlled within a temperature fluctuation of ± (1×10^{-2}) K, measured with a resolution better than 1×10^{-3} K and with an overall uncertainty better than ± (2×10^{-2}) K in the working temperature range. The programming of the temperature steps is performed with a LABVIEW software application, the programming of the temperature step is divided into two segments, in order to decrease the temperature overshoot.

3.1.6.3. Quartz crystal microbalance

The quartz crystal microbalance is based on a commercial Inficon - Maxtek liquid cool drawer single sensor head and feedthrough model CDS-A0F38. The quartz crystal is placed in a circular support, where the surface of the crystal is exposed to the condensation of the compound, as illustrated in figure 3.5. The refrigeration of the microbalance is achieved by means of a cooled circulator bath, Huber, model CC1-K6, in order to maintain the system at low temperatures (263.0 ± 0.5) K. The quartz crystal resonance frequency is measured using a high accurate crystal impedance meter, Agilent model E4915A, in a network analyzer resonator measuring mode.

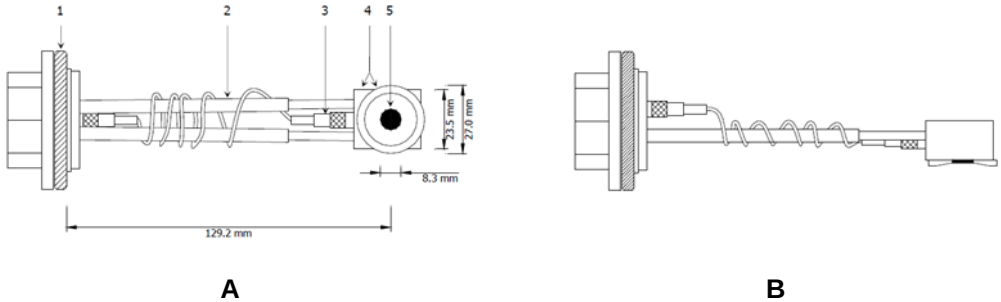

Figure 3.5. Technical drawing of the quartz crystal microbalance used in KEQCM I. **A** − bottom view: 1 − o-ring; 2 − refrigeration; 3 − coaxial cable; 4 − quartz crystal support; 5 − quartz crystal. **B** − side view. (adapted from source[2]).

3.1.6.4. Data acquisition and control

The software of the instrument was developed in LABVIEW 8.2, which is used for programming, control and data acquisition of the KEQCM I. The program of the temperature profile in the PID temperature controller and the acquisition of the vacuum data from the Varian is done using an RS485 interface. The programming and data acquisition of the 7½ digit resolution digital multimeter (Keithley, model 2010,) and the crystal impedance meter (Agilent, model E4915A) is performed by via IEEE488 interface.

The program of the experimental setup (temperature steps, stabilization time and time intervals) is done using the same software (figure 3.6).

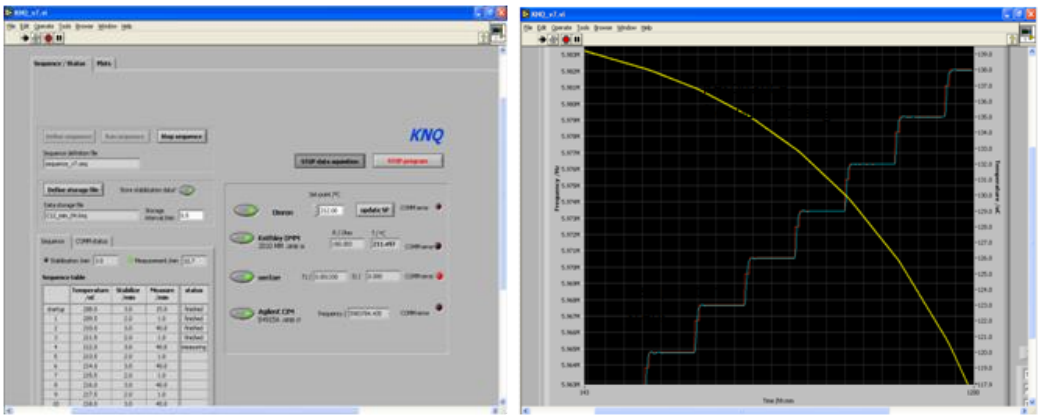

Figure 3.6. Screen shot of the program during a typical experiment in the KEQCM I.

Knudsen Effusion Apparatus II - KEQCM II

The Knudsen effusion apparatus combined with a quartz crystal microbalance, installation II (KEQCM II) was designed, developed and constructed in our Laboratory, as part of this thesis. The second installation was constructed with the same working principle as the previous installation I. The KEQCM II installation can be divided in five main parts:

3.1.6.5. Vacuum line and Vacuum pumping system;
3.1.6.6. Vacuum chamber;
3.1.6.7. Temperature measurement and control;
3.1.6.8. Quartz crystal microbalance;
3.1.6.9. Data acquisition and control.

In figure 3.7, the scheme of the Knudsen effusion apparatus combined with a quartz crystal microbalance, KEQCM II, is presented.

3.1.6.5. Vacuum line and Vacuum pumping system

The vacuum line is made of stainless steel (type 304) tubing with connections KF-40 (ISO-KF Flange Size NW-40), using KF-40 hinge clamp vacuum fittings. The turbo pumping station is connected to the vacuum line by means of a stainless steel bellows flex coupling KF-40. A cold trap (Kurt J. Lesker, KF-40, inline LN2 cooled traps, single fill tube, 0.75 L), cooled with liquid nitrogen, is placed between the vacuum chamber and the turbo pumping station. The vacuum pumping system consists of a turbo pumping station Adixen/Alcatel ATP80/ACT200TH with 2005SD backing pump. The pumping station is equipped with a rotary vane pump (Adixen/Alcatel model Pascal 2005SD), a turbomolecular pump (Adixen/Alcatel model ATP80), a turbomolecular pump controller (Adixen/Alcatel model ACT200TH) and a single-channel pressure controller (Adixen/Alcatel model ACS 2000). The pressure of the vacuum chamber and line is monitored using a cold cathode/Pirani gauge (Adixen/Alcatel model ACC2009) which is connected to a single-channel controller (Adixen/Alcatel model ACS2000). The ACS2000 controller provides power, control and pressure display for the operation of the ACC2009 gauge.

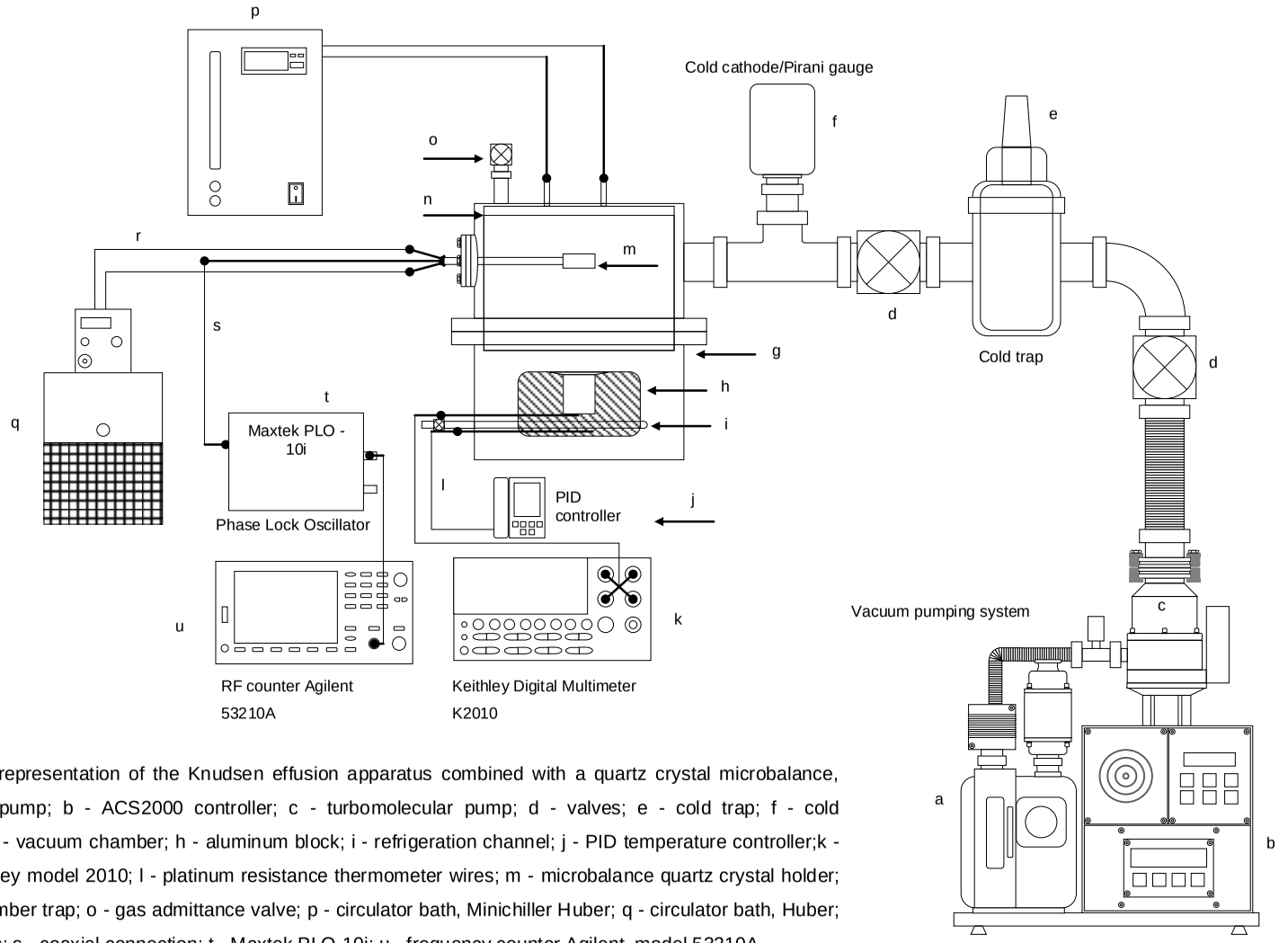

Figure 3.7. Schematic representation of the Knudsen effusion apparatus combined with a quartz crystal microbalance, KEQCM II. a - rotary pump; b - ACS2000 controller; c - turbomolecular pump; d - valves; e - cold trap; f - cold cathode/Pirani gauge; g - vacuum chamber; h - aluminum block; i - refrigeration channel; j - PID temperature controller;k - Digital Multimeter, Keithley model 2010; l - platinum resistance thermometer wires; m - microbalance quartz crystal holder; n - internal vacuum chamber trap; o - gas admittance valve; p - circulator bath, Minichiller Huber; q - circulator bath, Huber; r - refrigerator fluid tubes; s - coaxial connection; t - Maxtek PLO-10i; u - frequency counter Agilent, model 53210A.

3.1.6.6. Vacuum chamber

The effusion cell is concentrically placed in the cylindrical hole inside the aluminum block that is inside the vacuum chamber, as represented in figure 3.8. The vacuum chamber is made of stainless steel and presents a cylindrical shape (diameter = 150 mm, height = 200 mm, thickness = 4 mm). The aluminum block (diameter = 80 mm) is connected to a stainless steel platform by means of a stainless steel tube, which is also used as a refrigeration channel to cool the oven block. The stainless steel platform is connected to the vacuum chamber by a KF-150 connection. A cold trap (diameter = 131.4 mm, height = 98.5 mm, thickness =1.2 mm) is placed inside the vacuum chamber, in order to decrease the background noise, $(df / dt)_{\text{drift}}$. The cold trap refrigeration is achieved by means of circulation of a water/ethylene glycol mixture, refrigerated at 265 K by a Huber, compact Minichiller.

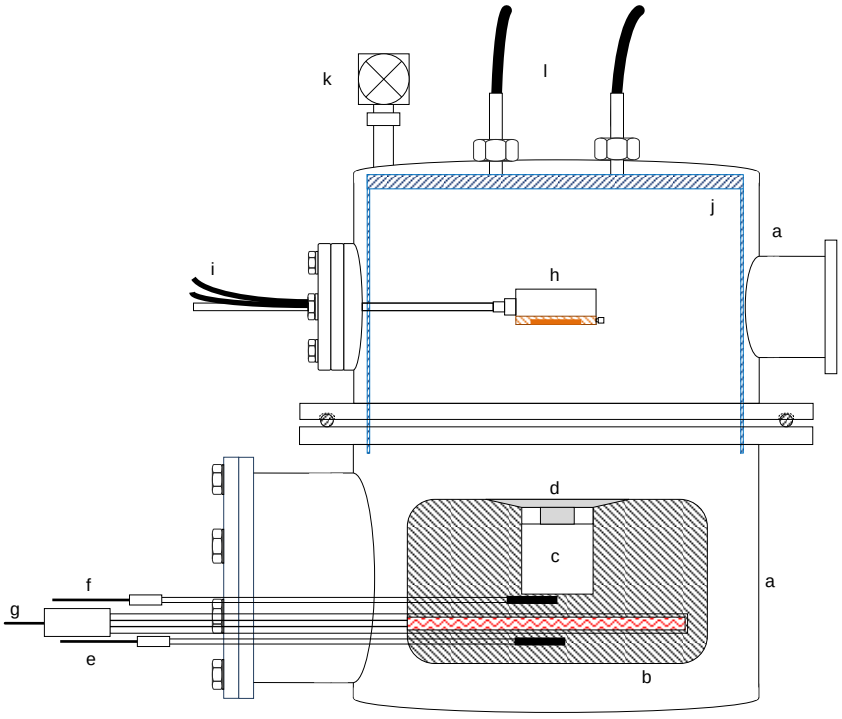

Figure 3.8. Schematic representation of the vacuum chamber of the Knudsen effusion apparatus combined with a quartz crystal microbalance, KEQCM II. a - vacuum chamber; b- aluminum block; c - cell cavity and effusion cell; d - thermal contact pressing disk; e - Pt100 for temperature control; f - Pt100 for temperature measurement of the effusion cell; g - electrical heaters; h - microbalance quartz crystal holder; i - quartz crystal holder cooling liquid circulation; j - internal vacuum chamber trap; k - gas admittance valve; l - chamber trap cooling liquid circulation.

3.1.6.7. Temperature measurement and control

The aluminum block is heated by two customized electrical heaters (100 watts at 230 VAC, "Resisterma", 8 mm external diameter, 100 mm heating length). Two heating modes are used: booster heating mode (electrical connection of the heaters in parallel; P = 200 watts) and temperature control mode (electrical connection of the heaters in series; P = 50 watts).

The temperature of the block is kept constant by a high speed and high precision PID (proportional, integral and differential) controller (OMRON, model E5ER) which receives the information of a platinum resistance thermometer, Pt100 class 1/10, located near to the electrical heater. The temperature of the block is measured using a platinum resistance thermometer, Pt100 class 1/10, positioned at the center of the block in close proximity to the base of the cavity containing the effusion cell. The Pt100 resistance is monitored in four wire measuring mode by a digital multimeter (K 2010). The temperature is controlled within a temperature fluctuation of $\pm(5\times10^{-3})$ K, measured with a resolution better than 1×10^{-3} K and with an overall uncertainty better than $\pm(2\times10^{-2})$ K in the working temperature range.

3.1.6.8. Quartz crystal microbalance

The vacuum quartz crystal microbalance (QCM) as well as the quartz crystals were acquired from Inficon. The quartz crystal microbalance is based on a commercial Inficon-Maxtek liquid cool drawer single sensor head and feedthrough CF40. The quartz crystal is placed in a rectangular support, where the surface of the crystal is exposed to the condensation of the compound. The microbalance is maintained at low temperatures, T = (263.0 ± 0.5) K, using a cooled circulator bath, Huber, model CC1-K6. The quartz crystal resonance frequency is locked using the Phase Lock Oscillator, Maxtek, model PLO-10i, and the output frequency is measured using a single channel frequency counter meter.

3.1.6.9. Data acquisition and control

The temperature of the Knudsen effusion cell is measured by a Digital Multimeter (Keithley, model 2010, 7½ digit resolution) and the quartz crystal resonance frequency is measured using a 350 MHz RF frequency counter (Agilent, model 53210A, 10 digit/second resolution), and the data is transferred to the

computer via IEEE488 interface. The data and time control is performed by the data acquisition and control software of the KEQCM II, developed in Agilent VEE, v9.0.[13] The data acquisition software shows the temperature, resonance frequency versus time, and the data is saved in real-time in text mode using the CSV (comma-separated values) format.

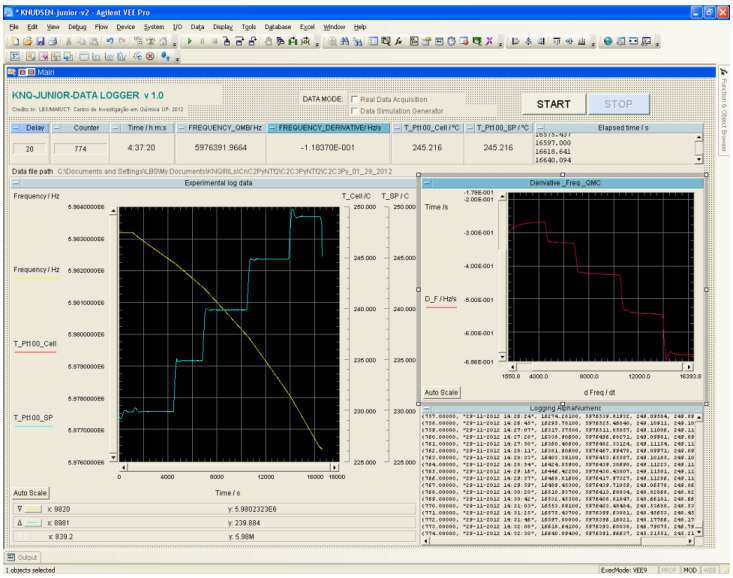

Figure 3.9. Screen shot of the program during a typical experiment in the KEQCM II.

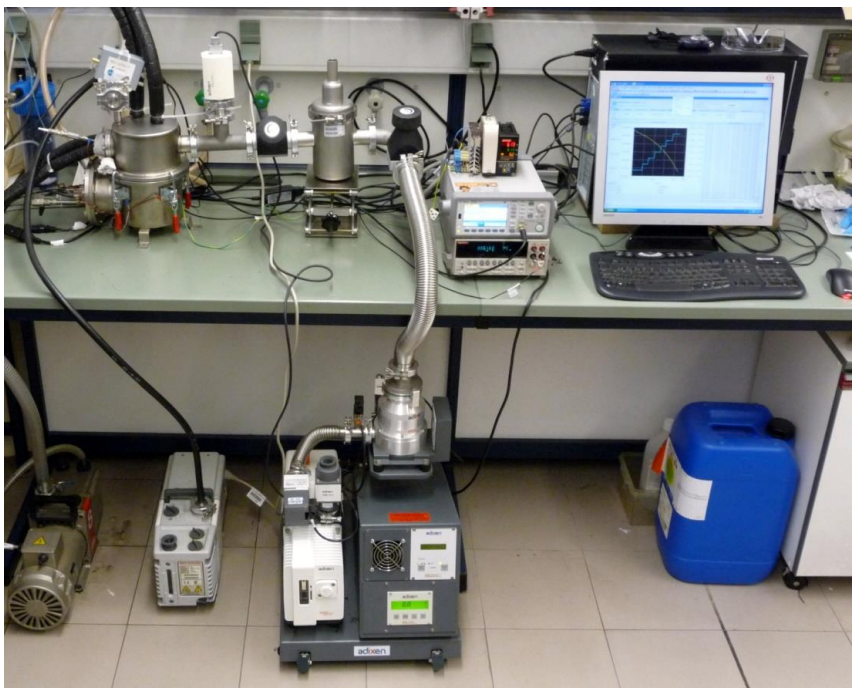

Figure 3.10. Overall view of the KEQCM II installation.

KEQCM I vs. KEQCM II

The new Knudsen effusion apparatus combined with a quartz crystal microbalance, installation II (KEQCM II), has some advantages compared to the KEQCM I. Besides of the already described advantages of KEQCM I[1,2], the new installation presents some improvements compared to installation I.

- easy assembling and disassembling of the experiment, since the opening of the chamber is carried out from the top. Additionally, all the components of the aluminum block, temperature sensors and thermal heaters are located in the fixed part of the vacuum chamber, thus increasing the reproducibility of the positioning of the oven.

- new design of the *in situ* effusion refrigerated and temperature controlled trap which covers the walls of the upper part of the vacuum chamber, reducing the background sign and increasing the repeatability, avoiding the probability of volatile compounds to condense in the quartz crystal microbalance.

- equipped with two refrigerated traps, one inside the vacuum chamber and the second in the vacuum line, which reduces the contamination of the vacuum system.

- the aluminum block features a new air refrigeration channel, allowing a faster temperature decrease at the end of the effusion experiment.

Effusion Cell and Evaluation of the Orifice Area and Roughness

The most crucial part of the Knudsen effusion cell is the effusion orifice that in this apparatus is made of a platinum disk, in order to minimize the effect of thermal expansion, and to maximize the shape stability as well as to avoid chemical reactivity. The platinum disk (diameter 21 mm and thickness 0.050 mm) is placed in the aluminum lid and compressed with a brass disk and ring, according to the scheme presented in figure 3.11. The platinum disk was acquired from Metal Goodfellow, where the circular orifice (diameter 1.2 mm) was made using a patented technology of the company, according to our specifications.

The size and roughness of the platinum disk orifice was evaluated using an optical microscope Leica, model M205 C, connected to a digital camera Leica, model DFC295, with a metric linear resolution of 0.002 mm, calibrated with an optical scale of (2.000 ± 0.002) mm. A typical image of the platinum disk orifice and scale are depicted in figure 3.12. The effusion orifice diameter was found to be (1.185 ± 0.004) mm, and the orifice circular regularity was better than 0.3%, with a maximum observed wall roughness of 0.01mm.

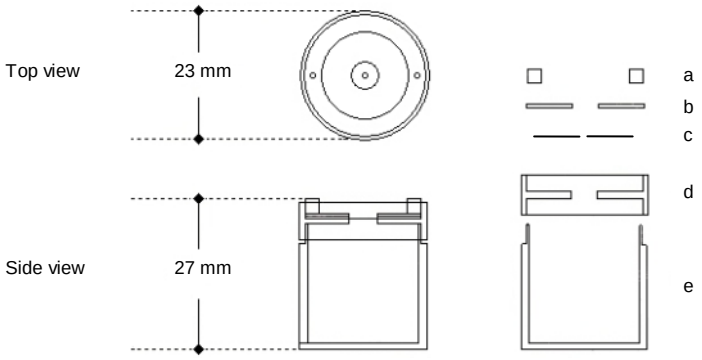

Figure 3.11. Side and top views of the effusion cell: a, brass ring; b, brass disk; c, platinum disk; d, aluminum lid; e, aluminum cell. (adapted from source [11])

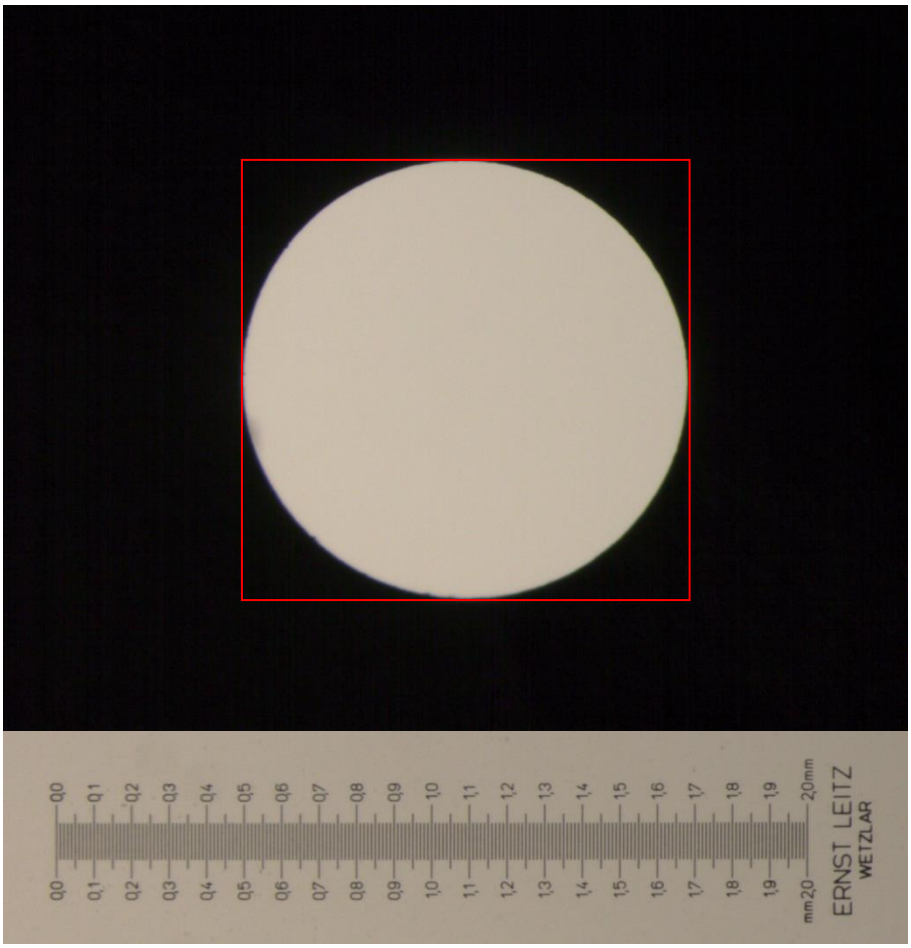

Figure 3.12. Image of the effusion orifice with a diameter of (1.185 ± 0.004) mm, together with the calibrated scale of (2.000 ± 0.002) mm.

Testing of the Apparatus

The new Knudsen effusion apparatus combined with a quartz crystal microbalance was tested based on the measurements of vapor pressures as a function of temperature of 1,3,5-triphenylbenzene, which is considered a tertiary reference material.[14] There are no recommended compounds to test Knudsen effusion installation for liquids. The recommended compounds for vapor pressures of liquids are usually high volatile and out of the temperature and pressure range of the Knudsen effusion apparatus combined with a quartz crystal microbalance. The 1,3,5-triphenylbenzene was chosen as a reference material due to the low volatility and stability at high temperatures, fitting in the working range of the apparatus,

which also has been done in the test of the previous installation.[1,11] The measurements of vapor pressures of liquids by the Knudsen effusion is not common in the literature[15] due to the usually high vapor pressures of the liquid phase.

The experimental vapor pressures data for 1,3,5-triphenylbenzene is presented in table 3.2. The graphical representation of ln(p/Pa) = f [(1/T) / K^{-1}] for the obtained data is depicted in figure 3.13.

Table 3.2. Experimental vapor pressures for 1,3,5-triphenylbenzene, as obtained with the quartz crystal microbalance Knudsen effusion apparatus.

T / K	p / Pa	Δp / Pa
408.16	0.1536	-0.0039
413.16	0.2528	0.0045
418.15	0.4157	0.0001
423.16	0.6722	0.0022
428.16	1.0811	-0.0029

$\Delta p = p - p_{calc}$, where p_{calc} is calculated from the Clarke and Glew equation (eq. 3.18) with the parameters given in Table 2.

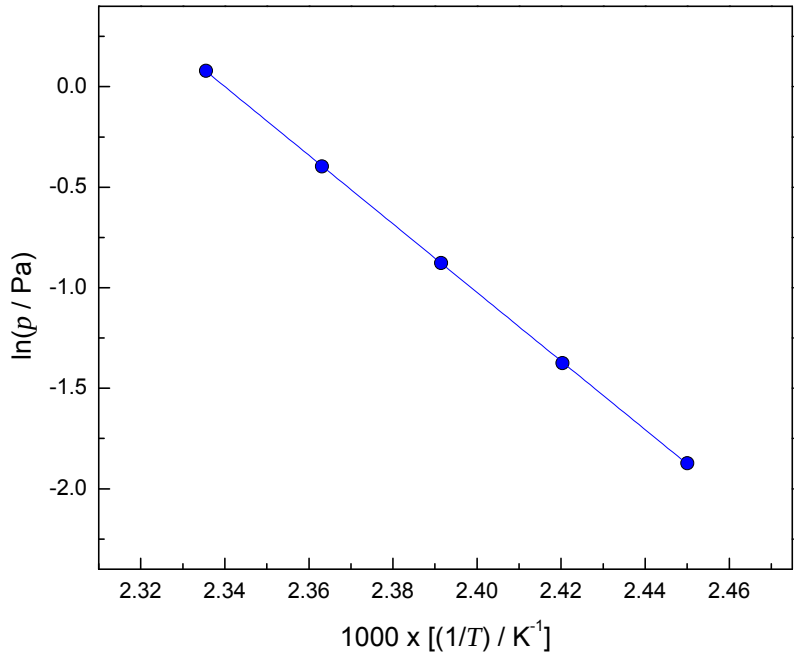

Figure 3.13. Plot of ln(p/Pa) = f [(1/T) / K^{-1}] for 1,3,5-triphenylbenzene.

The thermodynamic properties of sublimation at the mean temperature, <T>, and reference temperature, θ = 298.15 K, were derived from the fitting of the experimental results of the vapor pressures by the truncated form of the Clarke and Glew equation (3.18).[3] For 1,3,5-triphenylbenzene, the value $\Delta_{cr}^{g} C_{p,m}^{o}$(298.15 K) = −(28 ± 8) J·K^{-1}·mol^{-1} was considered, and was calculated with the values of $C_{p,m}^{o}$(cr) = 361 J·K^{-1}·mol^{-1} [11,16], and $C_{p,m}^{o}$(g) = 333 J·K^{-1}·mol^{-1} .as derived by computational thermochemistry reported in reference.[1] The thermodynamic properties of sublimation derived from equations (3.18) and (3.24) at the mean temperature,<T>, and reference temperature, θ = 298.15 K, are presented in table 3.3.

Table 3.3. Parameters of Clarke and Glew equation fitted from the vapor pressure results and the derived standard (p^o = 10^5 Pa) molar entropy of sublimation for 1,3,5-triphenylbenzene at the reference temperature, θ.

T interval / K	θ / K	$\Delta_{cr}^{g} G_m^o(\theta)$ / J·mol^{-1}	$\Delta_{cr}^{g} H_m^o(\theta)$ / J·mol^{-1}	$\Delta_{cr}^{g} S_m^o(\theta)$ / J·K^{-1}·mol^{-1}	r^2
408 to 429	418.16	43076 ± 471	141837 ± 331	236.2 ± 0.8	0.9999
	298.15	71956 ± 1314	145197 ± 1015	245.7 ± 2.8	

Table 3.4 lists a compilation of the thermodynamic properties of sublimation at reference temperature, T = 298.15 K, for 1,3,5-triphenylbenzene obtained in this work using the KEQCM II, as well as some selected literature values. The obtained results for thermodynamic properties of sublimation at reference temperature, T = 298.15 K, for 1,3,5-triphenylbenzene, are in excellent agreement with the literature values.

Table 3.4. Thermodynamic properties of sublimation at reference temperature, T = 298.15 K, for 1,3,5-triphenylbenzene, obtained in this work, together with some selected literature values.

<T> /K	$\Delta_{cr}^{g} H_{m}^{o}$ (298.15 K) / kJ·mol^{-1}	$\Delta_{cr}^{g} S_{m}^{o}$ (298.15 K) / J·K^{-1}·mol^{-1}	$\Delta_{cr}^{g} G_{m}^{o}$ (298.15 K) / kJ·mol^{-1}	
418.16	145.2 ± 1.0	245.7 ± 2.8	72.0 ± 1.3	This work (KEQCM II)
416.40	146.8 ± 1.1	249.2 ± 3.0	72.5 ± 1.4	Santos *et al.*[1] (Test 4#, KEQCM I)
415.89	147.4 ± 1.0	250.5 ± 2.8	72.7 ± 1.3	Santos *et al.*[1] (Test 5#, KEQCM I)
418.32	144.5 ± 1.2	244.3 ± 3.4	71.7 ± 1.6	Ribeiro da Silva *et al.*[11] (NECKA)
376	147.7 ± 1.3	253.3 ± 3.5	72.2 ± 1.6	Verevkin *et al.*[17] (TM)
427	145.6 ± 2.1	243.8 ± 5.3	72.9 ± 2.6	Malaspina *et al.*[18] (KEM)
409	145.7 ± 1.3	242.5 ± 3.6	73.4 ± 1.6	Wakayama and Inokuchi [19] (KEM)

All the values were corrected from <T> to reference temperature, T = 298.15 K, using the same $\Delta_{cr}^{g} C_{p,m}^{o}$ (298.15 K) = −(28 ± 8) J·K^{-1}·mol^{-1}. KEQCM - Knudsen Effusion Quartz Crystal Microbalance; NECKA - Nine Effusion Cell Knudsen Apparatus; TM - Transpiration Method; KEM - Knudsen Effusion Method.

3.1.7. Methodology for Vapor Pressure Measurements of Ionic Liquids

The Knudsen effusion methodology for the measurements of vapor pressure of ionic liquids was developed and refined in this Ph.D. project. The measurement of vapor pressure of ionic liquids is experimentally not trivial due to their low vapor pressures at the usual temperature range of the Knudsen effusion, as well as the useful short temperature interval in the thermal stability region. Along the methodology development and optimization, the following challenges/problems have been encountered:

- In situ (vacuum) purification of the ionic liquids before the vapor pressure measurements experiments;
- Experimental, namely the so-called "temperature window of opportunity" for the vaporization study of the ionic liquids without decomposition;
- Optimization of the temperature step and isothermal mode procedure, such as the temperature step and time interval;
- Stability and repeatability of the QCM background sign;

- Gravimetric mass loss detection process and measurement procedure for a highly hygroscopic liquid;
- Evaluation of the ionic liquid decomposition in the effusion experiment.
- High vacuum compatibility and high temperature stability of all the materials used in the oven and Knudsen effusion cell;
- Accurate high temperature measurement and control in vacuum;
- Sensitivity saturation/stability of the Quartz crystal microbalance;
- Condensation of ionic liquid in the effusion platinum disk orifice.

Some of the challenges mentioned in this section are quite specific of the Knudsen effusion measurement of an ionic liquid sample and were never faced simultaneously before.

In Situ Purification of the Ionic Liquid Sample

The *in situ* purification of the ionic liquid was performed using the Knudsen effusion installation. For that purpose, the effusion cell, without the platinum disk orifice, was loaded with the purified ionic liquid and placed in the oven, inside the vacuum chamber. The purification temperature is chosen, typically (20 – 30) K below the usual measuring temperature interval (470 to 520 K).

Afterwards, the ionic liquid sample inside the open effusion cell is kept in high vacuum conditions, while the temperature of the oven is raised until the purification temperature. The purification of the ionic liquid in high vacuum and high temperature is prolonged typically for about one hour.

This procedure proved to be very effective in degassing and minimizing the volatile contents of the sample that were not removed in the initial/standard purification procedure. It was found that the *in situ* purification is an essential step in the methodology for the accurate measurement of vapor pressures of ionic liquids.

Experimental and Temperature Step Mode Procedure

After the in situ purification, the effusion cell is prepared to start the experimental vapor pressures measurements.

The effusion cell is weighed in an analytical balance, Mettler, model AE163 with a resolution of 0.00001 g, and placed into the oven of the apparatus. An aluminum disk is placed above the cell to improve the thermal contact between the cell and the oven. The vacuum chamber is partially evacuated by means of a rotary vane pump, in order to reduce the risk of decomposition of the sample, while the temperature of the oven increases gradually until it reaches a fixed temperature. After thermal stabilization, the vacuum chamber is connected to a diffusion pump (KEQCM I) or a turbomolecular pumping station (KEQCM II). The effusion period is considered to start when the pressure of the vacuum chamber drops below 1 Pa, and the final pressure is lower than 1×10^{-5} Pa. When the effusion period (usually between 4 to 6 hours), and the temperature step profile is over, the connection valve to the turbomolecular pumping station is closed and the vacuum chamber is filled with gaseous N_2 (0.9999). When the oven reaches the temperature of 313 K, the vacuum chamber is opened, and the effusion cell is removed from the oven, cleaned and weighed in the same balance, in order to measure the total mass loss from the Knudsen effusion experiment.

Concerning the temperature step mode procedure, initially a 2 K temperature step mode was used, and the effusion time in each step was 1800 s. From the beginning of the measurements of the vapor pressure of an ionic liquid, usually it takes around 15 to 20 days to finish the measurements. In the new Knudsen effusion apparatus (KEQCM II), a new temperature step mode procedure was tested, a 5 K temperature step mode, and the effusion time in each step was around (1800 to 2400) s with good results, and the time for measuring the ionic liquids is around 10 days.

Isothermal Mode Procedure

In each studied ionic liquid, an isothermal experiment at a defined temperature was performed, where only the gravimetric mass loss method is considered. The isothermal procedure was adopted in the vapor pressure measurements of the ionic liquids, in order to verify the mass sensitivity coefficient obtained in the effusion experiments.

QCM Background Measurement

The background noise, $(df/dt)_{\text{drift}}$, is measured as an independent experiment using an identical empty effusion cell, considering the same temperature step and effusion time used for the ionic liquid. Usually, the background noise is in the order of (0.005 - 0.01) $Hz \cdot s^{-1}$, and tends to be lower along the effusion experiments. During the effusion experiments, the vacuum chamber's walls are contaminated with the ionic liquid under study, and with the increase of the number of experiments, the ionic liquid thin film on the walls decreases the background noise which is affected by the inevitable contamination of the vacuum chamber's walls. The background noise experiments are performed independently for each ionic liquid, and for each individual effusion experiment.

Optimization of Gravimetric Mass Loss Detection

One of the most sensitive steps in the vapor pressure measurement is the weighing of the effusion cell. In fact, the effusion cell is stored in an exicator before the weighing procedure. In order to minimize the effect of water in the effusion cell weighing, a chamber made of stainless steel and a brass lid, with an output to connect to the vacuum, was developed. The image and schematic representation of the weighing / drying chamber are represented in figures 3.14 and 3.15. Before the weighing procedure, the effusion cell was placed inside the chamber and then evacuated for 15 min at room temperature. Afterwards, the output of the chamber was protected with a Teflon cap, to reduce the contact with the air.

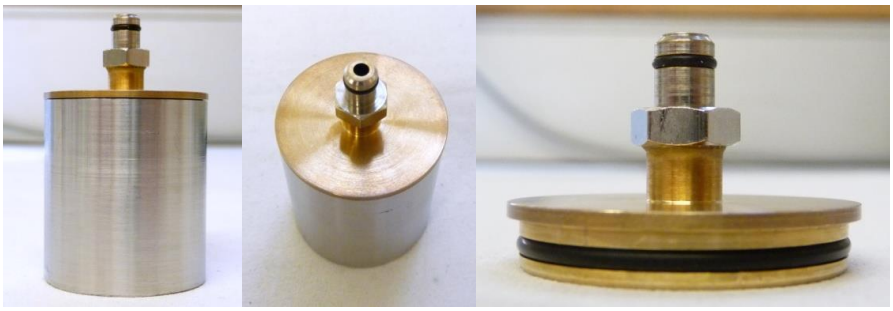

Figure 3.14. Image of the weighing / drying chamber (side and top view).

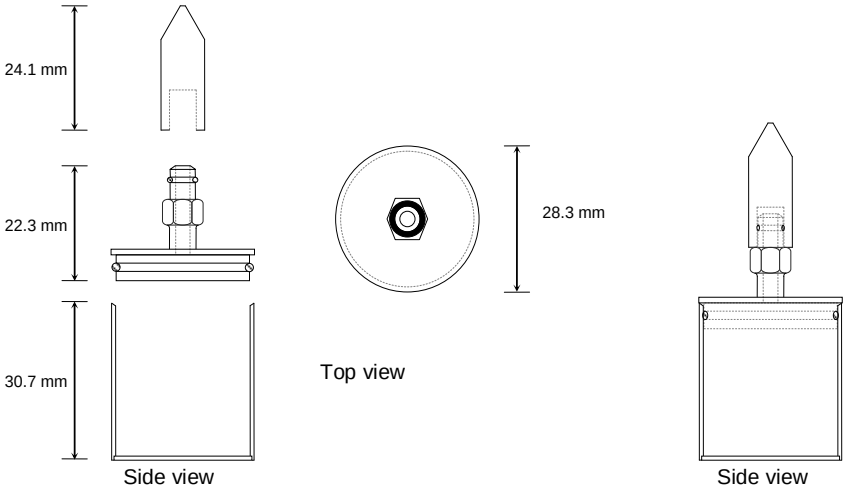

Figure 3.15. Schematic representation of the weighing / drying chamber (side and top view).

3.2 Heat Capacity Measurements

3.2.1. General Introduction

Heat capacity is one of the most important thermophysical properties which can be used to characterize a substance. It is intimately related with the temperature dependence of fundamental thermodynamic functions and consequently essential for the calculation and interpretation of their temperature dependence. Heat capacities are widely used in several areas such as: thermodynamics for obtaining entropy and enthalpy values, thermochemistry for calculating changes in reaction enthalpies, and in chemical engineering for establishing energy balances.[20–22]

The heat capacity is defined by the following differential relation:

$$C = \left(\frac{\partial Q}{\partial T}\right)_x , \tag{3.38}$$

where Q is the heat exchanged between the system and the surroundings when the temperature changes under the specified conditions, x. In the literature, several different thermodynamic functions that represent the heat capacity can be found:

1. heat capacity at constant volume (or isochoric heat capacity), C_V

$$C_V = \left(\frac{\partial U}{\partial T}\right)_V = T \cdot \left(\frac{\partial S}{\partial T}\right)_V = -T \cdot \left(\frac{\partial^2 A}{\partial T^2}\right)_V \tag{3.39}$$

2. heat capacity at constant pressure (or isobaric heat capacity), C_p

$$C_p = \left(\frac{\partial H}{\partial T}\right)_p = T \cdot \left(\frac{\partial S}{\partial T}\right)_p = -T \cdot \left(\frac{\partial^2 G}{\partial T^2}\right)_p \tag{3.40}$$

3. heat capacity at the saturation vapor pressure of the liquid, C_{sat}

$$C_{sat} = T \cdot \left(\frac{\partial S}{\partial T} \right)_{sat} \tag{3.41}$$

The thermodynamic functions U, H, S, A, and G represents, the internal energy, enthalpy, entropy, Helmholtz, and Gibbs functions, respectively.

Heat capacities of a sample can be measured in any calorimeter able of simultaneously measuring the amount of heat input or output as well as monitoring the temperature change in the sample. [20–23] The measurements can be performed either by continuously scanning temperature or by stepwise measurements. For the case of continuous scanning measurements, the heat capacity is derived as the ratio $(\mathrm{d}Q/\mathrm{d}t)/(\mathrm{d}T/\mathrm{d}t)$, and, depending on the conditions, a correction for the instrument response may be applied. If the calorimeter response can be expressed with a first-order exponential in time, the Tian equation can be used [20]:

$$\left(\frac{\partial Q}{\partial t} \right)_{c} = \left(\frac{\partial Q}{\partial t} \right)_{m} + \tau \cdot \left[\frac{\partial}{\partial t} \left[\left(\partial Q / \partial t \right)_{m} \right] \right] \tag{3.42}$$

Where, $\left(\partial Q / \partial t\right)_{c}$ is the corrected heat rate, $\left(\partial Q / \partial t\right)_{m}$ is the heat rate measured, and τ is the time constant for the response of the calorimeter and sample to a temperature change. In the case of stepwise measurements, a correction for the time response is not necessary; however, ΔT must be small, in order to assure the differential definition of heat capacity.

Differential scanning calorimetry, DSC, is the most common calorimeter used for heat capacity measurements. Typically, sample volumes of <0.1 cm^3 are used in the DSC. Taking into account that ΔQ is proportional to the sample size, the larger sample volume is useful in order to decrease the relative error in the ΔQ measurements. [20–23] Therefore, DSCs with sample volumes higher than 1 cm^3 and better heat detection limits present advantages.[20–23] In this method, two types of ampoules can be used: sealed ampoules with some vapor space which measure the C_{sat} and overflow ampoules which measures the C_p. Obviously, the sealed ampoules require a hermetic seal, in order to avoid loss of the sample during the experiment, and taking into account that the vapor pressure of the liquids vary with temperature,

the measurements give C_{sat}. For very small pressure changes, C_{sat} is identical to C_p. The overflow ampoules consist of a cylindrical ampoule with a filling tube extending outside the calorimeter.[20,24] In order to obtain high accuracy in the heat capacity measurements using a DSC, a correction for the thermal expansion of the ampoule might be required.

Another accurate method for heat capacity measurement is based on the isoperibol temperature-change calorimetry. Despite not having the temperature range or pressure range of the DSC, isoperibol calorimetry works with larger volumes (≥ 25 cm^3) and allows a very accurate determination of ΔT. [20,25] The isoperibol temperature-change calorimeter typically consists of a Dewar vessel flask, in which the temperature changes are measured with a thermistor (micro-degree resolution), and ΔQ is given by an electrical heater submerged in the liquid. [20,25] This method requires the correction for the heat exchange with the surroundings, a procedure that becomes more complex, since the physical size of the reaction vessel tends to decrease, the rate of the heat exchange with the surroundings and the reaction time increases. This method is not recommended to volatile liquids. [20,25]

Isothermal flow calorimetry is considered the best alternative for the heat capacity at constant pressure measurements over wide temperature range. In this method, no correction for vapor-liquid equilibrium is required. Temperature control, careful calibration and maintenance of the pumps is crucial to achieve good accuracy on the measurements. Since viscous liquids present difficulties when pumped through the tubing and viscous flow will generate sufficient heat to obstruct the measurements, this method is limited to low viscous liquids. For measurements of C_p, two methods can be used:

- temperature of the input flow is controlled, heat is added to the liquid at a constant rate, and the temperature of the output flow is measured;
- temperature of the input flow is controlled at a different temperature comparative to the isothermal calorimeter, as a result the output flow is at the calorimeter temperature.

Drop calorimetry is the simplest method for measuring heat capacities over a wide range of temperatures and was used not only for heat capacity measurements, but also for studies of enthalpies of phase transitions.[20,26–29] In this method, an ampoule containing the sample is moved from a fixed temperature to a calorimeter

at a different temperature. The applicable temperature range depends on the type of heat flow sensors. For high temperature calorimeters reaching 1300 K, platinum-platinum/rhodium thermocouples in series are frequently used, whereas for temperatures under 420 K, high sensitive heat flow plates (usually semiconductor Peltier plates) are used. Drop calorimeters of the heat conduction type take the advantage of the improved sensitivity arising from the isothermal working mode of the heat flow sensors. The twin design has proven to be suitable for very long reaction periods, as the surrounding disturbances will be significantly reduced. These characteristics (sensitivity and long term stability) are very important when the calorimeters are used in solution chemistry, in particular for biological and pharmaceutical applications .[20,30–32]

3.2.2. High-Precision Heat Capacity Drop Calorimeter

The heat capacities of the ionic liquids were measured using a twin high-precision drop calorimeter, reassembled, improved and tested as part of this Ph.D. project. This calorimeter was designed and constructed in the Wadsö's group in Lund, Sweden, and is described in the literature in an initial version [27], and some years later a description of an improved version of the same apparatus, with some modifications concerning instrumentation and working methodology to allow measurements on dilute solutions, was presented.[26] In our group, the same apparatus was reassembled and modernized with significant changes in the electronics, data acquisition and data treatment, as well as by creating a user-friendly software environment. The main design and hardware of the twin heat flux detectors were kept as in the originally apparatus[26], except the calorimeter optocoupler voltage pre-amplifier installed in the calorimeter block that was removed.

The full description of the reassembly and testing of the drop calorimeter used for the heat capacity measurements is available in Chapter 4 (Paper I). Since the publication, the apparatus was calibrated and tested frequently, and the only technical modification was concerned with the installation and tuning of two new PID temperature controllers, OMRON model E5CC, for the temperature control of the furnace and the calorimetric block of the calorimeter.

3.3 Viscosity and Density Measurements

3.3.1. General Introduction

Viscosity

Viscosity (viscosity coefficient) is a fundamental characteristic property of all liquids and is related with the internal resistance to the liquid flow. Therefore, viscosity is a measure of this resistance to an applied flow or shear. This is an important property which characterizes the behavior of liquids and is the viscosity due to fact that relates the shear stress in a moving fluid to the strain rate of the fluid, which is caused by intermolecular interactions present in the fluid. Although the viscosity is a function of temperature and pressure, this work will be focused on the dependence of the viscosity on temperature, exclusively.

The dynamic viscosity corresponds to the tangential force per unit area required to move one plane (*A*) with respect to the other (*B*) at unit velocity when a unit distance is maintained, as depicted in figure 3.16.

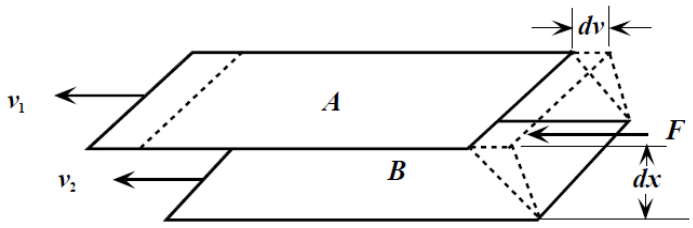

Figure 3.16. Simple shear of a liquid film. (source [33])

Taking into account that the viscosity of a liquid is a measure of the resistance to a flow, therefore the viscosity can be described as:

$$\sigma = \eta \cdot \dot{\gamma} \tag{3.43}$$

Where, σ is the shear stress, η is the dynamic viscosity, and $\dot{\gamma}$ is the strain rate (or rate of deformation) usually expressed as:

$$\dot{\gamma} = \frac{1}{x} \cdot \frac{dx}{dt} = \frac{v}{x} \tag{3.44}$$

Where, x is the length, t is time, and (dx / dt) is the velocity v. Consequently, the dynamic viscosity can be written as:

$$\eta = \sigma \cdot \frac{v}{x} \tag{3.45}$$

The kinematic viscosity is the ratio between the dynamic viscosity and the density (ρ) of the liquid at the considered temperature and pressure and is defined as:

$$\upsilon = \frac{\eta}{\rho} \tag{3.46}$$

The flow characteristics of the liquids are essentially dependent on the viscosity and are divided into two broad categories: Newtonian and non-Newtonian. A fluid for which the viscosity does not change with the shear rate is defined as Newtonian fluid. The fluids in which the viscosity varies with the shear rate, are termed a non-Newtonian fluid.[33,34] The behavior of Newtonian fluid can be represented by a straight line in figure 3.17. The slope of this line is determined by the viscosity. The horizontal axis represents the ideal fluid, with no viscosity, while the vertical axis represents the ideal elastic. The ideal plastic represents a plastic body which sustains a certain amount of stress before suffering a plastic flow.[33–35]

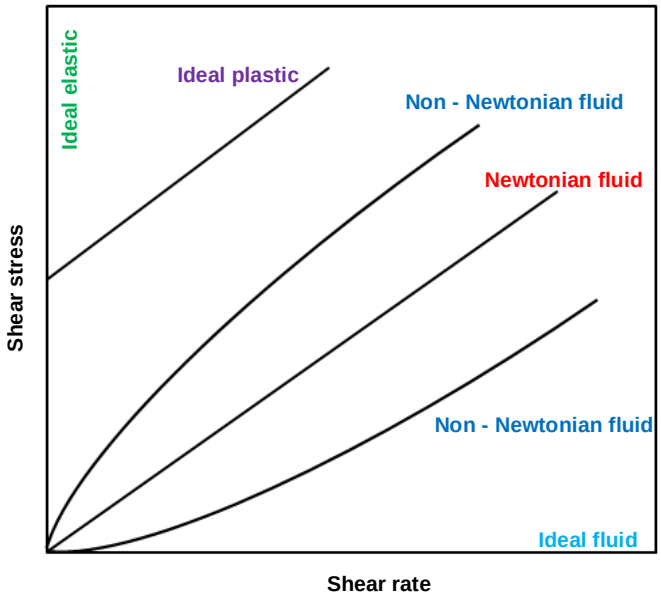

Figure 3.17. Various types of fluid behavior.

The fluids in which the viscosity, η, varies with the shear rate, are termed a non-Newtonian fluid. A particular characteristic of the non-Newtonian fluids is the preservation of a "memory" of their flow history which is termed elasticity. The liquids which are partly or wholly formed of macromolecules, or two-phase materials (i.e. high concentration suspensions of solid particles in a liquid carrier solution), are frequently representatives of non-Newtonian fluids.[35]

A variety of theoretical models and empirical or semi–empirical expressions are available in the literature, which relates the viscosity of liquids as function of pressure and temperature.[33] In this work, the Vogel-Tammann-Fulcher equation (VTF)[33] was used to correlate the experimental viscosity data:

$$\ln(\eta) = \ln(A_\eta) + \frac{B_\eta}{(T - C_\eta)} \tag{3.47}$$

where η is the dynamic viscosity in mPa·s, T is the temperature in K, and A_η, B_η and C_η are adjustable parameters. The parameters were determined from the fitting of the experimental data using the equation (3.46) for the studied ionic liquids.

The viscosity describes the internal resistance of a fluid to a shear stress. As

the viscosity arises from intermolecular interactions an increase in temperature will substantially decrease their intensity and therefore the viscosity. The energy barrier of the fluid to a shear stress, E, can be evaluated based on the viscosity dependence on temperature using the following equation:

$$E = R \cdot \frac{\partial(\ln \eta)}{\partial(1/T)} = R \cdot \left(\frac{B_\eta}{\left(\frac{C_\eta^2}{T^2} - \frac{2.C_\eta}{T} + 1 \right)} \right) \quad (3.48)$$

Density

Density, by definition, is mass per unit volume, and is a property required for industrial process design and implementation as well as for the development of equations of state.[36–39] Density can be measured with pycnometers, dilatometers, vibrating tube density meters and the buoyancy method. [36] In this work the densities of ionic liquids were measured using the Anton Paar rotational Stabinger viscometer – densimeter that applies the vibrating tube density methodology. Usually, the densities of ionic liquids do not shown a marked dependency on temperature and the density decreases almost linear the temperature increase.

The experimental density data, in the temperature range, was described using a second order polynomial equation correlation, according to equation 3.49

$$\ln(\rho) = a + b \cdot T + c \cdot T^2 \quad (3.49)$$

The isobaric thermal expansion coefficients (α_p), which considers the volumetric changes with temperature, were calculated using equation 3.50,

$$\alpha_p = -\frac{1}{\rho}\left(\frac{\partial \rho}{\partial T}\right)_p = -\left(\frac{\partial \ln \rho}{\partial T}\right)_p, \quad (3.50)$$

where ρ is the density, T is the temperature, and p is the pressure.

3.3.2. Anton Paar Rotational Stabinger Viscometer - Densimeter

In this work, the viscosities and densities were measured using an automated SVM 3000 Anton Paar rotational Stabinger viscometer - densimeter, as described in the literature.[40] The viscosity measurement is based on the simultaneous measurement of rotation speed and torque. A rotating magnet produces an eddy current field with an exact speed-dependent brake torque. The eddy current torque is measured with a resolution of about 50 pN·m. The measurement cell contains a rotor with a constant speed of rotation. The cell is filled with the sample in which the rotor is centered in the heavier liquid by the buoyancy effect, taking into account that the rotor needs no bearing, and therefore, no friction occurs (figure 3.18).

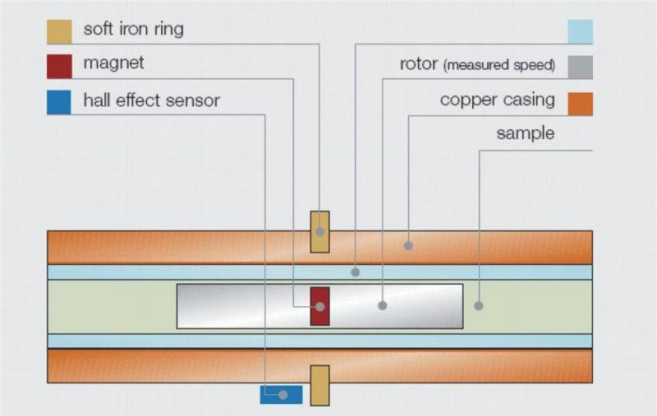

Figure 3.18. Schematic representation of the measuring principle. (source of the scheme[41])

The rotating rotor is forced to rotate by shear stress in the fluid and is guided axially by a built-in magnet, which interacts with the soft iron ring. The rotor reaches a constant rotation speed by the equilibrium between the effect of the eddy current and the shear forces at work in the fluid. The dynamic viscosity is derived from the rotor speed. The SVM 3000 is also equipped with a vibrating tube densimeter. Both measuring cells can be filled in one step and the measurements are performed simultaneously. The small sample volume allows extremely quick temperature changes and very short equilibration times. The SVM 3000 uses integrated Peltier elements for fast and efficient thermostability. The reproducibility of the dynamic viscosity and density measurements is according to the manufacturer 0.35 % and 0.5 $kg \cdot m^{-3}$, respectively from 288.15 K to 378.15 K. SVM 3000 viscometer -

densimeter is rapid, compact and versatile in use, with only small amounts of sample and solvents required.

3.3.3. Viscometer - Densimeter Calibration

The SVM 3000 viscometer - densimeter was calibrated using Anton Paar standard calibration samples, APN7.5, APN26 and APN415. The calibration of the SVM 3000 was performed at the same experimental conditions as the measurements of the studied ionic liquids. The apparatus was calibrated by measuring the viscosity and density of the three standard calibration samples in steps of 5 K in the temperature range from 293.15 to 393.15 K. During the calibration procedure, the reference data of the standard calibration samples are requested to be entered into the software of the apparatus in where the deviations of the obtained results from the respective standard calibration samples values are derived.

Preceding the viscosity and density measurements of the studied ionic liquids, the consistency of the apparatus calibration was checked with standard calibration sample, and the accuracy was additionally checked on the basis of the results obtained for $[C_7C_1im][NTf_2]$ already published in the literature.[42] The obtained results of the dynamic viscosity and density measurements were in agreement with the literature data, showing deviations in the order of with 0.5% for the viscosity and 0.03% for the density, respectively.

3.4 Refractive Index Measurements

3.4.1. General Introduction

The refractive index of a liquid, n, is defined as the ratio between the velocity of light in vacuum and the velocity of light in the liquid, describing its ability to refract light as it moves from one medium to another and therefore, the higher the refractive index, the more the light is refracted.[43]

The total polarizability of a liquid, α, is given by the Clausius-Mossotti equation[36] 3.51:

$$\frac{\alpha}{4\cdot\pi\cdot\varepsilon_{o}}=\left(\frac{\varepsilon-1}{\varepsilon+2}\right)\cdot\left(\frac{3\cdot M}{4\cdot\pi\cdot\rho\cdot N_{A}}\right) \tag{3.51}$$

where ε is the dielectric constant, ε_{o} is the vacuum permittivity, M is the molar mass, ρ is the density, and N_A is the Avogadro constant. When ε is measured in the visible range of frequencies, it equals n^2, where n is the refractive index of the medium. Usually, the reported data concerning refractive indices refers to the sodium D line (λ = 589 nm) and are denoted as, n_{D} .[44] Considering that $\left(M/\rho\cdot N_{A}\right)$ is related with the molecular volume, v, the electronic polarizability, α_{o}, is given by:

$$\frac{\alpha_{o}}{\varepsilon_{o}}=3\cdot v\cdot\left(\frac{n_{D}^{2}-1}{n_{D}^{2}+2}\right) \tag{3.52}$$

which is the known as Lorenz-Lorentz equation.[45] According to this equation, the electronic polarizability is related with the refractive index, which provides important information concerning the importance of the dispersion forces to the cohesion of the liquid.[46,47] Therefore, solvents with a large refractive indices, and hence large polarizabilities, should present strong dispersive forces.[46]

The refractive indices are temperature dependent and their dependence, $\left(\frac{\partial n_{D}}{\partial T}\right)_{p}$, is negative and essentially related with the thermal expansion coefficient, α_p, of the

material according the following equation considering a negligible effect of temperature on the polarizability:

$$\left(\frac{\partial n_D}{\partial T}\right)_p \cong \frac{1}{\rho}\left(\frac{\partial \rho}{\partial T}\right)_p \cdot (n_D - 1) \cong \alpha_p \cdot (1 - n_D) \tag{3.53}$$

Taking into account that α_p is very small and only slightly temperature dependent, the temperature dependence of the refractive index will be also small and for a short temperature range could be described by a linear function as follow:

$$n_D(T_2) = n_D(T_1) + \left(\frac{\partial n_D}{\partial T}\right)_p \cdot (T_2 - T_1) \tag{3.54}$$

If the temperature dependence of the refractive index is not known, a reasonable prediction could be achieved from equation 3.53.

3.4.2. Bellingham Refractometer, RFM340

The refractive indices were measured at the sodium D-line using a Bellingham model RFM340 refractometer (± 3×10^{-5} stated precision), as a function of temperature (288.15 to 318.15) K. The refractometer features a presser with a seal ring made of fluoropolymer Kalrez® which is closed over the sample on the prism. This presser improves the accuracy and repeatability by: improving the contact between the sample and prism, providing an "enclosed" environment which minimize the contact with the air and limiting the evaporation, and preventing strong ambient light from affecting the measurement quality. The presser incorporates a micro flow cell, which is used to introduce the sample into the refractometer, without opening the presser. The presser and the internal prism water jacket assembly is temperature controlled by an external bath through the presser hinge and integral channels in the presser arm. The temperature in the refractometer cell is controlled by an external refrigerated thermostatic bath, Huber, model CC1-K6. The temperature is typically controlled within a temperature fluctuation of (± 5×10^{-3}) K, measured with a resolution better than 1×10^{-3} K and an uncertainty within ± 0.02 K.

The temperature of the sample is measured with a sensor located at the centre of the presser.

3.3.3. Refractometer and Temperature Calibration

The calibration of the refractometer is essential to ensure accurate data and should be performed at low end (ZERO adjustment) and the high end (SPAN adjustment) scale of samples with well known values. Additionally to the calibration, the quality of the calibration should be checked daily with the samples used in the calibration, in order to check any deviations. In this work, the refractometer was calibrated with degassed water (Millipore® quality) and toluene (Spectranal®, 99.9 %). The temperature in the refractometer cell is controlled using an external thermostatic bath and measured by a 1/10 class Pt100 RTD in a data acquisition system in four-wire mode, Keithley model 2700/7700 DMM/MUX. The Pt100 temperature probe was previously calibrated against a calibrated platinum resistance thermometer, SPRT100 (Fluke-Hart Scientific 1529 Chub-E4), traceable to the National Institute of Standards and Technology (NIST) with an uncertainty lower than ($2x10^{-3}$) K.

3.5 Summary of Measurements / Ionic Liquids

The compilation of the measurements performed for each ionic liquid is listed in table 3.5. For the properties measured as a function of the temperature, the experimental temperature range is presented.

Table 3.5. Measurements overview for each ionic liquid.

Ionic Liquid Abbreviation	Knudsen effusion / quartz crystal microbalance		Heat Capacity Drop Calorimeter	Viscometer - Densimeter SVM 3000	Refractometer RFM340
	T range / K	Apparatus	T = 298.15 K	T range / K	T range / K
$[C_1C_1im][NTf_2]$	476 − 494	KEQCM I	✓	293 − 363	×
$[C_2C_1im][NTf_2]$	445 − 483	KEQCM I	✓	×	×
$[C_3C_1im][NTf_2]$	453 − 493	KEQCM I	✓	×	×
$[C_4C_1im][NTf_2]$	463 − 487	KEQCM I	✓	×	×
$[C_5C_1im][NTf_2]$	457 − 493	KEQCM I	✓	278 − 363	×
$[C_6C_1im][NTf_2]$	465 − 489	KEQCM I	✓	×	×
$[C_7C_1im][NTf_2]$	465 − 493	KEQCM I	✓	×	×
$[C_8C_1im][NTf_2]$	473 − 495	KEQCM I	✓	×	×
$[C_9C_1im][NTf_2]$	×	×	×	278 − 363	×
$[C_{10}C_1im][NTf_2]$	479 − 495	KEQCM I	✓	×	×
$[C_{11}C_1im][NTf_2]$	×	×	×	278 − 363	×
$[C_{12}C_1im][NTf_2]$	481 − 493	KEQCM I	✓	×	×
$[C_{14}C_1im][NTf_2]$	×	×	×	323 − 363	×
$[C_{16}C_1im][NTf_2]$	×	×	×	323 − 363	×
$[C_4C_1im][PF_6]$	×	×	✓	293 − 363	288 − 318
$[C_5C_1im][PF_6]$	×	×	✓	293 − 363	288 − 318
$[C_6C_1im][PF_6]$	×	×	✓	293 − 363	288 − 318
$[C_7C_1im][PF_6]$	×	×	✓	293 − 363	288 − 318
$[C_8C_1im][PF_6]$	×	×	✓	293 − 363	288 − 318
$[C_9C_1im][PF_6]$	×	×	✓	293 − 363	288 − 318
$[C_2C_2im][NTf_2]$	455 − 480	KEQCM I	✓	278 − 363	×
$[C_2C_3im][NTf_2]$	464 − 490	KEQCM I	✓	278 − 363	×
$[C_3C_3im][NTf_2]$	453 − 490	KEQCM I	✓	278 − 363	×
$[C_4C_4im][NTf_2]$	455 − 488	KEQCM I	✓	278 − 363	×
$[C_5C_5im][NTf_2]$	463 − 496	KEQCM I	✓	278 − 363	×
$[C_6C_6im][NTf_2]$	463 − 496	KEQCM I	✓	278 − 363	×
$[C_7C_7im][NTf_2]$	483 − 504	KEQCM I	✓	278 − 363	×
$[C_8C_8im][NTf_2]$	483 − 506	KEQCM I	✓	278 − 363	×
$[C_9C_9im][NTf_2]$	493 − 523	KEQCM II	✓	278 − 363	×
$[C_{10}C_{10}im][NTf_2]$	491 − 514	KEQCM I	✓	278 − 363	×
$[C_{12}C_{12}im][NTf_2]$	×	×	×	323 − 363	×
$[C_2Py][NTf_2]$	493 − 504	KEQCM I	×	×	×
$[C_3Py][NTf_2]$	497 − 512	KEQCM I	×	×	×
$[C_4Py][NTf_2]$	498 − 516	KEQCM I	×	×	×

... / ...

... / ...

$[^2C_2{}^1C_2Py][NTf_2]$	493 − 524	KEQCM II	✓	293 − 363	×
$[^2C_3{}^1C_2Py][NTf_2]$	498 − 524	KEQCM II	✓	293 − 363	×
$[^2C_4{}^1C_2Py][NTf_2]$	488 − 514	KEQCM II	✓	293 − 363	×
$[^2C_5{}^1C_2Py][NTf_2]$	493 − 424	KEQCM II	✓	293 − 363	×
$[^2C_6{}^1C_2Py][NTf_2]$	493 − 519	KEQCM II	✓	293 − 363	×
$[^2C_7{}^1C_2Py][NTf_2]$	498 − 419	KEQCM II	✓	293 − 363	×
$[^2C_8{}^1C_2Py][NTf_2]$	493 − 413	KEQCM II	✓	293 − 363	×

References

(1) Santos, L. M. N. B. F.; Lima, L. M. S. S.; Lima, C. F. R. A. C.; Magalhães, F. D.; Torres, M. C.; Schröder, B.; Ribeiro da Silva, M. A. V. *J. Chem. Thermodyn.* 43 (**2011**) 834–843.

(2) Lima, L. M. S. S., Ph.D. Thesis, University of Porto, **2009**.

(3) Clarke, E. C. W.; Glew, D. N. *Trans. Faraday Soc.* 62 (**1966**) 539–547.

(4) Dushman, S., *Scientific Foundations of Vacuum Technique*, John Wiley & Sons, New York, **1949**.

(5) Oonk, H. A. J.; Van der Linde, P. R.; Huinink, J.; Blok, J. G. *J. Chem. Thermodyn.* 30 (**1998**) 897–907.

(6) Vanderlinde, P.; Blok, J.; Oonk, H. *J. Chem. Thermodyn.* 30 (**1998**) 909–917.

(7) Mohr, P. J.; Taylor, B. N.; Newell, D. B. *Rev. Mod. Phys.* 84 (**2012**) 1527–1605.

(8) Knudsen, M. *Annalen der Physik* 333 (**1909**) 75–130.

(9) Knudsen, M. *Annalen der Physik* 333 (**1909**) 999–1016.

(10) Knudsen, M. *Annalen der Physik* 334 (**1909**) 179–193.

(11) Ribeiro da Silva, M. A. V.; Monte, M. J. S.; Santos, L. M. N. B. F. *J. Chem. Thermodyn.* 38 (**2006**) 778–787.

(12) Sauerbrey, G. *Z. Phys.* 155 (1959) 206–222. (cited in the reference 2)

(13) Agilent VEE Pro (Agilent Technologies, Inc., Santa Clara, CA).

(14) Sabbah, R.; Xu-wu, A.; Chickos, J. S.; Leitão, M. L. P.; Roux, M. V.; Torres, L. A. *Thermochim. Acta* 331 (**1999**) 93–204.

(15) Rocha, M. A. A.; Lima, C. F. R. A. C.; Santos, L. M. N. B. F. *J. Chem. Thermodyn.* 40 (**2008**) 1458–1463.

(16) Chickos, J. S.; Acree, W. E. *J. Phys. Chem. Ref. Data* 31 (**2002**) 537–698.

(17) Verevkin, S. P. *J. Chem. Thermodyn.* 29 (**1997**) 1495–1501.

(18) Malaspina, L.; Bardi, G.; Gigli, R. *J. Chem. Thermodyn.* 6 (**1974**) 1053–1064.

(19) Wakayama, N.; Inokuchi, H. *Bull. Chem. Soc. Jpn.* 40 (**1967**) 2267–2271.

(20) E. Wilhelm, T. M. Letcher, Eds., *Heat Capacities: Liquids, Solutions and Vapours*, The Royal Society of Chemistry, Cambridge, UK, **2010**.

(21) Zábranský, M.; Růžička Jr., V.; Domalski, E. S. *J. Phys. Chem. Ref. Data* 30 (**2001**) 1199–1689.

(22) Zábranský, M.; Kolská, Z.; Růžička Jr., V.; Domalski, E. S. *J. Phys. Chem. Ref. Data* 39 (**2010**) 013103.

(23) Kasper, M. *Anal. Bioanal. Chem.* 380 (**2004**) 366–367.

(24) González-Salgado, D.; Valencia, J. L.; Troncoso, J.; Carballo, E.; Peleteiro, J.; Romaní, L.; Bessières, D. *Rev. Sci. Instrum.* 78 (**2007**) 055103.

(25) Hansen, L. D.; Hart, R. M. *Thermochim. Acta* 417 (**2004**) 257–273.

(26) Suurkuusk, J.; Wadsö, I. *J. Chem. Thermodyn.* 6 (**1974**) 667–679.

(27) Konicek, J.; Suurkuusk, J.; Wadsö, I. *Chem. Scr.* 1 (**1971**) 217–220.

(28) Santos, L. M. N. B. F.; Schröder, B.; Fernandes, O. O. P.; Ribeiro da Silva, M. A. V. *Thermochim. Acta* 415 (**2004**) 15–20.

(29) Bernardes, C. E. S.; Santos, L. M. N. B. F.; Piedade, M. E. M. *Meas. Sci. Technol.* 17 (**2006**) 1405–1408.

(30) Bastos, M.; Volkova, N. N.; Wadso, I. *J. Chem. Soc., Faraday Trans.* 89 (**1993**) 1351–1352.

(31) Ng, K.; Rosenberg, A.; Bastos, M.; Wadsö, I. *Thermochim. Acta* 169 (**1990**) 339–346.

(32) Wadsö, I. *Thermochim. Acta* 267 (**1995**) 45–59.

(33) Viswanath, D. S., Ghosh, T. K., Prasad, D. H. L., Dutt, N. V. K., Rani, K. Y. *Viscosity of Liquids: Theory, Estimation, Experiment, and Data*, Springer, The Netherlands, **2007**.

(34) Brujan, E.-A. *Cavitation in Non-Newtonian Fluids With Biomedical and Bioengineering Applications*, Springer-Verlag, Berlin, Heidelberg, **2011**.

(35) Chhabra, R. P.; Richardson, J. F. *Non-Newtonian Flow and Applied Rheology: Engineering Applications*, Butterworth-Heinemann, **2008**.

(36) Goodwin, A. R. H.; Marsh, K. N.; W.akeham, A. W., Eds., *Measurement of the Thermodynamic Properties of Single Phases.* Experimental Thermodynamics, Vol. VI; Elsevier Science, Amsterdam, The Netherlands, **2003**.

(37) Rooney, D. W.; Jacquemin, J.; Gardas, R. *Top. Curr. Chem.* 209 (**2010**) 185–212.

(38) Dean, P. M.; Pringle, J. M.; MacFarlane, D. R. *Phys. Chem. Chem. Phys.* 12 (**2010**) 9144–9153.

(39) Wasserscheid, P.; Welton, T., Eds.; *Ionic Liquids in Synthesis*, Wiley-VCH Verlag GmbH, Weinheim, Germany, **2007**.

(40) Carvalho, P. J.; Regueira, T.; Santos, L. M. N. B. F.; Fernandez, J.; Coutinho, J. A. P. *J. Chem. Eng. Data* 55 (**2010**) 645–652.

(41) Viscosities and Rheology, http://www.ltp-oldenburg.de/index.php/viscosities.html (accessed Jun 11, **2013**).

(42) Tariq, M.; Carvalho, P. J.; Coutinho, J. A. P.; Marrucho, I. M.; Lopes, J. N. C.; Rebelo, L. P. N. *Fluid Phase Equilib.* 301 (**2011**) 22–32.

(43) Born, M.; Wolf, E. *Principles of Optics: Electromagnetic Theory of Propagation, Interference and Diffraction of Light*; 7th Ed.; Cambridge University Press, **1999**.

(44) Reinhard, M.; Drefahl, A. *Handbook for Estimating Physicochemical Properties of Organic Compounds*; John Wiley and Sons, Inc., **1998**.

(45) Israelachvili, J. N. *Intermolecular and Surface Forces*; 3rd Ed.; Academic Press, **2011**.

(46) Reichardt, C.; Welton, T. *Solvents and Solvent Effects in Organic Chemistry*; 4th Ed.; Wiley-VCH Verlag GmbH, Weinheim, Germany, **2010**;

(47) Tariq, M.; Forte, P. A. S.; Gomes, M. F. C.; Lopes, J. N. C.; Rebelo, L. P. N. *J. Chem. Thermodyn.* 41 (**2009**) 790–798.

CHAPTER 4

Results and Discussion

4.1 List of Papers

Details about the methodologies, experimental results and discussion are presented in article format. The articles are referred as "Paper I", etc.

Paper I. Luís M. N. B. F. Santos, Marisa A. A. Rocha, Ana S. M. C. Rodrigues, Vojtěch Štejfa, Michal Fulem, Margarida Bastos
"Reassembling and testing of a high-precision heat capacity drop calorimeter. Heat capacity of some polyphenyls at *T* = 298.15 K"
The Journal of Chemical Thermodynamics (2012), 43, 1818–1823.
doi: 10.1016/j.jct.2011.06.010

Paper II. Marisa A. A. Rocha, Carlos F. R. A. C. Lima, Lígia R. Gomes, Bernd Schröder, João A. P. Coutinho, Isabel M. Marrucho, José M. S. S. Esperança, Luís P. N. Rebelo, K. Shimizu, José N. Canongia Lopes, Luís M. N. B. F. Santos
"High-Accuracy Vapor Pressure Data of the Extended $[C_nC_1im][Ntf_2]$ Ionic Liquid Series: Trend Changes and Structural Shifts"
Journal of Physical Chemistry B (2011), 115, 10919–10926.
doi: 10.1021/jp2049316

Paper III. Marisa A. A. Rocha, Margarida Bastos, João A. P. Coutinho, Luís M. N. B. F. Santos
"Heat Capacities at 298.15 K of the Extended $[C_nC_1im][Ntf_2]$ Ionic Liquid Series"
The Journal of Chemical Thermodynamics (2012), 53, 140–143.
doi: 10.1016/j.jct.2012.04.025

Paper IV. Marisa A. A. Rocha, João A. P. Coutinho, Luís M. N. B. F. Santos
"Cation Symmetry Effect on the Volatility of Ionic Liquids"
Journal of Physical Chemistry B (2012), 116, 10922–10927.
doi: 10.1021/jp306937f

Paper V. Marisa A. A. Rocha, João A. P. Coutinho, Luís M. N. B. F. Santos
"Evidence of Nanostructuration from the Heat Capacities of the 1,3-Dialkylimidazolium Bis(trifluoromethylsulfonyl)imide Ionic Liquid Series "
Journal of Chemical Physics (2013), 139, 104502.
doi: 10.1063/1.4820825

Paper VI. Marisa A. A. Rocha, Filipe M. S. Ribeiro, Bernd Schröder, João A. P. Coutinho, Luís M. N. B. F. Santos
"Volatility Study of $[C_1C_1im][NTf_2]$ and $[C_2C_3im][NTf_2]$ Ionic Liquids "
The Journal of Chemical Thermodynamics (2014), 68, 317-321.
doi: 10.1016/j.jct.2013.09.020

Paper VII. Marisa A. A. Rocha, Catarina M. S. S. Neves, Mara G. Freire, Olga Russina, Alessandro Triolo, João A. P. Coutinho, Luís M. N. B. F. Santos
"Alkylimidazolium Based Ionic Liquids: Impact of Cation Symmetry on their Nanoscale Structural Organization"
Journal of Physical Chemistry B (2013) 117, 10889–10897.
doi: 10.1021/jp406374a

Paper VIII. Marisa A. A. Rocha, João A. P. Coutinho, Luís M. N. B. F. Santos
"Vapor Pressures of 1,3-Dialkylimidazolium Bis(trifluoromethylsulfonyl)imide Ionic Liquid Series with Long Alkyl Chain Length"
Manuscript

Paper IX. Marisa A. A. Rocha, Filipe M. S. Ribeiro, Ana I. M. C. Lobo Ferreira, João A. P. Coutinho, Luís M. N. B. F. Santos
"Thermophysical Properties of $[C_{N\text{-}1}C_1im][PF_6]$ Ionic Liquids"
Journal of Molecular Liquids (2013), 188, 196-202.
doi: 10.1016/j.molliq.2013.09.031

Paper X. Marisa A. A. Rocha, Filipe M. S. Ribeiro, João A. P. Coutinho, Luís M. N. B. F. Santos
"Heat Capacities at 298.15 K of $[C_{N\text{-}1}C_1im][PF_6]$ Ionic Liquids Series"
Manuscript

Paper XI. Marisa A. A. Rocha, Luís M. N. B. F. Santos
"First Volatility Study of the 1-Alkylpyridinium based Ionic Liquids by Knudsen Effusion"
Chemical Physics Letters (2013) 585, 59–62.
doi: 10.1016/j.cplett.2013.08.095

Paper XII. Miguel Vilas, Marisa A. A. Rocha, Emilia Tojo, Luís M. N. B. F. Santos
"Novel 1-Ethyl-2-Alkylpyridinium based Ionic Liquids: Synthesis and Volatility"
Manuscript.

Paper XIII. Marisa A. A. Rocha, Miguel Vilas, Ana S. M. C. Rodrigues, Emilia Tojo, Luís M. N. B. F. Santos
"Thermophysical Properties of a Novel Pyridinium Based Ionic Liquids Family"
Manuscript

4.2 Summary of Papers

High-Precision Heat Capacity Drop Calorimeter

The description of the reassembling and testing of a twin heat conduction, high-precision, drop microcalorimeter for the measurement of heat capacities of small samples that was used on the heat capacities measurements of the ionic liquids is presented in **Paper I**. This calorimeter was designed and constructed in the Thermochemistry Laboratory, Lund, Sweden, being afterwards transferred to Porto, Portugal, where it was reassembled, modernized and tested as a part of this Ph.D. Thesis. The apparatus was reassembled and modernized with significant changes in the electronics, data acquisition and data treatment, as well as by the development and test of a new user-friendly software environment. The performance of the apparatus was evaluated from the results obtained in the heat capacity measurements of benzoic acid and hexafluorobenzene. The results of the calibration experiments, the heat capacities derived for the test compounds as well as the quality of the data obtained for the polyphenyl compounds shows that this apparatus can be used to measure heat capacity at T = 298.15 K with high level of precision and accuracy.

[$C_{N-1}C_1$im][NTf_2] Ionic Liquids

In the papers II and III the effect of nanostructuration of ionic liquids on the thermodynamic properties of vaporization and heat capacity data was explored. The obtained results and conclusions were a significant contribution for the thermodynamic support of the nanostructuration in the ionic liquids. This feature in the ionic liquids was only possible to detect due to the study of the extended series of [$C_{N-1}C_1$im][NTf_2].

Paper II is dedicated to the vapor pressure measurements of the extended [$C_{N-1}C_1$im][NTf_2] ionic liquid series. For the first time, two distinct trends were clearly evidenced for the enthalpies and entropies of vaporization along the [$C_{N-1}C_1$im][NTf_2] series. The trend shift observed on the thermodynamic properties of vaporization, which occurs at [C_6C_1im][NTf_2], was related to the structural modifications along the series. This work represents a significant contribution to the better understanding of the relationship among cohesive energies, volatilities, and liquid structure of ionic liquids. It is important to stress that previous studies, only based on a handful of cations with an even number of carbon atoms in the alkyl side chain, did not allow

the complete characterization of the important trend changes of the thermodynamic properties of vaporization, including the outlier character of $[C_2C_1im][NTf_2]$. Additionally, in order to evaluate if the nanostructuration might be related to the trend changes observed in the thermodynamic properties, a MD study of the $[C_{N-1}C_1im][NTf_2]$ ionic liquid series was carried out, in collaboration with another research group. It was found that the trend shifts observed for $\Delta_l^g H_m^o$ and $\Delta_l^g S_m^o$ are related to the structural modifications that occur when the number of alkyl carbon atoms nears six.

In **Paper III**, the study was extended for the measurement of the heat capacities at 298.15 K using a drop heat capacity calorimeter reassembled and modernized during this Ph.D. project (Paper I). In this work, the trend of the heat capacities of the $[C_{N-1}C_1im][NTf_2]$ ionic liquids along the alkyl side chain length in the cation was investigated, in order to evaluate the effect of nanostructuration in the heat capacity data. It was found, that the dependence of the specific heat capacity on the alkyl side chain length for the extended ionic liquid series displays a trend shift at $[C_6C_1im][NTf_2]$, providing an additional experimental evidence for the nanostructuration in ionic liquids and its impact on their thermophysical properties. The observed subtle changes in the heat capacity with the length of the cation alkyl side chain was only possible due to the high precision of the heat capacity results obtained in the reassembled drop calorimeter (Paper I).

$[C_{N/2}C_{N/2}im][NTf_2]$ Ionic Liquids

Papers IV - VIII deals with the effect of the symmetry of the imidazolium cation on the thermophysical properties. This effect was investigated in order to obtain additional insights concerning the nanostructuration of ionic liquids. Therefore, in this ionic liquid family, the effect of the symmetry and the dependence of the thermophysical properties along the alkyl chain length were explored.

Paper IV is focused in the study of the cation symmetry effect on the volatility of ionic liquids. In this work, the first data of vapor pressures at several temperatures of the ionic liquids, $[C_{N/2}C_{N/2}im][NTf_2]$ (N = 4, 6, 8, 10, 12) series, using the Knudsen/Quartz crystal effusion technique (KEQCM I), was reported. The thermodynamic properties of vaporization derived from the vapor pressures, where compared with those of the $[C_{N-1}C_1im][NTf_2]$ series (Paper II). It was found that the volatility of $[C_{N/2}C_{N/2}im][NTf_2]$ is significantly higher than the asymmetric series, with the same total number of carbons in the alkyl side chains, *N*. The symmetric ionic liquids show lower entropies of vaporization when compared with the asymmetric

series, indicating an increase of the absolute liquid entropy in the symmetric cation ionic liquid series. Additionally, the obtained vaporization results of the $[C_{N/2}C_{N/2}im][NTf_2]$ ionic liquids, shows an enthalpic and entropic differentiation with a clearly discernible odd−even effect, with higher enthalpies and entropies of vaporization for the odd numbered $[C_3C_3im][NTf_2]$ and $[C_5C_5im][NTf_2]$.

The heat capacities at T = 298.15 K of $[C_{N/2}C_{N/2}im][NTf_2]$, were measured, for the first time, using a high-precision heat capacity drop calorimeter (Paper I), with an uncertainty of less than 0.15 % (**Paper V**). Based in the obtained results, it was possible to evaluate the effect of the cation symmetry on the heat capacity data through a comparative analysis with the $[C_{N-1}C_1im][NTf_2]$ ionic liquid series (Paper III). The molar heat capacities of the $[C_{N/2}C_{N/2}im][NTf_2]$ ionic liquids series present a less pronounced deviation from the linearity along the alkyl chain length than the asymmetric based ionic liquids series. Lower molar heat capacities for the symmetric than the asymmetric series were observed, being this difference more evidenced for the specific and volumic heat capacities. As observed previously for the $[C_{N-1}C_1im][NTf_2]$ series, a trend shift in the heat capacities at $[C_6C_6im][NTf_2]$ was found. Based on the obtained results, a clear indication that for the symmetric series, $[C_{N/2}C_{N/2}im][NTf_2]$, the starting of the liquid phase nanostructuration / alkyl chain segregation occurs around $[C_6C_6im][NTf_2]$, was found.

The vapor pressures as a function of temperatures of the short alkyl chain length, 1,3-dimethylimidazolium bis(trifluoromethylsulfonyl)imide, ($[C_1C_1im][NTf_2]$) and 1-ethyl-3-propylimidazolium bis(trifluoromethylsulfonyl)imide, ($[C_2C_3im][NTf_2]$) ionic liquids are presented in **Paper VI**. Based on the previous results, the thermodynamic properties of vaporization were derived. The thermodynamic properties of vaporization of the ionic liquids with short alkyl chains are reported, discussed and evaluated considering the effect of the cation's symmetry and alkyl side chain length. $[C_1C_1im][NTf_2]$ presents a higher enthalpy and entropy of vaporization than the neighboring members of the series. The enthalpy of vaporization of $[C_2C_3im][NTf_2]$ lies in between the asymmetric and symmetric ionic liquid series, reflecting a decrease in the electrostatic interactions due to a decrease of the charge accessibility between the ionic pairs when the methyl group is replaced by an ethyl group. The obtained higher volatility of $[C_2C_3im][NTf_2]$ arises from its asymmetric character, leading to a higher entropic contribution that compensates the enthalpic penalty.

The densities and viscosities as a function of temperature, and Small-Wide Angle X-ray Scattering (SWAXS) patterns at ambient conditions were determined and analyzed for asymmetric ($[C_{N-1}C_1im][NTf_2]$) and symmetric ($[C_{N/2}C_{N/2}im][NTf_2]$) ionic liquid series (**Paper VII**). The experimental results were used to evaluate the impact of the cation symmetry on the nanostructuration of ionic liquids. A lower viscosity for the symmetric ionic liquids than the asymmetric ionic liquid family was found. The analysis of the viscosity data along the alkyl side chain length shows a trend shift that occurs at $[C_6C_1im][NTf_2]$ for the asymmetric and at $[C_6C_6im][NTf_2]$ for the symmetric series, which is related with structural modifications in the liquid. These results have been supported by SWAXS measurements at ambient conditions. Data indicates that both asymmetric and symmetric members are characterized by the occurrence of a distinct degree of mesoscopic structural organization above a given threshold in the side alkyl chain length, regardless the cation symmetry. This threshold could be related to the development of well-established clusters stemming from the segregation of long enough alkyl tails.

The vapor pressures at several temperatures and the derived thermodynamic properties of vaporization for $[C_{N/2}C_{N/2}im][NTf_2]$ ionic liquid series with long alkyl chain length (N = 14, 16, 18, 20), are presented in **Paper VIII**. The analysis and rationalization of the results was done considering the thermodynamic properties of vaporization of the symmetric ionic liquids with short alkyl side chains recently published in the literature, $[C_{N/2}C_{N/2}im][NTf_2]$ (Paper IV, VI), in order to evaluate the effect of the alkyl side chains of the cation and to get more insights about the so-called nanostructuration / segregation of ionic liquids. The effect symmetry of the long alkyl side chain cations was investigated based on the comparison with the asymmetric imidazolium based ionic liquids, $[C_{N-1}C_1im][NTf_2]$ (Paper II). In the enthalpies and entropies of vaporization a shift on the trend of the odd-even effect along the symmetric ionic liquids, was found. Starting from $[C_6C_6im][NTf_2]$ an amplification of the odd-even effect is observed, with higher enthalpies and entropies of vaporization for the odd numbered ionic liquids, $[C_7C_7im][NTf_2]$ and $[C_9C_9im][NTf_2]$. This effect is related with the predominant orientation of the terminal methyl group of the alkyl chain to the imidazolium ring and their influence in the cation-anion interaction. In the previous work, were we report the volatility study for the asymmetric ionic liquids, $[C_{N-1}C_1im][NTf_2]$ (Paper II), a shift in the enthalpies and entropies of vaporization profiles along the alkyl side chain length was reported, which is related to a change in the molecular structure organization of the liquid phase, around $[C_6C_1im][NTf_2]$. The symmetry of the ionic

liquid cation, changes considerably the thermophysical properties, as it was already shown in the work presented in Papers IV - VII. The present results are well supported by the previous studies, where the heat capacities, viscosities, densities and SWAX (Paper V and VII) in the extended series of $[C_{N/2}C_{N/2}im][NTf_2]$ ionic liquids were studied and two regions, with a shift around $[C_6C_6im][NTf_2]$ were detected.
Based on these works (Papers II - VIII), it was found a clear indication that for imidazolium bis(trifluoromethylsulfonyl)imide ionic liquids, the limit for the beginning of the nanostructuration / alky chain segregation is around C_6.

$[C_{N-1}C_1im][PF_6]$ Ionic Liquids

Papers IX and X explores the effect of the chemical nature of the anion, sphericity, and size, as well as the overall impact of the nanostructuration on the thermophysical properties of $[C_{N-1}C_1im][PF_6]$ series.
The densities, viscosities, and refractive indices as a function of temperature, were determined and analyzed for $[C_{N-1}C_1im][PF_6]$ ionic liquid series (**Paper IX**). The refractive index and viscosity show a trend shift along the series around the $[C_7C_1im][PF_6]$ that could be associated to the impact of the change in the nanostructuration of the ionic liquids. The sphericity of the $[PF_6]^-$ anion is reflected in the lower pre-exponential VTF parameter, A_η , and the higher viscosity of the $[C_{N-1}C_1im][PF_6]$, when compared with the $[C_{N-1}C_1im][NTf_2]$ series (Paper VII), was found to be ruled by the higher shear energy barriers, which are related with stronger electrostatic interaction due to the low charge dispersion of the $[PF_6]^-$.anion. The effect of the increase of the alkyl side chain on the interaction between the cation and anion is more pronounced in the ionic liquids with shorter alkyl side chain due to the high impact of the alkyl chain steric hindrance in the cation - anion electrostatic interaction, in agreement with findings in the previous works (Papers II, VI and VII). The results obtained in the this work clear indicates that for the $[C_{N-1}C_1im][PF_6]$ series, the liquid phase nanostructuration / alkyl chain segregation starts around $[C_7C_1im][PF_6]$.

In **Paper X**, the study was extended for the measurement of the heat capacities at 298.15 K using a drop heat capacity calorimeter (Paper I). At 298.15 K, the molar heat capacities for the $[C_{N-1}C_1im][NTf_2]$ ionic liquids (Paper III) are (159 $J\cdot K^{-1}\cdot mol^{-1}$) higher than the obtained for the $[C_{N-1}C_1im][PF_6]$ series, which reflects the higher large molar heat capacity contribution of the bis(trifluoromethylsulfonyl)imide anion in comparison to the hexafluorophosphate anion, which is obviously related with the significant higher number of atoms of the bis(trifluoromethylsulfonyl)imide

anion and also related to their higher configurational contribution. The $[C_{N-1}C_1im][PF_6]$ series presents higher specific and volumic heat capacities than the $[NTf_2]^-$ based ionic liquids. In addition, unlike to the trend shift found around $[C_6C_1im][NTf_2]$ for $[C_{N-1}C_1im][NTf_2]$ series (Paper III), a subtle odd-even effect for the specific heat capacities, was found for the $[C_{N-1}C_1im][PF_6]$, where the even numbered ILs presents higher c_p^o. The higher specific / volumic heat capacities shown for the $[C_6C_1im][PF_6]$ and $[C_8C_1im][PF_6]$ indicates higher entropies in the liquid phase, that could be related with their low alkyl chain interdigitation capability for these two ILs, and consequently a less efficient rearrangement in the liquid. The $[C_4C_1im][PF_6]$ shows a different behavior than the trend of the homologous series, presenting a higher volumic heat capacities, in agreement with recent works reported in the literature for the short members of the bistriflamide ILs series (Papers II, V, IX). A support for the trend change observed for the $[C_4C_1im][PF_6]$ would be given if the data for the heat capacity of the other short members of the series $[C_2C_1im][PF_6]$ and $[C_3C_1im][PF_6]$ (that are solids at 298.15 K), were available.

Pyridinium Based Ionic Liquids

Papers XI - XIII explores the effect of the cation, size and structure on the thermophysical properties for the $[C_NPy][NTf_2]$ and $[^1C_2{}^2C_NPy][NTf_2]$ ionic liquid series. The obtained results were evaluated based on a comparative analysis with the $[C_{N-1}C_1im][NTf_2]$ ionic liquid series, where it is evaluated the increase from a five membered cation (imidazolium) to a six membered ring (pyridinium), and additionally, to obtain more insights of the nanostructuration of ionic liquids, based on the dependence of the thermophysical properties along the alkyl chain length for the $[^1C_2{}^2C_NPy][NTf_2]$ ionic liquids.

Paper XI presents the volatility study of the $[C_2Py][NTf_2]$, $[C_3Py][NTf_2]$, and $[C_4Py][NTf_2]$ ionic liquids. The analysis and the rationalization of the thermodynamic properties of vaporization of the studied alkylpyridinium based ionic liquids was done taking into account the literature data for the $[C_{N-1}C_1im][NTf_2]$ (N = 3, 4, 5) ionic liquids (Paper II). At the measurement temperature interval, $[C_2Py][NTf_2]$ and $[C_3Py][NTf_2]$ are exceptions within the considered ionic liquids, presenting lower volatility than $[C_4Py][NTf_2]$. The volatility differentiation is not very significant for the shorter alkyl chain members of at T = 298.15 K. It was found that the lower volatility of the pyridinium (five times lower than the imidazolium based ionic liquids) is enthalpically driven. The entropic profile is very identical than the observed in the imidazolium base ionic liquids.

Paper XII presents the synthesis and the volatility study of the new $[^2C_{N-2}{}^1C_2Py][NTf_2]$, (N = 4 − 10) ionic liquid series. The 1-ethyl-2-alkylpyridinium bis(trifluoromethylsulfonyl)imide ionic liquid family were synthesized, characterized and purified by a researcher at the Faculty of Chemistry of the University of Vigo. The vapor pressure measurements of the studied ionic liquid series were carried out using the Knudsen/Quartz crystal effusion technique (KEQCM II). The analysis and rationalization of the obtained thermodynamic properties of vaporization for the $[^2C_{N-2}{}^1C_2Py][NTf_2]$ ionic liquids by comparative analysis of the data for the $[C_{N-1}C_1im][NTf_2]$ (Papers II and VI) and $[C_NPy][NTf_2]$ (Paper XI), in order to get more insights on the effect of the topology and nature of the cation on the thermophysical properties of ionic liquids. From the analysis of the enthalpic and entropic contribution to the volatility, it was found that the lower volatility of the $[^2C_{N-2}{}^1C_2Py][NTf_2]$ with shorter alkyl side chain results from their highest enthalpies of vaporization however, starting form $[^2C_3{}^1C_2Py][NTf_2]$ the low volatility is ruled and a consequence of the lower entropies of vaporization.

The thermophysical properties of $[^2C_{N-2}{}^1C_2Py][NTf_2]$, (N = 4 − 10) such as the density and viscosity, their dependency with temperature, and heat capacities at a constant temperature, are presented in **Paper XIII**. The effect of the cation, size and structure was evaluated based on a comparative analysis with the $[C_{N-1}C_1im][NTf_2]$ ionic liquid series (Papers III, VII). The pyridinium based ionic liquids exhibits higher densities than the imidazolium ionic liquids, which is related with a denser packing in the liquid phase for the pyridinium ionic liquids. The $[^2C_{N-2}{}^1C_2Py][NTf_2]$ ionic liquid family presents higher viscosities than the $[C_{N-1}C_1im][NTf_2]$ ionic liquids series, where a shift trend in the viscosities starting from $[^2C_5{}^1C_2Py][NTf_2]$ was found. From $[^2C_3{}^1C_2Py][NTf_2]$ to $[^2C_5{}^1C_2Py][NTf_2]$, the viscosity does not show a significant dependency with the increasing of the alkyl side length, which could be related with the balance between the decrease in the electrostatic interactions between the cation and anion, and the increasing in the non-electrostatic interactions arising from the increase of the alkyl side length. The detected trend shift was related with the structural organization of the liquid above a Critical Alkyl Length Size, CALS, previously reported in the literature around $[C_6C_1im][NTf_2]$ (Papers II, III, V, VII, VIII and IX), for the imidazolium ionic liquids series.

Paper I

"Reassembling and testing of a high-precision heat capacity drop calorimeter. Heat capacity of some polyphenyls at *T* = 298.15 K"

Luís M. N. B. F. Santos, Marisa A. A. Rocha, Ana S.M.C. Rodrigues, Vojtěch Štejfa, Michal Fulem Margarida Bastos

The Journal of Chemical Thermodynamics (2012), 43, 1818–1823.
doi: 10.1016/j.jct.2011.06.010

Note: The author of this thesis contribute to the reassembling, testing, heat capacity measurements, data analysis and contribute to the discussion and conclusions

J. Chem. Thermodynamics 43 (2011) 1818–1823

Contents lists available at ScienceDirect

J. Chem. Thermodynamics

journal homepage: www.elsevier.com/locate/jct

Reassembling and testing of a high-precision heat capacity drop calorimeter. Heat capacity of some polyphenyls at $T = 298.15$ K

Luís M.N.B.F. Santos [a,*], Marisa A.A. Rocha [a], Ana S.M.C. Rodrigues [a], Vojtěch Štejfa [b], Michal Fulem [b], Margarida Bastos [a]

[a] Centro de Investigação em Química, Departamento de Química e Bioquímica, Faculdade de Ciências, Universidade do Porto, Rua do Campo Alegre, 687, 4169-007 Porto, Portugal
[b] Department of Physical Chemistry, Institute of Chemical Technology, Technická 5, CZ-166 28 Prague 6, Czech Republic

ARTICLE INFO

Article history:
Received 9 June 2011
Received in revised form 15 June 2011
Accepted 16 June 2011
Available online 23 June 2011

Keywords:
Heat capacity
Calibration
Accuracy
Drop method
Polyphenyls
Calorimetry: isomerisation effect

ABSTRACT

The description of the reassembling and testing of a twin heat conduction, high-precision, drop microcalorimeter for the measurement of heat capacities of small samples are presented. The apparatus, originally developed and used at the Thermochemistry Laboratory, Lund, Sweden, has now been reassembled and modernized, with changes being made as regarding temperature sensors, electronics and data acquisition system. The apparatus was thereafter thoroughly tested, using benzoic acid and hexafluorobenzene as test substances. The accuracy of the $C^{\circ}_{p,m}$ (298.15 K) data obtained with this apparatus is comparable to that achieved by high-precision adiabatic calorimetry. Here we also present the results of heat capacity measurements on of some polyphenyls (1,2,3-triphenylbenzene, 1,3,5-triphenylbenzene, *p*-terphenyl, *m*-terphenyl, *o*-terphenyl, *p*-quaterphenyl) at $T = 298.15$ K, measured with the renewed high precision heat capacity drop calorimeter system. The high resolution and accuracy of the obtained heat capacity data enabled differentiation among the *ortho*-, *meta*-, and *para*-phenyl isomers.

1. Introduction

Drop calorimeters have been used for heat capacity measurements as well as for studies of enthalpies of phase transitions [1–4]. The applicable temperature range depends on the type of heat flow sensors. For high temperature calorimeters reaching 1300 K, platinum–platinum/rhodium thermocouples in series are frequently used, whereas for temperatures under 420 K, high sensitive heat flow plates (usually semiconductor Peltier plates) are used. Drop calorimeters of the heat conduction type take the advantage of the improved sensitivity arising from the isothermal working mode of the heat flow sensors. The twin design has proven to be suitable for very long reaction periods as the surroundings disturbances will be significantly reduced and in some cases even cancelled. These characteristics (sensitivity and long term stability) are very important when the calorimeters are used in solution chemistry, in particular for applications in biology and pharmaceutical industry [5–7].

This work presents the reassembling, improvement and testing of a twin high-precision drop calorimeter for the precise measurement of heat capacities that was previously designed in Wadsö's group in Lund, Sweden, and described in the literature in an initial version [1] and some years later as an improved version of the same apparatus where some modifications concerning instrumentation and working methodology are presented, in order to allow measurements on dilute solutions [2]. The apparatus was now reassembled and modernized with significant changes at the level of electronics, data acquisition and data treatment, as well as by creating a user-friendly environment. The design and hardware of the twin heat flux detectors were kept as in the originally apparatus [2], except for the optocoupler voltage pre-amplifier that was originally installed in the calorimeter block which was deactivated.

The apparatus was tested and used to determine the heat capacities at $T = 298.15$ K of the following polyphenyls: 1,2,3-triphenylbenzene: 123tPhB; 1,3,5-triphenylbenzene: 135tPhB; *p*-terphenyl: *p*-tPh; *m*-terphenyl: *m*-tPh; *o*-terphenyl: *o*-tPh; *p*-quaterphenyl: *p*-quatPh. The aim of this study was to evaluate the performance of the apparatus in the measurement of the heat capacity of this type of compounds as well as to evaluate whether it is possible to discriminate between the heat capacity of the phenyl isomers (*ortho*-, *meta*-, *para*-) in the solid phase. The use and test of the apparatus with this series of compounds is part of an extended research project concerning structural and thermodynamic study of polyphenyls and their derivatives [8–10].

2. Apparatus and experimental procedure

In figure 1, a schematic diagram of the apparatus in the current configuration is presented. The apparatus comprises two main

* Corresponding author. Tel.: +351 220402536; fax: +351 220402520.
E-mail address: lbsantos@fc.up.pt (L.M.N.B.F. Santos).

0021-9614/$ - see front matter © 2011 Elsevier Ltd. All rights reserved.
doi:10.1016/j.jct.2011.06.010

parts: the furnace and the calorimetric receiving block. The receiving calorimeter is a twin heat conduction calorimeter, of the type used in Lund's instruments [11].

The ampoules (shown schematically in figure 2) are weighted in a precision analytical balance (with a readability of 0.00001 g) both empty and after filling with the liquid or solid sample and closed tightly by means of the existing o-ring. Thereafter the ampoule is inserted in the furnace. The ampoules are maintained in the furnace in the well defined positions by means of a magnet connect to the drop and lift mechanism system. The ampoule is first maintained in the furnace for temperature equilibration at a well defined temperature, and after a pre-defined time, it is dropped into the receiving calorimetric block, also kept at a well defined temperature (a more detailed description concerning the drop and lift mechanism was presented previously in the literature [2]). After the end of the period of the calorimetric measurement, the ampoules are transferred back to the furnace by the same magnetic lift. The drop experiment is automatically repeated using the same ampoule and the same pre-defined time intervals.

In the experiments reported here, the furnace temperature was 303.15 K and the receiving calorimeter was kept at 293.15 K. The twin calorimeter thus measures the heat exchange resulting from the ampoule cooling from the initial temperature (T_i = 303.15 K) to the final temperature (T_f = 293.15 K).

This heat exchange is recorded as the change in voltage signal across the thermopiles (U) as a function of time, and thus the relevant quantity to be considered is the integrated heat flow normalized to the temperature difference between the furnace and receiving calorimeter, *i.e.*, the integrated area divided by ($T_i - T_f$), according to equation (1)

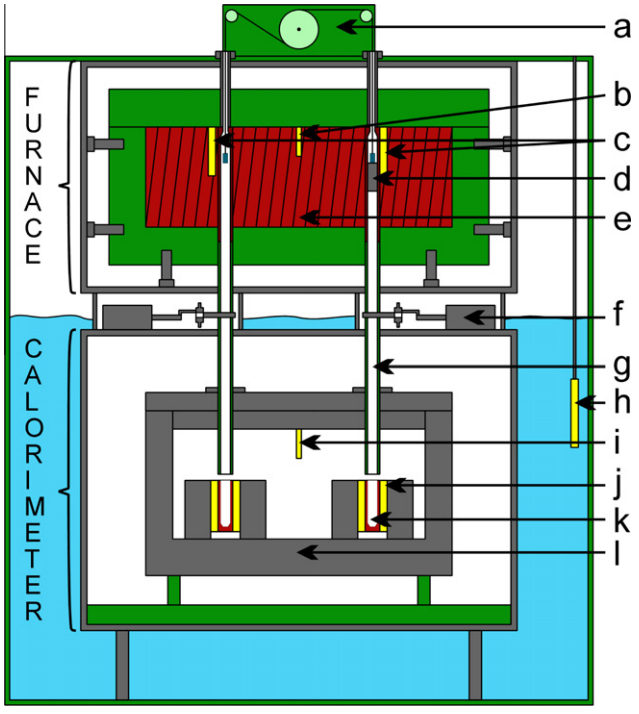

FIGURE 1. Drop calorimeter apparatus. Materials: (■): water; (■): PVC; (■): metal; (■): copper; (■): measuring elements; a: automatic lift; b: thermistor for temperature control; c: Pt100, temperature sensors; d: magnet holding ampoule; e: copper block (T_i) with manganin heater wound; f: electromechanical shutter; g: tube for the ampoule (top copper, bottom plastic); h: thermistor; i: Pt100, temperature sensor located in wall of block; j: Peltier plates; k: ampoule receiver; l: aluminum calorimeter block (T_f). Adapted and modified from Suurkuusk and Wadsö [2].

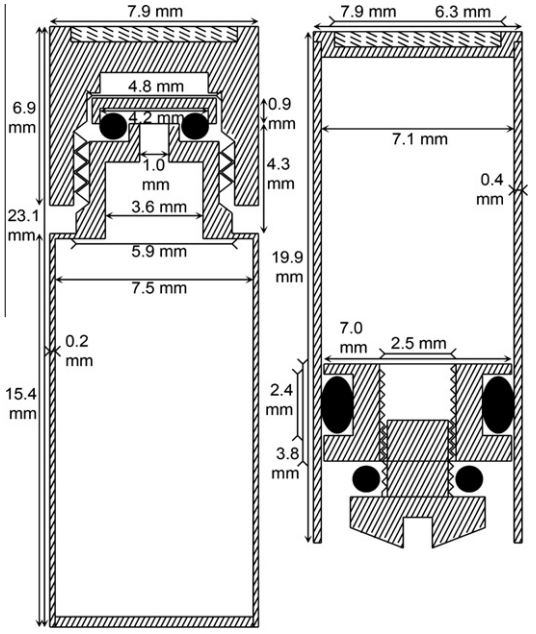

FIGURE 2. Detailed view of the ampoules used for drop calorimetry: liquid (left) and solid (right) ampoule ≋: soft iron plate; ⬬: o-rings. Adapted and modified from Suurkuusk and Wadsö [2].

$$A = \frac{\int U\,dt}{(T_i - T_f)}. \tag{1}$$

The integral is calculated by the new data treatment program developed for this application, described below in Section 2.2 and expressed in V · s.

The calibration constant, ε, is temperature dependent and must be known for each temperature interval. It was previously proven that the calibration constant is independent of sample mass and the compounds thermal conductivity [2]. Calibration constants can be obtained by two different approaches: (i) electrical calibration, where heat pulses are provided to the sample side through heaters (in this apparatus two 25 Ω manganin calibrations heaters coupled in series are located in each side of the receiver calorimeter as described previously [2]); (ii) chemical calibration, from a drop experiment in the conditions to be used in the experiments using samples of accurately known heat capacity. It was found that in this type of calorimeters it is preferable and more accurate to derive the calibration constant from chemical calibration [2], as electrical calibration does not take into account or is not able to reproduce several factors like: the air movements arising from dropping the ampoule, heat leakages in the heat flow cell, thermal conductivity from the cell to the calorimetric block, thermal gradients along the drop experiment, etc. The chemical calibration method is thus to be preferred because it cancels systematic errors inherent to the drop methodology, including the error associated with the measurement of the temperature drop interval and small deviations from the temperature considered as reference. The calibration constant is calculated from equation (2)

$$\varepsilon = \frac{C^{\circ}_{p,m} \cdot m_{sample}}{(A_{amp+sample} - A_{amp}) \cdot M}, \tag{2}$$

where $C^{\circ}_{p,m}$ is the available heat capacity of the reference material used in the calibration experiment, m_{sample} is the mass of sample, and A_{amp} and $A_{amp+sample}$, are the normalized integrated areas of the empty ampoule (blank) and of the ampoule with compound,

respectively, and M the molar mass of the sample (reference material – primary). It should be stressed that it is very important to fill the whole volume of ampoule with the sample, especially in case of more volatile compounds, otherwise, vaporization or sublimation will take place into the air gap and will affect the results. Solid compounds are easy to compress in the ampoule with wide orifice (solid ampoule) while the liquid ampoule has a narrow orifice, which can be filled without leaving any empty space.

Considering the heat content of the ampoule both empty and filled with sample, the calibration constant previously determined as describe above, and the integrated areas of the empty and filled ampoules, the heat capacity of the compound can be calculated by equation (3):

$$C^{\circ}_{p,m} = \frac{\varepsilon \cdot (A_{amp+sample} - A_{amp}) \cdot M}{m_{sample}}, \quad (3)$$

where M and m_{sample} are the molar mass and mass of the sample in the ampoule, respectively, ε is the determined calibration constant and A_{amp} and $A_{amp+sample}$, are the normalized integrated areas of the empty ampoule (blank) and of the ampoule with compound, respectively. The obtained $C^{\circ}_{p,m}$ values are thus expressed as $J \cdot K^{-1} \cdot mol^{-1}$.

2.1. Temperature measurement and control

Accurate temperature measurement and control are crucial for the overall quality and precision of the results obtained with this apparatus. The furnace is maintained at constant temperature (T_i = 303.17 ± 0.01 K) and the calorimetric block at (T_f = 293.15 ± 0.01) K, using two EUROTHERM PID process controllers modified to allow the temperature measurements based on a 2000 Ω (at 298.15 K) thermistor. The temperature of the furnace is measured by a platinum resistance thermometer Pt100 (class 1/10), which is located near the ampoule channel. The temperature of the block is also measured by a platinum resistance thermometer Pt100 (class 1/10), positioned symmetrically in one of the walls of the calorimetric block (as depicted in figure 1). The two Pt100 sensors were calibrated against a calibrated platinum resistance thermometer, PTR100 (Fluke – Hart Scientific, Model 5626), traceable to the National Institute of Standards and Technology (NIST) based on the ITS-90 temperature scale, with an uncertainty smaller than 0.002 K. The temperatures is typically controlled to within $\pm(3 \cdot 10^{-3})$ K and measured with a resolution better than $1 \cdot 10^{-3}$ K.

2.2. Data acquisition and control

The differential heat flow voltage signal and the temperature measurements are obtained through a data acquisition switch unit multimeter, 6½ digits, Agilent (model 34401A) interfaced to a computer. A switch unit board is used for the control of the drop and lift mechanism system. A virtual instrument software application has been developed in Agilent VEE, v9.0 [12], which is used to: (i) define and program the experimental setup; (ii) perform real time data acquisition and monitoring; (iii) control of the time interval between each drop; (iv) define the number of drop repeats per run. A dedicated and independent data evaluation program was developed for the temperature step evaluation and heat flow sign integration. The details of the tests and validation of the program are described in the supporting information. In order to test the new set-up and associated data acquisition and data treatment programs, the heat capacities were calculated from areas obtained from integrations using both a conventional program, Origin 8 [13], and the program here developed. This program evaluation/comparison allowed us to define optimized, standard time intervals to be used routinely in data acquisition and data treatment programs. Intervals for voltage baseline readings and temperature averaging are identical and taken to be 10 min long. The time required for equilibrium to be achieved after each drop is about 20 min. Therefore, the chosen conditions to be used are 10–20–10 (representing 10 min pre-period, 20 min main period and 10 min after period) and the length of integrating interval is 30 min. A typical drop calorimeter experiment profile and an amplified view of the experimental results provide a qualitative picture of the temperature control and heat flow noise level, and are presented in figures 3 and 4.

As shown in figures 3 and 4, the temperature fluctuation is in the mK range, without a significant long time drift. As it was already observed in the previous setup [2], a small but detectable increase (1 mK) of the calorimetric block temperature is observed after each drop. The temperature signal shows small and fast oscillations associated with the electronic noise. This lead us to adopt an averaging temperature procedure in the data evaluation methodology, as it represents a signal noise filter that in practice

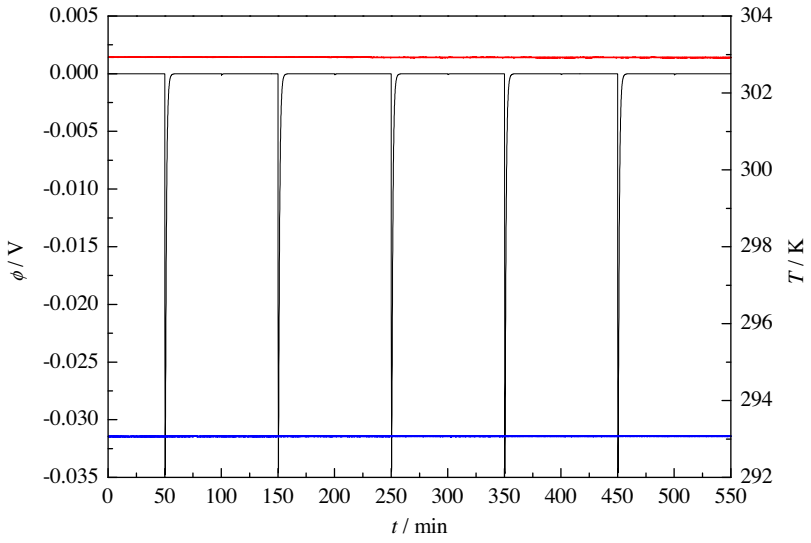

FIGURE 3. Typical experimental run results with five drop experiments, N_{drop} = 5: (—): furnace temperature; (—): heat flow; (—): calorimeter temperature.

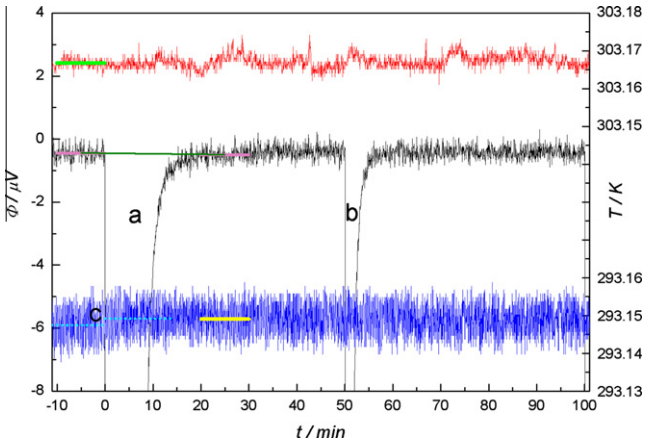

FIGURE 4. Detailed view on data gathered during one drop calorimetry experiment. (—) furnace temperature; (—) average temperature T_i; (—) heat flow; (—) heat flow baseline; (—) calorimeter temperature; (—) average temperature T_f; (—) average temperatures before and after drop; a: drop peak; b: withdraw peak (area of withdraw peak is approximately 0.2% of drop peak); c: drop causes detectable raising of temperature.

turns out to increase the temperature resolution. The noise level of the heat flow is of the order of ±1 μV. The time constant of the calorimeter proper (empty calorimetric block) was found by electrical calibration to be $\tau = (50 \pm 1)$ s. In figure 4 the withdraw peak, indicated as **b**, corresponds to the heat power effect caused by the lift finger when it touch the ampoule during the withdraw process (area of withdraw peak is typically 0.2% of drop peak).

2.3. Calibration and test

The ampoules (figure 2) used in the measurements have already been described in the original description of the apparatus [2]. In the present work, the apparatus was used in single-drop mode (drop experiment without simultaneously drop of a reference ampoule), since it was previously demonstrated that the use of the double-drop method (drop experiment with simultaneously drop of a reference ampoule) does not improve the quality of the obtained heat capacity data [2]. In order to measure the energetic effect associated with the heat capacity of the empty ampoules and heat flow associated with the transfer of the ampoules from the furnace to the receiving calorimeter, experiments are performed with the empty ampoules (blanks) as part of the apparatus calibration and the sample measurement. In these experiments, the empty ampoule is dropped into sample cell of the receiving calorimeter at the same experimental conditions as the ones to be used in the calibration and sample experiments. Table 1 presents the experimental results for the drop experiments obtained with different empty ampoules, coded with "S" for solids and with "L" liquid type ampoules.

The drop calorimeter was calibrated using recommended primary standards, as well as test substances [14]. The calibration of the calorimeter when using the solid ampoules was performed with sapphire (α-aluminum oxide, NBS standard sample, SRM 720) using the heat capacity value $C^{\circ}_{p,m}(\text{sapphire}) = (79.03 \pm 0.08)\ \text{J} \cdot \text{K}^{-1} \cdot \text{mol}^{-1}$ [14]. For cases where the liquid ampoules were used, the calorimeter was calibrated with Millipore water, using the $C^{\circ}_{p,m}(\textit{water}) = (75.32 \pm 0.01)\ \text{J} \cdot \text{K}^{-1} \cdot \text{mol}^{-1}$ [14]. The calibration constant of the drop calorimeter was found to be ε(sapphire) = (6.6329 ± 0.0046) W · V^{-1} and ε(water) = (6.6316 ± 0.0032) - W · V^{-1}, respectively. Table 2 presents the results of the calibration experiments using sapphire and water as calibration standards at $T = 298.15$ K, using a 10 K temperature interval.

TABLE 1
Experimental results obtained in experimental runs, with empty ampoules. (S – solid; L – liquid type ampoules).

Code	m_{amp}/g	N_{drop}	$T_{furnace}$/K	$T_{calorimeter}$/K	A_{amp}/V · s · K^{-1}
1S	2.94269	13	303.160	293.146	0.21439 ± 0.0005
2S	2.76588	13	303.173	293.153	0.20156 ± 0.0010
3S	2.92606	9	303.166	293.149	0.21348 ± 0.0005
4L	3.72258	11	303.160	293.152	0.26064 ± 0.0007
5L	4.52679	12	303.163	293.149	0.31987 ± 0.0016

N_{drop} = number of drop experiments; Code = ampoule code; the uncertainty reported is twice the standard deviation of the mean.

TABLE 2
Results of calibration experiments at $T = 298.15$ K using sapphire and water as calibration standards.

Code	m_{sample}/g	N_{drop}	$T_{furnace}$/K	$T_{calorimeter}$/K	ε/W · V^{-1}
		Sapphire (α-Al_2O_3, NIST-RM 720)			
1S	1.16000	5	303.144	293.152	6.6321 ± 0.0071
1S	1.28036	15	303.186	293.147	6.6470 ± 0.0073
2S	1.08045	7	303.158	293.154	6.6150 ± 0.0128
3S	1.03358	13	303.176	293.151	6.6373 ± 0.0081
				Average	6.6329 ± 0.0046
		Water			
4L	0.58454	5	303.169	293.170	6.6283 ± 0.0063
4L	0.58406	18	303.164	293.159	6.6372 ± 0.0022
5L	0.49126	6	303.164	293.164	6.6294 ± 0.0069
				Average	6.6316 ± 0.0032

N_{drop} = number of drop experiments; $T_{furnace}$ = average temperature of the furnace; $T_{calorimeter}$ = average temperature of the calorimeter; the uncertainty reported is twice the standard deviation of the mean.

The calibration constants obtained in the set of experiments with solid type ampoules and with liquid type ampoules are in excellent agreement within their uncertainty intervals, showing that, as stated above, the calibration constant is independent of sample mass, thermal conductivity of the compound, and the type of ampoule used. The overall uncertainty obtained is also quite similar, but will obviously be dependent on the heat power ratio between the blank and blank + sample.

The calorimeter was tested with benzoic acid, a primary reference material (NIST Standard Reference Material 39j), and was used after previous drying under reduced pressure (at 300 K; $p < 10$ Pa; 24 h), and hexafluorobenzene, a secondary reference material (Aldrich, mass fraction purity 0.998), that was used without further purification. Tables 3 and 4 contain the molar heat capacity values obtained, at $T = 298.15$ K, for benzoic acid and hexafluorobenzene obtained using in each case two independent experimental runs, each consisting of N_{drops} as indicated in the tables.

3. Heat capacities of some polyphenyls

Heat capacities of some polyphenyls at $T = 298.15$ K were obtained using the improved drop heat capacity calorimeter.

TABLE 3
Molar heat capacities values at $T = 298.15$ K for benzoic acid, obtained using two different solid ampoules. The calibration constant used to calculate the C_p values was the one derived from the sapphire calibration, (6.6329 ± 0.0046 W · V^{-1}).

Code	m_{sample}/g	N_{drop}	$T_{furnace}$/K	$T_{calorimeter}$/K	$C^{\circ}_{p,m}$/(J · K^{-1} · mol^{-1})
1S	0.49558	8	303.169	293.150	145.93 ± 0.31
2S	0.47335	9	303.169	293.151	146.18 ± 0.35
				Average	146.06 ± 0.33

N_{drop} = number of drop experiments; $T_{furnace}$ = average temperature of the furnace; $T_{calorimeter}$ = average temperature of the calorimeter; the uncertainty reported is twice the standard deviation of the mean.

TABLE 4
Molar heat capacities values at $T = 298.15$ K for hexafluorobenzene, obtained using two independent experimental runs and the same liquid ampoule. The calibration constant used to calculate the C_p values was the one derived from the water calibration, $(6.6316 \pm 0.0032\ W \cdot V^{-1})$.

Code	m_{sample}/g	N_{drop}	$T_{furnace}$/K	$T_{calorimeter}$/K	$C^{\circ}_{p,m}/(J \cdot K^{-1} \cdot mol^{-1})$
4L	0.92600	10	303.159	293.157	221.21 ± 0.23
4L	0.92666	15	303.170	293.146	221.63 ± 0.19
				Average	221.42 ± 0.21

N_{drop} = number of drop experiments; $T_{furnace}$ = average temperature of the furnace; $T_{calorimeter}$ = average temperature of the calorimeter; the uncertainty reported is twice the standard deviation of the mean.

1,2,3-Triphenylbenzene (CAS Number 1165-14-6), 1,3,5-triphenylbenzene (CAS No. 612-71-5), *o*-terphenyl (CAS No. 84-15-1), *m*-terphenyl (CAS No. 92-06-8), *p*-terphenyl (CAS No. 92-94-4), and *p*-quaterphenyl (CAS No. 135-70-6) were commercially acquired from Sigma–Aldrich. All studied compounds were purified by sublimation under reduced pressure (<10 Pa). The purity was checked by gas chromatography, using an HP 4890 apparatus equipped with an HP-5 column, cross-linked, 5% diphenyl and 95% dimethylpolysiloxane. All compounds showed a mass fraction purity greater than 0.999 after sublimation. The relative atomic masses used were those recommended by the IUPAC Commission in 2007 [15]. For the calculation of the heat capacities the calibration constant derived from the sapphire calibration, $(6.6329 \pm 0.0046\ W \cdot V^{-1})$ was used. Table 5 presents the obtained molar heat capacity and specific heat capacity values for the studied polyphenyls, at $T = 298.15$ K.

4. Discussion

The quality and performance of the apparatus were evaluated from the results obtained in the heat capacity measurements of benzoic acid and hexafluorobenzene. Table 6 presents the values for the heat capacity of the test substances here obtained together with some selected literature values. The results obtained with the present setup are in excellent agreement with the literature results. The obtained uncertainty interval of the respective heat capacity value was 0.2% for benzoic acid and 0.1% for hexafluorobenzene, reflecting the high sensitivity of the apparatus and being comparable to the one obtained in high precision adiabatic calorimetry. The overall uncertainty is obviously dependent on the sample size used in each independent experimental run, as is apparent in the improved uncertainty obtained for hexafluorobenzene as compared to benzoic acid, due to the higher volumetric heat capacity of the former.

The heat capacities of the polyphenyls studied, at $T = 298.15$ K, together with literature values are presented in table 7. For 123tPhB, no data were found in the literature. The available values for 135tPhB, *o*-tPh, *p*-tPh and *p*-quatPh were obtained by aneroid calorimetry and adiabatic calorimetry [16–20]. The heat capacities of the terphenyl isomers have also been measured using a DSC [21]. The heat capacity data obtained in this work are in excellent agreement with the data obtained by adiabatic calorimetry.

TABLE 5
Values of the molar heat capacity and specific heat capacity at $T = 298.15$ K for the polyphenyls studied. The calibration constant used to calculate the C_p values is the one derived from the sapphire calibration, $(6.6329 \pm 0.0046\ W \cdot V^{-1})$.

Compound	$M/(g \cdot mol^{-1})$	N_{drop}	$C^{\circ}_{p,m}/(J \cdot K^{-1} \cdot mol^{-1})$	$c^{\circ}_{p}/(J \cdot K^{-1} \cdot g^{-1})$
o-tPh	230.3053	9	274.73 ± 0.53	1.1929 ± 0.0023
m-tPh	230.3053	14	277.42 ± 0.32	1.2046 ± 0.0014
p-tPh	230.3053	8	279.58 ± 0.36	1.2140 ± 0.0016
123tPhB	306.4018	20	356.20 ± 0.80	1.1625 ± 0.0026
135tPhB	306.4018	24	357.96 ± 0.53	1.1683 ± 0.0017
p-quatPh	306.4018	7	363.45 ± 0.75	1.1862 ± 0.0024

N_{drop} = number of drop experiments; For 123tPhB, 135tPhB and *m*-tPh, the number of drops are the sum of the drops that were obtained in two independent experimental.

TABLE 6
Standard molar heat capacity values at $T = 298.15$ K, for benzoic acid and hexafluorobenzene, along with selected literature data, expressed in $(J \cdot K^{-1} \cdot mol^{-1})$.

Compound	This work	Selected literature data
Benzoic acid	146.06 ± 0.33	146.81 ± 0.30 [23] 146.79 ± 0.15 [24]
Hexafluorobenzene	221.42 ± 0.21	221.58 ± 0.44 [25] 221.77 ± 0.44 [26] 221.60 ± 0.40 [27]

TABLE 7
Standard molar heat capacity values at $T = 298.15$ K, for the polyphenyls studied, together with selected literature data, expressed in $(J \cdot K^{-1} \cdot mol^{-1})$.

Compound	This work	Literature data
o-Terphenyl	274.73 ± 0.53	274.75 ± 0.27 (AdC) [19] 276 (DSC) [21]
m-Terphenyl	277.42 ± 0.32	299 (DSC) [21]
p-Terphenyl	279.58 ± 0.36	278.12 (AdC) [17] 278.68 ± 0.06 (AdC) [18] 278 (DSC) [21]
1,2,3-Triphenylbenzene	356.20 ± 0.80	
1,3,5-Triphenylbenzene	357.96 ± 0.53	358.32 ± 2.51 (AnC) [16]
p-Quaterphenyl	363.45 ± 0.75	362.52 (AdC) [20]

AnC – aneroid calorimeter; AdC – adiabatic calorimeter; DSC – differential scanning calorimetry.

The aim of this study was to evaluate the performance of the apparatus for the measurement of heat capacities of these types of compounds as well as to evaluate whether it is possible to experimentally differentiate among the solid phase heat capacity values for the various isomers, as a consequence of the change in phenyl relative position (*ortho*-, *meta*-, *para*-). Figure 5A shows the graphic representation of the obtained molar heat capacities as a function of the number of phenyl groups. The plotted line represents the linear fitting derived from the $C^{\circ}_{p,m}$ data of the *para* derivatives (including the molar heat capacity of biphenyl, $C^{\circ}_{p,m}(\text{biphenyl},298.15\ K) = (198.39 \pm 0.20)\ J \cdot K^{-1} \cdot mol^{-1}$) [22] *versus* the number of phenyl rings that was used as a reference data trend, to analyze the effect of *ortho* and *meta* substitution in the molar heat capacity.

Some subtle deviations are observed for the *ortho* and *meta* polyphenyl isomers as shown in figure 5B and listed in table 5. We suggest that the lower heat capacity experimentally obtained here for the *ortho* and *meta* isomers as compared to the value that can be derived from the previous correlation, could be partially related to, the ring rotation restrictions in the *ortho* isomers and the supramolecular structural differentiation among the isomers.

In conclusion, the results of our calibration experiments, the heat capacities derived for the test compounds as well as the quality of the data obtained for the polyphenyl compounds show that this apparatus can be used to measure heat capacity at $T = 298.15$ K with high precision and accuracy, as the method is capable of detecting subtle heat capacity differences among position isomers. Further, the inherent excellent capabilities of the original apparatus are now updated to a fully automated set-up, designed in a user-friendly environment, with integrated automatic data treatment, providing a reliable means of obtaining high quality heat capacity data at $T = 298.15$ K for solid and liquid samples.

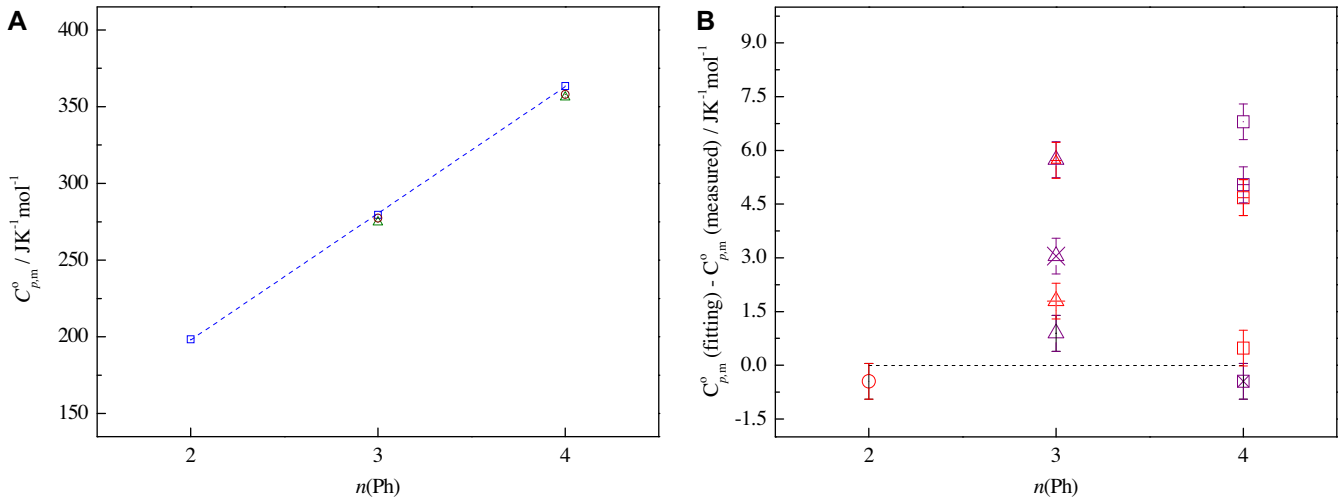

FIGURE 5. Plot of the molar heat capacity as a function of the total number of phenyl groups (A); Deviation of the $C^{\circ}_{p,m}$ (fitting) from the $C^{\circ}_{p,m}$ (measured) as a function of the total number of phenyl groups (B). Plot (A): □ – *p*-polyphenyls; ○ – *m*-polyphenyls; △ – *o*-polyphenyls. Plot (B): ○ – biphenyl [22]; ◬ – *p*-terphenyl (this work); ⧫ – *p*-terphenyl [18]; ⧋ – *o*-terphenyl (this work); ⧊ – *o*-terphenyl [19]; ⧓ – *m*-terphenyl (this work); ⊠ – *p*-quaterphenyl (this work); ◫ – *p*-quaterphenyl [20]; ⊞ – 1,3,5-triphenylbenzene (this work); ⊟ – 1,3,5-triphenylbenzene, [16]; ⊡ – 1,2,3-triphenylbenzene (this work).

Acknowledgements

Thanks are due to Fundação para a Ciência e Tecnologia (FCT), Lisbon, Portugal and to FEDER for financial support to Centro de Investigação em Química, University of Porto. Marisa A.A. Rocha acknowledges the financial support from FCT and the European Social Fund (ESF) under the Community Support Framework (CSF) for the award of a Ph.D. Research Grant with reference: SFRH/BD/60513/2009. Margarida Bastos and Luís M.N.B.F. Santos gratefully acknowledge Prof. Ingemar Wadsö and Dr. Gerd Olofsson, Lund University, Sweden, for the generous offer of the calorimeter.

Appendix A. Supplementary material

Supplementary data associated with this article can be found, in the online version, at doi:10.1016/j.jct.2011.06.010.

References

[1] J. Konicek, J. Suurkuusk, I. Wadsö, Chem. Scr. 1 (1971) 217–220.
[2] J. Suurkuusk, I. Wadsö, J. Chem. Thermodyn. 6 (1974) 667–679.
[3] L.M.N.B.F. Santos, B. Schröder, O.O.P. Fernandes, M.A.V. Ribeiro da Silva, Thermochim. Acta 415 (2004) 15–20.
[4] C.E.S. Bernardes, L.M.N.B.F. Santos, M.E. Minas da Piedade, Meas. Sci. Technol. 17 (2006) 1405–1408.
[5] I. Wadsö, Thermochim. Acta 267 (1995) 45–59.
[6] M. Bastos, N.N. Volkova, I. Wadsö, J. Chem. Soc., Faraday Trans. 89 (1993) 1351–1352.
[7] K. Ng, A. Rosenberg, M. Bastos, I. Wadsö, Thermochim. Acta 169 (1990) 339–346.
[8] J.C.S. Costa, C.F.R.A.C. Lima, M.A.A. Rocha, L.R. Gomes, L.M.N.B.F. Santos, J. Chem. Thermodyn. 43 (2011) 133–139.
[9] M.A.A. Rocha, L.R. Gomes, J.N. Low, L.M.N.B.F. Santos, J. Phys. Chem. A 113 (2009) 11015–11027.
[10] J.C.S. Costa, L.R. Gomes, L.M.N.B.F. Santos, J.N. Low, Acta Cryst. E66 (2010) o916.
[11] J. Suurkuusk, I. Wadsö, Chem. Scr. 20 (1982) 155–163.
[12] Agilent VEE Pro (Agilent Technologies, Inc., Santa Clara, CA).
[13] Origin (OriginLab, Northampton, MA).
[14] R. Sabbah, A. Xu-Wu, J.S. Chickos, M.L. Planas Leitão, M.V. Roux, L.A. Torres, Thermochim. Acta 331 (1999) 93–208.
[15] M.E. Wieser, M. Berglund, Pure Appl. Chem. 81 (2009) 2131–2156.
[16] G.S. Parks, S.S. Todd, W.A. Moore, J. Am. Chem. Soc. 58 (1936) 398–401.
[17] K. Saito, T. Atake, H. Chihara, Bull. Chem. Soc. Jpn. 61 (1988) 2327–2336.
[18] S.-S. Chang, J. Chem. Phys. 79 (1983) 6229–6236.
[19] S.-S. Chang, A.B. Bestul, J. Chem. Phys. 56 (1972) 503–516.
[20] K. Saito, T. Atake, H. Chihara, J. Chem. Thermodyn. 17 (1985) 539–548.
[21] S.P. Verevkin, J. Chem. Thermodyn. 29 (1997) 1495–1501.
[22] R.D. Chirico, S.E. Knipmeyer, A. Nguyen, W.V. Steele, J. Chem. Thermodyn. 21 (1989) 1307–1331.
[23] G.T. Furukawa, R.E. McCoskey, G.J. King, J. Res. Natl. Bur. Stand. 47 (1951) 256–261.
[24] K. Arvidsson, B. Falk, S. Sunner, Chem. Scr. 10 (1976) 193–200.
[25] J.F. Counsell, J.H.S. Green, J.L. Hales, J.F. Martin, Trans. Faraday Soc. 61 (1965) 212–218.
[26] J.F. Messerly, H.L. Finke, J. Chem. Thermodyn. 2 (1970) 867–880.
[27] N.I. Gorbunova, V.A. Grigoriev, V.M. Simonov, V.A. Shipova, J. Thermophys. 3 (1982) 1–15.

Supporting Information

Reassembling and Test of a High-Precision Heat Capacity Drop Calorimeter. Heat Capacities of Some Polyphenyls at 298.15 K

Luís M. N. B. F. Santos[¥,*], *Marisa A. A. Rocha*[¥], *Ana S. M. C. Rodrigues*[¥], *Vojtěch Štejfa*[£], *Michal Fulem*[£], *Margarida Bastos*[¥]

[¥]Centro de Investigação em Química, Departamento de Química e Bioquímica, Faculdade de Ciências, Universidade do Porto, Rua do Campo Alegre, 687, 4169-007 Porto, Portugal

[£] Department of Physical Chemistry, Institute of Chemical Technology, Prague, Technická 5, CZ-166 28 Prague 6, Czech Republic

*Corresponding author. Tel.: +351 220 402 836; Fax: +351 220 402 659

E-mail address: lbsantos@fc.up.pt (Luís M. N. B. F. Santos)

DC- evaluation program

The level of accuracy of the Cp measurements by high precision drop calorimetry is highly dependent on the experimental methodology as well as on the adopted numerical data integration procedure in order to minimize numeric calculation errors and maximise the error cancellation between the calibration, blanks and sample experiments. After several preliminary experiments with this apparatus, optimal conditions were found to be routinely used. The last part of process remaining to be standardized before this work was the data evaluation. Doing manual evaluation of the data was a tedious and very time consuming process, and thus a suitable automatic program was needed. Moreover, the manual peak integration done in Origin (OriginLab, Northampton, MA) and separated temperature average calculating was still very time-consuming.

The optimization and standardization of the measurement procedure enabled easy automatic evaluation with requirement of only minimal human contribution. This program was written in Agilent VEE in two steps. Firstly, a program that evaluates single peak by setting its beginning and end intervals. And secondly a program that automatically integrates all peaks, requiring only the first peak edge and preset lengths of all intervals and time difference between two consecutive drops. Both programs also automatically calculate and correlate temperatures according to preset correlation equation parameters.

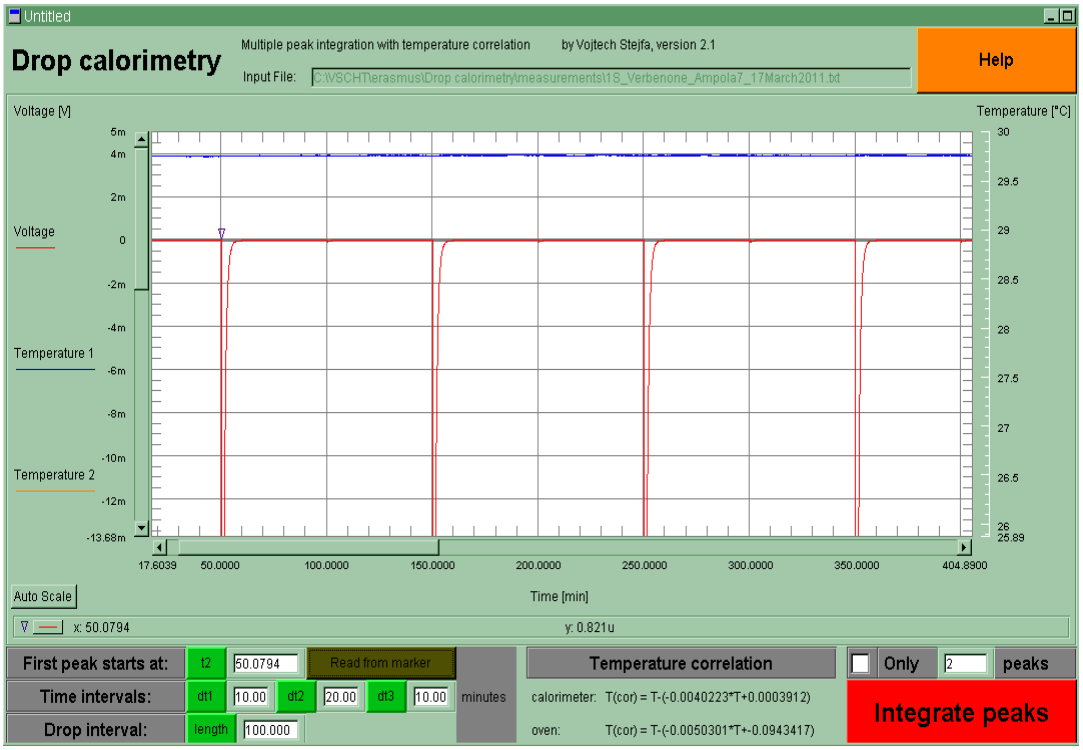

Figure S1. Automatic DC evaluation program written in Agilent VEE

The use of different time intervals was properly tested in order to evaluate the dependence of results on the interval length. Five different compounds were used for the testing: benzoic acid, hexafluorobenzene, o-terphenyl, m-terphenyl, and 1,3,5-triphenylbenzene; and up to 60 different intervals. Optimal interval lengths were determined to be 10-20-10 minutes based on the optimization of the integration procedure in order to achieve the highest precision in the numeric integration.

It was found that greatest systematic errors could be caused by interference of peak voltage values into the initial interval. Moreover, this cannot be perceived by the user, because all peak area integrals are “falsified” equally. Therefore, it was important to install a safety procedure into the program, which monitors this overflow..Data deviating by more than 0.5 % are not displayed.

Recalculation of previous measurements by this program gives results that are in better agreement with the literature than the original manual evaluation. In the case of the three tested compounds (benzoic acid, o-terphenyl, and 1,3,5-triphenylbenzene), results are significantly better. For hexafluorobenzene, deviation against the literature data is comparable using manual or automatic integration. For m-terphenyl, there are no reliable literature data. Comparison with literature data is summarized in Figure .

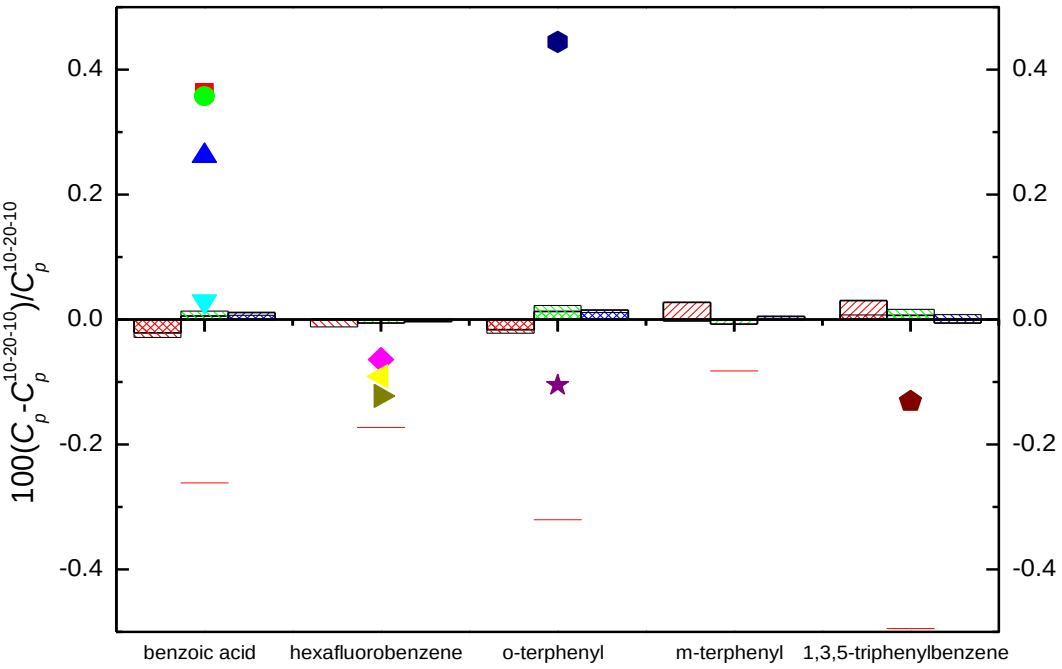

Figure S2. DC evaluation program results comparison with manual results and literature data.

1st (red), 2nd (green) and 3rd (blue) column indicate 20-20-10, 10-30-10 and 10-20-20 method; (///): chemical calibration constant and empty cell correlation calculated by the same method; (\\\): mixed calculation: calibration constant and correlation calculated by the 10-20-10 method; (—): Results obtained by manual evaluation;

(!)Konicek, J.; Wadso, I.; Suurkuus, J.[1]; (,)Arvidsson, K.; Falk, B.; Sunner, S.[2]; (7)Shakirov, R. F.; Lyubarskii, M. V.[3]; (B)Kolesov, V.; Seregin, E. A.; Skuratov, S. M.[4]; (Λ)J. Messerly, J. F.; Finke, H. L.[5]; (Ω)Counsell, J. F. et al.[6]; (β)Gorbunova, N. et al.[7]; (μ)Verevkin, S.P.[8]; (ξ)Chang, S.S.; Bestul, A.B.[9]; (□)Parks, G.S.; Todd, S.S.; Moore, W.A.[10]

References

(1) Konicek, J.; Wadso, I.; Suurkuus, J. Precise drop heat-capacity calorimeter for small samples. *Chemica Scripta* **1971,** *1*, 217.

(2) Arvidsson, K.; Falk, B.; Sunner, S. Small sample low-temperature adiabatic heat-capacity calorimeter with an automatic data acquisition-system - heat-capacity of benzoic acid from 5 to 350 K. *Chemica Scripta* **1976,** *10*, 193-200.

(3) Shakirov, R. F.; Lyubarskii, M. V., Low-temperature heat capacity and thermodynamic functions of methyl trichlorothioacrylate. In *SPSTL Deposited Publication 3 KhP-D80*, 1980; Vol. 19p.

(4) Kolesov, V.; Seregin, E. A.; Skuratov, S. M. Adiabatic calorimeter of small volume for the determination of true heat capacity over the range 12-340K. **1962,** *36*, 647-651.

(5) Messerly, J. F.; Finke, H. L. Hexafluorobenzene and 1,3-difluorobenzene low-temperature calorimetric studies and chemical thermodynamic properties. *The Journal of Chemical Thermodynamics* **1970,** *2*, 867-880.

(6) Counsell, J. F.; Green, J. H. S.; Hales, J. L.; Martin, J. F. Thermodynamic properties of fluorine compounds. Part 2.-Physical and thermodynamic properties of hexafluorobenzene. *Transactions of the Faraday Society* **1965,** *61*, 212-218.

(7) Gorbunova, N.; Grigoriev, V.; Simonov, V.; Shipova, V. Heat capacity of liquid benzene and hexafluorobenzene at atmospheric pressure. *International Journal of Thermophysics* **1982,** *3*, 1-15.

(8) Verevkin, S. P. Thermochemistry of substituted benzenes. Experimental standard molar enthalpies of formation of o-, m-, and p-terphenyls and 1,3,5-triphenylbenzene. *The Journal of Chemical Thermodynamics* **1997,** *29*, 1495-1501.

(9) Chang, S. S.; Bestul, A. B. Heat Capacity and Thermodynamic Properties of o-Terphenyl Crystal, Glass, and Liquid. *The Journal of Chemical Physics* **1972,** *56*, 503-516.

(10) Parks, G. S.; Todd, S. S.; Moore, W. A. Thermal data on organic compounds. XVI. Some heat capacity, entropy and free energy data for typical benzene derivatives and heterocyclic compounds. *J. Am. Chem. Soc.* **1936,** *58*, 398-401.

Paper II

"High-Accuracy Vapor Pressure Data of the Extended [$C_nC_1$im][Ntf_2] Ionic Liquid Series: Trend Changes and Structural Shifts"

Marisa A. A. Rocha, Carlos F. R. A. C. Lima, Lígia R. Gomes, Bernd Schröder, João A. P. Coutinho, Isabel M. Marrucho, José M. S. S. Esperança, Luís P. N. Rebelo, K. Shimizu, José N. Canongia Lopes, Luís M. N. B. F. Santos

Journal of Physical Chemistry B (2011), 115, 10919-10926.
doi: 10.1021/jp2049316

Note: The author of this thesis performed the vapor pressure measurements of the ionic liquids, data analysis and contribute to the discussion and conclusions.

THE JOURNAL OF PHYSICAL CHEMISTRY B

ARTICLE

pubs.acs.org/JPCB

High-Accuracy Vapor Pressure Data of the Extended $[C_nC_1im][Ntf_2]$ Ionic Liquid Series: Trend Changes and Structural Shifts

Marisa A. A. Rocha,[†] Carlos F. R. A. C. Lima,[†] Lígia R. Gomes,[§] Bernd Schröder,[‡] João A. P. Coutinho,[‡] Isabel M. Marrucho,[‡,∥] José M. S. S. Esperança,[∥] Luís P. N. Rebelo,[∥] Karina Shimizu,[#] José N. Canongia Lopes,[∥,#] and Luís M. N. B. F. Santos*[,†]

[†]Centro de Investigação em Química, Departamento de Química e Bioquímica, Faculdade de Ciências da Universidade do Porto, R. Campo Alegre 687, P-4169-007 Porto, Portugal

[‡]CICECO, Departamento de Química, Universidade de Aveiro, P-3810-193 Aveiro, Portugal

[§]CIAGEB, Faculdade de Ciências da Saúde da UFP, Universidade Fernando Pessoa, R. Carlos da Maia 296, P-4200-150 Porto, Portugal

[∥]Instituto de Tecnologia Química e Biológica, ITQB2, Universidade Nova de Lisboa, Av. República, Apartado 127, P-2780-901 Oeiras, Portugal

[#]Centro de Química Estrutural/IST, Av. Rovisco Pais, P-1049-001 Lisboa, Portugal

Supporting Information

ABSTRACT: For the first time, two distinct trends are clearly evidenced for the enthalpies and entropies of vaporization along the $[C_nmim][Ntf_2]$ ILs series. The trend shifts observed for $\Delta_l^g H_m^o$ and $\Delta_l^g S_m^o$, which occur at $[C_6mim][Ntf_2]$, are related to structural modifications. The thermodynamic results reported in the present article constitute the first quantitative experimental evidence of the structural percolation phenomenon and make a significant contribution to better understanding of the relationship among cohesive energies, volatilities, and liquid structures of ionic liquids. A new Knudsen effusion apparatus, combined with a quartz crystal microbalance, was used for the high-accuracy volatility study of the 1-alkyl-3-methylimidazolium bis(trifluoromethylsulfonyl)imide series ($[C_nmim][Ntf_2]$, where n = 2, 3, 4, 5, 6, 7, 8, 10, 12). Vapor pressures in the (450−500) K temperature range were measured, and the molar standard enthalpies, entropies, and Gibbs energies of vaporization were derived. The thermodynamic parameters of vaporization were reported, along with molecular dynamic simulations of the liquid phase structure, allowing the establishment of a link between the thermodynamic properties and the percolation phenomenon in ILs.

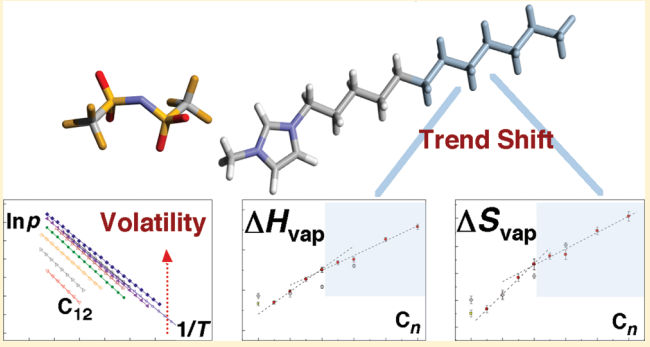

1. INTRODUCTION

Many properties of ionic liquids, for example, melting temperature, acidity and basicity, surface tension, or solubility in water and organic solvents can be adjusted by modifying the cations, anions, or both. Many authors have claimed that ionic liquids share common characteristics such as moderate-to-low electrical conductivity, moderate-to-high viscosity, good thermal stability, and extremely low vapor pressure at room temperature. However, extensive studies on the properties of ILs in the past decade[1] have shown that almost none of these properties are shared across the IL range; therefore, none of them can be considered in and of themselves as a defining characteristic of an ionic liquid.

Over recent years, a growing number of applications for these fluids have been developed. Nowadays, they can be used in multiple industrial processes,[2] including, cellulose processing,[3,4] gas handling, solar energy conversion,[5] and waste recycling. Besides their advantages for specific applications (catalytic activity, solvent effects, separation phenomena), ionic liquids have been designated as "green solvents" because of their low volatility, which prevents their spread into the atmosphere. Nonetheless, it has been also found that they are not free of toxicity, with aquatic toxicities at the same level of some organic solvents,[6] causing some controversy concerning the application of the "green solvent" label.[7] In fact, their extremely low volatilities limit the range of techniques available for their separation and purification, reducing the options for multiple recycling cycles during or after the manufacturing process as well as their recovery, storage, and so on.

It has been discovered that, at moderate temperatures, some ionic liquids may present a range of non-negligible vapor

Received: May 26, 2011
Revised: July 31, 2011
Published: August 04, 2011

pressures.[8] Earle et al.[8] have also shown that by fine-tuning the thermal stability of those ionic liquids it was possible to achieve their distillation.[9] Hence, during the past decade, the volatility of ionic liquids has been the subject of several studies to determine their vapor pressure and vaporization enthalpy with accuracy.[10] Additional information regarding these properties should shed light on the structural arrangement of the ions in the liquid phase, their cohesive energy, as well as the nature of the corresponding vapor phase. Moreover, accurate thermodynamic parameters of vaporization equilibrium are required to validate the models (force fields) used to describe ionic liquids in different simulation techniques (quantum and molecular mechanics, molecular dynamics (MD), Monte Carlo) and to anchor the parameters used in $P-V-T$ equations of state and other semiempirical prediction methods.

Previous works in this field focused on indirect determinations of vapor pressure at moderate temperatures (generally >400 K). Several approaches to measuring and predicting this quantity have been proposed, including MD simulations.[11] Direct experimental determinations have been carried out by the integral Knudsen effusion method,[12] transpiration method,[13] mass spectrometry,[14,15] high-precision vacuum vaporization drop microcalorimetry,[16] and thermogravimetry.[17] Despite all of these efforts, most of them centered on the determination of the vapor pressure and enthalpy of vaporization of ionic liquids of the 1-alkyl-3-methylimidazolium bis(trifluoromethylsulfonyl)imide family, $[C_nC_1im][Ntf_2]$, discrepancies still remain within the state-of-the-art data. Because the majority of the experiments have to be performed at moderate-to-high temperatures (>400 K and below the decomposition temperatures of the ionic liquids) and under very low pressure conditions, most of the expected systematic errors are related to the purity and thermal stability of the ionic liquid during the measurement.

In this work, we present for the first time a high-accuracy study of the volatility of 1-alkyl-3-methylimidazolium bis(trifluoromethylsulfonyl)imide ionic liquids ($[C_nC_1im][Ntf_2]$ with n = 2, 3, 4, 5, 6, 7, 8, 10, 12). The vapor pressure of each pure ionic liquid has been determined as a function of temperature in the [440−495] K range using a new quartz microbalance Knudsen effusion apparatus[18] and applying a methodology developed for this purpose. On the basis of the experimental results, the standard molar enthalpy, entropy, and Gibbs energy of vaporization have been derived. These properties were used to evaluate and rationalize the relationship among cohesive energy, volatility, and structural organization in the liquid phase of this homologous series of ionic liquids.

2. EXPERIMENTAL SECTION

2.1. Synthesis, Purification, and Characterization of Compounds. The ionic liquids used in this work, the 1-alkyl-3-methylimidazolium bis(trifluoromethylsulfonyl)imide series, $[C_nC_1im][Ntf_2]$ (n = 2, 3, 4, 5, 6, 8, 10, 12), were synthesized and purified at QUILL (The Queen's University Ionic Liquid Laboratories, Belfast) following reported procedures.[19] The sample 1-heptyl-3-methylimidazolium bis(trifluoromethylsulfonyl)imide, $[C_7C_1im][Ntf_2]$ was purchased from IOLITEC with a stated purity of better than 99%.^{1}H NMR analysis showed no major impurities except for the presence of water. Chloride analysis using a chloride electrode and the standard addition method indicated chloride contents smaller than 150 ppm.

Before each effusion experiment, the ionic liquids were dried under reduced pressure (<10 Pa) and stirred constantly for a minimum of 48 h at 373 K to reduce the presence of water or other volatile contents. The purity of the samples was verified by ^{1}H and ^{19}F NMR spectroscopy. Karl Fischer titration of the degassed samples revealed <100 ppm of water before the sample was inserted in the vacuum chamber. Inside the vacuum chamber, an additional cleaning experiment was performed at high temperature that reduces the water level in the sample inside the Knudsen cell. It was found that the differences in the derived vapor pressure (in different sets of data with the same IL obtained in independent experiments) do not correlate with the initial water content. The hypothetical effect of the water mass loss in the gravimetric weighing is considered to be negligible.

2.2. Quartz Crystal Microbalance Knudsen Effusion Apparatus. The vapor pressure of each ionic liquid was measured as a function of temperature using a new Knudsen effusion apparatus combined with a quartz crystal microbalance, KEQCM, recently described by Santos et al.[18] This simultaneous gravimetric and quartz crystal microbalance mass loss detection technique enables us to decrease both sample size and effusion times while achieving temperatures of up to 650 K. The combination of two mass loss determination techniques permits the instrument to measure vapor pressures from 0.005 to 1 Pa. The temperature step effusion procedure allows for vapor pressure measurements at different temperatures in one single experiment. The apparatus is essentially a closed system under high vacuum, comprising a quartz crystal positioned above the effusion cell; it is placed in an oven at controlled temperature. Like a typical Knudsen effusion experiment, the system is kept at high vacuum, allowing free effusion of the vapor from the cell, and at a fixed temperature, T. The temperature is controlled within a temperature fluctuation of $\pm(1 \times 10^{-2})$ K, measured with a resolution better than 1×10^{-3} K and with an overall uncertainty better than $\pm(2 \times 10^{-2})$ K along the entire working temperature range. At the working temperature, the quartz crystal microbalance is not sensitive to the water. The vapor pressure data obtained with this apparatus presents a maximum deviation of 1%.

At the temperature T, the mass m of the sample vaporized from the effusion cell, during the time period t, is related to the equilibrium vapor pressure of the liquid compound by the Knudsen equation

$$p(T) = (\Delta m/\Delta t)_T \cdot (1/A_o \cdot w_o) \cdot (2\pi RT/M)^{1/2} \quad (1)$$

where M is the molar mass of the sample, R is the gas constant (R = 8.314472 J·K^{-1}·mol^{-1}), A_o is the area of the orifice, and w_o is the transmission probability factor ($w_o = \{1 + (l/2r)\}^{-1}$). The relative atomic masses used were those recommended by the IUPAC Commission in 2007.[20]

3. RESULTS AND DISCUSSION

The detailed experimental results for vapor pressure, p, obtained in the KEQCM for the nine $[C_nC_1im][Ntf_2]$ ionic liquids as a function of temperature, are given in Table S1 of the Supporting Information. Figure 1 represents $\ln(p/Pa)$ as a function of $\{(1/T)/K^{-1}\}$. The higher working temperature was limited by the thermal stability of the ILs, and the lower temperature was limited by the mass loss detection limited. The vapor pressure experimental results were fitted to the Clarke and

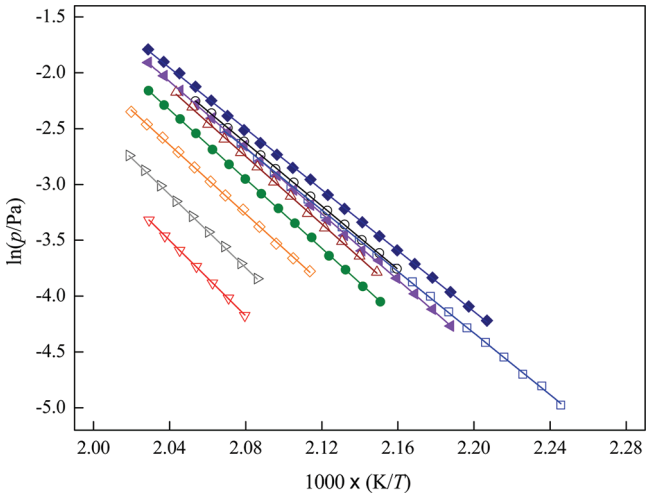

Figure 1. Plot of $\ln(p/\mathrm{Pa}) = f[(1/T)/\mathrm{K}^{-1}]$ for each studied ionic liquid: □, (blue), $[C_2C_1im][Ntf_2]$; ◆ (blue),$[C_3C_1im][Ntf_2]$; ○ (black), $[C_4C_1im][Ntf_2]$; ◀ (pink), $[C_5C_1im][Ntf_2]$; △ (brown), $[C_6C_1im]$-$[Ntf_2]$; ● (green), $[C_7C_1im][Ntf_2]$; ◇ (orange), $[C_8C_1im][Ntf_2]$; ▷ (gray), $[C_{10}C_1im][NTf_2]$; ▽ (red), $[C_{12}C_1im][Ntf_2]$.

Glew eq 2[21]

$$R\ln\left[\frac{p(T)}{p^{o}}\right] = -\frac{\Delta_l^g G_m^o(\theta)}{\theta} + \Delta_l^g H_m^o(\theta)\cdot\left(\frac{1}{\theta}-\frac{1}{T}\right) + \Delta_l^g C_{p,m}^o\cdot\left[\frac{\theta}{T}-1+\ln\left(\frac{T}{\theta}\right)\right] \quad (2)$$

where p is the vapor pressure, p^o is the standard pressure ($p^o = 10^5$ Pa), θ is a selected reference temperature, R is the molar gas constant ($R = 8.314472\ \mathrm{J\cdot K^{-1}\cdot mol^{-1}}$), $\Delta_l^g G_m^o$ is the standard molar Gibbs energy of vaporization at the selected reference pressure, $\Delta_l^g H_m^o$ is the standard molar enthalpy of vaporization, and $\Delta_l^g C_{p,m}^o$ is the difference between the heat capacities of the gaseous and of the liquid phases $[\Delta_l^g C_{p,m}^o = C_{p,m}^o(g) - C_{p,m}^o(l)]$. The values of $\Delta_l^g C_{p,m}^o$ were estimated considering the same temperature for all ILs, $T = 388$ K, and the available literature values for $C_{p,m}^o(l)$ and $C_{p,m}^o(g)$.[22−25] Hence, the values of $\Delta_l^g C_{p,m}{}^o$ ($T = 388$ K) were estimated using the linear fitted function ($\Delta_l^g C_{p,m}^o = -5.40\cdot n(\mathrm{C}) - 100.47$) derived from fitting the literature data of $\Delta_l^g C_{p,m}^o(T = 388\ \mathrm{K})$ as a function of the cationic alkyl chain length. (See Figure S1 of the Supporting Information.) A more detailed explanation of the $\Delta_l^g C_{p,m}^o$ ($T = 388$ K) estimate for the nine studied ionic liquids is presented as Supporting Information. Taking the values of $\Delta_l^g C_{p,}^o$m (Table 1) into account, the standard molar enthalpies, entropies, and Gibbs energies of vaporization at reference temperature, $T = 298.15$ K, were derived. Table 1 lists the derived standard ($p^o = 10^5$ Pa) molar enthalpies, entropies, and Gibbs energies of vaporization at the mean temperature, <T>, and at reference temperature, $T = 298.15$ K, as derived from the fitting of eq 2 and related to each other by the following eq 3

$$\Delta_l^g G_m^o(T) = -RT\ln\left[\frac{p(T)}{p^o}\right] = \Delta_l^g H_m^o(T) - T\cdot\Delta_l^g S_m^o(T) \quad (3)$$

The plots of $\ln(p/\mathrm{Pa})$ as a function of $\{(1/T)/\mathrm{K}^{-1}\}$ presented in Figure 1 show that the volatility of the $[C_nC_1im][Ntf_2]$ ionic liquids decreases along the homologous series, from $[C_3C_1im][Ntf_2]$ to $[C_{12}C_1im][Ntf_2]$. $[C_2C_1im][Ntf_2]$ is an exception to this trend, with lower volatilities than $[C_3C_1im][Ntf_2]$ in the measured temperature range.

Zaitsau et al.[12] also measured the vapor pressure of $[C_2C_1im][Ntf_2]$, $[C_4C_1im][Ntf_2]$, $[C_6C_1im][Ntf_2]$ and $[C_8C_1im][Ntf_2]$ by the effusion Knudsen method. Figure S2, presented as Supporting Information, compares their data with the present results. A reasonable agreement between the two data sets is observed. Nevertheless, small, systematic deviations between the data will affect the derived thermodynamic properties of vaporization, as discussed below.

The thermodynamic properties of vaporization, at $T = 298.15$ K, as derived from the data presented by Zaitsau et al.[12] were recalculated in this work using the same $\Delta_l^g C_{p,m}^o$. The graphic representation of the standard molar Gibbs energies of vaporization, $\Delta_l^g G_m^o(298.15\ \mathrm{K})$, as a function of the alkyl side chain length of the cation, $n(\mathrm{C})$, is presented in Figure 2. The Figure shows that the thermodynamic parameters of vaporization for $[C_2C_1im][Ntf_2]$ and $[C_4C_1im][Ntf_2]$ are in reasonable agreement, whereas those for $[C_6C_1im][Ntf_2]$ and $[C_8C_1im][Ntf_2]$ show differences of around $-5\ \mathrm{kJ\cdot mol^{-1}}$.

The volatility is directly related to the $\Delta_l^g G_m^o(298.15\ \mathrm{K})$: as this quantity rises, with increasing $n(\mathrm{C})$, the volatility along the ionic liquid homologous series falls. Figure 2 depicts an ill-defined trend in the literature data[12] in contrast with the steady increase in $(1.9 \pm 0.1)\ \mathrm{kJ\cdot mol^{-1}}$ per each methylene group $(-CH_2-)$ from $[C_3C_1im][Ntf_2]$ to $[C_{12}C_1im][Ntf_2]$ obtained in the present work. At the reference temperature, $[C_2C_1im][Ntf_2]$ and $[C_3C_1im][Ntf_2]$ exhibit the highest volatilities in the series.

The standard molar enthalpies of vaporization, $\Delta_l^g H_m^o(298.15\ \mathrm{K})$, as a function of the alkyl side chain length of the cation, $n(\mathrm{C})$, are represented in Figure 3.

The previous literature data of $\Delta_l^g H_m^o(298.15\ \mathrm{K})$ are in reasonably good agreement with the present results, with the exception of the value for $[C_6C_1im][Ntf_2]$, which is clearly lower. Santos et al.[16] performed direct measurements of the enthalpies of vaporization by Calvet microcalorimetry. Figure S3 (Supporting Information) presents a detailed comparison of those data with the current ones. Considering the associated uncertainty, only the $\Delta_l^g H_m^o(298.15\ \mathrm{K})$ results for $[C_2C_1im][Ntf_2]$ and $[C_4C_1im][Ntf_2]$ from Santos et al.[16] are in reasonable agreement with the present set of results or most of the results found in the literature.[12,16] The systematically higher results measured by Calvet microcalorimetry[16] may be attributable to a systematic error arising from the high experimental temperatures of the calorimetric measurements, some sample decomposition in the vaporization experiments, or both.

The current results show, for the first time, two distinct trends for the enthalpy of vaporization along the series. In the $[C_3C_1im][Ntf_2]$ to $[C_6C_1im][Ntf_2]$ range, $\Delta_l^g H_m^o(298.15\ \mathrm{K})$ increases $(5.5 \pm 0.2)\ \mathrm{kJ\cdot mol^{-1}}$ per $-CH_2-$ group added to the alkyl side chain of the cation. Between $[C_6C_1im][Ntf_2]$ and $[C_{12}C_1im][Ntf_2]$, the corresponding growth accounts only for $(3.7 \pm 0.2)\ \mathrm{kJ\cdot mol^{-1}}$. The decrease in the$\Delta_l^g H_m^o$ along the series (from 5.5 to 3.7 $\mathrm{kJ\cdot mol^{-1}}$·per $-CH_2-$ group), indicates a falling the contribution per methylene group to the cohesive energies from $[C_6C_1im][Ntf_2]$ to $[C_{12}C_1im][Ntf_2]$. It is interesting to observe that the enthalpies of vaporization, $\Delta_l^g H_m^o$, obtained for $[C_2C_1im][Ntf_2]$ and $[C_3C_1im][Ntf_2]$ are similar, which points out a balance between the decrease in electrostatic interaction and the increase in the intermolecular

Table 1. Parameters of Clarke and Glew Equation Fitted from the Vapor Pressure Results and the Derived Standard Molar Entropy of Vaporization for Each Studied IL at the Reference Temperature, θ, and at the Standard Pressure, $p^o = 10^5$ Pa

T interval/K	θ/K	$\Delta_f^g G_m^o(\theta)$/J·mol^{-1}	$\Delta_f^g H_m^o(\theta)$/J·mol^{-1}	$\Delta_f^g S_m^o(\theta)$/J·K^{-1}·mol^{-1}	r^2	$\Delta_f^g C_{p,m}^o$ (T = 388 K)/J·K^{-1}·mol^{-1}
			[C_2C_1im][Ntf$_2$]			
445 to 483	464.36[a]	58 683 ± 11	114 562 ± 445	120.4 ± 0.9	0.9997	−112
	298.15	82 504 ± 1150	133 177 ± 930	170.0 ± 2.6		
			[C_3C_1im][Ntf$_2$]			
453 to 493	473.04[a]	56 926 ± 14	113 331 ± 539	119.3 ± 0.9	0.9996	−117[b]
	298.15	82 140 ± 884	133 793 ± 475	173.4 ± 2.8		
			[C_4C_1im][Ntf$_2$]			
463 to 487	475.01[a]	57 248 ± 7	117 752 ± 445	127.4 ± 0.8	0.9998	−121
	298.15	84 374 ± 881	139 152 ± 470	183.8 ± 2.6		
			[C_5C_1im][Ntf$_2$]			
457 to 493	474.99[a]	57 479 ± 12	122 978 ± 526	138.0 ± 0.9	0.9997	−127[b]
	298.15	86 690 ± 893	145 437 ± 491	196.9 ± 2.8		
			[C_6C_1im][Ntf$_2$]			
465 to 489	477.35[a]	57 490 ± 16	126 053 ± 990	143.7 ± 1.9	0.9993	−134
	298.15	88 438 ± 372	150 065 ± 798	206.9 ± 4.0		
			[C_7C_1im][Ntf$_2$]			
465 to 493	478.92[a]	58 085 ± 7	128 729 ± 387	147.6 ± 0.8	0.9999	−138[b]
	298.15	90 196 ± 887	153 675 ± 480	213.0 ± 2.4		
			[C_8C_1im][Ntf$_2$]			
473 to 495	484.10[a]	58 582 ± 12	128 608 ± 857	144.7 ± 1.8	0.9996	−143
	298.15	91 406 ± 1222	155 199 ± 837	214.0 ± 3.7		
			[$C_{10}C_1$im][Ntf$_2$]			
479 to 495	487.38[a]	59 960 ± 5	136 028 ± 500	156.1 ± 0.9	0.9999	−154[b]
	298.15	96 071 ± 964	165 169 ± 573	231.8 ± 2.8		
			[$C_{12}C_1$im][Ntf$_2$]			
481 to 493	486.85[a]	61 731 ± 7	140 348 ± 809	161.5 ± 1.8	0.9998	−165[b]
	298.15	99 215 ± 1210	171 484 ± 815	242.5 ± 3.5		

[a] Mean temperature. r^2 is the linear regression coefficient. [b] $\Delta_f^g C_{p,m}^o$(388 K) estimated using the linear fitted function ($\Delta_f^g C_{p,m}^o = -5.40\,n(C) - 100.47$) derived from fitting of the literature data of $\Delta_f^g C_{p,m}^o$(388 K) as a function of the cationic alkyl chain length. It was considered an uncertainty of 5 J·K^{-1}·mol^{-1}.

interactions arising from the increment of the −CH_2− group from [C_2C_1im][Ntf$_2$] to [C_3C_1im][Ntf$_2$] (further discussion follows).

The entropies of vaporization profile along the series in Figure 4 are analogous to those observed for the enthalpies of vaporization.

The results show a steady increase in $\Delta_f^g S_m^o$ along the homologous series and a trend shift in the increase in $\Delta_f^g S_m^o$ with n(C), around n(C) = 6, identical to that observed for the enthalpies of vaporization profile. Because the absolute standard molar entropies in the gaseous phase increase linearly along the homologous series,[22] the observed change should be due to an additional increase in the absolute entropy in the liquid phase, starting at [C_6C_1im][Ntf$_2$]. The derived results for the standard molar entropies of vaporization and the absolute standard molar entropies in the gaseous and liquid phases are presented in Table S3 of the Supporting Information.

The accuracy and resolution of these results for the extended series of [$C_nC_1$im][Ntf$_2$] are sufficient to demonstrate that the two (entropic and enthalpic) trend changes at n(C) = 6 compensate for each other and that there is a steady increase in the resulting Gibbs energy values from [C_3C_1im][Ntf$_2$] to [$C_{12}C_1$im][Ntf$_2$].

It is important to stress that previous studies, utilizing only a handful of cations with an even number of carbon atoms in the alkyl side chain, did not allow for a complete characterization of the important trend changes of the thermodynamic parameters of vaporization, including the outlier character of [C_2C_1im][Ntf$_2$], as evidenced in this work.

Figure 5 demonstrates the increments per −CH_2− group in the vaporization thermodynamic properties in the ILs and some alkyl derivatives.

It is interesting to observe that the ILs present a regular increase of (1.9 ± 0.1) kJ·mol^{-1} per methylene group on the Gibbs energies of vaporization as compared with an increment of 2.86 kJ·mol^{-1} observed on alkanes, 1-alcohols, and 1-amino alkanes.[26−28] The smaller increase in the Gibbs energies of vaporization of the ILs reflects the increase in the chemical potential of the liquid phase. This results from a balance between the decrease in the electrostatic potential and the increase in the nonelectrostatic interactions with the increase in the cationic alkyl chain length. The contribution per methylene unit to $\Delta_f^g H_m^o$(298.15

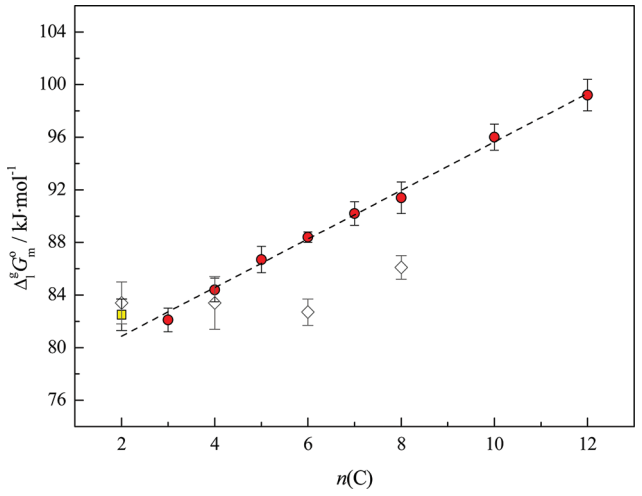

Figure 2. Graphic representation of standard molar Gibbs energies of vaporization at reference temperature (T = 298.15 K) as a function of the number of carbon atoms in the alkyl side chain of the cation, n(C). □ (yellow),○ (red), this work (Knudsen effusion/quartz crystal microbalance method); ◇, Zaitsau et al.[12] (Knudsen effusion method).

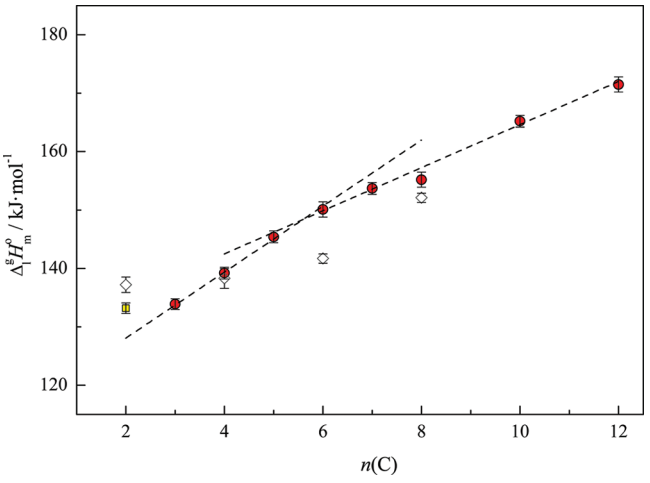

Figure 3. Graphic representation of standard molar enthalpies of vaporization at reference temperature (T = 298.15 K) as a function of the number of carbon atoms in the alkyl side chain of the cation, n(C). □ (yellow), ○ (red), this work (Knudsen effusion/quartz crystal microbalance method); ◇, Zaitsau et al.[12] (Knudsen effusion method).

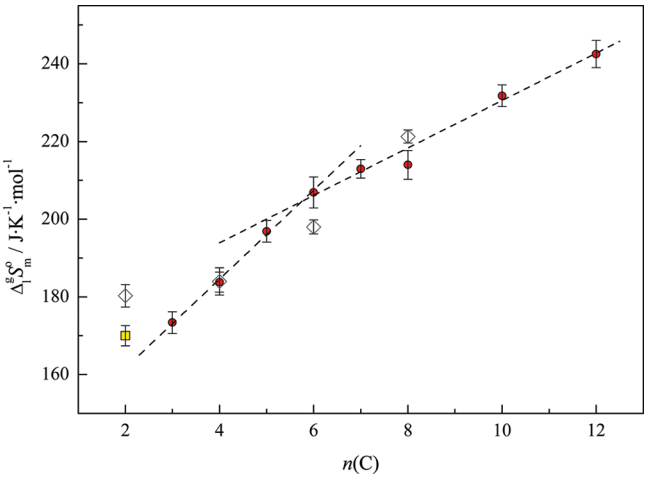

Figure 4. Graphic representation of standard molar entropies of vaporization, at reference temperature (T = 298.15 K), as a function of the number of carbon atoms in the alkyl side chain of the cation, n(C). □, (yellow), ○ (red), this work (Knudsen effusion/Quartz crystal microbalance method); ◇, Zaitsau et al.[12] (Knudsen effusion method).

K), in the range from $[C_3C_1im][Ntf_2]$ to $[C_6C_1im][Ntf_2]$, is comparable to that observed for the liquid phase in the alkyl derivatives and decreases after $[C_6C_1im][Ntf_2]$, directly reflecting the regular decrease in the electrostatic interaction; it indicates the beginning of a new regular type of molecular interaction.

The relatively smaller increase per methylene unit to the entropy of vaporization of the ILs as compared with the increment observed for the alkyl derivatives from $[C_3C_1im][Ntf_2]$ to $[C_6C_1im][Ntf_2]$ must be related to the decrease in rotational entropy contribution of the alkyl groups in the region of strong electrostatic interaction. The profile of the $\Delta_l^g S_m^o$ trend in the series, above $[C_6C_1im][Ntf_2]$, is identical to that observed in the alkyl derivatives and is identical to those observed along the alkane homologous series.

The enthalpic and entropic vaporization trend changes along the $[C_nC_1im][Ntf_2]$ series and must be related to a change in the molecular structure of the liquid phase around $[C_6C_1im][Ntf_2]$. The existing models for the structure of ionic liquids at a molecular level consider them to be nanosegregated fluids. To evaluate if this nanosegregation might be related to the trend changes observed in the thermodynamic properties of vaporization, we carried out MD studies for the $[C_nC_1im][Ntf_2]$ ionic liquid series. These MD studies[29−31] and subsequently X-ray diffraction studies[32] recognized the nanosegregated structures of ionic liquids. Although those first studies focused on the 1-alkyl-3-methylimidazolium hexafluorophosphate series, $[C_nC_1im][PF_6]$, the conclusions were quickly extended to the $[C_nC_1im][Ntf_2]$ series and contained two basic types of conclusion: (i) ionic liquids are highly structured fluids composed of high-charge density areas (the "polar heads" of the anions and cations forming a polar network) permeated by low-charge density regions (the alkyl side chains present in some of the ions forming nonpolar domains); (ii) the topology of the nonpolar domains is strongly dependent on the relative volumes occupied by the polar and nonpolar moieties of the molecules. For very small alkyl side chains, the nonpolar domains are isolated islands in a continuous polar domain; for longer alkyl side chains, those islands start to coalesce, and after a certain threshold value is reached, they form a second, continuous nonpolar domain. This corresponds to a kind of percolation limit of the nonpolar network regions and the formation of a bicontinuous fluid phase.[31,33]

The trend shifts observed for $\Delta_l^g H_m^o$ and $\Delta_l^g S_m^o$ as a function of the cationic alkyl side chain length (Figures 3 and 4) are related to the structural modifications that occur when the number of alkyl carbon atoms nears six.

For the $[C_nC_1im][PF_6]$ ionic liquids,[31,32] the percolation limit of the nonpolar islands was found to occur around n(C)= 4 to 5. With bulkier anions like $[Ntf_2]^-$ and a concomitantly larger polar network, as can be inferred from Figure S5 (Supporting Information), this threshold value was predicted to be larger.[33] New simulation runs were performed for all $[C_nC_1im][Ntf_2]$ ionic liquids between n(C)= 2 and 10, in order to verify if the

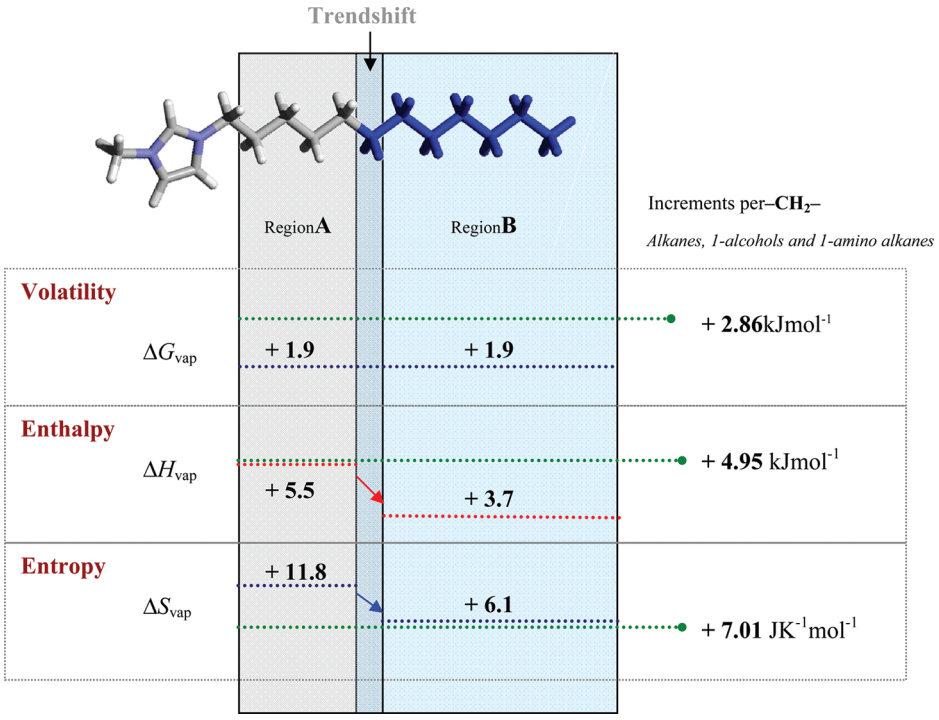

Figure 5. Schematic comparative diagram of the increments per methylene group of the thermodynamic vaporization properties between the studied ILs (before and after the trend shift n(C)) and the typical alkane derivatives data.[26−28]

percolation limit was attained around n(C)= 6, as occurred for the $\Delta_l^g H_m^o[n(C)]$ and $\Delta_l^g S_m^o[n(C)]$. Figure 6 shows the CT−CT radial distribution functions for the different ionic liquids and two snapshots of the simulation boxes for $[C_4C_1im][Ntf_2]$ and $[C_8C_1im][Ntf_2]$ (CT, carbons of the terminal methyl groups of the chain).

All RDFs show an intense first peak that tends to be higher as the alkyl side chain gets longer; that is, the terminal carbon atoms of the alkyl side chains tend to separate from the polar regions of the ionic liquid and come to rest in proximity to each other. This is particularly true for ionic liquids from $[C_2C_1im][Ntf_2]$ to $[C_5C_1im][Ntf_2]$, where the small clusters (islands) containing the adjoining CT groups (cf. circled areas in Figure 6a) are growing. However, above a certain alkyl side chain length (around $[C_6C_1im][Ntf_2]$), the intensities of the first peaks start to become almost constant. This suggests that to segregate from the nonpolar network, the CT atoms do not have to form a small cluster (the percolation limit was reached and a more ample and continuous nonpolar region is now available) and that the first peak intensities tend to increase because of the overall decrease in the volume fraction of the CT groups. (Radial distribution functions are normalized taking into account the average density of the pair under scrutiny in the total system volume.) Additionally, the structural modification from small clusters to a continuous nonpolar nanophase can be ascertained from a new type of analysis based on the second peaks: a string of CT atoms like those depicted in Figure 6b will exhibit shorter second neighbor distances than those found between CT atoms from neighboring, independent clusters. This is indeed the situation observed in the RDFs from $[C_4C_1im][Ntf_2]$ to $[C_{10}C_1im][Ntf_2]$: the peak around 1 nm in $[C_4C_1im][Ntf_2]$ starts decreasing and shifting in $[C_5C_1im][Ntf_2]$ and forms an incipient peak at 0.8 nm (twice the distance of the first peak at 0.4 nm) in $[C_6C_1im][Ntf_2]$, which then grows continuously from $[C_7C_1im][Ntf_2]$ to $[C_{10}C_1im][Ntf_2]$.

The simulations show a structural shift around $[C_6C_1im]$-$[Ntf_2]$ when the nonpolar island percolation limit is reached for this series of ionic liquids. This is consistent with higher $S_m^o(l)$ values from $[C_6C_1im][Ntf_2]$ onward, as inferred from the experimental results of this work (Figure 4). For n(C) > 6, the absolute entropy in the liquid phase increases more rapidly as the distances and segregation between the terminal alkyl groups and polar domains increase and the corresponding interactions decrease. The same argument also justifies the trend found for the cohesive energy of the liquid phase (Figure 3).

The $[C_2C_1im][Ntf_2]$ outlier character can also be analyzed taking into account possible structural changes occurring in the liquid phase, as evidenced by other simulation studies. (See the Supporting Information.)

The relation between the $\Delta_l^g H_m^o$ and $\Delta_l^g S_m^o$ trends and the structural changes in the liquid phase observed for the $[C_nC_1im][Ntf_2]$ series shed further light on recently reported experimental viscosity data and their temperature dependence for this same series of ionic liquids.[34] Figure 7 shows the trends of the viscosity and the corresponding parameters (A, E) of the Vogel−Tammann−Fulcher (VTF) equation used to fit the temperature dependence of the viscosity data along the $[C_nC_1im][Ntf_2]$ series. (See the details in the Supporting Information.) The Figure also clearly shows changes around $[C_6C_1im][Ntf_2]$.

The particularly conspicuous change observed in the pre-exponential factor of the VTF equation, A, around $[C_6C_1im]$ $[Ntf_2]$ indicates (and is in agreement with) an additional increase in liquid phase entropy. On the other hand, the decrease in the change of cohesive energies is only slightly reflected in the decrease of the viscosity activation energy, E. Interestingly, $[C_2C_1im][Ntf_2]$

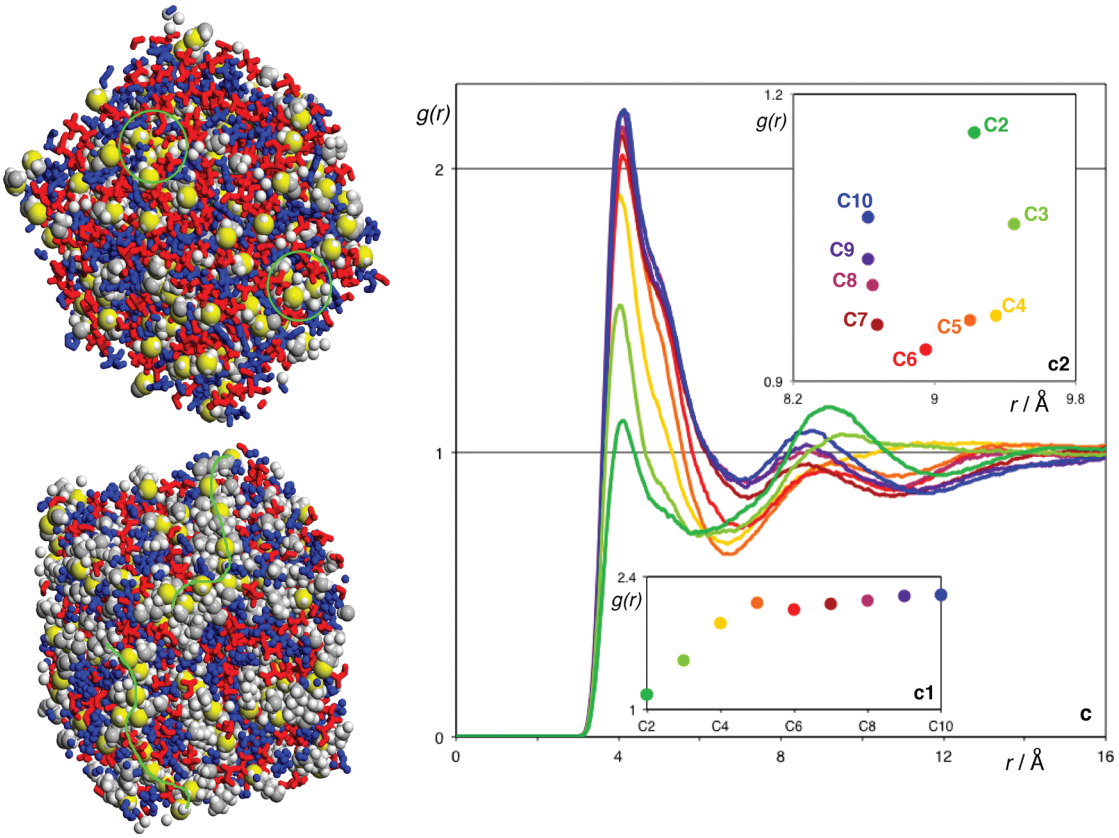

Figure 6. Two snapshots of simulation boxes containing $[C_4C_1im][Ntf_2]$ (top) and $[C_8C_1im][Ntf_2]$ ionic liquids (bottom). The high-charge density regions of the cations and anions are colored as blue and red sticks to highlight the continuity of the polar network. The alkyl side chains (from C2 onward) are colored using space-filled atoms and the SPK convention (carbon, gray; hydrogen, white). The terminal atoms (CT) of each alkyl side chain are colored in yellow and given a larger space filling radius. The green lines emphasize the relations between the CT atoms, as discussed in the text. The CT−CT radial distribution functions of all $[C_nC_1im][Ntf_2]$ (n = 2−10) are given next to the snapshots.

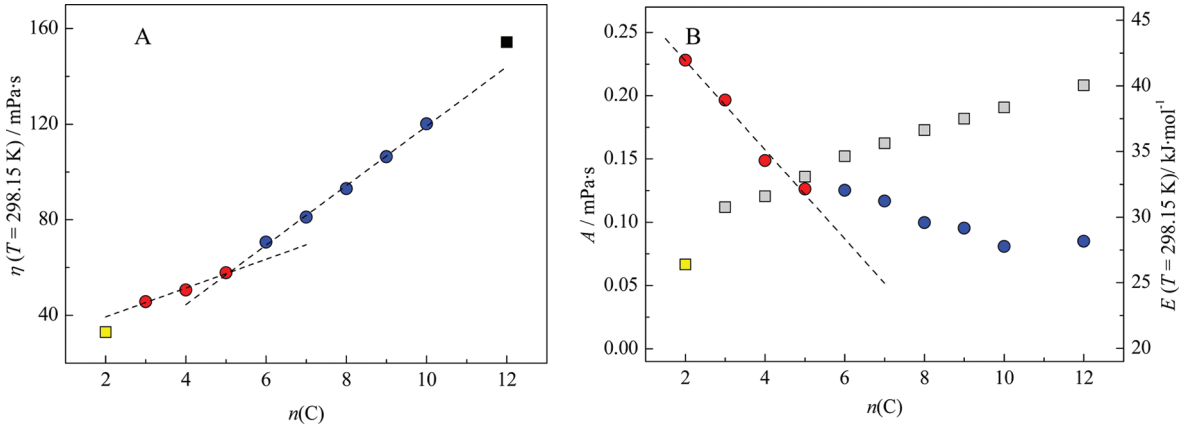

Figure 7. Plots of viscosity (η/mPa·s) at T = 298.15 K, pre-exponential coefficient of the Vogel−Tammann−Fulcher equation (A/mPa·s), and activation energy (E/kJ·mol^{-1}) at T = 298.15 K as a function of the number of carbon atoms in the alkyl side chain of the cation, n(C). (B) □ (yellow), □ (gray), E/kJ·mol^{-1}; ○ (red), ○ (blue), A/mPa·s. Derived from the data presented in ref 34.

is again an outlier relative to the rest of the homologous series. In this case, however, its varying viscosity is dominated by a significant lower contribution from its activation energy.

4. FINAL REMARKS

The study of the nine imidazolium-based ionic liquids enabled us to detect important trends in the thermodynamic parameters, which would have been impossible to verify with a smaller number of ILs. The high accuracy and resolution of the present vapor pressure results were sufficient to extract the individual thermodynamic entropic and enthalpic contributions to the liquid−vapor equilibrium.

The thermodynamic results herein reported constitute the first experimental quantitative evidence of the structural percolation

dx.doi.org/10.1021/jp2049316 |J. Phys. Chem. B 2011, 115, 10919–10926

phenomenon and represent an important contribution to increased understanding of the relationship between ionic liquids, cohesive energies, volatility and liquid structures. They also clarify the existent discrepancy between the thermodynamic properties of vaporization encountered in the literature and consequently provide strong experimental validation of the accurate parametrization of molecular force fields used in computer simulations.

■ ASSOCIATED CONTENT

Supporting Information. Experimental vapor pressures for the nine imidazolium-based ILs; literature data regarding heat capacities in the gaseous and liquid phases together with the calculated values, comparisons of the vapor pressures and enthalpies of vaporization with literature data, absolute standard molar entropies in gaseous and liquid phases, and molecular dynamics results. This material is available free of charge via the Internet at http://pubs.acs.org.

■ AUTHOR INFORMATION

Corresponding Author
*Tel: +351 220 402 836. Fax: +351 220 402 659. E-mail: lbsantos@fc.up.pt.

■ ACKNOWLEDGMENT

This work was supported by the *Fundação para a Ciência e a Tecnologia*. B.S., K.S., C.F.R.A.C.L., and M.A.A.R. acknowledge the financial support from *Fundação para a Ciência e a Tecnologia* for the research grants, specifically: SFRH/BPD/38637/2007, SFRH/BPD/38339/2007, SRFH/BD/29394/2006, and SFRH/BD/60513/2009, respectively. We also thank FCT for financial support for the project PTDC/QUI/72903/2006.

■ REFERENCES

(1) Greaves, T. L.; Drummond, C. J. *Chem. Rev.* **2008**, *108*, 206–237.
(2) Plechkova, N. V.; Seddon, K. R. *Chem. Soc. Rev.* **2008**, *37*, 123–150.
(3) Swatloski, R. P.; Spear, S. K.; Holbrey, J. D.; Rogers, R. D. *J. Am. Chem. Soc.* **2002**, *124*, 4974–4975.
(4) Ohno, H.; Fukaya, Y. *Chem. Lett.* **2009**, *38*, 2–7.
(5) Wu, B.; Reddy, R. G.; Rogers, R. D. Novel Ionic Liquid Thermal Storage for Solar Thermal Electric Power Systems, Proceedings of the Solar Forum 2001, Washington, D.C., 2001.
(6) Zhao, D.; Liao, Y.; Zhang, Z. *Clean* **2007**, *35*, 42–48.
(7) Scammells, P. J.; Scott, J. L.; Singer, R. D. *Aust. J. Chem.* **2005**, *58*, 155–169.
(8) Earle, M. J.; Esperança, J. M. S. S.; Gilea, M. A.; Canongia Lopes, J. N.; Rebelo, L. P. N.; Magee, J. W.; Seddon, K. R.; Widegren, J. A. *Nature* **2006**, *439*, 831–834.
(9) MacFarlane, D. R.; Pringle, J. M.; Johansson, K. M.; Forsyth, S. A.; Forsyth, M. *Chem. Commun.* **2006**, 1905–1917.
(10) Esperança, J. M. S. S.; Canongia Lopes, J. N.; Tariq, M.; Santos, L. M. N. B. F.; Magee, J. W.; Rebelo, L. P. R. *J. Chem. Eng. Data* **2010**, *55*, 3–12.
(11) Köddermann, T.; Paschek, D.; Ludwig, R. *Chem. Phys. Chem.* **2007**, *8*, 2464–2470.
(12) Zaitsau, D. H.; Kabo, G. J.; Strechan, A. A.; Paulechka, Y. U.; Tschersich, A.; Verevkin, S. P.; Heintz, A. *J. Phys. Chem. A* **2006**, *110*, 7303–7306.
(13) Emel'yanenko, V. N.; Verevkin, S. P.; Heintz, A. *J. Am. Chem. Soc.* **2007**, *129*, 3930–3937.
(14) Armstrong, J. P.; Hurst, C.; Jones, R. G.; Licence, P.; Lovelock, K. R. J.; Satterley, C. J.; Villar-Garcia, I. J. *Phys. Chem. Chem. Phys.* **2007**, *9*, 982–990.
(15) Deyko, A.; Lovelock, K. R. J.; Corfield, J.-A.; Taylor, A. W.; Gooden, P. N.; Villar-Garcia, I. J.; Licence, P.; Jones, R. G.; Krasovskiy, V. G.; Chernikova, E. A.; Kustov, L. M. *Phys. Chem. Chem. Phys.* **2009**, *11*, 8544–8555.
(16) Santos, L. M. N. B. F.; Canongia Lopes, J. N.; Coutinho, J. A. P.; Esperanca, J. M. S. S.; Gomes, L. R.; Marrucho, I. M.; Rebelo, L. P. N. *J. Am. Chem. Soc.* **2007**, *129*, 284–285.
(17) Luo, H.; Baker, G. A.; Dai, S. *J. Phys. Chem. B* **2008**, *112*, 10077–10081.
(18) Santos, L.M.N.B.F.; Lima, L. M. S. S.; Lima, C.F.R.A.C.; Magalhães, F. D.; Torres, M. C.; Schröder, B.; Ribeiro da Silva, M. A. V. *J. Chem. Thermodyn.* **2011**, *43*, 834–843.
(19) Bonhôte, P.; Dias, A. P.; Armand, M.; Papageorgiou, N.; Kalyanasundaram, K.; Grätzel, M. *Inorg. Chem.* **1996**, *35*, 1168–1178.
(20) Wieser, M. E.; Berglund, M. *Pure Appl. Chem.* **2009**, *81*, 2131–2156.
(21) Clarke, E. C. W.; Glew, D. N. *Trans. Faraday Soc.* **1966**, *62*, 539–547.
(22) Paulechka, Y. U.; Kabo, G. J.; Emel'yanenko, V. N. *J. Phys. Chem. B* **2008**, *112*, 15708–15717.
(23) Blokhin, A. V.; Paulechka, Y. U.; Kabo, G. J. *J. Chem. Eng. Data* **2006**, *51*, 1377–1388.
(24) Paulechka, Y. U.; Blokhin, A. V.; Kabo, G. J.; Strechan, A. A. *J. Chem. Thermodyn.* **2007**, *39*, 866–877.
(25) Blokhin, A. V.; Paulechka, Y. U.; Strechan, A. A.; Kabo, G. J. *J. Phys. Chem. B* **2008**, *112*, 4357–4364.
(26) Růžička, K.; Majer, V. *J. Phys. Chem. Ref. Data* **1994**, *23*, 1–39.
(27) Matulis, D. *Biophys. Chem.* **2001**, *93*, 67–82.
(28) Chickos, J. S.; Hanshaw, W. *J. Chem. Eng. Data* **2004**, *49*, 77–85.
(29) Urahata, S. M.; Ribeiro, M. C. C. *J. Chem. Phys.* **2004**, *120*, 1855–1863.
(30) Wang, Y.; Voth, G. A. *J. Am. Chem. Soc.* **2005**, *127*, 12192–12193.
(31) Canongia Lopes, J. N.; Pádua, A. A. H. *J. Phys. Chem. B* **2006**, *110*, 3330–3335.
(32) Triolo, A.; Russina, O.; Bleif, H.-J.; Di Cola, E. *J. Phys. Chem. B* **2007**, *111*, 4641–4644.
(33) Shimizu, K.; Gomes, M. F. C.; Pádua, A. A. H.; Rebelo, L. P. N.; Canongia Lopes, J. N. *THEOCHEM* **2010**, *946*, 70–76.
(34) Tariq, M.; Carvalho, P. J.; Coutinho, J. A.P.; Marrucho, I. M.; Canongia Lopes, J. N.; Rebelo, L. P.N. *Fluid Phase Equilib.* **2011**, *301*, 22–32.

Supporting Information

High-Accuracy Vapor Pressure Data of the Extended $[C_nC_1im][Ntf_2]$ Ionic Liquid Series: Trend Changes and Structural Shifts

Marisa A. A. Rocha [†, §], *Carlos F. R. A. C. Lima* [†], *Lígia R. Gomes* [#], *Bernd Schröder* [§], *João A. P. Coutinho* [§], *Isabel M. Marrucho* [§,¥], *José M. S. S. Esperança* [¥], *Luís P. N. Rebelo* [¥] *K. Shimizu* [£], *José N. Canongia Lopes* [£], *Luís M. N. B. F. Santos* [†,*]

[†] Centro de Investigação em Química, Faculdade de Ciências da Universidade do Porto, R. Campo Alegre 687, P-4169-007 Porto, Portugal

[§] CICECO, Departamento de Química, Universidade de Aveiro, 3810-193 Aveiro, Portugal

[#] CIAGEB, Faculdade de Ciências da Saúde da UFP, Universidade Fernando Pessoa, R. Carlos da Maia 296, P-4200-150 Porto, Portugal

[¥] Instituto de Tecnologia Química e Biológica, ITQB2, Universidade Nova de Lisboa, AV. República, Apartado 127, 2780-901 Oeiras, Portugal

[£] Centro de Química Estrutural/IST, Av. Rovisco Pais 1049 001 Lisboa, Portugal

*Corresponding author. Tel.: +351 220 402 836; Fax: +351 220 402 659

E-mail address: lbsantos@fc.up.pt (Luís M. N. B. F. Santos)

Vapor pressures measurements using Quartz crystal microbalance Knudsen effusion apparatus

The experimental vapor pressures for each IL, obtained by the quartz microbalance Knudsen effusion apparatus, appear in Table S1.

Table S1 Experimental vapor pressures for the nine imidazolium based ILs, obtained by the quartz crystal microbalance Knudsen effusion apparatus.

T / K	p / Pa	Δp / Pa	T / K	p / Pa	Δp / Pa	T / K	p / Pa	Δp / Pa
				[C_2C_1im][Ntf_2]				
445.30	0.0069	-0.0001	459.32	0.0183	0.0002	473.32	0.0436	-0.0002
447.30	0.0082	0.0002	461.32	0.0208	0.0002	475.33	0.0488	-0.0007
449.31	0.0091	-0.0001	463.34	0.0235	0.0000	477.33	0.0552	-0.0006
451.31	0.0106	0.0000	465.34	0.0264	-0.0003	479.34	0.0625	-0.0004
453.31	0.0121	0.0000	467.36	0.0303	0.0000	481.34	0.0720	0.0012
455.32	0.0138	-0.0001	469.34	0.0340	-0.0003	483.41	0.0821	0.0023
457.32	0.0159	0.0001	471.35	0.0383	-0.0006			
				[C_3C_1im][Ntf_2]				
453.13	0.0147	0.0003	467.02	0.0355	-0.0002	480.98	0.0809	-0.0023
455.11	0.0167	0.0002	469.04	0.0400	-0.0005	482.98	0.0919	-0.0015
457.11	0.0190	0.0002	471.00	0.0453	-0.0004	484.98	0.1054	0.0006
459.11	0.0216	0.0001	473.04	0.0520	0.0002	486.96	0.1194	0.0021
461.08	0.0244	0.0000	475.12	0.0577	-0.0010	488.95	0.1347	0.0035
463.06	0.0276	-0.0001	477.00	0.0649	-0.0008	490.95	0.1492	0.0025
465.06	0.0313	-0.0002	478.99	0.0721	-0.0019	492.95	0.1669	0.0030
				[C_4C_1im][Ntf_2]				
463.07	0.0234	0.000	473.02	0.0447	0.000	482.95	0.0825	0.000
465.06	0.0269	0.000	475.00	0.0506	0.000	484.97	0.0942	0.001
467.06	0.0303	0.000	477.18	0.0572	-0.001	486.95	0.1051	0.000
469.05	0.0348	0.000	478.96	0.0646	0.000			
471.05	0.0394	0.000	480.96	0.0730	0.000			

				[C_5C_1im im][Ntf_2]				
457.09	0.0140	0.0001	471.03	0.0361	-0.0006	484.93	0.0901	0.0000
459.08	0.0163	0.0002	473.01	0.0414	-0.0005	486.91	0.1021	0.0002
461.06	0.0187	0.0002	475.01	0.0474	-0.0004	488.90	0.1154	0.0003
463.07	0.0215	0.0002	476.98	0.0540	-0.0004	490.90	0.1318	0.0018
465.06	0.0252	0.0007	479.01	0.0615	-0.0005	492.89	0.1482	0.0017
467.05	0.0275	-0.0006	480.96	0.0704	0.0002			
469.04	0.0315	-0.0006	482.95	0.0796	0.0000			
				[C_6C_1im][Ntf_2]				
465.33	0.0227	0.0003	475.35	0.0448	0.0000	485.38	0.0853	-0.0011
467.33	0.0262	0.0004	477.35	0.0509	-0.0003	487.35	0.0996	0.0017
469.33	0.0299	0.0002	479.36	0.0582	-0.0003	489.37	0.1137	0.0026
471.35	0.0337	-0.0004	481.36	0.0663	-0.0004			
473.34	0.0384	-0.0007	483.37	0.0748	-0.0011			
				[C_7C_1im][Ntf_2]				
464.95	0.0174	0.0000	474.86	0.0352	0.0002	484.85	0.0680	-0.0006
466.94	0.0200	-0.0001	476.82	0.0402	0.0001	486.90	0.0786	0.0003
468.93	0.0232	0.0001	478.88	0.0458	-0.0003	488.88	0.0894	0.0004
470.86	0.0263	-0.0002	480.83	0.0522	-0.0004	490.89	0.1014	0.0002
472.88	0.0310	0.0005	482.81	0.0595	-0.0005	492.88	0.1152	0.0005
				[C_8C_1im][Ntf_2]				
473.10	0.0229	0.0003	481.08	0.0397	0.0006	489.09	0.0665	0.0004
475.08	0.0257	-0.0003	483.27	0.0451	-0.0001	491.08	0.0757	0.0006
477.10	0.0293	-0.0005	485.08	0.0511	0.0002	493.08	0.0852	0.0000
479.10	0.0341	-0.0001	487.08	0.0580	-0.0001	495.09	0.0955	-0.0012
				[$C_{10}C_1$im][Ntf_2]				
479.37	0.0214	0.0001	485.36	0.0325	-0.0001	491.37	0.0492	0.0000
481.35	0.0245	-0.0001	487.36	0.0374	0.0000	493.38	0.0564	0.0001
483.35	0.0285	0.0002	489.39	0.0428	-0.0002	495.38	0.0645	0.0002
				[$C_{12}C_1$im][Ntf_2]				
480.89	0.0154	-0.0001	486.84	0.0239	0.0001	492.81	0.0362	0.0000
482.87	0.0180	0.0001	488.94	0.0276	0.0000			
484.85	0.0206	0.0000	490.81	0.0314	-0.0001			

$\Delta p = p - p_{calc}$, where p_{calc} is calculated from the Clarke and Glew equation (eq. 5) with the parameters given in Table 1.

Estimation of the $\Delta_l^g C_{p,m}^o$ for the ionic liquids studied:

The heat capacities in the gaseous phase, $C_{p,m}^o(g)$, for [C_2mim][NTf_2], [C_4mim][NTf_2], [C_6mim][NTf_2] and [C_8mim][NTf_2], were calculated by Paulechka *et al.*[1] by quantum chemical calculations using B3LYP/6-31+G(2df,p) level of theory. The heat capacities in the liquid phase, $C_{p,m}^o(l)$, for the mentioned IL, were determined via adiabatic calorimetry, by the same research group.[2-4] The values of $\Delta_l^g C_{p,m}^o$ were estimated considering the same temperature for all ILs, T = 388 K. Therefore, the values of $\Delta_l^g C_{p,m}^o(T = 388\ K)$ for the other ILs ([C_3mim][NTf_2], [C_5mim][NTf_2], [C_7mim][NTf_2], [C_{10}mim][NTf_2] and [C_{12}mim][NTf_2]), were estimated using the linear fitted function ($\Delta_l^g C_{p,m}^o$ = -5.40 n(C) − 100.47) derived from fitting the literature data of $\Delta_l^g C_{p,m}^o(T = 388\ K)$ as a function of the cation alkyl chain length (Figure S1). The estimated values of $\Delta_l^g C_{p,m}^o(T = 388\ K)$ for the nine ionic liquids studied are presented in table S2.

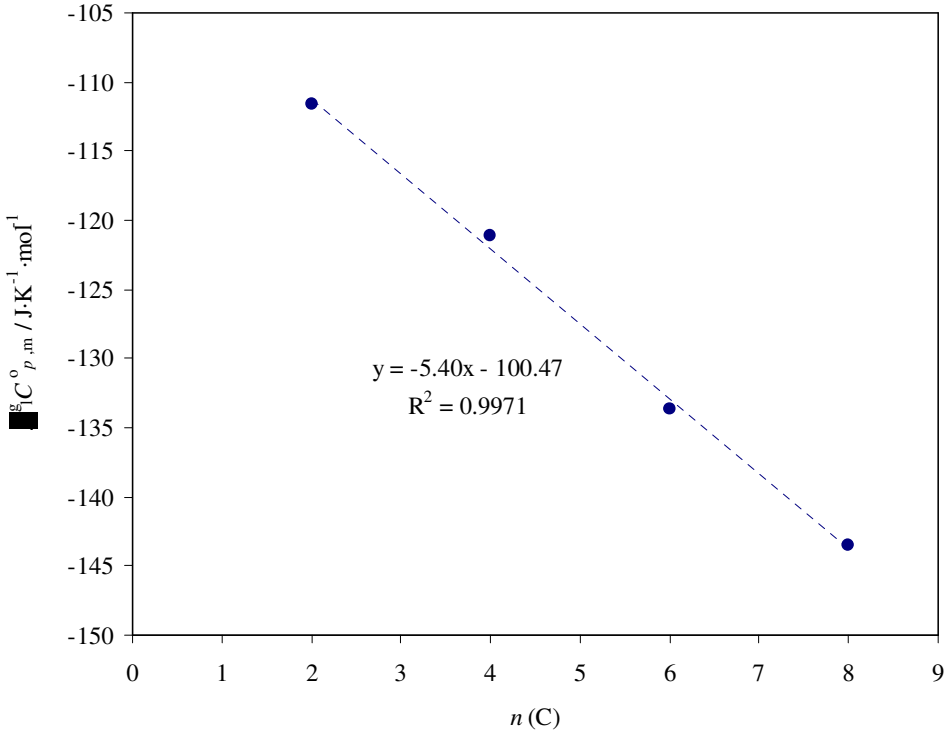

Figure S1 - lLiterature data of $\Delta_l^g C_{p,m}^o$ (T = 388 K) as a function of the cation alkyl chain length.

Table S2. Values of heat capacities in the gaseous and liquid phases available in literature and the calculated values of $\Delta_l^g C_{p,m}^o$ at T = 388 K.

Ionic Liquid	$C_{p,m}^o$ (l) / J·K^{-1}·mol^{-1}	$C_{p,m}^o$ (g) / J·K^{-1}·mol^{-1} (1)	$\Delta_l^g C_{p,m}^o$ (T = 388 K)* / J·K^{-1}·mol^{-1}
[C_2mim][NTf_2]	548.7 [3]	437.1	-112
[C_3mim][NTf_2]	-	-	-117 [a]
[C_4mim][NTf_2]	617.1 [4]	496.0	-121
[C_5mim][NTf_2]	-	-	-127 [a]
[C_6mim][NTf_2]	689.3 [2]	555.6	-134
[C_7mim][NTf_2]	-	-	-138 [a]
[C_8mim][NTf_2]	759.9 [3]	616.5	-143
[C_{10}mim][NTf_2]	-	-	-154 [a]
[C_{12}mim][NTf_2]	-	-	-165 [a]

[a] $\Delta_l^g C_{p,m}^o$ (388 K) estimated using the linear fitted function ($\Delta_l^g C_{p,m}^o$ = -5.40 n(C) - 100.47) derived from fitting of the literature data of $\Delta_l^g C_{p,m}^o$ (388 K) as a function of the cation alkyl chain length. * Uncertainty was set as 5 J·K^{-1}·mol^{-1}.

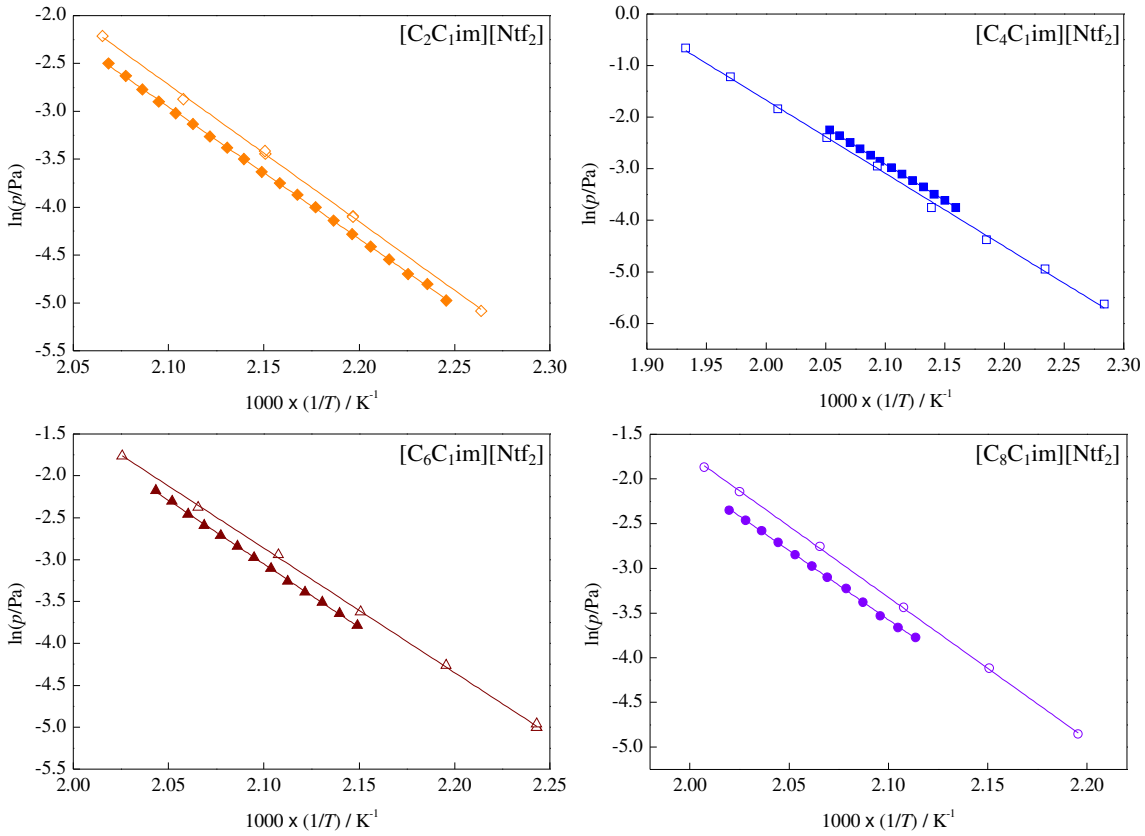

Figure S2. Plots of ln(p/Pa) = f [(1/T)/K^{-1}] for the values obtained in this work and those by Zaitsau *et al.*[5]. [C_2C_1im][Ntf_2]: ◆ - this work, ◇- Zaitsau *et al*; [C_4C_1im][Ntf_2]: ■ - this work, □- Zaitsau *et al.*; [C_6C_1im][Ntf_2]: ▲ - this work, △- Zaitsau *et al.*; [C_8C_1im][Ntf_2]: ● - this work, ○- Zaitsau *et al.*.

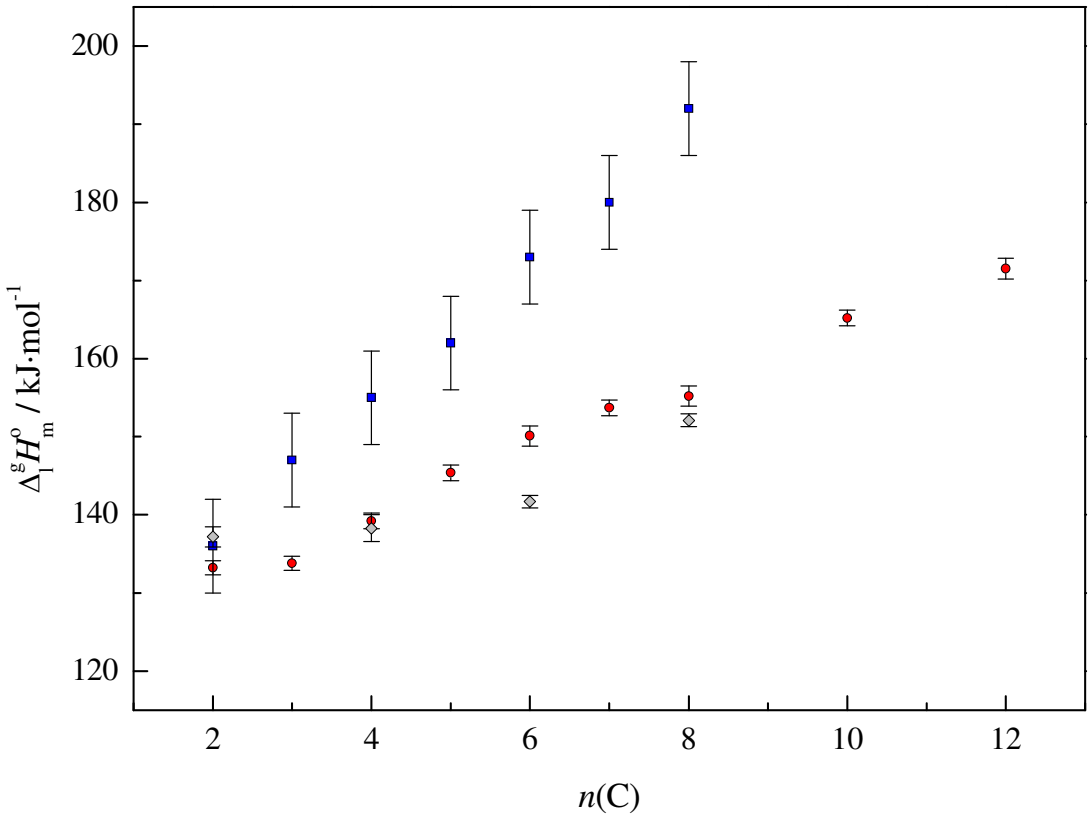

Figure S3. Comparison of the standard molar enthalpies of vaporization, at T=298.15 K, in comparison with the literature. ● - This work (Knudsen effusion / Quartz crystal microbalance method); ■ - Santos *et al.* (Calvet microcalorimetry)[6]; ◇ - Zaitsau *et al.* (Knudsen effusion method)[5].

Absolute standard molar entropies in gaseous and liquid phases:

Table S3. Values of standard molar entropies of vaporization and the absolute standard molar entropies in gaseous and liquid phases at reference temperature, T = 298.15 K. SI

Ionic Liquid	$\Delta_l^g S_m^o$ / J·K^{-1}·mol^{-1}	S_m^o(g) / J·K^{-1}·mol^{-1}	S_m^o(l) / J·K^{-1}·mol^{-1}
$[C_2C_1im][Ntf_2]$	170.0 ± 2.6	777.9 *	607.9
$[C_3C_1im][Ntf_2]$	173.4 ± 2.8	814.9[a]	641.5
$[C_4C_1im][Ntf_2]$	183.8 ± 2.6	853.8 *	670.0
$[C_5C_1im][Ntf_2]$	196.9 ± 2.8	893.0[a]	696.1
$[C_6C_1im][Ntf_2]$	206.9 ± 4.0	926.2 *	719.3
$[C_7C_1im][Ntf_2]$	213.0 ± 2.4	971.0[a]	758.0
$[C_8C_1im][Ntf_2]$	214.0 ± 3.7	1014.0 *	800.0
$[C_{10}C_1im][Ntf_2]$	231.8 ± 2.8	1088.2[a]	856.4
$[C_{12}C_1im][Ntf_2]$	242.5 ± 3.5	1166.2[a]	923.7

* reference [1];

[a] S_m^o(g) , at T = 298.15 K, calculated using the the linear fitted function (S_m^o(g) = 39.035 n(C) + 697.8)derived from fitting of the literature data of S_m^o(g) as a function of the cation alkyl chain length.

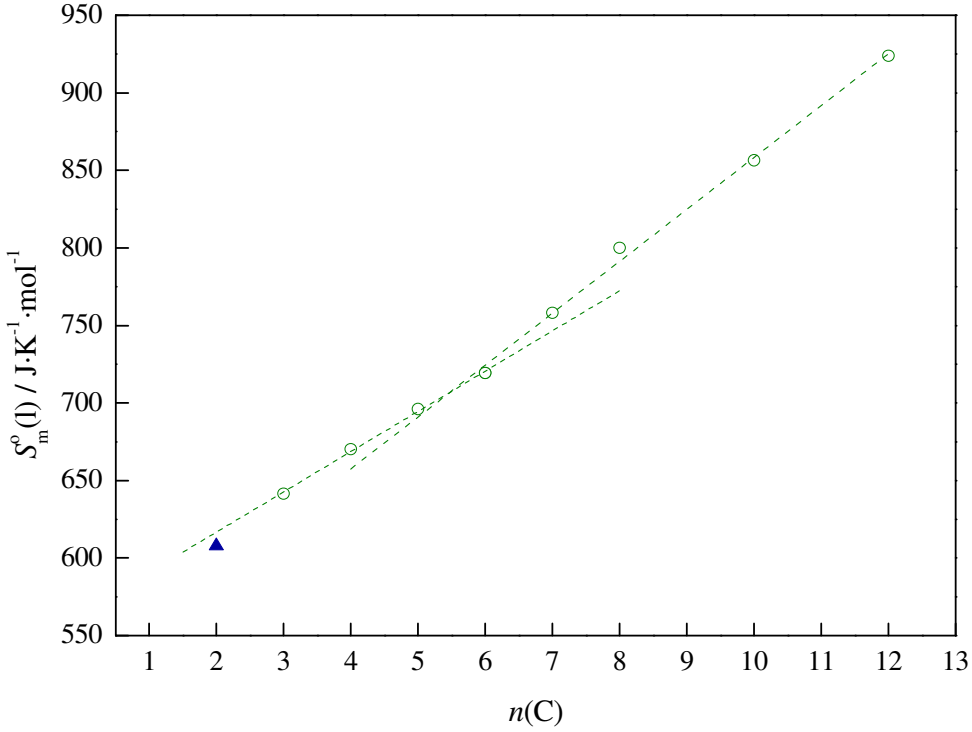

Figure S4 - Absolute standard molar entropies in liquid phase, at (T=298.15 K), as a function of the number of carbon atoms in the alkyl side chain of the cation, n(C).

Molecular Dynamics

Ionic liquids based on $[Ntf_2]^-$ exhibit particularly low viscosity, a fact attributable to the flexibility of the anion. This issue has been investigated by various authors[1,7] who have confirmed that $[Ntf_2]^-$ can exist as different interconvertible conformational isomers both as isolated ions or as constituents of ionic pairs in the gas phase or condensed ions in ionic liquids. The alkyl side chain of $[C_nC_1im]^+$ ions with n>1, can also exhibit distinct conformations, namely different preferred dihedral angles around the CR-N-C1-C2 (planar or non-planar conformations) and N-C1-C2-C3 (gauche or trans conformations) bonds.[8] The combination of these two types of flexible ions in the $[C_nC_1im][Ntf_2]$ series yields ionic liquids whose structure and energetics are dominated by complex potential energy surfaces[1,9], a fact which can explain the different trends found for the vaporization properties. The .character of $[C_2C_1im][Ntf_2]$ relative to the rest of the $[C_nC_1im][Ntf_2]$ series and the corresponding $\Delta_l^g H_m^o$ [n(C)] and $\Delta_l^g S_m^o$ [n(C)] gata presented in figures 3 and 4 can be interpreted in terms of structural modifications occurring both in the condensed and vapor phases as n(C) changes from 2 to 3. In this case the main structural alteration occurs around the CR-N-C1-C2 dihedral. Whereas in the $[C_2C_1im]^+$ cation the planar isomer represents a stable configuration (local energy minimum), in the $[C_2C_1im]^+$ and all other $[C_nC_1im]^+$ cations, the planar isomer is just a transition state. This state of affairs (observed spectroscopically[8] and corroborated by ab initio calculation[1,8,9] and molecular dynamics simulations[9]) can be observed in figure S5, which compares the distribution of conformational isomers in the condensed phase of $[C_2C_1im][Ntf_2]$ and $[C_4C_1im][Ntf_2]$. The central (red) peak corresponding to stable planar conformers in $[C_2C_1im][Ntf_2]$ is replaced by a flat region corresponding to transition states between the two non-planar conformers of $[C_4C_1im][Ntf_2]$. In other

words, only in the case of $[C_2C_1im]^+$ is it possible for (short) alkyl side chain to remain in a coplanar position with the ring. From $[C_3C_1im]^+$ onwards, the alkyl side chain (the C2 carbon) atom will begin either above or below the aromatic plane, facilitating inter-conversion between the two states. It is hard to estimate the effect of this obvious structural modification on the vaporization process. As it is an intramolecular change that can occur in both the condensed and vapor phases, the net effect may be quite small. However one can infer that the enhanced flexibility of the alkyl side chain at the C2 carbon due to the substitution of the planar peak by an interconversion plateau when one goes from $[C_2C_1im][Ntf_2]$ to $[C_3C_1im][Ntf_2]$ will ease interaction between the ions in the condensed phase. The peak/plateau substitution also indicates the possibility of a more entropic condensed phase of $[C_3C_1im][Ntf_2]$ relative to that of $[C_2C_1im][Ntf_2]$. In spite of the limitation to two stable conformers in the former ionic liquid and three in the latter, the number of intermediate transitional forms is enhanced in $[C_3C_1im][Ntf_2]$.

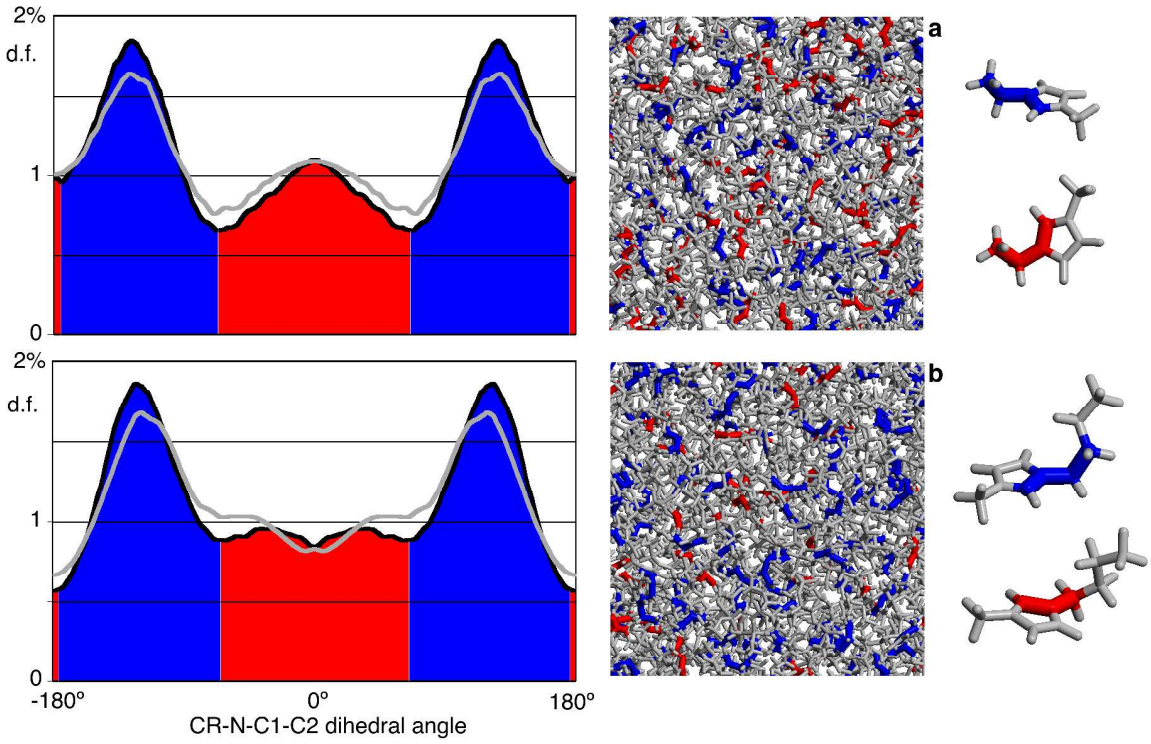

Figure S5. Probability distribution function (d.f.) of the conformational isomers of $[C_2C_1im]^+$ (top) and $[C_4C_1im]^+$ (bottom) around the CR-N-C1-C2 dihedral angle. The red and blue codes refer to isomers with planar (red) or non-planar (blue) conformations. The two snapshots are of simulated condensed phases of $[C_2C_1im][Ntf_2]$ and $[C_4C_1im][Ntf_2]$ used to calculate the distribution functions. Snapshot (b) reveals a prevalence of non-planar (blue) conformers relative to snapshot (a). The black and gray lines correspond to simulation runs performed at 303 and 343 K, respectively.

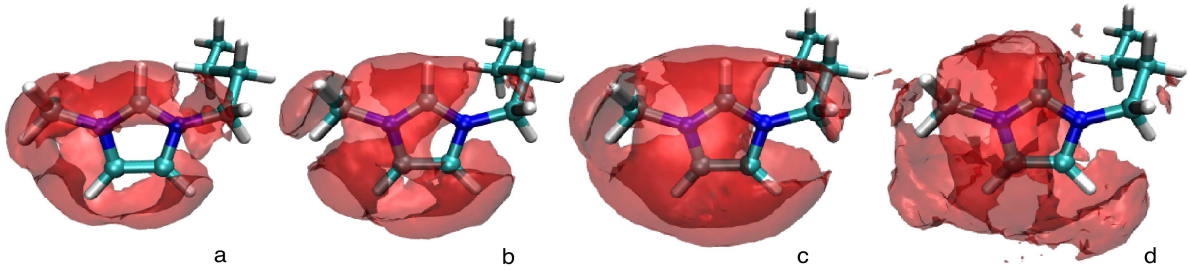

Figure S6. Spatial distribution functions of the anion center-of-mass around the $[C_4C_1im]^+$cation in the condensed phase of different $[C_4C_1im][X]$ ionic liquids. The anion size (indicated between parentheses as effective molar volumes in $cm^3 \cdot mol^{-1}$ at 298 K)[10] increases from left to right: (a) Cl^-(25.9); (b) $[BF_4]^-$ (53.4); (c) $[PF_6]^-$(73.7); (d) $[Ntf_2]^-$ (158.7).

Viscosity Data for $[C_nmim][NTf_2]$

The viscosity data available in the literature[11] was fitted using Vogel–Fulcher–Tammann (VFT) (equation 1),

$$\eta = A \times e^{B/(T-Tg)} \qquad (1)$$

where *A*, *B* and *C* are fitting parameters. Table S4, lists the fitting coefficients and the activation energy of viscosity, $\left[\frac{\partial \ln(\eta)}{\partial(1/T)}\right]$, for the ionic liquids studied in this work. [11]

Table S4. Fitting coefficients of VFT equation and the activation energy for the viscosity data available in the literature.[11]

Ionic Liquid	*A* /mPa.s	*B*	*C* / K	*E* /kJ·mol^{-1}
$[C_2mim][NTf_2]$	0.22810	692.5	158.9	26.40
$[C_3mim][NTf_2]$	0.19660	713.7	167.2	30.76
$[C_4mim][NTf_2]$	0.14880	794.7	161.8	31.59
$[C_5mim][NTf_2]$	0.12630	838.2	161.3	33.08
$[C_6mim][NTf_2]$	0.12540	855.9	163.0	34.63
$[C_7mim][NTf_2]$	0.11680	888.1	162.4	35.62
$[C_8mim][NTf_2]$	0.09972	943.3	160.2	36.64
$[C_9mim][NTf_2]$	0.09534	971	159.8	37.49
$[C_{10}mim][NTf_2]$	0.08095	1028	157.4	38.35
$[C_{12}mim][NTf_2]$	0.08497	1040	159.6	40.04

References:

(1) Paulechka, Y. U.; Kabo, G. J.; Emel'yanenko, V. N. *J. Phys. Chem. B* **2008**, *112*, 15708–15717.

(2) Blokhin, A. V.; Paulechka, Y. U.; Kabo, G. J. *J. Chem. Eng. Data* **2006**, *51*, 1377–1388.

(3) Paulechka, Y. U.; Blokhin, A. V.; Kabo, G. J.; Strechan, A. A. *J. Chem. Thermodynamics* **2007**, *39*, 866–877.

(4) Blokhin, A. V.; Paulechka, Y. U.; Strechan, A. A.; Kabo, G. J. *J. Phys. Chem. B* **2008**, *112*, 4357–4364.

(5) Zaitsau, D. H.; Kabo, G. J.; Strechan, A. A.; Paulechka, Y. U.; Tschersich, A.; Verevkin, S. P.; Heintz, A. *J. Phys. Chem. A* **2006**, *110*, 7303-7306.

(6) Santos, L. M. N. B. F.; Canongia Lopes, J. N.; Coutinho, J. A. P.; Esperança, J. M. S. S.; Gomes, L. R.; Marrucho, I. M.; Rebelo, L. P. N. *J. Am. Chem. Soc.* **2007**, *129*, 284-285.

(7) Canongia Lopes, J. N.; Shimizu, K.; Pádua, A. A. H.; Umebayashi, Y.; Fukuda, S.; Fujii, K.; Ishiguro, S.-i. *J. Phys. Chem. B* **2008**, *112*, 1465-1472.

(8) Umebayashi, Y.; Fujimori, T.; Sukizaki, T.; Asada, M.; Fujii, K.; Kanzaki, R.; Ishiguro, S.-i. *J. Phys. Chem. A* **2005**, *109*, 8976-8982.

(9) Canongia Lopes, J. N.; Pádua, A. A. H. *J. Phys. Chem. B* **2006**, *110*, 7485-7489.

(10) Rebelo, L. P. N.; Canongia Lopes, J. N.; Esperança, J. M. S. S.; Guedes, H. J. R.; Łachwa, J.; Najdanovic-Visak, V.; Visak, Z. P. *Acc. Chem. Res*. **2007**, *40*, 1114–1121.

(11) Tariq, M.; Carvalho, P. J.; Coutinho, J. A.P.; Marrucho, I. M.; Canongia Lopes, J. N.; Rebelo, L. P.N. *Fluid Phase Equilibria* **2011**, *301*, 22–32.

Paper III

"Heat Capacities at 298.15 K of the Extended [$C_nC_1$im][Ntf_2] Ionic Liquid Series"
Marisa A.A. Rocha, Margarida Bastos, João A.P. Coutinho, Luís M.N.B.F. Santos
The Journal of Chemical Thermodynamics (2012), 53, 140-143.
doi: 10.1016/j.jct.2012.04.025

Note: The author of this thesis performed the all the experimental work, data analysis and contribute to the discussion and conclusions.

J. Chem. Thermodynamics 53 (2012) 140–143

Contents lists available at SciVerse ScienceDirect

J. Chem. Thermodynamics

journal homepage: www.elsevier.com/locate/jct

Heat capacities at 298.15 K of the extended $[C_nC_1im][Ntf_2]$ ionic liquid series

Marisa A.A. Rocha [a,*], Margarida Bastos [a], João A.P. Coutinho [b], Luís M.N.B.F. Santos [a,*]

[a] Centro de Investigação em Química, Departamento de Química e Bioquímica, Faculdade de Ciências, Universidade do Porto, Rua do Campo Alegre, 687, 4169-007 Porto, Portugal
[b] CICECO, Departamento de Química, Universidade de Aveiro, Campus Santiago, 3810-193 Aveiro, Portugal

ARTICLE INFO

Article history:
Received 13 February 2012
Received in revised form 12 April 2012
Accepted 27 April 2012
Available online 8 May 2012

Keywords:
Heat capacity
Drop calorimeter
Bis(triflamide)
Ionic liquids
Imidazolium
Calorimetry
Percolation
Volumic heat capacities
Specific heat capacities
Thermophysics

ABSTRACT

High-precision heat capacities at 298.15 K of the $[C_nC_1im][Ntf_2]$ ionic liquid series were measured with an uncertainty of less than ±0.3%, using a drop heat capacity apparatus that was recently updated. The dependence of the c_p^o values on the alkyl side chain length for the extended ionic liquid series $[C_nC_1im][Ntf_2]$ (with $n = 2$ to 8, 10, and 12) displays a trend shift at $[C_6C_1im][Ntf_2]$, which is taken as an evidence for percolation limit. Above this limit there is an increase in the methylene group contribution to the molar heat capacity which is in agreement with the higher molar absolute entropies change observed from the (liquid + vapor) equilibrium results. The obtained experimental results support the model that the ionic liquids tend to be segregated into a polar network and non-polar domains, being followed by an increase of the entropy contribution of the non-polar domains.

1. Introduction

Research on ionic liquids (ILs) is growing at a very fast rate, due to their distinctive properties, such as low vapor pressure, stable liquid phase over a wide temperature range, low-flammability and thermal stability at high temperatures [1]. They are nanostructured fluids in which the ion pairs arrange themselves into polar and nonpolar domains. The structural segregation in these systems will depend on the size of the polar and nonpolar regions in each ion may exist as dispersed or continuous microphases. The transition between these two phases is related with the percolation phenomenon, and depends on the relative size of the high-charge and low-charge regions in each ion and the size of the alkyl chain length [2]. These characteristics are the basis for an increasing number of their potential applications in sensors, thermal fluids, batteries, capacitors, lubricants, ionogels, extractants and as solvents in analysis, synthesis, catalysis, and separation [3–5]. At odds with the exhaustive fundamental and applied studies on an extensive number of these systems, only few works are available in the literature providing reliable physicochemical properties for pure ILs [6,7]. For the interpretation of their properties and a successful modeling of ionic liquids, highly accurate data regarding these physicochemical properties are needed, such as heat capacities, vapor pressures, viscosities, densities, refraction index, etc. Heat capacity is one of the most important thermophysical properties of matter, since it is an important thermodynamic link between the fluid structure and dynamics. For a constant pressure process, the heat capacity, C_p, which is an extensive property, is defined as:

$$C_p = \frac{dq_p}{dT}. \quad (1)$$

The specific heat capacity, at constant pressure, is represented by c_p and is defined as the heat capacity per unit mass, or C_p/m, where m is the mass of the substance. Accordingly, the volumic heat capacity, denoted by C_p/V, is defined as the heat capacity per volume. Molar heat capacity, specific heat capacity, and volumic heat capacity are intensive properties, which is characteristic of each system and related with their structure and dynamics. Heat capacity data for a large number of aprotic ionic liquids have been published before [6]. However, a large fraction of the known data presents large uncertainties that are related to the calorimetric methods used as well as to the quality and purity of the samples.

Recently, we reported a thermodynamic study concerning the vaporization of the extended series of ILs $[C_nC_1im][Ntf_2]$ with $n = 2$ to 8, 10, and 12, where it was possible to detect important trends in the thermodynamic parameters, which would have been impossible to verify with a smaller number of ILs [8].

* Corresponding authors. Tel.: +351 220 402 836; fax: +351 220 402 659.
E-mail addresses: marisa.alexandra.rocha@gmail.com (M.A.A. Rocha), lbsantos@fc.up.pt (L.M.N.B.F. Santos).

0021-9614/$ - see front matter © 2012 Elsevier Ltd. All rights reserved.
http://dx.doi.org/10.1016/j.jct.2012.04.025

TABLE 1
Molar heat capacity values, at $T = 298.15$ K, for the studied ionic liquids. Calibration constant of the drop calorimeter used in the heat capacity calculation ($6.6329 \pm 0.0046\ W \cdot V^{-1}$).

Ionic liquid	$M/(g \cdot mol^{-1})$	N_{drop}	$C^o_{p,m}/(J \cdot K^{-1} \cdot mol^{-1})$
$[C_2C_1im][Ntf_2]$	391.313	10	504.8 ± 1.2
$[C_3C_1im][Ntf_2]$	405.340	13	534.9 ± 0.5
$[C_4C_1im][Ntf_2]$	419.366	10	565.9 ± 0.6
$[C_5C_1im][Ntf_2]$	433.393	17	595.6 ± 0.5
$[C_6C_1im][Ntf_2]$	447.420	15	629.4 ± 1.2
$[C_7C_1im][Ntf_2]$	461.446	16	659.2 ± 0.7
$[C_8C_1im][Ntf_2]$	475.473	6	690.2 ± 0.7
$[C_{10}C_1im][Ntf_2]$	503.526	18	754.5 ± 0.9
$[C_{12}C_1im][Ntf_2]$	531.580	18	820.2 ± 0.9

N_{drop} = number of drop experiments; for the $[C_nC_1im][Ntf_2]$, with $n = 3$, 5, 6, 7, 10, and 12, the number of drops are the sum of the drops that were obtained in two independent experiments.

In order to evaluate the linearity in the heat capacity of the $[C_nC_1im][Ntf_2]$ ionic liquid series as a function of the alkyl side chain length in the cation and any possible shift that could be related with the percolation phenomenon [2,8], high precision heat capacity data at $T = 298.15$ K have been measured, for the extended alkyl series (odd and even). The heat capacities of the nine ILs were measured by means of a high-precision heat capacity drop calorimeter developed by Wadsö [9,10] and recently modernized at our laboratory [11]. The quality of the heat capacity data, is comparable, in accuracy, with the best literature data measured by adiabatic calorimetry [12–17]. The observed subtle changes in the heat capacity with the length of the cation alkyl side chain was only possible due to the high precision of the heat capacity drop calorimeter.

2. Experimental section

The 1-alkyl-3-methylimidazolium bis(trifluoromethylsulfonyl)imide series, $[C_nC_1im][Ntf_2]$ ($n = 2$ to 8, 10, and 12), used in this work, were purchased from IOLITEC with a stated purity of better than 99%. All ionic liquids were dried under reduced pressure (<10 Pa) and stirred constantly for a minimum of 48 h at 373 K, in order to reduce the presence of water or other volatile contents. Karl Fischer titration of the degassed samples revealed less than 100 ppm of water.

2.1. High-precision heat capacity drop calorimeter

The heat capacities at 298.15 K of $[C_nC_1im][Ntf_2]$ were measured by a high-precision heat capacity drop calorimeter, developed by Wadsö [9,10] at the Thermochemistry Laboratory, Lund, Sweden, being afterwards transferred to Porto, Portugal, where its temperature sensors and electronics were modernized to enable the use of computer data acquisition in a user-friendly environment [11]. The apparatus comprises two main parts: the furnace and the receiving calorimeter. The receiving calorimeter consists in a twin heat conduction calorimeter of the type used in Lund's instruments. The furnace temperature was 303.15 K and the receiving calorimeter was kept at 293.15 K. The twin calorimeter measures the heat exchange resulting from the ampoule cooling from the initial temperature ($T_i = 303.15$ K) to the final temperature ($T_f = 293.15$ K). For the calculation of the heat capacities, the apparatus calibration constant was derived from the sapphire and water calibrations, and the value ($6.6329 \pm 0.0046\ W \cdot V^{-1}$) was used. The accuracy of the apparatus for the measurements of the heat capacities for liquids and solids was evaluated before, based on the measurements of benzoic acid and hexafluorobenzene [11]. Since the calorimeter was now used to measure the heat capacity of ionic liquids, the accuracy was additionally checked on the basis of the results obtained for $[C_6C_1im][Ntf_2]$ [18]. The determined $C^o_{p,m}$ ($[C_6C_1im][Ntf_2]$, 298.15 K) = $(629.4 \pm 1.2)\ J \cdot K^{-1} \cdot mol^{-1}$ was obtained from the average of two independent experimental runs, using different ampoules, and is in excellent agreement with the recommended value, $C^o_{p,m}$ ($[C_6C_1im][Ntf_2]$, 298.15 K) = $(631.6 \pm 1.3)\ J \cdot K^{-1} \cdot mol^{-1}$ [18].

The relative atomic masses used were those recommended by the IUPAC Commission in 2007 [19]. The molar masses, M ($g \cdot mol^{-1}$), number of drop experiments, N_{drop}, and molar heat capacities at 298.15 K, $C^o_{p,m}$ ($J \cdot K^{-1} \cdot mol^{-1}$), for each studied ionic liquid are presented in table 1. The masses of the samples were corrected for the buoyancy effect, and it was done both for calibration and experiments of ionic liquids. The reported uncertainty is the twice of the standard deviation of the mean and includes the calibration uncertainty.

3. Results and discussion

Table 2 presents heat capacity data for the studied ionic liquids at $T = 298.15$ K, together with available literature values. The volumic heat capacities (C^o_p/V) were calculated from the determined specific heat capacities, c^o_p, and the available experimental density values published by Tariq *et al.* [20]. The literature data for the molar heat capacities ($C^o_{p,m}$) here considered for comparison were obtained by adiabatic calorimetry [12–17]. The heat capacities of the studied ILs were measured with an uncertainty of less than ±0.3%

TABLE 2
Derived heat capacity results at $T = 298.15$ K, for each ionic liquid, together with selected literature data.

Ionic liquid	$c^o_p/(J \cdot K^{-1} \cdot g^{-1})$	$C^o_p/V/(J \cdot K^{-1} \cdot cm^{-3})$	$C^o_{p,m}/(J \cdot K^{-1} \cdot mol^{-1})$	$C^o_{p,m}/(J \cdot K^{-1} \cdot mol^{-1})$
	This work			Literature
$[C_2C_1im][Ntf_2]$	1.2900 ± 0.0031	1.9608 ± 0.0047	504.8 ± 1.2	506.5 ± 0.5 [14] 505.7 ± 2.0 [16]
$[C_3C_1im][Ntf_2]$	1.3197 ± 0.0013	1.9473 ± 0.0019	534.9 ± 0.5	
$[C_4C_1im][Ntf_2]$	1.3494 ± 0.0015	1.9399 ± 0.0022	565.9 ± 0.6	565.4 ± 1.1 [13] 564.1 ± 1.1 [14] 565.1 ± 2.3 [17]
$[C_5C_1im][Ntf_2]$	1.3743 ± 0.0012	1.9286 ± 0.0017	595.6 ± 0.5	
$[C_6C_1im][Ntf_2]$	1.4067 ± 0.0026	1.9321 ± 0.0036	629.4 ± 1.2	631.6 ± 0.6 [12] 629.2 ± 2.5 [15] 631.6 ± 1.3 [18]
$[C_7C_1im][Ntf_2]$	1.4286 ± 0.0015	1.9215 ± 0.0020	659.2 ± 0.7	
$[C_8C_1im][Ntf_2]$	1.4515 ± 0.0015	1.9189 ± 0.0020	690.2 ± 0.7	692.7 ± 2.8 [16]
$[C_{10}C_1im][Ntf_2]$	1.4984 ± 0.0018	1.9187 ± 0.0023	754.5 ± 0.9	
$[C_{12}C_1im][Ntf_2]$	1.5429 ± 0.0018	1.9212 ± 0.0022	820.2 ± 0.9	

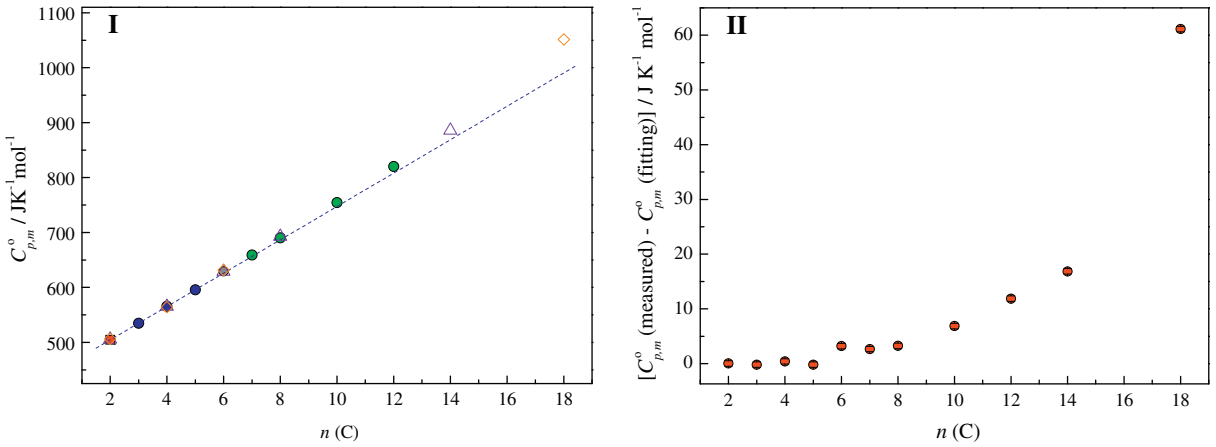

FIGURE 1. Molar heat capacities as a function of the number of carbon atoms in the alkyl side chain of the cation (I); deviation of the $C^o_{p,m}$ (fitting [C_3C_1im][Ntf_2]–[C_5C_1im][Ntf_2]) from the $C^o_{p,m}$ (measured) as a function of the number of carbon atoms in the alkyl side chain of the cation (II). This work: ■, [C_2C_1im][Ntf_2]; ●, [C_3C_1im][Ntf_2]–[C_5C_1im][Ntf_2]; and ●, [C_6C_1im][Ntf_2]–[$C_{14}C_1$im][Ntf_2]. Literature data: ◇ – [$C_nC_1$im][Ntf_2], n = 2, 4, 6, 8, 14 [15–17,23] and △ – [$C_nC_1$im][Ntf_2], n = 2, 4, 6, 18 [12–14].

and the obtained results differ less than 0.4%, from the literature data which is considered in the field an excellent agreement.

Figure 1(I) shows the representation of the molar heat capacity data ($C^o_{p,m}$) against the number of carbon atoms in the alkyl side chain, n(C), of the cation. Figure 1(II) shows the deviation plot derived from the fitting of the data for [C_3C_1im][Ntf_2] to [C_5C_1im][Ntf_2]. An apparent linearity along the IL series is shown in the representation of $C^o_{p,m}$ against the n(C). However, when considering the deviation plot from the line representing the lower members of the series as shown in figure 1(II), we can observe a strong indication of a trend shift starting from [C_6C_1im][Ntf_2], in the direction of higher molar heat capacities. This finding is an indication for an increase of the methylene group, –CH_2–, contribution to the heat capacity after n(C) = 6. Despite the excellent agreement between the data obtained in this work and the available in the literature, the fact that before only six ILs (even numbered carbons, n = 2, 4, 6, 8, 14, and 18) of these series were studied [12–17] prevented the detection of the trend shift as found now in this work. The trend shift starting from n(C) = 6 is in agreement with the findings reported on the study of the (liquid + vapor) equilibrium for the extended series of [$C_nC_1$im][Ntf_2], recently published [8]. The reported trend shift found previously in the enthalpies and entropies of vaporization was related with the structural modifications that occur when the number of alkyl carbon atoms nears six, which corresponds to a kind of limit of the polar network regions and the formation of a continuous non-polar domains. The observed higher –CH_2– contribution to the molar heat capacity obtained, also after [C_6C_1im][Ntf_2], is in line with the higher liquid entropy, as well as with the trend shift in the viscosity that was observed for the liquid phase after the limit, n(C) = 6 [8]. The limit at n(C) = 6 is also clearly revealed from the trend of the volumic enthalpies of vaporization, $\Delta^g_l h^o_V$, (derived from literature data [8]) against the n(C) presented in figure 2.

The [C_2C_1im][Ntf_2] shows the highest volumic enthalpies of vaporization in the series, that we relate with its outlier character in the series, due to the proximity of the methylene group to the imidazolium ring, leading to higher density and stronger electrostatic interactions for this IL. From [C_3C_1im][Ntf_2] to [C_6C_1im][Ntf_2], a constant value in the volumic enthalpies of vaporization is observed. This can be explained as the result of a balance between the decrease in density [20] and the increase in specific enthalpies of vaporization per –CH_2– group [8]. The limit at n(C) = 6 is clearly observed in figure 2, together with a trend shift in the direction of lower volumic enthalpies of vaporization. The gradual decrease of the volumic enthalpies of vaporization after n(C) = 6, besides being an evidence for the percolation phenomenon in ionic liquids, it is also in agreement with the expected decrease of the volumic cohesive enthalpies. This decrease arises from the decrease of the electrostatic interactions due to the formation of a larger continuous non-polar domain, and the decrease of the density.

Figure 3 presents the plots of the specific heat capacity (I) and the volumic heat capacity (II) against the number of carbon atoms in the alkyl side chain of the cation. A subtle trend shift at n(C) = 6 in the specific heat capacity is clearly evidenced. There is a gradual increase in the c^o_p along the alkyl side chain of cation, that is explained by an increase in the contribution of the alkyl fraction to the heat capacity of the ionic liquid, which has a higher specific heat capacity (typical value for alkanes is 2.2 $J \cdot K^{-1} \cdot g^{-1}$) [21].

The volumic heat capacity plot, instead of the constant value previously postulated [22,23] shows from [C_2C_1im][Ntf_2] to [C_5C_1im][Ntf_2] a gradual decrease in C^o_p/V, that reaches a constant value of 1.92 $J \cdot K^{-1} \cdot cm^{-3}$ in [C_7C_1im][Ntf_2] to [$C_{12}C_1$im][Ntf_2], showing a clear trend shift in this thermophysical property at [C_6C_1im][Ntf_2], in agreement with recent observations concerning the enthalpies and entropies of vaporization, and viscosities, as referred above [8]. The decrease in C^o_p/V from [C_2C_1im][Ntf_2] to [C_5C_1im][Ntf_2] is mainly due to the decrease of the ionic liquid den-

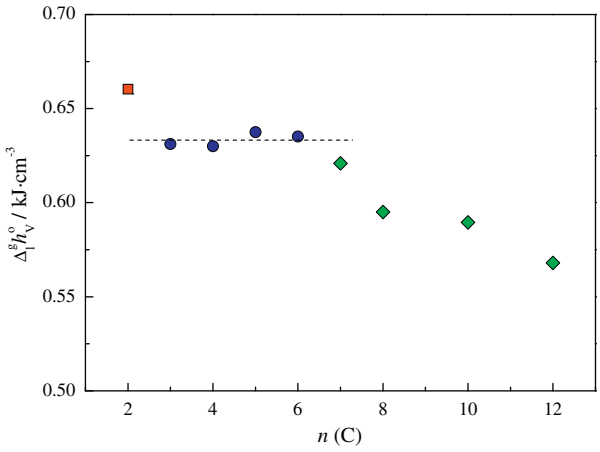

FIGURE 2. Volumic enthalpies of vaporization, $\Delta^g_l h^o_V$, as a function of the number of carbon atoms in the alkyl side chain of 1-alkyl-3-methylimidazolium bis(trifluoromethylsulfonyl)imide series, [$C_nC_1$im][Ntf_2] (n = 2 to 8, 10, and 12). ■, [C_2C_1im][Ntf_2]; ●, [C_3C_1im][Ntf_2]–[C_6C_1im][Ntf_2]; and ●, [C_7C_1im][Ntf_2]–[$C_{12}C_1$im][Ntf_2].

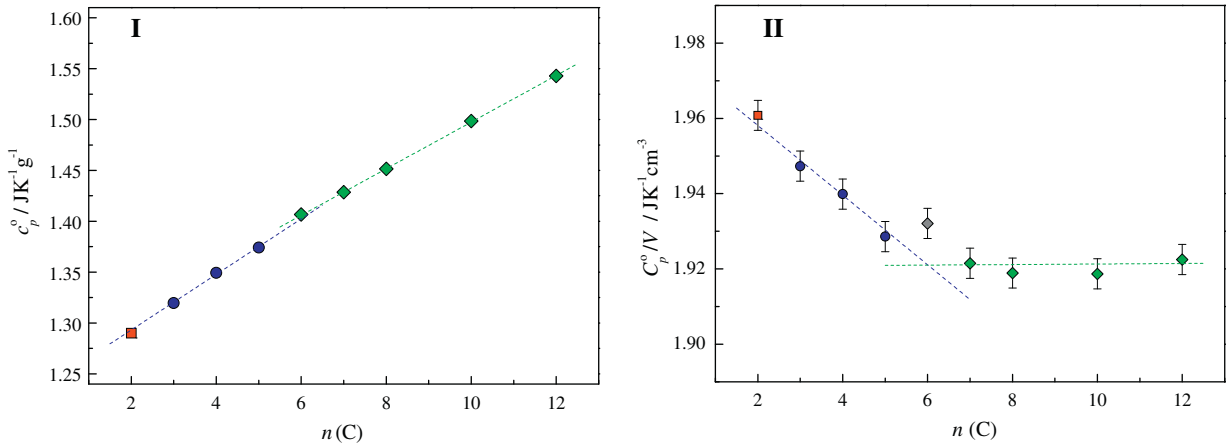

FIGURE 3. Specific heat capacities as a function of the number of carbon atoms in the alkyl side chain of the cation (I); volumic heat capacities as a function of the number of carbon atoms in the alkyl side chain of the cation (II). ■, [C_2C_1im][Ntf_2]; ●, [C_3C_1im][Ntf_2]–[C_5C_1im][Ntf_2]; and ●, [C_6C_1im][Ntf_2]–[$C_{12}C_1$im][Ntf_2].

sity along the series [20]. The constant value observed in C_p^o/V from [C_7C_1im][Ntf_2] to [$C_{12}C_1$im][Ntf_2], could be the result of a balance between the decrease in density and the increase in volumic heat capacity per $-CH_2-$ group. If we take this together with the decrease of the volumic cohesive enthalpy in this region, reflected in the decrease of $\Delta_l^g h_V^o$ (figure 2), one is led to the conclusion that the two phenomena must have the same origin, *i.e.*, the balance between electrostatic and non-polar interactions as the alkyl chain in the IL increases after n(C) = 6.

Finally we would like to stress the fact that the trend shift is much clearer when we use the heat capacities or the enthalpies of vaporization on a volumetric basis. This reflects the fact that the trends discussed here in these properties are related to the cohesive strength/energy in the liquid.

4. Final remarks

The heat capacities at 298.15 K of the [$C_nC_1$im][Ntf_2] ionic liquid series were measured with an uncertainty of less than ±0.3%. A trend shift in the heat capacities with the cation alkyl chain length starting at n(C) = 6 was found, providing and additional experimental evidence for the percolation phenomenon in ionic liquids and its impact on their thermophysical properties.

The recently proposed schematic model [8] of the two molecular regions for the [$C_nC_1$im][Ntf_2] ionic liquids and their different contribution to the thermodynamic properties gives a strong contribution for the interpretation of the percolation phenomenon after a critical number of carbons in the chain and is also supported by the experimental results obtained in this work. Above this limit there is an increase in the methylene group contribution to the molar heat capacity, in agreement with the higher molar absolute entropies change observed from the (liquid + vapor) equilibrium results, as well as the trend shift observed in the viscosity measurements of these compounds.

Acknowledgements

Thanks are due to Fundação para a Ciência e Tecnologia (FCT), Lisbon, Portugal and to FEDER for financial support to Centro de Investigação em Química, University of Porto. Marisa A.A. Rocha acknowledges the financial support from FCT and the European Social Fund (ESF) under the Community Support Framework (CSF) for the award of a Research Grants SFRH/BD/60513/2009. Thanks are also due to FCT for financial support for the project PTDC/CTM/103664/2008.

References

[1] P. Wasserscheid, T. Welton (Eds.), Ionic Liquids in Synthesis, Wiley-VCH, Weinheim, 2003.
[2] K. Shimizu, M.F.C. Gomes, A.A.H. Pádua, L.P.N. Rebelo, J.N. Canongia Lopes, J. Mol. Struct. – THEOCHEM 946 (2010) 70–76.
[3] H. Olivier-Bourbigou, L. Magna, D. Morvan, Appl. Catal. A: Gen. 373 (2010) 1–56.
[4] G. Quijano, A. Courvert, A. Amrane, Bioresource Technol. 101 (2010) 8923–8930.
[5] T.E. Sutto, T.T. Duncan, T.C. Wong, K. McGrady, Electrochim. Acta 56 (2011) 3375–3379.
[6] Y.U. Paulechka, J. Phys. Chem. Ref. Data 39 (2010) 033108.
[7] J.M.S.S. Esperança, J.N. Canongia Lopes, M. Tariq, L.M.N.B.F. Santos, J.W. Magee, L.P.N. Rebelo, J. Chem. Eng. Data 55 (2010) 3–12.
[8] M.A.A. Rocha, C.F.R.A.C. Lima, L.R. Gomes, B. Schröder, J.A.P. Coutinho, I.M. Marrucho, J.M.S.S. Esperança, L.P.N. Rebelo, K. Shimizu, J.N. Canongia Lopes, L.M.N.B.F. Santos, J. Phys. Chem. B 115 (2011) 10919–10926.
[9] J. Konicek, J. Suurkuusk, I. Wadsö, Chem. Scr. 1 (1971) 217–220.
[10] J. Suurkuusk, I. Wadsö, J. Chem. Thermodyn. 6 (1974) 667–679.
[11] L.M.N.B.F. Santos, M.A.A. Rocha, A.S.M.C. Rodrigues, V. Štejfa, M. Fulem, M. Bastos, J. Chem. Thermodyn. 43 (2011) 1818–1823.
[12] Y. Shimizu, Y. Ohte, Y. Yamamura, K. Saito, T. Atake, J. Phys. Chem. B 110 (2006) 13970–13975.
[13] Y. Shimizu, Y. Ohte, Y. Yamamura, K. Saito, Chem. Lett. 36 (2007) 1484–1485.
[14] Y. Shimizu, Y. Ohte, Y. Yamamura, K. Saito, Chem. Phys. Lett. 470 (2009) 295–299.
[15] A.V. Blokhin, Y.U. Paulechka, G.J. Kabo, J. Chem. Eng. Data 51 (2006) 1377–1388.
[16] Y.U. Paulechka, A.V. Blokhin, G.J. Kabo, A.A. Strechan, J. Chem. Thermodyn. 39 (2007) 866–877.
[17] A.V. Blokhin, Y.U. Paulechka, A.A. Strechan, G.J. Kabo, J. Phys. Chem. B 112 (2008) 4357–4364.
[18] R.D. Chirico, V. Diky, J.W. Magee, M. Frenkel, K.N. Marsh, Pure Appl. Chem. 81 (2009) 791–828.
[19] M.E. Wieser, M. Berglund, Pure Appl. Chem. 81 (2009) 2131–2156.
[20] M. Tariq, A.P. Serro, J.L. Mata, B. Saramago, J.M.S.S. Esperança, J.N. Canongia Lopes, L.P.N. Rebelo, Fluid Phase Equilib. 294 (2010) 131–138.
[21] D. Huang, S.L. Simon, G.B. McKenna, J. Chem. Phys. 122 (2005) 084907.
[22] R.L. Gardas, J.A.P. Coutinho, Ind. Eng. Chem. Res. 47 (2008) 5751–5757.
[23] Y.U. Paulechka, A.G. Kabo, A.V. Blokhin, G.J. Kabo, M.P. Shevelyova, J. Chem. Eng. Data 55 (2010) 2719–2724.

Paper IV

"The Cation Symmetry Effect on the Volatility of Ionic Liquids"
Marisa A.A. Rocha, João A.P. Coutinho, Luís M.N.B.F. Santos
Journal of Physical Chemistry B (2012), 116, 10922–10927.
doi: 10.1021/jp306937f

Note: The author of this thesis performed the all the experimental work, data analysis and contribute to the discussion and conclusions.

THE JOURNAL OF PHYSICAL CHEMISTRY B

Article

pubs.acs.org/JPCB

Cation Symmetry effect on the Volatility of Ionic Liquids

Marisa A. A. Rocha,*[,†] João A. P. Coutinho,[‡] and Luís M. N. B. F. Santos*[,†]

[†]Centro de Investigação em Química, Departamento de Química e Bioquímica, Faculdade de Ciências, Universidade do Porto, Rua do Campo Alegre, 687, 4169-007 Porto, Portugal

[‡]CICECO, Departamento de Química, Universidade de Aveiro, 3810-193 Aveiro, Portugal

Supporting Information

ABSTRACT: This work reports the first data for the vapor pressures at several temperatures of the ionic liquids, $[C_{N/2}C_{N/2}im][NTf_2]$ (N = 4, 6, 8, 10, 12) measured using a Knudsen effusion apparatus combined with a quartz crystal microbalance. The morphology and the thermodynamic parameters of vaporization derived from the vapor pressures, are compared with those for the 1-alkyl-3-methylimidazolium bis-(trifluoromethylsulfonyl)imide series, $[C_{N-1}C_1im][NTf_2]$ (N = 3 − 9, 11, and 13). It was found that the volatility of $[C_{N/2}C_{N/2}im][NTf_2]$ series is significantly higher than the asymmetric cation ILs with the same total number of carbons in the alkyl side chains, $[C_{N-1}C_1im][NTf_2]$. The observed higher volatility is related with the lower enthalpy of vaporization. The symmetric cation, $[C_{N/2}C_{N/2}im][NTf_2]$, presents lower entropies of vaporization compared with the asymmetric $[C_{N-1}C_1im][NTf_2]$, indicating an increase of the absolute liquid entropy in the symmetric cation ILs, being a reflection of a change of the ion dynamics in the IL liquid phase. Moreover both the enthalpy and entropy of vaporization of the $[C_{N/2}C_{N/2}im][NTf_2]$ ILs, present a clear odd−even effect with higher enthalpies/entropies of vaporization for the odd number of carbons in each alkyl chain ($[C_3C_3im][NTf_2]$ and $[C_5C_5im][NTf_2]$).

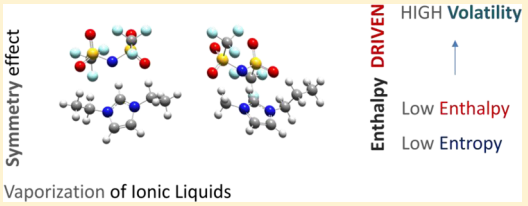

1. INTRODUCTION

Since 2001, room temperature ionic liquids, RTILs, have gained popularity, mainly because of their particular properties.[1] The research in these systems have been performed in a fundamental and applied way, contributing to a better understanding at a molecular level and consequently to an advance in the applied field of the ionic liquids.[2−5] For the interpretation of their properties and a successful modeling of ionic liquids, highly accurate data regarding these physicochemical properties are needed, such as heat capacities, vapor pressures, viscosities, densities, refractive index, etc.

Volatility of ionic liquids has been a topic of several studies, to determine their vapor pressures or enthalpies of vaporization with accuracy. Accurate thermodynamic parameters, of liquid−vapor equilibrium, are not only important to provide information on the liquid phase structure and cohesive energy, and the nature of the vapor phase, but are also essential to validate force-fields models used in several simulation techniques to describe ionic liquids.[2,3]

Earle et al. reported the first measurements of the volatility of some ILs, showing that many ionic liquids can be distilled at low pressure without decomposition.[6] Since then, a number of works addressing vapor pressure measurements and measurements/predictions of enthalpies of vaporization have emerged. Several approaches to measuring and predicting these quantities have been proposed, including molecular dynamics simulations.[7] Experimental determinations have been carried out by the integral Knudsen effusion method,[8,9] Knudsen effusion method combined with a quartz crystal microbalance,[10] quartz crystal microbalance method,[11] transpiration method,[12] mass spectrometry,[13−16] vacuum vaporization drop microcalorimetry,[17] and thermogravimetry.[18]

Recently, we reported a thermodynamic study concerning the vaporization of the extended series of ILs $[C_{N-1}C_1im][NTf_2]$ (with N = 3−9, 11, and 13), where the trends of the thermodynamic parameters of vaporization with the alkyl chain length were established.[10] In this work it was shown that the enthalpy and entropy of vaporization presented trend shifts along the $[C_{N-1}C_1im][NTf_2]$ series, related to a change in the molecular structure of the liquid phase around $[C_6C_1im][NTf_2]$.[10,19] It is well-known today that ILs are nanostructured fluids in which the ion pairs arrange themselves into polar and nonpolar domains. The structural segregation on these systems will depend on the size of the polar and nonpolar regions in each ion may exist as dispersed or continuous microphases. The transition between these two states depends on the relative size of the high-charge and low-charge regions in each ion and the size of the alkyl chain length.[19] In this previous work, it was possible to highlight the effect of the nanoscale-organization of $[C_{N-1}C_1im][NTf_2]$ family, on the thermodynamic properties of vaporization and viscosity.[10,20] On another recent work by us the effect of the nanoscale-organization on the heat capacities was also presented.[21]

The symmetry of the cation provides a different structural organization which can be used to tune the physicochemical properties of the ionic liquids. Xiao et al.,[22] based on small-

Received: July 12, 2012
Revised: August 2, 2012
Published: August 8, 2012

wide-angle X-ray scattering (SWAXS) data and optical Kerr effect (OKE) spectra, found that the symmetric ILs series, $[C_{N/2}C_{N/2}im][NTf_2]$, presents higher local order and higher intermolecular dynamics in frequency than the asymmetric series, $[C_{N-1}C_1im][NTf_2]$. SWAXS measurements provide information related with the structural heterogeneities in ILs. On the basis of this data, Zheng et al.[23] found that, for the asymmetric imidazolium based ILs, the structural heterogeneities take place over a large spatial scale, comparing with the results obtained for the symmetric ILs. In the same work, the authors observed that the densities for a symmetric/asymmetric IL pair, with a given total number carbons, are similar and the viscosity of the asymmetric IL is greater than the observed for the symmetric ILs. Also, it was observed an odd−even effect on the viscosity data, similar to what it was found in simulations of the ion diffusion coefficients.

In the present work, the thermodynamic properties of vaporization of 1,3-dialkylimidazolium bis-(trifluoromethylsulfonyl)imide series, $[C_{N/2}C_{N/2}im][NTf_2]$ (N = 4, 6, 8, 10, 12) are compared to those of 1-alkyl-3-methylimidazolium bis(trifluoromethylsulfonyl)imide series, $[C_{N-1}C_1im][NTf_2]$ (N = 3 − 9, 11 and 13). The vapor pressures at several temperatures of the ILs series, $[C_{N/2}C_{N/2}im][NTf_2]$, were measured by the Knudsen effusion apparatus combined with a quartz crystal microbalance.[24] Based on the previous results, the standard molar enthalpies, entropies and Gibbs energies of vaporization were derived at the reference temperature, T = 298.15 K. This work aims to explore the enthalpic and entropic contribution to the volatility of the symmetric $[C_{N/2}C_{N/2}im][NTf_2]$ and to assess the effect of the cation topological symmetry on the liquid−vapor equilibrium. The schematic representation of the considered imidazolium based ionic liquids, are presented in Figure 1.

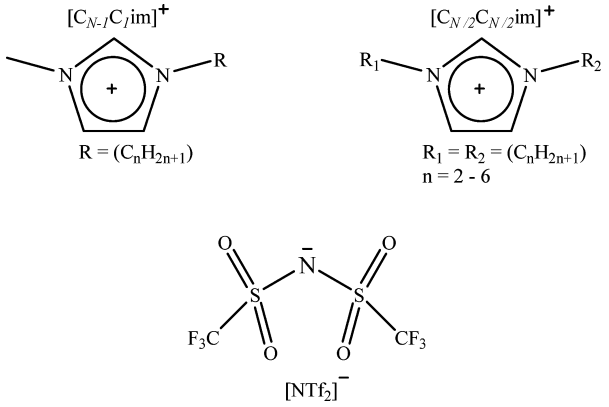

Figure 1. Schematic representation of the imidazolium based ionic liquids, where N corresponds to the total number of carbons in the two alkyl side chains in the cation.

2. EXPERIMENTAL SECTION

2.1. Purification and Characterization of Compounds. The ionic liquids used in this work, the 1,3-dialkylimidazolium bis(trifluoromethylsulfonyl)imide series, $[C_{N/2}C_{N/2}im][NTf_2]$ (N = 4, 6, 8, 10, 12), were purchased from IOLITEC with a stated purity of better than 98%. All the ionic liquids were dried under reduced pressure (<10 Pa) and stirred constantly for a minimum of 72 h at 373 K, in order to reduce the presence of water or other volatile contents. Karl Fischer titration of the degassed samples revealed less than 100 ppm of water. The purity of each ionic liquid after purification was further evaluated by ^{1}H, ^{13}C, and ^{19}F NMR spectra and for all ionic liquids the mass fraction was found to be >0.99.

2.2. Quartz Crystal Microbalance Knudsen Effusion Apparatus. The vapor pressure of each ionic liquid was measured as a function of temperature using a new Knudsen effusion apparatus combined with a quartz crystal microbalance, KEQCM, recently described in the literature.[24] This apparatus comprises two mass loss detection techniques, gravimetric, and quartz crystal microbalance, which enables the decrease of effusion times and the sample size. Furthermore the combination of two mass loss determination techniques permits the instrument to measure vapor pressures from 0.005 Pa up to 1 Pa. For the measurements of pressures below 0.01 Pa, a flow-concentrator device, placed between the oven and the quartz crystal, was used.[25] The temperature step effusion procedure allows for vapor pressure measurements at different temperatures in a single experiment and it can reach temperatures up to 650 K. The temperature is controlled within a temperature fluctuation of $\pm$ (1×10^{-2}) K, measured with a resolution better than 1×10^{-3} K and with an overall uncertainty better than $\pm$ (2×10^{-2}) K along the entire working temperature range. The vapor pressure data obtained with this apparatus for the ionic liquid samples, presents a pressure dependent uncertainty between (1 and 5) %, that is the typical uncertainty obtained in this apparatus using this methodology.[24] Due to the low volatility of the ionic liquids, the vapor pressure range under 0.05 Pa was explored in some cases, but below this pressure and for a particular individual experimental point, the relative uncertainty increases dramatically exceeding the indicated interval. The claimed uncertainty is done based on the overall results obtained from the fitting of the Clarke and Glew equation and is valid for the middle of the experimental pT region.

Like a typical Knudsen effusion experiment, the system is kept at high vacuum, allowing free effusion of the vapor from the cell, and at a fixed temperature, T. During an effusion experiment, the mass loss rate from the effusion cell, dm (cell)/dt, is proportional to the rate of change of the mass deposited on the quartz crystal, dm/dt, according to eq 1

$$\frac{dm(\text{cell})}{dt} = -g \times \frac{dm}{dt} = -g \times \frac{A_q}{S_q} \times \left(\frac{df}{dt}\right) \quad (1)$$

where g is a geometric factor of the mass detection, A_q is the area of the quartz crystal, S_q is the mass sensitivity of the crystal, and (df/dt) is the rate of change of the resonance frequency of the quartz crystal. Taking into account that

$$W = -\frac{S_q}{A_q \times g} \quad (2)$$

where, W, is the effective mass sensitivity coefficient, the eq 1 becomes

$$\left(\frac{df}{dt}\right) = W \times \left(\frac{dm(\text{cell})}{dt}\right) \quad (3)$$

To derive the vapor pressure, the value, W, must be known for each studied compound. The value can be determined by weighing the total mass loss of the effusion cell, Δm(cell), during an independent experiment, and considering the integrated form of the eq 3

dx.doi.org/10.1021/jp306937f | J. Phys. Chem. B 2012, 116, 10922−10927

$$W = \frac{\Delta f}{\Delta m(\text{cell})} \tag{4}$$

where Δf is the total change in the crystal's resonance frequency during the experiment.

The equilibrium vapor pressure of the liquid compound is obtained using the following eq 5:

$$p = \left(\frac{df}{dt}\right) \times \left(\frac{1}{w_o A_o W}\right) \times \left(\frac{2\pi RT}{M}\right)^{1/2} \tag{5}$$

where M is the molar mass of the sample, R is the gas constant (R = 8.3144621 J·K^{-1}·mol^{-1}), A_o is the area of the orifice, and w_o is the transmission probability factor (w_o= {1 + (l/2r)}$^{-1}$). The relative atomic masses used were those recommended by the IUPAC Commission in 2007.[26]

3. RESULTS AND DISCUSSION

The vapor pressures for the studied imidazolium based ionic liquids ([$C_{N/2}C_{N/2}$im][NTf_2], N = 4, 6, 8, 10, 12), were measured at several temperatures, using the Knudsen effusion apparatus combined with a quartz crystal microbalance. The experimental vapor pressures data for each IL, are listed in Table S1 of the Supporting Information.

Figure 2, presents the ln(p/Pa) = f(K/T) plots for the experimental results obtained for the studied ILs.

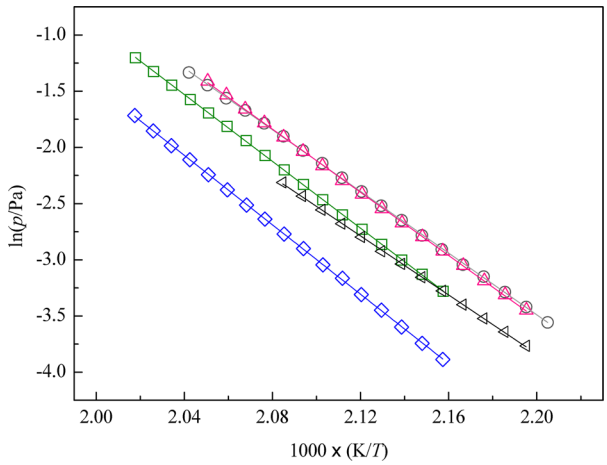

Figure 2. Plot of ln(p/Pa) = f (K/T) for each studied ionic liquid: black triangle, [C_2C_2im][NTf_2]; gray circle, [C_3C_3im][NTf_2]; pink triangle, [C_4C_4im][NTf_2]; green square, [C_5C_5im][NTf_2]; blue diamond, [C_6C_6im][NTf_2].

The experimental results of the vapor pressures were fitted by the Clarke and Glew eq 6[27]

$$R \ln \frac{p}{p^o} = -\frac{\Delta_l^g G_m^o(\theta)}{\theta} + \Delta_l^g H_m^o(\theta)\left(\frac{1}{\theta} - \frac{1}{T}\right) + \Delta_l^g C_{p,m}^o\left[\frac{\theta}{T} - 1 + \ln\left(\frac{T}{\theta}\right)\right] \tag{6}$$

where p is the vapor pressure, p^o is a selected reference pressure (p^o = 10^5 Pa), θ is a selected reference temperature, R is the gas constant (R = 8.3144621 J·K^{-1}·mol^{-1}), $\Delta_l^g G_m^o$ is the standard molar Gibbs energy of vaporization at the selected reference pressure, $\Delta_l^g H_m^o$ is the standard molar enthalpy of vaporization, and $\Delta_l^g G_{p,m}^o$ is the difference between the heat capacities of the gaseous and of the liquid phases [$\Delta_l^g G_{p,m}^o = C_{p,m}^o(g) - C_{p,m}^o(1)$].

The values of $\Delta_l^g C_{p,m}^o$ were estimated considering the same temperature for all the ILs, T = 388 K (mean temperature between the average temperature and 298.15K) using a procedure recently proposed in the literature.[10] Table 1 presents the derived standard (p^o = 10^5 Pa) molar enthalpies, entropies, and Gibbs energies of vaporization at the mean temperature, $\langle T \rangle$, at T = 460.0 K and at reference temperature, T = 298.15 K, as derived from the fitting of eq 6 and related to each other by the following eq 7:

$$\Delta_l^g G_m^o(T) = -RT \ln\left[\frac{p(T)}{p^o}\right] = \Delta_l^g H_m^o(T) - T\Delta_l^g S_m^o(T) \tag{7}$$

The graphic representations of standard molar Gibbs energy of vaporization at reference temperature (460 and 298.15 K) as a function of total number of carbon atoms in the two alkyl side chains of the cation, N are presented in figure 3. At the temperature of 460 K, the following order of volatility for the studied series was found:

$$[C_3C_3\text{im}][NTf_2] \approx [C_4C_4\text{im}][NTf_2] > [C_2C_2\text{im}][NTf_2] \approx [C_5C_5\text{im}][NTf_2] > [C_6C_6\text{im}][NTf_2]$$

The [C_2C_2im][NTf_2] is an exception within this sequence, showing a lower volatility than [C_3C_3im][NTf_2] and [C_4C_4im]-[NTf_2]. This is the typical outlier behavior observed before for the ILs with a short alkyl chain length (e.g., [C_2C_1im]-[NTf_2]),[10] that can be explained based on the stronger polar interactions contribution observed in the border members (methyl, ethyl) of the alkyl series.

Taking into account the estimated volatility at 298.15 K depicted in Figure 3 panel II, a slightly change in the volatility order arising from the differentiation effect of the enthalpies of vaporization, and in smaller scale from the $\Delta_l^g C_{p,m}^o$ correction to the volatility, that leads to a crossover of the pressure to temperature dependence along the series was identified. At 298.15 K, the estimated following order of volatility was derived:

$$[C_2C_2\text{im}][NTf_2] > [C_3C_3\text{im}][NTf_2] > [C_4C_4\text{im}][NTf_2] \gg [C_5C_5\text{im}][NTf_2] \gg [C_6C_6\text{im}][NTf_2]$$

In Figure 3 panel II, the derived standard molar Gibbs energies of vaporization, at T = 298.15K, of the studied ILs and the asymmetric ILs, [$C_{N-1}C_1$im][NTf_2], are compared.[10] It can be observed that the volatility of [$C_{N/2}C_{N/2}$im][NTf_2] is significantly higher than the asymmetric cation ILs with the same total number of carbons in the alkyl side chains, [$C_{N-1}C_1$im][NTf_2]. At reference temperature, 298.15 K, the [C_2C_2im][NTf_2] presents the highest volatility ever observed for the alkylimidazolium bis(trifluoromethylsulfonyl)imide based ionic liquids.

Unlike what happens for the asymmetric ILs series, which presents in one of the nitrogens of the imidazolium a methyl group and in the other an alkyl side chain of increasing length, the symmetric ILs presents a simultaneous increase of the two alkyl side chains. The existence of a permanent methyl group in the imidazolium ring, in the asymmetric ILs series, enhances their electrostatic interactions between the cations and anions which affects the charge distribution and accessibility as well as the dynamics, increasing in this way their interaction potential. The standard molar enthalpies of vaporization, $\Delta_l^g H_m^o$ (298.15

dx.doi.org/10.1021/jp306937f | J. Phys. Chem. B 2012, 116, 10922−10927

Table 1. Parameters of Clarke and Glew Equation Fitted from the Vapor Pressure Results and the Derived Standard Molar Entropy of Vaporization for Each Studied IL at the Reference Temperature, θ, and at the Standard Pressure, $p^o = 10^5$ Pa

T interval/K	θ/K	$\Delta_l^g G_m^o(\theta)$/J·mol^{-1}	$\Delta_l^g H_m^o(\theta)$/J·mol^{-1}	$\Delta_l^g S_m^o(\theta)$/J·K^{-1}·mol^{-1}	r^2	$\Delta_l^g C_{p,m}^o$ (T = 388 K)/J·K^{-1}·mol^{-1}
			[C_2C_2im][NTf_2]			
455−480	467.61[a]	56539 ± 654	109212 ± 462	111.7 ± 1.0	0.9998	−117[b]
	460.00	57404 ± 651	110102 ± 464	114.6 ± 1.0		
	298.15	79755 ± 1212	129038 ± 965	165.3 ± 2.5		
			[C_3C_3im][NTf_2]			
453−490	471.60[a]	54529 ± 444	114013 ± 314	126.1 ± 0.7	0.9999	−127[b]
	460.00	56010 ± 446	115487 ± 319	129.3 ± 0.7		
	298.15	81073 ± 1165	136041 ± 922	184.4 ± 2.4		
			[C_4C_4im][NTf_2]			
455−488	471.58[a]	54564 ± 529	116836 ± 374	132.0 ± 0.8	0.9998	−138[b]
	460.00	56113 ± 529	118434 ± 378	135.5 ± 0.8		
	298.15	82534 ± 1189	140769 ± 944	195.3 ± 2.4		
			[C_5C_5im][NTf_2]			
463−496	479.54[a]	54675 ± 290	123575 ± 205	143.7 ± 0.4	0.9999	−149[b]
	460.00	57543 ± 316	126486 ± 227	149.9 ± 0.5		
	298.15	86652 ± 1176	150602 ± 930	214.5 ± 2.4		
			[C_6C_6im][NTf_2]			
463−496	479.60[a]	56928 ± 354	138362 ± 250	148.9 ± 0.5	0.9999	−160[b]
	460.00	59912 ± 373	131498 ± 269	155.6 ± 0.6		
	298.15	90310 ± 1188	157394 ± 941	225.0 ± 2.4		

[a]Mean experimental temperature. r^2 is the linear regression coefficient. [b]$\Delta_l^g C_{p,m}^o$ (388 K) estimated using the linear fitted function ($\Delta_l^g C_{p,m}^o$/J·K^{-1}·mol^{-1} = −5.40 n(C) - 100.47). [10] An uncertainty of ±5 J·K^{-1}·mol^{-1} was considered for the $\Delta_l^g C_{p,m}^o$.

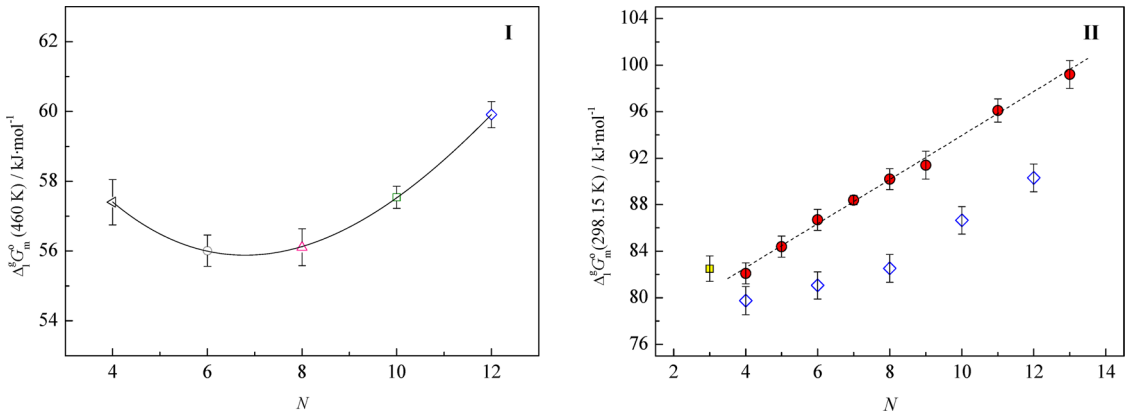

Figure 3. Graphic representation of standard molar Gibbs energy of vaporization at reference temperature as a function of total number of carbon atoms in the two alkyl side chains of the cation, N. (**I**) $\Delta_l^g G_m^o$(460 K): black triangle, [C_2C_2im][NTf_2]; gray circle, [C_3C_3im][NTf_2]; pink triangle, [C_4C_4im][NTf_2]; green square, [C_5C_5im][NTf_2]; blue diamond, [C_6C_6im][NTf_2]; (**II**) $\Delta_l^g C_m^o$(298 K): yellow square and red circle, [$C_{N-1}C_1$im][NTf_2];[10] blue diamond, [$C_{N/2}C_{N/2}$im][NTf_2].

K), as a function of the total number of the alkyl side chains of the cation, N, for the studied compounds ([$C_{N/2}C_{N/2}$im][NTf_2]) is presented in Figure 4 and compared with the previous data for the [$C_{N-1}C_1$im][NTf_2] series.

In the previous work on the asymmetric imidazolium ILs series, [$C_{N-1}C_1$im][NTf_2], an enthalpic and entropic trend shift was observed with the increase of the cation alkyl chain length, is related to a change in the molecular structure of the liquid phase around [C_6C_1im][NTf_2].[10,19] The symmetry of the IL cation changes dramatically the thermodynamic vaporization parameters. The enthalpies of vaporization are lower for the symmetric [$C_{N/2}C_{N/2}$im][NTf_2] than for the asymmetric imidazolium ILs, [$C_{N-1}C_1$im][NTf_2], indicating a decrease of the polar interactions in the symmetric imidazolium ILs. Moreover the vaporization results of the [$C_{N/2}C_{N/2}$im][NTf_2] ILs, show an enthalpic differentiation with a clearly discernible odd−even effect with higher enthalpies of vaporization for the odd numbered [C_3C_3im][NTf_2] and [C_5C_5im][NTf_2]. An odd−even effect was also reported in the viscosity data for the same ILs series and is also consistent with the solid phase crystallization behavior, recently published.[23] The odd numbered ILs, which presents higher enthalpies of vaporization, show also higher viscosities in agreement with the observed increase of their cohesive energies.[23]

The standard molar entropies of vaporization, $\Delta_l^g S_m^o$ (298.15K), as a function of the total number of the alkyl side chains of the cation, N, for the studied compounds ([$C_{N/2}C_{N/2}$im][NTf_2]) is presented in figure 5 and compared with the data for the [$C_{N-1}C_1$im][NTf_2] series.

Similarly to what was observed for the enthalpies of vaporization, a differentiation between the asymmetric and symmetric ILs series, was found. The ILs with symmetric cations, [$C_{N/2}C_{N/2}$im][NTf_2], present lower entropies of vaporization compared with the asymmetric imidazolium,

dx.doi.org/10.1021/jp306937f | J. Phys. Chem. B 2012, 116, 10922−10927

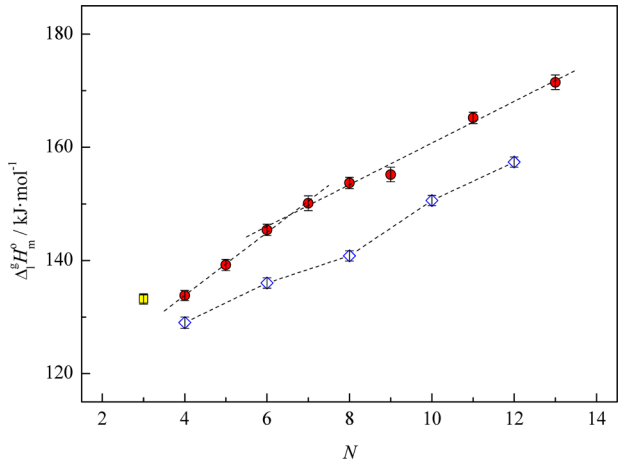

Figure 4. Graphic representation of standard molar enthalpy of vaporization at reference temperature (T = 298.15K) as a function of the total number of carbon atoms in the alkyl side chains of the cation, N. Yellow square and red circle $[C_{N-1}C_1im][NTf_2]$;[10] blue diamond, $[C_{N/2}C_{N/2}im][NTf_2]$.

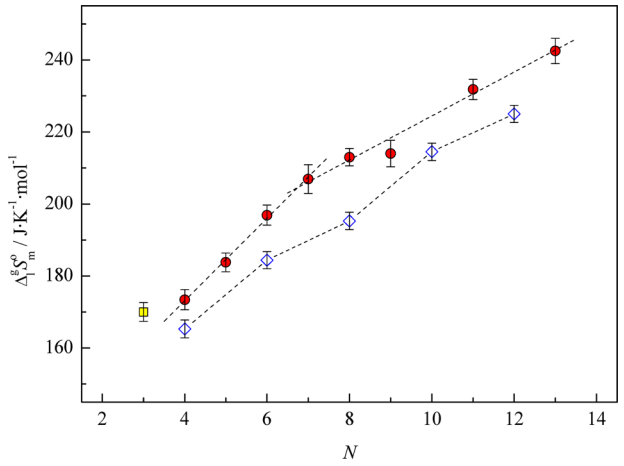

Figure 5. Graphic representation of standard molar entropy of vaporization at reference temperature (T = 298.15 K) as a function of the total number of carbon atoms in the alkyl side chains of the cation, N. Yellow square and red circle, $[C_{N-1}C_1im][NTf_2]$;[10] blue diamond, $[C_{N/2}C_{N/2}im][NTf_2]$.

$[C_{N-1}C_1im][NTf_2]$, indicating an entropic increase of the absolute liquid entropy for the symmetric cation ILs, that could be related with a molecular entropy increase as well as being a reflection of the change of the ion dynamics in the IL liquid phase.

The observed lower entropies of vaporization are in opposition with the higher volatility observed for the symmetric ILs series, which shows that the higher volatility of the symmetric ILs, when compared with the asymmetric series, is ruled by their enthalpy of vaporization.

The odd−even effect is also clearly discernible in the entropies of vaporization of the $[C_{N/2}C_{N/2}im][NTf_2]$ ILs, with higher entropies of vaporization for the odd numbered $[C_3C_3im][NTf_2]$ and $[C_5C_5im][NTf_2]$, indicating a decrease in the absolute entropies of the liquid for the odd numbers.

The observed odd−even effect in the entropy and enthalpy of vaporization in the symmetrical series are attenuated in the volatility because of an entropic−enthalpic compensation.

4. FINAL REMARKS

The study of the five symmetric imidazolium based ionic liquids, $[C_{N/2}C_{N/2}im][NTf_2]$, enabled the evaluation the effect of the symmetry of the cation on the thermodynamic parameters of vaporization, taking into account the previous results for the $[C_{N-1}C_1im][NTf_2]$ series. The volatility of $[C_{N/2}C_{N/2}im][NTf_2]$ series is significantly higher than the asymmetric cation ILs It was found that the higher volatility is ruled by the enthalpy of vaporization. The symmetric ILs show lower entropies of vaporization compared with the asymmetric, indicating an increase of the absolute liquid entropy in the symmetric cation ILs. The obtained vaporization results of the $[C_{N/2}C_{N/2}im][NTf_2]$ ILs, shows an enthalpic and entropic differentiation with a clearly discernible odd−even effect, with higher enthalpies and entropies of vaporization for the odd numbered $[C_3C_3im][NTf_2]$ and $[C_5C_5im][NTf_2]$.

■ ASSOCIATED CONTENT

Supporting Information

This section presents the experimental vapor pressures for the five studied imidazolium based ILs. This material is available free of charge via the Internet at http://pubs.acs.org.

■ AUTHOR INFORMATION

Corresponding Author

*Tel.: +351 220 402 836. Fax: +351 220 402 659. E-mail: lbsantos@fc.up.pt (L.M.N.B.F.S.); marisa.alexandra.rocha@gmail.com (M.A.A.R.).

Notes

The authors declare no competing financial interest.

■ ACKNOWLEDGMENTS

Thanks are due to Fundação para a Ciência e Tecnologia (FCT), Lisbon, Portugal and to FEDER for financial support to Centro de Investigação em Química, University of Porto. Marisa A. A. Rocha acknowledges the financial support from FCT and the European Social Fund (ESF) under the Community Support Framework (CSF) for the award of a Research Grants SFRH/BD/60513/2009. Thanks are also due to FCT for financial support for the project PTDC/CTM/103664/2008.

■ REFERENCES

(1) Wasserscheid, P., Welton, T., Eds. *Ionic Liquids in Synthesis*; Wiley-VCH: Weinheim, Germany, 2003.

(2) Esperança, J. M. S. S.; Canongia Lopes, J. N.; Tariq, M.; Santos, L. M. N. B. F.; Magee, J. W.; Rebelo, L. P. N. *J. Chem. Eng. Data* **2010**, *55*, 3−12.

(3) Paulechka, Y. U. J. *Phys. Chem. Ref. Data* **2010**, *39*, 033108.

(4) Chirico, R. D.; Diky, V.; Magee, J. W.; Frenkel, M.; Marsh, K. N. *Pure Appl. Chem.* **2009**, *81*, 791−828.

(5) Wieser, M. E.; Berglund, M. *Pure Appl. Chem.* **2009**, *81*, 2131−2156.

(6) Earle, M. J.; Esperança, J. M. S. S.; Gilea, M. A.; Lopes, J. N. C.; Rebelo, L. P. N.; Magee, J. W.; Seddon, K. R.; Widegren, J. A. *Nature* **2006**, *439*, 831−834.

(7) Köddermann, T.; Paschek, D.; Ludwig, R. *Chem. Phys. Chem.* **2007**, *8*, 2464−2470.

(8) Zaitsau, D. H.; Kabo, G. J.; Strechan, A. A.; Paulechka, Y. U.; Tschersich, A.; Verevkin, S. P.; Heintz, A. *J. Phys. Chem. A* **2006**, *110*, 7303−7306.

(9) Paulechka, Y. U.; Zautsau, D. H.; Kabo, G. J.; Strechan, A. A. *Thermochim. Acta* **2005**, *439*, 158−160.

(10) Rocha, M. A. A.; Lima, C. F. R. A. C.; Gomes, L. R.; Schröder, B.; Coutinho, J. A. P.; Marrucho, I. M.; Esperança, J. M. S. S.; Rebelo, L. P. N.; Shimizu, K.; Canongia Lopes, J. N.; Santos, L. M. N. B. F. *J. Phys. Chem. B* **2011**, *115*, 10919−10926.
(11) Zaitsau, D. H.; Verevkin, S. P.; Emel'yanenko, V. N.; Heintz, A. *ChemPhysChem* **2011**, *12*, 3609−3613.
(12) Emel'yanenko, V. N.; Verevkin, S. P.; Heintz, A. *J. Am. Chem. Soc.* **2007**, *129*, 3930−3937.
(13) Armstrong, J. P.; Hurst, C.; Jones, R. G.; Licence, P.; Lovelock, K. R. J.; Satterley, C. J.; Villar-Garcia, I. J. *Phys. Chem. Chem. Phys.* **2007**, *9*, 982−990.
(14) Deyko, A.; Lovelock, K. R. J.; Corfield, J.-A.; Taylor, A. W.; Gooden, P. N.; Villar-Garcia, I. J.; Licence, P.; Jones, R. G.; Krasovskiy, V. G.; Chernikova, E. A.; Kustov, L. M. *Phys. Chem. Chem. Phys.* **2009**, *11*, 8544−8555.
(15) Deyko, A.; Lovelock, K. R. J.; Licence, P.; Jones, R. G. *Phys. Chem. Chem. Phys.* **2011**, *13*, 16841−16850.
(16) Deyko, A.; Hessey, S. G.; Licence, P.; Chernikova, E. A.; Krasovskiy, V. G.; Kustov, L. M.; Jones, R. G. *Phys. Chem. Chem. Phys.* **2012**, *14*, 3181−3193.
(17) Santos, L. M. N. B. F.; Canongia Lopes, J. N.; Coutinho, J. A. P.; Esperanca, J. M. S. S.; Gomes, L. R.; Marrucho, I. M.; Rebelo, L. P. N. *J. Am. Chem. Soc.* **2007**, *129*, 284−285.
(18) Luo, H.; Baker, G. A.; Dai, S. *J. Phys. Chem. B* **2008**, *112*, 10077−10081.
(19) Shimizu, K.; Costa Gomes, M. F.; Pádua, A. A. H.; Rebelo, L. P. N.; Canongia Lopes, J. N. *THEOCHEM* **2010**, *946*, 70−76.
(20) Tariq, M.; Carvalho, P. J.; Coutinho, J. A.P.; Marrucho, I. M.; Canongia Lopes, J. N.; Rebelo, L. P.N. *Fluid Phase Equilib.* **2011**, *301*, 22−32.
(21) Rocha, M. A. A.; Lima; Coutinho, J. A. P.; Bastos, M.; Santos, L. M. N. B. F. *J. Chem. Thermodynamics* **2012**, *53*, 140−143.
(22) Xiao, D.; Hines, L. G., Jr.; Li, S.; Bartsch, R. A.; Quitevis, E. L.; Russina, O.; Triolo, A. *J. Phys. Chem. B* **2009**, *113*, 6426−6433.
(23) Zheng, W.; Mohammed, A.; Hines, L. G., Jr.; Xiao, D.; Martinez, O. J.; Bartsch, R. A.; Simon, S. L.; Russina, O.; Triolo, A.; Quitevis, E. L. *J. Phys. Chem. B* **2011**, *115*, 6572−6584.
(24) Santos, L. M. N. B. F.; Lima, L. M. S. S.; Lima, C. F. R. A. C.; Magalhães, F. D.; Torres, M. C.; Schröder, B.; Ribeiro da Silva, M. A. V. *J. Chem. Thermodynamics* **2011**, *43*, 834−843.
(25) Lima, C. F. R. A. C.; Rocha, M. A. A.; Melo, A.; Gomes, L. R.; Low, J. N.; Santos, L. M. N. B. F. *J. Phys. Chem. A* **2011**, *115*, 11876−11888.
(26) Wieser, M. E.; Berglund, M. *Pure Appl. Chem.* **2009**, *81*, 2131−2156.
(27) Clarke, E. C. W.; Glew, D. N. *Trans. Faraday Soc.* **1966**, *62*, 539−547.

Supporting Information

The Cation Symmetry effect on the Volatility of Ionic Liquids

Marisa A. A. Rocha [†,*], *João A. P. Coutinho*[§], *Luís M. N. B. F. Santos* [†,*]

[†] Centro de Investigação em Química, Faculdade de Ciências da Universidade do Porto,

R. Campo Alegre 687, P-4169-007 Porto, Portugal

[§] CICECO, Departamento de Química, Universidade de Aveiro, 3810-193 Aveiro, Portugal

*Corresponding author. Tel.: +351 220 402 836; Fax: +351 220 402 659
E-mail address: lbsantos@fc.up.pt (Luís M. N. B. F. Santos);
marisa.alexandra.rocha@gmail.com (Marisa A. A. Rocha)

Vapor pressures measurements using Quartz crystal microbalance Knudsen effusion apparatus

Table S1 Experimental vapor pressures for the studied imidazolium based ILs, obtained by the quartz crystal microbalance Knudsen effusion apparatus.

T / K	p / Pa	Δp / Pa	T / K	p / Pa	Δp / Pa	T / K	p / Pa	Δp / Pa
				[C_2C_2im][Ntf_2]				
455.54	0.0231	-0.0127	465.61	0.0426	0.0050	475.64	0.0776	-0.0016
457.58	0.0262	-0.0073	467.62	0.0479	0.0092	477.65	0.0877	-0.0078
459.57	0.0295	0.0000	469.58	0.0537	0.0132	479.68	0.0989	-0.0137
461.59	0.0333	0.0037	471.61	0.0610	0.0052			
463.59	0.0377	0.0035	473.60	0.0687	0.0031			
				[C_3C_3im][Ntf_2]				
453.52	0.0285	-0.0065	467.60	0.0707	0.0056	481.63	0.1677	-0.0058
455.54	0.0327	-0.0071	469.61	0.0805	0.0030	483.65	0.1880	-0.0026
457.56	0.0373	-0.0056	471.60	0.0914	-0.0011	485.67	0.2095	0.0051
459.58	0.0428	-0.0088	473.59	0.1034	-0.0018	487.67	0.2355	0.0023
461.59	0.0476	0.0166	475.60	0.1177	-0.0098	489.68	0.2636	0.0023
463.62	0.0546	0.0119	477.61	0.1316	-0.0010			
465.58	0.0618	0.0124	479.62	0.1495	-0.0089			
				[C_4C_4im][Ntf_2]				
455.52	0.0317	-0.0139	469.55	0.0784	0.0130	483.63	0.1902	-0.0063
457.53	0.0365	-0.0141	471.55	0.0891	0.0123	485.64	0.2155	-0.0127
459.52	0.0413	-0.0033	473.56	0.1006	0.0180	487.65	0.2436	-0.0180
461.53	0.0473	-0.0050	475.57	0.1147	0.0117			
463.54	0.0538	-0.0007	477.58	0.1305	0.0062			
465.53	0.0611	0.0035	479.61	0.1483	0.0014			
467.54	0.0690	0.0118	481.62	0.1684	-0.0040			
				[C_5C_5im][Ntf_2]				
463.49	0.0375	-0.0014	475.54	0.0849	0.0048	487.55	0.1838	0.0006
465.54	0.0437	-0.0098	477.52	0.0972	-0.0003	489.55	0.2071	0.0045
467.56	0.0497	0.0026	479.52	0.1108	-0.0013	491.56	0.2353	-0.0004
469.57	0.0570	0.0020	481.53	0.1258	0.0011	493.58	0.2655	0.0002
471.54	0.0653	0.0004	483.55	0.1437	-0.0032	495.59	0.3006	-0.0037
473.55	0.0742	0.0076	485.56	0.1631	-0.0036			

[C_6C_6im im][Ntf_2]

463.53	0.0205	-0.0037	475.53	0.0476	0.0063	487.58	0.1063	0.0030
465.56	0.0236	0.0017	477.52	0.0549	-0.0024	489.59	0.1211	0.0006
467.58	0.0274	0.0014	479.54	0.0626	0.0040	491.60	0.1375	0.0013
469.59	0.0317	-0.0033	481.56	0.0715	0.0052	493.60	0.1566	-0.0038
471.61	0.0366	-0.0025	483.50	0.0810	0.0084	495.66	0.1795	-0.0128
473.54	0.0422	-0.0110	485.55	0.0928	0.0074			

$\Delta p = p - p_{calc}$, where p_{calc} is calculated from the Clarke and Glew equation (eq. 6) with the parameters given in Table1.

Paper V

"Evidence of Nanostructuration from the Heat Capacities of the [$C_{N/2}C_{N/2}$im][NTf_2] Ionic Liquid Series"

Marisa A.A. Rocha, João A.P. Coutinho, Luís M.N.B.F. Santos

Journal of Chemical Physics (2013), 139, 104502.
doi: 10.1063/1.4820825

Note: The author of this thesis performed the all the experimental work, data analysis and contribute to the discussion and conclusions.

Evidence of nanostructuration from the heat capacities of the 1,3-dialkylimidazolium bis(trifluoromethylsulfonyl)imide ionic liquid series

Marisa A. A. Rocha,[1,a)] João A. P. Coutinho,[2] and Luís M. N. B. F. Santos[1,a)]
[1]*Centro de Investigação em Química, Departamento de Química e Bioquímica, Faculdade de Ciências, Universidade do Porto, Rua do Campo Alegre, 687, P-4169-007 Porto, Portugal*
[2]*CICECO, Departamento de Química, Universidade de Aveiro, P-3810-193 Aveiro, Portugal*

(Received 29 May 2013; accepted 26 August 2013; published online 12 September 2013)

In the present work, the heat capacities at $T = 298.15$ K of 1,3-dialkylimidazolium bis(trifluoromethylsulfonyl)imide, $[C_{N/2}C_{N/2}im][NTf_2]$, were measured, for the first time, using a high-precision heat capacity drop calorimeter, with an uncertainty of less than 0.15%. Based on the obtained results, it was possible to evaluate the effect of the cation symmetry on the heat capacity data through a comparative analysis with the $[C_{N-1}C_1im][NTf_2]$ ionic liquid series. The molar heat capacities of the $[C_{N/2}C_{N/2}im][NTf_2]$ ionic liquids series present a less pronounced deviation from the linearity along the alkyl chain length than the asymmetric based ionic liquids series. Lower molar heat capacities for the symmetric than the asymmetric series were observed, being this difference more evident for the specific and volumic heat capacities. As observed for the $[C_{N-1}C_1im][NTf_2]$ series, a trend shift in the heat capacities at $[C_6C_6im][NTf_2]$ was found that reflects the impact of nonpolar region nanostructuration on the thermophysical properties of the ionic liquids. The profile of the two regions is in agreement with the expected effect arising from the nanostructuration in ionic liquids. The results obtained in the present work show a clear indication that for the symmetric series, $[C_{N/2}C_{N/2}im][NTf_2]$, the starting of the liquid phase nanostructuration/alkyl chain segregation occurs around $[C_6C_6im][NTf_2]$. © *2013 AIP Publishing LLC*. [http://dx.doi.org/10.1063/1.4820825]

I. INTRODUCTION

Heat capacity is one of the most important thermophysical properties characterizing the liquid phase, and is intimately linked to the temperature dependence of fundamental thermodynamic properties. Heat capacities are essential for the temperature correction of entropy and enthalpy in any chemical or physical process, it can be used to evaluate molecular and supramolecular interactions, as well as, highlight some structural and dynamics properties of materials. Accurate heat capacity data have a wide field of application in thermochemistry for calculating changes in reaction enthalpies and in chemical engineering for establishing energy balances.[1–3] The possible use of ionic liquids (ILs) as heat transfer for heat exchange in chemical plants and solar thermal power generation was discussed, and it was found that the imidazolium based ionic liquids present higher heat capacities per unit of volume that two high performance commercial thermal fluids.[4–6] The knowledge of the heat capacity is required for the evaluation of the applicability of the ionic liquids as heat transfer fluids.[4–6]

During the past decade, the research in ionic liquids has gained popularity, mainly due to their particular properties. Hence, intense research in these systems was performed both in fundamental and applied fields, contributing to the progress in the understanding of the ionic liquids at a molecular level, and consequently, to the advance in the applied field.[7–9] The comprehension of the physical chemical properties of ionic liquids and their adequate tuning, relies on the adequate understanding of the molecular structure of the ILs in the liquid phase. The structural organization of the liquid phase of ionic liquids comprises high charge density organized themselves in order to satisfy the electroneutrality conditions and to enhance the electrostatic interactions between the cation and anion, and the alkyl chains of the cation (low charge density) segregate elsewhere.[10–14] The interaction between these two types of regions (polar and nonpolar) led to the recognition of ionic liquids as high-charge density (polar) network permeated by low-charge density (non-polar) regions.[10–14] This characteristic of the structural organization in ionic liquids was later supported experimentally by X-ray diffraction[15] and by small-wide angle X-ray scattering (SWAXS).[16,17] Recently, the studies exploring mesoscopic structural heterogeneities in ionic liquids has been compiled and discussed in order to give a better understanding on the nature of structural heterogeneities in ILs.[18] Shimizu *et al.*,[19] based on molecular dynamics simulation, have shown that the structural segregation in ILs depends on the size of the polar and nonpolar regions. These regions can exist as isolated (dispersed) islands or a second continuous phase, in which the transition from a dispersed to a continuous non-polar phase corresponds to the nanostructuration limit.[19] Recently we have reported the heat capacities at $T = 298.15$ K of the extended series of ionic liquids, $[C_{N-1}C_1im][NTf_2]$ (with N = 3–9, 11, and 13), where the effect of the nanostructuration of ionic liquids in

[a)]Authors to whom correspondence should be addressed. Electronic addresses: marisa.alexandra.rocha@gmail.com and lbsantos@fc.up.pt. Tel.: +351 220 402 836. Fax: +351 220 402 659.

this property was evaluated.[20] In this work a trend shift along the alkyl side chain length, related to a change in the molecular structure of the liquid phase around $[C_6C_1im][NTf_2]$, in agreement with the thermodynamic study of vaporization published, for the same ionic liquid family[21] was disclosed. It was also shown that the effect of the nanostructuration is more visible when the heat capacities and enthalpies of vaporization on a volumetric basis are used. This being a result of the relationship of the trend shift with the cohesive energy of the liquid.[20]

In the present work, the heat capacities at $T = 298.15$ K of 1,3-dialkylimidazolium bis(trifluoromethylsulfonyl)imide, $[C_{N/2}C_{N/2}im][NTf_2]$, were measured using a high-precision heat capacity drop calorimeter developed by Wadsö[22,23] and recently updated in our laboratory.[24] This work complements and extends the previous study concerning the heat capacities of the $[C_{N-1}C_1im][NTf_2]$ ionic liquid series, aiming at evaluating the effect of the symmetry and nanostructuration on the heat capacities of an ionic liquid homologous series.

II. EXPERIMENTAL DETAILS

The 1,3-dialkylimidazolium bis(trifluoromethylsulfonyl)imide series, $[C_{N/2}C_{N/2}im][NTf_2]$ (N = 2, 4, 6, 8, 10, 12, 14, 16, 18, 20), used in this work, were purchased from IOLITEC with a stated purity of better than 98%. All ionic liquids were dried under reduced pressure (<10 Pa) and stirred constantly at 323 K, in order to reduce the presence of water or other volatile contents. This process was performed systematically before and during the heat capacity measurements. The purity of each ionic liquid was further evaluated by ^{1}H, ^{13}C, and ^{19}F NMR spectra and all ionic liquids found to be >99 wt.% purity. The water contents of the degassed samples were determined with a Metrohm 737 Karl Fischer coulometer, using the Hydranal®- Coulomat AG from Riedel-de Haën, and revealed less than 200 ppm of water.

A. High-precision heat capacity drop calorimetry

The heat capacities at $T = 298.15$ K of the extended series of $[C_{N/2}C_{N/2}im][NTf_2]$ (N = 2, 4, 6, 8, 10, 12, 14, 16, 18, 20) ionic liquids were measured by a high-precision heat capacity drop calorimeter, which is described in detail in the literature.[22–24] The calorimeter, was originally developed and used at the Thermochemistry Laboratory, Lund, Sweden,[22,23] being afterwards transferred to Porto, Portugal, where it was reassembled, modernized, and tested.[24] The apparatus comprises two main parts: the furnace and the calorimetric receiving block. The furnace is maintained at a constant temperature $T = 303.15$ K and the receiving calorimeter is kept at $T = 293.15$ K. The ampoules were weighted in a Mettler Toledo AG245 dual range analytical balance (sensitivity of 0.00001 g and repeatability of 0.00002 g) both empty and after filling with the ionic liquid. The ampoule was maintained in the furnace for temperature equilibration, in a fixed position, by means of a drop and lift mechanism system. After a pre-defined time, the ampoule was dropped into the receiving calorimetric block at a well-defined temperature, and was kept there for a fixed time interval. In each independent drop experiment, the drop procedure was automatically repeated using the same experimental conditions, used for the blanks and calibration experiments. In the present work the apparatus was used in single-drop mode (no reference ampoule was used) with blank correction that was measured independently using empty ampoules.

The calorimeter was calibrated with water and sapphire (α-Al_2O_3), using the respective standard molar heat capacities at 298.15 K reported in literature, $C^o_{p,m}$ (H_2O) = (75.32 ± 0.01) J K^{-1} mol^{-1} and $C^o_{p,m}$ (α-aluminum oxide) = (79.03 ± 0.08) J K^{-1} mol^{-1}.[25] The calibration constant was found to be ε = (6.6040 ± 0.0036) W V^{-1}. Since the calorimeter was used to measure the heat capacity of ionic liquids, the accuracy was checked on the basis of the results obtained for $[C_6C_1im][NTf_2]$. The determined $C^o_{p,m}$ ($[C_6C_1im][NTf_2]$, 298.15 K) = (629.24 ± 0.43) J K^{-1} mol^{-1} was obtained from the average of two independent experiments, using different ampoules, and is in excellent agreement with the recommended value, $C^o_{p,m}$ ($[C_6C_1im][NTf_2]$, 298.15 K) = (631.6 ± 1.3) J K^{-1} mol^{-1}.[26]

The relative atomic masses of the 11 elements have been presented as an interval, in the latest IUPAC technical report 2009.[27] Since the values reported in the IUPAC Commission in 2007[28] are within the presented interval, we choose to use the relative atomic masses recommended by the IUPAC report 2007 in this work.[28] All the uncertainties are given as twice of the standard deviation of the mean, and include the calibration uncertainty. The buoyancy effect correction was considered both for the calibration and experiments of the ionic liquids.

III. RESULTS AND DISCUSSION

The molar masses, M (g mol^{-1}), number of drop experiments, N_{drop}, and the measured molar heat capacities at 298.15 K, $C^o_{p,m}$ (J K^{-1} mol^{-1}), for the studied ionic liquids are presented in Table I.

Table II lists a compilation of the heat capacity data for the studied ionic liquids at $T = 298.15$ K. The volumic heat capacities, C^o_p/V, were calculated taking into account the

TABLE I. Molar heat capacity values, at $T = 298.15$ K, for the studied ionic liquids.

Ionic liquid	M (g mol^{-1})	N_{drop}	$C^o_{p,m}$ (J K^{-1} mol^{-1})
$[C_1C_1im][NTf_2]$	377.286	14	472.33 ± 0.46
$[C_2C_2im][NTf_2]$	405.340	20	532.64 ± 0.52
$[C_3C_3im][NTf_2]$	433.393	16	594.52 ± 0.49
$[C_4C_4im][NTf_2]$	461.446	33	656.79 ± 0.82
$[C_5C_5im][NTf_2]$	489.500	17	718.19 ± 0.71
$[C_6C_6im][NTf_2]$	517.553	14	778.50 ± 0.77
$[C_7C_7im][NTf_2]$	545.606	23	838.71 ± 0.62
$[C_8C_8im][NTf_2]$	573.660	20	906.36 ± 1.23
$[C_9C_9im][NTf_2]$	601.713	15	966.17 ± 1.38
$[C_{10}C_{10}im][NTf_2]$	629.766	19	1027.00 ± 0.86

N_{drop}. = Number of drop experiments; the number of drops is the sum of the drops that were obtained in two or more independent experiments.

TABLE II. Densities, ρ, specific heat capacities, c_p^o, volumic heat capacities, C_p^o/V, and molar heat capacities, $C_{p,m}^o$, at $T = 298.15$ K, for each ionic liquid.

Ionic liquid	ρ (298.15 K) (g cm^{-3}) [Ref. 29]	c_p^o (J K^{-1} g^{-1})	C_p^o/V (J K^{-1} cm^{-3}) [a]	$C_{p,m}^o$ (J K^{-1} mol^{-1})
[C_1C_1im][NTf_2]	1.5692	1.2519 ± 0.0012	1.9645 ± 0.0019	472.33 ± 0.46
[C_2C_2im][NTf_2]	1.4749	1.3141 ± 0.0013	1.9382 ± 0.0019	532.64 ± 0.52
[C_3C_3im][NTf_2]	1.3990	1.3718 ± 0.0011	1.9191 ± 0.0015	594.52 ± 0.49
[C_4C_4im][NTf_2]	1.3428	1.4233 ± 0.0018	1.9112 ± 0.0024	656.79 ± 0.82
[C_5C_5im][NTf_2]	1.2924	1.4672 ± 0.0015	1.8962 ± 0.0019	718.19 ± 0.71
[C_6C_6im][NTf_2]	1.2550	1.5042 ± 0.0015	1.8878 ± 0.0019	778.50 ± 0.77
[C_7C_7im][NTf_2]	1.2252	1.5372 ± 0.0011	1.8834 ± 0.0013	838.71 ± 0.62
[C_8C_8im][NTf_2]	1.1948	1.5800 ± 0.0021	1.8878 ± 0.0025	906.36 ± 1.23
[C_9C_9im][NTf_2]	1.1692	1.6057 ± 0.0023	1.8774 ± 0.0027	966.17 ± 1.38
[$C_{10}C_{10}$im][NTf_2]	1.1522	1.6308 ± 0.0014	1.8790 ± 0.0016	1027.00 ± 0.86

[a] C_p^o/V values were calculated taking into account the specific heat capacities, c_p^o, and the experimental density values available in the literature.[29]

specific heat capacities, c_p^o, and the experimental density values available in the literature.[29] For this series of ionic liquids, no literature data were found. The heat capacities of the studied ionic liquids were measured with an uncertainty of less than 0.15%.

The graphic representations of the molar heat capacity data, $C_{p,m}^o$, and the specific heat capacity data, c_p^o, as a function of the total number of carbons atoms in the alkyl side chains of the cation, N, are presented in Figure 1.

Unlike to what it was observed for the series of ionic liquids, [$C_{N-1}C_1$im][NTf_2] (asymmetric ILs)[20], the $C_{p,m}^o$ ($T = 298.15$ K) of the [$C_{N/2}C_{N/2}$im][NTf_2] series (symmetric ILs) increases near linearly along the alkyl chain length, with a contribution of (30.88 ± 0.09) J K^{-1} mol^{-1} per methylene group (–CH_2–).

From Figure 1(I) it can be observed that, for the same total number of carbons in the alkyl chains, the symmetric series presents slightly lower molar heat capacities than the asymmetric ones, being this difference larger above [C_6C_1im][NTf_2]. This difference becomes more evident in the specific heat capacities, presented in Figure 1(II), where the asymmetric ionic liquids present higher specific heat capacities than the symmetric. Instead of two regions in the c_p^o values, as observed for the asymmetric series, the specific heat capacities of the symmetric ionic liquids could be described by a curvilinear function with a decrease of the derivative, without a clear distinction of two regions with a discontinuity of a derivative. The contribution per –CH_2– group for the c_p^o values is higher for the symmetric ILs with shorter alkyl side chains, reaching a region where a subtle decrease in the $-CH_2-$ group contribution is observed, with a clear odd-even effect for longer alkyl side chains, as depicted in Figure 1(II).

Figure 2 presents the volumic heat capacities against the total number of carbons in the alkyl side chains of the cation. In this graphic representation it is clear that the symmetric imidazolium based ionic liquids present lower volumic heat capacities than those observed for the asymmetric ILs.[20] For the asymmetric ionic liquids,[20] the volumic heat capacity reaches a constant value (1.92 J K^{-1} cm^{-3}) above [C_6C_1im][NTf_2] (Figure 2 "Region B" in the asymmetric series). In the case of the symmetric series, the volumic heat capacities present an identical decrease in the volumic heat capacities, from [C_2C_2im][NTf_2] to [C_6C_6im][NTf_2], reaching a constant value of 1.88 J K^{-1} cm^{-3} (Figure 2 "Region B" in the symmetric series) significantly lower than the observed value for the asymmetric ILs from [C_7C_7im][NTf_2] to [$C_{10}C_{10}$im][NTf_2]. The lower constant value for the volumic

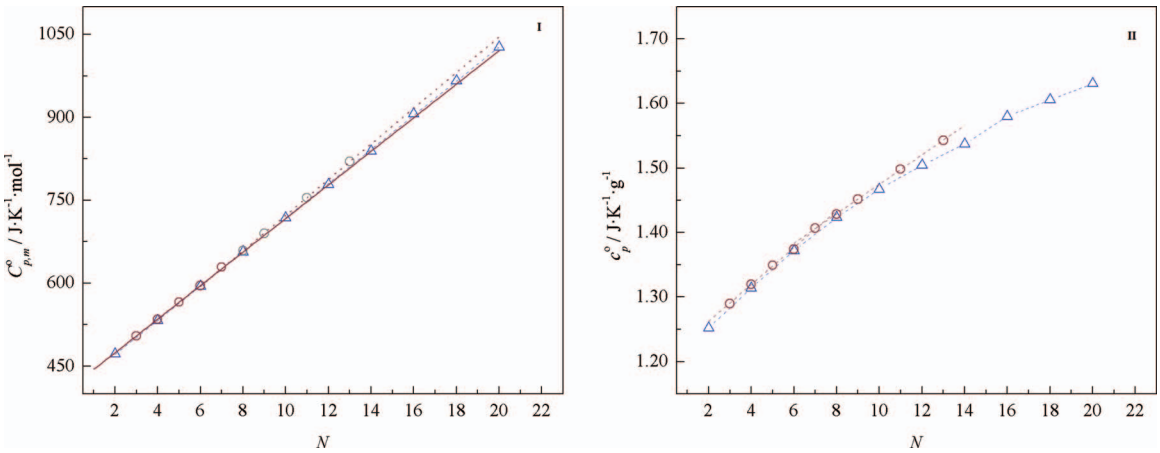

FIG. 1. Molar heat capacities (**I**) and specific heat capacities (**II**) as a function of the total number of carbon atoms in the alkyl side chains of the cation. Graph (**I**) ○ (gray), [$C_{N-1}C_1$im][NTf_2] (N = 3–9, 11, and 13);[20] — (gray), fitting of $C_{p,m}^o$ values of [C_3C_1im][NTf_2]-[C_5C_1im][NTf_2]; — (gray), fitting of $C_{p,m}^o$ values of [C_7C_1im][NTf_2]-[$C_{12}C_1$im][NTf_2]; △ (blue), [$C_{N/2}C_{N/2}$im][NTf_2] (N = 2, 4, 6, 8, 10, 12, 14, 16, 18, 20); – – – (blue), fitting of $C_{p,m}^o$ values of [C_1C_1im][NTf_2]-[$C_{10}C_{10}$im][NTf_2]. Graph (**II**) ○ (gray), [$C_{N-1}C_1$im][NTf_2];[20] △ (blue), [$C_{N/2}C_{N/2}$im][NTf_2].

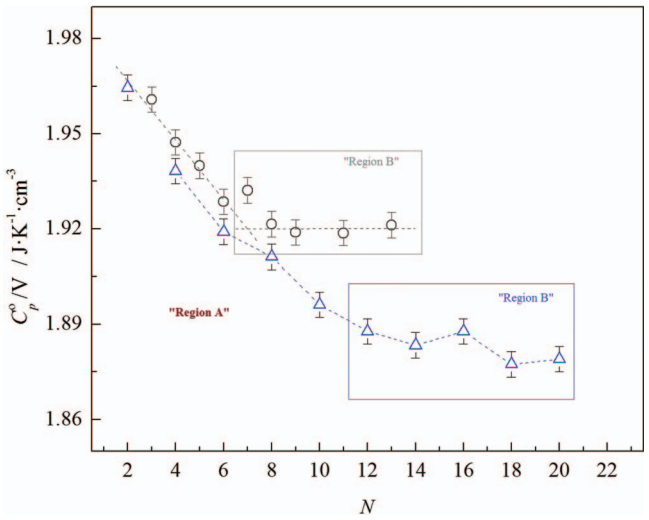

FIG. 2. Volumic heat capacities as a function of the total number of carbon atoms in the alkyl side chains of the cation. ◯ (gray), $[C_{N-1}C_1im][NTf_2]$ (N = 3–9, 11, and 13);[20] △ (blue), $[C_{N/2}C_{N/2}im][NTf_2]$ (N = 2, 4, 6, 8, 10, 12, 14, 16, 18, 20).

heat capacity obtained for the symmetric series is related with the higher separations between the ions in the charged region, due to the high steric hindrance arising from the alkyl chains present in both sides of the cation. This lowers the contribution for the heat capacity of the alkyl chain located in the charged region more significantly than in the asymmetrical ILs.

The observed trend shift in the volumic heat capacities at $[C_6C_6im][NTf_2]$ is in good agreement with the trend shift previously found in the viscosity data.[29] Moreover, the volumic heat capacities result from $[C_2C_2im][NTf_2]$ to $[C_{10}C_{10}im][NTf_2]$ show a differentiation with a visible odd-even effect with higher C_p^o/V for the even numbered ionic liquids, $[C_2C_2im][NTf_2]$, $[C_4C_4im][NTf_2]$, $[C_6C_6im][NTf_2]$, $[C_8C_8im][NTf_2]$, and $[C_{10}C_{10}im][NTf_2]$. The higher values of C_p^o/V of the even numbered ionic liquids are related with the some lower vibrational frequencies modes of the ionic liquids, and are in qualitative agreement with their lower cohesive energies and higher liquid absolute entropy derived previously from the thermodynamic properties of vaporization obtained for the $[C_{N/2}C_{N/2}im][NTf_2]$ (N = 4, 6, 8, 10, 12).[30]

The decrease in the C_p^o/V from $[C_1C_1im][NTf_2]$ to $[C_6C_6im][NTf_2]$ is mainly due to the decrease of the ionic liquid densities along the alkyl chain length of the cation.[29] The observed constant value for the C_p^o/V for the heavier symmetrical ionic liquids probably results from a balance between the decrease of the density and the increase of the contribution per methylene group, $-CH_2-$, in the volumic heat capacities. The profile of the two regions (Figure 2, "Region A," "Region B"), found for the heat capacity data for the extended series of $[C_{N/2}C_{N/2}im][NTf_2]$, is in agreement with the expected effect arising from the nanostructuration in ionic liquids.[20] The constant value of C_p^o/V (Figure 2), reached after $[C_6C_6im][NTf_2]$ ("Region B"), indicates that the volumic heat capacity of the $-CH_2-$ group remains unchanged in agreement with the expected behaviour of continuous non-polar segregated region.

It is well established that in the liquid phase of ionic liquids, the polar regions tend to organize themselves in order to enhance the electrostatic interactions between the cation and anion and the alkyl chains of the cation for a non-polar segregated network.[13,14,19] In previous studies, the experimental evidence for the nanostructuration in ionic liquids was verified to occur above $[C_6C_1im][NTf_2]$.[20,21,29] Based on the results obtained in the present work, we found a clear indication that for the symmetric series, $[C_{N/2}C_{N/2}im][NTf_2]$, the limit for the beginning of the nanostructuration/alkyl chain segregation is around $[C_6C_6im][NTf_2]$.

ACKNOWLEDGMENTS

Thanks are due to Fundação para a Ciência e Tecnologia (FCT), Lisbon, Portugal and to FEDER for financial support to Centro de Investigação em Química, University of Porto through the project Pest-C/QUI/UI0081/2011, and CICECO, University of Aveiro, through the project Pest-C/CTM/LA0011/2011. Marisa A. A. Rocha acknowledges the financial support from FCT and the European Social Fund (ESF) under the Community Support Framework (CSF) for the award of a Ph.D. Research Grant No. SFRH/BD/60513/2009.

[1] *Heat Capacities: Liquids, Solutions and Vapours*, edited by E. Wilhelm and T. M. Letcher (The Royal Society of Chemistry, Cambridge, UK, 2010).
[2] M. Zábranský, Z. Kolskaá, V. Růžička, Jr., and E. S. Domalski, J. Phys. Chem. Ref. Data **39**, 013103 (2010).
[3] M. Zábranský, V. Růžička, Jr., and E. S. Domalski, J. Phys. Chem. Ref. Data **30**, 1199 (2001).
[4] Y. U. Paulechka, J. Phys. Chem. Ref. Data **39**, 033108 (2010).
[5] J. M. P. França, C. A. Nieto de Castro, M. M. Lopes, and V. M. B. Nunes, J. Chem. Eng. Data **54**, 2569 (2009).
[6] V. V. Chaban and O. V. Prezhdo, J. Phys. Chem. Lett. **4**, 1423 (2013).
[7] *Ionic Liquids in Synthesis*, edited by P. Wasserscheid and T. Welton, (Wiley-VCH Verlag GmbH, Weinheim, Germany, 2007).
[8] *Ionic Liquids*, edited by B. Kirchner (Springer, Berlin, 2010).
[9] *Ionic Liquids—New Aspects for the Future*, edited by J.-I. Kadokawa (InTech, 2013).
[10] S. M. Urahata and M. C. C. Ribeiro, J. Chem. Phys. **122**, 024511 (2005).
[11] Y. Wang and G. A. Voth, J. Am. Chem. Soc. **127**, 12192 (2005).
[12] S. Izvekov and G. A. Voth, J. Chem. Phys. **123**, 134105 (2005).
[13] J. N. A. Canongia Lopes and A. A. H. Pádua, J. Phys. Chem. B **110**, 3330 (2006).
[14] M. F. C. Gomes, J. N. C. Lopes and A. A. H. Padua, Top. Curr. Chem. **290**, 161 (2010).
[15] A. Triolo, O. Russina, H.-J. Bleif and E. Di Cola, J. Phys. Chem. B **111**, 4641 (2007).
[16] O. Russina, A. Triolo, L. Gontrani, R. Caminiti, D. Xiao, L. G. Hines, Jr., R. A. Bartsch, E. L. Quitevis, N. Pleckhova and K. R. Seddon, J. Phys.: Condens. Matter **21**, 424121 (2009).
[17] A. Triolo, O. Russina, B. Fazio, G. B. Appetecchi, M. Carewska, and S. Passerini, J. Chem. Phys. **130**, 164521 (2009).
[18] O. Russina, A. Triolo, L. Gontrani, and R. Caminiti, J. Phys. Chem. Lett. **3**, 27 (2012).
[19] K. Shimizu, M. F. C. Gomes, A. A. H. Pádua, L. P. N. Rebelo, and J. N. Canongia Lopes, J. Mol. Struct.: THEOCHEM **946**, 70 (2010).
[20] M. A. A. Rocha, M. Bastos, J. A. P. Coutinho, and L. M. N. B. F. Santos, J. Chem. Thermodyn. **53**, 140 (2012).
[21] M. A. A. Rocha, C. F. R. A. C. Lima, L. R. Gomes, B. Schröder, J. A. P. Coutinho, I. M. Marrucho, J. M. S. S. Esperança, L. P. N. Rebelo, K. Shimizu, J. N. C. Lopes, and L. M. N. B. F. Santos, J. Phys. Chem. B **115**, 10919 (2011).
[22] J. Konicek, J. Suurkuusk, and J. Wadsö, Chem. Scr. **1**, 217 (1971).
[23] J. Suurkuusk and I. Wadsö, J. Chem. Thermodyn. **6**, 667 (1974).

[24]L. M. N. B. F. Santos, M. A. A. Rocha, A. S. M. C. Rodrigues, V. Štejfa, M. Fulem, and M. Bastos, J. Chem. Thermodyn. **43**, 1818 (2011).
[25]R. Sabbah, A. Xu-wu, J. S. Chickos, M. L. P. Leitão, M. V. Roux, and L. A. Torres, Thermochim. Acta **331**, 93 (1999).
[26]R. D. Chirico, V. Diky, J. W. Magee, M. Frenkel, and K. N. Marsh, Pure Appl. Chem. **81**, 791 (2009).
[27]M. E. Wieser and T. B. Coplen, Pure Appl. Chem. **83**, 359 (2011).
[28]M. E. Wieser and M. Berglund, Pure Appl. Chem. **81**, 2131 (2009).
[29]M. A. A. Rocha, C. M. S. S. Neves, M. G. Freire, O. Russina, A. Triolo, J. A. P. Coutinho, and L. M. N. B. F. Santos, "Alkylimidazolium Based Ionic Liquids: Impact of Cation Symmetry on Their Nanoscale Structural Organization," J. Phys. Chem. B (published online).
[30]M. A. A. Rocha, J. A. P. Coutinho, and L. M. N. B. F. Santos, J. Phys. Chem. B **116**, 10922 (2012).

Paper VI

"Volatility Study of [C_1C_1im][NTf_2] and [C_2C_3im][NTf_2] Ionic Liquids "

Marisa A. A. Rocha, Filipe M. S. Ribeiro, Bernd Schröder João A. P. Coutinho, Luís M. N. B. F. Santos

The Journal of Chemical Thermodynamics (2014), 68, 317-321.
doi: 10.1016/j.jct.2013.09.020

Note: The author of this thesis performed the all the experimental work, data analysis and contribute to the discussion and conclusions.

J. Chem. Thermodynamics 68 (2014) 317–321

Contents lists available at ScienceDirect

J. Chem. Thermodynamics

journal homepage: www.elsevier.com/locate/jct

Volatility study of $[C_1C_1im][NTf_2]$ and $[C_2C_3im][NTf_2]$ ionic liquids

Marisa A.A. Rocha [a,*], Filipe M.S. Ribeiro [a], Bernd Schröder [b], João A.P. Coutinho [b], Luís M.N.B.F. Santos [a,*]

[a] Centro de Investigação em Química, Departamento de Química e Bioquímica, Faculdade de Ciências da Universidade do Porto, R. Campo Alegre 687, P-4169-007 Porto, Portugal
[b] CICECO, Departamento de Química, Universidade de Aveiro, 3810-193 Aveiro, Portugal

ARTICLE INFO

Article history:
Received 10 June 2013
Received in revised form 14 September 2013
Accepted 16 September 2013
Available online 3 October 2013

Keywords:
Volatility
Ionic liquids
Vapor pressure
Thermodynamics
Entropy
Enthalpy
Vaporization
Knudsen effusion
1-Ethyl-3-propylimidazolium
1,3-Dimethylimidazolium
Bis(trifluoromethylsulfonyl)imide

ABSTRACT

Vapor pressures of 1,3-dimethylimidazolium bis(trifluoromethylsulfonyl)imide, ($[C_1C_1im][NTf_2]$) and 1-ethyl-3-propylimidazolium bis(trifluoromethylsulfonyl)imide, ($[C_2C_3im][NTf_2]$) ionic liquids were measured as a function of temperature using a Knudsen effusion apparatus combined with a quartz crystal microbalance. Enthalpies and entropies of vaporization were derived from the fitting of vapor pressure and temperature results to the Clarke and Glew equation. $[C_1C_1im][NTf_2]$ presents a higher enthalpy and entropy of vaporization than the neighboring members of the series. The enthalpy of vaporization of $[C_2C_3im][NTf_2]$ lies in between the asymmetric and symmetric ionic liquid series, reflecting a decrease in the electrostatic interactions due to a decrease of the charge accessibility between the ionic pairs when the methyl group is replaced by an ethyl group. The obtained higher volatility of $[C_2C_3im][NTf_2]$ arises from its asymmetric character, leading to an higher entropic contribution that compensates the enthalpic penalty. The border conditions ($[C_1C_1im][NTf_2]$, $[C_2C_1im][NTf_2]$ and $[C_2C_2im][NTf_2]$), topology ($[C_2C_3im][NTf_2]$) and symmetry/asymmetry of the ILs effect were evaluated and rationalized based on a comparative analysis of the thermodynamic properties, enthalpies and entropies of vaporization.

1. Introduction

Recently, we have reported on the (vapor + liquid) equilibrium study of the extended series of ILs, $[C_{N-1}C_1im][NTf_2]$ (with $N = 3$ to 9, 11, and 13), were the effect of nanostructuration of the $[C_{N-1}C_1im][NTf_2]$ series on the thermodynamic properties of vaporization and viscosity was highlighted [1]. In the previous work, the thermodynamic properties of vaporization presented trend shifts along the alkyl side chain length, related to a change in the molecular structure of the liquid phase around $[C_6C_1im][NTf_2]$ [1,2]. On another recent work, the effect of the cation's topological symmetry on the thermodynamic properties of vaporization for the symmetric ILs $[C_{N/2}C_{N/2}im][NTf_2]$, with $N = 4$, 6, 8, 10, 12, was reported [3]. Based on this work, it was possible to observe that the symmetry of the cation, $[C_{N/2}C_{N/2}im][NTf_2]$, leads to higher volatilities and lower enthalpies and entropies of vaporization, when compared with the asymmetric ILs, $[C_{N-1}C_1im][NTf_2]$.

The present work is an extension of the previous studies, which deals with the thermophysical properties of imidazolium based ionic liquids, ILs [1,3,4]. The vapor pressures of 1,3-dimethylimidazolium bis(trifluoromethylsulfonyl)imide, $[C_1C_1im][NTf_2]$, and 1-ethyl-3-propylimidazolium bis(trifluoromethylsulfonyl)imide, $[C_2C_3im][NTf_2]$, were determined at different temperatures, using a quartz microbalance Knudsen effusion apparatus [5]. Based on the previous results, the thermodynamic properties of vaporization of the ionic liquids with short alkyl chains are reported, discussed and evaluated considering the effect of the cation's symmetry and alkyl side chain length. The schematic representation of the studied imidazolium based ionic liquids is presented in figure 1.

2. Experimental

2.1. Synthesis, purification and characterization of compounds

1,3-Dimethylimidazolium bis(trifluoromethylsulfonyl)imide ($[C_1C_1im][NTf_2]$) has been synthesized by means of halide-free Carbonate Based Ionic Liquid Synthesis (CBILS©), of proionic/Sigma–Aldrich [6–8]. 1,3-Dimethylimidazolium hydrogen carbonate solution (~50% in methanol: water (2:3) (Sigma–Aldrich) has been treated with an stoichiometric amount of bis(trifluoromethylsulfonyl)imide lithium salt (Sigma–Aldrich). After separating from the precipitate, the aqueous phase has been discarded. The remaining organic phase has been washed with water. After further phase separation, remaining water and methanol has been removed in vacuum, leaving $[C_1C_1im][NTf_2]$. The sample was characterized by ^{1}H-NMR (chloroform-d, δ/ppm relative to TMS): 8.86 (s,1H),

* Corresponding authors. Tel.: +351 220 402 836; fax: +351 220 402 659.
E-mail addresses: marisa.alexandra.rocha@gmail.com (M.A.A. Rocha), lbsantos@fc.up.pt (L.M.N.B.F. Santos).

0021-9614/$ - see front matter © 2013 Elsevier Ltd. All rights reserved.
http://dx.doi.org/10.1016/j.jct.2013.09.020

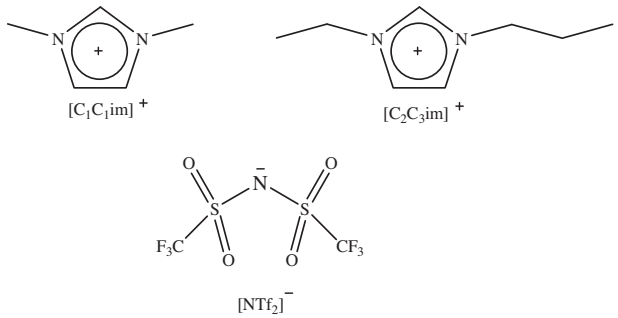

FIGURE 1. Schematic representation of the studied ionic liquids.

7.25 (d,2H), 3.97 (s,6H). 1-Ethyl-3-propylimidazolium bis(trifluoromethylsulfonyl)imide $[C_2C_3im][NTf_2]$ was acquired from IOLITEC with a stated purity of better than 99%. The studied ionic liquids were dried under reduced pressure (<10 Pa) and stirred constantly for a minimum of 48 h at 353 K, in order to reduce the presence of water or other volatile contents. Karl Fischer titration of the degassed samples revealed less than 100 ppm of water.

2.2. Quartz crystal microbalance Knudsen effusion apparatus

The vapor pressures of the two ionic liquids were measured as a function of temperature using a Knudsen effusion apparatus combined with a quartz crystal microbalance, KEQCM [5]. This apparatus comprises two mass loss detection techniques, gravimetric and quartz crystal microbalance, which enables the decrease of effusion times and the sample size. Furthermore, the combination of two mass loss determination techniques permits the instrument to measure vapor pressures from 0.005 Pa up to 1 Pa. The temperature is controlled within a temperature fluctuation of $\pm(1 \cdot 10^{-2})$ K, measured with a resolution better than $1 \cdot 10^{-3}$ K and along the working temperature range, the overall uncertainty is better than $\pm(2 \cdot 10^{-2})$ K. The vapor pressure data obtained with this apparatus for the ionic liquid have a typical pressure dependent uncertainty of 1% to 5% [5]. The relative atomic masses used were those recommended by the IUPAC Commission in 2007 [9]. The claimed uncertainty is done based on the overall results obtained from the fitting of the Clarke and Glew equation and is valid for the middle of the experimental p, T region.

3. Results and discussion

The vapor pressures of the studied imidazolium based ionic liquids were measured at several temperatures, using the Knudsen effusion apparatus combined with a quartz crystal microbalance. The experimental vapor pressures data are listed in table 1 and depicted in graphical representation as $\ln(p/\text{Pa}) = f[(1/T)/\text{K}^{-1}]$ in figure 2.

The experimental vapor pressures data as a function of the temperature were fitted using the Clarke and Glew equation (1) [10]:

$$R \cdot \ln\left[\frac{p(T)}{p^{o}}\right] = -\frac{\Delta_{l}^{g}G_{m}^{o}(\theta)}{\theta} + \Delta_{l}^{g}H_{m}^{o}(\theta) \cdot \left(\frac{1}{\theta} - \frac{1}{T}\right) + \Delta_{l}^{g}C_{p,m}^{o} \cdot \left[\frac{\theta}{T} - 1 + \ln\left(\frac{T}{\theta}\right)\right], \quad (1)$$

where $p(T)$ is the vapor pressure at the temperature T, p^{o} is the standard pressure ($p^{o} = 10^{5}$ Pa), θ is a selected reference temperature, R is the gas constant ($R = 8.3144621$ J · K^{-1} · mol^{-1}) [11], $\Delta_{l}^{g}G_{m}^{o}$ is the standard molar Gibbs energy of vaporization, $\Delta_{l}^{g}H_{m}^{o}$ is the standard molar enthalpy of vaporization, and $\Delta_{l}^{g}C_{p,m}^{o}$ is the difference between the heat capacities of the gaseous and of the liquid phases [$\Delta_{l}^{g}C_{p,m}^{o} = C_{p,m}^{o}(g) - C_{p,m}^{o}(l)$]. The values of $\Delta_{l}^{g}C_{p,m}^{o}$ were estimated for the same temperature, $T = 388$ K (mean temperature between 298.15 K and the working temperature interval), based on linear correlation of the literature values for $C_{p,m}^{o}(l)$ and $C_{p,m}^{o}(g)$ [12–15] as a function of the cation's alkyl chain length, using previously described methodology [1]. Considering the values of $\Delta_{l}^{g}C_{p,m}^{o}$, the

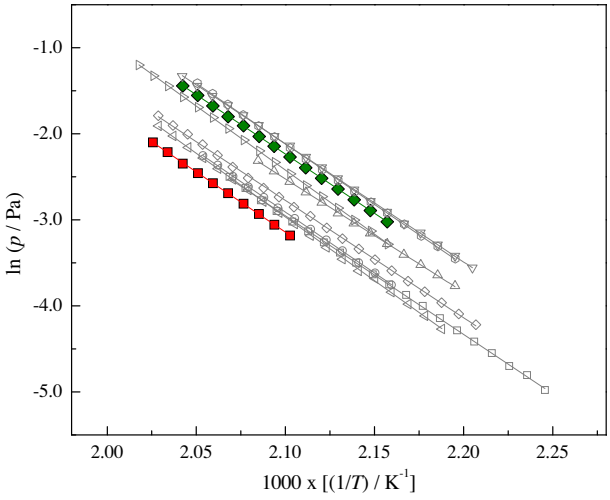

FIGURE 2. Plot of $\ln(p/\text{Pa}) = f[(1/T)/\text{K}^{-1}]$ for the studied ionic liquid: ■ (red) – $[C_1C_1im][NTf_2]$; ◆ (green) – $[C_2C_3im][NTf_2]$. Rocha *et al.* [1]: □ (gray) – $[C_2C_1im][NTf_2]$; ◇ (gray) – $[C_3C_1im][NTf_2]$; ○ (gray) – $[C_4C_1im][NTf_2]$; ◁ (gray) – $[C_5C_1im][NTf_2]$. Rocha *et al.* [3]: △ (gray) – $[C_2C_2im][NTf_2]$; ▽ (gray) – $[C_3C_3im][NTf_2]$; ⬡ (gray) – $[C_4C_4im][NTf_2]$; ▷ (gray) – $[C_5C_5im][NTf_2]$. (For interpretation of the references to color in this figure legend, the reader is referred to the web version of this article.)

TABLE 1
Experimental vapor pressures for the studied imidazolium based ILs, as obtained with the quartz crystal microbalance Knudsen effusion apparatus.

T/K	p/Pa	Δp/Pa	T/K	p/Pa	Δp/Pa	T/K	p/Pa	Δp/Pa
				$[C_1C_1im][NTf_2]$				
475.62	0.0415	0.0013	483.59	0.0678	−0.0002	491.67	0.1095	−0.0058
477.60	0.0470	0.0001	485.60	0.0763	−0.0005	493.68	0.1225	−0.0029
479.60	0.0533	−0.0033	487.60	0.0856	0.0034			
481.59	0.0601	−0.0018	489.62	0.0957	0.0096			
				$[C_2C_3im][NTf_2]$				
463.58	0.0486	−0.0016	473.62	0.0911	0.0051	483.60	0.1651	0.0094
465.61	0.0555	−0.0037	475.62	0.1034	0.0008	485.61	0.1872	0.0004
467.59	0.0629	−0.0015	477.63	0.1172	−0.0020	487.62	0.2112	−0.0044
469.60	0.0712	0.0016	479.56	0.1311	0.0014	489.62	0.2364	−0.0030
471.62	0.0807	0.0024	481.58	0.1487	−0.0046			

$\Delta p = p - p_{calc}$, where p_{calc} is calculated from the Clarke and Glew equation (equation (1)) with the parameters given in table 2.
Standard uncertainties, u, are $u(T) = 0.02$ K, $u(p) = (0.001 + 0.05 \cdot p)$ Pa, the 0.95 confidence level ($k \approx 2$).

TABLE 2
Parameters of Clarke and Glew equation fitted from the vapor pressure results and the derived standard ($p^o = 10^5$ Pa) molar entropy of vaporization for each studied IL at the reference temperature, θ.

T[a] interval/K	θ/K	$\Delta_l^g G_m^o(\theta)$/J · mol^{-1}	$\Delta_l^g H_m^o(\theta)$/J · mol^{-1}	$\Delta_l^g S_m^o(\theta)$/J · K^{-1} · mol^{-1}	r^2	$\Delta_l^g C_{p,m}^o$ (T = 388 K)[b]/J · K^{-1} · mol^{-1}
			[C_1C_1im][NTf$_2$]			
476 to 494	484.65[a]	56,990 ± 684	116,658 ± 482	123.1 ± 1.0	0.99986	−106 ± 5
	460.00	60,092 ± 678	119,271 ± 498	128.7 ± 1.0		
	298.15	84,366 ± 1305	136,427 ± 1050	174.6 ± 2.6		
			[C_2C_3im][NTf$_2$]			
464 to 490	476.60[a]	54,373 ± 327	114,523 ± 225	126.2 ± 0.5	0.99995	−121 ± 5
	460.00	56,504 ± 332	116,532 ± 239	130.5 ± 0.5		
	298.15	81,565 ± 1166	136,116 ± 920	183.0 ± 2.4		

r^2 is the linear regression coefficient.
[a] Mean temperature.
[b] $\Delta_l^g C_{p,m}^o$ (T = 388 K) estimated using the linear fitted function [$\Delta_l^g C_{p,m}^o$ (T = 388 K)/J · K^{-1} · mol^{-1} = −5.40 n(C) − 100.47] derived from fitting of the literature data of $\Delta_l^g C_{p,m}^o$ (T = 388 K) as a function of the cationic alkyl chain length [1].

standard ($p^o = 10^5$ Pa) molar enthalpies, entropies and Gibbs energies of vaporization at reference temperature, T = 298.15 K, were derived. The thermodynamic properties of vaporization at the mean temperature, $\langle T \rangle$, T = 460 K and at 298.15 K, derived from equation (1), are presented in table 2.

The analysis and the rationalization of the thermodynamic properties of vaporization of the studied ILs will be done taking into account the literature data for the [$C_{N-1}C_1$im][NTf$_2$] (N = 3, 4, 5, 6) [1,16], and [$C_{N/2}C_{N/2}$im][NTf$_2$] (N = 4, 6, 8, 10) ionic liquid series [3]. Although, the thermodynamic properties of vaporization of the extended series [$C_{N-1}C_1$im][NTf$_2$] (N = 7, 8, 9, 11, 12) are available in the literature [1], in this work we will be only focused on imidazolium based ionic liquids of short alkyl length (C_2C_1 to C_5C_1).

The standard molar Gibbs energies, enthalpies and entropies of vaporization at reference temperatures (460 and 298.15) K, as a function of the sum of the number of carbon atoms in the two alkyl side chains of the cation, are presented in figures 3–5.

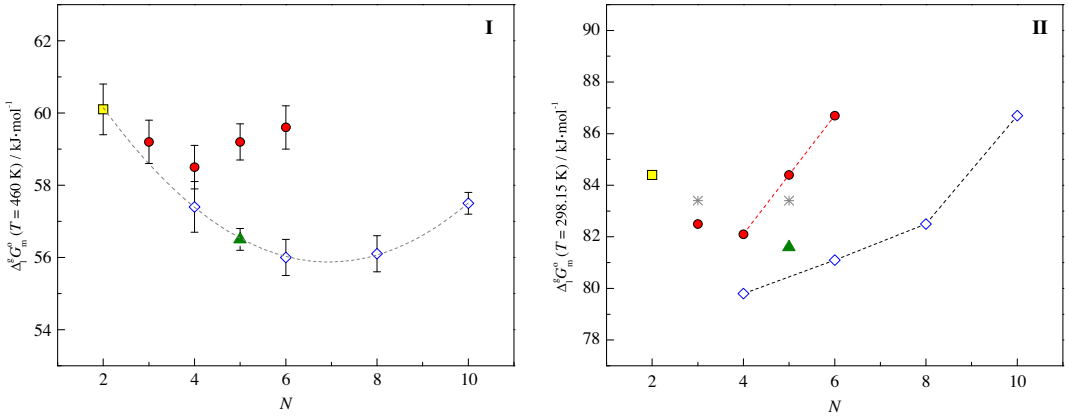

FIGURE 3. Standard ($p^o = 10^5$ Pa) molar Gibbs energy of vaporization as a function of the total number of carbons in the alkyl side chains of the cation, N: (I) $\Delta_l^g G_m^o$ (T = 460 K) and (II) $\Delta_l^g G_m^o$ (T = 298.15 K). ■ (yellow) – [C_1C_1im][NTf$_2$]; ▲ (green) – [C_2C_3im][NTf$_2$]; ● (red) – [$C_{N-1}C_1$im][NTf$_2$], N = 3, 4, 5, 6 [1]; ◇ (blue) – [$C_{N/2}C_{N/2}$im][NTf$_2$], N = 4, 6 [3]; ✳ (gray) – [$C_{N-1}C_1$im][NTf$_2$], N = 3, 4 [16]. (For interpretation of the references to color in this figure legend, the reader is referred to the web version of this article.)

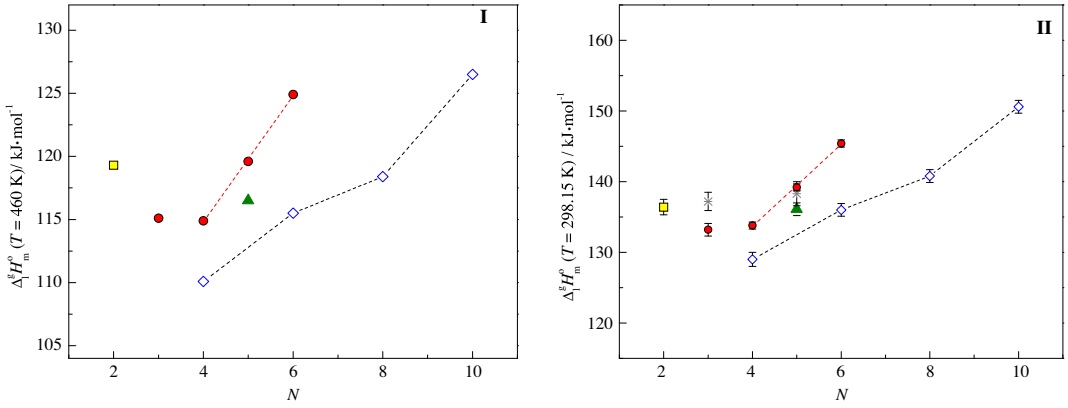

FIGURE 4. Standard ($p^o = 10^5$ Pa) molar enthalpies of vaporization as a function of the total number of carbons in the alkyl side chains of the cation, N: (I) $\Delta_l^g H_m^o$ (T = 460 K) and (II) $\Delta_l^g H_m^o$ (T = 298.15 K). ■ (yellow) – [C_1C_1im][NTf$_2$]; ▲ (green) – [C_2C_3im][NTf$_2$]; ● (red) – [$C_{N-1}C_1$im][NTf$_2$], N = 3, 4, 5, 6 [1]; ◇ (blue) – [$C_{N/2}C_{N/2}$im][NTf$_2$], N = 4, 6 [3]; ✳ (gray) – [$C_{N-1}C_1$im][NTf$_2$], N = 3, 4 [16]. (For interpretation of the references to color in this figure legend, the reader is referred to the web version of this article.)

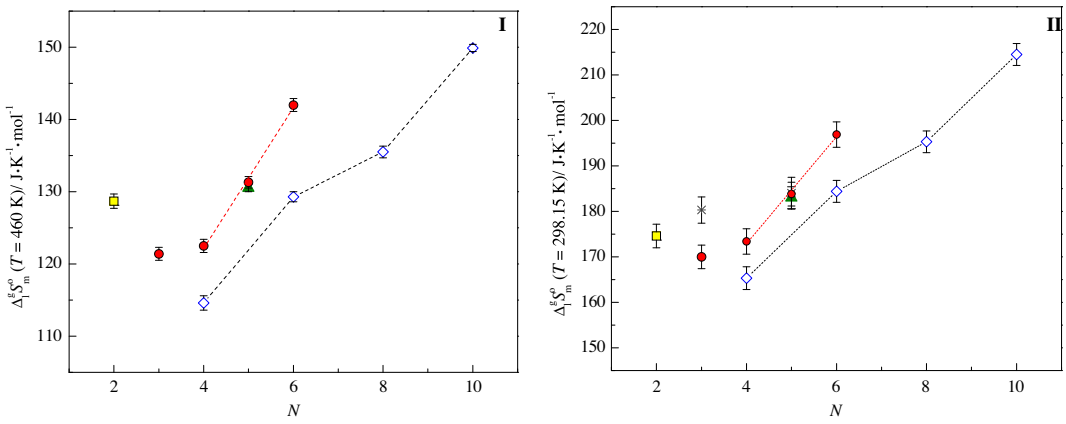

FIGURE 5. Standard (p^o = 10^5 Pa) molar entropy of vaporization as a function of the total number of carbons in the alkyl side chains of the cation, N: (I) $\Delta_l^g S_m^o$ (T = 460 K) and (II) $\Delta_l^g S_m^o$ (T = 298.15 K). ■ (yellow) – [C_1C_1im][NTf_2]; ▲ (green) – [C_2C_3im][NTf_2]; ● (red) – [$C_{N-1}C_1$im][NTf_2], N = 3, 4, 5, 6 [1]; ◇ (blue) – [$C_{N/2}C_{N/2}$im][NTf_2], N = 4, 6 [3]; ✳ (gray) – [$C_{N-1}C_1$im][NTf_2], N = 3, 4 [16]. (For interpretation of the references to color in this figure legend, the reader is referred to the web version of this article.)

In order to give an overview of the available data, the thermodynamic properties of vaporization published previously [1,16] were included in the graphical representations. The comparative analysis between the thermodynamic properties of vaporization obtained by our group [1] and the ones published by Zaitsau *et al.* [16] presented in the literature. Experimental vapor pressure data of ionic liquids is very scarce in the literature, and for the case of [C_1C_1im][NTf_2] and [C_2C_3im][NTf_2] no vapor pressure data was found. In order to avoid the mix-up of different levels of accuracy we will be restrict the comparison of the obtained results with literature data derived from direct experimental vapor pressures measurements.

The two studied ionic liquids and the eight imidazolium based ionic liquids published in the literature can be grouped schematically in a matrix diagram (figure 6), in which a relation between the alkyl side chains in positions 1 and 3 of the imidazolium is presented.

The asymmetric series, [$C_{N-1}C_1$im][NTf_2], is represented in the first line (red dots) and the symmetric, [$C_{N/2}C_{N/2}$im][NTf_2], as the diagonal (blue diamonds) of the diagram. [C_1C_1im][NTf_2] (yellow square) is the shortest alkyl side chain ionic liquid and is represented as the beginning of the symmetric and asymmetric homologous series. [C_2C_3im][NTf_2] (green triangle), despite being asymmetric, is located in an intermediate position in relation with the two homologous series.

A decrease of $\Delta_l^g G_m^o$, $\Delta_l^g H_m^o$ and $\Delta_l^g S_m^o$ starting from [C_1C_1im][NTf_2] to a minimum for the [C_2C_1im][NTf_2] and [C_3C_1im][NTf_2] (asymmetric series) and at [C_2C_2im][NTf_2] (symmetric series) and then increases with the alkyl chain length was observed. The expected increase of non-electrostatic interactions between ion pairs with the alkyl chain size is followed by a stronger decrease of the electrostatic potential due to the increase of the steric hindrance. This is supported and in agreement with the observed decrease of the $\Delta_l^g H_m^o$ and $\Delta_l^g S_m^o$ from [C_1C_1im][NTf_2] > [C_2C_1im][NTf_2] > [C_2C_2im][NTf_2]. Due to their singular molecular topology, a methyl group connected to the positions 1 and 3 of the imidazolium cation, the [C_1C_1im][NTf_2] presents an outlier behavior in the thermodynamic properties of vaporization. The lowest charge dispersion and the highest electrostatic ion pair interactions, which enhances the electrostatic interactions [17] between the ionic species (higher organization of the bulk). As a consequence, $\Delta_l^g H_m^o$ and $\Delta_l^g S_m^o$ is higher than for the rest of the nearest members of the series. It was found that the volatility of the ionic liquids, at T = 460 K, is ruled by the enthalpic contribution in which [C_1C_1im][NTf_2] presents

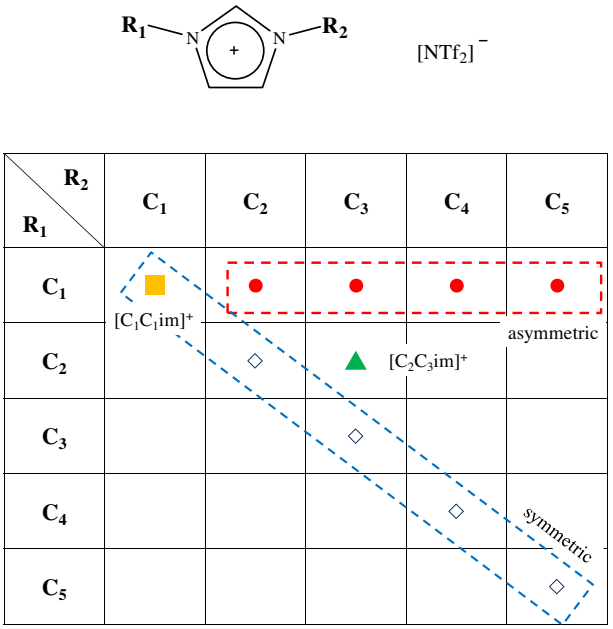

FIGURE 6. Schematic representation of the relations between the alkyl side chains of the cation of the ionic liquids under discussion.

the lower volatility compared with the other ionic liquids under discussion.

The [C_2C_3im][NTf_2] is located in an intermediate position between the asymmetric and symmetric ILs of the diagram. At the temperature of 460 K, their volatility fits the volatility trend of the symmetric series, however due to the higher enthalpies of vaporization and in smaller scale from the $\Delta_l^g C_{p,m}^o$ correction, at 298.15 K, the volatility of [C_2C_3im][NTf_2] is lower than the symmetric series. The entropy of vaporization of the [C_2C_3im][NTf_2] is similar to the [C_4C_1im][NTf_2], due to the asymmetric character of the cation. On the other hand, the enthalpy of vaporization is in between the asymmetric and symmetric ionic liquid series, reflecting a decrease in the electrostatic interactions between the ionic species arising from the decrease of charge accessibility between the ionic pairs (ethyl and a propyl group connected to the positions 1 and 3 of the cation). That is in agreement with the decrease of the $\Delta_l^g H_m^o$ from [C_1C_1im][NTf_2] > [C_2C_1im][NTf_2] > [C_2C_2im][NTf_2] discussed above.

Acknowledgments

Thanks are due to Fundação para a Ciência e Tecnologia (FCT), Lisbon, Portugal and to FEDER for financial support to Centro de Investigação em Química, University of Porto through the project Pest-C/QUI/UI0081/2011, and CICECO, University of Aveiro, through the project Pest-C/CTM/LA0011/2011. Marisa A.A. Rocha and Bernd Schröder acknowledges the financial support from FCT and the European Social Fund (ESF) under the Community Support Framework (CSF) for the award of a Ph.D. Research Grants SFRH/BD/60513/2009 and a Post-Doctoral Grant, SFRH/BPD/38637/2007, respectively.

References

[1] M.A.A. Rocha, C.F.R.A.C. Lima, L.R. Gomes, B. Schröder, J.A.P. Coutinho, I.M. Marrucho, J.M.S.S. Esperança, L.P.N. Rebelo, K. Shimizu, J.N. Canongia Lopes, L.M.N.B.F. Santos, J. Phys. Chem. B 115 (2011) 10919.
[2] K. Shimizu, M.F. Costa Gomes, A.A.H. Pádua, L.P.N. Rebelo, J.N. Canongia Lopes, J. Mol. Struct. – THEOCHEM 946 (2010) 70.
[3] M.A.A. Rocha, J.A.P. Coutinho, L.M.N.B.F. Santos, J. Phys. Chem. B 116 (2012) 10922.
[4] M.A.A. Rocha, M. Bastos, J.A.P. Coutinho, L.M.N.B.F. Santos, J. Chem. Thermodyn. 53 (2012) 140.
[5] L.M.N.B.F. Santos, L.M.S.S. Lima, C.F.R.A.C. Lima, F.D. Magalhães, M.C. Torres, B. Schröder, M.A.V. Ribeiro da Silva, J. Chem. Thermodyn. 43 (2011) 834.
[6] P.L. Short, Chem. Eng. News 84 (2006) 15.
[7] M. Freemantle, Chem. Eng. News 85 (2007) 23.
[8] http://www.sigmaaldrich.com/chemistry/chemical-synthesis/technology-spotlights/cbils.html.
[9] M.E. Wieser, M. Berglund, Pure Appl. Chem. 81 (2009) 2131–2156.
[10] E.C.W. Clarke, D.N. Glew, Trans. Faraday Soc. 62 (1966) 539.
[11] P.J. Mohr, B.N. Taylor, D.B. Newell, Rev. Mod. Phys. 84 (2012) 1527.
[12] Y.U. Paulechka, G.J. Kabo, V.N. Emel'yanenko, J. Phys. Chem. B 112 (2008) 15708.
[13] A.V. Blokhin, Y.U. Paulechka, G.J. Kabo, J. Chem. Eng. Data 51 (2006) 1377.
[14] Y.U. Paulechka, A.V. Blokhin, G.J. Kabo, A.A. Strechan, J. Chem. Thermodyn. 39 (2007) 866.
[15] A.V. Blokhin, Y.U. Paulechka, A.A. Strechan, G.J. Kabo, J. Phys. Chem. B 112 (2008) 4357.
[16] D.H. Zaitsau, G.J. Kabo, A.A. Strechan, Y.U. Paulechka, A. Tschersich, S.P. Verevkin, A. Heintz, J. Phys. Chem. A 110 (2006) 7303.
[17] A.M. Fernandes, M.A.A. Rocha, M.G. Freire, I.M. Marrucho, J.A.P. Coutinho, L.M.N.B.F. Santos, J. Phys. Chem. B 115 (2011) 4033.

JCT 13-328

Paper VII

"Alkylimidazolium Based Ionic Liquids: Impact of Cation Symmetry on their Nanoscale Structural Organization"

Marisa A. A. Rocha, Catarina M. S. S. Neves, Mara G. Freire, Olga Russina, Alessandro Triolo, João A. P. Coutinho, Luís M. N. B. F. Santos

Journal of Physical Chemistry B (2013) 117, 10889–10897.
doi: 10.1021/jp406374a

Note: The author of this thesis performed part of the viscosity and density measurements of the ionic liquids, data analysis and contribute to the discussion and conclusions.

THE JOURNAL OF PHYSICAL CHEMISTRY B

Article

pubs.acs.org/JPCB

Alkylimidazolium Based Ionic Liquids: Impact of Cation Symmetry on Their Nanoscale Structural Organization

Marisa A. A. Rocha,[†] Catarina M. S. S. Neves,[‡] Mara G. Freire,[‡] Olga Russina,[§] Alessandro Triolo,[∥] João A. P. Coutinho,*[,‡] and Luís M. N. B. F. Santos*[,†]

[†]Centro de Investigação em Química, Departamento de Química e Bioquímica, Faculdade de Ciências, Universidade do Porto, R. Campo Alegre 687, P-4169-007 Porto, Portugal

[‡]Departamento de Química, CICECO, Universidade de Aveiro, P-3810-193 Aveiro, Portugal

[§]Department of Chemistry, University of Rome "Sapienza", Piazzale Aldo Moro 5, I-00185 Rome, Italy

[∥]Istituto di Struttura della Materia, Consiglio Nazionale delle Ricerche, Via del Fosso del Cavaliere 100, I-00133 Rome, Italy

Supporting Information

ABSTRACT: Aiming at evaluating the impact of the cation symmetry on the nanostructuration of ionic liquids (ILs), in this work, densities and viscosities as a function of temperature and small−wide angle X-ray scattering (SWAXS) patterns at ambient conditions were determined and analyzed for 1-alkyl-3-methylimidazolium bis(trifluoromethylsulfonyl)imide (asymmetric) and 1,3-dialkylimidazolium bis-(trifluoromethylsulfonyl)imide (symmetric) series of ionic liquids. The symmetric IL series, $[C_{N/2}C_{N/2}im][NTf_2]$, presents lower viscosities than the asymmetric $[C_{N-1}C_1im][NTf_2]$ counterparts. For ionic liquids from $[C_1C_1im][NTf_2]$ to $[C_6C_6im][NTf_2]$, an odd−even effect in the viscosity along the cation alkyl side chain length was observed, in contrast with a linear increase found for the ones ranging between $[C_6C_6im][NTf_2]$ and $[C_{10}C_{10}im][NTf_2]$. The analysis of the viscosity data along the alkyl side chain length reveals a trend shift that occurs at $[C_6C_1im][NTf_2]$ for the asymmetric series and at $[C_6C_6im][NTf_2]$ for the symmetric series. These results are further supported by SWAXS measurements at ambient conditions. The gathered data indicate that both asymmetric and symmetric members are characterized by the occurrence of a distinct degree of mesoscopic structural organization above a given threshold in the side alkyl chain length, regardless the cation symmetry. The data also highlight a difference in the alkyl chain dependence of the mesoscopic cluster sizes for symmetric and asymmetric cations, reflecting a different degree of interdigitation of the aliphatic tails in the two families. The trend shift found in this work is related to the structural segregation in the liquid after a critical alkyl length size (CALS) is attained and has particular relevance in the cation structural isomerism with higher symmetry.

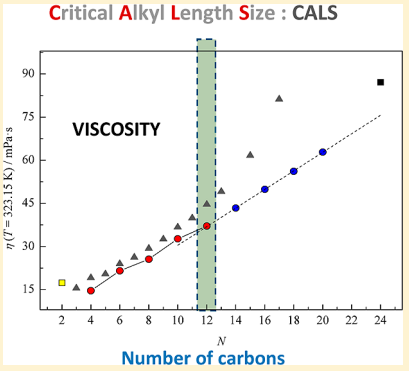

1. INTRODUCTION

The physical properties of ionic liquids (ILs) depend on the nature, size, and shape of both their cations and anions. Therefore, the properties of ILs can be tuned over a wide range by adjusting the structure and chemical composition of the constituting ions. This tunability feature, achieved with the high number of possible ILs that can be formed by combining different cation and anion pairs, by introducing isomerization effects and variations in the alkyl side chains, has made of ILs a focus of intensive research.[1,2] Some ILs can be considered as nanostructurated fluids in which the ion pairs arrange themselves into polar and nonpolar domains. It is the interplay of these two domains/interactions that eventually leads to the formation of medium-range nanoscale domains. This was first recognized by computer simulations studies[3,4] and then confirmed experimentally.[5−7] It was later shown, by molecular dynamics (MD) simulation, that the structural segregation in ILs depends on the size of the polar and nonpolar regions in which each ion may exist as dispersed or continuous microphases.[8,9] On the basis of these works[8,9] it was possible to detect that the transition between these two phases depends on the relative size of the high-charge and low-charge regions in each ion and on the size of the aliphatic moiety. These findings were later experimentally confirmed by a thermodynamic study concerning the vaporization of an extended series of ILs, $[C_{N-1}C_1im][NTf_2]$, where it was found, for the first time, that their thermodynamic properties of vaporization and their heat capacities present trend shifts along the studied series, which are related to a change in the molecular structure of the liquid for compounds larger than $[C_6C_1im][NTf_2]$.[10,11]

Additionally, the cation symmetry provides a different structural organization which also allows the fine-tuning of IL's physicochemical properties. Dzyuba and Bartsch[12] showed that the $[C_{N/2}C_{N/2}im][PF_6]$, with N = 8, 10, 14, 16, 18, and 20,

Received: June 27, 2013
Revised: August 5, 2013
Published: August 5, 2013

present melting temperatures below 373 K. These results demonstrated that one important factor that determines the low melting points of ILs is the asymmetric nature of the cation. Xiao et al.,[13] based on small−wide angle X-ray scattering (SWAXS) data and optical Kerr effect (OKE) spectra, showed that the symmetric IL series, $[C_{N/2}C_{N/2}im][NTf_2]$, presents higher local order and higher intermolecular dynamics in frequency than the asymmetric series, $[C_{N-1}C_1im][NTf_2]$. SWAXS measurements provide information related to the structural heterogeneities in ILs, and on the basis of the data gathered by this technique, Zheng et al.[14] found that, for the asymmetric imidazolium-based ILs, the structural heterogeneities extend over a large spatial scale when compared with the symmetric ILs. In the same work,[14] the authors observed that the densities for a symmetric/asymmetric IL pair, with a given total number of carbons, are similar and the viscosity of the asymmetric ILs is larger than that found for the symmetric fluids. Also, it was observed an odd−even effect on the viscosity data similar to what is found in simulations of ion diffusion coefficients.[14] A recent atomistic MD simulation[15] study and coarse grained molecular dynamics (CG-MD)[16] from the group of Balasubramanian focused on the exploration of mesoscopic order in symmetric imidazolium cations. The authors[15,16] studied symmetric and asymmetric cations with relatively short alkyl chains (the same ILs experimentally investigated by Xiao and co-workers[13]) with N = 4−6 and the bistriflamide anion. This study[15,16] essentially confirmed the structural scenario observed experimentally, providing atomistic inspection into the morphological properties of these systems, by mimicking the experimental data. The authors have also previously investigated the IL 1,3-didecylimidazolium hexafluorophosphate that, although bearing a different anion with respect to the ones for which experimental data are available, is characterized by the cation bearing two relatively long decyl chains. In this case the authors observed a peculiar structural behavior as the sample turned out to be characterized by a pseudolamellar structural organization.

Recently, Rocha et al.[17] assessed the effect of the cation topological symmetry on the thermodynamic properties of vaporization for the symmetric $[C_{N/2}C_{N/2}im][NTf_2]$ ILs, with N = 4, 6, 8, 10, and 12. It was found that the symmetric imidazolium-based ILs present a higher volatility than the asymmetric counterparts, $[C_{N-1}C_1im][NTf_2]$. The obtained vaporization results showed an enthalpic and entropic differentiation with a clearly discernible odd−even effect, with higher enthalpies and entropies of vaporization for the odd-numbered ILs, and in agreement with the trend observed by Zheng et al.[14]

Tariq et al.[18,19] explored the effect of temperature, cation alkyl side chain length, and cation and anion nature on a systematic study of densities, viscosities, surface tensions, and refractive indices in order to obtain some insights on the intermolecular forces and behavior in solutions of different ILs. The authors[18,19] suggested that the structural segregation in ILs does not affect, or at most it has a negligible effect on, the trends found for the volumetric behavior, in terms of both temperature and alkyl side chain length. However, based on the reanalysis of the viscosity data published by Tariq et al.[19] for the series of the $[C_{N-1}C_1im][NTf_2]$ ILs, Rocha et al.[10] have shown the existence of two regions in the viscosity dependency of the alkyl chain, and could relate it to the structural segregation occurring in longer alkyl chain ILs.

On the basis of all the described scenarios and aiming at evaluating the impact of the cation symmetry on the nanostructuration of ILs, in the present work, the densities and viscosities, and their dependence on temperature, of 1,3-dialkylimidazolium bis(trifluoromethylsulfonyl)imide, $[C_{N/2}C_{N/2}im][NTf_2]$, are compared to those of 1-alkyl-3-methylimidazolium bis(trifluoromethylsulfonyl)imide, $[C_{N-1}C_1im][NTf_2]$, for a wide set of N values. Moreover, SWAXS data have been collected at ambient temperature for the same group of fluids. The combined approaches were then used to properly evaluate the influence of the structural segregation of ILs as well as the symmetry effect on their thermophysical properties. The schematic representation of the studied ILs is presented in Figure 1.

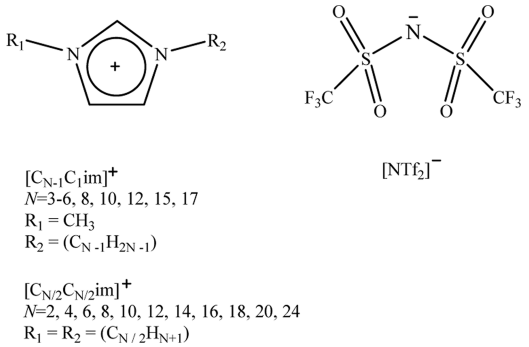

Figure 1. Schematic representation of the imidazolium based ionic liquids, where N corresponds to the total number of carbons in the two alkyl side chains in the cation. υ, number of alkyl groups in the longest chain that is either $\upsilon = N - 1$ in the case of asymmetric or $\upsilon = N/2$ in the case of symmetric.

2. EXPERIMENTAL SECTION

2.1. Materials. The densities, viscosities, and small−wide angle X-ray scattering (SWAXS) spectra were measured for the following imidazolium-based ionic liquids: 1-alkyl-3-methylimidazolium bis(trifluoromethylsulfonyl)imide, $[C_{N-1}C_1im][NTf_2]$ (with N = 3−6, 8, 10, 12, 15, 17), and 1,3-dialkylimidazolium bis(trifluoromethylsulfonyl)imide, $[C_{N/2}C_{N/2}im][NTf_2]$ (with N = 2−20, 24). All ILs were purchased from Iolitec. Before the measurements, the ionic liquids were dried and purified under high vacuum (10^{-3} Pa) and at moderate temperature (353 K) for at least 48 h. The purity of each ionic liquid was further evaluated by ^{1}H, ^{13}C, and ^{19}F NMR spectra, and all samples found to be >99 wt % pure. The water mass fraction contents were determined with a Metrohm 831 Karl Fischer coulometer, using a Hydranal-Coulomat AG from Riedel-de Haën. The water content, in all samples, was below 100 ppm.

2.2. Densities and Viscosities. Density and viscosity measurements for the pure ionic liquids were performed at atmospheric pressure in the temperature range from 278.15 to 363.15 K. Only for $[C_{14}C_1im][NTf_2]$, $[C_{16}C_1im][NTf_2]$, $[C_1C_1im][NTf_2]$, and $[C_{12}C_{12}im][NTf_2]$ were the measurements performed in a narrower temperature range since these compounds are solid at room temperature. The measurements were carried out using an automated SVM 3000 Anton Paar rotational Stabinger viscometer−densimeter, and the detailed description concerning the operation of the system, calibration, and validation is described elsewhere.[20] The SVM 3000 uses Peltier elements for fast and efficient thermostability, where the uncertainty in temperature is within ±0.02 K. The apparatus was calibrated by measuring the viscosity/density of three

Table 1. Fitting Parameters of eq 1 and Thermal Expansion Coefficients, α_p, at 323.15 K and 0.1 MPa for the Studied Ionic Liquids

ionic liquid	a	$(10^4 \times b)/K^{-1}$	$(10^7 \times c)/K^{-2}$	$(10^3 \times \alpha_p(T=323.15\ K))/K^{-1}$
		$[C_{N-1}C_1im][NTf_2]$		
$[C_2C_1im][NTf_2]$	7.5304 ± 0.0010	−7.004 ± 0.064	0.49 ± 0.10	0.669 ± 0.009
$[C_3C_1im][NTf_2]$	7.5029 ± 0.0010	−7.098 ± 0.066	0.60 ± 0.10	0.671 ± 0.009
$[C_4C_1im][NTf_2]$	7.4734 ± 0.0013	−7.125 ± 0.084	0.70 ± 0.13	0.667 ± 0.012
$[C_5C_1im][NTf_2]$	7.4570 ± 0.0010	−7.384 ± 0.061	1.099 ± 0.096	0.667 ± 0.009
$[C_7C_1im][NTf_2]$	7.4059 ± 0.0018	−6.83 ± 0.11	0.17 ± 0.18	0.672 ± 0.016
$[C_9C_1im][NTf_2]$	7.3787 ± 0.0014	−7.310 ± 0.090	0.92 ± 0.14	0.672 ± 0.013
$[C_{11}C_1im][NTf_2]$	7.3524 ± 0.0013	−7.417 ± 0.080	0.99 ± 0.12	0.678 ± 0.011
$[C_{14}C_1im][NTf_2]$	7.3274 ± 0.0064	−8.20 ± 0.37	2.03 ± 0.54	0.689 ± 0.051
$[C_{16}C_1im][NTf_2]$	7.3114 ± 0.0049	−8.30 ± 0.29	2.06 ± 0.41	0.697 ± 0.039
		$[C_{N/2}C_{N/2}im][NTf_2]$		
$[C_1C_1im][NTf_2]$	7.5675 ± 0.0013	−7.344 ± 0.078	1.10 ± 0.12	0.663 ± 0.011
$[C_2C_2im][NTf_2]$	7.5010 ± 0.0009	−6.970 ± 0.053	0.348 ± 0.082	0.675 ± 0.007
$[C_3C_3im][NTf_2]$	7.4571 ± 0.0010	−7.518 ± 0.065	1.19 ± 0.10	0.675 ± 0.009
$[C_4C_4im][NTf_2]$	7.4157 ± 0.0010	−7.530 ± 0.066	1.27 ± 0.10	0.671 ± 0.009
$[C_5C_5im][NTf_2]$	7.3750 ± 0.0009	−7.338 ± 0.058	0.907 ± 0.090	0.675 ± 0.008
$[C_6C_6im][NTf_2]$	7.3487 ± 0.0016	−7.49 ± 0.10	1.07 ± 0.15	0.680 ± 0.014
$[C_7C_7im][NTf_2]$	7.3216 ± 0.0016	−7.322 ± 0.097	0.86 ± 0.15	0.677 ± 0.014
$[C_8C_8im][NTf_2]$	7.2979 ± 0.0017	−7.36 ± 0.11	0.81 ± 0.16	0.684 ± 0.015
$[C_9C_9im][NTf_2]$	7.2761 ± 0.0024	−7.35 ± 0.15	0.79 ± 0.23	0.684 ± 0.021
$[C_{10}C_{10}im][NTf_2]$	7.2666 ± 0.0016	−7.63 ± 0.10	1.17 ± 0.15	0.687 ± 0.014
$[C_{12}C_{12}im][NTf_2]$	7.2361 ± 0.0070	−7.69 ± 0.41	1.28 ± 0.59	0.686 ± 0.056

Anton Paar standard calibration samples, APN7.5, APN26, and APN415, in steps of 5 K in the temperature range from 293.15 to 393.15 K. The reproducibility of the dynamic viscosity and density measurements is in accordance to the levels given by the manufacturer, namely ±0.35% and ±0.5 kg·m^{-3}, from 288.15 to 378.15 K.

2.3. Small−Wide Angle X-ray Scattering. SWAXS data were collected at the ID15b beamline at the ESRF synchrotron in Grenoble, using an instrumental setup that covers a wide momentum transfer range (namely, using a monochromatic beam with energy of 60 keV, one can access from 0.2 to ca. 20 Å^{-1}). Measurements were performed using a thermostat, maintaining the temperature at 298.15 K, and the samples were kept in a quartz capillary with an outer diameter of 2 mm. The corresponding empty cell contribution was subtracted. In the present paper we focus attention on the low Q portion of the data sets, limiting the range from 0.2 to 1.7 Å^{-1}. Measurements were also performed at the SWAXS beamline ID02 at ESRF (Grenoble), aiming to cover the lower Q range (0.03−1.2 Å^{-1}), using a monochromatic beam with energy of 19.8 keV and the same sample environment.

3. RESULTS AND DISCUSSION

3.1. Densities. Densities for pure ionic liquids were determined at atmospheric pressure and in the temperature range from 278.15 to 363.15 K, with the exception of $[C_{14}C_1im][NTf_2]$, $[C_{16}C_1im][NTf_2]$, $[C_1C_1im][NTf_2]$, and $[C_{12}C_{12}im][NTf_2]$ that display melting temperatures higher than room temperature. The experimental densities of the studied compounds are reported in Tables 1S and 2S as Supporting Information. The experimental density data (ρ), in the studied temperature (T) range, was further correlated using the second order polynomial equation:

$$\ln(\rho) = a + bT + cT^2 \quad (1)$$

where a, b, and c are constants obtained from the fitting. The graphic representation of the logarithm of density as a function of temperature and the respective relative deviations between the experimental density measured in this work and those reported in the literature[14,18,21−25] are presented as Supporting Information. The experimental density data gathered in this work are in good agreement with literature results showing deviations on the order of 0.2% for the majority of the studied ionic liquids. Two exceptions were observed for $[C_4C_1im][NTf_2]$[21,23] and $[C_2C_1im][NTf_2]$,[18] where significantly larger deviations were found. These higher deviations could be related to the IL sample purity (such as water content), deficiencies in the experimental methodologies, and lower apparatus accuracy.

The isobaric thermal expansion coefficient, α_p, which considers the volumetric changes with temperature, was calculated using eq 2:

$$\alpha_p = -\frac{1}{\rho}\left(\frac{\partial \rho}{\partial T}\right)_p = -\left(\frac{\partial \ln \rho}{\partial T}\right)_p = -(b + 2cT) \quad (2)$$

where ρ is the density in kg·m^{-3}, T is the temperature in K, and p is the standard pressure (10^5 Pa), while b and c are the fitting parameters of eq 1. Furthermore, based on the propagation of errors from the standard deviations coupled to each parameter adjustment, very small, i.e., no statistically significant, temperature dependence can be assigned to α_p. Table 1 lists the fitting parameters of eq 1 and the thermal expansion coefficients, at 323.15 K and 0.1 MPa, for all the investigated ionic liquids. The graphic representations of the density and thermal expansion coefficients, at 323.15 K and 0.1 MPa, as a function of the total number of carbons of the alkyl side chains length, N, are depicted in Figure 2. Due to the fact that some of the studied ionic liquids are solid at 298.15 K, the comparison between the two studied families is presented at T = 323.15 K.

Above N = 6 and for the same total number of carbons in the alkyl chains, the symmetric series seems to present a somewhat lower density than the asymmetric ones. The explanation of

dx.doi.org/10.1021/jp406374a | J. Phys. Chem. B 2013, 117, 10889−10897

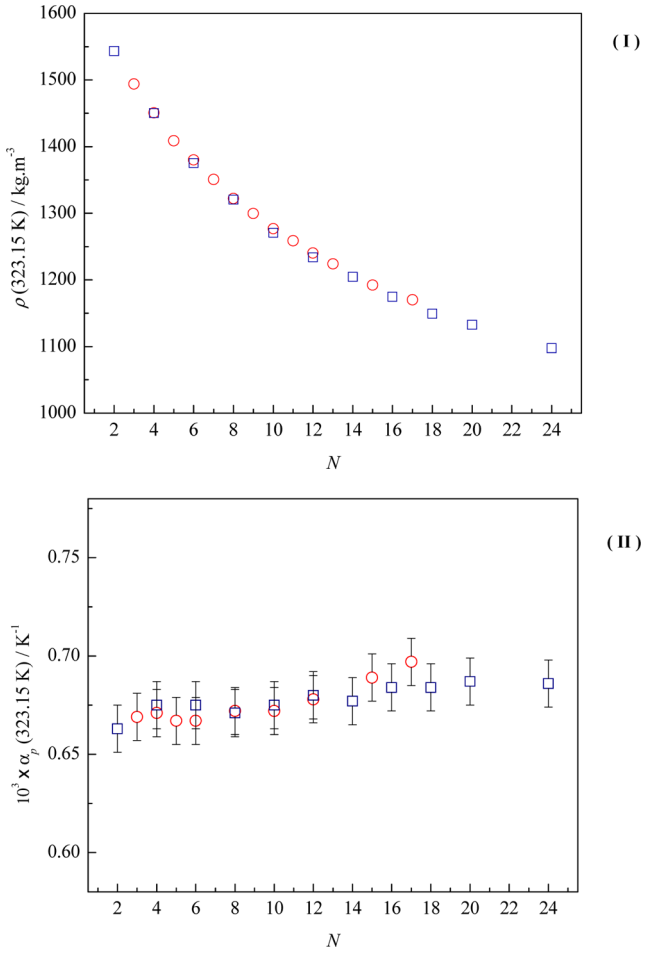

Figure 2. Graphic representation of the (I) density and (II) thermal expansion coefficient, at 323.15 K and 0.1 MPa, as a function of the total number of carbons of the alkyl side chain length, *N*. Red open circles, $[C_{N-1}C_1im][NTf_2]$; blue open squares, $[C_{N/2}C_{N/2}im][NTf_2]$.

that subtle difference is, in our opinion, quite challenging due to the small differentiation of the data. Concerning the thermal expansion coefficients, they are very similar, increasing only slightly with the alkyl chain length from 6.6×10^{-4} K^{-1} for $[C_1C_1im][NTf_2]$ to 7.0×10^{-4} K^{-1} for $[C_{16}C_1im][NTf_2]$. No significant differentiation could be detected in the thermal expansion coefficients between the asymmetry and symmetric IL series.

3.2. Viscosities. The experimental viscosity data (η) for the studied ionic liquids are reported in Tables 3S and 4S in the Supporting Information, and the graphic representations of ln(η/mPa·s) against the temperature and the deviations between the experimental viscosity measured in this work and those reported in the literature[14,19,25] are presented in Figures 3S and 4S in the Supporting Information. The experimental viscosity data for the $[C_{N-1}C_1im][NTf_2]$ series are in good agreement with the literature data, within 1%, with the exception of $[C_5C_1im][NTf_2]$,[19] which presents a relative deviation on the order of 8%. The higher positive deviation observed with this ionic liquid could be related to the higher water content which thus leads to a significant decrease in viscosity. In the case of the $[C_{N/2}C_{N/2}im][NTf_2]$ ionic liquids, the data presented for $[C_4C_4im][NTf_2]$ are in excellent agreement with the literature data.[25]

The data published previously by Zheng et al.[14] present a deviation of ±15% from our results, which indicates a systematic deviation in their viscosity sensitivity coefficient that could arise from the procedure used in the apparatus calibration based on a single viscosity standard. The experimental viscosity data were correlated using the Vogel–Tammann–Fulcher (VTF) model described in eq 3:

$$\eta(T) = A_\eta \exp\left[\frac{B_\eta}{T - C_\eta}\right] \quad (3)$$

where $\eta(T)$ is the viscosity in mPa·s, T is the temperature in K, and A_η, B_η, and C_η are adjustable parameters. The adjustable parameters were determined from the fitting of the experimental data using eq 3. The derived coefficients of the VTF equation are presented in Table 2. The correlated viscosities are in good agreement with the experimental data. For the studied ionic liquids a maximum relative deviation of 1% for the correlated values was achieved. Some of the data were already available in the literature[19] and are here used in the discussion/analysis aiming for better understanding of the results and related accuracy obtained in this work.

The viscosity describes the internal resistance of a fluid to a shear stress, and as is well-known, ionic liquids show higher viscosities than common molecular solvents show. The ionic liquid high viscosities are a direct consequence of their high molecular weights as well as their multiple intermolecular interactions (H-bonding, dispersive and electrostatic interactions). As the viscosity arises from intermolecular interactions, an increase in temperature will substantially decrease their intensity and therefore the viscosity. The energy barrier of the fluid to a shear stress, E, can be evaluated based on the viscosity dependence with the temperature using the following equation:

$$E = R\,\frac{\partial(\ln[\eta(T)])}{\partial(1/T)} = R\left(\frac{B_\eta}{\frac{C_\eta^{\,2}}{T^2} - \frac{2C_\eta}{T} + 1}\right) \quad (4)$$

The derived energy barrier, E, at T = 323.15 K, is listed in Table 2. The graphic representations of the viscosity and energy barrier at 323.15 K, and the pre-exponential coefficient, A_η, of the VTF equation as a function of the total number of carbon atoms in the alkyl chains of the cation, are presented in Figures 3 and 4.

As previously shown by us for other properties,[10,11,17] in Figures 3I and 4I there is a shift in the viscosity trend above $[C_6C_1im][NTf_2]$ for the asymmetric series and $[C_6C_6im]$-$[NTf_2]$ for the symmetric ILs. This trend shift is related to the structural organization of the liquid above a critical alkyl length size, CALS, and that is particularly emphasized by the cation structural isomerism with a higher symmetry for the $[C_{N/2}C_{N/2}im][NTf_2]$ series. In "Region A", in Figure 3I, a subtle but clearly visible odd–even effect for the viscosity with increasing alkyl side chain length was found in asymmetric ionic liquids (from $[C_2C_1im][NTf_2]$ to $[C_6C_1im][NTf_2]$), in contrast with the linear increase for the "Region B" (from $[C_7C_1im][NTf_2]$ to $[C_{12}C_1im][NTf_2]$). Starting from $[C_{12}C_1im][NTf_2]$, the ionic liquids show a progressive positive deviation (toward higher viscosities) from the linear behavior observed in "Region B". The positive deviation for the long alkyl side chain ionic liquids is identical to that observed for the long chain alkane derivatives[27,28] and is related to the increase of the conformational entropy and possibility of alkyl chain

dx.doi.org/10.1021/jp406374a | J. Phys. Chem. B 2013, 117, 10889–10897

Table 2. Fitting Coefficients of the VTF Equation for Viscosity Data of the Studied Ionic Liquids and the Derived Energy Barrier at 323.15 K

ionic liquid	A_η/(mPa·s)	B_η/K	C_η/K	$E(T=323.15\ K)/(kJ\cdot mol^{-1})$
		$[C_{N-1}C_1im][NTf_2]$		
$[C_2C_1im][NTf_2]$	0.215 ± 0.003	709.7 ± 4.0	157.1 ± 0.4	22.35 ± 0.24
$[C_3C_1im][NTf_2]$	0.194 ± 0.001	717.4 ± 1.6	166.8 ± 0.2	25.48 ± 0.15
$[C_4C_1im][NTf_2]$	0.160 ± 0.002	774.2 ± 4.4	163.6 ± 0.4	26.41 ± 0.31
$[C_5C_1im][NTf_2]$	0.156 ± 0.001	790.6 ± 2.0	166.2 ± 0.2	27.87 ± 0.16
$[C_6C_1im][NTf_2]$	0.134 ± 0.001	837.1 ± 2.6	164.6 ± 0.2	28.91 ± 0.17
$[C_7C_1im][NTf_2]$	0.119 ± 0.001	883.5 ± 1.6	162.8 ± 0.1	29.83 ± 0.09
$[C_8C_1im][NTf_2]$	0.113 ± 0.002	908.8 ± 4.5	162.8 ± 0.4	30.69 ± 0.34
$[C_9C_1im][NTf_2]$	0.108 ± 0.003	937.4 ± 7.8	162.4 ± 0.6	31.50 ± 0.54
$[C_{10}C_1im][NTf_2]$	0.096 ± 0.002	978.1 ± 6.8	160.9 ± 0.5	32.26 ± 0.46
$[C_{11}C_1im][NTf_2]$	0.096 ± 0.003	995 ± 10	161.3 ± 0.8	32.99 ± 0.74
$[C_{12}C_1im][NTf_2]$	0.087 ± 0.002	1034.5 ± 7.4	160.0 ± 0.6	33.74 ± 0.55
$[C_{14}C_1im][NTf_2]$	0.092 ± 0.009	1040 ± 34	163.4 ± 2.9	35.4 ± 2.9
$[C_{16}C_1im][NTf_2]$	0.097 ± 0.008	1039 ± 28	168.7 ± 2.3	37.8 ± 2.6
		$[C_{N/2}C_{N/2}im][NTf_2]$		
$[C_1C_1im][NTf_2]$	0.219 ± 0.003	716.7 ± 5.0	159.2 ± 0.6	23.15 ± 0.37
$[C_2C_2im][NTf_2]$	0.148 ± 0.004	821.0 ± 8.8	144.5 ± 0.9	22.33 ± 0.47
$[C_3C_3im][NTf_2]$	0.150 ± 0.001	782.2 ± 1.7	165.8 ± 0.2	27.43 ± 0.16
$[C_4C_4im][NTf_2]$	0.120 ± 0.002	863.9 ± 3.9	162.1 ± 0.3	28.92 ± 0.25
$[C_5C_5im][NTf_2]$	0.095 ± 0.002	948.7 ± 6.7	160.7 ± 0.5	31.21 ± 0.44
$[C_6C_6im][NTf_2]$	0.084 ± 0.002	998.7 ± 8.1	159.4 ± 0.6	32.34 ± 0.54
$[C_7C_7im][NTf_2]$	0.079 ± 0.005	1039 ± 19	158.6 ± 1.4	33.3 ± 1.3
$[C_8C_8im][NTf_2]$	0.067 ± 0.003	1104 ± 15	156.4 ± 1.0	34.47 ± 0.92
$[C_9C_9im][NTf_2]$	0.065 ± 0.002	1127.4 ± 8.1	156.4 ± 0.6	35.20 ± 0.55
$[C_{10}C_{10}im][NTf_2]$	0.079 ± 0.009	1086 ± 37	160.7 ± 2.8	35.7 ± 2.7
$[C_{12}C_{12}im][NTf_2]$	0.0704 ± 0.0003	1153.5 ± 1.4	161.2 ± 0.1	38.19 ± 0.10

folding. This is in agreement also with the higher energy barriers arising from the increase of shear stress.

In Figure 4I, the viscosities at 323.15 K of the symmetric IL series, $[C_{N/2}C_{N/2}im][NTf_2]$, and the asymmetric series, $[C_{N-1}C_1im][NTf_2]$, are compared. It can be observed that the ILs with symmetric cations present a significantly lower viscosity than the asymmetric series present. Moreover, the viscosity results for the $[C_{N/2}C_{N/2}im][NTf_2]$ series show a clearly discernible odd−even effect in "Region A" ($[C_2C_2im][NTf_2]$ to $[C_6C_6im][NTf_2]$), in which the odd-numbered ILs ($[C_3C_3im][NTf_2]$ to $[C_5C_5im][NTf_2]$) present higher viscosities. An odd−even effect was also recently reported for the thermodynamic study of vaporization for the same IL series, where higher enthalpies and entropies of vaporization for the odd-numbered $[C_3C_3im][NTf_2]$ and $[C_5C_5im][NTf_2]$ were found.[17] In "Region B", starting at $[C_7C_7im][NTf_2]$ and going until $[C_{10}C_{10}im][NTf_2]$, the odd−even effect ceases and a linear increase of the viscosity of 3.23 ± 0.03 mPa·s per methylene group, $-CH_2-$, is observed, essentially identical to the increment found for the asymmetric series of 3.6 ± 0.1 mPa·s. As observed for the $[C_{N-1}C_1im][NTf_2]$ series, above $[C_{12}C_1im][NTf_2]$, the viscosity of the ionic liquid $[C_{12}C_{12}im][NTf_2]$ deviates toward higher viscosities from the linear behavior observed in "Region B". The odd−even effect in "Region A" reflects and supports the existence of structuration on the charged region and highlights the effect of the short alkyl chain ILs in that interaction.[17] This effect is related to the predominant orientation of the terminal methyl group of the alkyl chain to the imidazolium ring and their influence in the cation−anion interaction. That phenomenon was also observed recently in the vapor−liquid equilibrium study for the same series[17] and is in qualitative agreement, with higher viscosities associated with higher enthalpies and entropies of vaporization. In Figures 3II and 4II, a fast decrease of the pre-exponential parameter of the VTF equation, A_η, is observed for "Region A", from $[C_3C_1im][NTf_2]$ to $[C_6C_1im][NTf_2]$ (for the asymmetric ILs) and from $[C_2C_2im][NTf_2]$ to $[C_6C_6im][NTf_2]$ (for the symmetric series). The sharp decrease of A_η in "Region A" is related to the decrease of the surface−volume ratio of the ion pair. In "Region B" the decrease of the A_η parameter with increasing chain length is significantly reduced and could be explained by the loss of the sphericity and increasing elongation shape of the ion pair above $[C_6C_1im][NTf_2]$ or $[C_6C_6im][NTf_2]$. The energy barrier at 323.15 K, E, increases monotonically in both IL series, with a faster increase in "Region A" and a linear increase around 1 $kJ\cdot mol^{-1}$ per methylene group in "Region B". This pattern is in qualitative agreement with the trend observed for the enthalpies of vaporization.[10,17] $[C_1C_1im][NTf_2]$ shows the typical and expected outlier behavior, for the viscosity and VTF parameters, relative to the homologues series, with a higher viscosity, higher A_η value, and higher energy barrier, E, than what would be obtained by the extrapolation of the homologues series trend.

3.3. Small−Wide Angle X-ray Scattering. SWAXS data from 1-alkyl-3-methylimidazolium bis(trifluoromethylsulfonyl)-imide, $[C_{N-1}C_1im][NTf_2]$ (with N = 3−13), and 1,3-dialkylimidazolium bis(trifluoromethylsulfonyl) imide, $[C_{N/2}C_{N/2}im][NTf_2]$ (with even members of N = 2−16, 20), are reported in Figure 5. SWAXS results for the asymmetric imidazolium-based ILs have been already reported, but only $[C_{N/2}C_{N/2}im][NTf_2]$ with N = 6, 8, and 10 have been studied so far.[13,14] Therefore, in the present work we present new findings using SWAXS data for the extended series of the

dx.doi.org/10.1021/jp406374a | J. Phys. Chem. B 2013, 117, 10889−10897

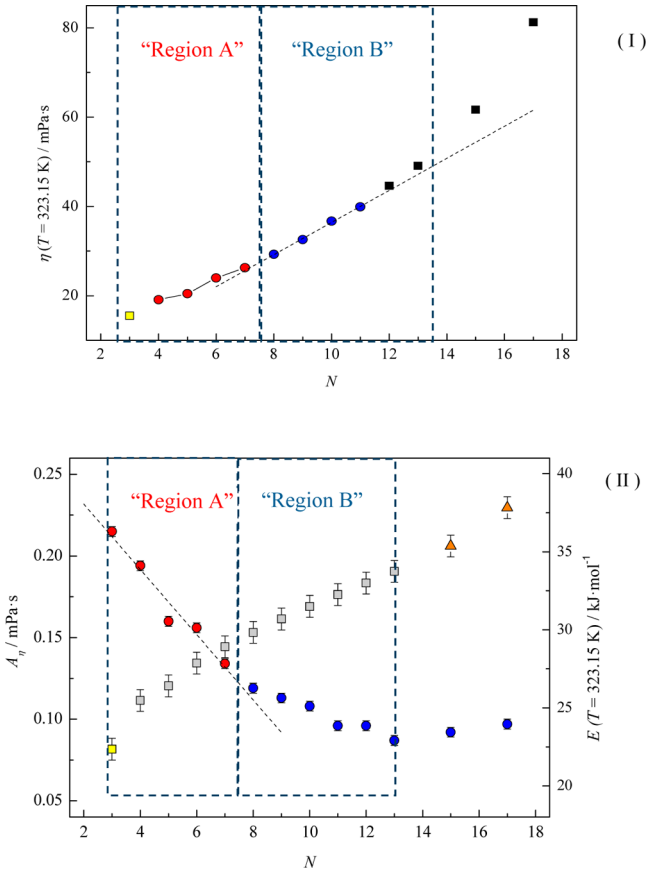

Figure 3. Plots of (I) viscosity (η/mPa·s) at T = 323.15 K and 0.1 MPa and (II) pre-exponential coefficient of the Vogel−Tammann−Fulcher equation (A_η/mPa·s) and energy barrier (E/kJ·mol^{-1}) at T = 323.15 K as a function of the total number of carbon atoms in the alkyl side chains of the cation, N, for the $[C_{N-1}C_1im][NTf_2]$ ionic liquid series. Yellow open squares and gray filled squares, E/kJ·mol^{-1}; red filled circles and blue filled circles, A_η/mPa·s.

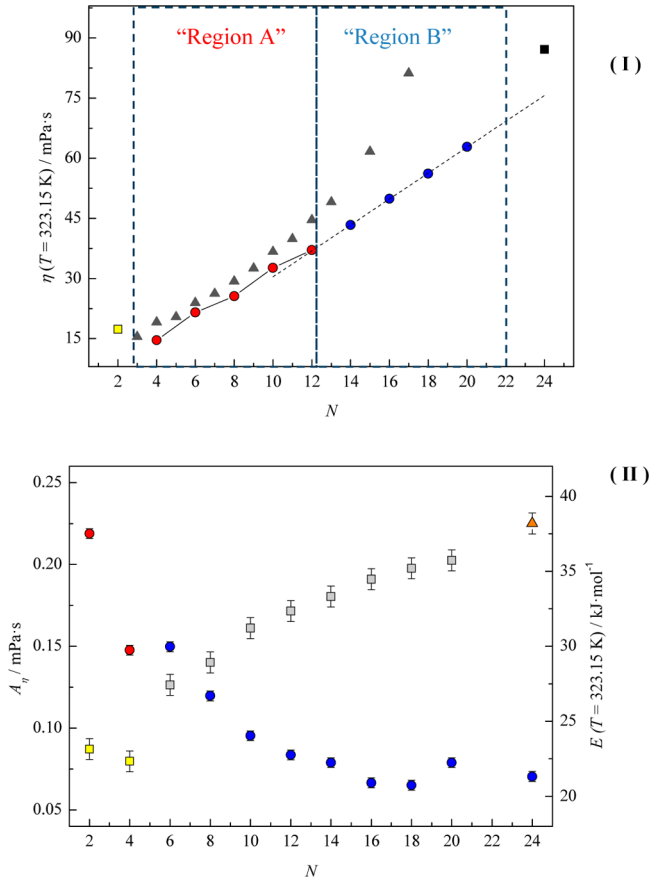

Figure 4. (I) Plots of $\eta(T$=323.15 K) = $f(N)$ for (yellow filled square, red filled circles, blue filled circles, black filled square) $[C_{N/2}C_{N/2}im][NTf_2]$and (gray filled triangles) $[C_{N-1}C_1im][NTf_2]$. (II) Graphic representation of the pre-exponential coefficient of the Vogel−Tammann−Fulcher equation (A_η/mPa·s) and energy barrier (E/kJ·mol^{-1}) at T = 323.15 K as a function of the total number of carbon atoms in the alkyl side chains of the cation, N, for $[C_{N/2}C_{N/2}im][NTf_2]$ ionic liquid family. Yellow filled squares and gray filled squares, E/kJ·mol^{-1}; red filled circles and blue filled circles, A_η/mPa·s.

$[C_{N-1}C_1im][NTf_2]$ and $[C_{N/2}C_{N/2}im][NTf_2]$ and further relate them to the density and viscosity data. It should be remarked that data were also collected over a wider Q range, but here we mainly focus on the low Q portion of the data, which contains information on the mesoscopic structural organization in these materials. Similarly to other ionic liquids, the diffraction patterns below 2 Å^{-1} are characterized by three amorphous peaks. In the family of dialkylimidazolium bistriflamide ionic liquids, these diffraction peaks are centered at ca. 0.2−0.5 (peak I), 0.9 (peak II), and 1.35 (peak III) Å^{-1}, for $[C_5C_5im][NTf_2]$, $[C_{10}C_1im][NTf_2]$, and $[C_{10}C_{10}im][NTf_2]$.

Samples such as $[C_5C_5im][NTf_2]$ and $[C_{10}C_1im][NTf_2]$ are characterized by comparable values for N, but inspection of Figure 6 indicates that the positions of the lowest Q peak, Q_I, are substantially different ($Q_I([C_5C_5im][NTf_2]) \approx 0.54$ Å^{-1} while $Q_I([C_{10}C_1im][NTf_2]) \approx 0.28$ Å^{-1}); on the other hand, the comparison between the data sets from $[C_{10}C_1im][NTf_2]$ ($Q_I \approx 0.28$ Å^{-1}) and $[C_{10}C_{10}im][NTf_2]$ ($Q_I \approx 0.32$ Å^{-1}) indicates that the corresponding values for Q_I are quite similar. This evidence indicates that the mesoscopic spatial order in these materials is mainly determined by the longest alkyl chain, regardless of the cation symmetry.

While volumetric quantities depend mostly on the total number carbons in the alkyl chain (N), the parameter that plays a role in determining the mesoscopic structure is υ, the number of alkyl groups in the longest chain that is either $\upsilon = N - 1$ in the case of asymmetric cations or $\upsilon = N/2$ in the case of symmetric cations. The available diffraction data (both data from ID15 (Figure 5) and from ID02 (data not shown)) were analyzed as a combination of three components (namely Lorentzian functions) in the Q range from 0.1 to 1.7 Å^{-1} in order to determine the alkyl chain length dependence of the peak positions, Q_i (with i = I−III), and, through Bragg's law ($D_i = 2\pi/Q_i$), of the corresponding characteristic sizes. These latter parameters are reported in Figure 7. The reported structural parameters are in excellent agreement with the existing data sets from other studies (e.g., our previous report for a more limited number of samples and the recent report from Martinelli and co-workers[29] that explores the asymmetric cation series up to $[C_{16}C_1im][NTf_2]$, at 323 K).

The higher Q peak centered at ca. 1.4 Å^{-1} (Q_{III}) shows barely any dependence on both alkyl chain length and the cation's symmetry/asymmetry, and the characteristic size associated with it, D_{III}, corresponds to ca. 4.6 Å.

This correlation length is related to characteristic distances between first neighbor opposite ions, which tends to organize in order to optimize their reciprocal distance, e.g., by imidazolium−imidazolium stacking. The intermediate peak

dx.doi.org/10.1021/jp406374a | J. Phys. Chem. B 2013, 117, 10889−10897

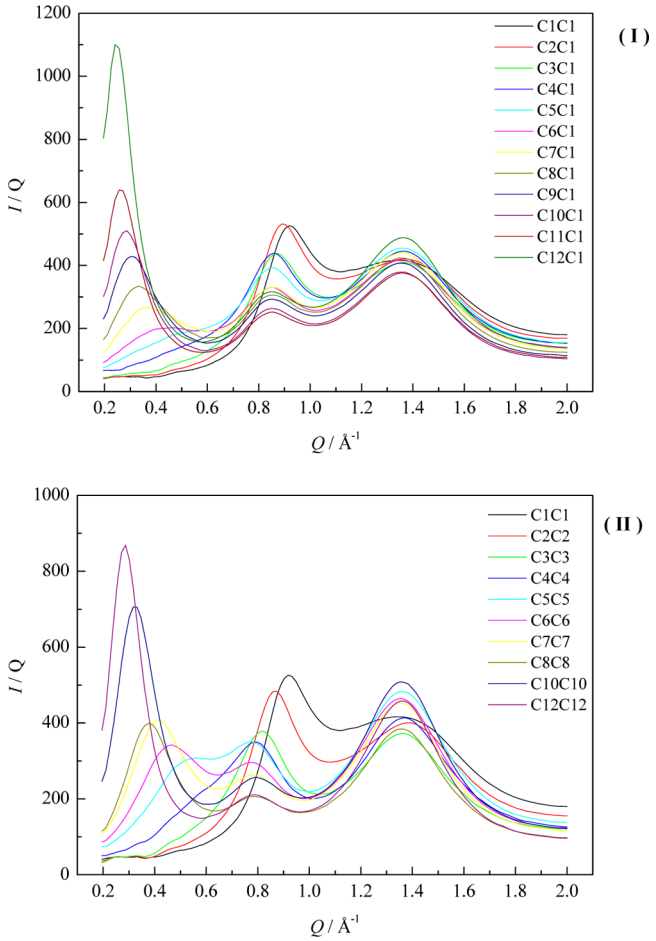

Figure 5. Comparison of SWAXS data for (I) $[C_{N-1}C_1im][NTf_2]$ (with N = 2−13) and (II) $[C_{N/2}C_{N/2}im][NTf_2]$ (with N = 2−16, 20, 24).

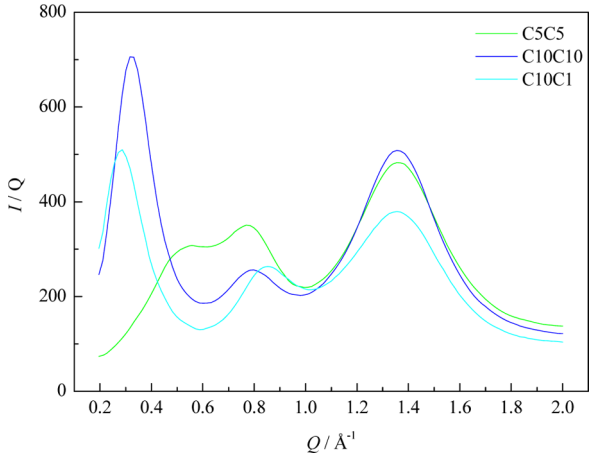

Figure 6. Comparison of SWAXS data for $[C_{10}C_1im][NTf_2]$, $[C_5C_5im][NTf_2]$, and $[C_{10}C_{10}im][NTf_2]$.

(Q_{II}) has a center at ca. 0.8 Å^{-1}. The position of this peak depends on the cation symmetry. The dependence from the alkyl chain length is negligible for $\upsilon \geq 6$, while it shifts substantially when increasing υ from 2 to 6. In particular in the case of dimethyl (υ = 1) D_{II} = 6.8 Å and upon increasing υ, D_{II} increases as well, reaching a plateau level at υ = 6, where D_{II} = 7.5 or 8.1 Å, for the case of asymmetric and symmetric cations,

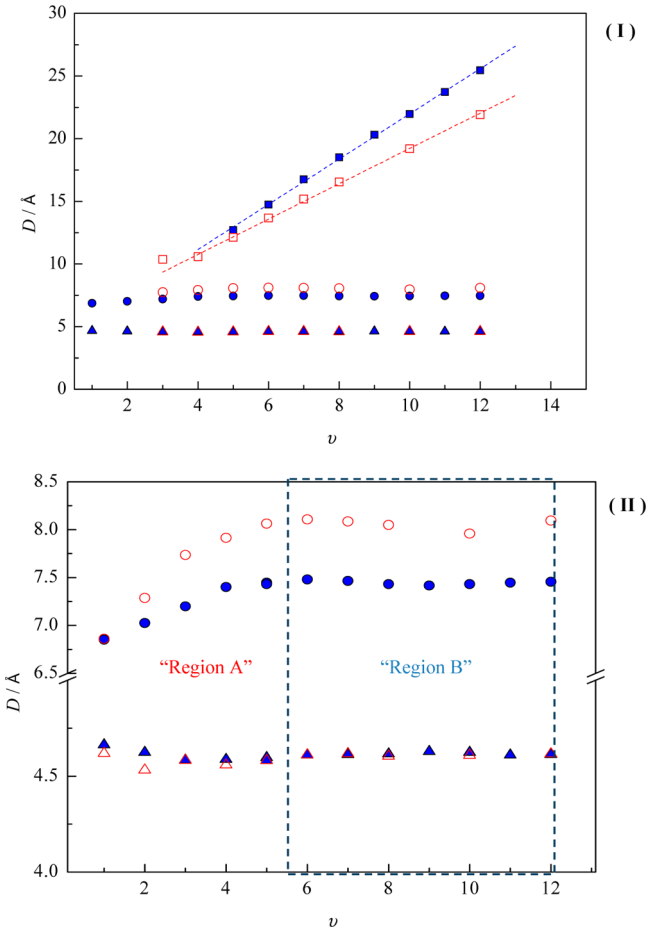

Figure 7. Alkyl chain length dependence of the characteristic size of nanoscale heterogeneities as obtained from the low Q peak position from SWAXS data for $[C_{N-1}C_1im][NTf_2]$ (with $\upsilon = N - 1$ = 2−12): blue filled squares, D_I, $dD/d\upsilon$ = (1.80 ± 0.02)Å; blue filled circles, D_{II}; blue filled triangles, D_{III}. Alkyl chain length dependence of the characteristic size of nanoscale heterogeneities as obtained from the low Q peak position from SWAXS data for $[C_{N/2}C_{N/2}im][NTf_2]$ (with $\upsilon = N/2$ = 1−8, 10, 12): red open squares, D_I, $dD/d\upsilon$ = (1.42 ± 0.02)Å; red open circles, D_{II}; red open triangles, D_{III}. υ, number of alkyl groups in the longest chain that is either $\upsilon = N - 1$ in the case of asymmetric or $\upsilon = N/2$ in the case of symmetric.

respectively. This spatial correlation length is related to the distance at which the closest ions of the same charge occur in the liquid. It is clear that above a threshold (υ = 6) this distance is no longer affected by the increasing of the alkyl chain length. These results are in agreement with the thermodynamic study concerning the vaporization of an extended series of ILs, $[C_{N-1}C_1im][NTf_2]$,[10,11] and with the viscosity data presented in this work, where two regions of different behaviors were found and a trend shift along the studied series was observed at $[C_6C_1im][NTf_2]$. Furthermore, it is noteworthy that a systematic difference of approximately 0.6 Å exists between these separations in the cases of symmetric and asymmetric cations. Presumably the steric hindrance stemming from the chains connected to the symmetric cations tends to separate the stacked imidazolium rings more than in the case of asymmetric cations. This may explain the slightly lower densities observed for the symmetric cations and is also in agreement with our recent work,[17] where a lower enthalpy of vaporization was found for the symmetric series $[C_{N/2}C_{N/2}im][NTf_2]$. The low

dx.doi.org/10.1021/jp406374a | J. Phys. Chem. B 2013, 117, 10889−10897

Q peak (Q_I) is centered at positions highly depending both on the cation symmetry and on the alkyl chain length. It can be appreciated that its detection is difficult for chains that are shorter than $\upsilon = 6$: in this range, it is both very broad and covered by the intermediate Q_{II} peak. Similarly to what has been reported in the past, the asymmetric series shows a linear trend for D vs υ.

A similar trend is here observed for the symmetric series over the whole accessible υ values. However, the characteristic slope for the two trends is substantially different well above the experimental uncertainties: namely, we find that the slopes $dD_I/d\upsilon$ are 1.80 ± 0.02 and 1.42 ± 0.02 Å per $-CH_2-$ unit for the asymmetric and symmetric cases, respectively. The large difference between these slopes indicates that the difference between D_I values for the symmetric and asymmetric series increases with increasing υ. This observation is at odds with the behavior found for the case of D_{II}, where the difference was maintained constant to ca. 0.6 Å for $\upsilon \geq 6$. Presumably these values for the slopes $dD_I/d\upsilon$ witness a different structural organization of the different classes of ILs. Wasserscheid and co-workers recently explored long chain symmetric imidazolium cation ILs, such as $[C_{12}C_{12}im][BF_4]$.[26]

In their report, they explore the crystalline structure of this class of ILs and find that the cations are organized in a rod shape with the two alkyl chains being stretched outward along the imidazolium plane, with the imidazolium/anion pair forming hydrophilic stacks and the long alkyl chains strongly interdigitating. This description of the crystalline phase of symmetric cation ILs is consistent with our present observation for the liquid state, as the value that we found for $dD_I/d\upsilon$ in the symmetric cation case is close to what one expects for full interdigitation (that corresponds to the $-CH_2-$ unit van der Waals diameter and equals ca. 1.27 Å per $-CH_2-$ unit). We already reported, including the case of bistriflamide anion, that asymmetric imidazolium cations are characterized by values for $dD_I/d\upsilon$ substantially larger than the $-CH_2-$ van der Waals diameter, thus indicating a poor interdigitation of the alkyl tails.[30,31]

The SWAXS technique probes merely structural effects and might be unable to detect purely dynamic effects that might affect the rheological measurements. We stress, however, that in a recent work[29] it was detected the existence of a nonnegligible deviation from linearity in the D vs υ trend plotted in Figure 7, for the alkyl chain length higher than $\upsilon > 12$, $[C_{12}C_1im][NTf_2]$. These measurements had been performed at higher temperatures (than room temperature); thus our data set probably is too limited to probe the existence of such a regime, which presumably is related to the higher conformational disorder in long alkyl chains. Such different structural conditions probably affect the viscosity of the corresponding ionic liquids.

4. CONCLUSIONS

The impact of the cation symmetry on the properties of imidazolium-based ionic liquid densities and viscosities as a function of temperature and small−wide angle X-ray scattering (SWAXS) patterns were evaluated for 1-alkyl-3-methylimidazolium bis(trifluoromethylsulfonyl)imide (asymmetric), $[C_{N-1}C_1im][NTf_2]$, and 1,3-dialkylimidazolium bis(trifluoromethylsulfonyl)imide (symmetric), $[C_{N/2}C_{N/2}im][NTf_2]$, series of ionic liquids. Above $N = 6$, the symmetric $[C_{N/2}C_{N/2}im][NTf_2]$ series presents a slightly lower density and lower viscosities than the asymmetric $[C_{N-1}C_1im][NTf_2]$ counterparts have. From $[C_2C_2im][NTf_2]$ to $[C_6C_6im][NTf_2]$, an odd−even effect was found in the viscosity along the alkyl side chain that vanishes in "Region B" where the structural segregation in ILs starts. A deviation toward higher viscosities for the long alkyl side chain ionic liquids was identified that could be related to the increase of the conformational entropy and possibility of alkyl chain folding, in agreement with the observed higher energy barriers arising from the increase of shear stress, identical to that observed for the long chain alkane derivatives.[27,28] Those observations were further supported by the small−wide angle X-ray scattering (SWAXS) pattern results. With reference to the observation of different chain length regimes in the density and viscosity determinations, it was observed that the SWAXS technique allows the detection of a major transition at $[C_5C_5im][NTf_2]$ for the symmetric series or at $[C_5C_1im][NTf_2]$ for the asymmetry series, where the low Q peak (Q_I) grows in a discernible way and the intermediate peak (Q_{II}) reaches a plateau level at $\upsilon = 6$. This threshold could be related to the development of well-established clusters stemming from the segregation of long enough alkyl tails in "Region B". This work highlights and gives an additional understanding of the change in the structural organization of ionic liquids above a critical alkyl length size (CALS).

■ ASSOCIATED CONTENT

Supporting Information

Experimental density and viscosity results at 0.1 MPa for the $[C_{N-1}C_1im][NTf_2]$ and $[C_{N/2}C_{N/2}im][NTf_2]$ ionic liquid series as a function of temperature. This material is available free of charge via the Internet at http://pubs.acs.org.

■ AUTHOR INFORMATION

Corresponding Authors

*E-mail: lbsantos@fc.up.pt.
*E-mail: jcoutinho@ua.pt.

Author Contributions

The manuscript was written through contributions of all authors. All authors have given approval to the final version of the manuscript. All authors contributed equally.

Notes

The authors declare no competing financial interest.

■ ACKNOWLEDGMENTS

This work was financed by national funding from FCT—Fundação para a Ciência e a Tecnologia, through the projects Pest-C/QUI/UI0081/2011, Pest-C/CTM/LA0011/2011, and PTDC/AAC-AMB/119172/2010. The authors also thank FCT for the Ph.D. and postdoctoral grants SFRH/BD/70641/2010, SFRH/BD/60513/2009, and SFRH/BPD/41781/2007 for C.M.S.S.N., M.A.A.R., and M.G.F., respectively. We acknowledge the European Synchrotron Radiation Facility for provision of synchrotron radiation facilities, and we would like to thank Dr. T. Narayanan and Dr. M. Di Michiel for assistance in using beamline ID02 and ID15b. A.T. acknowledges financial support from FIRB-Futuro in Ricerca (RBFR086BOQ) and PRIN (2009WHPHRH).

■ REFERENCES

(1) *Ionic Liquids in Synthesis*; Wasserscheid, P., Welton, T., Eds.; Wiley-VCH: Weinheim, Germany, 2003.

(2) Plechkova, N. V.; Seddon, K. R. In *Methods and Reagents for Green Chemistry: An Introduction*; Tundo, P., Perosa, A., Zecchini, F., Eds.; John Wiley & Sons, Inc.: New York, 2007; pp 105−130.
(3) Urahata, S. M.; Ribeiro, M. C. C. *J. Chem. Phys.* **2004**, *120*, 1855.
(4) Wang, Y.; Voth, G. A. *J. Am. Chem. Soc.* **2005**, *127*, 12192.
(5) Tokuda, H.; Ishii, K.; Susan, M. A. B. H.; Watanabe, M. *J. Phys. Chem. B* **2005**, *109*, 6103.
(6) Triolo, A.; Russina, O.; Bleif, H.-J.; Di Cola, E. *J. Phys. Chem. B* **2007**, *111*, 4641.
(7) Russina, O.; Triolo, A.; Gontrani, L.; Caminiti, R.; Xiao, D.; Hines, L. G., Jr.; Bartsch, R. A.; Quitevis, E. L.; Plechkova, N.; Seddon, K. R. *J. Phys.: Condens. Matter* **2009**, *21*, 424121.
(8) Pádua, A. A. H.; Canongia Lopes, J. N. *J. Phys. Chem. B* **2006**, *110*, 3330.
(9) Shimizu, K.; Costa Gomes, M. F.; Pádua, A. A. H.; Rebelo, L. P. N.; Canongia Lopes, J. N. *J. Mol. Struct.: THEOCHEM* **2010**, *946*, 70.
(10) Rocha, M. A. A.; Lima, C. F. R. A. C.; Gomes, L. R.; Schröder, B.; Coutinho, J. A. P.; Marrucho, I. M.; Esperança, J. M. S. S.; Rebelo, L. P. N.; Shimizu, K.; Canongia Lopes, J. N.; Santos, L. M. N. B. F. *J. Phys. Chem. B* **2011**, *115*, 10919.
(11) Rocha, M. A. A.; Bastos, M.; Coutinho, J. A. P.; Santos, L. M. N. B. F. *J. Chem. Thermodyn.* **2012**, *53*, 140.
(12) Dzyuba, S. V.; Bartsch, R. A. *Chem. Commun.* **2001**, 1466.
(13) Xiao, D.; Hines, L. G., Jr.; Li, S.; Bartsch, R. A.; Quitevis, E. L.; Russina, O.; Triolo, A. *J. Phys. Chem. B* **2009**, *113*, 6426.
(14) Zheng, W.; Mohammed, A.; Hines, L. G., Jr.; Xiao, D.; Martinez, O. J.; Bartsch, R. A.; Simon, S. L.; Russina, O.; Triolo, A.; Quitevis, E. L. *J. Phys. Chem. B* **2011**, *115*, 6572.
(15) Raju, S. G.; Balasubramanian, S. *J. Phys. Chem. B* **2010**, *114*, 6455.
(16) Raju, S. G.; Balasubramanian, S. *J. Mater. Chem.* **2009**, *19*, 4343.
(17) Rocha, M. A. A.; Coutinho, J. A. P.; Santos, L. M. N. B. F. *J. Phys. Chem. B* **2012**, *116*, 10922.
(18) Tariq, M.; Forte, P. A. S.; Costa Gomes, M. F.; Canongia Lopes, J. N.; Rebelo, L. P. N. *J. Chem. Thermodyn.* **2009**, *41*, 790.
(19) Tariq, M.; Carvalho, P. J.; Coutinho, J. A. P.; Marrucho, I. M.; Canongia Lopes, J. N.; Rebelo, L. P. N. *Fluid Phase Equilib.* **2011**, *301*, 22.
(20) Carvalho, P. J.; Regueira, T.; Santos, L. M. N. B. F.; Fernandez, J.; Coutinho, J. A. P. *J. Chem. Eng. Data* **2010**, *55*, 645.
(21) Tariq, M.; Serro, A. P.; Mata, J. L.; Saramago, B.; Esperança, J. M. S. S.; Canongia Lopes, J. N.; Rebelo, L. P. N. *Fluid Phase Equilib.* **2010**, *294*, 131.
(22) Jacquemin, J.; Husson, P.; Padua, A. A. H.; Majer, V. *Green Chem.* **2006**, *8*, 172.
(23) Tokuda, H.; Hayamizu, K.; Ishii, K.; Susan, M. A. B. H.; Watanabe, M. *J. Phys. Chem. B* **2005**, *108*, 16593.
(24) Costa Gomes, M. F.; Pison, L.; Pensado, A. S.; Padua, A. A. H. *Faraday Discuss.* **2012**, *154*, 41.
(25) Hasse, B.; Lehmann, J.; Assenbaum, D.; Wasserscheid, P.; Leipertz, A.; Fröba, A. P. *J. Chem. Eng. Data* **2009**, *54*, 2576.
(26) Wang, X.; Heinemann, F. W.; Yang, M.; Melcher, B. U.; Fekete, M.; Mudring, A. V.; Wasserscheid, P.; Meyer, K. *Chem. Commun.* **2009**, 7405.
(27) Queimada, A. J.; Stenby, E. H.; Marrucho, I. M.; Coutinho, J. A. P. *Fluid Phase Equilib.* **2003**, *212*, 303.
(28) Queimada, A. J.; Quiñones-Cisneros, S. E.; Marrucho, I. M.; Coutinho, J. A. P.; Stenby, E. H. *Int. J. Thermophys.* **2003**, *21*, 1221.
(29) Martinelli, A.; Maréchal, M.; Östlund, Å.; Cambedouzou, J. *Phys. Chem. Chem. Phys.* **2013**, *15*, 5510.
(30) Russina, O.; Triolo, A.; Gontrani, L.; Caminiti, R. *J. Phys. Chem. Lett.* **2012**, *3*, 27.
(31) Russina, O.; Triolo, A. *Faraday Discuss.* **2012**, *154*, 97.

Supporting Information

Alkylimidazolium Based Ionic Liquids: Impact of Cation Symmetry on the Nanoscale Structural Organization

Marisa A. A. Rocha [a], *Catarina M. S. S. Neves* [b], *Mara G. Freire* [b], *Olga Russina* [c], *Alessandro Triolo* [d], *João A. P. Coutinho* [*b], *Luís M. N. B. F. Santos* [*a]

[a] Centro de Investigação em Química, Departamento de Química e Bioquímica, Faculdade de Ciências da Universidade do Porto, R. Campo Alegre 687, P-4169-007 Porto, Portugal

[b] Departamento de Química, CICECO, Universidade de Aveiro, P-3810-193 Aveiro, Portugal

[c] Department of Chemistry, University of Rome "Sapienza", Rome, Italy

[d] Consiglio Nazionale delle Ricerche, Istituto di Struttura dellaMateria, Via del Fosso del Cavaliere 100, I-00133 Roma, Italy

*Corresponding authors

Fax: +351220402520; Tel: +351220402536; E-mail: lbsantos@fc.up.pt

Fax: +351234370084; Tel: +351234370200; E-mail: jcoutinho@ua.pt

TABLES

Table 1S. Experimental density results at 0.1 MPa, ρ, for the $[C_{N-1}C_1im][NTf_2]$ ionic liquid series as a function of temperature.

T / K	ρ / (kg·m^{-3})								
	$[C_2C_1im][NTf_2]$	$[C_3C_1im][NTf_2]$	$[C_4C_1im][NTf_2]$	$[C_5C_1im][NTf_2]$	$[C_7C_1im][NTf_2]$	$[C_9C_1im][NTf_2]$	$[C_{11}C_1im][NTf_2]$	$[C_{14}C_1im][NTf_2]$	$[C_{16}C_1im][NTf_2]$
278.15	1539.8	1495.3	1452.0	1422.5	1363.0	1316.4	1279.1		
283.15	1534.6	1490.3	1447.0	1417.6	1358.2	1311.8	1274.5		
288.15	1529.5	1485.3	1442.2	1412.9	1353.6	1307.3	1270.1		
293.15	1524.4	1480.3	1437.4	1408.1	1349.1	1302.8	1265.7		
298.15	1519.3	1475.3	1432.5	1403.4	1344.6	1298.4	1261.4		
303.15	1514.2	1470.4	1427.8	1398.7	1340.1	1294.1	1257.1		
308.15	1509.1	1465.4	1423.0	1394.0	1335.6	1289.7	1252.9		
313.15	1504.1	1460.5	1418.3	1389.3	1331.1	1285.4	1248.6		
318.15	1499.0	1455.6	1413.5	1384.7	1326.7	1281.1	1244.4		
323.15	1494.0	1450.7	1408.8	1380.1	1322.3	1276.8	1240.2	1192.2	1170.0
328.15	1489.0	1445.8	1404.1	1375.5	1317.8	1272.5	1236.0	1188.1	1165.9
333.15	1484.1	1441.0	1399.4	1370.9	1313.4	1268.3	1231.8	1184.1	1161.9
338.15	1479.1	1436.2	1394.8	1366.4	1309.0	1264.0	1227.6	1180.0	1157.9
343.15	1474.2	1431.4	1390.2	1361.8	1304.6	1259.8	1223.5	1176.0	1153.9
348.15	1469.3	1426.6	1385.5	1357.3	1300.2	1255.6	1219.4	1172.0	1149.9
353.15	1464.4	1421.9	1381.0	1352.8	1295.9	1251.4	1215.3	1168.0	1146.0
358.15	1459.6	1417.2	1376.4	1348.4	1291.5	1247.3	1211.2	1164.1	1142.1
363.15				1344.0	1287.2	1243.1	1207.2	1160.2	1138.2

Table 2S. Experimental density results at 0.1 MPa, ρ, for the $[C_{N/2}C_{N/2}im][NTf_2]$ ionic liquid series as a function of temperature.

	ρ / (kg·m^{-3})										
	$[C_1C_1im]$	$[C_2C_2im]$	$[C_3C_3im]$	$[C_4C_4im]$	$[C_5C_5im]$	$[C_6C_6im]$	$[C_7C_7im]$	$[C_8C_8im]$	$[C_9C_9im]$	$[C_{10}C_{10}im]$	$[C_{12}C_{12}im]$
T / K	$[NTf_2]$	$[NTf_2]$	$[NTf_2]$	$[NTf_2]$	$[NTf_2]$	$[NTf_2]$	$[NTf_2]$	$[NTf_2]$	$[NTf_2]$	$[NTf_2]$	$[NTf_2]$
278.15		1495.1	1418.3	1361.2	1310.3	1272.6	1242.4	1211.8	1185.9	1168.6	
283.15		1489.6	1413.4	1356.5	1305.7	1268.1	1237.9	1207.4	1181.5	1164.3	
288.15		1484.9	1408.6	1351.9	1301.2	1263.7	1233.6	1203.1	1177.4	1160.3	
293.15	1574.5	1479.9	1403.8	1347.3	1296.8	1259.3	1229.4	1198.9	1173.2	1156.2	
298.15	1569.2	1474.9	1399.0	1342.8	1292.4	1255.0	1225.2	1194.8	1169.2	1152.2	
303.15	1564.0	1469.9	1394.2	1338.2	1288.0	1250.7	1221.0	1190.7	1165.2	1148.2	
308.15	1558.8	1465.0	1389.5	1333.7	1283.7	1246.5	1216.9	1186.6	1161.2	1144.2	
313.15	1553.6	1460.0	1384.8	1329.3	1279.3	1242.2	1212.8	1182.6	1157.3	1140.3	
318.15	1548.5	1455.1	1380.2	1324.8	1275.0	1238.0	1208.7	1178.6	1153.4	1136.4	
323.15	1543.3	1450.2	1375.5	1320.3	1270.7	1233.8	1204.6	1174.5	1149.4	1132.5	1097.6
328.15	1538.2	1445.3	1370.9	1315.9	1266.4	1229.6	1200.6	1170.5	1145.5	1128.7	1093.9
333.15	1533.1	1440.5	1366.3	1311.5	1262.2	1225.5	1196.5	1166.5	1141.6	1124.8	1090.1
338.15	1528.1	1435.6	1361.7	1307.2	1257.9	1221.4	1192.5	1162.6	1137.7	1120.9	1086.4
343.15	1523.1	1430.8	1357.1	1302.8	1253.7	1217.2	1188.5	1158.6	1133.9	1117.1	1082.7
348.15	1518.1	1426.0	1352.6	1298.5	1249.5	1213.1	1184.4	1154.7	1130.0	1113.3	1079.0
353.15	1513.1	1421.2	1348.0	1294.2	1245.3	1209.0	1180.5	1150.7	1126.2	1109.5	1075.4
358.15	1508.1	1416.4	1343.6	1289.9	1241.2	1204.9	1176.5	1146.9	1122.3	1105.7	1071.7
363.15	1503.2	1411.7	1339.1	1285.6	1237.0	1200.9	1172.6	1143.0	1118.5	1102.0	1068.1

Table 3S. Experimental viscosity results at 0.1 MPa, η, for the $[C_{N-1}C_1im][NTf_2]$ ionic liquid series as a function of temperature.

T / K	η / (mPa·s)				
	$[C_5C_1im]$ $[NTf_2]$	$[C_9C_1im]$ $[NTf_2]$	$[C_{11}C_1im]$ $[NTf_2]$	$[C_{14}C_1im]$ $[NTf_2]$	$[C_{16}C_1im]$ $[NTf_2]$
278.15	181.43	354.64	475.42		
283.15	134.44	254.28	336.89		
288.15	101.97	187.03	244.85		
293.15	78.996	140.50	179.87		
298.15	62.384	107.90	138.02		
303.15	50.122	84.330	106.70		
308.15	40.871	67.020	83.910		
313.15	33.807	54.242	66.821		
318.15	28.317	44.260	54.337		
323.15	23.990	36.683	44.626	61.672	81.237
328.15	20.544	30.761	37.099	50.589	65.697
333.15	17.749	26.310	31.407	42.104	54.004
338.15	15.469	22.301	26.476	35.234	44.712
343.15	13.587	19.250	22.689	29.861	37.542
348.15	12.020	16.753	19.614	25.539	31.871
353.15	10.704			22.079	27.301
358.15	9.5897	12.970	14.999	19.137	23.480
363.15	8.6394	11.527	13.255	16.739	20.388

Table 4S. Experimental viscosity results at 0.1 MPa, η, for the $[C_{N/2}C_{N/2}im][NTf_2]$ ionic liquid series as a function of temperature.

T / K	η / (mPa·s)										
	$[C_1C_1im]$ $[NTf_2]$	$[C_2C_2im]$ $[NTf_2]$	$[C_3C_3im]$ $[NTf_2]$	$[C_4C_4im]$ $[NTf_2]$	$[C_5C_5im]$ $[NTf_2]$	$[C_6C_6im]$ $[NTf_2]$	$[C_7C_7im]$ $[NTf_2]$	$[C_8C_8im]$ $[NTf_2]$	$[C_9C_9im]$ $[NTf_2]$	$[C_{10}C_{10}im]$ $[NTf_2]$	$[C_{12}C_{12}im]$ $[NTf_2]$
278.15			157.39	204.75	305.55	372.75	465.71	575.61	684.41		
283.15			117.13	150.67	220.39	266.69	330.56	404.83	475.01		
288.15		44.808	89.324	113.75	163.09	195.54	240.46	292.06	339.25		
293.15	46.228	36.890	69.517	87.625	123.25	146.49	176.75	212.10	249.93		
298.15	38.058	30.784	55.111	68.739	94.970	111.92	135.49	161.77	185.49	211.59	
303.15	31.807	26.020	44.429	54.845	74.473	87.049	104.62	123.87	141.54	160.75	
308.15	26.902	22.207	36.364	44.435	59.352	68.762	82.094	96.548	109.70	124.24	
313.15	23.016	19.149	30.173	36.506	48.011	55.214	65.265	75.967	86.875	96.836	
318.15	19.891	16.654	25.348	30.374	39.369	44.973	52.931	61.309	69.230	77.761	
323.15	17.343	14.611	21.534	25.569	32.685	37.099	43.372	49.891	56.164	62.827	87.146
328.15	15.233	12.896	18.484	21.748	27.450	30.960	35.959	41.083	46.106	51.416	70.405
333.15	13.490	11.460	16.008	18.679	23.293	26.111	30.387	34.460	38.392	42.767	57.594
338.15	12.025	10.246	13.981	16.183	19.951	22.258	25.543	28.836	32.134	35.628	47.655
343.15	10.785	9.2098	12.304	14.135	17.242	19.136	21.840	24.529	27.245	30.114	39.842
348.15	9.7307	8.3154	10.903	12.440	15.021	16.582	18.834	21.057	23.278	25.687	33.629
353.15	8.8211	7.5397	9.7271	11.025	13.184	14.481	16.721		20.116	22.485	28.637
358.15	8.0304	6.8706	8.7290	9.8310	11.653	12.733	14.359	15.879	17.418	19.150	24.584
363.15	7.3432	6.2895	7.8756	8.8163	10.369	11.270	12.638	13.939	15.227	16.718	21.269

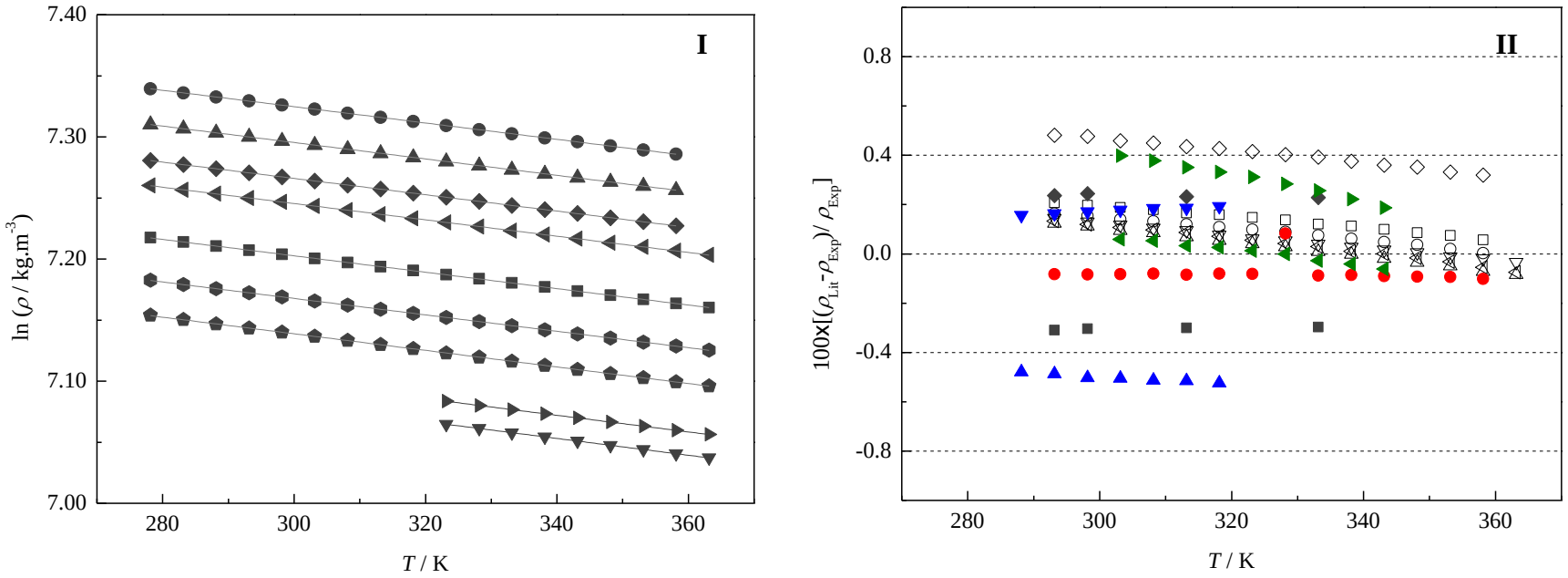

Figure 1S. (I) Logarithm of density as a function of temperature for the $[C_{N\text{-}1}C_1im][NTf_2]$ ionic liquid series: ● - $[C_2C_1im][NTf_2]$; ▲- $[C_3C_1im][NTf_2]$; ◆ - $[C_4C_1im][NTf_2]$; ◀ - $[C_5C_1im][NTf_2]$; ■ - $[C_7C_1im][NTf_2]$; ⬢ - $[C_9C_1im][NTf_2]$; ⬟ - $[C_{11}C_1im][NTf_2]$; ▶ - $[C_{14}C_1im][NTf_2]$; ▼ - $[C_{16}C_1im][NTf_2]$. The thin lines represent from the linear fitting of the experimental results by eq 1. **(II)** Relative deviations between the experimental density measured in this work (ρ_{exp}) and those reported in the literature (ρ_{exp}) as a function of temperature for the $[C_{N\text{-}1}C_1im][NTf_2]$ ionic liquid series. Tariq *et al.*[21] : □ - $[C_2C_1im][NTf_2]$; ○ - $[C_3C_1im][NTf_2]$; ◇ - $[C_4C_1im][NTf_2]$; ◁ - $[C_5C_1im][NTf_2]$; ▽ - $[C_7C_1im][NTf_2]$; △ - $[C_9C_1im][NTf_2]$; ▷ - $[C_{14}C_1im][NTf_2]$. Tariq *et al.* [18]: ■ - $[C_2C_1im][NTf_2]$; ◆ - $[C_4C_1im][NTf_2]$; Jacquemin *et al.*[22] : ● - $[C_2C_1im][NTf_2]$. Tokuda *et al.*[23] : ▼- $[C_2C_1im][NTf_2]$; ▲ - $[C_4C_1im][NTf_2]$. M.F. Costa Gomes *et al.*[24] ◀ - $[C_2C_1im][NTf_2]$, ▶ - $[C_4C_1im][NTf_2]$.

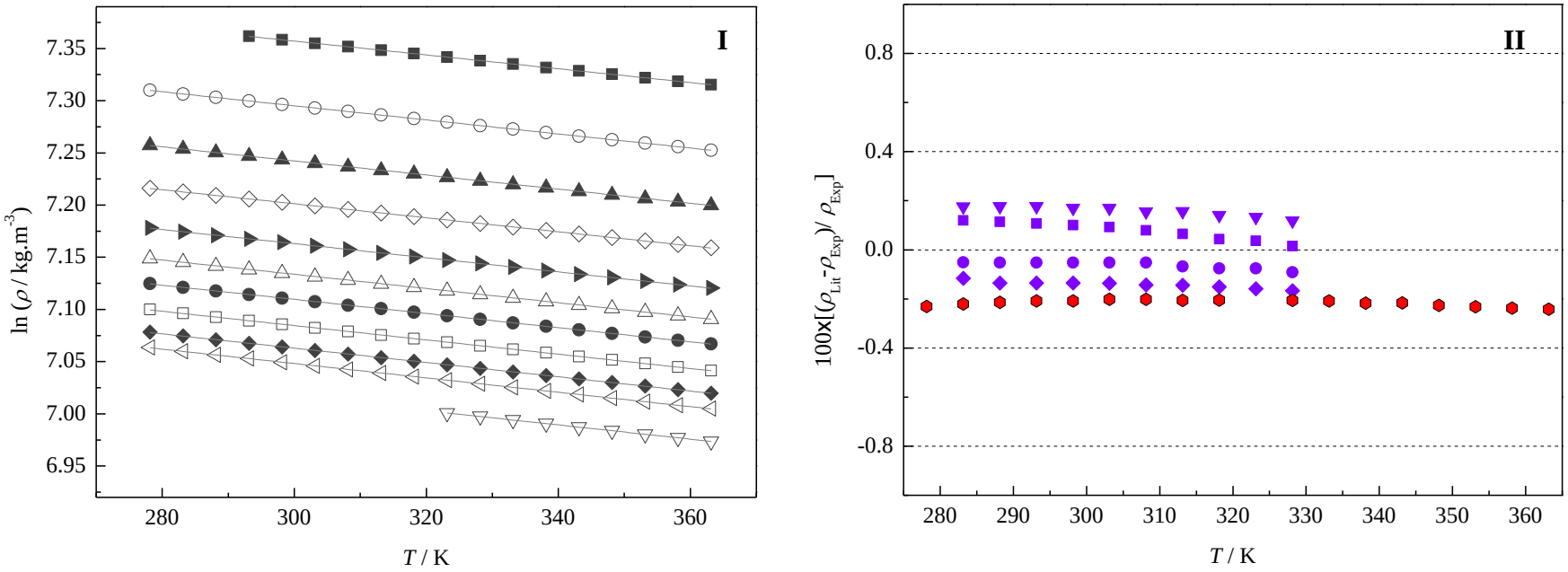

Figure 2S. (I) Logarithm of density as a function of temperature for the $[C_{N/2}C_{N/2}im][NTf_2]$ ionic liquid series: ■ - $[C_1C_1im][NTf_2]$; ○ - $[C_2C_2im][NTf_2]$; ▲- $[C_3C_3im][NTf_2]$; ◇ - $[C_4C_4im][NTf_2]$; ▶ - $[C_5C_5im][NTf_2]$; △ - $[C_6C_6im][NTf_2]$; ● - $[C_7C_7im][NTf_2]$; □ - $[C_8C_8im][NTf_2]$; ◆ - $[C_9C_9im][NTf_2]$; ◁ - $[C_{10}C_{10}im][NTf_2]$; ▽ - $[C_{12}C_{12}im][NTf_2]$. The thin lines results from the linear fitting of the experimental results. **(II)** Relative deviations between the experimental density measured in this work (ρ_{exp}) and those reported in the literature (ρ_{exp}) as a function of temperature for $[C_{N/2}C_{N/2}im][NTf_2]$ ionic liquid series. Zheng *et al.* [14]: ◆- $[C_2C_2im][NTf_2]$; ●- $[C_3C_3im][NTf_2]$; ■ - $[C_4C_4im][NTf_2]$; ▼ - $[C_5C_5im][NTf_2]$. Hasse *et al.* [25]: ⬢ - $[C_4C_4im][NTf_2]$.

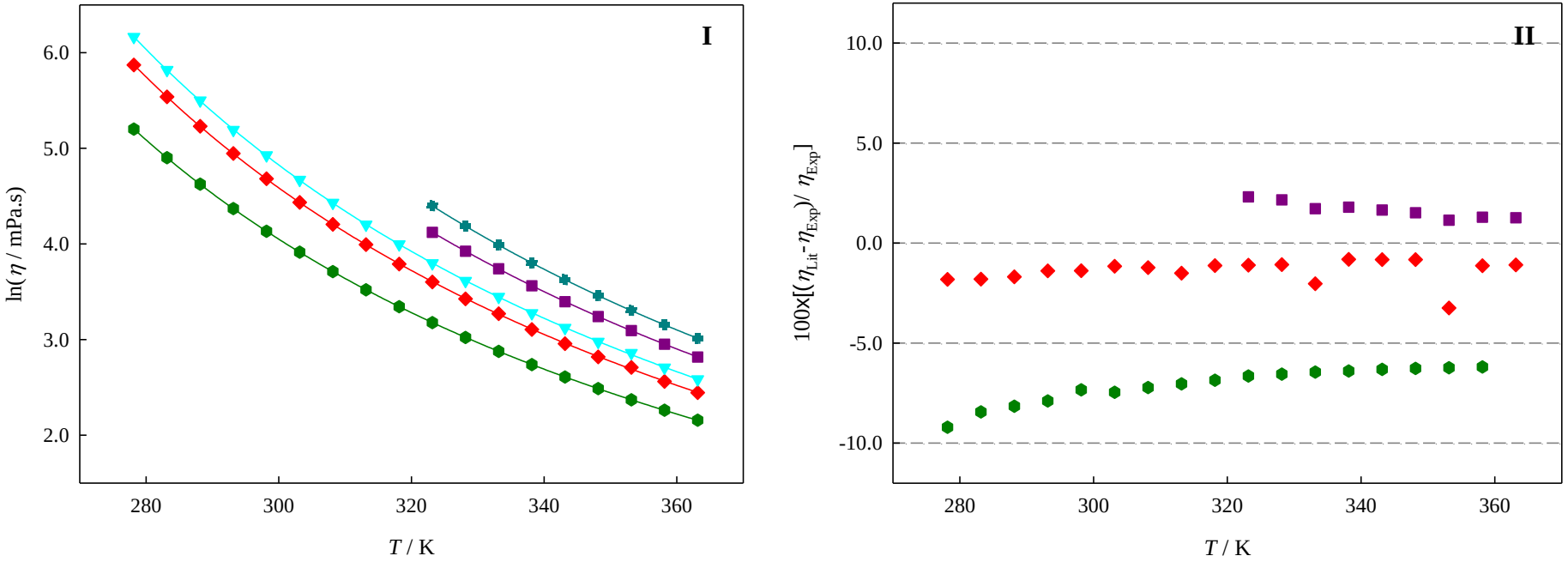

Figure 3S. (I) Graphic representation of ln(η / mPa·s) = f(T) for [$C_{N-1}C_1$im][NTf_2] ionic liquid family: ⬢ - [C_5C_1im][NTf_2]; ◆ - [C_9C_1im][NTf_2]; ▼ - [$C_{11}C_1$im][NTf_2]; ■ - [$C_{14}C_1$im][NTf_2]; ✚ - [$C_{16}C_1$im][NTf_2]. . The solid lines represent the Vogel-Tammann-Fulcher fitting (equation 5). **(II)** Relative deviations between the experimental viscosity measured in this work (η_{exp}) and those reported in the literature (η_{exp}) as a function of temperature. Tariq *et al.*[19]: ⬢ - [C_5C_1im][NTf_2]; ◆ - [C_9C_1im][NTf_2]; ■ - [$C_{14}C_1$im][NTf_2].

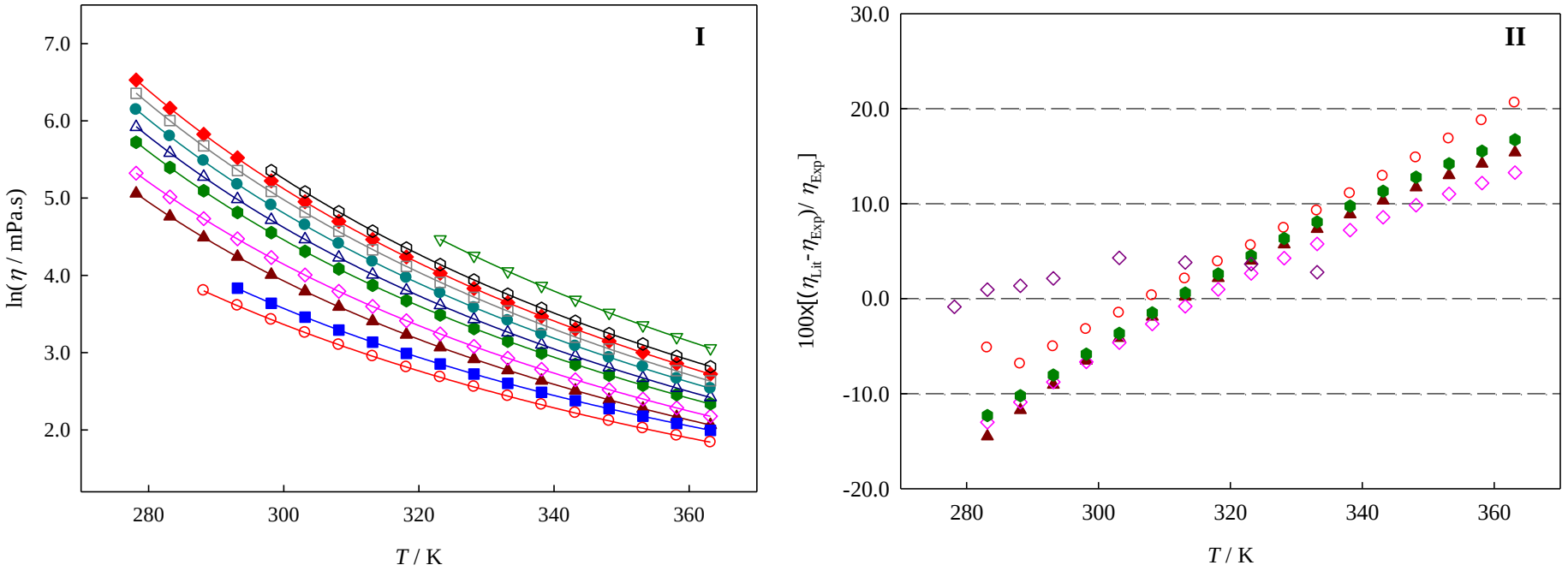

Figure 4S. (I) Graphic representation of ln(η / mPa·s) = f(T) for the [$C_{N/2}C_{N/2}$im][NTf_2] ionic liquid series: ■ - [C_1C_1im][NTf_2]; ○ - [C_2C_2im][NTf_2]; ▲- [C_3C_3im][NTf_2]; ◇ - [C_4C_4im][NTf_2]; ⬢ - [C_5C_5im][NTf_2]; △ - [C_6C_6im][NTf_2]; ● - [C_7C_7im][NTf_2]; □ - [C_8C_8im][NTf_2]; ◆ - [C_9C_9im][NTf_2]; ⬡ - [$C_{10}C_{10}$im][NTf_2]; ▽ - [$C_{12}C_{12}$im][NTf_2]. The solid lines represent the Vogel-Tammann-Fulcher fittings (equation 5). **(II)** Relative deviations between the experimental viscosity measured in this work (η_{exp}) and those reported in the literature (η_{exp}) as a function of temperature, for [$C_{N/2}C_{N/2}$im][NTf_2] ionic liquid series. Zheng *et al.* [14]: ○- [C_2C_2im][NTf_2]; ▲- [C_3C_3im][NTf_2]; ◇ - [C_4C_4im][NTf_2]; ⬢ - [C_5C_5im][NTf_2]. Hasse *et al.* [25]: ◇ - [C_4C_4im][NTf_2].

References

1 P. Wasserscheid, T. Welton, Eds. Ionic Liquids in Synthesis; Wiley-VCH: Weinheim, Germany, 2003.
2 N. V. Plechkova, K. R. Seddon, In Methods and Reagents for Green Chemistry: An Introduction; P. Tundo; A. Perosa; F. Zecchini, Eds.; John Wiley & Sons, Inc.: New York, 2007, 105-130.
3 S. M. Urahata, M. C. C. Ribeiro, *J. Chem. Phys.*, 2004, **120**, 1855.
4 Y. Wang, G. A. Voth, *J. Am. Chem. Soc.*, 2005, **127**, 12192.
5 H. Tokuda, K. Ishii, M. A. B. H. Susan, M. Watanabe, *J. Phys. Chem. B*, 2005, **109**, 6103.
6 A. Triolo, O. Russina, H.-J.Bleif, E. Di Cola, *J. Phys. Chem. B*, 2007, **111**, 4641.
7 O. Russina, A.Triolo, L. Gontrani, R. Caminiti, D. Xiao, L. G. Hines Jr., R. A. Bartsch, E. L. Quitevis, N. Plechkova, K. R. Seddon, *J. Phys.: Condens. Matter*, 2009, **21**, 424121.
8 A. A. H. Pádua, J. N. Canongia Lopes, *J. Phys. Chem. B*, 2006, **110**, 3330.
9 K. Shimizu, M. F. Costa Gomes, A. A. H. Pádua, L. P. N. Rebelo, J. N. Canongia Lopes, *J. Mol. Struct: Theochem*, 2010, **946**, 70.
10 M. A. A. Rocha, C. F. R. A. C. Lima, L. R. Gomes, B. Schröder, J. A. P. Coutinho, I. M. Marrucho, J. M. S. S. Esperança, L. P. N. Rebelo, K. Shimizu, J. N. Canongia Lopes, L. M. N. B. F. Santos, *J. Phys. Chem. B*, 2011, **115**, 10919.
11 M. A. A. Rocha, M. Bastos, J. A. P. Coutinho, L. M. N. B. F. Santos, *J. Chem. Thermodyn.* , 2012, 53, 140-143.
12 S. V. Dzyuba, R. A. Bartsch, *Chem. Commun.*, 2001, 1466.
13 D. Xiao; L. G. Hines, Jr., S. Li, R. A. Bartsch, E. L. Quitevis, O. Russina, A. Triolo, *J. Phys. Chem. B*, 2009, **113**, 6426.
14 W. Zheng, A. Mohammed, L. G. Hines, Jr., D. Xiao, O. J. Martinez, R. A. Bartsch, S. L. Simon, O. Russina, A. Triolo, E. L. Quitevis, *J. Phys. Chem. B*, 2011, **115**, 6572.
15 S. G. Raju, S. Balasubramanian, *J. Phys. Chem. B*, 2010, **114**, 6455.
16 S. G. Raju, S.Balasubramanian, *J. Mater. Chem.*, 2009, **19**, 4343.
17 M. A. A. Rocha, J. A. P. Coutinho, L. M. N. B. F. Santos, *J. Phys. Chem. B*, 2012, **116**, 10922.
18 M. Tariq, P. A. S. Forte, M. F. Costa Gomes, J. N. Canongia Lopes, L. P. N. Rebelo, *J. Chem. Thermodyn.*, 2009, **41**, 790.

Paper VIII

"Vapor Pressures of 1,3-Dialkylimidazolium Bis(trifluoromethylsulfonyl)imide Ionic Liquid Series with Long Alkyl Chain Length"

Marisa A.A. Rocha, João A.P. Coutinho, Luís M.N.B.F. Santos

Manuscript version

Note: The author of this thesis performed the all the experimental work, data analysis and contribute to the discussion and conclusions.

Vapor Pressures of 1,3-Dialkylimidazolium Bis(trifluoromethylsulfonyl)imide Ionic Liquid Series with Long Alkyl Chain Length

Marisa A. A. Rocha [†,*], *João A. P. Coutinho*[§], *Luís M. N. B. F. Santos* [†,*]

[†] Centro de Investigação em Química, Departamento de Química e Bioquímica, Faculdade de Ciências, Universidade do Porto, Rua do Campo Alegre, 687, P-4169-007 Porto, Portugal

[§] CICECO, Departamento de Química, Universidade de Aveiro, P-3810-193 Aveiro, Portugal

*Corresponding author. Tel.: +351 220 402 836; Fax: +351 220 402 659

E-mail address: lbsantos@fc.up.pt (Luís M. N. B. F. Santos); marisa.alexandra.rocha@gmail.com (Marisa A. A. Rocha)

ABSTRACT

This works presents the vapor pressure at several temperatures for the 1,3-dialkylimidazolium bis(trifluoromethylsulfonyl)imide series, $[C_{N/2}C_{N/2}im][NTf_2]$ (N = 14, 16, 18, 20), measured by a Knudsen effusion method combined with a quartz crystal microbalance. The thermodynamic properties of vaporization of the ionic liquids under study, are analysed together with the results obtained previously for the shorter alkyl chain length $[C_{N/2}C_{N/2}im][NTf_2]$ (N =2, 4, 6, 8, 10, 12), in order to evaluate the effect of the alkyl side chains of the cation and to get more insights about the nanostructuration of ionic liquids. The effect symmetry is explored, based on the comparison with the asymmetric imidazolium based ionic liquids, $[C_{N-1}C_1im][NTf_2]$. A trend shift on the thermodynamic properties of vaporization along the alkyl side chains of the extended symmetric ionic liquids, around $[C_6C_6im][NTf_2]$, was detected. Starting from $[C_6C_6im][NTf_2]$ an intensification of the odd-even effect is observed, with higher enthalpies and entropies of vaporization for the odd numbered ionic liquids, $[C_7C_7im][NTf_2]$ and $[C_9C_9im][NTf_2]$. Similar, but less pronounced, odd-even effect was found for the symmetric ionic liquids with lower alkyl side chains length, $[C_{N/2}C_{N/2}im][NTf_2]$ (with N=4, 6, 8, 10, 12). This effect is related with the predominant orientation of the terminal methyl group of the alkyl chain to the imidazolium ring and their influence in the cation-anion interaction. The results presented in this work are a strong contribution for the understanding of the nanostructuration of the imidazolium bistriflamide ionic liquids in which the same Critical Alkyl length size (CALS) at the hexyl, $C_{6,}$ for was founded in the symmetric and asymmetric series

KEYWORDS: vapor pressures; dialkylimidazolium; bistriflamide; ionic liquids; Knudsen effusion method; quartz crystal microbalance; thermodynamic properties of vaporization; trend shift; nanostructuration;

1. INTRODUCTION

Until recently, the ionic liquids were regarded as non-volatile, and thus did not exhibit measurable vapor pressure, even at higher temperatures. In fact, at room temperature the vapor pressures of ionic liquids are too low to be detected. However, Earle *et al.*[1] have shown that some ionic liquids can be distillated at low pressure without decomposition. This work was followed by that of Paulechka *et al.*[2] who determined the thermal stability of 1-butyl-3-methylimidazolium bis(trifluoromethylsulfonyl)amide, $[C_4C_1im][NTf_2]$, in vacuum, and evaluated the possibility of measurement of vapor pressure and enthalpy of vaporization of this ionic liquid. Kabo and collaborators[3] reported the first experimental determinations of vapor pressures for a series of 1-alkyl-3-methylimidazolium bis(trifluoromethylsulfonyl)imide, $[C_{N-1}C_1im][NTf_2]$ (N = 2, 4, 6, and 8), ionic liquids, using an integral effusion Knudsen method. In the same year, Santos *et al.*[4] presented the first proof that the vaporization of ionic liquids occurs as a direct liquid to gas transfer of the intact ionic pair. This was (vaporization of the ionic liquids via neutral ion pairs) where supported by studies using photoionization[5], line of sight mass spectrometry [6–8], Fourier transform ion cyclotron resonance[9,10], and by tunable vacuum ultraviolet photoionization [11], and more recently by molecular dynamics simulations.[12,13]

For most of the ionic liquids, the determination of vapor pressures is extremely difficulty due to the competition between the vaporization and decomposition mechanisms as well as the effect of the presence impurities.[14] Therefore, for many of the ionic liquid families, the vaporization does not occur due to the limit imposed by the decomposition temperature, as reported for the $[C_4C_1im][PF_6]$ ionic liquid.[15,16] These pioneering works[1–4] contributed to the knowledge of a "window of opportunity" for the vaporization of some ionic liquids without decomposition.[14] Furthermore, it was possible to knowledge that some ionic liquids can be vaporized under moderated temperatures and vacuum conditions and the gaseous phase is most likely to be

composed by neutral ion pairs. Several techniques/strategies have been used in order to determine the enthalpies of vaporization, at a reference temperature, for a wide range of ionic liquids determined using both experimental[7,8,11,17–22] and theoretical methods[23,24].

Accurate thermodynamic properties of vaporization equilibrium of ionic liquids are scarce and yet crucial for the better understanding of the liquid phase of ionic liquids, evaluation of the cohesive energy, as well as the nature of the gaseous phase. Furthermore, are required for validation and parameterization of the models (force fields) used to describe ionic liquids in different simulation techniques.[14,25,26] Despite of the importance of the vapor pressures of the ionic liquids and the related thermodynamic properties of vaporization (enthalpies, entropies and Gibbs energies of vaporization), most of the works performed until know, is focused in estimate / determine the enthalpies of vaporization.[7,8,11,14,17–22]

Recently, we reported the thermodynamic study concerning the vaporization of the $[C_{N-1}C_1im][NTf_2]$ (N = 3-9, 11, and 13) ionic liquid series, where important trends for the enthalpies and entropies of vaporization were found, which are related to a change in the molecular structure of the liquid phase around $[C_6C_1im][NTf_2]$.[27] Later on, the volatility study for the symmetric ionic liquids, $[C_{N/2}C_{N/2}im][NTf_2]$ (N = 4, 6, 8, 10, 12), was reported and was found that the symmetry of the imidazolium cation leads to higher volatilities and lower enthalpies and entropies of vaporization, when compared with the asymmetric ILs, $[C_{N-1}C_1im][NTf_2]$.[27] The effect of short alkyl chain length as well as the symmetry of the cation on the vaporization thermodynamics was evaluated based on the thermodynamic properties of vaporization of the $[C_1C_1im][NTf_2]$ and $[C_2C_3im][NTf_2]$. [28] The previous studies are related with the effect of nanostructuration of ionic liquids on the thermodynamic properties of vaporization, that until recently it was only described by molecular simulation dynamics. [25,29,30] Actually, the nanostructuration in ionic liquids was already detected in several thermophysical properties such as heat capacities[31,32], viscosities[27,33,34] and refractive indices.[34]

This work presents the vapor pressure data for the 1,3-dialkylimidazolium bis(trifluoromethylsulfonyl)imide series, $[C_{N/2}C_{N/2}im][NTf_2]$ (N = 14, 16, 18, 20), with longer alkyl side chains. This is an extension of the thermodynamic study of vaporization for the $[C_{N/2}C_{N/2}im][NTf_2]$ (N = 4, 6, 8, 10, 12), reported recently in the literature.[35] The analysis and rationalization of the obtained results will be done considering the thermodynamic properties of vaporization of the symmetric ionic liquids with shorter alkyl side chains, $[C_{N/2}C_{N/2}im][NTf_2]$ (N =2, 4, 6, 8, 10, 12)[28,35], in order to evaluate the effect of the alkyl side chains of the cation and to get more insights about the so-called nanostructuration / segregation of ionic liquids.[25,29] The effect symmetry of the long alkyl side chain cations, $[C_{N/2}C_{N/2}im][NTf_2]$ (N =14, 16, 18, 20), presented in this work, will be investigated based on the comparison with the asymmetric imidazolium based ionic liquids, $[C_{N-1}C_1im][NTf_2]$.[27]

2. EXPERIMENTAL DETAILS

The 1,3-dialkylimidazolium bis(trifluoromethylsulfonyl)imide series, $[C_{N/2}C_{N/2}im][NTf_2]$ (N = 14, 16, 18, 20), used in this work, were purchased from IOLITEC with a stated purity of better than 98%. The purity of each ionic liquid was further evaluated by ^{1}H, ^{13}C, and ^{19}F NMR spectra and all ionic liquids found to be > 99 wt % purity. All ionic liquids were dried under reduced pressure (< 10 Pa) and stirred constantly at 323 K, in order to reduce the presence of water or other volatile contents.

Quartz crystal microbalance Knudsen effusion apparatus

The vapor pressures of the studied ionic liquids were measured as a function of the temperature using Knudsen effusion apparatus combined with a quartz crystal microbalance, KEQCM, described in detail in the literature.[36] Basically, this apparatus results on the combination of the

Knudsen effusion technique and quartz crystal microbalance. The combination of two mass loss detection techniques (gravimetric and quartz crystal microbalance) presents several advantages: small effusion times; smaller sample sizes; higher control of the vaporization process, since it is possible to detect some problem during the experiment by the monitoring the change of the crystal's resonant frequency with time. Additionally, the instrument enables the measurement of vapor pressures from 0.005 Pa up to 1 Pa. The temperature is controlled within a temperature fluctuation of $\pm(1\times10^{-2})$ K, measured with a resolution better than 1×10^{-3} K and along the working temperature range, the overall uncertainty is better than $\pm(2\times10^{-2})$ K. The vapor pressure data obtained with this apparatus for the ionic liquid have a typical pressure dependent uncertainty of (1 to 5) %.[27] The relative atomic masses used were those recommended by the IUPAC Commission in 2007.[37]

3. RESULTS AND DISCUSSION

The vapor pressures were measured at different temperatures intervals, $[C_7C_7im][NTf_2]$ (483 to 504)K, $[C_8C_8im][NTf_2]$ (483 to 506)K, $[C_9C_9im][NTf_2]$ (493 to 523)K, and $[C_{10}C_{10}im][NTf_2]$ (491 to 514)K, using a Knudsen effusion apparatus combined with a quartz crystal microbalance. The experimental vapor pressures data for each studied ionic liquids, is presented in table 1. Figure 1, presents the graphical representation of $\ln(p/\text{Pa}) = f\,[(1/T) / \text{K}^{-1}]$ for the studied ionic liquids.

Table 1. Experimental vapor pressures for the studied imidazolium based ILs, as obtained with the quartz crystal microbalance Knudsen effusion apparatus.

T / K	p / Pa	Δp / Pa	T / K	p / Pa	Δp / Pa	T / K	p / Pa	Δp / Pa
				$[C_7C_7im][NTf_2]$				
483.37	0.0540	-0.0101	491.17	0.0896	0.0046	499.29	0.1517	-0.0021
485.37	0.0613	-0.0013	493.17	0.1020	0.0052	501.41	0.1738	-0.0063
487.38	0.0698	0.0041	495.28	0.1176	-0.0016	503.41	0.1948	0.0033
489.27	0.0789	0.0069	497.28	0.1338	-0.0031			
				$[C_8C_8im][NTf_2]$				
483.29	0.0368	0.0104	493.33	0.0712	-0.0056	503.36	0.1301	0.0005
485.31	0.0423	0.0036	495.34	0.0801	0.0013	505.37	0.1462	0.0019
487.32	0.0486	-0.0050	497.34	0.0902	0.0053			
489.33	0.0554	-0.0070	499.35	0.1019	0.0054			
491.32	0.0629	-0.0078	501.36	0.1159	-0.0028			
				$[C_9C_9im][NTf_2]$				
493.11	0.0448	-0.0034	508.11	0.1115	0.0216	523.09	0.2765	-0.0242
498.13	0.0626	-0.0158	513.11	0.1510	0.0140			
503.16	0.0843	0.0006	518.11	0.2027	0.0073			
				$[C_{10}C_{10}im][NTf_2]$				
491.35	0.0251	0.0056	499.36	0.0416	-0.0021	507.37	0.0669	-0.0009
493.34	0.0287	-0.0029	501.35	0.0466	0.0051	509.38	0.0750	0.0007
495.34	0.0326	-0.0051	503.36	0.0528	-0.0003	511.38	0.0843	-0.0016
497.35	0.0368	-0.0023	505.36	0.0594	0.0005	513.38	0.0941	0.0015

$\Delta p = p - p_{calc}$, where p_{calc} is calculated from the Clarke and Glew equation (eq. 1) with the parameters given in Table 2.
Standard uncertainties, u, are $u(T) = 0.02$ K, $u(p) = (0.001 + 0.05 \cdot p)$ Pa, the 0.95 confidence level ($k \approx 2$).

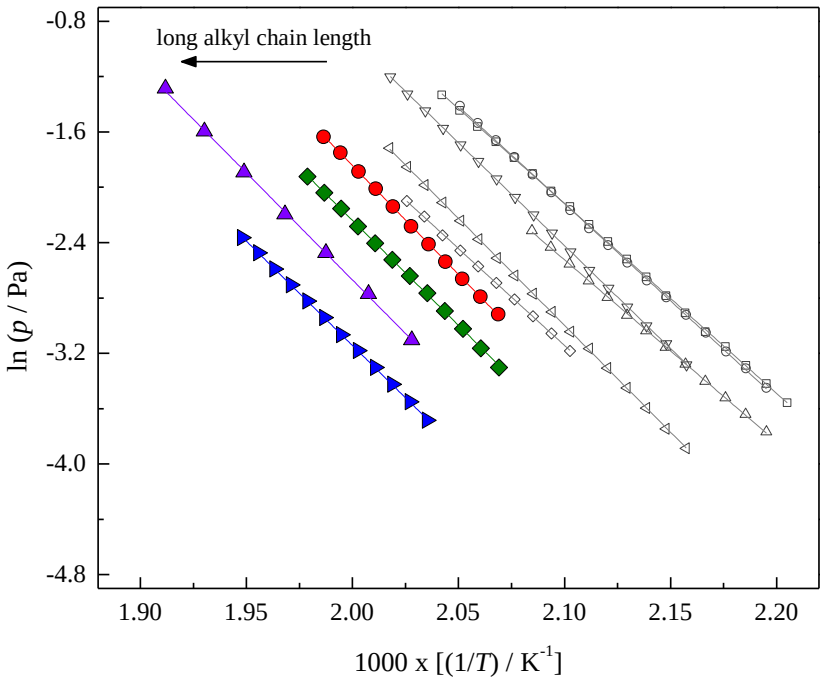

Figure 1. Plot of ln(p/Pa) = f [(1/T) / K^{-1}] for the studied ionic liquid: ● (red) - [C_7C_7im][NTf_2]; ◆ (green) - [C_8C_8im][NTf_2]; ▲ (violet) - [C_9C_9im][NTf_2]; ▶ (blue) - [$C_{10}C_{10}$im][NTf_2]. Rocha *et al.* [35]: ◇ (gray) - [C_1C_1im][NTf_2];△ (gray) - [C_2C_2im][NTf_2]; □ (gray) - [C_3C_3im][NTf_2]; ○ (gray) - [C_4C_4im][NTf_2]; ▽ (gray) - [C_5C_5im][NTf_2]; ◁ (gray) - [C_6C_6im][NTf_2].

The thermodynamic properties of vaporization at the mean temperature,<T>, and references temperatures, θ, 460 K and 298.15 K, were derived from the fitting of the experimental results of the vapor pressures by the truncated form of the Clarke and Glew equation[38]:

$$R \cdot \ln \frac{p}{p^{\circ}} = -\frac{\Delta_l^g G_m^{\circ}(\theta)}{\theta} + \Delta_l^g H_m^{\circ}(\theta) \cdot \left(\frac{1}{\theta} - \frac{1}{T}\right) + \Delta_l^g C_{p,m}^{\circ} \cdot \left[\frac{\theta}{T} - 1 + \ln\left(\frac{T}{\theta}\right)\right] \qquad (1)$$

where p is the vapor pressure, p° is a selected reference pressure (p° = 10^5 Pa), θ is a selected reference temperature, R is the gas constant (R = 8.3144621 $J \cdot K^{-1} \cdot mol^{-1}$)[39], $\Delta_l^g G_m^{\circ}$ is the standard molar Gibbs energy of vaporization at the selected reference pressure, $\Delta_l^g H_m^{\circ}$ is the standard molar enthalpy of vaporization, and $\Delta_l^g C_{p,m}^{\circ}$ is the difference between the heat capacities of the gaseous

and of the liquid phases [$\Delta_l^g C_{p,m}^o = C_{p,m}^o(g) - C_{p,m}^o(l)$]. The values of $\Delta_l^g C_{p,m}^o$ imposed in equation (1) are presented in table 2, and were estimated for the same temperature, T = 388 K, based on the linear correlation of the literature values [40–43] for $C_{p,m}^o(l)$ and $C_{p,m}^o(g)$ as a function of the cation's alkyl chain length, n(C) ([$C_{N/2}C_{N/2}$im][NTf_2] where n(C) = N − 1), using the previously described methodology. [27,28,35] The thermodynamic properties of vaporization derived from equation (1) at the mean temperature,<T>, and references temperatures, θ, 460 K and 298.15 K, together with the used $\Delta_l^g C_{p,m}^o$, are presented in table 2.

Table 2. Parameters of Clarke and Glew equation fitted from the vapor pressure results and the derived standard (p^o = 10^5 Pa) molar entropy of vaporization for each studied IL at the reference temperature, θ.

T interval / K	θ / K	$\Delta_l^g G_m^o(\theta)$ / J·mol^{-1}	$\Delta_l^g H_m^o(\theta)$ / J·mol^{-1}	$\Delta_l^g S_m^o(\theta)$ / J·K^{-1}·mol^{-1}	r^2	$\Delta_l^g C_{p,m}^o(T = 388\ K)^*$ / J·K^{-1}·mol^{-1}
			[C_7C_7im][NTf_2]			
483 to 504	493.39 [a]	56514 ± 692	130835 ± 485	150.6 ± 1.0	0.9999	-171
	460.00	61741 ± 692	136544 ± 513	162.6 ± 1.0		
	298.15	93629 ± 786	164221 ± 1090	236.7 ± 2.7		
			[C_8C_8im][NTf_2]			
483 to 506	494.33 [a]	57946 ± 852	126063 ± 612	137.8 ± 1.2	0.9998	-181
	460.00	62898 ± 852	132277 ± 635	150.8 ± 1.3		
	298.15	93203 ± 932	161572 ± 1156	229.3 ± 2.8		
			[C_9C_9im][NTf_2]			
493 to 523	508.10 [a]	57816 ± 1669	128653 ± 1192	139.4 ± 2.3	0.9996	-192
	460.00	64974 ± 1669	137888 ± 1216	158.5 ± 2.4		
	298.15	96880 ± 1725	168963 ± 1589	241.8 ± 3.6		
			[$C_{10}C_{10}$im][NTf_2]			
491 to 514	502.37 [a]	60621 ± 515	125391 ± 376	128.9 ± 0.7	0.9998	-203
	460.00	66457 ± 515	133992 ± 432	146.8 ± 0.9		
	298.15	96829 ± 658	166847 ± 1088	234.8 ± 2.7		

[a] mean temperature. r^2 is the linear regression coefficient. * $\Delta_l^g C_{p,m}^o$ (T = 388 K) estimated using the linear fitted function [$\Delta_l^g C_{p,m}^o$ (T = 388 K) = -5.40 n(C) - 100.47] derived from fitting of the literature data of $\Delta_l^g C_{p,m}^o$ (T = 388 K) as a function of the cationic alkyl chain length. [27,28,35,40–43] For [$C_{N/2}C_{N/2}$im][NTf_2], n(C) = N-1. Uncertainty associated with the $\Delta_l^g C_{p,m}^o$ (T = 388 K), ± 5 J·K^{-1}·mol^{-1}.

The analysis and rationalization of the present results will be done considering the thermodynamic properties of vaporization of the symmetric ionic liquids with short alkyl side chains recently published in the literature, $[C_{N/2}C_{N/2}im][NTf_2]$ (N =2, 4, 6, 8, 10, 12)[28,35], in order to evaluate the effect of the alkyl side chains of the cation and to get more insights about the so-called nanostructuration / segregation of ionic liquids.[25,29] The effect symmetry of the long alkyl side chain cations, $[C_{N/2}C_{N/2}im][NTf_2]$ (N =14, 16, 18, 20), presented in this work, will be investigated based on the comparison with the asymmetric imidazolium based ionic liquids, $[C_{N-1}C_1im][NTf_2]$.[27]

The plots of ln(p/Pa) as a function of [(1/T) / K^{-1}] presented in figure 1, show that, in the measured temperature range, the volatility of the $[C_{N/2}C_{N/2}im][NTf_2]$ ionic liquids decreases along the homologous series, from $[C_3C_3im][NTf_2]$ to $[C_{10}C_{10}im][NTf_2]$, where $[C_3C_3im][NTf_2]$ presents a similar volatility than the $[C_4C_4im][NTf_2]$ and $[C_{10}C_{10}im][NTf_2]$ is the lowest volatile ionic liquid in the studied series. As previously observed, $[C_1C_1im][NTf_2]$ and $[C_2C_2im][NTf_2]$ presents an outlier behaviour, with lower volatilities than $[C_3C_3im][NTf_2]$ and $[C_4C_4im][NTf_2]$.[28,35]

The graphic representations of the standard molar enthalpies, entropies and Gibbs energies of vaporization at reference temperature (460 K and 298.15 K) as a function of the total number of carbon atoms in the two alkyl side chains of the cation, N, are presented in figures 2, 3 and 4. The thermodynamic properties of vaporization of $[C_{N/2}C_{N/2}im][NTf_2]$ (with N=14, 16, 18, 20), are compared with $[C_{N/2}C_{N/2}im][NTf_2]$ (with N=2, 4, 6, 8, 10, 12)[28,35], and with $[C_{N-1}C_1im][NTf_2]$ (with N= 3 - 9, 11 and 13)[31]. The data at reference temperature, T = 460K, are presented to show that the considered $\Delta_l^g C_{p,m}^o$ does not affect the trends observed on the thermodynamic properties of vaporization at 298.15 K.

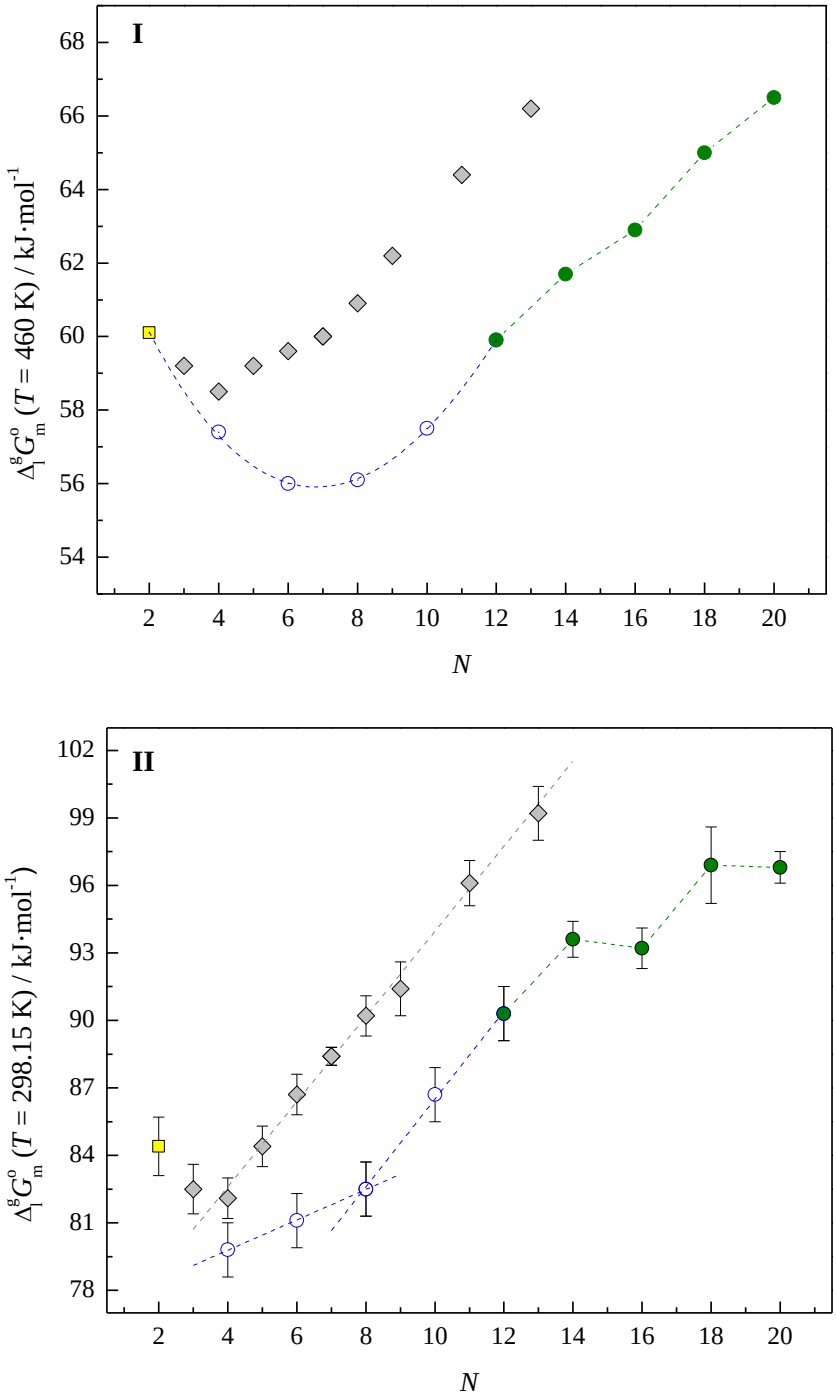

Figure 2. Standard (p^o=10^5 Pa) molar Gibbs energy of vaporization as a function of the total number of carbons in the alkyl side chains of the cation, N. (**I**) $\Delta_l^g G_m^o$ (T = 460 K) and (**II**) $\Delta_l^g G_m^o$ (T = 298.15 K). Literature: ■ (yellow) - [C_1C_1im][NTf_2] [28]; ◆ (gray) - [$C_{N-1}C_1$im][NTf_2] (N=3 - 9, 11, 13) [27]; ○ (blue) - [$C_{N/2}C_{N/2}$im][NTf_2] (N= 4, 6, 8, 10, 12)[35]. This work: ● (green) - [$C_{N/2}C_{N/2}$im][NTf_2] (N= 14, 16, 18, 20).

If we consider the linear trend of standard molar Gibbs energies of vaporization, at T = 298.15 K, of the asymmetric ionic liquids ($[C_{N-1}C_1im][NTf_2]$) [27], the volatility of the symmetric ionic liquids with longer alkyl side chains is significantly higher than the asymmetric ILs. Instead of a gradual linear increase of the $\Delta_l^g G_m^o$ (decrease of the volatility) along the alkyl side chain length of the asymmetric ionic liquids[27], the symmetric ionic liquid series with longer alkyl side chain length presents the following order of volatility, at T=298.15 K:

$[C_2C_2im][NTf_2] > [C_3C_3im][NTf_2] > [C_4C_4im][NTf_2] >> [C_5C_5im][NTf_2] >>$

$[C_6C_6im][NTf_2] >>$ **$[C_7C_7im][NTf_2] \approx [C_8C_8im][NTf_2] >> [C_9C_9im][NTf_2] \approx [C_{10}C_{10}im][NTf_2]$**

In figure 2 (II), a gradual linear increase of (1.8 ± 0.1) kJ·mol^{-1} per methylene group, $-CH_2-$, on the $\Delta_l^g G_m^o(298.15\,K)$, from $[C_4C_4im][NTf_2]$ to $[C_7C_7im][NTf_2]$, is observed, similar to the one found for the asymmetric ionic liquids, $[C_{N-1}C_1im][NTf_2]$. However, starting from $[C_6C_6im][NTf_2]$ a decrease on the contribution per $-CH_2-$ group of (0.8 ± 0.2) kJ·mol^{-1}, with a clear odd-even effect on the standard molar Gibbs energies is found, with higher $\Delta_l^g G_m^o(298.15\,K)$ (lower volatility) values for the odd numbered ionic liquids, $[C_7C_7im][NTf_2]$ and $[C_9C_9im][NTf_2]$. Considering the associated uncertainty the volatility is similar, at T = 298.15 K, between $[C_7C_7im][NTf_2]$ with $[C_8C_8im][NTf_2]$, and between $[C_9C_9im][NTf_2]$ with $[C_{10}C_{10}im][NTf_2]$. This can be rationalized based on the enthalpic and entropic contributions to the volatility of the ionic liquids. In the present work, the discussion will focus on the symmetric ionic liquids with longer alkyl chains, since the rest of the series, $[C_{N/2}C_{N/2}im][NTf_2]$ (with N=2, 4, 6, 8, 10, 12), were already addressed in the literature. [28,35]

Figures 3 and 4 shows the graphic representations of the standard molar enthalpies and entropies of vaporization at reference temperature, T = 460 K and T = 298.15 K.

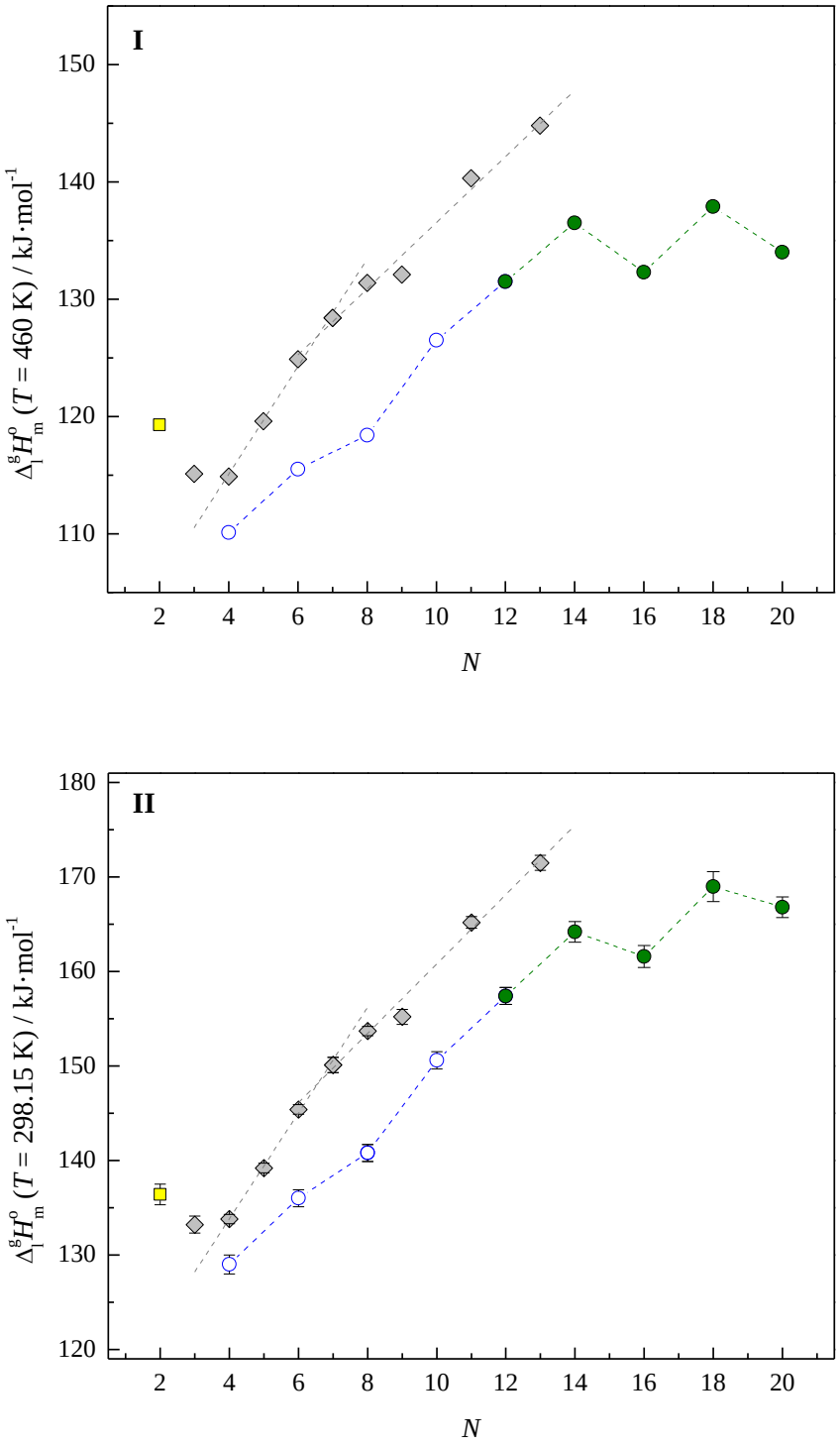

Figure 3. Standard (p^o=10^5 Pa) molar enthalpy of vaporization as a function of the total number of carbons in the alkyl side chains of the cation, *N*. (**I**) $\Delta_l^g H_m^o$ (T = 460 K) and (**II**) $\Delta_l^g H_m^o$ (T = 298.15 K) .Literature: ■ (yellow) - [C_1C_1im][NTf_2] [28]; ◆ (gray) - [$C_{N-1}C_1$im][NTf_2] (N=3 - 9, 11, 13) [27]; ○ (blue) - [$C_{N/2}C_{N/2}$im][NTf_2] (N= 4, 6, 8, 10, 12)[35]. This work: ● (green) - [$C_{N/2}C_{N/2}$im][NTf_2] (N= 14, 16, 18, 20).

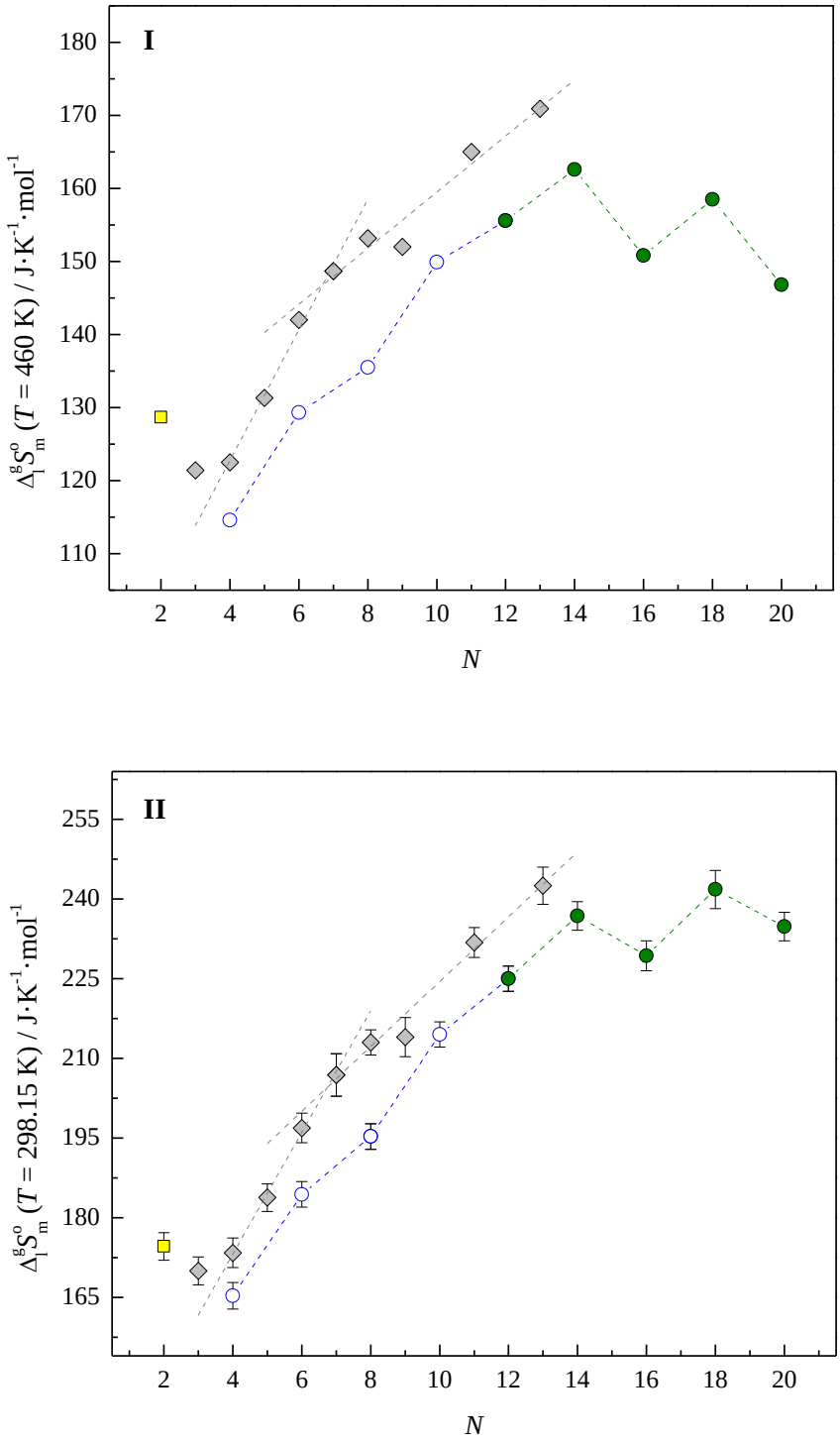

Figure 4. Standard (p^o=10^5 Pa) molar entropy of vaporization as a function of the total number of carbons in the alkyl side chains of the cation, N. (**I**) $\Delta_l^g S_m^o$ (T = 460 K) and (**II**) $\Delta_l^g S_m^o$ (T = 298.15 K) .Literature: ■ (yellow) - [C_1C_1im][NTf_2] [28]; ◆ (gray) - [$C_{N-1}C_1$im][NTf_2] (N=3 - 9, 11, 13) [27]; ○ (blue) - [$C_{N/2}C_{N/2}$im][NTf_2] (N= 4, 6, 8, 10, 12)[35]. This work: ● (green) - [$C_{N/2}C_{N/2}$im][NTf_2] (N= 14, 16, 18, 20).

In both thermodynamic properties, enthalpies and entropies of vaporization, a trend shift on the odd-even effect along the symmetric ionic liquids was found. Starting from $[C_6C_6im][NTf_2]$ an intensification of the odd-even effect is observed, with higher enthalpies and entropies of vaporization for the odd numbered ionic liquids, $[C_7C_7im][NTf_2]$ and $[C_9C_9im][NTf_2]$. Similar, but less pronounced, odd-even effect was found for the symmetric ionic liquids with lower alkyl side chains length, $[C_{N/2}C_{N/2}im][NTf_2]$ (with N=4, 6, 8, 10, 12)[35], where $[C_3C_3im][NTf_2]$ and $[C_5C_5im][NTf_2]$ presented higher enthalpies and entropies of vaporization. [35] This effect is related with the predominant orientation of the terminal methyl group of the alkyl chain to the imidazolium ring and their influence in the cation-anion interaction. [32,33,35]

Considering the same nomenclature used for the previous works [27,28,31], from $[C_2C_2im][NTf_2]$ to $[C_6C_6im][NTf_2]$, is "Region A", and from $[C_6C_6im][NTf_2]$ to $[C_{10}C_{10}im][NTf_2]$, is "Region B". In the $[C_2C_2im][NTf_2]$ to $[C_6C_6im][NTf_2]$ region (Region A), $\Delta_l^g H_m^o(298.15\,K)$ increases (3.6 ± 0.2) kJ·mol^{-1} per methylene group, $-CH_2-$, added to the alkyl side chains of the cation. This is followed by a decrease of the $-CH_2-$ group contribution of (1.2 ± 0.5) kJ·mol^{-1}, from $[C_6C_6im][NTf_2]$ to $[C_{10}C_{10}im][NTf_2]$ (Region B), which indicates a decrease of the $-CH_2-$ group contribution for the cohesive energies in Region B. This could be related with the higher separations between the charged region, due to the steric hindrance arising from the longer alkyl chains present in both sides of the cation, from $[C_6C_6im][NTf_2]$ to $[C_{10}C_{10}im][NTf_2]$, leading to a decline on the overall electrostatic interactions.

The entropies of vaporization, $\Delta_l^g S_m^o(298.15\,K)$, profile along the series in figure 4 (II), are analogous to the observed for the enthalpies of vaporization. In addition to the intensification of the odd-even effect from "Region A" to "Region B", it can be observed a decrease of the contribution per $-CH_2-$ group on the $\Delta_l^g S_m^o(298.15\,K)$, from $[C_2C_2im][NTf_2]$ to $[C_6C_6im][NTf_2]$ of (7.5 ± 0.4) J·K^{-1}·mol^{-1}, and from $[C_6C_6im][NTf_2]$ to $[C_{10}C_{10}im][NTf_2]$ of (1.2 ± 0.9) J·K^{-1}·mol^{-1}. Considering that the absolute standard entropies in the gaseous phase increases linearly, the observed change

should be due to an intensification of the increase of the absolute standard entropies in the liquid phase, starting from $[C_6C_6im][NTf_2]$, in agreement with the literature.[33]

For the same number of carbons in the alkyl chain, the observed higher volatility of the symmetric ionic liquids than the asymmetric, is ruled by the lower enthalpies of vaporization of the symmetric series. The lower enthalpies of vaporization of the symmetric series are only partial entropically compensated leading to a volatility increase reflecting the steric hindrance arising from the alkyl chains present in both sides of the cation.

4. FINAL REMARKS

In the previous work, were we report the volatility study for the asymmetric ionic liquids, $[C_{N-1}C_1im][NTf_2]$, a shift in the enthalpies and entropies of vaporization profiles along the alkyl side chain length was observed, which is related to a change in the molecular structure organization of the liquid phase, around $[C_6C_1im][NTf_2]$. The symmetry of the ionic liquid cation, changes dramatically the thermophysical properties, as it was already shown in the literature. [28,32,33,35,44] In fact, only until recently, the extended series of $[C_{N/2}C_{N/2}im][NTf_2]$ ionic liquids was fully studied concerning the heat capacities, viscosities, densities and SWAX[32,33,44], and was detected two regions, with a shift around $[C_6C_6im][NTf_2]$. Above $[C_6C_6im][NTf_2]$ the symmetric ionic liquids presents lower enthalpies and entropies of vaporization than the expected, with an accentuated odd-even effect, with higher values for the odd numbered ionic liquids, $[C_7C_7im][NTf_2]$ and $[C_9C_9im][NTf_2]$. The profile of the two regions found for the thermodynamic properties of vaporization for the extended series of $[C_{N/2}C_{N/2}im][NTf_2]$, is in agreement with the expected effect arising from the nanostructuration in ionic liquids. It is well established that in the liquid phase of ionic liquids, the polar regions tend to organize themselves in order to enhance the electrostatic interactions between the cation and anion and the alkyl chains of the cation for a non-polar segregated network.[25,29,30] Based on the results obtained in the present work, we found a clear

indication that for the symmetric series, $[C_{N/2}C_{N/2}im][NTf_2]$, that the limit for the beginning of the nanostructuration / alkyl chain segregation, Critical Alkyl Length Size (CALS) is $[C_6C_6im][NTf_2]$, presenting the same size for the longer alkyl chain than the asymmetric series $[C_6C_1im][NTf_2]$,.

ACKNOWLEDGEMENTS

Thanks are due to Fundação para a Ciência e Tecnologia (FCT), Lisbon, Portugal and to FEDER for financial support to Centro de Investigação em Química, University of Porto through the project Pest-C/QUI/UI0081/2011, and CICECO, University of Aveiro, through the project Pest-C/CTM/LA0011/2011. Marisa A. A. Rocha acknowledges the financial support from FCT and the European Social Fund (ESF) under the Community Support Framework (CSF) for the award of a Ph.D. Research Grant, SFRH/BD/60513/2009.

REFERENCES

(1) Earle, M. J.; Esperança, J. M. S. S.; Gilea, M. A.; Lopes, J. N. C.; Rebelo, L. P. N.; Magee, J. W.; Seddon, K. R.; Widegren, J. A. *Nature* **2006**, *439*, 831–834.

(2) Paulechka, Y. U.; Zaitsau, D. H.; Kabo, G. J.; Strechan, A. A. *Thermochim. Acta* **2005**, *439*, 158–160.

(3) Zaitsau, D. H.; Kabo, G. J.; Strechan, A. A.; Paulechka, Y. U.; Tschersich, A.; Verevkin, S. P.; Heintz, A. *J. Phys. Chem. A* **2006**, *110*, 7303–7306.

(4) Santos, L. M. N. B. F.; Lopes, J. N. C.; Coutinho, J. A. P.; Esperança, J. M. S. S.; Gomes, L. R.; Marrucho, I. M.; Rebelo, L. P. N. *J. Am. Chem. Soc.* **2007**, *129*, 284–285.

(5) Strasser, D.; Goulay, F.; Kelkar, M. S.; Maginn, E. J.; Leone, S. R. *J. Phys. Chem. A* **2007**, *111*, 3191–3195.

(6) Emel'yanenko, V. N.; Verevkin, S. P.; Heintz, A.; Corfield, J.-A.; Deyko, A.; Lovelock, K. R. J.; Licence, P.; Jones, R. G. *J. Phys. Chem. B* **2008**, *112*, 11734–11742.

(7) Armstrong, J. P.; Hurst, C.; Jones, R. G.; Licence, P.; Lovelock, K. R. J.; Satterley, C. J.; Villar-Garcia, I. J. *Phys. Chem. Chem. Phys.* **2007**, *9*, 982–990.

(8) Lovelock, K. R. J.; Deyko, A.; Corfield, J.-A.; Gooden, P. N.; Licence, P.; Jones, R. G. *Chem. Phys. Chem.* **2009**, *10*, 337–340.

(9) Leal, J. P.; Da Piedade, M. E. M.; Canongia Lopes, J. N.; Tomaszowska, A. A.; Esperança, J. M. S. S.; Rebelo, L. P. N.; Seddon, K. R. *J. Phys. Chem. B* **2009**, *113*, 3491–3498.

(10) Leal, J. P.; Esperança, J. M. S. S.; Da Piedade, M. E. M.; Lopes, J. N. C.; Rebelo, L. P. N.; Seddon, K. R. *J. Phys. Chem. A* **2007**, *111*, 6176–6182.

(11) Chambreau, S. D.; Vaghjiani, G. L.; To, A.; Koh, C.; Strasser, D.; Kostko, O.; Leone, S. R. *J. Phys. Chem. B* **2010**, *114*, 1361–1367.

(12) Chaban, V. V.; Prezhdo, O. V. *J. Phys. Chem. Lett.* **2012**, *3*, 1657–1662.

(13) Neto, B. A. D.; Meurer, E. C.; Galaverna, R.; Bythell, B. J.; Dupont, J.; Cooks, R. G.; Eberlin, M. N. *J. Phys. Chem. Lett.* **2012**, *3*, 3435–3441.

(14) M. S. S. Esperança, J.; Canongia Lopes, J. N.; Tariq, M.; Santos, L. M. N. B. F.; Magee, J. W.; Rebelo, L. P. N. *J. Chem. Eng. Data* **2010**, *55*, 3–12.

(15) Kabo, G. J.; Blokhin, A. V.; Paulechka, Y. U.; Kabo, A. G.; Shymanovich, M. P.; Magee, J. W. *J. Chem. Eng. Data* **2004**, *49*, 453–461.

(16) Paulechka, Y. U.; Kabo, G. J.; Blokhin, A. V.; Vydrov, O. A.; Magee, J. W.; Frenkel, M. *J. Chem. Eng. Data* **2003**, *48*, 457–462.

(17) Deyko, A.; Lovelock, K. R. J.; Corfield, J.-A.; Taylor, A. W.; Gooden, P. N.; Villar-Garcia, I. J.; Licence, P.; Jones, R. G.; Krasovskiy, V. G.; Chernikova, E. A.; Kustov, L. M. *Phys. Chem. Chem. Phys.* **2009**, *11*, 8544–8555.

(18) Verevkin, S. P.; Zaitsau, D. H.; Emel'yanenko, V. N.; Ralys, R. V.; Yermalayeu, A. V.; Schick, C. *J. Chem. Thermodyn.* **2012**, *54*, 433–437.

(19) Fumino, K.; Wulf, A.; Verevkin, S. P.; Heintz, A.; Ludwig, R. *Chem. Phys. Chem.* **2010**, *11*, 1623–1626.

(20) Wang, C.; Luo, H.; Li, H.; Dai, S. *Phys. Chem. Chem. Phys.* **2010**, *12*, 7246–7250.

(21) Deyko, A.; Hessey, S. G.; Licence, P.; Chernikova, E. A.; Krasovskiy, V. G.; Kustov, L. M.; Jones, R. G. *Phys. Chem. Chem. Phys.* **2012**, *14*, 3181–3193.

(22) Verevkin, S. P.; Ralys, R. V.; Zaitsau, D. H.; Emel'yanenko, V. N.; Schick, C. *Thermochim. Acta* **2012**, *538*, 55–62.

(23) Köddermann, T.; Paschek, D.; Ludwig, R. *Chem. Phys. Chem.* **2008**, *9*, 549–555.

(24) Ludwig, R. *Phys. Chem. Chem. Phys.* **2008**, *10*, 4333–4339.

(25) Canongia Lopes, J. N. A.; Pádua, A. A. H. *J. Phys. Chem. B* **2006**, *110*, 3330–3335.

(26) Dommert, F.; Wendler, K.; Berger, R.; Delle Site, L.; Holm, C. *Chem. Phys. Chem.* **2012**, *13*, 1625–1637.

(27) Rocha, M. A. A.; Lima, C. F. R. A. C.; Gomes, L. R.; Schröder, B.; Coutinho, J. A. P.; Marrucho, I. M.; Esperança, J. M. S. S.; Rebelo, L. P. N.; Shimizu, K.; Lopes, J. N. C.; Santos, L. M. N. B. F. *J. Phys. Chem. B* **2011**, *115*, 10919–10926.

(28) Rocha, M. A. A.; Schröder, B.; Coutinho, J. A. P.; Santos, L. M. N. B. F. *J. Chem. Thermodyn.* **2013**, Submitted (Paper VI).

(29) Shimizu, K.; Costa Gomes, M. F.; Pádua, A. A. H.; Rebelo, L. P. N.; Canongia Lopes, J. N. *J. Mol. Struct.: THEOCHEM* **2010**, *946*, 70–76.

(30) Gomes, M. F. C.; Lopes, J. N. C.; Padua, A. A. H. *Top. Curr. Chem.* **2010**, *290*, 161–83.

(31) Rocha, M. A. A.; Bastos, M.; Coutinho, J. A. P.; Santos, L. M. N. B. F. *J. Chem. Thermodyn.* **2012**, *53*, 140–143.

(32) Rocha, M. A. A.; Coutinho, J. A. P.; Santos, L. M. N. B. F. *J. Chem. Phys.* **2013**, 139, 104502.

(33) Rocha, M. A. A.; Neves, C. M. S. S.; Freire, M. G.; Russina, O.; Triolo, A.; Coutinho, J. A. P.; Santos, L. M. N. B. F. *J. Phys. Chem. B* **2013**, doi: 10.1021/jp406374a.

(34) Rocha, M. A. A.; Ribeiro, F. M. S.; Ferreira, A. I. M. C. L.; Coutinho, J. A. P.; Santos, L. M. N. B. F. *J. Mol. Liq.* **2013**, accepted.

(35) Rocha, M. A. A.; Coutinho, J. A. P.; Santos, L. M. N. B. F. *J. Phys. Chem. B* **2012**, *116*, 10922–10927.

(36) Santos, L. M. N. B. F.; Lima, L. M. S. S.; Lima, C. F. R. A. C.; Magalhães, F. D.; Torres, M. C.; Schröder, B.; Ribeiro da Silva, M. A. V. *J. Chem. Thermodyn.* **2011**, *43*, 834–843.

(37) Wieser, M. E.; Berglund, M. *Pure Appl. Chem.* **2009**, *81*, 2131–2156.

(38) Clarke, E. C. W.; Glew, D. N. *Trans. Faraday Soc.* **1966**, *62*, 539–547.

(39) Mohr, P. J.; Taylor, B. N.; Newell, D. B. *Rev. Mod. Phys.* **2012**, *84*, 1527–1605.

(40) Paulechka, Y. U.; Kabo, G. J.; Emel'yanenko, V. N. *J. Phys. Chem. B* **2008**, *112*, 15708–15717.

(41) Blokhin, A. V.; Paulechka, Y. U.; Kabo, G. J. *J. Chem. Eng. Data* **2006**, *51*, 1377–1388.

(42) Blokhin, A. V; Paulechka, Y. U.; Strechan, A. A.; Kabo, G. J. *J. Phys. Chem. B* **2008**, *112*, 4357–4364.

(43) Paulechka, Y. U.; Blokhin, A. V.; Kabo, G. J.; Strechan, A. A. *J. Chem. Thermodyn.* **2007**, *39*, 866–877.

(44) Zheng, W.; Mohammed, A.; Hines, L. G.; Xiao, D.; Martinez, O. J.; Bartsch, R. A.; Simon, S. L.; Russina, O.; Triolo, A.; Quitevis, E. L. *J. Phys. Chem. B* **2011**, *115*, 6572–6584.

Paper IX

"Thermophysical Properties of [$C_{N-1}C_1$im][PF_6] Ionic Liquids"

Marisa A. A. Rocha, Filipe M. S. Ribeiro, Ana I.M.C. Lobo Ferreira, João A. P. Coutinho, Luís M. N. B. F. Santos

Journal of Molecular Liquids (2013), 188, 196-202.
doi: 10.1016/j.molliq.2013.09.031

Note: The author of this thesis performed part of the experimental work, data analysis and contribute to the discussion and conclusions.

Journal of Molecular Liquids 188 (2013) 196–202

Contents lists available at ScienceDirect

Journal of Molecular Liquids

journal homepage: www.elsevier.com/locate/molliq

Thermophysical properties of $[C_{N-1}C_1im][PF_6]$ ionic liquids

Marisa A.A. Rocha [a,*], Filipe M.S. Ribeiro [a], Ana I.M.C. Lobo Ferreira [a], João A.P. Coutinho [b], Luís M.N.B.F. Santos [a,*]

[a] CIQ, Departamento de Química e Bioquímica, Faculdade de Ciências da Universidade do Porto, R. Campo Alegre 687, P-4169-007, Porto, Portugal
[b] CICECO, Departamento de Química, Universidade de Aveiro, P-3810-193 Aveiro, Portugal

ARTICLE INFO

Article history:
Received 25 June 2013
Received in revised form 30 August 2013
Accepted 9 September 2013
Available online 18 October 2013

Keywords:
Refractive indices
Viscosities
Densities
Hexafluorophosphate
Nanostructuration
Ionic liquids
Trend shift
Imidazolium
Alkyl chain effect

ABSTRACT

Densities, viscosities and refractive index, as a function of temperature, and isobaric thermal expansion coefficient, were determined for 1-alkyl-3-methylimidazolium hexafluorophosphate, $[C_{N-1}C_1im][PF_6]$ (where N = 5 to 10) series of ionic liquids. The density presents a regular decrease along the ionic liquid series, with no detectable alkyl chain length dependence of the thermal expansion coefficient. Both the refractive index and viscosity show a trend shift along the series around the $[C_6C_1im][PF_6]$ that could be associated to the impact of the change in the nanostructuration of the ionic liquids. The experimental results are compared with the analogous $[C_{N-1}C_1im][NTf_2]$ series and the effect of the anion is analyzed. The sphericity of the $[PF_6]^-$ anion is reflected in the lower pre-exponential VTF parameter, A_η, and the higher viscosity of the $[C_{N-1}C_1im][PF_6]$, when compared with the $[C_{N-1}C_1im][NTf_2]$ series, is ruled by the higher energy barriers, which are related with stronger electrostatic interaction due to the low charge dispersion of the $[PF_6]^-$.anion.

1. Introduction

The physicochemical properties of ionic liquids can vary considerably depending on the combination of cations and anions. Therefore, for the interpretation of their properties and a successful modeling of ionic liquids, highly accurate data regarding these physicochemical properties are needed, such as heat capacities, vapor pressures, viscosities, densities and refraction index. Recently, we reported several thermodynamic studies of the extended series of ILs $[C_{N-1}C_1im][NTf_2]$ (with N = 3–9, 11, and 13), and of the symmetric $[C_{N/2}C_{N/2}im][NTf_2]$ (with N = 4–24) [1–4]. Based on these works, it was possible to highlight the effect of the nanostructuration of $[C_{N-1}C_1im][NTf_2]$ and $[C_{N/2}C_{N/2}im][NTf_2]$ ionic liquid series and to evaluate the effect of the cation topological symmetry on the thermodynamic properties of vaporization, heat capacities and viscosity data. Understanding the impact of nanostructuration on the thermophysical properties of ionic liquids is highly relevant but previous works used only the even numbered ionic liquids, and consequently the complete characterization of important trends which are related with the nanostructuration is not possible, neither the identification of the outlier character of $[C_1C_1im][NTf_2]$ and $[C_2C_1im][NTf_2]$ [1–4].

In this work, the thermophysical properties of 1-alkyl-3-methylimidazolium hexafluorophosphate, $[C_{N-1}C_1im][PF_6]$ (with N = 5–10), specifically density, viscosity and refractive index, and their dependency with temperature were measured. Concerning this family of ionic liquids, most of the thermophysical studies have been focused on the following liquids: $[C_4C_1im][PF_6]$, $[C_6C_1im][PF_6]$ and $[C_8C_1im][PF_6]$, which prevent the identification of the nanostructuration on these ionic liquids [5–31]. The experimental results obtained will be used to evaluate the effect of the chemical nature of the anion, sphericity, and size, as well as the overall impact of the nanostructuration on the thermophysical properties of these ionic liquids.

2. Experimental section

2.1. Materials and purification

The 1-alkyl-3-methylimidazolium hexafluorophosphate, $[C_{N-1}C_1im][PF_6]$ (with N = 5–10), used in this work, was purchased from IOLITEC with a stated purity of better than 99%. All the ionic liquids were dried and purified under vacuum (<10 Pa) at moderate temperature (323 K) and constant stirring, in order to reduce the

* Corresponding authors. Tel.: +351 220402836; fax: +351 220402659.
E-mail addresses: marisa.alexandra.rocha@gmail.com (M.A.A. Rocha), lbsantos@fc.up.pt (L.M.N.B.F. Santos).

0167-7322/$ – see front matter © 2013 Elsevier B.V. All rights reserved.
http://dx.doi.org/10.1016/j.molliq.2013.09.031

Table 1
Experimental results of density, ρ, at 0.1 MPa for the $[C_{N-1}C_1im][PF_6]$ ionic liquid series as a function of temperature.

T/K	ρ/(kg·m^{-3})					
	$[C_4C_1im][PF_6]$	$[C_5C_1im][PF_6]$	$[C_6C_1im][PF_6]$	$[C_7C_1im][PF_6]$	$[C_8C_1im][PF_6]$	$[C_9C_1im][PF_6]$
293.15	1371.8	1332.2	1298.5	1266.7	1240.9	1217.0
298.15	1367.4	1327.8	1294.2	1262.6	1236.9	1213.1
303.15	1363.2	1323.7	1290.1	1258.5	1232.9	1209.2
308.15	1359.0	1319.6	1286.1	1254.5	1229.0	1205.3
313.15	1354.9	1315.5	1282.1	1250.6	1225.1	1201.5
318.15	1350.8	1311.6	1278.2	1246.8	1221.3	1197.8
323.15	1346.8	1307.6	1274.3	1243.0	1217.6	1194.1
328.15	1342.7	1303.7	1270.5	1239.3	1213.9	1190.4
333.15	1338.7	1299.8	1266.7	1235.5	1210.2	1186.8
338.15	1334.7	1295.9	1262.9	1231.8	1206.6	1183.2
343.15	1330.6	1292.0	1259.1	1228.1	1202.9	1179.6
348.15	1326.6	1288.1	1255.3	1224.4	1199.3	1176.0
353.15	1322.7	1284.3	1251.5	1220.7	1195.6	1172.4
358.15	1318.7	1280.4	1247.7	1217.0	1192.0	1168.8
363.15	1314.8	1276.6	1244.0	1213.3	1188.4	1165.3

Note: the magnitude of the experimental differentiation between the two independent set of density data: ±0.2 kg·m^{-3}.

presence of water or other volatile contents. This process was performed systematically before and during the thermophysical property measurements.

2.2. Density and viscosity

The density, ρ, and dynamic viscosity, η, measurements were performed with an automated SVM 3000 Anton Paar rotational Stabinger viscometer–densimeter. The description concerning the operation of this equipment is available in the literature [32]. The measurements were carried out at atmospheric pressure in the temperature range from 293.15 to 363.15 K for the pure ionic liquids. The apparatus was calibrated using the three standard calibration samples, APN7.5, APN26 and APN415 in the same experimental conditions of the ionic liquid measurements. The reproducibility of the dynamic viscosity and density measurements is, according to the manufacturer, 0.35% and ± 0.5 kg·m^{-3}, respectively from 288.15 K to 378.15 K and the uncertainty of temperature is within ±0.02 K. For each ionic liquid, at least two independent measurements of the density and viscosity were performed, using the same experimental conditions and different samples.

2.3. Refractive index

The refractive indices were measured at the sodium D-line using a Bellingham model RFM340 refractometer ($\pm 3\times10^{-5}$ stated precision), as a function of temperature (288.15 to 318.15) K. The apparatus was calibrated with degassed water (Millipore quality) and toluene (Spectranal, 99.9%). The temperature in the refractometer cell is controlled using an external thermostatic bath within a temperature fluctuation of ($\pm 5\times10^{-3}$) K, measured with a resolution better than 1×10^{-3} K and an uncertainty within ±0.02 K. Samples were directly introduced into the flow cell (prism assembly) using a syringe; the flow cell was kept closed after sample injection. For each ionic liquid at least two independent experiment were performed and in each experiment at least three measurements were taken at each temperature. The refractive indices were measured with respect to air and no corrections were applied.

3. Results and discussion

3.1. Density

The experimental density data for the studied ionic liquids are presented in Table 1. Fig. 1 displays the logarithm of density as a function of temperature and the respective relative deviations between the experimental density measured in this work and those reported in the literature.

The experimental density data, in the temperature range, was described using a second order polynomial equation correlation, according to Eq. (1):

$$\ln(\rho/\mathrm{kg\cdot m^{-3}}) = a + b\cdot T + c\cdot T^2 \quad (1)$$

The comparison with the literature data was limited due to the lack of data for the odd number of the studied ionic liquids series ($[C_5C_1im][PF_6]$, $[C_7C_1im][PF_6]$ $[C_9C_1im][PF_6]$). Only densities of three ionic liquids, $[C_4C_1im][PF_6]$, $[C_6C_1im][PF_6]$ and $[C_8C_1im][PF_6]$, were found in the literature. The densities obtained in this work are in good agreement with the literature results, with deviations under 0.1% [12,33]. Higher

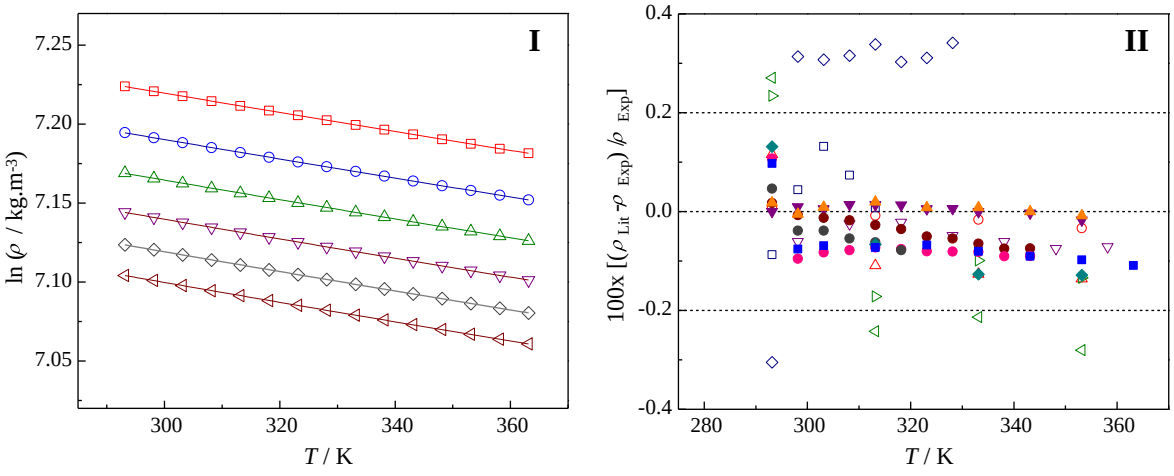

Fig. 1. (I) Logarithm of density as a function of temperature for $[C_{N-1}C_1im][PF_6]$ ionic liquid family. The thin lines results from the linear fitting of the experimental results. □ – $[C_4C_1im][PF_6]$; ○ – $[C_5C_1im][PF_6]$; △ – $[C_6C_1im][PF_6]$; ▽ – $[C_7C_1im][PF_6]$; ◇ – $[C_8C_1im][PF_6]$; ◁ – $[C_9C_1im][PF_6]$.(II) Relative deviations between the experimental density measured in this work (ρ_{exp}) and those reported in the literature (ρ_{exp}) as a function of temperature for $[C_{N-1}C_1im][PF_6]$ ionic liquid series. Tomida et al. [13] ◆ – $[C_4C_1im][PF_6]$; Y. Geng et al. [14] ◇ – $[C_4C_1im][PF_6]$; D. Tomida et al. [15] ◁ – $[C_6C_1im][PF_6]$, ▷ – $[C_8C_1im][PF_6]$; Taguchi et al. [16] △ – $[C_6C_1im][PF_6]$, ○ – $[C_8C_1im][PF_6]$; A.B. Pereiro et al. [20] ● – $[C_4C_1im][PF_6]$, ● – $[C_8C_1im][PF_6]$; W. Fan et al. [21] ▼ – $[C_4C_1im][PF_6]$; K. R. Harris et al. [22] ▲ – $[C_8C_1im][PF_6]$; K. R. Harris et al. [23] ■ – $[C_6C_1im][PF_6]$; Tokuda et al. [25] □ – $[C_4C_1im][PF_6]$; A. Muhammad et al. [26] ▽ – $[C_6C_1im][PF_6]$; A.B. Pereiro et al. [31] ● – $[C_6C_1im][PF_6]$.

Table 2
Fitting parameters of the equation, $\ln(\rho/\mathrm{kg}\cdot\mathrm{m}^{-3}) = a + b.T + c.T^2$, density, molar volume and the thermal expansion coefficients, α_p, at 323.15 K and 0.1 MPa for the studied ionic liquids.

Ionic liquid	a	$10^4 \times b$ / K^{-1}	$10^7 \times c$ / K^{-2}	ρ (T = 323.15 K) / (kg·m^{-3})	V_m (T = 323.15 K) / (cm^3·mol^{-1})	$10^3 \times \alpha_p$(T = 323.15 K) / K^{-1}
[C_4C_1im][PF_6]	7.4175 ± 0.0035	−7.07 ± 0.21	1.56 ± 0.33	1346.8	211.0	0.606 ± 0.030
[C_5C_1im][PF_6]	7.3974 ± 0.0048	−7.62 ± 0.29	2.38 ± 0.44	1307.6	228.1	0.608 ± 0.041
[C_6C_1im][PF_6]	7.3765 ± 0.0055	−7.89 ± 0.34	2.74 ± 0.51	1274.3	245.0	0.612 ± 0.047
[C_7C_1im][PF_6]	7.3562 ± 0.0058	−8.14 ± 0.36	3.08 ± 0.54	1243.0	262.5	0.615 ± 0.050
[C_8C_1im][PF_6]	7.3381 ± 0.0049	−8.27 ± 0.30	3.22 ± 0.45	1217.6	279.5	0.619 ± 0.042
[C_9C_1im][PF_6]	7.3175 ± 0.0039	−8.17 ± 0.24	3.02 ± 0.36	1194.1	296.7	0.622 ± 0.033

relative deviations on density, in the range between −0.32% and 0.25% for [C_4C_1im][PF_6] [13–34], [C_6C_1im][PF_6] [14,15], and [C_8C_1im][PF_6] [14] were observed, which in these cases could be attributed to the low quality of the ionic liquid samples (namely water and halide content) [12–17,32,34–41].

From the parameters obtained from the fitting of the density data using Eq. (1), the temperature dependence of the isobaric thermal expansion coefficients (α_p) were derived, using the following equation:

$$\alpha_p = -\frac{1}{\rho}\left(\frac{\partial\rho}{\partial T}\right)_p = -\left(\frac{\partial \ln\rho}{\partial T}\right)_p = -(b + 2c\cdot(T/\mathrm{K})) \quad (2)$$

where, ρ is the density in kg·m^{-3}, T is the temperature in K, p is the pressure, and b and c represent the parameters of Eq. (1). The fitting parameters of Eq. (1) and the thermal expansion coefficients, at 323.15 K and 0.1 MPa, for all the studied ionic liquids are listed in Table 2. The graphic representations of the molar volumes and thermal expansion coefficients, at 323.15 K (data is presented at T = 323.15 K, in order to compare with the data available in the literature for the [$C_{N-1}C_1$im][NTf_2] series [4,42] and for [C_3C_1im][PF_6]. [43]) and 0.1 MPa, against the total number of carbons of the alkyl side chains length, N, are presented in Fig. 2.

It can be observed that the derived molar volume increment at (323.15 K) for each $-CH_2-$ is identical for both IL series ([PF6]$^-$, [NTf_2]$^-$) and very close to the typical value for alkanes [45]. For the same number of carbons in the alkyl chain, N, the hexafluorophosphate based ionic liquids presents lower density and lower thermal expansion coefficients when compared with the [$C_{N-1}C_1$im][NTf_2] IL series [4,42]. Considering the associated uncertainty, the thermal expansion coefficients are constant with the alkyl side chain of the cation. The lower thermal expansion coefficients observed for the IL with the [PF_6]$^-$ anion when compared with the [NTf_2]$^-$ should be related with the higher conformational flexibility of the [NTf_2]$^-$ anion. The increase of the molar volume arising from the [PF_6]$^-$ anion is due only to the increase of the translation dynamics of the spherical anion and the small increase of the occupied vibrational mode. In the case of the [NTf_2]$^-$ anion, the higher increase of the molar volume with the temperature and consequently higher thermal expansion coefficient is related with the high flexibility and several possible configurationally conformers of the bistriflamide anion, and additionally several internal rotors will also contribute. Fig. 1(II) depicts the predicted thermal expansion coefficients by the Gardas and Coutinho [44] group contribution method for comparison.

3.2. Viscosity

The experimental viscosity data for the studied ionic liquids are reported in Table 3. Fig. 3 depicts the graphic representations of the ln(η/mPa·s) against the temperature and the deviations between the experimental viscosity measured in this work and those reported in the literature, respectively.

The data presented in this work show a good agreement with several literature data sources, as shown in Fig. 3(II) [12,13,15,19–23]. The data reported by Branco et al. [24] for [C_4C_1im][PF_6] and [C_8C_1im][PF_6] and by Geng et al. [14] for [C_4C_1im][PF_6], present a large negative deviation between 22% and 50% from our results, which could be related with the higher water content, which leads to a significant decrease of the viscosity [14,24,25]. The data published previously by Huddleston et al. [8], presents a positive deviations of 40% for [C_4C_1im][PF_6] and 17% for [C_6C_1im][PF_6] from our data. The positive deviation for these ionic liquids is usually related with the higher chloride impurities, which lead to a significant increase of the viscosity [8,12,17,26]. The effect of water content and chloride impurities on the viscosity and density of ionic liquids has been already evaluated in the literature, and was shown that the presence of very low concentrations of chloride

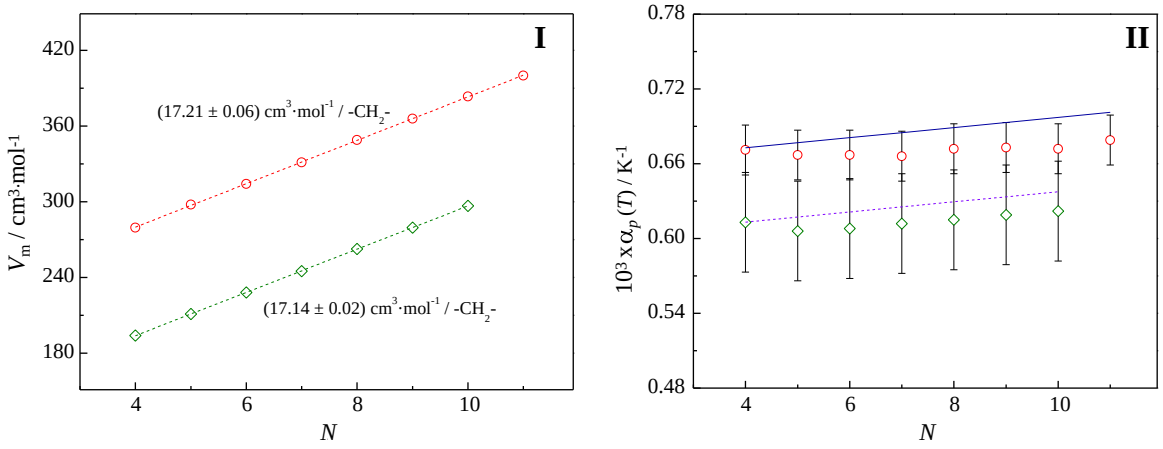

Fig. 2. Graphical representation of the (I) molar volumes and (II) thermal expansion coefficient, at 323.15 K and 0.1 MPa, as a function of the total number of carbons of the alkyl side chains length, N. ○ – [$C_{N-1}C_1$im][NTf_2] (with N = 4–11) [4].; ◇ - [C_3C_1im][PF_6] [29]; [$C_{N-1}C_1$im][PF_6] (with N = 5–10). Gardas and Coutinho group contribution [44], values calculated at 298.15 K: – – – [$C_{N-1}C_1$im][PF_6] (N = 4–10) and – – [$C_{N-1}C_1$im][NTf_2] (with N = 4–11).

Table 3
Experimental viscosity results, η, at 0.1 MPa for the $[C_{N-1}C_1im][PF_6]$ ionic liquid series as a function of temperature.

T/K	η/(mPa·s)					
	[C_4C_1im][PF_6]	[C_5C_1im][PF_6]	[C_6C_1im][PF_6]	[C_7C_1im][PF_6]	[C_8C_1im][PF_6]	[C_9C_1im][PF_6]
293.15	373.95	537.91	694.11	821.98	1044.8	1319.90
298.15	269.03	380.06	482.86	568.36	711.88	892.92
303.15	200.02	277.57	347.71	407.03	503.46	624.37
308.15	151.96	207.41	256.98	298.44	364.84	447.45
313.15	118.20	158.86	194.75	224.76	271.98	330.25
318.15	92.709	122.70	148.68	170.48	204.31	245.78
323.15	74.230	96.844	116.11	132.43	157.08	187.13
328.15	60.266	77.608	92.133	104.44	122.76	144.94
333.15	49.717	63.228	74.355	83.812	97.641	114.29
338.15	41.372	51.907	60.514	67.831	78.386	91.025
343.15	34.872	43.210	49.976	55.725	63.89	73.660
348.15	29.678	36.347	41.732	46.321	52.664	60.366
353.15	25.550	30.932	35.255	38.946	43.974	49.986
358.15	22.074	26.469	29.987	32.984	37.024	41.848
363.15	19.261	22.878	25.769	28.220	31.489	35.378

Note: the magnitude of the experimental differentiation between the two independent set of viscosity data: ±[0.005 mPa·s + 0.001.(η/mPa·s)].

Table 4
Fitting coefficients of VFT equation for the viscosity data of the studied ionic liquids and the derived energy barrier at 323.15 K.

Ionic Liquid	A_η/(mPa.s)	B_η/K	C_η/K	$E(T = 323.15\ K)$/(kJ·mol^{-1})
[C_4C_1im][PF_6]	0.133 ± 0.004	934 ± 8	175.6 ± 0.7	37.2 ± 0.8
[C_5C_1im][PF_6]	0.100 ± 0.003	1036 ± 9	172.6 ± 0.6	39.7 ± 0.8
[C_6C_1im][PF_6]	0.088 ± 0.003	1084. ± 11	172.3 ± 0.8	41.4 ± 1.0
[C_7C_1im][PF_6]	0.077 ± 0.003	1137 ± 11	170.6 ± 0.8	42.4 ± 1.0
[C_8C_1im][PF_6]	0.066 ± 0.003	1192 ± 13	169.9 ± 0.8	44.1 ± 1.1
[C_9C_1im][PF_6]	0.055 ± 0.002	1260 ± 13	168.2 ± 0.8	45.6 ± 1.1

in the ionic liquid sample drastically increases the viscosity, whereas the presence of water reduces the viscosity [12,17,46,47].

Various theoretical models and empirical or semi-empirical expressions are available in the literature to correlate the viscosity of liquids as a function of pressure and temperature [48]. In this work, the Vogel–Tammann–Fulcher equation (VTF) [48–51] was used to correlate the experimental viscosity data:

$$\ln(\eta/\mathrm{mPa\cdot s}) = \ln\left(A_\eta/\mathrm{mPa\cdot s}\right) + \frac{B_\eta}{\left(T - C_\eta\right)} \tag{3}$$

where η is the viscosity in mPa·s, T is the temperature in K, and A_η, B_η and C_η are the adjustable parameters. The parameters were determined from the fitting of the experimental data using the Eq. (3) for the studied ionic liquids. The parameters of VTF equation are presented in Table 4. The correlated viscosities, represented as the solid lines in Fig. 3(I), are in good agreement with the experimental data.

The energy barrier of the fluid to a shear stress, E, can be evaluated based in the viscosity dependence with the temperature using the following equation:

$$E = R\cdot\frac{\partial(\ln\eta)}{\partial(1/T)} = R\cdot\left(\frac{B_\eta}{\left(\frac{C_\eta^2}{T^2} - \frac{2\cdot C_\eta}{T} + 1\right)}\right). \tag{4}$$

In this work, the energy barrier, E, was derived at $T = 323.15$ K in order to compare with the literature data for $[C_{N-1}C_1im][NTf_2]$ and evaluate the effect of the anion [4,52]. The plots of viscosity at $T = 323.15$ K as a function of the total number of carbon atoms in the alkyl chains in the cation, for the $[C_{N-1}C_1im][PF_6]$ and their comparison with the $[C_{N-1}C_1im][NTf_2]$, are depicted in Fig. 4. The literature values obtained for the $[C_3C_1im][PF_6]$ for the discussion was considered [43]. The pre-exponential coefficient of the VTF equation, A_η, and the energy barrier at $T = 323.15$ K as a function of the total number of carbon atoms in the alkyl chains of the cation, are presented in Fig. 5. The predicted parameters, A_η and energy barriers from the Gardas and Coutinho [44] group contribution method (plotted in Fig. 5) are in quite reasonable agreement with the experimental results.

Unlike the dependency of the density with the alkyl side chain length previously observed, there is an increase of the viscosity along the studied ionic liquid series as shown in Fig. 4. A shift in the viscosities

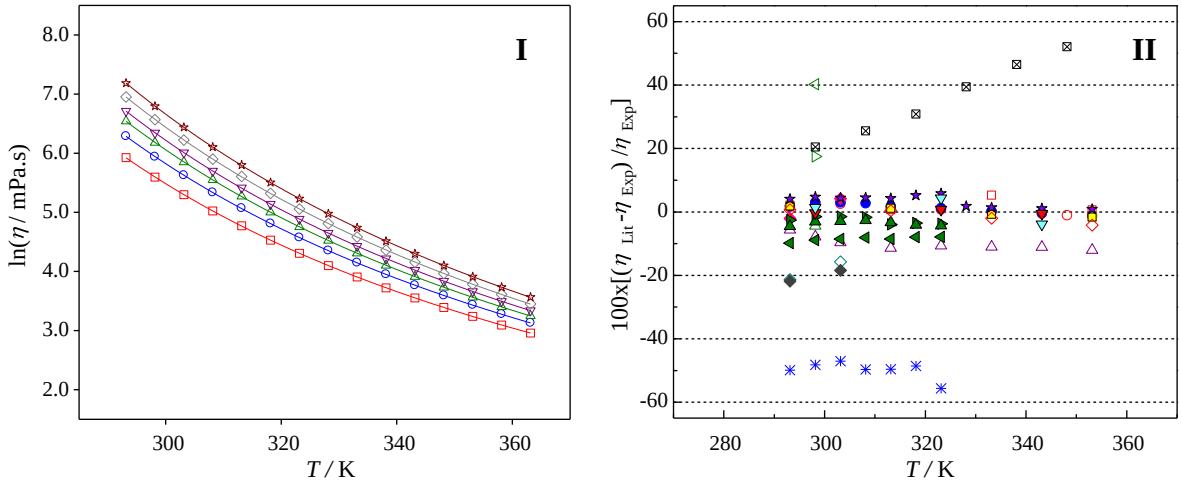

Fig. 3. (I) Graphic representation of $\ln(\eta/\mathrm{mPa\cdot s}) = f(T)$ for for$[C_{N-1}C_1im][PF_6]$ ionic liquid family. The solid lines represent the Vogel–Tammann–Fulcher fittings (Eq. (3)). □ – [C_4C_1im][PF_6]; ○ – [C_5C_1im][PF_6]; △ – [C_6C_1im][PF_6]; ▽ – [C_7C_1im][PF_6]; ◇ – [C_8C_1im][PF_6]; ☆ – [C_9C_1im][PF_6]. (II) Relative deviations between the experimental density measured in this work (ρ_{exp}) and those reported in the literature (ρ_{exp}) as a function of temperature for $[C_{N-1}C_1im][PF_6]$ ionic liquid series. J. G. Huddleston et al. [8] ▷ – [C_4C_1im][PF_6], ◁ – [C_6C_1im][PF_6], △ – [C_8C_1im][PF_6]; D. Tomida et al. [13] □ – [C_4C_1im][PF_6]; Y. Geng et al. [14] ✳ – [C_4C_1im][PF_6]; D. Tomida et al. [15] ■ – [C_6C_1im][PF_6]; A. Ahosseini et al. [19] ▼ – [C_6C_1im][PF_6] (Oscillating-piston viscosimeter), ▼ – [C_6C_1im][PF_6] (Cone-and-plate viscosimeter); A. B. Pereiro et al. [20] ◀ – [C_4C_1im][PF_6], ▶ – [C_6C_1im][PF_6], ▲ – [C_8C_1im][PF_6]; ◇ – [C_8C_1im][PF_6]; W. Fan et al. [21] ★ – [C_4C_1im][PF_6]; K. R. Harris et al. [22] ● – [C_8C_1im][PF_6]; K. R. Harris et al. [23] ○ – [C_6C_1im][PF_6]; L. C. Branco et al. [24] ◇ – [C_4C_1im][PF_6], ◆ – [C_6C_1im][PF_6], ◆ – [C_8C_1im][PF_6]; H. Tokuda et al. [25] △ – [C_4C_1im][PF_6]; A. Muhammad et al. [26] ⊠ – [C_6C_1im][PF_6].

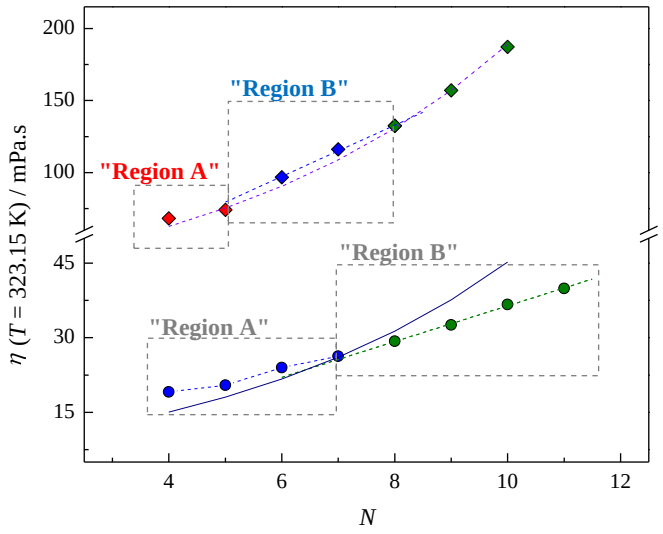

Fig. 4. Plots of viscosity (η/mPa··s) at $T = 323.15$ K and 0.1 MPa for the $[C_{N-1}C_1im][PF_6]$ and the Comparison of the viscosity (η/mPa·s) at $T = 323.15$ K and 0.1 MPa. ♦ — $[C_3C_1im][PF_6]$ [43]; $[C_{N-1}C_1im][PF_6]$ (with $N = 5$–10); ● — $[C_{N-1}C_1im][NTf_2]$ (with $N = 4$–11) [4,51]. Gardas and Coutinho group contribution [44]: – – – — $[C_{N-1}C_1im][PF_6]$ ($N = 4$–10) and – – $[C_{N-1}C_1im][NTf_2]$ (with $N = 4$–10).

along the $[C_{N-1}C_1im][PF_6]$ ILs series starting at $[C_5C_1im][PF_6]$, similar to that previously identified in the bistriflamide, $[C_{N-1}C_1im][NTf_2]$, series, was here observed [4]. This trend shift is related with the structural organization of the liquid above a Critical Alkyl Length Size, (CALS). Due to the bulkier, $[NTf_2]^-$ anion the CALS for $[PF_6]^-$ is shifted to shorter alkyl side chains. This is in good agreement with MD results showing that the CALS for $[PF_6]$-based ILs [53] takes place at shorter chain lengths than for $[NTf_2]$-based ILs [1].

In "Region A" ($[C_3C_1im][PF_6]$ and $[C_4C_1im][PF_6]$), the increase on the viscosity, is smaller than the observed in "Region B" ($[C_5C_1im][PF_6]$ and $[C_7C_1im][PF_6]$) which presents a linear and more pronounced increase on the viscosity. Starting from $[C_7C_1im][PF_6]$, the viscosity shows a progressive positive deviation (higher viscosities) from the linear behavior in "Region B". The ionic liquids with the $[PF_6]^-$ anion present significantly higher viscosities than the bistriflamide based ILs and the higher contribution of the $[PF_6]^-$ anion to the viscosity increases with the alkyl side chain length. In Fig. 5(I), two regions in the pre-exponential parameter of the VTF equation, A_η, could be identified. Starting from $[C_5C_1im][PF_6]$ until $[C_9C_1im][PF_6]$, a linear decrease of the pre-exponential parameter, similar to that present in the $[C_{N-1}C_1im][NTf_2]$ series, is observed [4]. Additionally $[C_{N-1}C_1im][PF_6]$ ILs present lower A_η comparing with the $[C_{N-1}C_1im][NTf_2]$ series, that is related with the sphericity of the $[PF_6]^-$ anion.

The energy barrier at 323.15 K, E, (Fig. 5(II)), for the $[C_{N-1}C_1im][PF_6]$ series increases monotonously in both regions and is ~10 kJ·mol^{-1} higher than in the $[NTf_2]$ ILs. The contribution per methylene group for the energy barriers for the $[C_{N-1}C_1im][PF_6]$ seems to be slightly higher than for the $[C_{N-1}C_1im][NTf_2]$ (1.5 kJ·mol^{-1}, against 1.0 kJ·mol^{-1} per $-CH_2-$) [4]. The shorter members $[C_3C_1im][PF_6]$ and $[C_4C_1im][PF_6]$ have identical and lower energy barrier, E, than would be expected from the extrapolation of the homolog series trend. This could be related with a balance between the decrease in the electrostatic interactions and the increase in the intermolecular interactions arising from the increase of the alkyl side length. The higher viscosity of the $[C_{N-1}C_1im][PF_6]$ when compared with the $[C_{N-1}C_1im][NTf_2]$ series is ruled by the higher energy barriers, which are related with their higher intermolecular interactions and could be understood considering the low charge dispersion of the $[PF_6]^-$ when compared

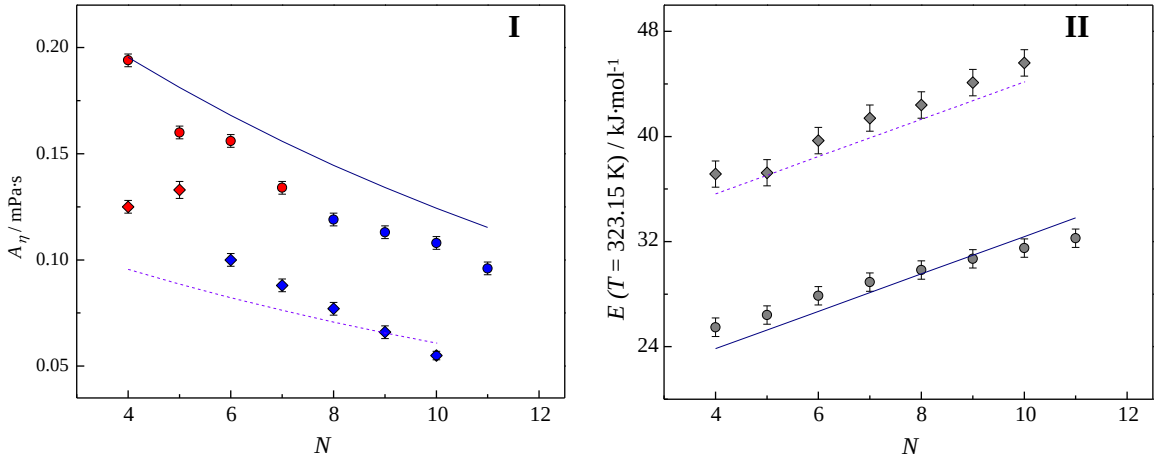

Fig. 5. Graphical representation of the pre-exponential coefficient of the Vogel–Tammann–Fulcher equation (A_η/mPa·s) (I), energy barrier (E/kJ·mol^{-1}) at $T = 323.15$ K (II) as function of the total number of carbon atoms in the alkyl side chains of the cation, N, for ♦ — $[C_3C_1im][PF_6]$ [43], $[C_{N-1}C_1im][PF_6]$ (with $N = 5$–10), this work; ● — $[C_{N-1}C_1im][NTf_2]$ (with $N = 4$–11) [4]. Gardas and Coutinho group contribution [44]: – – – — $[C_{N-1}C_1im][PF_6]$ ($N = 4$–10) and – – $[C_{N-1}C_1im][NTf_2]$ (with $N = 4$–11).

Table 5
Experimental refractive indices at the sodium D-line, n_D, at 0.1 MPa, for the studied ionic liquids as a function of temperature.

T/K	n_D					
	$[C_4C_1im][PF_6]$	$[C_5C_1im][PF_6]$	$[C_6C_1im][PF_6]$	$[C_7C_1im][PF_6]$	$[C_8C_1im][PF_6]$	$[C_9C_1im][PF_6]$
288.15	1.41211	1.41657	1.41980	1.42311	1.42576	1.42823
293.15	1.41078	1.41522	1.41844	1.42172	1.42434	1.42681
298.15	1.40945	1.41387	1.41708	1.42033	1.42293	1.42538
303.15	1.40812	1.41252	1.41572	1.41894	1.42152	1.42396
308.15	1.40679	1.41117	1.41436	1.41755	1.42011	1.42253
313.15	1.40546	1.40982	1.41300	1.41616	1.41869	1.42111
318.15	1.40413	1.40847	1.41164	1.41477	1.41727	1.41968

The data presented in this table were obtained taking into account the linear fitting of the raw experimental results for the refractive indices. Experimental data is presented as supporting information.
Note: the magnitude of the experimental differentiation between the two independent set of refractive indices data: ±0.00005.

Table 6
Experimental refractive indices at the sodium D-line, n_D, for the studied ionic liquids as a function of temperature at 0.1 MPa.

Ionic liquid	n_D (298.15 K)	$10^4 \cdot (dn_D/dT)/(K^{-1})$ [a]	n_D (298.15 K) literature
$[C_4C_1im][PF_6]$	1.40945	−2.66 ± 0.01	1.40890 [5]
			1.40937 [6]
			1.40950 [7]
			1.40900 [8]
			1.40925 [9]
			1.40844 [18]
$[C_5C_1im][PF_6]$	1.41387	−2.70 ± 0.01	
$[C_6C_1im][PF_6]$	1.41708	−2.72 ± 0.02	1.41787 [6]
			1.4169 [26]
			1.41648 [18]
$[C_7C_1im][PF_6]$	1.42033	−2.78 ± 0.01	
$[C_8C_1im][PF_6]$	1.42293	−2.846 ± 0.005	1.4230 [8]
			1.42302 [6]
			1.42351 [18]
$[C_9C_1im][PF_6]$	1.42538	−2.85 ± 0.01	

[a] In the temperature interval, any value of n_D, at a specific temperature, T, can be estimated using the following equation: $n_D(T/K) = n_D\ (298.15\ K) + dn_D/dT \cdot (T/K - 298.15\ K)$.

with the $[NTf_2]^-$ that will be reflected on higher cohesive energies [49] of the $[C_{N-1}C_1im][PF_6]$ series. These findings are in agreement with molecular simulation results reported in the literature [50]. The authors found that for the $[C_{N-1}C_1im][PF_6]$, which possesses a smaller anion and higher charge density compared to the bistriflamide anion, the non-polar domains consist of islands in the continuous medium of polar network ($[C_3C_1im][PF_6]$ to $[C_4C_1im][PF_6]$), whereas starting from $[C_5C_1im][PF_6]$, a bi continuous segregated phase is established [50]. For the case of the bistriflamide anion, which is a bulkier anion, and possesses a lower charge density, the limit to start the nanostructuration is around $[C_6C_1im][NTf_2]$ as previously shown by us [1–4].

3.3. Refractive index

The measured refractive index data in the temperature range from 288 K to 318 K, are presented in Table 5. The graphic representation of the refractive indices as a function of the temperature for the studied ionic liquids is depicted in Fig. 6(I). Table 6 lists the refractive indices of all studied ionic liquids, at $T = 298.15$ K, the literature values, and the temperature derivative of the refractive index, dn_D/dT.

For all the ionic liquids, the refractive index values at 298.15 K obtained in this work are in good agreement with those previously reported in the literature (relative deviations are between 0.03% and −0.05%). As observed before [27], the temperature dependence of the refractive indices is less pronounced than the verified for the usual molecular solvents. For the studied ILs, a decrease in the refractive index of 0.00027 to 0.00029 per Kelvin along the alkyl side chain of the cation was found .

The plots of the refractive indices, at $T = 298.15$ K as a function of the total number of carbon atoms in the alkyl chains in the cation, for the $[C_{N-1}C_1im][PF_6]$ and their comparison with the $[C_{N-1}C_1im][NTf_2]$ [18], are shown in Fig. 6(II). The lower refractive indices of the $[PF_6]^-$ compared with $[NTf_2]^-$ the series arise from the lower polarizability of the $[PF_6]^-$ anion. A shift in the refractive indices trend along the alkyl side chain of the cation for the studied hexafluorophosphate based ILs, around $[C_7C_1im][PF_6]$, was found. Above this Critical Alkyl Length Size (CALS), $[C_7C_1im][PF_6]$, a decrease of the contribution per methylene group ($-CH_2-$) is observed. The shift in the refractive indices trend could be related with the nanostructuration/segregation that occurs after the CALS. After that, there is no significant change in the nearest cation–anion interaction potential and as consequence, the charge dispersion and the

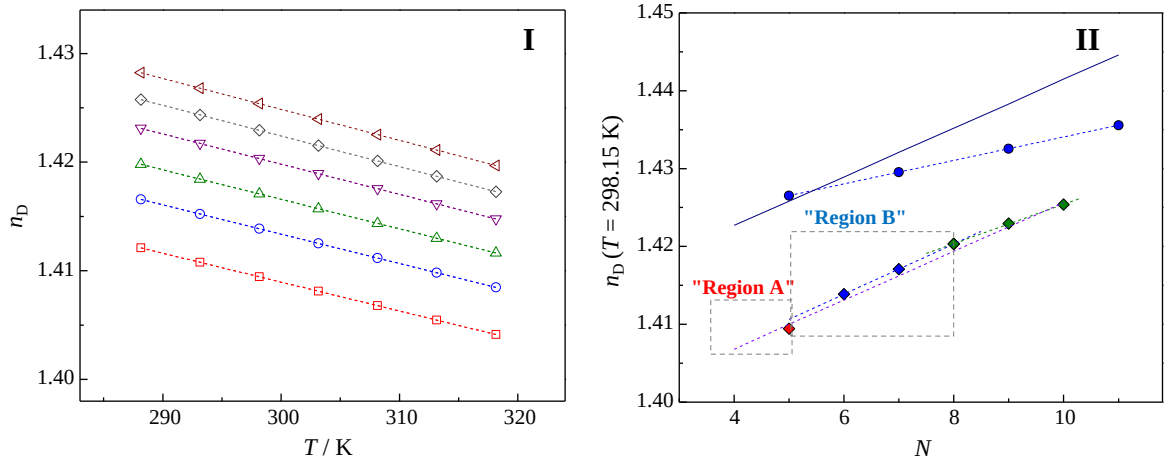

Fig. 6. (**I**) Graphical representation of the refractive indices as a function of temperature for $[C_{N-1}C_1im][PF_6]$ ionic liquid series. □ - $[C_4C_1im][PF_6]$; ○ - $[C_5C_1im][PF_6]$; △ - $[C_6C_1im][PF_6]$; ▽ - $[C_7C_1im][PF_6]$; ◇ - $[C_8C_1im][PF_6]$; ◁ - $[C_9C_1im][PF_6]$. (**II**) Refractive indices, n_D, at $T = 298.15$ K as function of the total number of carbon atoms in the alkyl side chains of the cation, *N*. ◆ - $[C_{N-1}C_1im][PF_6]$ (with $N = 5$ - 10) and ● - $[C_{N-1}C_1im][NTf_2]$ (with $N = 5, 7, 9, 11$) [18]. Gardas and Coutinho group contribution [44]: – – – - $[C_{N-1}C_1im][PF_6]$ ($N = 4$ - 10) and — - $[C_{N-1}C_1im][NTf_2]$ (with $N = 4$ - 11).

polarizability of the charged region remains almost unchanged, and with it the contribution to the refractive indices due to the polarizability.

4. Final remarks

The molecular interpretation of the thermophysical properties of the hexafluorophosphate based ionic liquids, and the comparison with the analogous NTf_2 series could only be done by taking into account the high degree of organization, the structural complexity, shape and size of the ions of the ionic liquids. For the same number of carbons in the alkyl chain, *N*, the hexafluorophosphate based ionic liquids present lower density and lower thermal expansion coefficients when compared with the $[C_{N-1}C_1im][NTf_2]$ IL series. The $[C_{N-1}C_1im][PF_6]$ ionic liquids present significantly higher viscosities than the bistriflamide based ILs, which are related with the higher energy barrier of the liquid to a shear stress. A trend shift along the alkyl side chain of the cation around $[C_7C_1im][PF_6]$, was found for the viscosities and refractive indices. The effect of the increase of the alkyl side chain on the interaction between the cation and anion is more pronounced in the ionic liquids with shorter alkyl side chain due to the high impact of the alkyl chain steric hindrance in the ions electrostatic interaction.

For ionic liquids with intermediate alkyl side chain lengths, there is a regular region where a decrease of the electrostatic interaction between the ions, is observed. From a critical alkyl length size, CALS (around $[C_7C_1im][PF_6]$) the nanostructuration into polar and non-polar regions begins and the effect of the decrease of the electrostatic interactions is partially compensated by the increase of the non-electrostatic interactions in the non-polar regions. After the CALS, the increase of the non-polar region leads to a new behavior where the $-CH_2-$ increment is similar to the one observed for the alkanes/alkane-derivatives where a smaller but progressive change of the overall polar network region is observed.

Acknowledgments

This work was supported by FCT, Lisbon, Portugal, and the European Social Fund through strategic projects Pest-C/QUI/UI0081/2011 awarded to CIQUP and Pest-C/CTM/LA0011/2011 to CICECO. M.A.A. Rocha and A.I.M.C.L. Ferreira acknowledge the financial support from FCT for the award of research grants with references, SFRH/BD/60513/2009 and SFRH/BPD/84891/2012 respectively.

Appendix A. Supplementary data

Experimental refractive indices at the sodium D-line, nD, at 0.1 MPa, for the studied ionic liquids as a function of temperature. Supplementary data to this article can be found online at http://dx.doi.org/10.1016/j.molliq.2013.09.031.

References

[1] M.A.A. Rocha, C.F.R.A.C. Lima, L.R. Gomes, B. Schröder, J.A.P. Coutinho, I.M. Marrucho, J.M.S.S. Esperança, L.P.N. Rebelo, K. Shimizu, J.N. Canongia Lopes, L.M.N.B.F. Santos, J. Phys. Chem. B 115 (2011) 10919.
[2] M.A.A. Rocha, M. Bastos, J.A.P. Coutinho, L.M.N.B.F. Santos, J. Chem. Thermodyn. 53 (2012) 140.
[3] M.A.A. Rocha, J.A.P. Coutinho, L.M.N.B.F. Santos, J. Phys. Chem. B 116 (2012) 10922.
[4] M.A.A. Rocha, C.M.S.S. Neves, M.G. Freire, O. Russina, A. Triolo, J.A.P. Coutinho, L.M.N.B.F. Santos, J. Phys. Chem. B (2013), http://dx.doi.org/10.1021/jp406374a.
[5] A. Kumar, J. Solut. Chem. 37 (2008) 203–214.
[6] A.B. Pereiro, A. Rodríguez, J. Chem. Eng. Data 52 (2007) 600–608.
[7] M.T. Zafarani-Moattar, R. Majdan-Cegincara, J. Chem. Eng. Data 52 (2007) 2359–2364.
[8] J.G. Huddleston, A.E. Visser, M. Reichert, H.D. Willauer, G.A. Broker, R.D. Rogers, Green Chem. 3 (2001) 156–164.
[9] M. Bendová, Z. Wagner, J. Chem. Eng. Data 51 (2006) 2126–2131.
[10] G.J. Kabo, A.V. Blokhin, Y.U. Paulechka, A.G. Kabo, M.P. Shymanovich, J.W. Magee, J. Chem. Eng. Data 49 (2004) 453–461.
[11] C.P. Fredlake, J.M. Crosthwaite, D.G. Hert, S.N.V.K. Aki, J.F. Brennecke, J. Chem. Eng. Data 49 (2004) 954–964.
[12] J. Jacquemin, P. Husson, A.A.H. Padua, V. Majer, Green Chem. 8 (2006) 172–180.
[13] D. Tomida, A. Kumagai, K. Qiao, C. Yokoyama, Int. J. Thermophys. 27 (2006) 39–47.
[14] Y. Geng, S. Chen, T. Wang, D. Yu, C. Peng, H. Liu, Y. Hu, J. Mol. Liq. 143 (2008) 100–108.
[15] D. Tomida, A. Kumagai, S. Kenmochi, K. Qiao, C. Yokoyama, J. Chem. Eng. Data 52 (2007) 577–579.
[16] R. Taguchi, H. Machida, Y. Sato, R.L. Smith Jr., J. Chem. Eng. Data 54 (2009) 22–27.
[17] J. Troncoso, C.A. Cerdeiriña, Y.A. Sanmamed, L. Romaní, L.P.N. Rebelo, J. Chem. Eng. Data 51 (2006) 1856.
[18] M. Tariq, P.A.S. Forte, M.F.C. Gomes, J.N.C. Lopes, L.P.N. Rebelo, J. Chem. Thermodyn. 41 (2009) 790–798.
[19] A. Ahosseini, A.M. Scurto, Int. J. Thermophys. 29 (2008) 1222–1243.
[20] A.B. Pereiro, J.L. Legido, A. Rodríguez, J. Chem. Thermodyn. 39 (2007) 1168–1175.
[21] W. Fan, Q. Zhou, J. Sun, S. Zhang, J. Chem. Eng. Data 54 (2009) 2307–2311.
[22] K.R. Harris, M. Kanakubo, L.A. Woolf, J. Chem. Eng. Data 51 (2006) 1161–1167.
[23] K.R. Harris, M. Kanakubo, L.A. Woolf, J. Chem. Eng. Data 52 (2007) 1080–1085.
[24] L.C. Branco, J.N. Rosa, J.J.M. Ramos, C.A.M. Afonso, Chem. Eur. J. 8 (2002) 3671–3677.
[25] H. Tokuda, S. Tsuzuki, Md.A.B.H. Susan, K. Hayamizu, M. Watanabe, J. Phys. Chem. B 110 (2006) 19593–19600.
[26] A. Muhammad, M.I. Abdul Mutalib, C.D. Wilfred, T. Murugesan, A. Shafeeq, J. Chem. Thermodyn. 40 (2008) 1433–1438.
[27] M.G. Freire, A.R.R. Teles, M.A.A. Rocha, B. Schröder, C.M.S.S. Neves, P.J. Carvalho, D.V. Evtuguin, L.M.N.B.F. Santos, J.A.P. Coutinho, J. Chem. Eng. Data 56 (2011) 4813–4822.
[28] Y. Yu, A.N. Soriano, M. Li, Thermochim. Acta 42 (2009) 482.
[29] John D. Holbrey, W. Matthew Reichert, Ramana G. Reddy, Robin D. Rogers, ACS Symp. Ser. 856 (2003) 121–133.
[30] C.A. Nieto de Castro, M.J.V. Lourenço, A.P.C. Ribeiro, E. Langa, S.I.C. Vieira, J. Chem. Eng. Data 55 (2010) 653–661.
[31] A.B. Pereiro, J.L. Legido, A. Rodríguez, J. Chem. Thermodyn. 38 (2006) 651–661.
[32] P.J. Carvalho, T. Regueira, L.M.N.B.F. Santos, J. Fernandez, J.A.P. Coutinho, J. Chem. Eng. Data 55 (2010) 645–652.
[33] R.L. Gardas, M.G. Freire, P.J. Carvalho, I.M. Marrucho, I.M.A. Fonseca, A.G.M. Ferreira, J.A.P. Coutinho, J. Chem. Eng. Data 52 (2007) 80–88.
[34] M.E. Wieser, M. Berglund, Pure Appl. Chem. 81 (2009) 2131–2156.
[35] J. Suurkuusk, I. Wadsö, J. Chem. Thermodyn. 6 (1974) 667–679.
[36] J. Konicek, J. Suurkuusk, I. Wadsö, Chem. Scr. 1 (1971) 217–220.
[37] L.M.N.B.F. Santos, M.A.A. Rocha, A.S.M.C. Rodrigues, V. Štejfa, M. Fulem, M. Bastos, J. Chem. Thermodyn. 43 (2011) 1818–1823.
[38] C.E.S. Bernardes, L.M.N.B.F. Santos, M.E. Minas da Piedade, Meas. Sci. Technol. 17 (2006) 1405–1408.
[39] R. Sabbah, A. Xu-wu, J.S. Chickos, M.L.P. Leitão, M.V. Roux, L.A. Torres, Thermochim. Acta 331 (1999) 93–204.
[40] R.D. Chirico, V. Diky, J.W. Magee, M. Frenkel, K.N. Marsh, Pure Appl. Chem. 81 (2009) 791–828.
[41] M.E. Wieser, T.B. Coplen, Pure Appl. Chem. 83 (2011) 359–396.
[42] M. Tariq, A.P. Serro, J.L. Mata, B. Saramago, J.M.S.S. Esperança, J.N. Canongia Lopes, L.P.N. Rebelo, Fluid Phase Equilib. 294 (2010) 131–138.
[43] C.M.S.S. Neves, M.L.S. Batista, A.F.M. Cláudio, L.M.N.B.F. Santos, I.M. Marrucho, M.G. Freire, J.A.P. Coutinho, J. Chem. Eng. Data 55 (2010) 5065–5073.
[44] R.L. Gardas, J.A.P. Coutinho, AIChE J. 55 (2009) 1274–1290.
[45] David R. Lide, CRC Handbook of Chemistry and Physics, 84th edition Taylor & Francis, 2003.
[46] K.R. Seddon, A. Stark, M. Torres, J. Pure Appl. Chem. 72 (2000) 2275–2287.
[47] K.R. Seddon, A. Stark, M. Torres, , Chapter 4 ACS Symp. Ser. (2002) 34–49.
[48] D.S. Viswanath, T.K. Ghosh, D.H.L. Prasad, N.V.K. Dutt, K.Y. Rani, Viscosity of Liquids: Theory, Estimation, Experiment, and Data, Springer, Netherlands, 2007.
[49] H. Vogel, Phys. Z. 22 (1921) 645.
[50] G.S. Fulcher, J. Am. Ceram. Soc. 8 (1925) 339.
[51] G. Tammann, W. Hesse, Z. Anorg. Allg. Chem. 156 (1926) 245.
[52] M. Tariq, P.J. Carvalho, J.A.P. Coutinho, I.M. Marrucho, J.N.C. Lopes, L.P.N. Rebelo, Fluid Phase Equilib. 301 (2011) 22–32.
[53] J.N.A. Canongia Lopes, A.A.H. Pádua, J. Phys. Chem. B 110 (2006) 3330–3335.

Thermophysical Properties of $[C_{N-1}C_1im][PF_6]$ Ionic Liquids

Marisa A. A. Rocha[1,], Filipe M. S. Ribeiro[1], Ana I.M.C. Lobo Ferreira[1], João A. P. Coutinho[2], Luís M. N. B. F. Santos[1,*]*

(Supporting Information)

[1] CIQ, Departamento de Química e Bioquímica, Faculdade de Ciências da Universidade do Porto, R. Campo Alegre 687, P-4169-007, Porto, Portugal

[2]CICECO, Departamento de Química, Universidade de Aveiro, P-3810-193 Aveiro, Portugal

Table S1. Experimental refractive indices at the sodium D-line, n_D, at 0.1 MPa, for the studied ionic liquids as a function of temperature.

Ionic Liquid	T / K	n_D
$[C_4C_1im][PF_6]$	287.98	1.41217
	293.25	1.41074
	298.25	1.40940
	303.25	1.40811
	308.15	1.40681
	313.15	1.40550
	318.00	1.40414
$[C_5C_1im][PF_6]$	288.25	1.41655
	293.25	1.41520
	298.05	1.41387
	302.95	1.41258
	308.05	1.41119
	313.12	1.40982
	318.05	1.40851
$[C_6C_1im][PF_6]$	288.30	1.41981
	293.25	1.41841
	298.15	1.41702
	303.15	1.41568
	308.15	1.41437
	313.15	1.41304
	318.05	1.41168
$[C_7C_1im][PF_6]$	288.25	1.42311
	293.15	1.42172
	298.25	1.42030
	303.15	1.41892
	308.05	1.41753
	313.05	1.41620
	318.02	1.41483
$[C_8C_1im][PF_6]$	288.28	1.42573
	293.15	1.42435
	298.18	1.42290
	303.22	1.42150
	308.05	1.42013
	313.05	1.41873
	317.95	1.41734
$[C_9C_1im][PF_6]$	288.23	1.42822
	293.15	1.42680
	298.25	1.42537
	303.15	1.42394
	308.00	1.42257
	312.95	1.42115
	317.95	1.41978

Paper X

"Heat Capacities at 298.15 K of [$C_{N-1}C_1$im][PF_6] Ionic Liquids Series"

Marisa A. A. Rocha, Filipe M. S. Ribeiro, João A. P. Coutinho, Luís M. N. B. F. Santos

Manuscript version

Note: The author of this thesis performed part of the experimental work, data analysis and contribute to the discussion and conclusions.

Heat Capacities at 298.15 K of $[C_{N-1}C_1im][PF_6]$ Ionic Liquids Series

Marisa A. A. Rocha[1,], Filipe M. S. Ribeiro[1], João A. P. Coutinho[2], Luís M. N. B. F. Santos[1,*]*

[1] CIQ, Departamento de Química e Bioquímica, Faculdade de Ciências da Universidade do Porto, R. Campo Alegre 687, P-4169-007, Porto, Portugal

[2]CICECO, Departamento de Química, Universidade de Aveiro, P-3810-193 Aveiro, Portugal

*Corresponding author

Tel: +351220402836. Fax:+351220402659; E-mail address:lbsantos@fc.up.pt (L.M.N.B.F.Santos), marisa.alexandra.rocha@gmail.com (M.A.A. Rocha)

ABSTRACT

The heat capacities at T = 298.15 K of the 1-alkyl-3-methylimidazolium hexafluorophosphate, $[C_{N-1}C_1im][PF_6]$ (where N = 5 to 10) ionic liquid series, are used to explore the effect of the alkyl size length in the nanostructuration of the ionic liquids. The heat capacities of the studied ionic liquids were measured with an uncertainty better than ± 0.15 % and are in excellent agreement with the available data in the literature. A subtle odd-even effect for the specific heat capacities of the $[C_{N-1}C_1im][PF_6]$ series was found, where the even numbered ILs presents higher c_p^o. The observed odd-even effect in the heat capacity was rationalized taking into account the preferential orientation of the terminal $-CH_3$ group. The higher specific / volumic heat capacities shown for the $[C_6C_1im][PF_6]$ and $[C_8C_1im][PF_6]$ is an indication of a additional conformational disorder increase in the liquid phase that could be related with a weaker alkyl chain interdigitation capability for these two ILs.

KEYWORDS: drop calorimeter; molar heat capacity; specific heat capacity; volumic heat capacity; hexafluorophosphate; ionic liquids; trend shift; imidazolium; alkyl chain effect; odd-even.

1. INTRODUCTION

The 1-alkyl-3-methylimidazolium hexafluorophosphate ionic liquids series is one of the most studied ionic liquid series due to their relative higher thermostability and the interesting differentiation of the hexafluorophosphate anion compared with the bistriflamide anion. The hexafluorophosphate anion is a spherical anion with an uniform charge distribution with a less complex conformation analysis in their interaction with the cation when compared with the bistriflamide anion.

In this work, the heat capacities at T = 298.15 K of 1-alkyl-3-methylimidazolium hexafluorophosphate, $[C_{N-1}C_1im][PF_6]$ (with N = 5 - 10), were measured by a high-precision heat capacity drop calorimeter, originally developed by Wadsö [1,2] and recently modernized and tested in our laboratory.[3] This work complements the previous thermophysical properties of the $[C_{N-1}C_1im][NTf_2]$ [4-6], $[C_{N/2}C_{N/2}im][NTf_2]$ [6-9] and $[C_{N-1}C_1im][PF_6]$ [10].

The experimental results obtained for the molar, specific and volumic heat capacities will be used to evaluate the effect of the nature and size of the anion, as well as the impact of the nanostucturation of ionic liquids on the thermophysical properties. This analysis will be performed in a comparative basis with the literature data for the $[C_{N-1}C_1im][NTf_2]$ ionic liquid series.

2. EXPERIMENTAL DETAILS

2.1. Materials and Purification

The 1-alkyl-3-methylimidazolium hexafluorophosphate, $[C_{N-1}C_1im][PF_6]$ (with N = 5 - 10), used in this work, were purchased from IOLITEC with a stated purity of better than 99%. All the ionic liquids were dried and purified under vacuum (< 10 Pa) at moderate temperature (323 K) and constant stirring, in order to reduce the presence of water or other volatile contents. This process was performed systematically before and during the thermophysical properties measurements.

2.2. High-Precision Heat Capacity Drop Calorimetry

The heat capacities of the studied ILs were measured at T = 298.15 K, by a high-precision heat capacity drop calorimeter, which is described in detail in the literature.[1-3] The calorimeter was calibrated with water and sapphire (α-Al_2O_3 pellets, NIST-RM 720) based on a drop temperature step procedure of ΔT = 10 K [1-3, 11,12], using the respective standard molar heat capacities at 298.15 K reported in literature, $C^{o}_{p,m}$(α-aluminum oxide) = (79.03 ± 0.08) $J \cdot K^{-1} \cdot mol^{-1}$ and $C^{o}_{p,m}(H_2O)$ = (75.32 ± 0.01) $J \cdot K^{-1} \cdot mol^{-1}$.[13] The calibration constant was found to be ε = (6.6040 ± 0.0036) $W \cdot V^{-1}$. The accuracy of the apparatus for the measurements of the heat capacities of liquids and solids was evaluated before, based on the measurements of benzoic acid and hexafluorobenzene.[3] The calorimeter was already used in the measurement of heat capacities for the extended $[C_{N-1}C_1im][NTf_2]$ ionic liquid series [4], and was found that the obtained results differ less than 0.4% from the literature data, which is in excellent agreement. Nevertheless, the calorimeter was additionally tested based on the results obtained for 1-hexyl-3-methylimidazolium bis(trifluoromethylsulfonyl)imide,

[C_6mim][NTf_2].[14] The determined $C^{o}_{p,m}$ ([C_6mim][NTf_2], 298.15 K) = (629.24 ± 0.43) $J \cdot K^{-1} \cdot mol^{-1}$ is in excellent agreement with the available literature data ($C^{o}_{p,m}$ ([C_6mim][NTf_2], 298.15 K) = (631.6 ± 0.5) $J \cdot K^{-1} \cdot mol^{-1}$).[14] The masses of the samples were corrected for the buoyancy effect, and it was done both for calibration and experiments of ionic liquids. The relative atomic masses used were those recommended by the IUPAC Commission in 2007. [15] The presented uncertainties are presented as twice the standard deviation of the mean and the calibration uncertainty is included.

3. RESULTS AND DISCUSSION

The molar masses, M ($g \cdot mol^{-1}$), number of drop experiments, N_{drop}, and the molar heat capacity at 298.15 K, $C^{o}_{p,m}$ ($J \cdot K^{-1} \cdot mol^{-1}$), for the each studied ionic liquids are presented in table 1.

Table 1. Molar heat capacity values, at T = (298.15 ± 0.02) K, for the studied ionic liquids. Calibration constant of the drop calorimeter used in the heat capacity calculation (6.6040 ± 0.0036 $W \cdot V^{-1}$).

Ionic Liquid	M /$g \cdot mol^{-1}$	N_{drop}	$C^{o}_{p,m}$ / $J \cdot K^{-1} \cdot mol^{-1}$
[C_4C_1im][PF_6]	284.183	21	406.68 ± 0.51
[C_5C_1im][PF_6]	298.210	19	435.49 ± 0.63
[C_6C_1im][PF_6]	312.236	22	468.73 ± 0.54
[C_7C_1im][PF_6]	326.263	43	500.81 ± 0.52
[C_8C_1im][PF_6]	340.290	30	535.16 ± 0.56
[C_9C_1im][PF_6]	354.316	21	566.89 ± 0.45

N_{drop}.= number of drop experiments; the number of drops are the sum of the drops that were obtained in at least two independent experiments.

Table 2 presents the heat capacity data at T = 298.15 K, together with the available literature values. For the ionic liquids [C_5C_1im][PF_6], [C_7C_1im][PF_6] and [C_9C_1im][PF_6], no literature data was found. The heat capacity data available in

literature for $[C_4C_1im][PF_6]$, $[C_6C_1im][PF_6]$ and $[C_8C_1im][PF_6]$ presents a large uncertainty that in some cases exceed 10%.[16-19] Taking into account the level of uncertainty of the data obtained in this work, only the available literature data with an uncertainty better than 3%.[20-23] was considered for comparison. The volumic heat capacities, C_p^o/V, were calculated taking into account the specific heat capacities, c_p^o, and the experimental density values at the same reference temperature already reported in the literature.[10] The heat capacities of the studied ionic liquids were measured with an uncertainty of less than ± 0.15 % and the obtained results for the $[C_4C_1im][PF_6]$ are in excellent agreement with the available literature data.

Table 2. Derived heat capacity results at T = (298.15 ± 0.02) K , for each ionic liquid, together with selected literature data.

Ionic Liquid	c_p^o / J·K^{-1}·g^{-1}	C_p^o/V / J·K^{-1}·cm^{-3}	$C_{p,m}^o$ / J·K^{-1}·mol^{-1}	$C_{p,m}^o$ / J·K^{-1}·mol^{-1}
	This work			Literature
$[C_4C_1im][PF_6]$	1.4310 ± 0.0018	1.9567 ± 0.0025	406.68 ± 0.51	408.7 ± 1.6 (AC) [20,23] 407.7 ± 2.5 (TC) [21,23] 405 ± 12 (TC)* [22,23]
$[C_5C_1im][PF_6]$	1.4603 ± 0.0021	1.9390 ± 0.0028	435.49 ± 0.63	
$[C_6C_1im][PF_6]$	1.5012 ± 0.0017	1.9429 ± 0.0022	468.73 ± 0.54	
$[C_7C_1im][PF_6]$	1.5350 ± 0.0016	1.9381 ± 0.0020	500.81 ± 0.52	
$[C_8C_1im][PF_6]$	1.5727 ± 0.0016	1.9453 ± 0.0020	535.16 ± 0.56	
$[C_9C_1im][PF_6]$	1.6000 ± 0.0013	1.9410 ± 0.0016	566.89 ± 0.45	

Note: AC - adiabatic calorimetry;TC - Tian-Calvet microcalorimetry;. * the heat capacity of $[C_4C_1im][PF_6]$ was extrapolated to T = 298.15 K.[22]

Figure 1 shows the graphic representation of the molar heat capacity data, $C_{p,m}^o$, against the total number of carbon atoms in the alkyl side chains of the cation, N, for the $[C_{N-1}C_1im][PF_6]$ together with the literature data for the $[C_{N-1}C_1im][NTf_2]$ ionic liquids.[4] An

apparent linearity behavior along the IL series is observed in the representation of $C^{o}_{p,m}$ = f (*N*) for the studied ionic liquids. At 298.15 K, the molar heat capacities for the [$C_{N-1}C_1$im][NTf_2] ionic liquids are (159 $J{\cdot}K^{-1}{\cdot}mol^{-1}$) higher than the obtained for the [$C_{N-1}C_1$im][PF_6] series, which reflects the higher large molar heat capacity contribution of the bistriflamide anion in comparison to the hexafluorophosphate anion which is obviously related with the significant higher number of atoms of the bistriflamide anion and also related to their higher configurational contribution.[24]

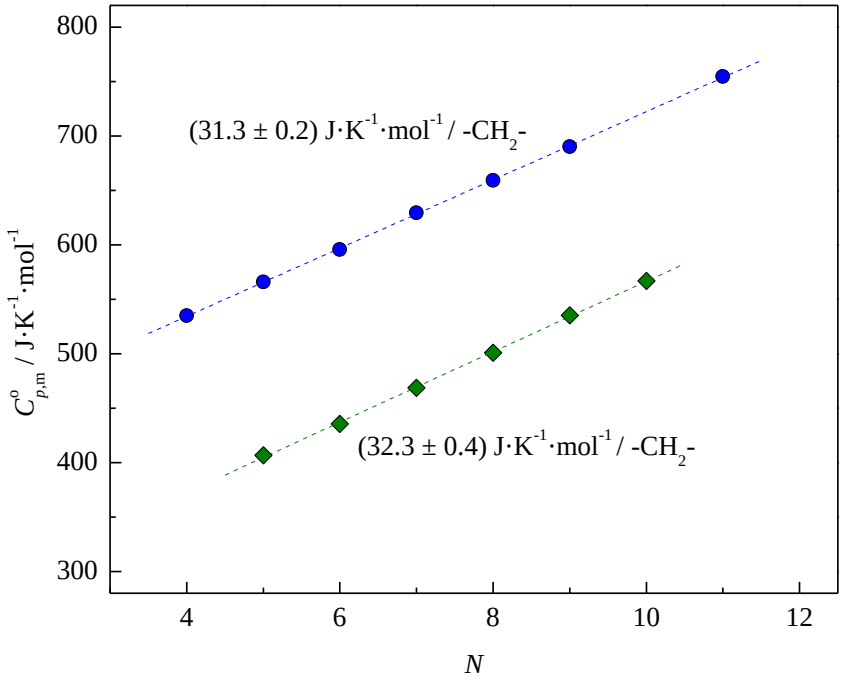

Figure 1. Molar heat capacities $C^{o}_{p,m}$, at *T* = 298.15 K as function of the total number of carbon atoms in the alkyl side chains of the cation, *N*, for ◆ - [$C_{N-1}C_1$im][PF_6] (with *N* = 5 - 10) and ● - [$C_{N-1}C_1$im][NTf_2] (with *N* = 4 - 11). [4]

Figure 2 presents the plots of the specific heat capacity (I) and the volumic heat capacity (II) against the total number of carbon atoms in the alkyl side chains of the cation, *N*, and their comparison with the [$C_{N-1}C_1$im][NTf_2].[4] As it can be observed, the [$C_{N-1}C_1$im][PF_6] presents higher specific heat capacities than the bistriflamide based

ionic liquids. In addition, unlike to the trend shift found around $[C_6C_1im][NTf_2]$ for $[C_{N-1}C_1im][NTf_2]$ series, a subtle odd-even effect for the specific heat capacities, was found for the $[C_{N-1}C_1im][PF_6]$, where the even numbered ILs presents higher c_p^o. The observed odd-even effect in the heat capacity of the $[C_{N-1}C_1im][PF_6]$ series could be rationalized considering the preferential orientation of the terminal $-CH_3$ group. The higher specific/volumic heat capacities shown for the $[C_6C_1im][PF_6]$ and $[C_8C_1im][PF_6]$ indicates higher entropies in the liquid phase that could be related with their low alkyl chain interdigitation capability for these two ILs, and consequently a less efficient rearrangement in the liquid. The odd-even effect was already observed in some thermodynamic properties of different kinds of compounds, such as paraffins [25], alcohols [26], fatty acids [27], and more recently in fluorotelomer alcohols [28] as well as, in ionic liquids [6,7,29,30]. However, for this case is still not clear why the sphericity and low charge dispersion of the hexafluorophosphate anion leads to a more pronounced odd-even effect on the heat capacities of ionic liquids than the bistriflamide anion.

The $[C_4C_1im][PF_6]$ shows an outlier behavior from the trend of the homologous series, presenting a higher volumic heat capacity, in agreement with recent works reported in the literature for the short members of the bistriflamide ILs series.[4,8,10] For a better understanding of the differentiation observed for the $[C_4C_1im][PF_6]$, accurate data for the heat capacity of the other short members of the series $[C_2C_1im][PF_6]$ and $[C_3C_1im][PF_6]$ (that are solids at 298.15 K), will be needed.

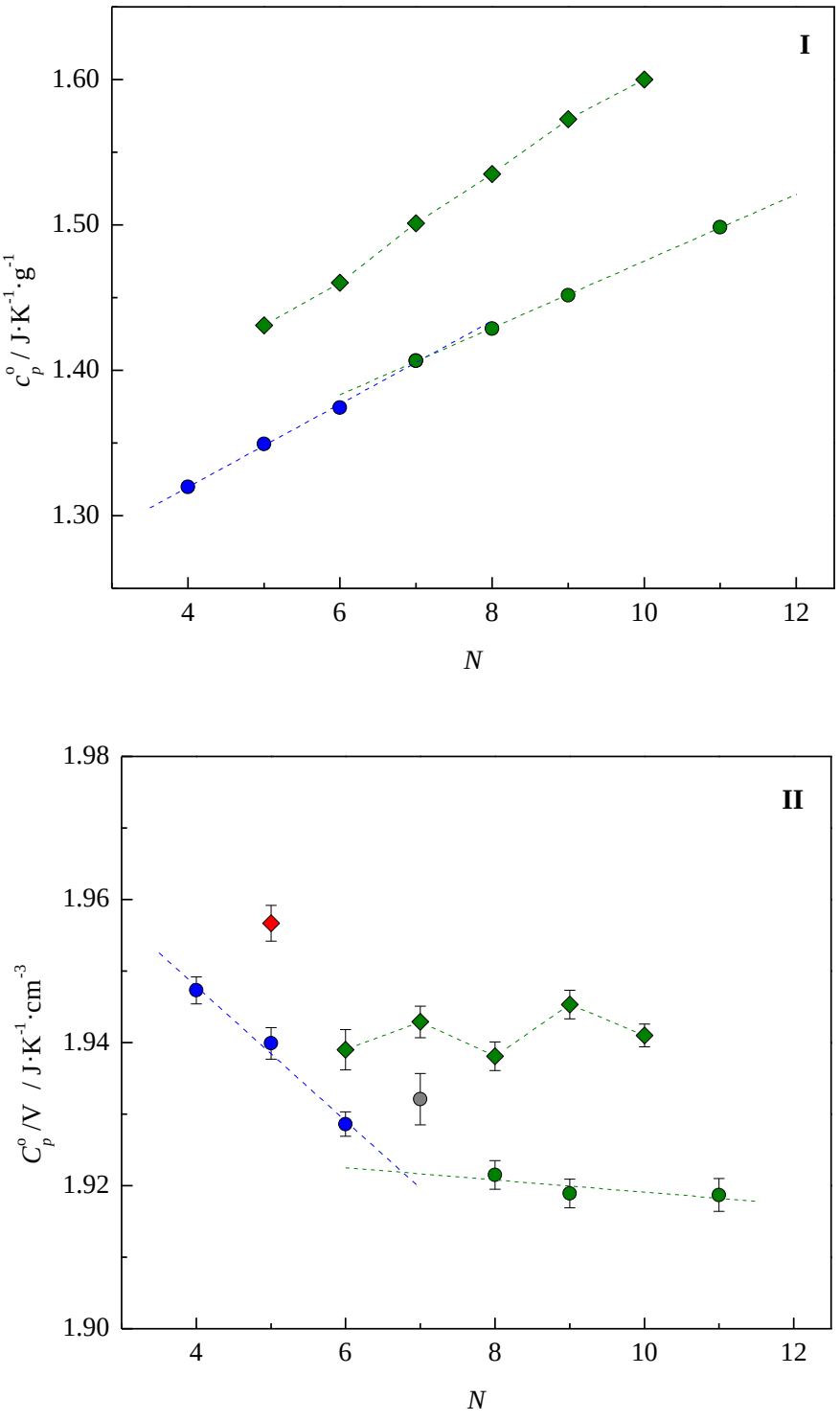

Figure 8. Specific heat capacities (**I**) and volumic heat capacities (**II**), at T = 298.15 K, as function of the total number of carbon atoms in the alkyl side chains of the cation, N, for, ◆ - $[C_{N\text{-}1}C_1im][PF_6]$ (with N = 5 - 10) and ● - $[C_{N\text{-}1}C_1im][NTf_2]$ (with N = 4 - 11). [4]

AKNOWLEDGMENTS

Thanks are due to Fundação para a Ciência e Tecnologia (FCT), Lisbon, Portugal and to FEDER for financial support to Centro de Investigação em Química, University of Porto through the project Pest-C/QUI/UI0081/2011, and CICECO, University of Aveiro, through the project Pest-C/CTM/LA0011/2011. Marisa A. A. Rocha acknowledge the financial support from FCT and the European Social Fund (ESF) under the Community Support Framework (CSF) for the award of a Ph.D. Research Grant, SFRH/BD/60513/2009.

REFERENCES

(1) J. Suurkuusk, I. Wadsö, J. Chem. Thermodyn. 6 (1974) 667.

(2) J. Konicek, J. Suurkuusk, I. Wadsö, Chemica Scripta 1 (1971) 217.

(3) L. M. N. B. F. Santos, M. A. A. Rocha, A. S. M. C. Rodrigues, V. Štejfa, M. Fulem, M. Bastos, J. Chem. Thermodyn. 43 (2011) 1818.

(4) M. A. A. Rocha, M. Bastos, J. A. P. Coutinho, L. M. N. B. F. Santos, J. Chem. Thermodyn. 53 (2012) 140.

(5) M. A. A. Rocha, C. F. R. A. C. Lima, L. R. Gomes, B. Schröder, J. A. P. Coutinho, I. M. Marrucho, J. M. S. S. Esperança, L. P. N. Rebelo, K. Shimizu, J. N. C. Lopes, L. M. N. B. F. Santos, J. Phys. Chem. B 115 (2011) 10919.

(6) M. A. A. Rocha, C. M. S. S. Neves, M. G. Freire, O. Russina, A. Triolo, J. A. P. Coutinho, L. M. N. B. F. Santos, J. Phys. Chem. B (2013), doi: 10.1021/jp406374a.

(7) M. A. A. Rocha, J. A. P. Coutinho, L. M. N. B. F. Santos, J. Phys. Chem. B 116 (2012) 10922.

(8) M. A. A. Rocha, J. A. P. Coutinho, L. M. N. B. F. Santos, J. Chem. Phys. (2013), doi: 10.1063/1.4820825.

(9) M. A. A. Rocha, J. A. P. Coutinho, L. M. N. B. F. Santos, Manuscript. (Paper VIII)

(10) M. A. A. Rocha, F. M. S. Ribeiro, A. I. M. C. Lobo Ferreira, J. A. P. Coutinho, L. M. N. B. F. Santos, J. Mol. Liq. (2013), accepted, Ref.:MOLLIQ-D-13-00329R1.

(11) C. E. S. Bernardes, L. M. N. B. F. Santos, M. E. Minas da Piedade, Meas. Sci. Technol. 17 (2006) 1405.

(12) L. M. N. B. F. Santos, B. Schröder, O. O. P. Fernandes, M. A. V. Ribeiro da Silva, Thermochim. Acta 415 (2004) 15.

(13) R. Sabbah, A. Xu-wu, J.S. Chickos, M.L.P. Leitão, M.V. Roux, L.A. Torres, Thermochim. Acta 331 (1999) 93.

(14) R. D. Chirico, V. Diky, J. W. Magee, M. Frenkel, K. N. Marsh, Pure and Appl. Chem. 81 (2009) 791.

(15) M. E. Wieser, M. Berglund, Pure Appl. Chem. 81 (2009) 2131.

(16) C. P. Fredlake, J. M. Crosthwaite, D. G. Hert, S. N. V. K. Aki, and J. F. Brennecke, J. Chem. Eng. Data 49 (2004) 954.

(17) Y.-H. Yu, A. N. Soriano, and M.-H. Li, J. of the Taiwan Institute of Chemical Engineers 40 (2009) 205.

(18) Y.-H. Yu, A. N. Soriano, and M.-H. Li, Thermochim. Acta 482 (2009) 42.

(19) J. D. Holbrey, W. M. Reichert, R. G. Reddy, and R. D. Rogers, in *Ionic Liquids as Green Solvents: Progress and Prospects,* ACS Symposium Series Vol. 856, edited by R. D. Rogers and K. R. Seddon, American Chemical Society, New York, 2003, pp. 121–133.

(20) G. J. Kabo, A. V. Blokhin, Y. U. Paulechka, A. G. Kabo, M. P. Shymanovich, and J. W. Magee, J. Chem. Eng. Data 49 (2004) 453.

(21) J. Troncoso, C. A. Cerdeirina, Y. A. Sanmamed, L. Romaní, and L. P. N. Rebelo, J. Chem. Eng. Data 51 (2006) 1856.

(22) C. A. Nieto de Castro, M. J. V. Lourenço, A. P. C. Ribeiro, E. Langa, and S. I. C. Vieira, J. Chem. Eng. Data 55 (2010) 653.

(23) Y. U. Paulechka, J. Phys. Chem. Ref. Data, 39 (2010) 033108.

(24) E. Wilhelm, T. M. Letcher, Eds., *Heat Capacities: Liquids, Solutions and Vapours*, The Royal Society of Chemistry, Cambridge, UK, 2010.

(25) G. L. Somayajulu, Int. J. Thermophys. 11 (1990) 555.

(26) H. Izumi, S. Yamagami, S. Futamura, L.A. Nafie, R.K. Dukor, J. Am. Chem. Soc.126 (2004) 194.

(27) D. Yablon, D. Wintgens, W. Flynn, J. Phys. Chem. B 106 (2002) 5470.

(28) J. C. S. Costa, M. Fulem, B. Schröder, J. A. P. Coutinho, M. J. S. Monte, L. M. N. B. F. Santos, J. Chem. Thermodyn. 54 (2012) 171.

(29) W. Zheng, A. Mohammed, L. G. Hines, Jr., D. Xiao, O. J. Martinez, R. A. Bartsch, S. L. Simon, O. Russina, A. Triolo, E. L. Quitevis, J. Phys. Chem. B 115 (2011) 6572.

(30) G. Adamová, R. L. Gardas, L. P. N. Rebelo, A. J. Robertson, K. R. Seddon, Dalton Trans. 40 (2011) 12750.

Paper XI

"First Volatility Study of the 1-Alkylpyridinium based Ionic Liquids by Knudsen Effusion"
Marisa A. A. Rocha, Luís M. N. B. F. Santos
Chemical Physics Letters (2013) 585, 59–62.
doi: 10.1016/j.cplett.2013.08.095

Note: The author of this thesis performed the all the experimental work, data analysis and contribute to the discussion and conclusions.

Chemical Physics Letters 585 (2013) 59–62

Contents lists available at ScienceDirect

Chemical Physics Letters

journal homepage: www.elsevier.com/locate/cplett

First volatility study of the 1-alkylpyridinium based ionic liquids by Knudsen effusion

Marisa A.A. Rocha, Luís M.N.B.F. Santos *

Centro de Investigação em Química, Departamento de Química e Bioquímica, Faculdade de Ciências da Universidade do Porto, R. Campo Alegre 687, P-4169-007 Porto, Portugal

ARTICLE INFO

Article history:
Received 26 June 2013
In final form 22 August 2013
Available online 29 August 2013

ABSTRACT

For the first time, a volatility study of the 1-ethylpyridinium bis(trifluoromethylsulfonyl)imide ([C_2Py][NTf_2], CAS: 712354-97-7), 1-propylpyridinium bis(trifluoromethylsulfonyl)imide ([C_3Py][NTf_2]) and 1-butylpyridinium bis(trifluoromethylsulfonyl)imide ([C_4Py][NTf_2], CAS: 187863-42-9) ionic liquids, is presented. The vapor pressures as a function of temperature, for this ionic liquids were measured and the thermodynamic properties of vaporization were derived. The analysis and rationalization of the obtained results for the alkylpyridinium based ionic liquids was done based on the comparison with the [$C_{N-1}C_1$im][NTf_2] (N = 3–5). The volatility of pyridinium is five times lower than the imidazolium based ionic liquids and that is driven by their higher enthalpy of vaporization.

1. Introduction

Some ionic liquids (ILs) can be considered as nanostructurated fluids in which the ion pairs arrange themselves into polar and nonpolar domains. It is the interplay of these two domains/interactions that eventually leads to the formation of medium-range nano-scale domains, as well as their dual character will affect significantly the physico-chemical properties of ionic liquids [1–3]. Compared to the conventional organic solvents, the unique properties of ionic liquids favor their application in diverse fields, such as synthesis, extraction, catalysis, and electrochemistry [4–7]. These liquids present desirable properties for such uses, including low vapor pressure, thermal stability up to high temperatures, wide electrochemical windows, good thermal conductivity, high miscibility with substances having a wide range of polarities and a capability of dissolving organic and inorganic substances [4,5].

In ionic liquids, the molecular interactions between the ions results from their configurational aspects and charge distribution, in which involves not only coulombic interactions [8–10], but also van der Waals interactions [11–15] and hydrogen bonding [14–20], leading to a complex but interesting structural/nanostructural organization. The alkylimidazolium and alkylpyridinium based ionic liquids presents also an aromatic character with significant contribution of the $\pi\cdots\pi$ interactions and charge delocalization on the aromatic moiety. Their aromatic character contributes also to the high thermal stability of both cations [21]. Accurate thermodynamic properties of vaporization equilibrium of ionic liquids are scarce and yet crucial for the better understanding of the liquid phase of ionic liquids, evaluation of the cohesive energy, as well as the nature of the vapor phase. Furthermore, thermodynamic properties are required for validation and parameterization of the models (force fields) used to describe ionic liquids in different simulation techniques [1,22,23]. It must be stressed that the data published concerning vapor liquid equilibrium, it consists mainly of repetitions using in some cases inappropriate techniques/methodologies, extrapolations and predictions for essentially the same ionic liquid family and for a relatively small set of experiments, which leads, sometimes, to inaccurate conclusions. Therefore accurate vapor pressure measurements are needed, and special effort should be done in order to obtain reliable data in new ionic liquid families. Recently, we have reported the volatility study of the extended series of ionic liquids (ILs), [$C_{N-1}C_1$im][NTf_2] (N = 3–13), where it was found, for the first time, a trend shift in the thermodynamic properties of vaporization and viscosity data along the studied ILs series, which are related to the nanostructuration of the liquid phase starting from [C_6C_1im][NTf_2] [24]. The effect of cation symmetry on the thermodynamic properties of vaporization for the 1,3-dialkylimidazolium based ILs, [$C_{N/2}C_{N/2}$im][NTf_2] (N = 2–12), where also evaluated [25]. Based in the previous letter, it was possible to detect an odd–even effect, with higher enthalpies and entropies of vaporization for the odd numbered ILs, in agreement with the trend observed in the letter published by Zheng et al. [26].

In the present study the vapor pressure of the 1-alkylpyridinium bis(trifluoromethylsulfonyl)imide, [C_NPy][NTf_2] (N = ethyl, propyl and butyl), were measured as a function of temperature, in the temperature range of (493–516 K), using the Knudsen effusion methodology combined with a quartz crystal microbalance. This is the first volatility study performed on the alkylpyridinium based ionic liquids, and the obtained results will be used to evaluate the

* Corresponding author. Fax: +351 220 402 659.
E-mail addresses: marisa.alexandra.rocha@gmail.com (M.A.A. Rocha), lbsantos@fc.up.pt (L.M.N.B.F. Santos).

0009-2614/$ - see front matter © 2013 Elsevier B.V. All rights reserved.
http://dx.doi.org/10.1016/j.cplett.2013.08.095

effect of the identity/nature of the cation on the volatility and on the thermodynamic properties of vaporization, by comparing with the vaporization thermodynamics data of the $[C_{N\text{-}1}C_1im][NTf_2]$ series [24].

2. Experimental

2.1. Materials and purification

The 1-alkylpyridinium bis(trifluoromethylsulfonyl)imide, $[C_NPy][NTf_2]$ (N = 2–4), were purchased from IOLITEC with a stated purity of better than 99%. The studied ionic liquids were dried and purified under vacuum (<10 Pa) at moderate temperature (323 K) and constant stirring, in order to reduce the presence of water or other volatile contents. In the Knudsen effusion methodology the most important is to remove any volatile impurity. The remaining impurities (non volatile impurities) do not interfere in the vapor pressures measurements. The optimized procedure for the vapor pressure of ILs by Knudsen effusion includes an additional step of in situ purification until the vapor pressure remains constant. The in situ purification is performed with the ionic liquid inside the effusion cell, typically at 500 K under high vacuum (<0.001 Pa).

2.2. Quartz crystal microbalance Knudsen effusion apparatus

The vapor pressures as a function of temperature were measured using a Knudsen effusion apparatus combined with a quartz crystal microbalance, described in detail in the literature [27]. This apparatus comprises two mass loss detection techniques, gravimetric and quartz crystal microbalance, weighed mass of the effusion cell before and after the respective experiment, and the change of the crystal's resonant frequency as the vapor condenses on its surface. The combination of these two mass loss detection techniques presents several advantages, such as, small effusion times, smaller sample size and higher control of the vaporization process. The temperature is controlled within a temperature fluctuation of $\pm(1 \times 10^{-2})$ K, measured with a resolution better than 1×10^{-3} K, with an overall uncertainty better than $\pm(2 \times 10^{-2})$ K along the entire working temperature range, and can reach temperatures up to 650 K. Usually in a typical Knudsen effusion experiment, the system is kept at high vacuum and at a fixed temperature, allowing free effusion of the vapor from the cell. During an effusion experiment, the mass loss rate from the effusion cell, $dm(\text{cell})/dt$, is proportional to the rate of change of the mass deposited on the quartz crystal, dm/dt, according to the following Eq. (1):

$$\frac{dm(\text{cell})}{dt} = -g \cdot \frac{dm}{dt} = -g \cdot \frac{A_q}{S_q} \cdot \left(\frac{df}{dt}\right) \tag{1}$$

where, g is a geometric factor of the mass detection, A_q is the area of the quartz crystal, S_q is the mass sensitivity of the crystal, and (df/dt) is the rate of change of the resonance frequency of the quartz crystal. Taking into account that:

$$W = -\frac{S_q}{A_q \cdot g} \tag{2}$$

where, W is the effective mass sensitivity coefficient, the Eq. (1) becomes:

$$\left(\frac{df}{dt}\right) = W \cdot \left(\frac{dm(\text{cell})}{dt}\right). \tag{3}$$

The value, W must be known for each studied compound and can be determined by weighing the total mass loss of the effusion cell, $\Delta m(\text{cell})$, during an independent experiment, and considering the integrated form of the Eq. (3):

$$W = \frac{\Delta f}{\Delta m(\text{cell})} \tag{4}$$

where Δf is the total change in the crystal's resonance frequency during the experiment. The equilibrium vapor pressure of the liquid compound is obtained using the following Eq. (5):

$$p = \left(\frac{df}{dt}\right) \cdot \left(\frac{1}{w_o \cdot A_o \cdot W}\right) \cdot \left(\frac{2 \cdot \pi \cdot R \cdot T}{M}\right)^{1/2} \tag{5}$$

where M is the molar mass of the sample, R is the gas constant ($R = 8.3144621$ J K^{-1} mol^{-1}) [28], A_o is the area of the orifice and w_o is the transmission probability factor ($w_o = \{1 + (l/2r)\}^{-1}$). The vapor pressure data obtained with this apparatus for the ionic liquid samples, presents a pressure dependent uncertainty between (1 and 5)%, that is the typical uncertainty obtained in this apparatus using this methodology [24]. The relative atomic masses used were those recommended by the IUPAC Commission in 2007 [29].

3. Results and discussion

The experimental vapor pressures data are presented in Table 1 and depicted in the graphical representation as $\ln(p/\text{Pa}) = f[(1/T)/\text{K}^{-1}]$ in Figure 1. The experimental results were fitted using the integrated form of the Clausius–Clapeyron equation:

$$\ln(p/p_o) = a - b/T \tag{6}$$

where b corresponds to $\Delta_l^g H_m^o(\langle T\rangle)/R, p^o = 0.1$ MPa, and a is a constant.

The parameters of the Clausius–Clapeyron equation, the calculated standard deviations, the mean temperature, $\langle T\rangle$, and the pressure at the mean temperature are listed in Table 2. The thermodynamic properties of vaporization at the mean temperature, $\langle T\rangle$, $T = 460$ and 298.15 K, are presented in Table 3.

The standard molar of enthalpies and entropies of vaporization were corrected to the reference temperature, 460 and 298.15 K, using the following equations:

$$\Delta_l^g H_m^o(T/K) = \Delta_l^g H_m^o(<T>) + \Delta_l^g C_{p,m}^o \cdot (T - <T>) \tag{7}$$

$$\Delta_l^g S_m^o(T/K) = \Delta_l^g S_m^o(<T>) + \Delta_l^g C_{p,m}^o \cdot ln\left(\frac{T}{<T>}\right) \tag{8}$$

Table 1
Experimental vapor pressures, p, and temperature, T, for the studied pyridinium based ILs, as obtained with the quartz crystal microbalance Knudsen effusion apparatus.

T/K	p/Pa	Δp/Pa	T/K	p/Pa	Δp/Pa
[C$_2$Py][NTf$_2$]					
493.55	0.0319	−0.0026	499.59	0.0454	−0.0016
495.56	0.0357	0.0036	501.60	0.0509	0.0000
497.58	0.0403	0.0007	503.61	0.0571	0.0000
[C$_3$Py][NTf$_2$]					
497.47	0.0333	−0.0028	505.51	0.0535	0.0004
499.48	0.0374	0.0019	507.49	0.0604	−0.0056
501.48	0.0421	0.0027	509.50	0.0674	0.0008
503.49	0.0475	0.0009	511.52	0.0756	0.0017
[C$_4$Py][NTf$_2$]					
498.07	0.0519	0.0018	508.06	0.0929	−0.0016
500.57	0.0608	−0.0094	510.56	0.1061	0.0068
503.07	0.0695	0.0024	513.04	0.1227	0.0003
505.57	0.0800	0.0058	515.56	0.1420	−0.0061

$\Delta p = p - p(\text{fitting})$; $p(\text{fitting})$ corresponds to the vapor pressures obtained from the fitted Clausius–Clapeyron equation.

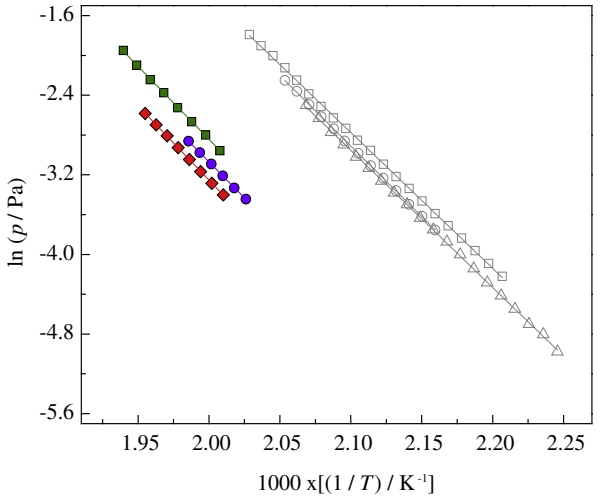

Figure 1. Plot of $\ln(p/\mathrm{Pa}) = f\,[(1/T)/\mathrm{K}^{-1}]$ for each studied ionic liquid: ● – $[C_2Py][NTf_2]$; ◆ – $[C_3Py][NTf_2]$; ■ – $[C_4Py][NTf_2]$. Literature data: △ – $[C_2C_1im][NTf_2]$; □ – $[C_3C_1im][NTf_2]$; ○ – $[C_4C_1im][NTf_2]$ [24].

Table 2
Fitted a and b parameters derived from the Clausius–Clapeyron Eq. (6) for the studied ionic liquids. $\langle T\rangle$ mean temperature of the pressure, p, temperature T, interval. $p(\langle T\rangle)$/Pa is the pressure derived from the fitting at the mean temperature $\langle T\rangle$.

Ionic liquid	a	b/K	r^2	$\langle T\rangle$/K	$p(\langle T\rangle)$/Pa
$[C_2Py][NTf_2]$	25.83 ± 0.14	14449 ± 70	0.9999	498.58	0.043
$[C_3Py][NTf_2]$	26.61 ± 0.12	14930 ± 59	0.9999	504.50	0.050
$[C_4Py][NTf_2]$	26.48 ± 0.19	14661 ± 96	0.9997	506.82	0.086

Table 3
Standard (p^o = 0.1 MPa) molar enthalpies, $\Delta_l^g H_m^o(T)$, entropies, $\Delta_l^g S_m^o(T)$, and Gibbs energies, $\Delta_l^g G_m^o(T)$, of vaporization for the studied ionic liquids.

T interval/K	T/K	$\Delta_l^g H_m^o(T)$/ kJ·mol^{-1}	$\Delta_l^g S_m^o(T)$/ J·K^{-1}·mol^{-1}	$\Delta_l^g G_m^o(T)$/ kJ·mol^{-1}
[C₂Py][NTf₂]				
493–504	498.58	120.1 ± 0.6	119.0 ± 1.2	60.8 ± 0.8
	460.00	124.0 ± 0.7	127.1 ± 1.4	65.5 ± 0.8
	298.15	140.2 ± 2.1	170.4 ± 5.3	89.4 ± 0.9
$[C_3Py][NTf_2]$				
497–512	504.50	124.1 ± 0.5	125.5 ± 1.0	60.8 ± 0.7
	460.00	128.6 ± 0.7	134.7 ± 1.3	66.6 ± 0.7
	298.15	144.8 ± 2.1	178.1 ± 5.3	91.7 ± 0.8
$[C_4Py][NTf_2]$				
498–516	506.82	121.9 ± 0.8	124.4 ± 1.6	58.8 ± 1.1
	460.00	126.6 ± 0.9	134.1 ± 1.8	64.9 ± 1.1
	298.15	142.8 ± 2.2	177.5 ± 5.5	89.8 ± 1.2

where, $\langle T\rangle$ is the average experimental temperature interval, $\Delta_l^g C_{p,m}^o = (-100 \pm 10)\ \mathrm{J\cdot K^{-1}\cdot mol^{-1}}$ was assumed as the average heat capacity difference between the liquid and gas for all the ILs under study. The value of (-100 J·K^{-1}·mol^{-1}) for the $\Delta_l^g C_{p,m}^o$ is a typical value for liquids and have been used before for the imidazolium based series [23]. The standard (p^o = 0.1 MPa) molar Gibbs energies of vaporization, $\Delta_l^g G_m^o$, at the references temperatures, were calculated using Eq. (4):

$$\Delta_l^g G_m^o(T/K) = \Delta_l^g H_m^o(T/K) - (T/K)\cdot\Delta_l^g S_m^o(T/K) \quad (9)$$

The linear fitting of the Clausius–Clapeyron equation is numerical equivalent to the Clarke and Glew Eq. [30] equation when only the first term is considered:

$$R\cdot ln\left[\frac{p(T)}{p^o}\right] = -\frac{\Delta_l^g G_m^o(\theta)}{\theta} + \Delta_l^g H_m^o(\theta)\cdot\left(\frac{1}{\theta}-\frac{1}{T}\right) + \Delta_l^g C_{p,m}^o \cdot\left[\frac{\theta}{T} - 1 + ln\left(\frac{T}{\theta}\right)\right] \quad (10)$$

where p is the vapor pressure, p^o is the standard pressure (p^o = 0.1 MPa), θ is a selected reference temperature. The uncertainty of standard molar Gibbs energy of vaporization $\Delta_l^g G_m^o$ was derived based in the temperature correction of the Clarke and Glew Eq. (10) in order to reflect the error cancelation in the temperature correction of the enthalpic and entropic terms.

The analysis and the rationalization of the thermodynamic properties of vaporization of the studied alkylpyridinium based ionic liquids will be done taking into account the literature data for the $[C_{N\text{-}1}C_1im][NTf_2]$ (N = 3–5) ionic liquids [24]. The standard molar Gibbs energies, enthalpies and entropies of vaporization at reference temperature, T = 298.15 K, as function of the number of carbons of the longest alkyl side chain of the cation, n(C), are presented in Figures 2–4. The graphic representations of the thermodynamic properties of vaporization at T = 460 K as a function of the number of carbons of the longest alkyl side chain of the cation, n(C), are presented as supporting information.

In the measured temperature range, the following order of volatility for the $[C_NPy][NTf_2]$ ionic liquids was found:

$$[C_3Py][NTf_2] > [C_2Py][NTf_2] > [C_4Py][NTf_2]$$

The $[C_2Py][NTf_2]$ and $[C_3Py][NTf_2]$ are exceptions within the considered ionic liquids, presenting lower volatilities than $[C_4Py][NTf_2]$. This is the typical outlier behavior observed before for the imidazolium based ILs with short alkyl chain length (e.g. $[C_{N\text{-}1}C_1im][NTf_2]$ and $[C_{N/2}C_{N/2}im][NTf_2]$) [24,25].

At the reference temperature, T = 298.15 K, the volatility differentiation is not very significant for members of the shorter alkyl chain. More interesting, is undoubtedly, the comparative analysis between the volatility of the imidazolium based ionic liquids with the studied alkylpyridinium ionic liquids. The volatility of the pyridinium based ionic liquids is approximately five times lower than the considered imidazolium, as it can be depicted easily in Figure 1 (e.g. at T = 490 K the vapor pressure of the $[C_NPy][NTf_2]$ ILs is ≈0.04 Pa and for the $[C_{N\text{-}1}C_1im][NTf_2]$ ILs is ≈0.2 Pa). That observation is in agreement with a higher charge localization of the pyridinium cation in contrast to the imidazolium cation that

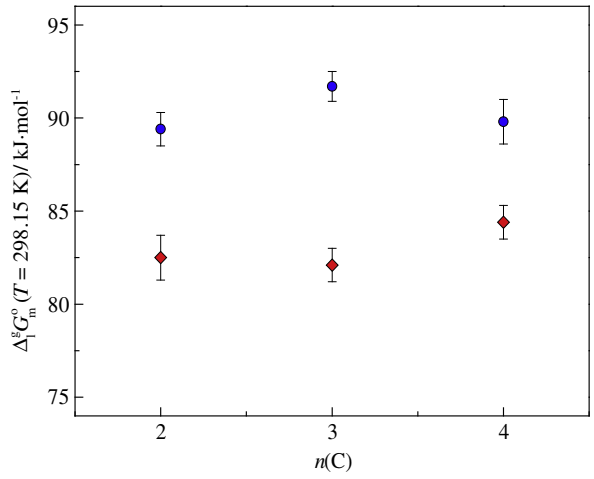

Figure 2. Standard (p^o = 0.1 MPa) molar Gibbs energy of vaporization $\Delta_l^g G_m^o$ (T = 298.15 K) as a function of the number of carbons in the alkyl side chain of the cation, n(C). ● – $[C_NPy][NTf_2]$, n(C) = N = 2–4; ◆ – $[C_{N\text{-}1}C_1im][NTf_2]$, n(C) = N-1 = 2–4 [24].

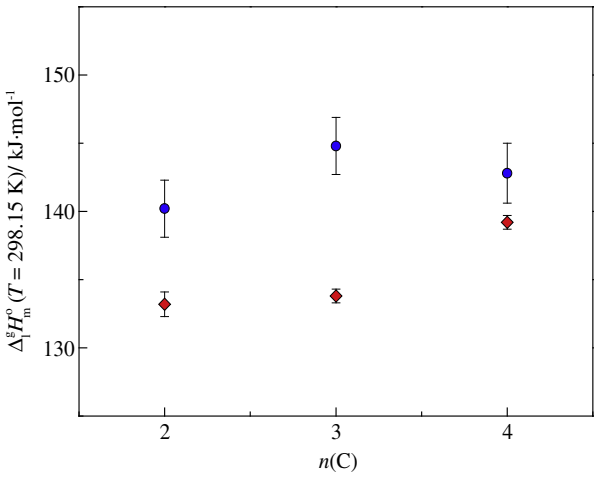

Figure 3. Standard (p^o = 0.1 MPa) molar enthalpies of vaporization $\Delta_l^g H_m^o$ (T = 298.15 K) as a function of the number of carbons in the alkyl side chain of the cation, n(C). ● – [C_NPy][NTf_2], n(C) = N = 2–4; ◆ – [$C_{N-1}C_1$im][NTf_2], n(C) = N-1 = 2–4 [24].

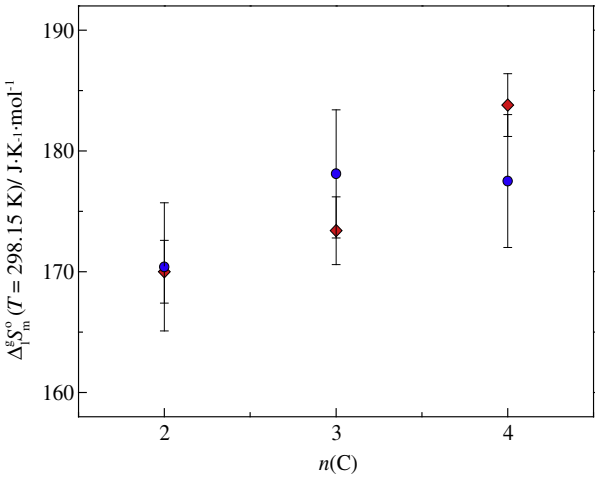

Figure 4. Standard (p^o = 0.1 MPa) molar entropies of vaporization $\Delta_l^g S_m^o$ (T = 298.15 K) as a function of the number of carbons in the alkyl side chain of the cation, n(C). ● – [C_NPy][NTf_2], n(C) = N = 2–4; ◆ – [$C_{N-1}C_1$im][NTf_2], n(C) = N-1 = 2–4 [24].

is reflected in their higher enthalpies and lower entropies of vaporization (Figures 3 and 4).

The obtained result indicates a significant lower volatility (with Gibbs energy of vaporization of 5–10 kJ·mol^{-1}higher) of the pyridinium based ionic liquids. It was found that the lower volatility is enthalpically driven, with an identically differentiation of 5–10 kJ·mol^{-1} in the enthalpy. The entropic profile seems very identical than the observed in the imidazolium based ILs. However, there is an indication of a crossover of the enthalpic and entropic profiles behavior starting from [C_4Py][NTf_2] that could only be demonstrated with further work concerning the volatility study for the extended alkyl chain length pyridinium based ionic liquids.

Acknowledgments

This letter was supported by FCT, Lisbon, Portugal, and the European Social Fund through strategic projects Pest-C/QUI/UI0081/2011 awarded to CIQUP. Marisa A.A. Rocha acknowledges the financial support from FCT for the award of research Grant with reference, SFRH/BD/60513/2009.

Appendix A. Supplementary data

Supplementary data associated with this article can be found, in the online version, at http://dx.doi.org/10.1016/j.cplett.2013.08.095.

References

[1] J.N.A. Canongia Lopes, A.A.H. Pádua, J. Phys. Chem. B 110 (2006) 3330.
[2] S.M. Urahata, M.C.C. Ribeiro, J. Chem. Phys. 122 (2005). 024511-1.
[3] K. Shimizu, M.F. Costa Gomes, A.A.H. Pádua, L.P.N. Rebelo, J.N. Canongia Lopes, J. Mol. Struct. THEOCHEM 946 (2010) 70.
[4] P. Wasserscheid, T. Welton (Eds.), Ionic Liquids in Synthesis, Wiley-VCH Verlag GmbH & Co. KGaA, Weinheim, Germany, 2007.
[5] B. Kirchner (Ed.), Ionic Liquids, Springer Berlin Heidelberg, Berlin, Heidelberg, 2010.
[6] K. Marsh, J. Boxall, R. Lichtenthaler, Fluid Phase Equilib. 219 (2004) 93.
[7] H. Weingärtner, Angew. Chem. Int. Ed. 47 (2008) 654.
[8] H.V. Spohr, G.N. Patey, J. Chem. Phys. 132 (2010). 154504-1.
[9] H.V. Spohr, G.N. Patey, J. Chem. Phys. 132 (2010). 234510-1.
[10] H.V. Spohr, G.N. Patey, J. Chem. Phys. 130 (2009). 104506-1.
[11] P. Ballone, C. Pinilla, J. Kohanoff, M.G. Del Pópolo, J. Phys. Chem. B 111 (2007) 4938.
[12] S. Zahn, G. Bruns, J. Thar, B. Kirchner, Phys. Chem. Chem. Phys. 10 (2008) 6921.
[13] S. Zahn, F. Uhlig, J. Thar, C. Spickermann, B. Kirchner, Angew. Chem. Int. Ed. 47 (2008) 3639.
[14] S.B.C. Lehmann, M. Roatsch, M. Schöppke, B. Kirchner, Phys. Chem. Chem. Phys. 12 (2010) 7473.
[15] S. Zahn, J. Thar, B. Kirchner, J. Chem. Phys. 132 (2010). 124506-1.
[16] K. Fumino, A. Wulf, R. Ludwig, Phys. Chem. Chem. Phys. 11 (2009) 8790.
[17] B. Qiao, C. Krekeler, R. Berger, L. Delle Site, C. Holm, J. Phys. Chem. B 112 (2008) 1743.
[18] M.F.C. Gomes, J.N.C. Lopes, A.A.H. Padua, Top. Curr. Chem. 290 (2010) 161.
[19] A. Stark, Top. Curr. Chem. 290 (2010) 41.
[20] C. Roth, T. Peppel, K. Fumino, M. Köckerling, R. Ludwig, Angew. Chem. Int. Ed. 49 (2010) 10221.
[21] M.J. Earle et al., Nature 439 (2006) 831.
[22] F. Dommert, K. Wendler, R. Berger, L. Delle Site, C. Holm, Chem. Phys. Chem. 13 (2012) 1625.
[23] J.M.S.S. Esperança, J.N. Canongia Lopes, M. Tariq, J. Chem. Eng. Data 55 (2010) 3.
[24] M.A.A. Rocha, J. Phys. Chem. B 115 (2011) 10919.
[25] M.A.A. Rocha, J.A.P. Coutinho, J. Phys. Chem. B 116 (2012) 10922.
[26] W. Zheng et al., J. Phys. Chem. B 115 (2011) 6572.
[27] L.M.N.B.F. Santos, L.M.S.S. Lima, C.F.R.A.C. Lima, F.D. Magalhães, M.C. Torres, B. Schröder, M.A.V. Ribeiro da Silva, J. Chem. Thermodyn. 43 (2011) 834.
[28] P.J. Mohr, B.N. Taylor, D.B. Newell, Rev. Mod. Phys. 84 (2012) 1527.
[29] M.E. Wieser, M. Berglund, Pure Appl. Chem. 81 (2009) 2131.
[30] E.C.W. Clarke, D.N. Glew, Trans. Faraday Soc. 62 (1966) 539.

First Volatility Study of the 1-Alkylpyridinium based Ionic Liquid by Knudsen Effusion

(Supporting Information)

Marisa A. A. Rocha and Luís M. N. B. F. Santos

† Centro de Investigação em Química, Departamento de Química e Bioquímica, Faculdade de Ciências da Universidade do Porto, P-4169-007 Porto, Portugal

* Corresponding author: email: lbsantos@fc.up.pt, phone: +351 220402536, fax : +351 220402520; E-mail: lbsantos@fc.up.pt ; marisa.alexandra.rocha@gmail.com

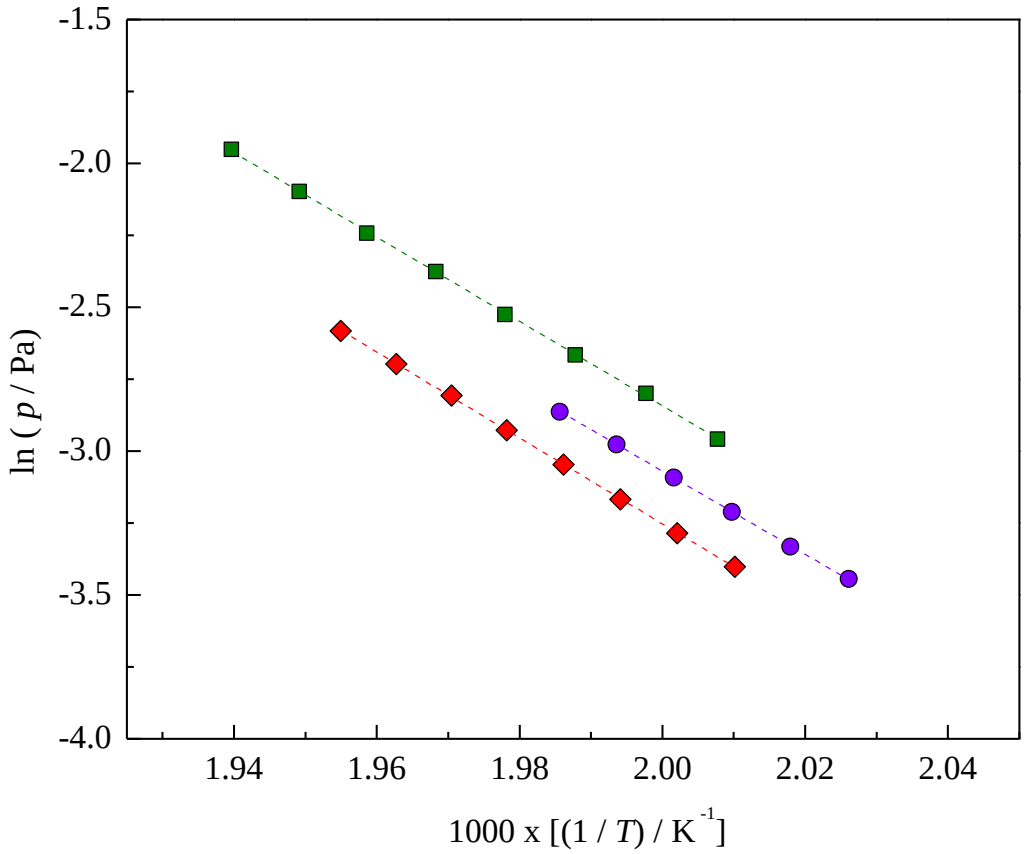

Fig. 1S. Plot of ln(p/Pa) = f [(1/T)/K^{-1}] for each studied ionic liquid: ● - [C_2Py][NTf_2]; ◆ - [C_3Py][NTf_2]; ■ - [C_4Py][NTf_2].

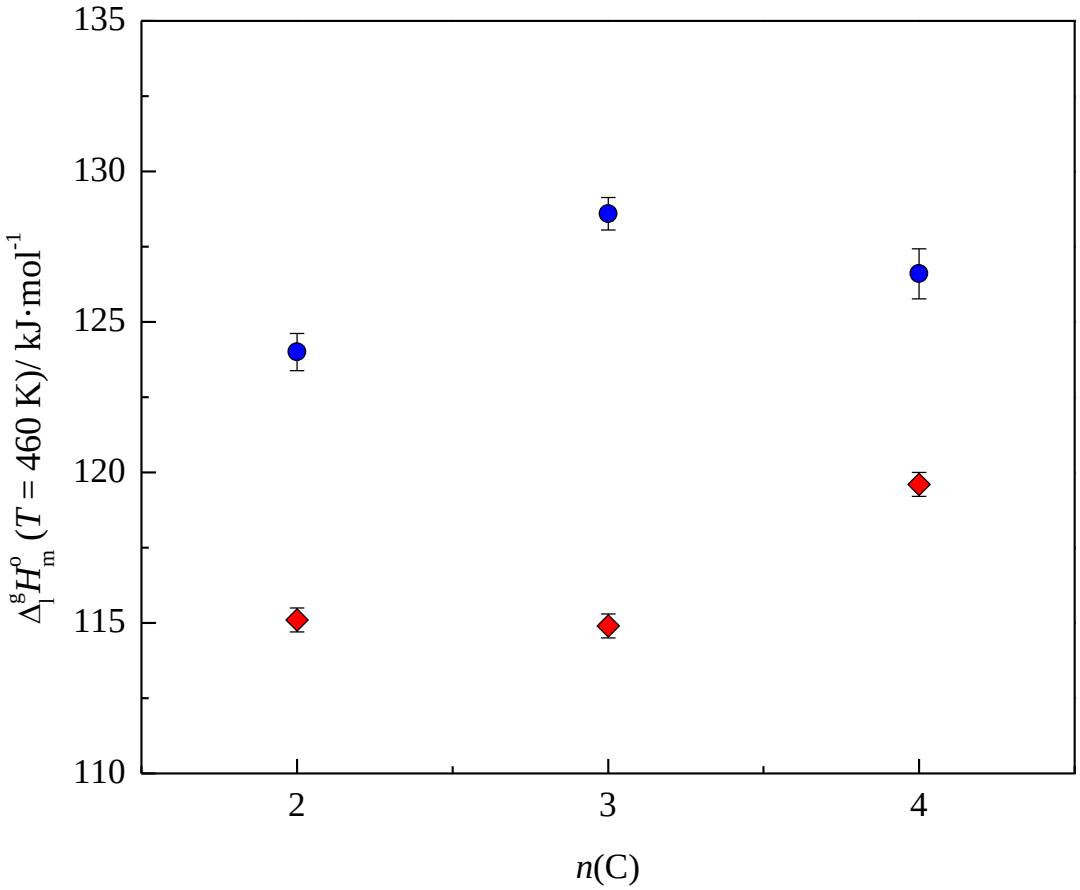

Fig. 2S. Standard (p^o=10^5 Pa) molar enthalpies of vaporization $\Delta_l^g H_m^o(T = 460\text{K})$ as a function of the number of carbons in the alkyl side chain of the cation, n(C). ● - [C_NPy][NTf_2], n(C)= 2, 3, 4; ◆ - [$C_{N-1}C_1$im][NTf_2], n(C)= 2, 3, 4. [1]

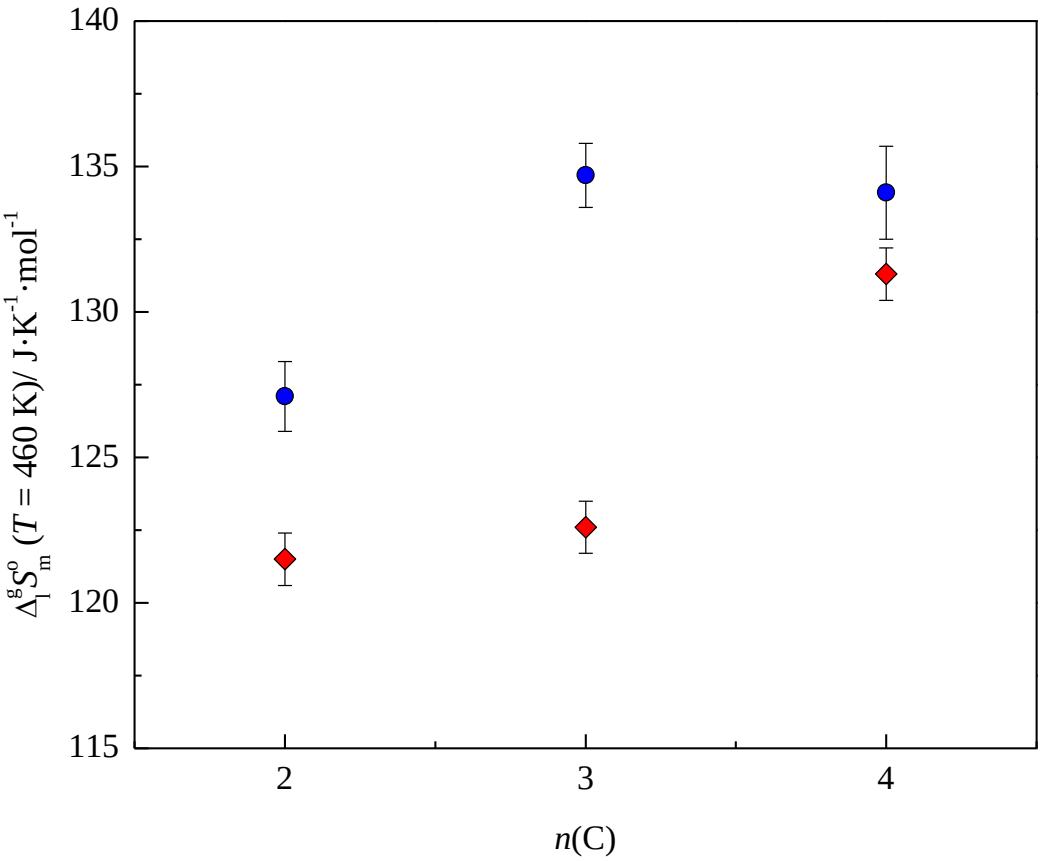

Fig. 3S. Standard (p^o=10^5 Pa) molar entropies of vaporization $\Delta_l^g S_m^o (T = 460\text{K})$ as a function of the number of carbons in the alkyl side chain of the cation, *n*(C). ● - [C_NPy][NTf_2], *n*(C)= 2, 3, 4; ◆ - [$C_{N-1}C_1$im][NTf_2], *n*(C)= 2, 3, 4. [1]

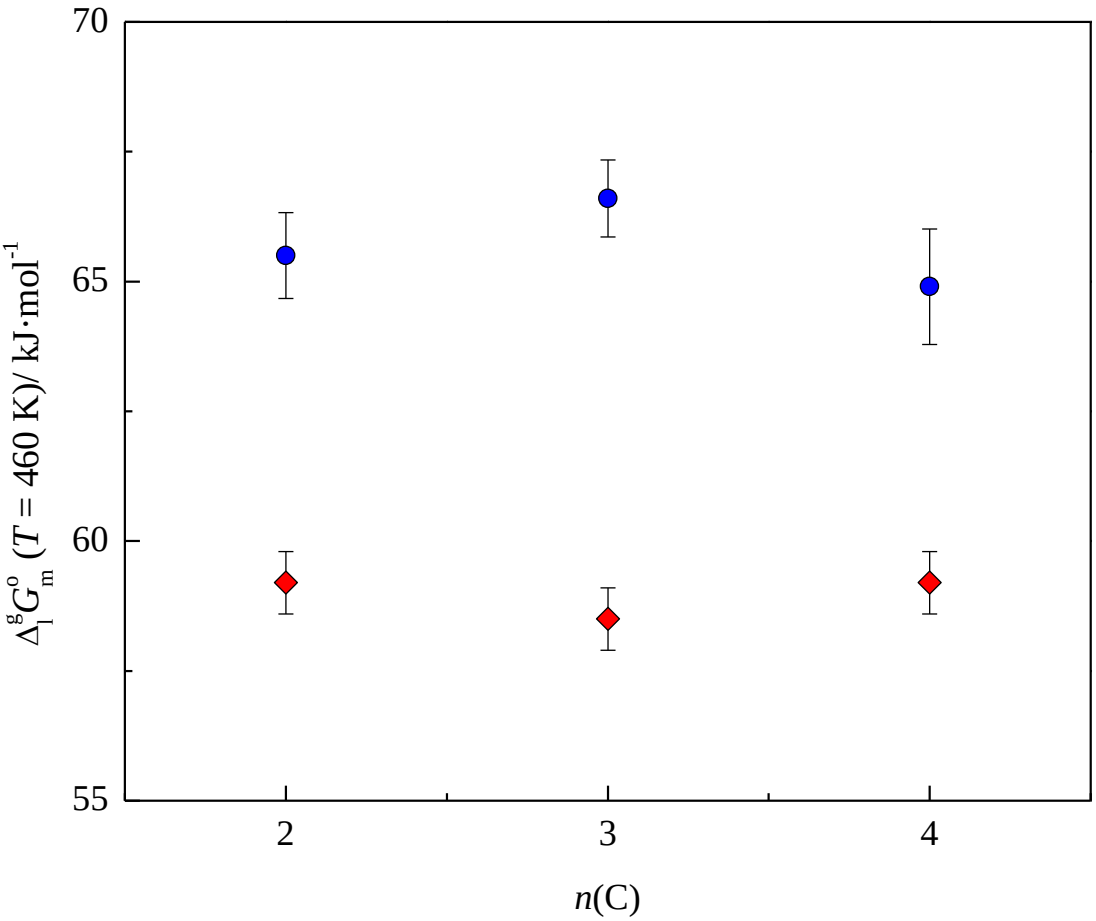

Fig. 4S. Standard (p^o=10^5 Pa) molar Gibbs energy of vaporization $\Delta_l^g G_m^o (T = 460\text{K})$ as a function of the number of carbons in the alkyl side chain of the cation, *n*(C). ● - [C_NPy][NTf_2], *n*(C)= 2, 3, 4; ◆ - [$C_{N-1}C_1$im][NTf_2], *n*(C)= 2, 3, 4. [1]

[1] M. A. A. Rocha, C. F. R. A. C. Lima, L. R. Gomes, B. Schröder, J. A. P. Coutinho, I. M. Marrucho, J. M. S. S. Esperança, L. P. N. Rebelo, K. Shimizu, J. N. C. Lopes, L. M. N. B. F. Santos, J. Phys. Chem. B 115 (2011) 10919–10926.

Paper XII

"Novel 1-Ethyl-2-Alkylpyridinium based Ionic Liquids: Synthesis and Volatility"
Miguel Vilas, Marisa A. A. Rocha, Emilia Tojo, Luís M. N. B. F. Santos
Manuscript version

Note:. The author of this thesis performed the vapor pressure measurements of the ionic liquids, data analysis and contribute to the discussion and conclusions.

CHEMISTRY
A EUROPEAN JOURNAL

FULL PAPER

DOI: 10.1002/chem.200((will be filled in by the editorial staff))

Novel 1-Ethyl-2-Alkylpyridinium based Ionic Liquids: Synthesis and Volatility

Miguel Vilas [b], Marisa A. A. Rocha[a], Emilia Tojo*[b], Luís M. N. B. F. Santos*[a]

Abstract: This work presents the synthesis and the volatility study of novel dialkylpyridinium based ionic liquids, $[^2C_{N-2}{}^1C_2Py][NTf_2]$. Compared to the imidazolium based ionic liquids, the new ionic liquid series presents a higher thermal stability as well as a lower volatility. It was found that for the $[^2C_{N-2}{}^1C_2Py][NTf_2]$ with shorter alkyl chain length, the lower volatility is due to their higher enthalpies of vaporization. Starting from $[^2C_3{}^1C_2Py][NTf_2]$, the lower volatility is ruled by the combination of slightly lower entropies and higher enthalpies of vaporization, that is also an indication of a higher structural disorder of the pyridinium based ionic liquids.

Keywords: 1-ethyl-2-alkylpyridinium • synthesis • vapor pressures • enthalpy • entropy• vaporization

Introduction

The understanding of the physical chemical properties of ionic liquids hinge on the proper comprehension of the molecular structure of the compounds in the liquid phase. It is well accepted nowadays that ionic liquids are highly structured fluids. The long-range structuration of ionic liquids was studied by Urahata and Ribeiro [1], using computer simulation to provide a perspective view of the ionic motions and the onset of distinct dynamical processes in ionic liquids. Later, Wang and Voth [2] explored the effect of the alkyl side chain length of the cation in ionic liquids, using a multiscale coarse-graining (MS-CG) method. [2,3] Based on this work, it was found for extended lengths of the alkyl chains, that the tail groups of the cations aggregate to form spatial heterogeneous tail domains, where the headgroups and the anions distribute reasonably homogeneous in order to maintain electroneutrality as well as to maximize the electrostatic interactions, while the tail groups tend to segregate elsewhere. [2] In 2006, for the first time, Lopes and Pádua [4] used atomistic simulation to study the nanostructuration of 1-alkyl-3-methylimidazolium based ionic liquids, $[C_{N-1}C_1im]^+$ (N = 3 up to 13), in the liquid phase, and to investigate the effect of the alkyl side chain length of the cations on the long-range structures. Based on this work it was possible to predict that the structure of the liquid phase of the studied ionic liquids exhibits microphase separation between polar and nonpolar regions. Additionally, it was observed that the polar regions has the structure of a tridimensional network of ionic channels, while the nonpolar regions are arranged as dispersed microphases, for the $[C_2C_1im]^+$ based ILs, and as a continuous phase for higher alkyl chains lengths.

The interaction between these two types of regions (polar and nonpolar) led to the recognition of ionic liquids as high-charge density (polar) network permeated by low-charge density (nonpolar) regions.[1–6] This characteristic of the structural organization in ionic liquids was first supported experimentally by X-ray diffraction [7] and later by small-wide angle X-ray scattering (SWAXS). [8,9] Neutron diffraction was used to study the structures of 1,3-dimethylimidazolium chloride [10], $[C_1C_1im][Cl]$, and hexafluorophosphate [11], $[C_1C_1im][PF_6]$, ionic liquids. The comparison of diffraction patterns of deuterated and protiated liquids enables a detailed picture of the anion-cation and cation-cation interactions. Based on this work, a strong charge ordering with similar anion-cation interactions for both anions was found. In both works, a strong correlation between the solid and liquid phases was detected, and along with the degree of charge ordering, becomes less pronounced for large anions and asymmetrical cations. [10–13] Recently, a combination of infrared (IR) spectroscopic techniques was used to characterize the degree of charge organization present in the imidazolium based ionic liquids family. [14] It was found that longer alkyl side chains attached onto the imidazolium ions increases the short-range repulsive interactions among the ions and disrupt the charge organization, in agreement with previous studies. [15,16]

The possibility of concisely tuning the physical chemical properties by changing the cation-anion combination is one of the biggest advantages of these systems. For this purpose, the knowledge and understanding of structure−property relationships of of ionic liquids is indispensable.[17,18] Therefore, great efforts have been made in order to determine these properties experimentally or by theoretical calculations. [17–26] Due to the large number of possible ionic liquids,

[a] Dr. L. M. N. B. F. Santos, M. A. A. Rocha
CIQ, Departamento de Química e Bioquímica
Faculdade de Ciências da Universidade do Porto
R. Campo Alegre 687, P-4169-007, Porto, Portugal
Fax: (+351)220402520
E-mail: lbsantos@fc.up.pt
[b] Dr. E. Tojo, M. Vilas
Department of Organic Chemistry
University of Vigo
Faculty of Chemistry, Marcosende, 36210 Vigo (Pontevedra), Spain
Fax: (+34)986812262
E-mail: etojo@uvigo.es

Supporting information for this article is available on the WWW under http://www.chemeurj.org/ or from the author.

predictive models have been proposed to overcome this limitation. [27–31]

Until recently, ionic liquids were regarded as non-volatile, and thus did not exhibit measurable vapor pressures, even at higher temperatures. However, Earle *et al.* [32] have shown that some ionic liquids can be distilled at low pressures without decomposition. Later on, Paulechka *et al.* [33] have evaluated the possibility of measuring the vapor pressure and enthalpy of vaporization of 1-butyl-3-methylimidazolium bis(trifluoromethylsulfonyl)amide in vacuum. Kabo and collaborators[34] reported the first experimental determinations of vapor pressures for a series of 1-alkyl-3-methylimidazolium bis(trifluoromethylsulfonyl)imide, $[C_{N\text{-}1}C_1im][NTf_2]$ (N = 2, 4, 6, and 8), ionic liquids, using an integral Knudsen effusion method. Based on this work, it was possible to prove that the balance of the thermal stability and volatility for $[C_{N\text{-}1}C_1im][NTf_2]$ allowed measurements of vapor pressures in a temperature range suitable for a proper evaluation of the thermodynamic properties of vaporization. In the same year, Santos *et al.* [35] presented the first proof that the vaporization of ionic liquids occurs as a direct liquid to gas transfer of the intact ionic pair. The proposed vaporization mechanism (vaporization of the ionic liquids via neutral ion pairs) where supported by studies using photoionization [36], line of sight mass spectrometry [37–39], Fourier transform ion cyclotron resonance [40,41], and by tunable vacuum ultraviolet photoionization [42]. These pioneering works [32–336] contributed to the knowledge of a window of opportunity [19] for the vaporization of some ionic liquids without decomposition. In addition to the already cited works concerning the vapor pressure measurements by the integral Knudsen effusion method [34] and the determination of enthalpies of vaporization by Calvet drop calorimetry [35], several other techniques and strategies were used to determine the enthalpies of vaporization. Nowadays, there are a number of publications reporting enthalpies of vaporization, at a reference temperature, for a wide range of ionic liquids determined using both experimental [37,38,42,43–49] and theoretical methods [50,51].
Accurate thermodynamic properties of vaporization equilibrium of ionic liquids are scarce and crucial for the better understanding of the liquid phase of ionic liquids, evaluation of the cohesive energy, as well as the nature of the vapor phase. Additionally, they are required for validation and parameterization of the models (force fields) used to describe ionic liquids in different simulation techniques. [3,5,19,52] Despite of the importance of the vapor pressures of ionic liquids and the related thermodynamic properties of vaporization, $\Delta_l^g H_m^o$, $\Delta_l^g S_m^o$, and $\Delta_l^g G_m^o$, respectively, most of the works performed until now are focused on estimation and determination of enthalpies of vaporization.[19]
Our group has been focused on the vapor pressure measurements of several families of ionic liquids [53–57], using the quartz microbalance Knudsen effusion apparatus.[58] In these works, the effect of the alkyl chain length of the cation was explored in order to get more insights about the nanostructuration of ionic liquids, which is related with the transition from a dispersed to a continuous non-polar phase, as the alkyl-side chain of the cation becomes longer.[6] Based on these works, it was possible to give a thermodynamic view of the nanostructuration of the imidazolium bistriflamide ionic liquids, for which a limit for the beginning of the nanostructuration / nano segregation at C_6 was observed.[53–55] Recently, the first volatility study of the 1-alkylpyridinium bis(trifluoromethylsulfonyl)imide, $[C_NPy][NTf_2]$ (N=ethyl, propyl, and butyl) was reported, and the analysis and rationalization of the obtained results was done based on the comparison with the $[C_{N\text{-}1}C_1im][NTf_2]$ (N = 3. 4, 5).[53,56] It was found that the volatility of pyridinium ionic liquids is five times lower than that of imidazolium and that it is driven by their higher enthalpy of vaporization. [56]
Imidazolium based ionic liquids are the most investigated family in several research areas. Compared to the imidazolium cation, the pyridinium cation have lower cost, low toxicity, chemical stability and a high extractive performance.[59–63] The change of the cation from a imidazolium to a pyridinium leads to a different kind of structural organization in the liquid phase, and the enlargement of the cation size increases the distance between charges while delocalizing them as well, thus resulting in a decrease in the ionic interaction energy.[64,65] Despite the decrease of the electrostatic interactions, the pyridinium based ionic liquids have found to be associated with a higher cohesion than the imidazolium ionic liquids, which is associated to the importance of cation-cation dispersive interactions.[66,67] The molecular interactions between the ions and their structural arrangement results in a complex structural / nanostructural organization recognized in the ionic liquids, and hence to interesting properties. Therefore, the knowledge of the dependence of the properties of the liquids on their molecular structures is of great importance.
The present work comprises the synthesis and volatility study of a novel 1-ethyl-2-alkylpyridinium bis(trifluoromethanesulfonyl)imide, $[^2C_{N\text{-}2}{}^1C_2Py][NTf_2]$ (N = 4, 5, 6, 7, 8, 9, 10). The vapor pressure of each pure ionic liquid has been determined as a function of temperature in the [493 − 524] K range, using a new quartz microbalance Knudsen effusion apparatus.[68] Based on the experimental results, the standard molar enthalpy, entropy and Gibbs energy of vaporization have been derived. In this work, we have designed and synthesized a new ionic liquid series based on the pyridinium cation in order to explore the effect of the nanostructuration in the pyridinium bistriflamide ionic liquids by means of a comparative analysis with the previous studies. [55,58] The inspiration for the design of the this novel pyridinium based ionic liquids series was based on the idea of mimetize the properties and thermal stability of the dialkylimidazolium base ILs, in a different chemical moiety that present some applicability advantages. [59-63]

Results and Discussion

Synthesis: The new 1-ethyl-2-alkylpyridinium ionic liquids were synthesized in a three-step process following the general route shown in Scheme 1. The introduction of different alkyl groups in position 2 of the pyridine ring was carried out by metalation of commercial 2-picoline (**1**) and subsequent alkylation with an appropriate alkyl halide. The 2-alkylpyridines **2-8** were then treated with ethyl bromide to afford the corresponding dialkylpyridinium bromides **9-15**. Optimization of the reaction conditions (concentrations, temperature, reaction time and base) for both metalation and alkylation were described in a previous report.[63] Finally, the subsequent metathesis with bis(trifluoromethane) sulfonimide lithium salt provided the 1-ethyl-2-alkylpyridinium bis(trifluoromethane)sulfonimides **16-22** with excellent purity and overall yield. Their structures were confirmed by ^{1}H NMR, ^{13}C NMR and ESI-HRMS.

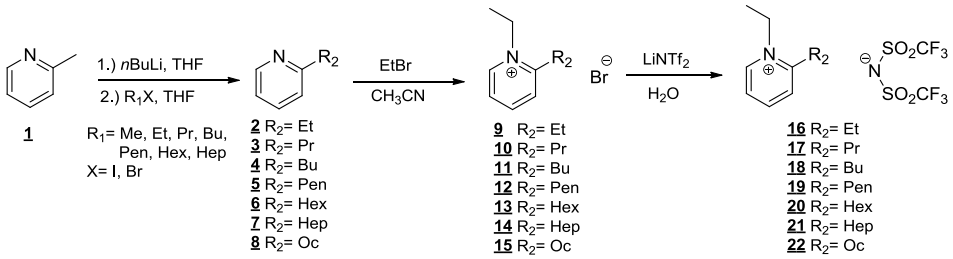

1 R1= Me, Et, Pr, Bu, Pen, Hex, Hep; X= I, Br

2 R2= Et; **3** R2= Pr; **4** R2= Bu; **5** R2= Pen; **6** R2= Hex; **7** R2= Hep; **8** R2= Oc

9 R2= Et; **10** R2= Pr; **11** R2= Bu; **12** R2= Pen; **13** R2= Hex; **14** R2= Hep; **15** R2= Oc

16 R2= Et; **17** R2= Pr; **18** R2= Bu; **19** R2= Pen; **20** R2= Hex; **21** R2= Hep; **22** R2= Oc

Scheme 1. General synthetic procedure employed to prepare new 1-ethyl-2-alkylpyridinium ILs.

Vapor pressure measurements: The vapor pressures of the synthesized ionic liquids were measured at different temperatures using a Knudsen effusion apparatus combined with a quartz crystal microbalance. [68] The experimental vapor pressure data for each ionic liquid is presented in table S1, and as supporting information SI. Figure 1 presents the graphical representation of ln(p/Pa) = f [(1/T) / K^{-1}] for the studied ionic liquids. Based on the previous results, the thermodynamic properties of vaporization at the mean temperature, <T>, and references temperatures, θ, 460 K and 298.15 K, were derived from the fitting of the experimental results of the vapor pressures by the truncated form of the Clarke and Glew equation [69]:

$$R\cdot\ln\frac{p}{p^{o}}=-\frac{\Delta_{l}^{g}G_{m}^{o}(\theta)}{\theta}+\Delta_{l}^{g}H_{m}^{o}(\theta)\cdot\left(\frac{1}{\theta}-\frac{1}{T}\right)+\Delta_{l}^{g}C_{p,m}^{o}\cdot\left[\frac{\theta}{T}-1+\ln\left(\frac{T}{\theta}\right)\right] \qquad (1)$$

where p is the vapor pressure, p^{o} is a selected reference pressure (p^{o} = 10^{5} Pa), θ is a selected reference temperature, R is the gas constant (R = 8.3144621 J·K^{-1}·mol^{-1}) [70], $\Delta_{l}^{g}G_{m}^{o}$ is the standard molar Gibbs energy of vaporization at the selected reference pressure, $\Delta_{l}^{g}H_{m}^{o}$ is the standard molar enthalpy of vaporization, and $\Delta_{l}^{g}C_{p,m}^{o}$ is the difference between the heat capacities of the gaseous and of the liquid phases [$\Delta_{l}^{g}C_{p,m}^{o}=C_{p,m}^{o}(g)-C_{p,m}^{o}(l)$]. In this work, $\Delta_{l}^{g}C_{p,m}^{o}$ = − 100 ± 10 J·K^{-1}·mol^{-1} was considered in the calculations for all ILs under study. The value of (− 100 J·K^{-1}·mol^{-1}) for $\Delta_{l}^{g}C_{p,m}^{o}$ is a typical value for liquids and have been used before in the literature.[19,57,71] Table 1 lists the thermodynamic properties of vaporization derived from equation (1) at the mean temperature, <T>, and references temperatures, θ, 460 K and 298.15 K.

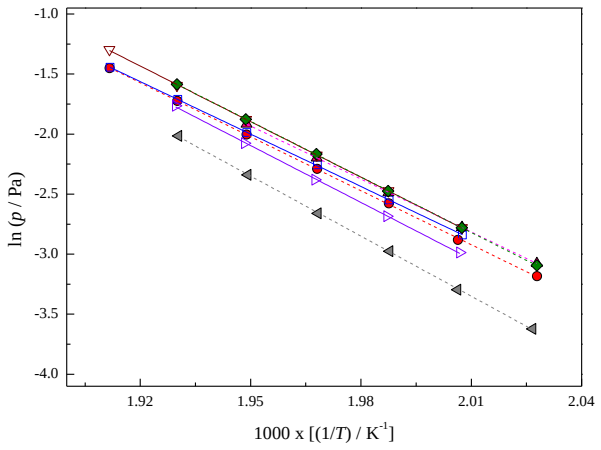

Figure 1. Plot of ln(p/Pa) = f [(1/T) / K^{-1}] for the studied ionic liquid: ● - [^{2}C$_{2}$^{1}C$_{2}$Py][NTf$_{2}$]; □ - [^{2}C$_{3}$^{1}C$_{2}$Py][NTf$_{2}$]; ▲ - [^{2}C$_{4}$^{1}C$_{2}$Py][NTf$_{2}$]; ▽ - [^{2}C$_{5}$^{1}C$_{2}$Py][NTf$_{2}$]; ◆ - [^{2}C$_{6}$^{1}C$_{2}$Py][NTf$_{2}$]; ▷ - [^{2}C$_{7}$^{1}C$_{2}$Py][NTf$_{2}$]; ◀ - [^{2}C$_{8}$^{1}C$_{2}$Py][NTf$_{2}$].

Table 1. Thermodynamic properties of vaporization derived from the vapor pressure results and the derived standard (p^{o} = 10^{5} Pa), at the reference temperature, θ.

T interval / K	θ / K	$\Delta_{l}^{g}G_{m}^{o}(\theta)$ / J·mol^{-1}	$\Delta_{l}^{g}H_{m}^{o}(\theta)$ / J·mol^{-1}	$\Delta_{l}^{g}S_{m}^{o}(\theta)$ / J·K^{-1}·mol^{-1}	r^{2}
		[^{2}C$_{2}$^{1}C$_{2}$Py][NTf$_{2}$]			
493 to 524	508.11 [a]	58315 ± 978	124553 ± 693	130.4 ± 1.4	0.9998
	460.00	64822 ± 978	129364 ± 843	140.3 ± 1.7	
	298.15	90787 ± 1039	145549 ± 2211	183.7 ± 5.5	
		[^{2}C$_{3}$^{1}C$_{2}$Py][NTf$_{2}$]			
498 to 524	510.59 [a]	57885 ± 617	120929 ± 436	123.5 ± 0.9	0.9999
	460.00	64390 ± 617	125988 ± 668	133.9 ± 1.3	
	298.15	89320 ± 716	142173 ± 2169	177.3 ± 5.4	
		[^{2}C$_{4}$^{1}C$_{2}$Py][NTf$_{2}$]			
493 to 523	503.12 [a]	58554 ± 235	122261 ± 166	126.6 ± 0.3	0.9999
	460.00	64204 ± 236	126573 ± 461	135.6 ± 1.0	
	298.15	89405 ± 424	142758 ± 2056	178.9 ± 5.2	
		[^{2}C$_{5}$^{1}C$_{2}$Py][NTf$_{2}$]			
498 to 524	510.63 [a]	57472 ± 839	128159 ± 593	138.4 ± 1.2	0.9999
	460.00	64741 ± 840	133222 ± 780	148.9 ± 1.6	
	298.15	92092 ± 915	149407 ± 2206	192.2 ± 5.5	
		[^{2}C$_{6}$^{1}C$_{2}$Py][NTf$_{2}$]			
493 to 519	505.65 [a]	58155 ± 385	128235 ± 235	138.6 ± 0.5	0.9999
	460.00	64694 ± 334	132800 ± 514	148.1 ± 1.1	
	298.15	91913 ± 485	148985 ± 2088	191.4 ± 5.3	
		[^{2}C$_{7}$^{1}C$_{2}$Py][NTf$_{2}$]			
498 to 519	508.27 [a]	58669 ± 1778	131425 ± 1257	143.1 ± 2.5	0.9997
	460.00	65816 ± 1778	136252 ± 1346	153.1 ± 2.7	
	298.15	93855 ± 1813	152437 ± 2448	196.5 ± 5.9	
		[^{2}C$_{8}$^{1}C$_{2}$Py][NTf$_{2}$]			
493 to 519	505.73 [a]	60203 ± 1066	138746 ± 754	155.3 ± 1.5	0.9999
	460.00	67518 ± 1066	143319 ± 881	164.8 ± 1.8	
	298.15	97445 ± 1122	159504 ± 2208	208.1 ± 5.5	

[a] mean temperature. r^{2} is the linear regression coefficient.

The analysis and the rationalization of the obtained thermodynamic properties of vaporization for the [^{2}C$_{N-2}$^{1}C$_{2}$Py][NTf$_{2}$] ionic liquids will be done considering the literature data for the [C$_{N-1}$C$_{1}$im][NTf$_{2}$] [53] and [C$_{N}$Py][NTf$_{2}$] [56], in order to get more insights on the effect of the topology of the cation (scheme 2) on the ionic liquid properties.

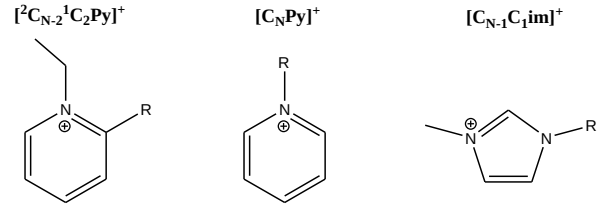

1-ethyl-2-alkylpyridinium; 1-alkylpyridinium; 1-methyl-3-alkylimidazolium

Scheme 2. Schematic molecular structure of the 1-ethyl-2-alkylpyridinium, N-alkylpyridinium and 1-methyl-3-alkylimidazolium cations.

In order to explore the effect of the nanostructuration in pyridinium bistriflamide ionic liquids, the dependence of the thermodynamic properties of vaporization of the $[^2C_{N-2}{}^1C_2Py][NTf_2]$ ionic liquids with the alkyl side chain length of the cation will be analysed and discussed.

Analysing the $\ln(p/Pa) = f[(1/T)/K^{-1}]$ representation and considering the experimental temperature range (figure 1), the following order of volatility for the $[^2C_{N-2}{}^1C_2Py][NTf_2]$ ionic liquids was found to be:

$[^2C_4{}^1C_2Py][NTf_2] \approx [^2C_5{}^1C_2Py][NTf_2] \approx [^2C_6{}^1C_2Py][NTf_2] > [^2C_2{}^1C_2Py][NTf_2] \approx [^2C_3{}^1C_2Py][NTf_2] > [^2C_7{}^1C_2Py][NTf_2] >> [^2C_8{}^1C_2Py][NTf_2]$

The shorter members, $[^2C_2{}^1C_2Py][NTf_2]$ and $[^2C_3{}^1C_2Py][NTf_2]$, of the series present an outlier behaviour, with lower volatilities than the $[^2C_4{}^1C_2Py][NTf_2]$, $[^2C_5{}^1C_2Py][NTf_2]$ and $[^2C_6{}^1C_2Py][NTf_2]$. The outlier behaviour is similar to the one recently observed in the imidazolium based ILs with short alkyl chain length (e.g. $[C_{N-1}C_1im][NTf_2]$ and $[C_{N/2}C_{N/2}im][NTf_2]$) and arises from the stronger initial effect of the steric hindrance of the alkyl chain on the cation-anion interaction. [53,57]

The graphic representation of the standard molar Gibbs energies of vaporization at reference temperature, T = 460 K, as a function of the total number of carbon atoms in the two alkyl side chains of the cation, N, is presented in figure 2. At the reference temperature, T = 460 K, the 1-ethyl-2-alkylpyridinium based ionic liquids presents lower volatility than the imidazolium ionic liquids.[53] Analogous to imidazolium based ionic liquids[53,57], the $\Delta_l^g G_m^o$ profile along the alkyl side chain presents a non-linear behaviour for the ionic liquids with shorter alkyl chain length, with an initial increase of volatility due to the marked effect of steric hindrance of the alkyl chain, reaching a maximum volatility plateau at $[^2C_3{}^1C_2Py][NTf_2]$ and $[^2C_4{}^1C_2Py][NTf_2]$. Starting from $[^2C_4{}^1C_2Py][NTf_2]$, the volatility decreases along the alkyl side chain length of the cation, similarly as it was observed for the imidazolium series. [53] It is observed that the electrostatic potential decreases gradually with the alkyl chain length increase, being sharper for shorter alkyl chain length, due to the highest impact of the steric hindrance. The non-electrostatic potential is expected to increase nearly linear along the alkyl chain length.[72-74] The volatility trend (figure 2) reflects the overlapping of the two main interaction potentials: electrostatic and non-electrostatic, reaching a nearly linear increment of the Gibbs energy of vaporization (volatility decrease) after $[C_3C_1im][NTf_2]$ (N=4) and $[^2C_3{}^1C_2Py][NTf_2]$ (N=5) indicating that the electrostatic potential reaches a linear decreasing functional, lower than the increment of the non-electrostatic interaction potential per methylene group, $-CH_2-$.

The graphic representations of the standard molar enthalpies and entropies of vaporization at reference temperature, T = 298.15 K, as a function of the total number of carbon atoms in the two alkyl side chains of the cation, N, are presented in figures 3 and 4. The 1-ethyl-2-alkylpyridinium and 1-alkylpyridinium ionic liquids with the shortest alkyl chains, present a significant higher $\Delta_l^g H_m^o$ than the imidazolium series. [53,57] After $[^2C_3{}^1C_2Py][NTf_2]$ and for the same total number of carbons in the alkyl side chains of the cation, N, the difference between the enthalpies of vaporization for the two ionic liquid families is smaller, being related with the comparable cohesive energies in the bulk and an indication that the trend of the electrostatic interactions contribution should be similar. [53,57]

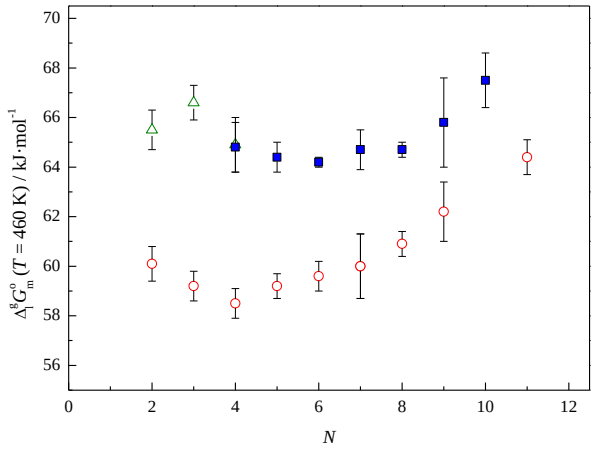

Figure 2. Standard (p^o=10^5 Pa) molar Gibbs energy of vaporization, at T = 460 K, as a function of the total number of carbons in the alkyl side chains of the cation, N. ○ - $[C_{N-1}C_1im][NTf_2]$ [53,57] (N = 2 - 9, 11, 13); △ - $[C_NPy][NTf_2]$ [56] (N = 2 - 4); ■ - $[^2C_{N-2}{}^1C_2Py][NTf_2]$ (N = 4 - 10).

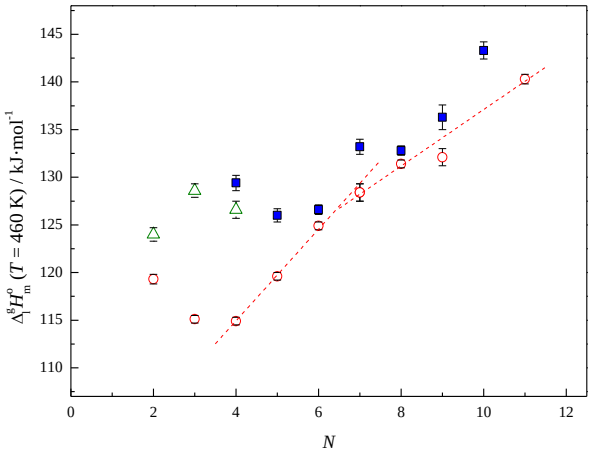

Figure 3. Standard (p^o=10^5 Pa) molar enthalpies of vaporization, at T = 460 K, as a function of the total number of carbons in the alkyl side chains of the cation, N. ○ - $[C_{N-1}C_1im][NTf_2]$ [53,57] (N = 2 - 9, 11, 13); △ - $[C_NPy][NTf_2]$ [56] (N = 2 - 4); ■ - $[^2C_{N-2}{}^1C_2Py][NTf_2]$ (N = 4 - 10).

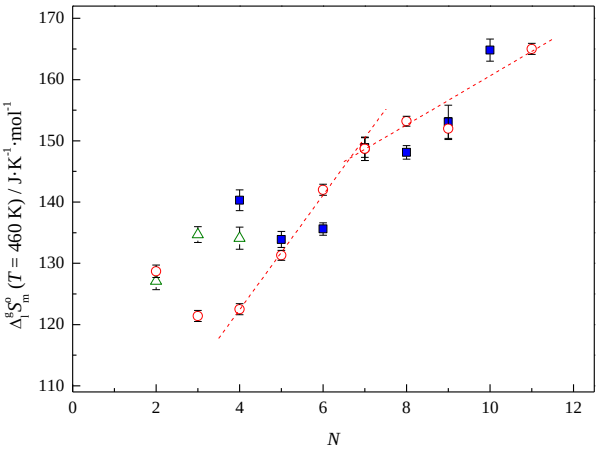

Figure 4. Standard (p^o=10^5 Pa) molar entropies of vaporization, at T = 460 K, as a function of the total number of carbons in the alkyl side chains of the cation, N. ○ - $[C_{N-1}C_1im][NTf_2]$ [53,57] (N = 2 - 9, 11, 13); △ - $[C_NPy][NTf_2]$ [56] (N = 2 - 4); ■ - $[^2C_{N-2}{}^1C_2Py][NTf_2]$ (N = 4 - 10).

The overview of the entropies of vaporization along the series (figure 4) shows a similar profile than the one of $\Delta_l^g H_m^o$, however the differentiation between the ionic liquid families, focused in this work, is smaller for $\Delta_l^g S_m^o$.[53,56,57] A decrease of the entropy from $[^2C_2{}^1C_2Py][NTf_2]$ to $[^2C_3{}^1C_2Py][NTf_2]$ is observed, which is related with an increase of the entropy of the liquid due to the increase of the alkyl chain length. After $[^2C_3{}^1C_2Py][NTf_2]$, the entropies of vaporization increases along the series and are in the same range than the slightly lower ones of the imidazolium based ionic liquids.[62]

It is interesting to observed that $[^2C_2{}^1C_2Py][NTf_2]$ presents higher enthalpies and entropies of vaporization than the isomer $[C_4Py][NTf_2]$ [56], which results in similar volatilities.

From the analysis of the enthalpic and entropic contribution to the volatility of the ionic liquids under study, it was found that the lower volatility of the $[^2C_{N-2}{}^1C_2Py][NTf_2]$ ionic liquids, than the $[C_{N-1}C_1im][NTf_2]$ series, is mainly due to the higher enthalpies of vaporization. However, starting from $[^2C_3{}^1C_2Py][NTf_2]$, it is a consequence of the combination of slightly lower entropies and higher enthalpies of vaporization.

This work presents the detailed synthesis, characterization and volatility study of new pyridinium based ionic liquids, $[^2C_{N-2}{}^1C_2Py][NTf_2]$. This new series presents higher thermal stability and lower volatility than the imidazolium based ionic liquids. The present work is a contribution to the molecular understanding of the thermodynamics of vaporization of new dialkylpyridinium based ionic liquids.

Experimental Section

Materials

Chemicals used in the synthesis*:* 2-Picoline (Acros organics, 98%), *n*-butyllithium (Sigma–Aldrich, 2.5 M in hexane), iodomethane (Acros organics, 99%, stabilized), bromoethane (Acros organics, 98%), 1-bromopropane (Acros organics, 99%), 1-bromobutane (Sigma–Aldrich, 99%), 1-iodopentane (Sigma–Aldrich, 98%, stabilized), 1-iodohexane (Sigma–Aldrich, 98%, stabilized), 1-bromoheptane (Acros organics, 99%), bis(trifluoromethanesulfonyl)imide lithium salt (Sigma-Aldrich, 99%) and acetonitrile (Sigma–Aldrich, ACS reagent, ≥99.5%) were commercially available and used without any further pre-treatment or pre-purification, except tetrahydrofuran (Panreac, 99.5%, stabilized),which was dried with suitable drying agents and distilled under argon prior to use.

General Methods: ^{1}H and ^{13}C NMR spectra of the obtained products were recorded in $CDCl_3$ on a Bruker ARX at 400.1621 and 100.6314 MHz respectively. Chemical shifts are reported in parts per million (ppm, δ) and coupling constants (*J*) in hertz. ESI mass spectra were recorded on an apex-Qe spectrometer.

General procedure for 2-picoline alkylation: A solution of 2-picoline (5 mL, 49.5 mmol) in anhydrous THF (75 mL) was introduced into a 250 mL round flask under inert atmosphere. The mixture was cooled to -78 °C with a dry ice-acetone bath and a solution of *n*-BuLi 2.5 M in hexane (19.8 mL, 49.5 mmol) was then slowly added over 10 min. After stirring for 1h, while keeping the temperature below -20 °C, the obtained deep red solution was cooled again to -78 °C and a solution of the appropriate 1-alkyl halide (2 equiv.) in anhydrous THF (50 mL) was slowly added. The reaction mixture was allowed to gradually warm up to room temperature and stirred for 1 to 5 h depending on the 1-alkyl halide. The reaction progress was monitored by t.l.c using silica gel 60 GF-254 aluminium sheets and hexane/ethyl acetate (1/1) as eluent. The reaction was worked up by adding of water (25 mL), neutralized with a saturated solution of ammonium chloride (25 mL) and extracted with dichloromethane (3 x 25 mL). The organic extracts were combined, dried over Na_2SO_4 and filtered. The solvent was removed on the rotary evaporator and the residue was further purified by chromatography over silica gel using gradient elution (starting with hexane to hexane/ethyl acetate 1.5/1).

2-Ethylpyridine (2).[75] Yield 83%. ^{1}H NMR (400 MHz, $[D_1]CDCl_3$, 25°C, TMS): δ= 8.49 (ddd, *J*(H,H) = 0.8 Hz, *J*(H,H) = 1.7 Hz, *J*(H,H) = 4.8 Hz, 1H; H-6), 7.56 (dt, *J*(H,H) = 1.9 Hz, *J*(H,H) = 7.7 Hz, 1H; H-4), 7.12 (d, *J*(H,H) = 7.8 Hz, 1H; H-3), 7.06 (m, 1H; H-5), 2.79 (q, *J*(H,H) = 7.6 Hz, 2H; (C-2)C*H*$_2$), 1.28 (t, *J*(H,H) = 7.6 Hz, 3H; (C-2)CH$_2$C*H*$_3$). ^{13}C NMR (100 MHz, $[D_1]CDCl_3$, 25°C, TMS): δ= 162.9 (C-2), 148.6 (C-6), 135.8 (C-4), 121.5 (C-3), 120.4 (C-5), 30.9 ((C-2)*C*H$_2$), 13.4 ((C-2)CH$_2$*C*H$_3$).

2-Propylpyridine (3).[76] Yield 87%. ^{1}H NMR (400 MHz, $[D_1]CDCl_3$, 25°C, TMS): δ= 8.48 (ddd, *J*(H,H) = 0.8 Hz, *J*(H,H) = 1.7 Hz, *J*(H,H) = 4.8 Hz, 1H; H-6), 7.53 (dt, *J*(H,H) = 1.6 Hz, *J*(H,H) = 7.7 Hz, 1H; H-4), 7.09 (d, *J*(H,H) = 7.8 Hz, 1H; H-3), 7.04 (m, 1H; H-5), 2.72 (m, 2H; (C-2)C*H*$_2$), 1.72 (m, 2H; (C-2)CH$_2$C*H*$_2$), 0.93 (t, *J*(H,H) = 7.4 Hz, 3H; (C-2)(CH$_2$)$_2$C*H*$_3$). ^{13}C NMR (100 MHz, $[D_1]CDCl_3$, 25°C, TMS): δ= 162.1 (C-2), 149.1 (C-6), 136.0 (C-4), 122.6 (C-3), 120.7 (C-5), 40.3, ((C-2)*C*H$_2$), 23.0 ((C-2)CH$_2$*C*H$_2$), 13.7 ((C-2)(CH$_2$)$_2$*C*H$_3$).

2-Butylpyridine (4).[77] Yield 82%. ^{1}H NMR (400 MHz, $[D_1]CDCl_3$, 25°C, TMS): δ= 8.49 (ddd, *J*(H,H) = 0.8 Hz, *J*(H,H) = 1.7 Hz, *J*(H,H) = 4.9 Hz, 1H; H-6), 7.54 (dt, *J*(H,H) = 1.9 Hz, *J*(H,H) = 7.7 Hz, 1H; H-4), 7.10 (d, *J*(H,H) = 7.8 Hz, 1H; H-3), 7.05 (ddd, *J*(H,H) = 1.0 Hz, *J*(H,H) = 4.9 Hz, *J*(H,H) = 7.5 Hz, 1H; H-5), 2.75 (m, 2H; (C-2)C*H*$_2$), 1.68 (m, 2H; (C-2)CH$_2$C*H*$_2$), 1.35 (m, 2H; (C-2)(CH$_2$)$_2$C*H*$_2$), 0.91 (t, *J*(H,H) = 7.4 Hz, 3H; (C-2)(CH$_2$)$_3$C*H*$_3$). ^{13}C NMR (100 MHz, $[D_1]CDCl_3$, 25°C, TMS): δ= 162.4 (C-2), 149.1 (C-6), 136.1 (C-4), 122.6 (C-3), 120.7 (C-5), 38.1 ((C-2)*C*H$_2$), 32.0 ((C-2)CH$_2$*C*H$_2$), 22.4 ((C-2) (CH$_2$)$_2$*C*H$_2$), 13.9 ((C-2)(CH$_2$)$_3$*C*H$_3$).

2-Pentylpyridine (5).[78] Yield 85%. ^{1}H NMR (400 MHz, $[D_1]CDCl_3$, 25°C, TMS): δ= 8.48 (ddd, *J*(H,H) = 0.8 Hz, *J*(H,H) = 1.7 Hz, *J*(H,H) = 4.9 Hz, 1H; H-6), 7.53 (dt, *J*(H,H) = 1.9 Hz, *J*(H,H) = 7.7 Hz, 1H; H-4), 7.09 (d, *J*(H,H) = 7.8 Hz, 1H; H-3), 7.04 (ddd, *J*(H,H) = 1.0 Hz, *J*(H,H) = 4.9 Hz, *J*(H,H) = 7.4 Hz, 1H; H-5), 2.74 (m, 2H; (C-2)C*H*$_2$), 1.69 (m, 2H; (C-2)CH$_2$C*H*$_2$), 1.30 (m, 4H; (C-2)(CH$_2$)$_2$(C*H*$_2$)$_2$), 0.85 (t, *J*(H,H) = 7.0 Hz, 3H; (C-2)(CH$_2$)$_4$C*H*$_3$). ^{13}C NMR (100 MHz, $[D_1]CDCl_3$, 25°C, TMS): δ= 162.5 (C-2), 149.2 (C-6), 136.2 (C-4), 122.7 (C-3), 120.8 (C-5), 38.4 ((C-2)*C*H$_2$), 31.6 ((C-2)(CH$_2$)$_2$CH$_2$), 29.6 ((C-2)CH$_2$*C*H$_2$), 22.5 ((C-2)(CH$_2$)$_3$CH$_2$), 14.0 ((C-2)(CH$_2$)$_4$*C*H$_3$).

2-Hexylpyridine (6).[79] Yield 85%. ^{1}H NMR (400 MHz, $[D_1]CDCl_3$, 25°C, TMS): δ= 8.51 (ddd, *J*(H,H) = 0.8 Hz, *J*(H,H) = 1.7 Hz, *J*(H,H) = 4.9 Hz, 1H; H-6), 7.56 (dt, *J*(H,H) = 1.9 Hz, *J*(H,H) = 7.7 Hz, 1H; H-4), 7.12 (d, *J*(H,H) = 7.8 Hz, 1H; H-3), 7.07 (ddd, *J*(H,H) = 1.0 Hz, *J*(H,H) = 4.9 Hz, *J*(H,H) = 7.4 Hz, 1H; H-5), 2.76 (m, 2H; (C-2)C*H*$_2$), 1.71 (m, 2H; (C-2)CH$_2$C*H*$_2$), 1.32 (m, 6H; (C-2)(CH$_2$)$_2$(C*H*$_2$)$_3$), 0.86 (t, *J*(H,H) = 7.1 Hz, 3H; (C-2)(CH$_2$)$_5$C*H*$_3$). ^{13}C NMR (100 MHz, $[D_1]CDCl_3$, 25°C, TMS): δ= 162.5 (C-2), 149.2 (C-6), 136.2 (C-4), 122.7 (C-3), 120.8 (C-5),

38.5 ((C-2)*C*H$_2$), 31.7 ((C-2)(CH$_2$)$_3$*C*H$_2$), 29.9 ((C-2)CH$_2$*C*H$_2$), 29.1 ((C-2)(CH$_2$)$_2$*C*H$_2$), 22.6 ((C-2)(CH$_2$)$_4$*C*H$_2$), 14.1 ((C-2)(CH$_2$)$_5$*C*H$_3$).

2-Heptylpyridine (7).[80] Yield 79%. ^{1}H NMR (400 MHz, [D$_1$]CDCl$_3$, 25°C, TMS): δ= 8.49 (ddd, *J*(H,H) = 0.8 Hz, *J*(H,H) = 1.7 Hz, *J*(H,H) = 4.9 Hz, 1H; H-6), 7.53 (dt, *J*(H,H) = 1.9 Hz, *J*(H,H) = 7.7 Hz, 1H; H-4), 7.10 (d, *J*(H,H) = 7.8 Hz, 1H; H-3), 7.04 (ddd, *J*(H,H) = 1.0 Hz, *J*(H,H) = 4.9 Hz, *J*(H,H) = 7.5 Hz, 1H; H-5), 2.75 (m, 2H; (C-2)C*H*$_2$), 1.70 (m, 2H; (C-2)CH$_2$C*H*$_2$), 1.30 (m, 8H; (C-2)(CH$_2$)$_2$(C*H*$_2$)$_4$), 0.84 (t, *J*(H,H) = 6.9 Hz, 3H; (C-2)(CH$_2$)$_6$C*H*$_3$). ^{13}C NMR (100 MHz, [D$_1$]CDCl$_3$, 25°C, TMS): δ= 162.4 (C-2), 149.0 (C-6), 136.0(C-4), 122.5(C-3), 120.7(C-5), 38.3 ((C-2)*C*H$_2$), 31.6 ((C-2)(CH$_2$)$_4$*C*H$_2$), 29.8 ((C-2)CH$_2$*C*H$_2$), 29.2 ((C-2)(CH$_2$)$_3$*C*H$_2$), 29.0 ((C-2)(CH$_2$)$_2$*C*H$_2$), 22.5 ((C-2)(CH$_2$)$_5$*C*H$_2$), 14.0 ((C-2)(CH$_2$)$_6$*C*H$_3$).

2-Octylpyridine (8).[81] Yield 83%. ^{1}H NMR (400 MHz, [D$_1$]CDCl$_3$, 25°C, TMS): δ= 8.49 (ddd, *J*(H,H) = 0.8 Hz, *J*(H,H) = 1.7 Hz, *J*(H,H) = 4.9 Hz, 1H; H-6), 7.54 (dt, *J*(H,H) = 1.9 Hz, *J*(H,H) = 7.7 Hz, 1H; H-4), 7.10 (d, *J*(H,H) = 7.8 Hz, 1H; H-3), 7.05 (ddd, *J*(H,H) = 1.0 Hz, *J*(H,H) = 4.9 Hz, *J*(H,H) = 7.5 Hz, 1H; H-5), 2.75 (m, 2H; (C-2)C*H*$_2$), 1.69 (m, 2H; (C-2)CH$_2$C*H*$_2$), 1.28 (m, 10H; (C-2)(CH$_2$)$_2$(C*H*$_2$)$_5$), 0.84 (t, *J*(H,H) = 6.9 Hz, 3H; (C-2)(CH$_2$)$_7$C*H*$_3$). ^{13}C NMR (100 MHz, [D$_1$]CDCl$_3$, 25°C, TMS): δ= 162.4 (C-2), 149.0 (C-6), 136.1(C-4), 122.6(C-3), 120.7(C-5), 38.4 ((C-2)*C*H$_2$), 31.8 ((C-2)(CH$_2$)$_5$*C*H$_2$), 29.9 ((C-2)CH$_2$*C*H$_2$), 29.4 ((C-2)(CH$_2$)$_3$*C*H$_2$), 29.3 ((C-2)(CH$_2$)$_2$*C*H$_2$), 29.1 ((C-2)(CH$_2$)$_4$*C*H$_2$), 22.6 ((C-2)(CH$_2$)$_6$CH$_2$), 14.0 ((C-2)(CH$_2$)$_7$*C*H$_3$).

General procedures for the synthesis of 1-ethyl-2-alkylpyridinium bromides

Bromoethane (5 equivalents) was added dropwise to a solution of the corresponding 2-alkylpyridine in acetonitrile (5 mL per mmol of starting 2-alkylpyridine). The reaction mixture was stirred at reflux until completion. The reaction progress was monitored by t.l.c using silica gel 60 GF-254 aluminium sheets and CH$_2$Cl$_2$/CH$_3$OH (95/5) as eluent. After removing the solvent under reduced pressure, the residue was purified by Al$_2$O$_3$ chromatography (neutral, activity II-III), using gradient elution (starting with CH$_2$Cl$_2$ to CH$_2$Cl$_2$/CH$_3$OH 9/1). The resulting fractions were combined and the solvent removed under reduced pressure to give the desired 1-ethyl-2-alkylpyridinium bromide that were dried by heating at 60 °C and stirring under high vacuum (2 x 10^{-1} Pa) for 48 h.

1,2-Diethylpyridinium bromide (9). Yield 96%. ^{1}H NMR (400 MHz, [D$_1$]CDCl$_3$, 25°C, TMS): δ= 9.70 (dd, *J*(H,H) = 1.1 Hz, *J*(H,H) = 6.2 Hz, 1H; H-6), 8.47 (dt, *J*(H,H) = 1.4 Hz, *J*(H,H) = 7.9 Hz, 1H; H-4), 7.94 (m, 2H ; H-3, H-5), 4.93 (q, *J*(H,H) = 7.3 Hz, 2H; NC*H*$_2$CH$_3$), 3.21 (q, *J*(H,H) = 7.5 Hz, 2H; (C-2)C*H*$_2$), 1.60 (t, *J*(H,H) = 7.3 Hz, 3H; NCH$_2$C*H*$_3$), 1.42 (t, *J*(H,H) = 7.5 Hz, 3H; (C-2)CH$_2$C*H*$_3$). ^{13}C NMR (100 MHz, [D$_1$]CDCl$_3$, 25°C, TMS): δ= 156.6 (C-2), 146.2 (C-6), 145.4 (C-4), 127.9 (C-3), 126.2 (C-5), 53.1 (N*C*H$_2$CH$_3$), 25.7 ((C-2)C*H*$_2$), 16.6 (NCH$_2$*C*H$_3$), 12.5 ((C-2)CH$_2$*C*H$_3$). ESI-HRMS (apex-Qe): m/z (%): 566.17302 (6) [(C$_9$H$_{14}$N)$_3$ (Br)$_2$]$^+$ calcd for 566.17400), 352 (9) [(C$_9$H$_{14}$N)$_2$ (Br) +1]$^+$, 351.14263 (43) [(C$_9$H$_{14}$N)$_2$ (Br)]$^+$ calcd for 351.14304), 136 (100) [(C$_9$H$_{14}$N)]$^+$.

1-Ethyl-2-propylpyridinium bromide (10). Yield 94%. ^{1}H NMR (400 MHz, [D$_1$]CDCl$_3$, 25°C, TMS): δ=8.48 (dd, *J*(H,H) =1.1 Hz, *J*(H,H) = 6.2 Hz, 1H; H-6), 7.53 (dt, *J*(H,H) = 1.6 Hz, *J*(H,H) = 7.7 Hz, 1H; H-4), 7.09 (d, *J*(H,H) = 7.8 Hz, 1H; H-3), 7.04 (m, 1H; H-5), 2.72 (m, 2H; (C-2)C*H*$_2$), 1.72 (m, 2H; (C-2)CH$_2$C*H*$_2$), 0.93 (t, *J*(H,H) = 7.4 Hz, 3H; (C-2)(CH$_2$)$_2$C*H*$_3$). ^{13}C NMR (100 MHz, [D$_1$]CDCl$_3$, 25°C, TMS): δ= 157.3 (C-2), 146.2 (C-6), 145.2 (C-4), 128.8 (C-3), 126.2 (C-5), 53.0 (N*C*H$_2$), 34.0 ((C-2)*C*H$_2$), 21.9 ((C-2)CH$_2$*C*H$_2$), 16.7 (NCH$_2$*C*H$_3$), 13.5 ((C-2)(CH$_2$)$_2$*C*H$_3$). ESI-HRMS (apex-Qe): m/z (%): 837 (47) [(C$_{10}$H$_{16}$N)$_4$ (Br)$_3$]$^+$, 608 (24) [(C$_{10}$H$_{16}$N)$_3$ (Br)$_2$]$^+$, 379.17400 (100) ([(C$_{10}$H$_{16}$N)$_2$ (Br)]$^+$ calcd for 379.17434).

2-Butyl-1-ethylpyridinium bromide (11). Yield 95%. ^{1}H NMR (400 MHz, [D$_1$]CDCl$_3$, 25°C, TMS): δ= 9.62 (dd, *J*(H,H) = 1.0 Hz, *J*(H,H) = 6.2 Hz, 1H; H-6), 8.41 (dt, *J*(H,H) = 1.5 Hz, *J*(H,H) = 7.9 Hz, 1H; H-4), 7.86 (m, 2H; H-3, H-5), 4.82 (q, *J*(H,H) = 7.3 Hz, 2H; NC*H*$_2$), 3.03 (m, 2H; (C-2)C*H*$_2$), 1.64 (m, 2H; (C-2)CH$_2$C*H*$_2$), 1.53 (t, *J*(H,H) = 7.3 Hz, 3H; NCH$_2$C*H*$_3$), 1.37 (m, 2H; (C-2)(CH$_2$)$_2$C*H*$_2$), 0.84 (t, *J*(H,H) = 7.3 Hz, 3H; (C-2)(CH$_2$)$_3$C*H*$_3$). ^{13}C NMR (100 MHz, [D$_1$]CDCl$_3$, 25°C, TMS): δ= 157.3 (C-2), 146.1 (C-6), 145.2 (C-4), 128.6 (C-3), 126.1 (C-5), 52.8 (N*C*H$_2$), 31.8 ((C-2)*C*H$_2$), 30.3 ((C-2)CH$_2$*C*H$_2$), 22.0 ((C-2)(CH$_2$)$_2$*C*H$_2$), 16.6 (NCH$_2$*C*H$_3$), 13.3 ((C-2)(CH$_2$)$_3$*C*H$_3$). ESI-HRMS (apex-Qe): m/z (%): 893 (27) [(C$_{11}$H$_{18}$N)$_4$ (Br)$_3$]$^+$, 650 (17) [(C$_{11}$H$_{18}$N)$_3$ (Br)$_2$]$^+$, 407.20529 (100) ([(C$_{11}$H$_{18}$N)$_2$ (Br)]$^+$ calcd for 407.20564).

1-Ethyl-2-pentylpyridinium bromide (12). Yield 91%. ^{1}H NMR (400 MHz, [D$_1$]CDCl$_3$, 25°C, TMS): δ= 9.69 (dd, *J*(H,H) = 1.0 Hz, *J*(H,H) = 6.1 Hz, 1H; H-6), 8.43 (dt, *J*(H,H) = 1.3 Hz, *J*(H,H) = 7.9 Hz, 1H; H-4), 7.88 (m, 2H; H-3, H-5), 4.85 (q, *J*(H,H) = 7.3 Hz, 2H; NC*H*$_2$CH$_3$), 3.04 (m, 2H; (C-2)C*H*$_2$), 1.68 (m, 2H; (C-2)CH$_2$C*H*$_2$), 1.55 (t, *J*(H,H) = 7.3 Hz, 3H; NCH$_2$C*H*$_3$), 1.37-1.20 (m, 4H; (C-2)(CH$_2$)$_2$(C*H*$_2$)$_2$), 0.78 (t, *J*(H,H) = 7.2 Hz, 3H; (C-2)(CH$_2$)$_4$C*H*$_3$). ^{13}C NMR (100 MHz, [D$_1$]CDCl$_3$, 25°C, TMS): δ= 157.4 (C-2), 146.1 (C-6), 145.2 (C-4), 128.7 (C-3), 126.1 (C-5), 52.8 (N*C*H$_2$), 32.1 ((C-2)*C*H$_2$), 30.9 ((C-2)(CH$_2$)$_2$*C*H$_2$), 28.1 ((C-2)CH$_2$*C*H$_2$), 21.9 ((C-2)(CH$_2$)$_3$CH$_2$), 16.6 (NCH$_2$*C*H$_3$), 13.5 ((C-2) (CH$_2$)$_4$*C*H$_3$). ESI-HRMS (apex-Qe): m/z (%): 949 (23) [(C$_{12}$H$_{20}$N)$_4$ (Br)$_3$]$^+$, 692 (25) [(C$_{12}$H$_{20}$N)$_3$ (Br)$_2$]$^+$, 435.23641 (100) ([(C$_{12}$H$_{20}$N)$_2$ (Br)]$^+$ calcd for 435.23694).

1-Ethyl-2-hexylpyridinium bromide (13). Yield 97%. ^{1}H NMR (400 MHz, [D$_1$]CDCl$_3$, 25°C, TMS): δ= 9.58 (dd, *J*(H,H) = 1.1 Hz, *J(H,H)* = 6.3 Hz, 1H; H-6), 8.38 (dt, *J*(H,H) = 1.4 Hz, *J*(H,H) = 7.9 Hz, 1H; H-4), 7.84 (dd, *J*(H,H) = 1.1 Hz, *J*(H,H) = 8.1 Hz, 1H; H-3), 7.79 (m, 1H; H-5), 4.76 (q, *J*(H,H) = 7.3 Hz, 2H; NC*H*$_2$CH$_3$), 2.97 (m, 2H; (C-2)C*H*$_2$), 1.59 (m, 2H; (C-2)CH$_2$C*H*$_2$), 1.47 (t, *J*(H,H) = 7.3 Hz, 3H; NCH$_2$C*H*$_3$), 1.27 (m, 2H; (C-2)(CH$_2$)$_2$C*H*$_2$), 1.10 (m, 4H; (C-2)(CH$_2$)$_3$(C*H*$_2$)$_2$), 0.66 (t, *J*(H,H) = 7.1 Hz, 3H; (C-2)(CH$_2$)$_5$C*H*$_3$). ^{13}C NMR (100 MHz, [D$_1$]CDCl$_3$, 25°C, TMS): δ= 157.2 (C-2), 145.8 (C-6), 145.1 (C-4), 128.6 (C-3), 125.9 (C-5), 52.6 (N*C*H$_2$), 31.9 (C(2)*C*H$_2$), 30.7 ((C-2)(CH$_2$)$_3$*C*H$_2$), 28.3 ((C-2)CH$_2$*C*H$_2$), 28.2 ((C-2)(CH$_2$)$_2$*C*H$_2$), 21.8 ((C-2)(CH$_2$)$_4$*C*H$_2$), 16.4 (NCH$_2$*C*H$_3$), 13.4 ((C-2)(CH$_2$)$_5$*C*H$_3$). ESI-HRMS (apex-Qe): m/z (%): 1005 (21) [(C$_{13}$H$_{22}$N)$_4$ (Br)$_3$]$^+$, 734 (39) [(C$_{13}$H$_{22}$N)$_3$ (Br)$_2$]$^+$, 463.26771 (100) ([(C$_{13}$H$_{22}$N)$_2$ (Br)]$^+$ calcd for 463.26824).

1-Ethyl-2-heptylpyridinium bromide (14). Yield 94%. ^{1}H NMR (400 MHz, [D$_1$]CDCl$_3$, 25°C, TMS): δ= 9.65 (dd, *J*(H,H) = 1.1 Hz, *J*(H,H) = 6.3 Hz, 1H; H-6), 8.41 (dt, *J*(H,H) = 1.4 Hz, *J*(H,H) = 7.9 Hz, 1H; H-4), 7.84 (m, 2H; H-3, H-5), 4.81 (q, *J*(H,H) = 7.3 Hz, 2H; NC*H*$_2$CH$_3$), 3.01 (m, 2H; (C-2)C*H*$_2$), 1.63 (m, 2H; (C-2)CH$_2$C*H*$_2$), 1.51 (t, *J*(H,H) = 7.3 Hz, 3H; NCH$_2$C*H*$_3$), 1.30 (m, 2H; (C-2)(CH$_2$)$_2$C*H*$_2$), 1.04-1.21 (m, 6H; (C-2)(CH$_2$)$_3$(C*H*$_2$)$_3$), 0.69 (t, *J*(H,H) = 6.9 Hz, 3H; (C-2)(CH$_2$)$_6$C*H*$_3$). ^{13}C NMR (100 MHz, [D$_1$]CDCl$_3$, 25°C, TMS): δ= 157.3 (C-2), 146.0 (C-6), 145.2 (C-4), 128.6 (C-3), 126.0 (C-5), 52.7 (N*C*H$_2$), 32.1 (C(2)*C*H$_2$), 31.0 ((C-

2)(CH_2)$_4$*C*H$_2$), 28.7 ((C-2)CH$_2$*C*H$_2$), 28.4* ((C-2)(CH_2)$_3$*C*H$_2$), 28.3* ((C-2)(CH_2)$_2$*C*H$_2$), 22.0 ((C-2)(CH_2)$_5$*C*H$_2$), 16.5 (NCH$_2$*C*H$_3$), 13.6 ((C-2) (CH_2)$_6$*C*H$_3$). ESI-HRMS (apex-Qe): m/z (%): 1061 (4) [($C_{14}H_{24}N$)$_4$ (Br)$_3$]$^+$, 776 (10) [($C_{14}H_{24}N$)$_3$ (Br)$_2$]$^+$, 491.29923 (64) [($C_{14}H_{24}N$)$_2$ (Br)]$^+$ calcd for 491.29954), 206.19024 (100) [($C_{14}H_{24}N$)]$^+$ calcd for 206.19033).

1-Ethyl-2-octylpyridinium bromide (15). Yield 96%. ^{1}H NMR (400 MHz, [D$_1$]CDCl$_3$, 25°C, TMS): δ= 9.81 (dd, *J*(H,H) = 1.1 Hz, *J*(H,H) = 6.3 Hz, 1H; H-6), 8.45 (dt, *J*(H,H) = 1.0 Hz, *J*(H,H) = 7.9 Hz, 1H; H-4), 7.96 (m, 1H; H-3), 7.88 (m, 1H; H-5), 4.94 (q, *J*(H,H) = 7.3 Hz, 2H; NC*H*$_2$CH$_3$), 3.09 (m, 2H; (C-2)C*H*$_2$), 1.75 (m, 2H; (C-2)CH$_2$C*H*$_2$), 1.63 (t, *J*(H,H) = 7.3 Hz, 3H; NCH$_2$C*H*$_3$), 1.42 (m, 2H; (C-2)(CH_2)$_2$C*H*$_2$), 1.13-1.35 (m, 8H; (C-2)(CH_2)$_3$(C*H*$_2$)$_4$), 0.82 (t, *J*(H,H) = 6.9 Hz, 3H; (C-2)(CH_2)$_7$C*H*$_3$). ^{13}C NMR (100 MHz, [D$_1$]CDCl$_3$, 25°C, TMS): δ= 157.6 (C-2), 146.3 (C-6), 145.5 (C-4), 128.9 (C-3), 126.4 (C-5), 53.0 (N*C*H$_2$), 32.4 (C(2)*C*H$_2$), 31.5 ((C-2)(CH_2)$_5$*C*H$_2$), 29.1 ((C-2)CH$_2$*C*H$_2$), 29.0((C-2)(CH_2)$_3$*C*H$_2$), 28.8* ((C-2)(CH_2)$_2$*C*H$_2$), 28.7* ((C-2)(CH_2)$_4$*C*H$_2$), 22.4 ((C-2)(CH_2)$_6$*C*H$_2$), 16.8 (NCH$_2$*C*H$_3$), 13.9 ((C-2) (CH_2)$_7$*C*H$_3$). ESI-HRMS (apex-Qe): m/z (%): 1118 (10) [($C_{15}H_{26}N$)$_4$ (Br)$_3$]$^+$, 818 (11) [($C_{15}H_{26}N$)$_3$ (Br)$_2$]$^+$, 519.33005 (100) [($C_{15}H_{26}N$)$_2$ (Br)]$^+$ calcd for 519.33084), 220.20583 (79) [($C_{15}H_{26}N$)]$^+$ calcd for 220.20598).

General procedures for the synthesis of 1-ethyl-2-alkylpyridinium bis(trifluoromethanesulfonyl)imide: An aqueous solution of bis(trifluoromethanesulfonyl)imide lithium salt was added at room temperature, to an equal amount of a stirred aqueous solution of the corresponding 1-ethyl-2-alkylpyridinium bromide and the mixture was stirred for an additional 1 h. Two phases were formed. After addition of dichloromethane (20 mL), the upper aqueous phase was decanted and the lower dichloromethane layer was washed with distilled water (5 x 25 mL). The resulting extracts were dried over anhydrous Na_2SO_4 and evaporated under reduced pressure to afford the desired product. The obtained ILs were dried by heating at 80 °C and stirring under high vacuum (2 x 10^{-1} Pa) for 48 h.

1,2-Diethylpyridinium bis(trifluoromethanesulfonyl)imide (16). Yield 93%. 1H NMR (400 MHz, [D1]CDCl3, 25°C, TMS): δ= 8.60 (dd, J(H,H) = 1.2 Hz, J(H,H) = 6.3 Hz, 1H; H-6), 8.29 (dt, J(H,H) = 1.4 Hz, J(H,H) = 7.9 Hz, 1H; H-4), 7.81 (m, 1H; H-5), 7.73 (m, 1H; H-3), 4.50 (q, J(H,H) = 7.3 Hz, 2H; NCH2CH3), 3.05 (q, J(H,H) = 7.5 Hz, 2H; (C-2)CH2), 1.50 (t, J(H,H) = 7.3 Hz, 3H; NCH2CH3), 1.35 (t, J(H,H) = 7.5 Hz, 3H; (C-2)CH2CH3). 13C NMR (100 MHz, [D1]CDCl3, 25°C, TMS): δ= 158.9 (C-2), 145.0 (C-4), 144.1 (C-6), 127.8 (C-5), 125.5 (C-3), 119.3 (q, J(C,F) = 321.3 Hz; N(SO2CF3)2), 52.7 (NCH2CH3), 25.0 (CH2CH3), 15.1 (NCH2CH3), 11.3 (CH2CH3). ESI-HRMS (apex-Qe): m/z (%): 553 (24) [(C9H14N)2 (C2F6NO4S2) + 1]+, 552.14065 (100) [(C9H14N)2 (C2F6NO4S2)]+ calcd for 552.14199)

1-Ethyl-2-propylpyridinium bis(trifluoromethanesulfonyl)imide (17). Yield 94%. 1H NMR (400 MHz, [D1]CDCl3, 25°C, TMS): δ= 8.74 (dd, J(H,H) = 1.4 Hz, J(H,H) = 6.7 Hz, 1H; H-6), 8.35 (dt, J(H,H) = 1.4 Hz, J(H,H) = 7.9 Hz, 1H; H-4), 7.85 (m, 2H; H-3, H-5), 4.61 (q, J(H,H) = 7.3 Hz, 2H; NCH2), 3.05 (m, 2H; (C-2)CH2), 1.85 (m, 2H; (C-2)CH2CH2), 1.62 (t, J(H,H) = 7.3 Hz, 3H; NCH2CH3), 1.10 (t, J(H,H) = 7.3 Hz, 3H; (C-2)(CH2)2CH3). 13C NMR (100 MHz, [D1]CDCl3, 25°C, TMS): δ= 157.8 (C-2), 144.9 (C-4), 144.4 (C-6), 128.8 (C-5), 125.8 (C-3), 119.41 (q, J(C,F) = 321.1 Hz; N(SO2CF3)2), 52.9 (NCH2), 33.5 ((C-2)CH2), 21.2 ((C-2)CH2CH2), 15.5 (NCH2CH3), 12.9 ((C-2)(CH2)2CH3). ESI-HRMS (apex-Qe): m/z (%): , 581 (24) [(C10H16N)2 (C2F6NO4S2) + 1]+, 580.17234 (100) [(C10H16N)2 (C2F6NO4S2)]+ calcd for 580.17329).

2-Butyl-1-ethylpyridinium bis(trifluoromethanesulfonyl)imide (18). Yield 96%. 1H NMR (400 MHz, [D1]CDCl3, 25°C, TMS): δ= 8.70 (dd, J(H,H) = 0.8 Hz, J(H,H) = 6.2 Hz, 1H; H-6), 8.33 (dt, J(H,H) = 1.3 Hz, J(H,H) = 8.0 Hz, 1H; H-4), 7.83 (m, 2H; H-5, H-3), 4.58 (q, J(H,H) = 7.3 Hz, 2H; NCH2), 3.05 (m, 2H; (C-2)CH2), 1.75 (m, 2H; (C-2)CH2CH2), 1.60 (t, J(H,H) = 7.3 Hz, 3H; NCH2CH3), 1.48 (m, 2H; (C-2)(CH2)2CH2), 0.96 (t, J(H,H) = 7.3 Hz, 3H; (C-2)(CH2)3CH3). 13C NMR (100 MHz, [D1]CDCl3, 25°C, TMS): δ= 158.2 (C-2), 145.2 (C-4), 144.8 (C-6), 128.9 (C-5), 126.1 (C-3), 119.68 (q, J(C,F) = 321.3 Hz; N(SO2CF3)2), 53.2 (NCH2), 32.0 (CH2), 30.2 ((C-2)CH2CH2), 22.2 ((C-2)(CH2)2CH2), 15.9 (NCH2CH3), 13.4 ((C-2)(CH2)3CH3). ESI-HRMS (apex-Qe): m/z (%): 609 (23) [(C11H18N)2 (C2F6NO4S2) + 1]+, 608.20327 (100) [(C11H18N)2 (C2F6NO4S2)]+ calcd for 608.20459).

1-Ethyl-2-pentylpyridinium bis(trifluoromethanesulfonyl)imide (19). Yield 94%. 1H NMR (400 MHz, [D1]CDCl3, 25°C, TMS): δ= 8.69 (dd, J(H,H) = 0.8 Hz, J(H,H) = 6.2 Hz, 1H; H-6), 8.33 (dt, J(H,H) = 1.3 Hz, J(H,H) = 7.9 Hz, 1H; H-4), 7.82 (m, 2H; H-5, H-3), 4.57 (q, J(H,H) = 7.3 Hz, 2H; NCH2CH3), 3.04 (m, 2H; (C-2)CH2), 1.76 (m, 2H; (C-2)CH2CH2), 1.58 (t, J(H,H) = 7.3 Hz, 3H; NCH2CH3), 1.46-1.31 (m, 4H; (C-2)(CH2)2(CH2)2), 0.88 (t, J(H,H) = 7.1 Hz, 3H; (C-2)(CH2)4CH3). 13C NMR (100 MHz, [D1]CDCl3, 25°C, TMS): δ= 158.1 (C-2), 145.2 (C-4), 144.8 (C-6), 128.9 (C-5), 126.1 (C-3), 119.6 (q, J(C,F) = 321.2 Hz; N(SO2CF3)2), 53.2 (NCH2CH3), 32.1 (C(2)CH2), 31.0 ((C-2)CH2CH2), 27.9 ((C-2)(CH2)2CH2), 22.0 ((C-2)(CH2)3CH2], 15.9 (NCH2CH3), 13.5 ((C-2) (CH2)4CH3). ESI-HRMS (apex-Qe): m/z (%): 637 (28) [(C12H20N)2 (N(SO2CF3)2) + 1]+, 636.22024 (100) [(C12H20N)2 (N(SO2CF3)2)]+ calcd for 636.23589).

1-Ethyl-2-hexylpyridinium bis(trifluoromethanesulfonyl)imide (20). Yield 96%. 1H NMR (400 MHz, [D1]CDCl3, 25°C, TMS): δ= 8.68 (dd, J(H,H) = 0.8 Hz, J(H,H) = 6.2 Hz, 1H; H-6), 8.32 (dt, J(H,H) = 1.3 Hz, J(H,H) = 7.9 Hz, 1H; H-4), 7.81 (m, 2H; H-3, H-5), 4.57 (q, J(H,H) = 7.3 Hz, 2H; NCH2CH3), 3.04 (t, J(H,H) = 7.9 Hz, 2H; (C-2)CH2), 1.75 (m, 2H; (C-2)CH2CH2), 1.58 (t, J(H,H) = 7.3 Hz, 3H; NCH2CH3), 1.44 (m, 2H; (C-2)(CH2)2CH2), 1.30 (m, 4H; (C-2)(CH2)3(CH2)2), 0.85 (t, J(H,H) = 7.0 Hz, 3H; (C-2)(CH2)5CH3). 13C NMR (100 MHz, [D1]CDCl3, 25°C, TMS): δ= 158.1(C-2), 145.2 (C-6), 144.7 (C-4), 128.9 (C-3), 126.1 (C-5), 119.6 (q, J(C,F) = 321.3 Hz; N(SO2CF3)2), 53.1 (NCH2), 32.2 (C(2)CH2), 31.1 ((C-2)(CH2)3CH2), 28.6 ((C-2)CH2CH2), 28.1 ((C-2)(CH2)2CH2), 22.2 ((C-2)(CH2)4CH2), 15.9 (NCH2CH3), 13.7 ((C-2) (CH2)5CH3). ESI-HRMS (apex-Qe): m/z (%): 664.26564 (100) [(C13H22N)2 (N(SO2CF3)2)]+ calcd for 664.26719).

1-Ethyl-2-heptylpyridinium bis(trifluoromethanesulfonyl)imide (21). Yield 97%. 1H NMR (400 MHz, [D1]CDCl3, 25°C, TMS): δ= 8.72 (dd, J(H,H) = 0.8 Hz, J(H,H) = 6.2 Hz, 1H; H-6), 8.34 (dt, J(H,H) = 1.3 Hz, J(H,H) = 8.0 Hz, 1H; H-4), 7.83 (m, 2H; H-3 and H-5), 4.59 (q, J(H,H) = 7.3 Hz, 2H; NCH2CH3), 3.05 (m, 2H; (C-2)CH2), 1.77 (m, 2H; (C-2)CH2CH2), 1.61 (t, J(H,H) = 7.3 Hz, 3H; NCH2CH3), 1.45 (m, 2H; (C-2)(CH2)2CH2), 1.32 (m, 6H; (C-2)(CH2)3(CH2)3), 0.86 (t, J(H,H) = 6.9 Hz, 3H; (C-2)(CH2)6CH3). 13C NMR (100 MHz, [D1]CDCl3, 25°C, TMS): δ= 158.3(C-2), 145.3 (C-6), 145.0 (C-4), 129.0 (C-3), 126.2 (C-5), 119.5 (q, J(C,F) = 321.3 Hz; N(SO2CF3)2), 53.3 (NCH2), 32.4 ((C-2)CH2), 31.5 ((C-2)(CH2)4CH2), 29.1 ((C-2)CH2CH2), 28.8* ((C-2)(CH2)3CH2), 28.4* ((C-2)(CH2)2CH2), 22.5 ((C-2)(CH2)5CH2), 16.0 (NCH2CH3), 14.0 ((C-2) (CH2)6CH3). ESI-HRMS (apex-Qe): m/z (%): 693 (26) [(C14H24N)2 (N(SO2CF3)2) + 1]+, 692.29796 (100) [(C14H24N)2 (N(SO2CF3)2)]+ calcd for 692.29849), 206 (47) [(C14H24N)]+.

1-Ethyl-2-octylpyridinium bis(trifluoromethanesulfonyl)imide (22). Yield 98%. 1H NMR (400 MHz, [D1]CDCl3, 25°C, TMS): δ=

8.72 (dd, J(H,H) = 0.9 Hz, J(H,H) = 6.2 Hz, 1H; H-6), 8.33 (dt, J(H,H) = 1.3 Hz, J(H,H) = 8.0 Hz, 1H; H-4), 7.81 (m, 2H; H-3, H-5), 4.58 (q, J(H,H) = 7.3 Hz, 2H; NCH2CH3), 3.04 (m, 2H; (C-2)CH2), 1.75 (m, 2H; (C-2)CH2CH2), 1.59 (t, J(H,H) = 7.3 Hz, 3H; NCH2CH3), 1.43 (m, 2H; (C-2)(CH2)2CH2), 1.29 (m, 8H; (C-2)(CH2)3(CH2)4), 0.84 (t, J(H,H) = 6.8 Hz, 3H; (C-2)(CH2)7CH3). 13C NMR (100 MHz, [D1]CDCl3, 25°C, TMS): δ= 158.0(C-2), 145.1 (C-6), 144.6 (C-4), 128.8 (C-3), 125.9 (C-5), 119.5 (q, J(C,F) = 321.3 Hz; N(SO2CF3)2), 53.0 (NCH2), 32.0 ((C-2)CH2), 31.4 ((C-2)(CH2)5CH2), 28.8* ((C-2)CH2CH2), 28.8*((C-2)(CH2)3CH2), 28.7 ((C-2)(CH2)2CH2), 28.0 ((C-2)(CH2)4CH2), 22.2 ((C-2)(CH2)6CH2), 15.7 (NCH2CH3), 13.7 ((C-2)(CH2)7CH3). ESI-HRMS (apex-Qe): m/z (%): 720 (11) [(C15H26N)2 (N(SO2CF3)2)]+, 220.20581 (100) ([(C14H24N)]+ calcd for 220.20598).

Vapor Pressure Measurements

Purification: Before the vapor pressure measurements, the ionic liquids were dried under reduced pressure (< 10 Pa) and stirred constantly for a minimum of 48 h at 323 K, in order to reduce the presence of water or other volatile contents. Afterwards, an *in situ* purification of the ionic liquids was performed using the Knudsen effusion installation, at high vacuum (1×10^{-7} Pa).

Quartz crystal microbalance Knudsen effusion apparatus:

The vapor pressures of the ionic liquids were measured as a function of temperature using a new Knudsen effusion method combined with a quartz crystal microbalance [68] , with the same working principle of the previous installation described in detail.[58] Basically, this apparatus results on the combination of the Knudsen effusion technique and quartz crystal microbalance. In a typical KEQCM experiment, the measurement of the equilibrium vapor pressure at a given temperature, *T*, is achieved by the vapor effusion through the orifice of a effusion cell and condensation of a fraction of the vapor on the surface of the cooled quartz crystal, placed above the effusion cell. This apparatus comprises two mass loss detection techniques, gravimetric and quartz crystal microbalance: the weighed mass of the effusion cell before and after the respective experiment, and the change of the crystal's resonant frequency as the vapor condenses on its surface. The combination of these two mass loss detection techniques presents several advantages, such as, small effusion times, small sample size and real time monitoring of the effusion experiment. The instrument enables the measurement of vapor pressures from 0.02 Pa up to 1 Pa and the temperature is controlled within a temperature fluctuation of $\pm(5\times10^{-3})$ K, measured with a resolution better than 1×10^{-3} K and along the working temperature range, the overall uncertainty is better than $\pm(2\times10^{-2})$ K. The vapor pressure data obtained with this apparatus for the ionic liquid have a typical pressure dependent uncertainty of (1 to 5) %. [58] The relative atomic masses used were those recommended by the IUPAC Commission in 2007. [82]

Supporting Information: The experimental vapor pressure results at different temperatures, the graphic representations of the thermodynamic properties of vaporization at T = 298.15 K as a function of the total number of carbon atoms in the two alkyl side chains of the cation, N, are presented as supporting information.

Acknowledgements

The authors are grateful to the Ministerio de Economía y Competitividad of Spain (Ref. DPI2012-38841-C02-02), to the Xunta de Galicia (project 2012/184) and the Galician Network on Ionic Liquids REGALIs (CN 2012/120) for financial support. Thanks are due to Fundação para a Ciência e Tecnologia (FCT), Lisbon, Portugal and to FEDER for financial support to Centro de Investigação em Química, University of Porto through the project Pest-C/QUI/UI0081/2011. Marisa A. A. Rocha acknowledges the financial support from FCT and the European Social Fund (ESF) under the Community Support Framework (CSF) for the award of a Ph.D. Research Grant, SFRH/BD/60513/2009.

[1] S. M. Urahata, M. C. C. Ribeiro, *J. Chem. Phys.* **2004**, *120*, 1855–1863.
[2] Y. Wang, G. A. Voth, *J. Am. Chem. Soc.* **2005**, *127*, 12192–12193.
[3] S. Izvekov, G. A. Voth, *J. Chem. Phys.* **2005**, *123*, 134105.
[4] J. N. A. C. Lopes, A. A. H. Pádua, *J. Phys. Chem. B* **2006**, *110*, 3330–3335.
[5] M. F. C. Gomes, J. N. C. Lopes, A. A. H. Padua, *Top. Curr. Chem.* **2010**, *290*, 161–183.
[6] K. Shimizu, M. F. Costa Gomes, A. A. H. Pádua, L. P. N. Rebelo, J. N. Canongia Lopes, *J. Mol. Struct. : THEOCHEM* **2010**, *946*, 70–76
[7] A. Triolo, O. Russina, H.-J. Bleif, E. Di Cola, *J. Phys. Chem. B* **2007**, *111*, 4641–4644.
[8] O. Russina, A. Triolo, L. Gontrani, R. Caminiti, D. Xiao, L. G. Hines Jr, R. A. Bartsch, E. L. Quitevis, N. Pleckhova, K. R. Seddon, *J. Phys.: Condens. Matter* **2009**, *21*, 424121.
[9] A. Triolo, O. Russina, B. Fazio, G. B. Appetecchi, M. Carewska, S. Passerini, *J. Chem. Phys.* **2009**, *130*, 164521.
[10] C. Hardacre, J. D. Holbrey, S. E. J. McMath, D. T. Bowron, A. K. Soper, *J. Chem. Phys.* **2003**, *118*, 273–279.
[11] C. Hardacre, S. E. J. McMath, M. Nieuwenhuyzen, D. T. Bowron, A. K. Soper, *J. Phys.: Condens. Matter* **2003**, *15*, S159–S166.
[12] A. Triolo, A. Mandanici, O. Russina, V. Rodriguez-Mora, M. Cutroni, C. Hardacre, M. Nieuwenhuyzen, H.-J. Bleif, L. Keller, M. A. Ramos, *J. Phys. Chem. B* **2006**, *110*, 21357–21364.
[13] K. Fujii, Y. Soejima, Y. Kyoshoin, S. Fukuda, R. Kanzaki, Y. Umebayahi, T. Yamaguchi, S.-I. Ishiguro, T. Takamuku, *J. Phys. Chem. B* **2008**, *112*, 4329–4336.
[14] C. M. Burba, J. Janzen, E. D. Butson, G. L. Coltrain, *J. Phys. Chem. B* **2013**, *117*, 8814–8820.
[15] A. Triolo, O. Russina, H.-J. Bleif, E. Di Cola, *J. Phys. Chem. B* **2007**, *111*, 4641–4644.
[16] O. Russina, A. Triolo, L. Gontrani, *R. Caminiti, J. Phys. Chem. Lett.* **2012**, *3*, 27–33.
[17] K. N. Marsh, A. Deer, A. C-T. Wu, Emma Tran, A. Klamt, *Korean J. Chem. Eng.* **2002**, *19*, 357–362.
[18] S. Zhang, N. Sun, X. He, X. Lu, X. Zhang, *J. Phys. Chem. Ref. Data* **2006**, *35*, 1475–1517.
[19] J. M. S. S. Esperança, J. N. Canongia Lopes, M. Tariq, L. M. N. B. F. Santos, J. W. Magee, L. P. N. Rebelo, *J. Chem. Eng. Data* **2010**, *55*, 3–12.
[20] H. Liu, E. Maginn, A. E. Visser, J. Bridges, E. B. Fox, *Ind. Eng. Chem. Res.* **2012**, *51*, 7242−7254.
[21] R. G. Seoane, S. Corderí, E. Gómez, N. Calvas, E. J. González, E. A. Macedo, Á. Domínguez, *Ind. Eng. Chem. Res.* **2012**, *51*, 2492−2504.
[22] S. Aparicio, M. Atilhan, F. Karadas, *Ind. Eng. Chem. Res.* **2010**, *49*, 9580–9595.
[23] Y. U. Paulechka, *J. Phys. Chem. Ref. Data* **2010**, *39*, 033108.
[24] P. J. Carvalho, I. Khan, A. Morais, J. F. O. Granjo, N. M. C. Oliveira, L. M. N. B. F. L. Santos, J. A. P. Coutinho, *Fluid Phase Equilib.* **2013**, *354*, 156–165.
[25] S. Stevanovic, M. F. Costa Gomes, *J. Chem. Thermodyn.* **2013**, *59*, 65–71.
[26] W. Zheng, A. Mohammed, L. G. Hines, Jr., D. Xiao, O. J. Martinez, R. A. Bartsch, S. L. Simon, O. Russina, A. Triolo, E. L. Quitevis, *J. Phys. Chem. B* **2011**, *115*, 6572–6584.
[27] D. Rooney, J. Jacquemin, R. Gardas, *Top. Curr. Chem.* **2010**, *290*, 185-212.
[28] J. A. P. Coutinho, P. J. Carvalho, M. C. Oliveira, *RSC Adv.* **2012**, *2*, 7322–7346.
[29] R. Gardas, J. A. P. Coutinho, *Fluid Phase Equilib.* **2008**, *266*, 195–201.
[30] A.-L. Revelli, F. Mutelet, J.-N. Jaubert, *Ind. Eng. Chem. Res.* **2010**, *49*, 3883–3892.
[31] R. Gardas, J. A. P. Coutinho, *AIChE J.* **2009**, *55*, 1274–1290.
[32] M. J. Earle, J. M. S. S. Esperança, M. A. Gilea, J. N. C. Lopes, L. P. N. Rebelo, J. W. Magee, K. R. Seddon, J. A. Widegren, *Nature* **2006**, *439*, 831–834.
[33] Y. U. Paulechka, D. H. Zaitsau, G. J. Kabo, A. A. Strechan, *Thermochim. Acta* **2005**, *439*, 158–160.
[34] D. H. Zaitsau, G. J. Kabo, A. A. Strechan, Y. U. Paulechka, A. Tschersich, S. P. Verevkin, A. Heintz, *J. Phys. Chem. A* 2006, *110*, 7303–7306.
[35] L. M. N. B. F. Santos, J. N. C. Lopes, J. A. P. Coutinho, J. M. S. S. Esperança, L. R. Gomes, I. M. Marrucho, L. P. N. Rebelo, *J. Am. Chem. Soc.* **2007**, *129*, 284–285.
[36] D. Strasser, F. Goulay, M. S. Kelkar, E. J. Maginn, S. R. Leone, *J. Phys. Chem. A* **2007**, *111*, 3191–3195.
[37] V. N. Emel'yanenko, S. P. Verevkin, A. Heintz, J.-A. Corfield, A. Deyko, K. R. J. Lovelock, P. Licence, R. G. Jones, *J. Phys. Chem. B* **2008**, *112*, 11734–11742.
[38] J. P. Armstrong, C. Hurst, R. G. Jones, P. Licence, K. R. J. Lovelock, C. J. Satterley, I. J. Villar-Garcia, *Phys. Chem. Chem. Phys.* **2007**, *9*, 982–990.
[39] K. R. J. Lovelock, A. Deyko, J.-A. Corfield, P. N. Gooden, P. Licence, R. G. Jones, *ChemPhysChem* **2009**, *10*, 337–340.
[40] J. P. Leal, M. E. M. Piedade, J. N. C. Lopes, A. A. Tomaszowska, J. M. S. S. Esperança, L. P. N. Rebelo, K. R. Seddon, *J. Phys. Chem. B* **2009**, *113*, 3491–3498.
[41] J. P. Leal, J. M. S. S. Esperança, M. E. M. Piedade, J. N. C. Lopes, L. P. N. Rebelo, K. R. Seddon, *J. Phys. Chem. A* **2007**, *111*, 6176–6182.
[42] S. D. Chambreau, G. L. Vaghjiani, A. To, C. Koh, D. Strasser, O. Kostko, S. R. Leone, *J. Phys. Chem. B* **2010**, *114*, 1361–1367.
[43] A. Deyko, K. R. J. Lovelock, J.-A. Corfield, A. W. Taylor, P. N. Gooden, I. J. Villar-Garcia, P. Licence, R. G. Jones, V. G. Krasovskiy, E. A. Chernikova, L. M. Kustov, *Phys. Chem. Chem. Phys.* **2009**, *11*, 8544–8555.
[44] S. P. Verevkin, D. H. Zaitsau, V. N. Emel'yanenko, R. V. Ralys, A. V. Yermalayeu, C. Schick, *J. Chem. Thermodyn.* **2012**, *54*, 433–437.
[45] K. Fumino, A. Wulf, S. P. Verevkin, A. Heintz, R. Ludwig, *ChemPhysChem* **2010**, *11*, 1623–1626.
[46] C. Wang, H. Luo, H. Li, S. Dai, *Phys. Chem. Chem. Phys.* **2010**, *12*, 7246–7250.
[47] A. Deyko, S. G. Hessey, P. Licence, E. A. Chernikova, V. G. Krasovskiy, L. M. Kustov, R. G. Jones, *Phys. Chem. Chem. Phys.* **2012**, *14*, 3181–3193.
[48] S. P. Verevkin, R. V. Ralys, D. H. Zaitsau, V. N. Emel'yanenko, C. Schick, *Thermochim. Acta* **2012**, *538*, 55–62.
[49] D. H. Zaitsau, A. V. Yermalayeu, V. N. Emel'yanenko, S. P. Verevkin, U. Welz-Biermann, T. Schubert, *Sci. China Chem.* **2012**, *55*, 1525–1531.

[50] T. Köddermann, D. Paschek, R. Ludwig, *ChemPhysChem* **2008**, *9*, 549–555.
[51] R. Ludwig, *Phys. Chem. Chem. Phys.* **2008**, *10*, 4333–4339.
[52] F. Dommert, K. Wendler, R. Berger, L. Delle Site, C. Holm, *ChemPhysChem* **2012**, *13*, 1625–1637.
[53] M. A. A. Rocha, C. F. R. A. C. Lima, L. R. Gomes, B. Schröder, J. A. P. Coutinho, I. M. Marrucho, J. M. S. S. Esperança, L. P. N. Rebelo, K. Shimizu, J. N. C. Lopes, L. M. N. B. F. Santos, *J. Phys. Chem. B* **2011**, *115*, 10919−10926.
[54] M. A. A. Rocha, J. A. P. Coutinho, L. M. N. B. F. Santos, *J. Phys. Chem. B* **2012**, *116*, 10922−10927.
[55] M. A. A. Rocha, J. A. P. Coutinho, L. M. N. B. F. Santos, Manuscript (Paper VIII).
[56] M. A. A. Rocha, L. M. N. B. F. Santos, *Chem. Phys. Lett.* **2013**, 585, 59-62.
[57] M. A. A. Rocha, F. M. S. Ribeiro, B. Schröder, J. A. P. Coutinho, L. M. N. B. F. Santos, *J. Chem. Thermodyn.* **2013**, doi: 10.1016/j.jct.2013.09.020.
[58] L. M. N. B. F. Santos, L. M. S. S. Lima, C. F. R. A. C. Lima, F. D. Magalhães, M. C. Torres, B. Schröder, M. A. V. Ribeiro da Silva, *J. Chem. Thermodyn.* **2011**, *43*, 834–843.
[59] M. B. Oliveira, F. Llovell, J. A. P. Coutinho, L. F. Vega, *J. Phys. Chem. B* **2012**, *116*, 9089–9100.
[60] C. Cadena, Q. Zhao, R. Q. Snurr, E. J.Maginn, *J. Phys. Chem. B* **2006**, *110*, 2821−2832
[61] J. M. Crosthwaite, M. J. Muldoon, J. K. Dixon, J. L. Anderson, J. F. Brennecke, *J. Chem. Thermodyn.* **2005**, *37*, 559−568.
[62] H. Gao, M. Luo, J. Xing, Y. Wu, Y. Li, W. Li, Q. Liu, H. Liu, *Ind. Eng. Chem. Res.* **2008**, *47*, 8384−8388.
[63] P. Verdía, E. J. González, B. Rodríguez-Cabo, E. Tojo, *Green Chem.* **2011**, *13*, 2768-2776.
[64] A. M. Fernandes, M. A. A. Rocha, M. G. Freire, I. M. Marrucho, J. A. P. Coutinho, L. M. N. B. F. Santos, *J. Phys. Chem. B* **2011**, *115*, 4033–4041.
[65] M. García-Mardones, I. Bandrés, M. C. López, I. Gascón, C. Lafuente, *J. Solution Chem.* **2012**, *41*, 1836–1852.
[66] W. Xu, L.-M. Wang, R. A. Nieman, C. A. Angell, *J. Phys. Chem. B* **2003**, *107*, 11749–11756.
[67] Y. Yoshida, O. Baba, G. Saito, *J. Phys. Chem. B* **2007**, *111*, 4742–4749.
[68] M. A. A. Rocha, *Thermophysical Study of Ionic Liquids*, Ph.D. Thesis, University of Porto, 2013.
[69] E. C. W. Clarke, D. N. Glew, *Trans. Faraday Soc.* **1966**, *62*, 539−547.
[70] P. J. Mohr, B. N. Taylor, D. B. Newell, *Rev. Mod. Phys.* **2012**, *84*, 1527−1605.
[71] D. H. Zaitsau, A. V. Yermalayeu, V. N. Emel'yanenko, A. Heintz, S. P. Verevkin, C. Schick, S. Berdzinski, V. Strehmel, *J. Mol. Liq.* **2013**, doi: 10.1016/j.molliq.2013.07.018
[72] K. Růžička, V. Majer, *J. Phys. Chem. Ref. Data* **1994**, *23*, 1 – 39.
[73] D. Matulis, *Biophysical Chemistry* **2001**, *93*, 67 – 82.
[74] J. S. Chickos, W. Hanshaw, *J. Chem. Eng. Data* **2004**, *49*, 77 – 85.
[75] C. Smit, M. W. Fraaije, A. J. Minnaard, *J. Org. Chem.* **2008**, *73*, 9482–9485.
[76] X. Chen, C. E. Goodhue, J-Q Yu, *J. Am. Chem. Soc.* **2006**, *128*, 12634–12635.
[77] K. Tamao, S. Kodama, I. Nakajima, M. Kumad, *Tetrahedron* **1982**, *38*, 3347–3354.
[78] L. Benli, G. Lianquan, *Huazhong Shifan Daxue Xuebao, Ziran Kexueban* **1989**, *23*, 51–53.
[79] J. W. Tilley, S. Zawoiski, *J. Org. Chem.* **1988**, *53*, 386–390.
[80] Z. Jia-Liang, S. Yi-Lin, C. Yu-Hui, C. I.-Chia, L. Chuan-Chen, *Heterocycles* **2009**, *78*, 369–387.
[81] I. Kondolff, H. Doucet, M. Santelli, *Tetrahedron* **2004**, *60*, 3813–3818.
[82] M. E. Wieser, M. Berglund, *Pure Appl. Chem.* **2009**, *81*, 2131–2156.

Received: ((will be filled in by the editorial staff))
Revised: ((will be filled in by the editorial staff))
Published online: ((will be filled in by the editorial staff))

Novel 1-Ethyl-2-Alkylpyridinium based Ionic Liquids: Synthesis and Volatility

Miguel Vilas [b], Marisa A. A. Rocha[a], Emilia Tojo*[b], Luís M. N. B. F. Santos*[a]

[a] CIQ, Departamento de Química e Bioquímica, Faculdade de Ciências da Universidade do Porto
R. Campo Alegre 687, P-4169-007, Porto, Portugal
Fax: (+351)220402520
E-mail: lbsantos@fc.up.pt

[b] Department of Organic Chemistry, University of Vigo, Faculty of Chemistry,
Marcosende, 36210 Vigo (Pontevedra), Spain
Fax: (+34)986812262
E-mail: etojo@uvigo.es

Supporting Information

Volatility of new 1-ethyl-2-alkylpyridinium ionic liquids

Table S1. Experimental vapor pressures for the nine pyridinium based ILs, obtained by the quartz crystal microbalance Knudsen effusion apparatus.

T / K	p / Pa	Δp / Pa	T / K	p / Pa	Δp / Pa
		$[^2C_2{}^1C_2Py][NTf_2]$			
493.11	0.0414	-0.0083	513.10	0.1348	-0.0003
498.41	0.0560	0.0159	518.10	0.1784	-0.0006
503.11	0.0759	-0.0058	523.10	0.2343	0.0005
508.10	0.1013	-0.0014			
		$[^2C_3{}^1C_2Py][NTf_2]$			
498.10	0.0584	0.0003	513.08	0.1369	0.0045
503.09	0.0781	0.0017	518.08	0.1806	-0.0001
508.09	0.1047	-0.0057	523.08	0.2358	-0.0006
		$[^2C_4{}^1C_2Py][NTf_2]$			
493.14	0.0461	-0.0016	508.13	0.1111	0.0003
498.14	0.0622	0.0000	513.10	0.1471	-0.0018
503.14	0.0832	0.0031			
		$[^2C_5{}^1C_2Py][NTf_2]$			
498.14	0.0620	-0.0040	513.15	0.1527	0.0034
503.16	0.0844	-0.0014	518.15	0.2029	0.0077
508.14	0.1135	0.0040	523.13	0.2735	-0.0096
		$[^2C_6{}^1C_2Py][NTf_2]$			
493.15	0.0453	-0.0021	508.15	0.1145	-0.0023
498.16	0.0620	0.0009	513.16	0.1530	0.0025
503.17	0.0843	0.0030	518.14	0.2048	-0.0021
		$[^2C_7{}^1C_2Py][NTf_2]$			
498.29	0.0505	-0.0093	513.24	0.1255	0.0058
503.25	0.0682	0.0046	518.24	0.1714	-0.0102
508.25	0.0925	0.0090			
		$[^2C_8{}^1C_2Py][NTf_2]$			
493.42	0.0267	-0.0082	508.06	0.0699	0.0076
498.43	0.0370	0.0079	513.03	0.0963	0.0043
503.07	0.0510	-0.0031	518.03	0.1332	-0.0085

$\Delta p = p - p_{calc}$, where p_{calc} is calculated from the Clarke and Glew equation (eq. 6) with the parameters given in Table 2.

Thermodynamic properties of vaporization

The graphic representations of the standard molar enthalpies, entropies and Gibbs energies of vaporization at reference temperature, T = 298.15K, as a function of the total number of carbon atoms in the two alkyl side chains of the cation, N, are presented in figures S1 − S6.

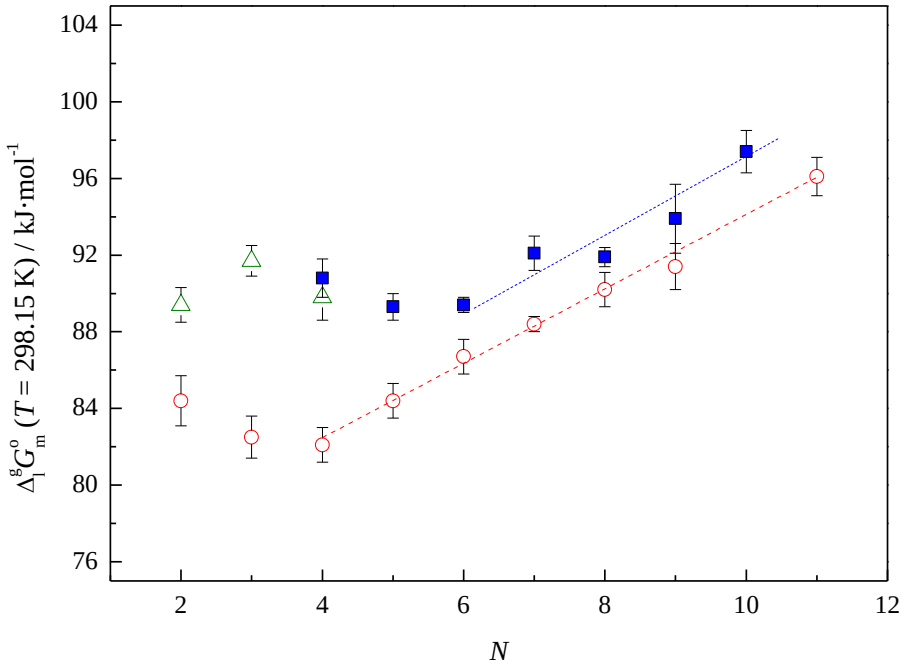

Figure S1. Standard (p^o=10^5 Pa) molar Gibbs energy of vaporization $\Delta_l^g G_m^o$ (T = 298.15K) as a function of the total number of carbons in the alkyl side chains of the cation, N. ○ - [$C_{N-1}C_1$im][NTf_2] [1,2] (N = 2 - 9, 11, 13); △ - [C_NPy][NTf_2] [3] (N = 2 - 4); ■ - [$^2C_{N-2}{}^1C_2$Py][NTf_2] (N = 4 - 10).

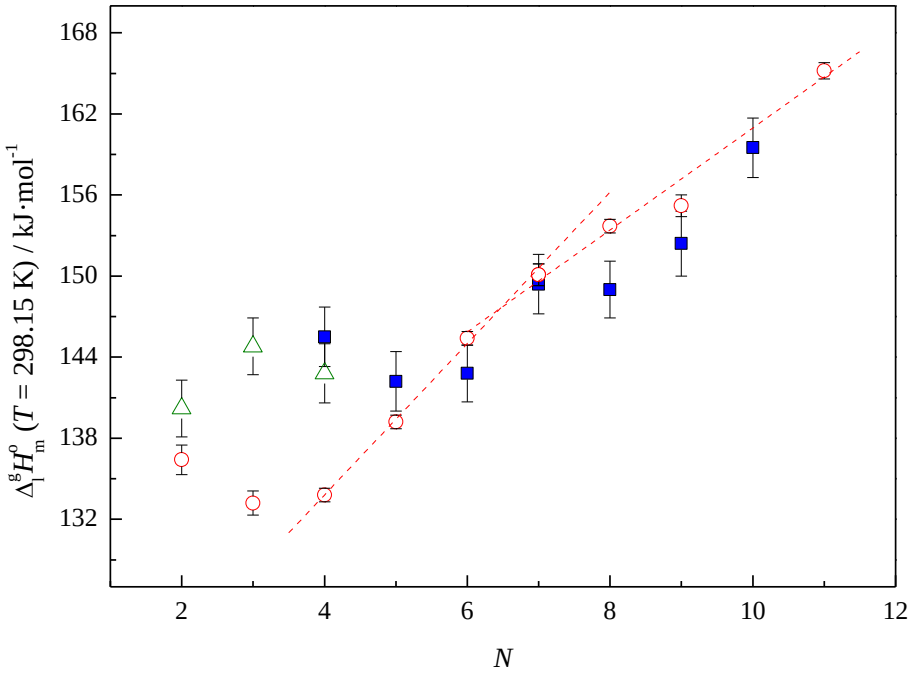

Figure S2. Standard (p^o=10^5 Pa) molar enthalpies of vaporization $\Delta_l^g H_m^o$ (T = 298.15 K) as a function of the total number of carbons in the alkyl side chains of the cation, *N*. ○ - [$C_{N-1}C_1$im][NTf_2] [1,2] (N = 2 - 9, 11, 13); △ - [C_NPy][NTf_2] [3] (N = 2 - 4); ■ - [$^2C_{N-2}{}^1C_2$Py][NTf_2] (N = 4 - 10).

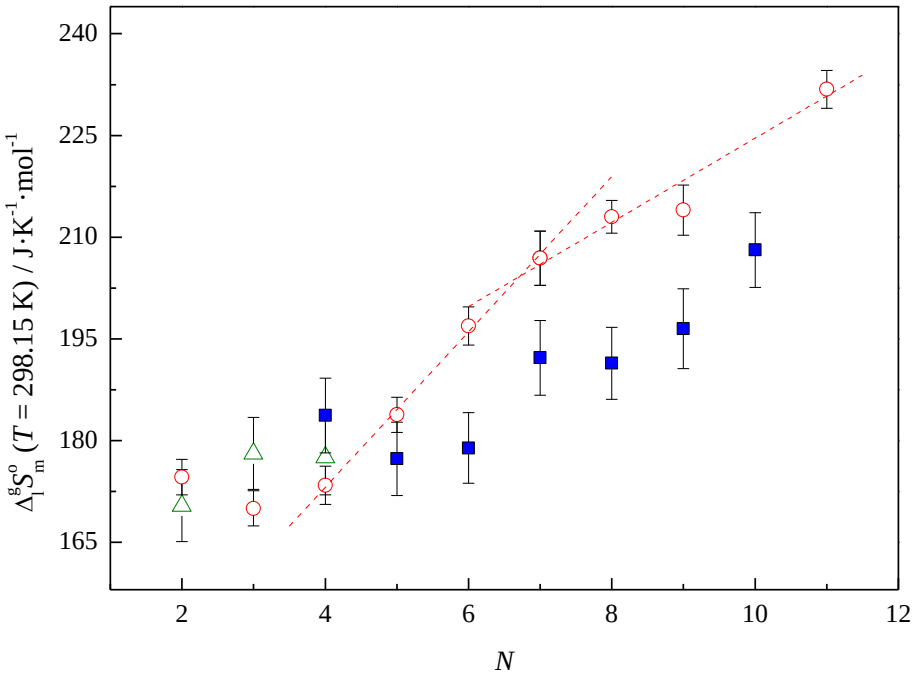

Figure S3. Standard (p^o=10^5 Pa) molar entropies of vaporization $\Delta_l^g S_m^o$ (T = 298.15 K) as a function of the total number of carbons in the alkyl side chains of the cation, *N*. ○ - [$C_{N-1}C_1$im][NTf_2] [1,2] (N = 2 - 9, 11, 13); △ - [C_NPy][NTf_2] [3] (N = 2 - 4); ■ - [$^2C_{N-2}{}^1C_2$Py][NTf_2] (N = 4 - 10).

References

[1] M. A. A. Rocha, C. F. R. A. C. Lima, L. R. Gomes, B. Schröder, J. A. P. Coutinho, I. M. Marrucho, J. M. S. S. Esperança, L. P. N. Rebelo, K. Shimizu, J. N. Canongia Lopes, L. M. N. B. F. Santos, J. Phys. Chem. B **2011**, 115, 10919.

[2] M. A. A. Rocha, F. M. S. Ribeiro, B. Schröder, J. A. P. Coutinho, L. M. N. B. F. Santos, *J. Chem. Thermodyn.* **2013**, accepted.

[3] M. A. A. Rocha, L. M. N. B. F. Santos, *Chem. Phys. Lett.* **2013**, doi: 10.1016/j.cplett.2013.08.095.

Paper XIII

"Thermophysical Properties of a Novel Pyridinium Based Ionic Liquids Family"
Marisa A. A. Rocha, Miguel Vilas, Ana S. M. C. Rodrigues, Emilia Tojo, Luís M. N. B. F. Santos
Manuscript version

Note: The author of this thesis performed part of the viscosity and density measurements and heat capacity measurements of the ionic liquids, data analysis and contribute to the discussion and conclusions.

Thermophysical Properties of a Novel Pyridinium Based Ionic Liquid Family

Marisa A. A. Rocha[1], *Miguel Vilas* [2], *Ana S. M. C. Rodrigues*[1], *Emilia Tojo* [2*],

Luís M. N. B. F. Santos[1*]

[1]Centro de Investigação em Química, Departamento de Química e Bioquímica, Faculdade de Ciências da Universidade do Porto, R. Campo Alegre 687, P-4169-007, Porto, Portugal

[2] Department of Organic Chemistry, Faculty of Chemistry of the University of Vigo, Marcosende, 36310, Vigo, Spain

*Corresponding author

Tel: +351 220 402 836. Fax:+351 220 402 659; E-mail address: Luís Santos (lbsantos@fc.up.pt); Emilia Tojo (etojo@uvigo.es)

ABSTRACT

In this work, the dependence of the heat capacities, at T = 298.15 K, as well as, the temperature dependencies of density and viscosity, all as a function of the alkyl chain length in the position 2 of the core 1-ethylpyridinium cation, is explored. Densities and viscosities and their dependence on temperature were measured for the 1-ethyl-2-alkylpyridinium bis(trifluoromethanesulfonyl)imide, $[^2C_{N-2}{}^1C_2Py][NTf_2]$ (N=4, 5, 6, 7, 8, 9, 10) ionic liquid series. Based on the previous results, the molar volume, thermal expansion coefficients, VTF parameters, as well as, the energy barrier related to the fluid shear stress at T = 298.15 K, were derived. High precision heat capacities, at T = 298.15 K, were measured using a heat capacity drop calorimeter. A trend shift on the thermophysical properties, which presents a clear indication that in the pyridinium based ionic liquids the nanostructuration starts at $[^2C_5{}^1C_2Py][NTf_2]$ was found, in agreement with the previously studied alkylimidazolium ionic liquids series. The observed trend shift in the viscosity and in the heat capacities of the pyridinium ionic liquids is more pronounced in the pyridinium than in the imidazolium ionic liquids series. This work confirms and is an additional support, for the understanding of the trend shift in the thermophysical properties of ionic liquids, as well as, to the molecular understanding of the relation between the structural organization of the ionic liquids, their physico-chemical properties, tuning, design and application potential.

KEYWORDS: Density; ionic liquids; thermodynamics;; viscosity; VTF; Vogel-Tammann-Fulcher; thermal expansion coefficients.

INTRODUCTION

The possible tuning of thermophysical properties by varying the nature of the anions and cations is one of the many advantages of ionic liquids, which contributes to a design of "greener" ionic liquids for a specific application. In order to benefit from this characteristic of ionic liquids, highly accurate data regarding their thermophysical properties is needed and essential to a deep understanding of ionic liquids on a molecular level, as well as for the application support and process optimization involving ionic liquids. Most of the experimental and modeling work to date has been focused on the imidazolium based ionic liquids.[1]

As it is well known, the ionic liquids presents a short range organization, in order to sustain electroneutrality and to enhance the electrostatic interactions.[2–4] Additionally these systems are regarded as nanostructurated liquids due to the complex structure with high charge density regions and low charge density.[2–4] The molecular understanding of nanostructuration of ionic liquids is of great interest due to their intrinsic relation with most of the physico-chemical properties, such as heat capacities [5–7], densities and viscosities[6,8–11], vapor pressures[12–16], vaporization properties[17–19], among others. The knowledge of the physico-chemical properties and their relation with the nanostructuration of ionic liquids has high importance, due to the fact that it could be helpful in the design of new ionic liquids, and consequently, in their use in industrial applications.[20–26]

The present work is part of a wider project concerning the understanding of the effect of nanostructuration of ionic liquids on their thermophysical properties. In previous works, the effect of the alkyl side chain length[8,12,14,27], together with the

evaluation of the symmetry effect[5,8,13,14] on thermophysical properties, have been explored for the imidazolium bistriflamide based ionic liquids. The effect of the chemical nature of the anion, sphericity and size, as well as the overall impact of the nanostructuration on the trend on the thermophysical properties of ionic liquids, was recently explored.[6] Based on these works, it was possible to give a thermodynamic view of the nanostructuration of ionic liquids.[2–4,28]

In this work, the thermophysical properties of 1-ethyl-2-alkylpyridinium bis(trifluoromethanesulfonyl)imide (figure 1), $[^2C_{N-2}{}^1C_2Py][NTf_2]$ (N=4, 5, 6, 7, 8, 9, 10), in particular the density and viscosity, and their dependency with temperature, and heat capacities at a constant temperature, were measured. To our knowledge, this is the first thermophysical study reported in the literature for the considered ionic liquids. García-Mardones *et al.*[7] reported the thermophysical data for the $[^2C_1{}^1C_2Py][NTf_2]$, which will be considered along this work. The effect of the cation, size and structure will be evaluated based on a comparative analysis with the $[C_{N-1}C_1im][NTf_2]$ ionic liquid series.[8,27,29]

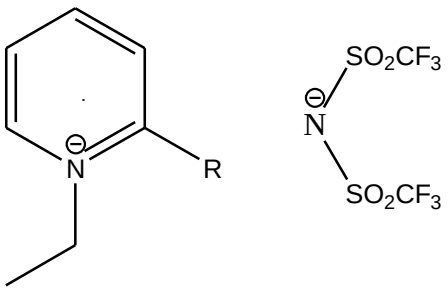

Figure 1. Schematic representation of the studied ionic liquids, $[^2C_{N-2}{}^1C_2Py][NTf_2]$. R = $C_{(N-2)}H_{(2N-3)}$, where N = 4, 5, 6, 7, 8, 9, 10.

EXPERIMENTAL SECTION

Synthesis, Purification, and Characterization of Ionic liquids. The ionic liquids used in this work, 1-ethyl-2-alkylpyridinium bis(trifluoromethanesulfonyl)imides, $[^2C_{N-2}{}^1C_2Py][NTf_2]$ (N = 4, 5, 6, 7, 8, 9, 10), were synthesized, purified and characterized at University of Vigo, following reported procedures.[30,31] The ionic liquids samples were characterized by ^{1}H-NMR, ^{13}C-NMR and ESI-HRMS, and the purity of the samples was found to be 99%. All the ionic liquids were dried under reduced pressure (< 10 Pa) and stirred constantly for a minimum at 323 K, in order to reduce the presence of water or other volatile contents. This process was performed systematically before and during the thermophysical properties measurements.

Densities and viscosities. The density and viscosity of all pure ionic liquids, at atmospheric pressure and a temperature range from (293.15 to 363.15)K, were measured using an automated Anton Paar rotational Stabinger viscometer-densimeter, SVM 3000, as described in the literature.[32] The SVM 3000 uses an integrated Peltier element for fast and efficient thermostability where the uncertainty in temperature is within ± 0.02 K, and the small sample volume allows extremely quick temperature changes and very short equilibrium times. The apparatus was calibrated by measuring the viscosity/density of three standard calibration samples, APN7.5, APN26 and APN415 in steps of 5 K in the temperature range from 293.15 to 393.15 K. The reproducibility of the dynamic viscosity and density measurements is according to the manufacturer, 0.35 % and ± 0.5 kg·m^{-3} uncertainty respectively, from 288.15 K to 378.15 K.

Heat Capacities. The heat capacities of the $[^2C_{N-2}{}^1C_2Py][NTf_2]$ (N = 4, 5, 6, 7, 8, 9, 10) ionic liquid series, were measured, at T = 298.15 K, with a high-precision heat capacity drop calorimeter, which is described in detail in the literature.[33–35] The heat capacity drop calorimeter apparatus comprises two main parts: the furnace and the calorimetric receiving block. The furnace is maintained at a constant temperature T = 303.15K, and the receiving calorimeter is kept at T = 293.15 K. The ampoules were weighted in a Mettler Toledo AG245 dual range analytical balance (readability of 0.00001 g and repeatability of ±0.00002 g) both empty and after filling with the ionic liquid. The single-drop mode (no reference ampoule was used) with blank correction that were measured independently using empty ampoules methodology was used. The calorimeter was calibrated with water and sapphire (α-Al_2O_3), using the respective standard molar heat capacities at 298.15 K reported in literature, $C^{o}_{p,m}(H_2O)$ = (75.32 ± 0.01) $J{\cdot}K^{-1}{\cdot}mol^{-1}$ and $C^{o}_{p,m}$ (α-aluminum oxide) = (79.03 ± 0.08) $J{\cdot}K^{-1}{\cdot}mol^{-1}$.[36] The calibration constant was found to be ε = (6.6040 ± 0.0036) $W{\cdot}V^{-1}$. The buoyancy effect correction was considered both for the calibration and experiments of the ionic liquids. Since the calorimeter was used to measure the heat capacity of ionic liquids, the accuracy was checked on the basis of the results obtained for $[C_6C_1im][NTf_2]$. The determined $C^{o}_{p,m}$ ($[C_6C_1im][NTf_2]$, 298.15 K) = (629.24 ± 0.43) $J{\cdot}K^{-1}{\cdot}mol^{-1}$ was obtained from the average of two independent experiments, using different ampoules, and is in excellent agreement with the recommended value, $C^{o}_{p,m}$ ($[C_6C_1im][NTf_2]$, 298.15 K) = (631.6 ± 1.3) $J{\cdot}K^{-1}{\cdot}mol^{-1}$.[37] The relative atomic masses used were those recommended by the IUPAC report 2007.[38] All the uncertainties are given as twice as the standard deviation of the mean, and include the calibration uncertainty.

RESULTS AND DISCUSSION

The thermophysical data obtained in this work, together with the data found for $[^2C_1{}^1C_2Py][NTf_2]$ reported by García-Mardones *et al.*[7], are compared with the available literature data for the $[C_{N-1}C_1im][NTf_2]$ ionic liquid series [8,27,29], in order to get better understanding of the effect of changing the cation on the studied thermophysical properties. The dependence of the heat capacities, at T = 298.15 K, as well as, the temperature dependencies of density and viscosity, all as a function of the alkyl chain length in the position 2 of the core 1-ethylpyridinium cation, is explored.

Density. The experimental density data determined, at atmospheric pressure, in the temperature range from (293.15 to 363.15) K, are listed in table 1. The graphic representation of $\ln(\rho / \text{kg}\cdot\text{m}^{-3}) = f(T/\text{K})$ is depicted in figure 2.

Table 1. Experimental density results at p^o = 0.1 MPa, ρ, for the $[^2C_{N-2}{}^1C_2Py][NTf_2]$ ionic liquid series as a function of temperature.

T / K	ρ / kg·m^{-3}						
	$[^2C_2{}^1C_2Py][NTf_2]$	$[^2C_3{}^1C_2Py][NTf_2]$	$[^2C_4{}^1C_2Py][NTf_2]$	$[^2C_5{}^1C_2Py][NTf_2]$	$[^2C_6{}^1C_2Py][NTf_2]$	$[^2C_7{}^1C_2Py][NTf_2]$	$[^2C_8{}^1C_2Py][NTf_2]$
293.15	1475.5	1452.0	1413.7	1375.6	1348.7	1325.1	1301.7
298.15	1470.6	1447.2	1409.1	1371.1	1344.3	1320.8	1297.4
303.15	1465.8	1442.5	1404.5	1366.6	1339.9	1316.5	1293.2
308.15	1461.1	1437.8	1400.0	1362.2	1335.5	1312.2	1289.0
313.15	1456.3	1433.1	1395.4	1357.8	1331.2	1307.9	1284.8
318.15	1451.6	1428.4	1390.9	1353.4	1326.8	1303.6	1280.6
323.15	1446.9	1423.8	1386.4	1349.0	1322.5	1299.4	1276.4
328.15	1442.2	1419.2	1381.9	1344.6	1318.2	1295.2	1272.3
333.15	1437.5	1414.6	1377.4	1340.2	1313.9	1290.9	1268.1
338.15	1432.9	1410.0	1373.0	1335.8	1309.7	1286.7	1264.0
343.15	1428.3	1405.4	1368.5	1331.5	1305.6	1282.5	1259.9
348.15	1423.7	1400.9	1364.1	1327.1	1301.4	1278.3	1255.8
353.15	1419.1	1396.4	1359.7	1322.8	1297.1	1274.2	1251.7
358.15	1414.6	1391.9	1355.4	1318.6	1292.9	1270.1	1247.6
363.15	1410.0	1387.5	1351.0	1314.3	1288.8	1266.0	1243.6

The experimental density data, in the temperature range, is described using a second order polynomial equation correlation, according to equation (1),

$$\ln(\rho) = a + b.T + c.T^2 . \qquad (1)$$

Table 2 lists the fitting parameters of equation (1). The isobaric thermal expansion coefficients (α_p), which considers the volumetric changes with temperature, were calculated using equation (2),

$$\alpha_p = -\frac{1}{\rho}\left(\frac{\partial \rho}{\partial T}\right)_p = -\left(\frac{\partial \ln \rho}{\partial T}\right)_p, \qquad (2)$$

where ρ is the density, T is the temperature, and p is the pressure.

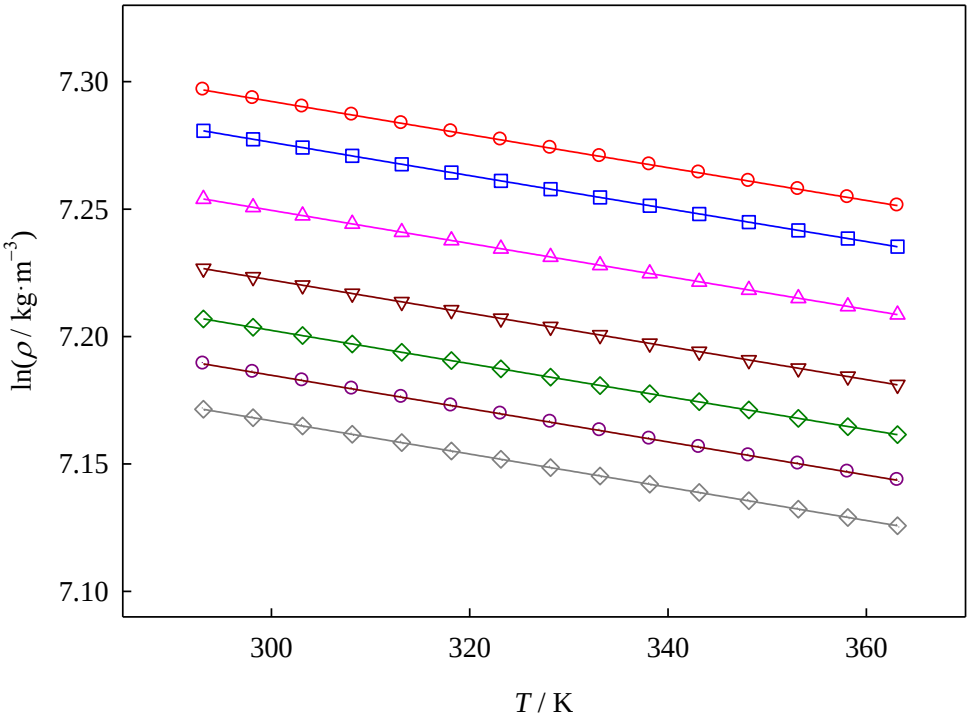

Figure 2. Logarithm of density as a function of temperature for $[^2C_{N\text{-}2}{}^1C_2Py][NTf_2]$ ionic liquid family. The thin lines results from the linear fitting of the experimental results. ○ - $[^2C_2{}^1C_2Py][NTf_2]$; □ - $[^2C_3{}^1C_2Py][NTf_2]$; △ - $[^2C_4{}^1C_2Py][NTf_2]$; ▽ - $[^2C_5{}^1C_2Py][NTf_2]$; ◇ - $[^2C_6{}^1C_2Py][NTf_2]$; ⊙ - $[^2C_7{}^1C_2Py][NTf_2]$; ◈ - $[^2C_8{}^1C_2Py][NTf_2]$.

Table 2. Fitting parameters of the equation, $\ln\left(\rho / \mathrm{kg \cdot m^{-3}}\right) = a + b.T + c.T^2$ for the studied ionic liquids.

Ionic Liquid	a	$10^4 \times b$ / K^{-1}	$10^7 \times c$ / K^{-2}
$[^2C_2{}^1C_2Py][NTf_2]$	7.4972 ± 0.0014	-7.127 ± 0.087	0.99 ± 0.13
$[^2C_3{}^1C_2Py][NTf_2]$	7.4827 ± 0.0013	-7.214 ± 0.078	0.11 ± 0.19
$[^2C_4{}^1C_2Py][NTf_2]$	7.4506 ± 0.0014	-6.888 ± 0.085	0.62 ± 0.13
$[^2C_5{}^1C_2Py][NTf_2]$	7.4180 ± 0.0021	-6.54 ± 0.13	0.40 ± 0.19
$[^2C_6{}^1C_2Py][NTf_2]$	7.4094 ± 0.0027	-7.25 ± 0.17	0.12 ± 0.25
$[^2C_7{}^1C_2Py][NTf_2]$	7.3857 ± 0.0019	-6.84 ± 0.12	0.48 ± 0.18
$[^2C_8{}^1C_2Py][NTf_2]$	7.3646 ± 0.0012	-6.644 ± 0.074	0.18 ± 0.11

From fitted coefficients (table 2), the temperature dependence of the isobaric thermal expansion coefficients (α_p) was derived from equation (3),

$$\alpha_p = -\left(\frac{\partial \ln \rho}{\partial T}\right)_p = -(b + 2c \cdot T) \qquad (3)$$

The molar mass, M , density, ρ, molar volumes ($V_m = M / \rho$) and the thermal expansion coefficients, α_p, at T = 298.15 K and p^o =0.1 MPa, of the studied ionic liquids are presented in table 3. The graphic representations of the density and molar volume at 298.15 K and 0.1 MPa, against the total number of carbon atoms in the alkyl side chains of the cation, N, are presented in figure 3.

Table 3. Molar mass, M, density, ρ, molar volume, V_m, and the derived thermal expansion coefficients, α_p, at T = 298.15 K and p^o = 0.1 MPa of the studied ionic liquids.

Ionic Liquid	M / g·mol^{-1}	ρ (298.15 K) / kg·m^{-3}	V_m (298.15 K) / cm^3·mol^{-1}	$10^4 \times \alpha_p$ (298.15 K) / K^{-1}
$[^2C_1{}^1C_2Py][NTf_2]$*	402.336	1505.7	267.21	6.40 ± 0.62
$[^2C_2{}^1C_2Py][NTf_2]$	416.362	1470.6	283.12	6.54 ± 0.12
$[^2C_3{}^1C_2Py][NTf_2]$	430.389	1447.2	297.39	6.56 ± 0.15
$[^2C_4{}^1C_2Py][NTf_2]$	444.416	1409.1	315.39	6.52 ± 0.12
$[^2C_5{}^1C_2Py][NTf_2]$	458.442	1371.1	334.36	6.52 ± 0.18
$[^2C_6{}^1C_2Py][NTf_2]$	472.469	1344.3	351.46	6.56 ± 0.23
$[^2C_7{}^1C_2Py][NTf_2]$	486.496	1320.8	368.33	6.55 ± 0.17
$[^2C_8{}^1C_2Py][NTf_2]$	500.522	1297.4	385.79	6.54 ± 0.10

*-derived from the data in reference 7

For the same total number of carbon atoms in the alkyl side chains of the cation, N, the pyridinium based ionic liquids present similar densities when compared with the imidazolium ionic liquids. It is interesting to observe that when changing a cation from a five (imidazolium) to a six membered ring (pyridinium), the contribution to the densities is maintained. However, considering the ionic liquids with similar molar masses (e.g. $[^2C_2{}^1C_2Py][NTf_2]$, M = 416 g·mol^{-1}, and $[C_4C_1im][NTf_2]$, M = 419 g·mol^{-1}), the pyridinium based ionic liquids exhibits higher densities than the imidazolium ionic liquids [8,29], related with a denser packing in the liquid phase for the pyridinium based ionic liquids. When representing the molar volume against the total number of carbons in the alkyl side chains of the cation, N, of the respective ionic liquid (figure 2(II)), reflecting the ions size, it can be observed that the pyridinium based ionic liquids display higher molar volume, related with the higher molar volume of the pyridinium than the imidazolium core.

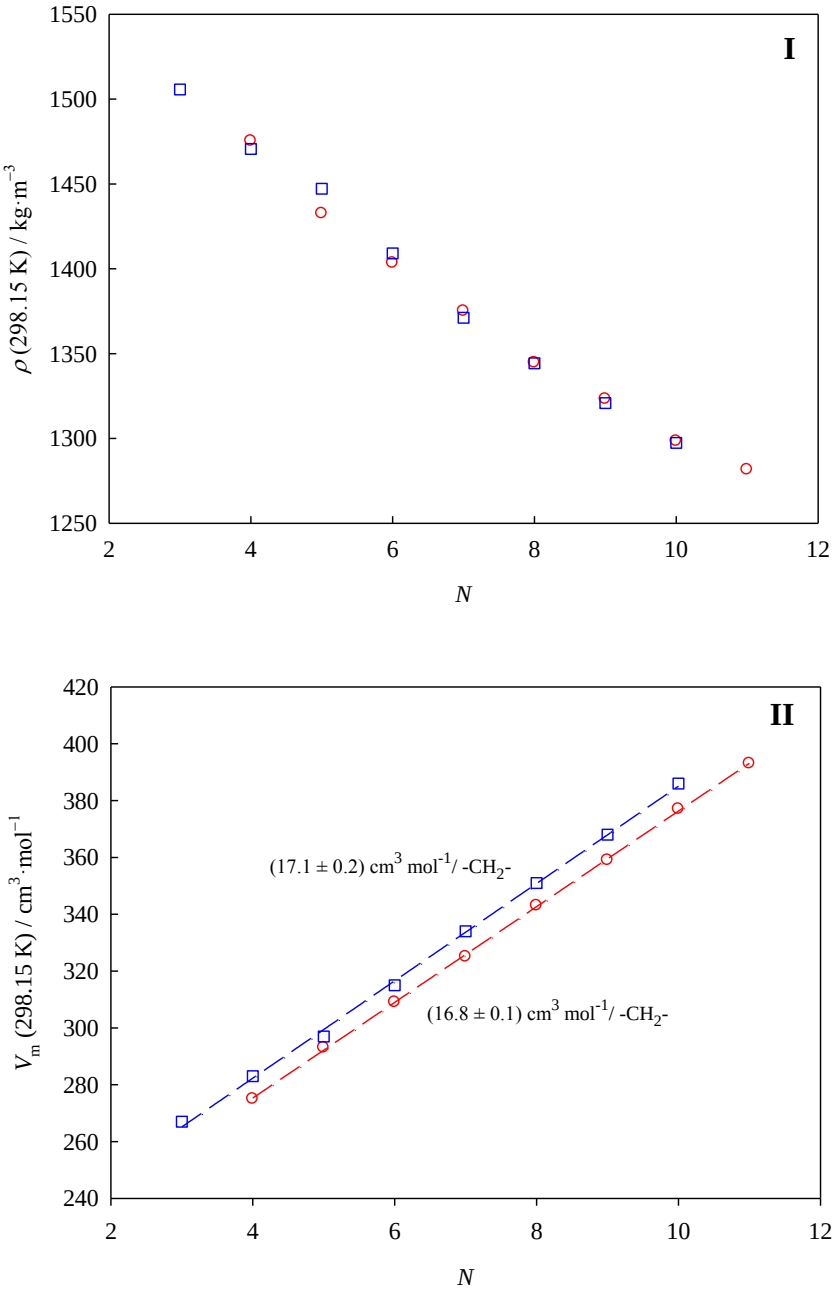

Figure 3. Graphic representation of the **(I)** density and **(II)** molar volume, at 298.15 K and p^{o} = 0.1MPa, as a function of the total number of carbon atoms in the alkyl side chains of the cation, *N*. ○ - [$C_{N-1}C_1$im][NTf_2][8,29] (N = 3 - 9, 11, 13); □ - [$^2C_{N-2}{}^1C_2$Py][NTf_2] (N = 4 - 10); [$^2C_1{}^1C_2$Py][NTf_2] [7].

The graphic representation of the thermal expansion coefficients at 298.15 K and 0.1 MPa, against the *N* of the ionic liquids, are presented in figure 4.

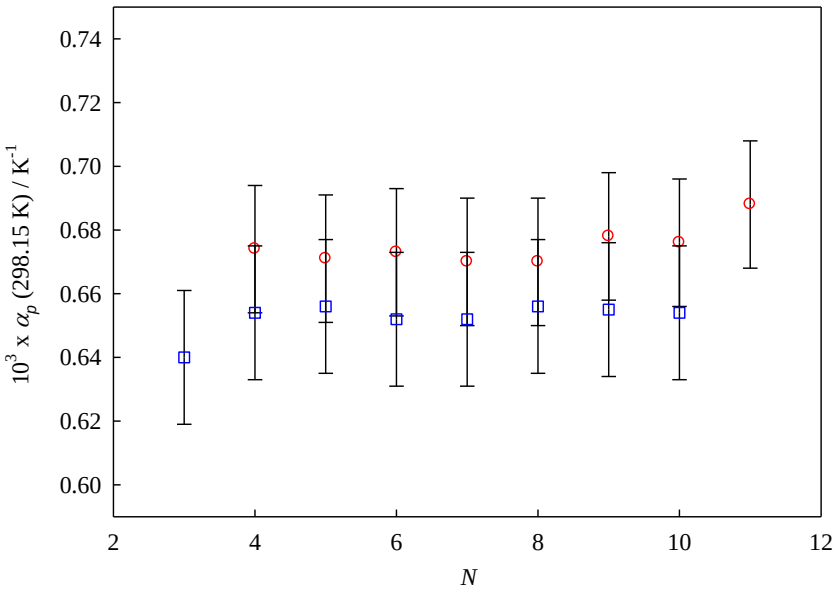

Figure 4. Graphic representation of the thermal expansion coefficients, at 298.15 K and p^o = 0.1MPa, as a function of the total number of carbon atoms in the alkyl side chains of the cation, *N*. ○ - $[C_{N-1}C_1im][NTf_2]$[8,29] (N = 3 - 9, 11, 13); □ - $[^2C_{N-2}{}^1C_2Py][NTf_2]$ (N = 4 - 10); $[^2C_1{}^1C_2Py][NTf_2]$ [7].

The pyridinium based ionic liquids present lower thermal expansion coefficients when compared with the $[C_{N-1}C_1im][NTf_2]$ ionic liquid series.[8,29] Considering the associated uncertainty, the thermal expansion coefficients are independent with the increase of the alkyl side chain size of the cation similar to the imidazolium series. [8,29]

Viscosity: The experimental viscosity data determined, at atmospheric pressure, in the temperature ranges from (293.15 to 363.15) K, are listed in table 4. The graphic representation of the ln (η / mPa·s) = f (T/K) is presented in figure 5.

Table 4. Experimental viscosity results at p^o = 0.1 MPa, η, for the $[C_2C_{N-2}Py][NTf_2]$ ionic liquid series as a function of temperature.

T / K	η / mPa·s						
	$[^2C_2{}^1C_2Py]$ $[NTf_2]$	$[^2C_3{}^1C_2Py]$ $[NTf_2]$	$[^2C_4{}^1C_2Py]$ $[NTf_2]$	$[^2C_5{}^1C_2Py]$ $[NTf_2]$	$[^2C_6{}^1C_2Py]$ $[NTf_2]$	$[^2C_7{}^1C_2Py]$ $[NTf_2]$	$[^2C_8{}^1C_2Py]$ $[NTf_2]$
293.15	87.870	139.89	146.84	144.37	159.82	180.53	216.19
298.15	68.771	105.02	109.82	108.78	119.41	134.10	159.29
303.15	54.952	81.090	84.492	83.992	91.773	102.47	120.76
308.15	44.686	63.904	66.343	66.144	71.934	79.904	93.450
313.15	36.907	51.366	53.173	53.002	57.525	63.598	73.883
318.15	30.875	41.805	43.107	43.061	46.514	51.171	59.000
323.15	26.160	34.572	35.545	35.525	38.222	41.881	47.971
328.15	22.384	28.962	29.704	29.654	31.826	34.727	39.540
333.15	19.402	24.590	25.144	25.110	26.870	29.212	33.065
338.15	16.899	21.005	21.416	21.396	22.802	24.709	27.821
343.15	14.857	18.151	18.455	18.441	19.591	21.156	23.706
348.15	13.156	15.824	16.039	16.019	16.977	18.279	20.385
353.15	11.754	13.938	14.087	14.062	14.864	15.968	17.717
358.15	10.516	12.297	12.393	12.361	13.036	13.972	15.436
363.15	9.4826	10.947	11.004	10.967	11.540	12.341	13.580

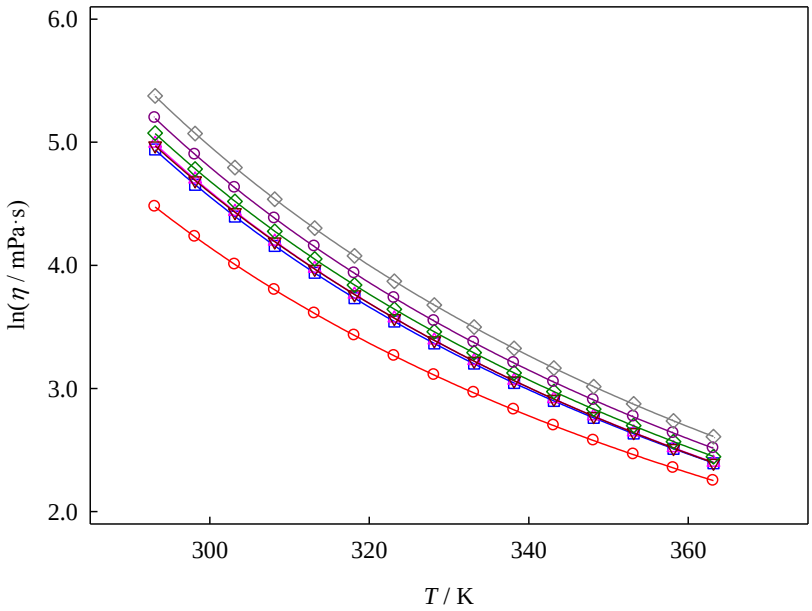

Figure 5. Logarithm of viscosity as a function of temperature for $[^2C_{N-2}{}^1C_2Py][NTf_2]$ ionic liquid family. The solid lines represents the Vogel-Tammann-Fulcher fitting (equation 4). ○ - $[^2C_2{}^1C_2Py][NTf_2]$; □ - $[^2C_3{}^1C_2Py][NTf_2]$; △ - $[^2C_4{}^1C_2Py][NTf_2]$; ▽ - $[^2C_5{}^1C_2Py][NTf_2]$; ◇ - $[^2C_6{}^1C_2Py][NTf_2]$; ⊙ - $[^2C_7{}^1C_2Py][NTf_2]$; ⟐ - $[^2C_8{}^1C_2Py][NTf_2]$.

The experimental viscosity data was correlated using the Vogel-Tammann-Fulcher (VTF) model described in equation (4),

$$\eta\,(T) = A_\eta \cdot \exp\left[\frac{B_\eta}{(T - C_\eta)}\right] \qquad (4)$$

where $\eta(T)$ is the viscosity in mPa·s, T is the temperature in K, and A_η, B_η and C_η are adjustable parameters. The derived coefficients of the VTF equation and the viscosity, at T=298.15 K, are presented in table 5. The correlated viscosities are in good agreement with the experimental data and a maximum relative deviation of 0.5 % for the correlated values was achieved.

As it is well known, the viscosity relates the shear stress in a moving fluid to the strain rate of the fluid. The energy related to this process is defined as energy barrier, E, which

can be evaluated based on the viscosity dependence with the temperature using the following equation (5):

$$E = R \cdot \frac{\partial(\ln \eta)}{\partial(1/T)} = R \cdot \left(\frac{B_\eta}{\left(\frac{C_\eta^2}{T^2} - \frac{2.C_\eta}{T} + 1 \right)} \right) \quad (5)$$

The derived energy barrier, E, at T = 298.15 K, for each ionic liquid is also listed in table 5.

Table 5. Fitting coefficients of VFT equation for the viscosity data of the studied ionic liquids, viscosity and the derived energy barrier at T = 298.15 K.

Ionic Liquid	A_η / mPa·s	B_η / K	C_η / K	η (298.15 K)/ mPa·s	E (298.15 K) / kJ·mol^{-1}
[^{2}C$_1$^{1}C$_2$Py][NTf$_2$] [7]	0.2010 ± 0.004	754.8 ± 5.0	171.4 ± 0.4	77.10	34.7 ± 0.8
[^{2}C$_2$^{1}C$_2$Py][NTf$_2$]	0.2240 ± 0.005	705.0 ± 6.2	175.1 ± 0.6	68.77	34.4 ± 0.7
[^{2}C$_3$^{1}C$_2$Py][NTf$_2$]	0.1810 ± 0.004	750.8 ±6.5	180.2 ± 0.6	105.02	39.9 ± 0.8
[^{2}C$_4$^{1}C$_2$Py][NTf$_2$]	0.1610 ± 0.004	780.1 ± 7.7	178.7 ± 0.7	109.82	40.4 ± 1.0
[^{2}C$_5$^{1}C$_2$Py][NTf$_2$]	0.1410 ± 0.003	821.6 ± 5.4	174.6 ± 0.5	108.78	39.8 ± 0.6
[^{2}C$_6$^{1}C$_2$Py][NTf$_2$]	0.1360 ± 0.004	837.0 ± 7.9	174.7 ± 0.7	119.41	40.6 ± 0.9
[^{2}C$_7$^{1}C$_2$Py][NTf$_2$]	0.1340 ± 0.003	850.5 ± 7.3	175.0 ± 0.6	134.10	41.4 ± 0.8
[^{2}C$_8$^{1}C$_2$Py][NTf$_2$]	0.1240 ± 0.003	887.9 ± 7.0	174.2 ± 0.6	159.29	42.7 ± 0.8

The graphic representation of the viscosity as a function of the total number of carbon atoms in the alkyl side chains of the cation, *N*, is depicted in figure 6. The [$^2C_{N-2}{}^1C_2Py$][NTf_2] ionic liquid family presents higher viscosities than the ones observed for the [$C_{N-1}C_1im$][NTf_2] ionic liquids, and the viscosity profile along the alkyl side chain length changes drastically when the cation is changed from an imidazolium to a pyridinium. The pre-exponential coefficient of the VTF equation, and the energy barrier at T = 298.15 K, as a function of the total number of carbon atoms in the alkyl side chains of the cation, *N*, are presented in figure 7.

Based on the viscosity results, three distinct regions could be identified. An initial region or so called outlier - region "Region O" for the ionic liquids with short alkyl chains ([$^2C_1{}^1C_2Py$][NTf_2] and [$^2C_2{}^1C_2Py$][NTf_2]) showing significant lower viscosity and lower energy barriers than the remaining members of the series, that could be explained by the small contribution of the alkyl chain in the position 2 of the cation to the increase of their cohesive interaction that is ruled by the size of the existent ethyl group in position 1 of the pyridinium. A regular and constant "Region A" is observed from [$^2C_3{}^1C_2Py$][NTf_2] to [$^2C_5{}^1C_2Py$][NTf_2], where the viscosity and the energy barriers, *E*, do not show any significant dependency with the increasing of the alkyl side length. In figure 7, panel **I**, a fast decrease of the pre-exponential parameter of the VTF equation, A_η, is observed for "Region A", from [$^2C_3{}^1C_2Py$][NTf_2] to [$^2C_5{}^1C_2Py$][NTf_2], related with the decrease with the surface - volume ratio of the ion pair. Starting from [$^2C_5{}^1C_2Py$][NTf_2], the decrease of A_η is attenuated. It is interesting to note that in "Region A", the pyridinium based ionic liquids have slightly higher A_η values and starting from [$^2C_5{}^1C_2Py$][NTf_2], the difference of A_η values between the pyridinium and the imidazolium ionic liquids increases. A similar A_η profile along the series is observed between the two ionic liquid families.

For longer alkyl chains in position 2, a "Region B" ([$^2C_6{}^1C_2Py$][NTf_2] to [$^2C_8{}^1C_2Py$][NTf_2]) in the viscosity and derived viscosity parameters trend was found. A shift in the viscosity trend starting from [$^2C_5{}^1C_2Py$][NTf_2] could be related with the balance between the decrease in the electrostatic interactions between cation and anion, and the increase in the van der Waals interactions arising from the increase of the alkyl side length. From [$^2C_5{}^1C_2Py$][NTf_2], the viscosity increases along the alkyl side length in "Region B" ([$^2C_6{}^1C_2Py$][NTf_2] to [$^2C_8{}^1C_2Py$][NTf_2]). This trend shift is related with the structural organization of the liquid above a Critical Alkyl Length Size, (CALS), already detected in the literature, for the imidazolium ionic liquids around [C_6C_1im][NTf_2].[2,4,6,8,12,13,27]

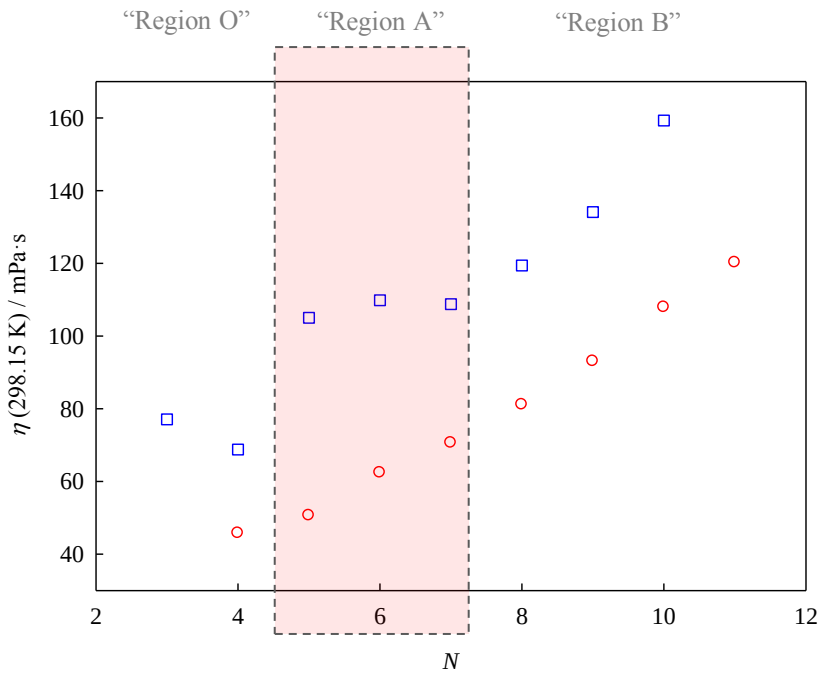

Figure 6. Graphic representation of the viscosity, at 298.15 K and 0.1MPa, as a function of the total number of carbon atoms in the alkyl side chains of the cation, *N*. ○ - [$C_{N-1}C_1im$][NTf_2][8,29] (N = 3 - 9, 11, 13); □ - [$^2C_{N-2}{}^1C_2Py$][NTf_2] (N = 4 - 10); [$^2C_1{}^1C_2Py$][NTf_2] [7].

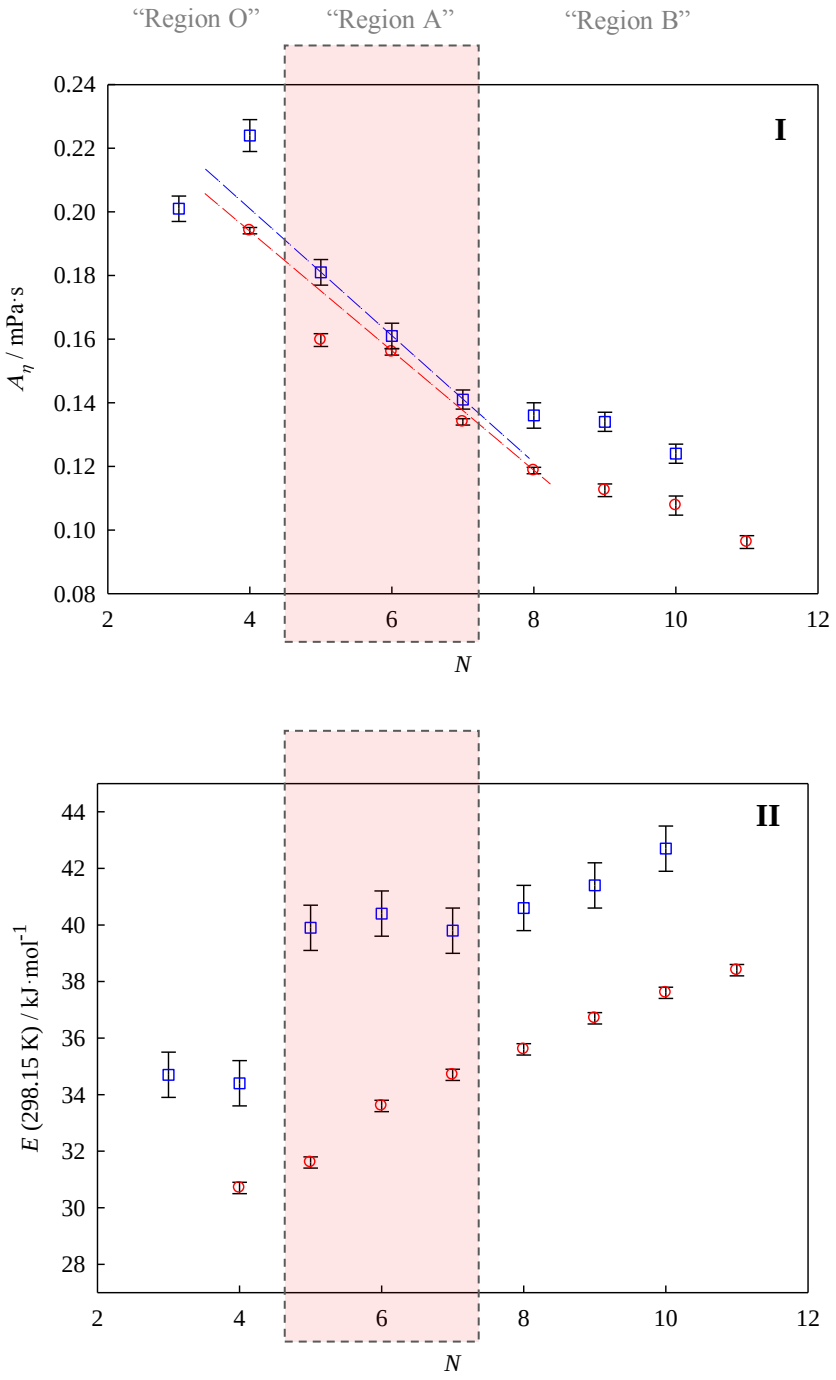

Figure 7. Graphic representation of the **(I)** pre-exponential coefficient, A_η, of the VTF equation and **(II)** energy barrier, at 298.15 K and 0.1MPa, as a function of the total number of carbon atoms in the alkyl side chains of the cation, *N*. ○ - $[C_{N-1}C_1im][NTf_2]$[8,29] (N = 3 - 9, 11, 13); □ - $[^2C_{N-2}{}^1C_2Py][NTf_2]$ (N = 4 - 10); $[^2C_1{}^1C_2Py][NTf_2]$ [7].

The energy barrier at T = 298.15 K, figure 7 (II), presents the same pattern as η = f(N), unlike to the one observed for the imidazolium based ionic liquids. The two regions are clearly visible in the energy barrier in the pyridinium ionic liquids, and are higher than the ones shown in the imidazolium ionic liquids. In ionic liquids, some of the structural features are expected, such as the short-range organization in order to maintain electroneutrality and to enhance electrostatic interactions.[2,3] Unlike to what was found for the $[C_{N-1}C_1im][NTf_2]$ ionic liquids, in the case of pyridinium ionic liquids, the $[NTf_2]^-$ anion is located near the pyridinium ring, with the N atom of the anion face towards the N of the pyridinium cation, with the anion placed above or below the pyridinium ring plane, respectively.[7] This leads to a different kind of structural organization in the liquid phase, and the cation size change from a five to a six membered ring increases the distance between charges while delocalizing them as well, resulting thus in a decrease in the ionic interaction energy.[39] Despite of the decrease of the electrostatic interaction, the pyridinium based ionic liquids have found to be associated with a higher cohesion than the imidazolium ionic liquids, which is associated to the importance of cation-cation dispersive interactions.[11,40] Actually this is in agreement with the obtained results in this work, where the viscosity and energy barrier profiles confirms the increase of the importance of dispersive over electrostatic interactions, since the latter are diminishing with the increase of the alkyl side chain length of the cation.[8,12,14]

"Region O", $[^2C_1{}^1C_2Py][NTf_2]$ [7] and $[^2C_2{}^1C_2Py][NTf_2]$ presents the typical outlier behavior for the viscosity and VTF parameters, with respect to the homologous series. From $[^2C_1{}^1C_2Py][NTf_2]$ [7] to $[^2C_2{}^1C_2Py][NTf_2]$ ionic liquids, there is a decrease of viscosity, governed by the somewhat lower energy barrier of the latter ionic liquid. This is related with the impact of adding a methylene group, $-CH_2-$, to the pyridinium cation

which leads to a decrease of the electrostatic interactions of the ionic liquids. This is reflected by the lowering of the viscosity and energy barrier from $[^2C_1{}^1C_2Py][NTf_2]$ [7] to $[^2C_2{}^1C_2Py][NTf_2]$ ionic liquids. For the pyridinium ionic liquids with longer alkyl chain lengths, the viscosity increases significantly compared with the ionic liquids with lower alkyl chain lengths, which is a reflection of the importance of dispersive over electrostatic interactions.

Heat Capacities. The number of drop experiments, N_{drop}, the molar heat capacity, $C^{o}_{p,m}$ ($J{\cdot}K^{-1}{\cdot}mol^{-1}$), specific heat capacities, c^{o}_{p} ($J{\cdot}K^{-1}{\cdot}g^{-1}$), and volumic heat capacities, C^{o}_{p}/V ($J{\cdot}K^{-1}{\cdot}cm^{-3}$), at T = 298.15 K are presented in table 6.

Table 6. Number of drop experiments, N_{drop}, the molar heat capacity, $C^{o}_{p,m}$ ($J{\cdot}K^{-1}{\cdot}mol^{-1}$), specific heat capacities, c^{o}_{p} ($J{\cdot}K^{-1}{\cdot}g^{-1}$), and volumic heat capacities, C^{o}_{p}/V ($J{\cdot}K^{-1}{\cdot}cm^{-3}$) at 298.15 K.

Ionic Liquid	N_{drop}	$C^{o}_{p,m}$ / $J{\cdot}K^{-1}{\cdot}mol^{-1}$	c^{o}_{p} / $J{\cdot}K^{-1}{\cdot}g^{-1}$	C^{o}_{p}/V / $J{\cdot}K^{-1}{\cdot}cm^{-3}$
$[^2C_2{}^1C_2Py][NTf_2]$	11	566.1 ± 0.9	1.3596 ± 0.0022	1.9994 ± 0.0032
$[^2C_3{}^1C_2Py][NTf_2]$	71	593.9 ± 0.4	1.3799 ± 0.0010	1.9970 ± 0.0014
$[^2C_4{}^1C_2Py][NTf_2]$	21	623.6 ± 0.9	1.4032 ± 0.0019	1.9772 ± 0.0027
$[^2C_5{}^1C_2Py][NTf_2]$	15	652.7 ± 0.5	1.4237 ± 0.0010	1.9520 ± 0.0014
$[^2C_6{}^1C_2Py][NTf_2]$	37	685.5 ± 0.6	1.4509 ± 0.0012	1.9504 ± 0.0016
$[^2C_7{}^1C_2Py][NTf_2]$	12	717.5 ± 0.9	1.4748 ± 0.0018	1.9479 ± 0.0024
$[^2C_8{}^1C_2Py][NTf_2]$	22	749.4 ± 0.7	1.4974 ± 0.0013	1.9427 ± 0.0017

N_{drop} = number of drop experiment; the number of drops are the sum of the drops that were obtained in at least two independent experiments.

The heat capacity data obtained for the ionic liquids under study were compared with the data for the $[C_{N-1}C_1im][NTf_2]$ ionic liquid series available in the literature.[27] García-Mardones *et al.*[7] recently published the heat capacities of $[^2C_1{}^1C_2Py][NTf_2]$ and their dependence with temperature determined using a differential scanning calorimetry, with an uncertainty no greater than 3 %. These values are considered in the analysis of the obtained data in this work.

The representation of the molar heat capacity data ($C^{o}_{p,m}$) against the total number of carbon atoms in the alkyl side chains of the cation, *N*, of the ionic liquids, [$^{2}C_{N-2}{}^{1}C_{2}Py$][NTf_2] and [$C_{N-1}C_1im$][NTf_2][27], is presented in figure 8 (I). As it was already reported for the [$C_{N-1}C_1im$][NTf_2] ionic liquids [27], an apparent linearity in the $C^{o}_{p,m}$ against *N* for the [$^{2}C_{N-2}{}^{1}C_{2}Py$][NTf_2] ionic liquids, is observed. However, considering the deviation plot from the linear fitting in the "Region A" ([$^{2}C_{3}{}^{1}C_{2}Py$] [NTf_2] - [$^{2}C_{5}{}^{1}C_{2}Py$] [NTf_2]), as represented in figure 7 (II), starting from [$^{2}C_{5}{}^{1}C_{2}Py$] [NTf_2], an indication of higher molar heat capacities is observed. At 298.15 K, the molar heat capacities for the pyridinium ionic liquids are around 28 $J\cdot K^{-1}\cdot mol^{-1}$ higher than the ones obtained for the imidazolium series, which reflects the increase in cation size from a five to a six membered ring and which is also related to the slightly higher configurational contribution of the two alkyl side chains of 1-ethyl-2-alkylpyridinium, when compared with the 1-ethyl-3-alkylimidazolium cation.

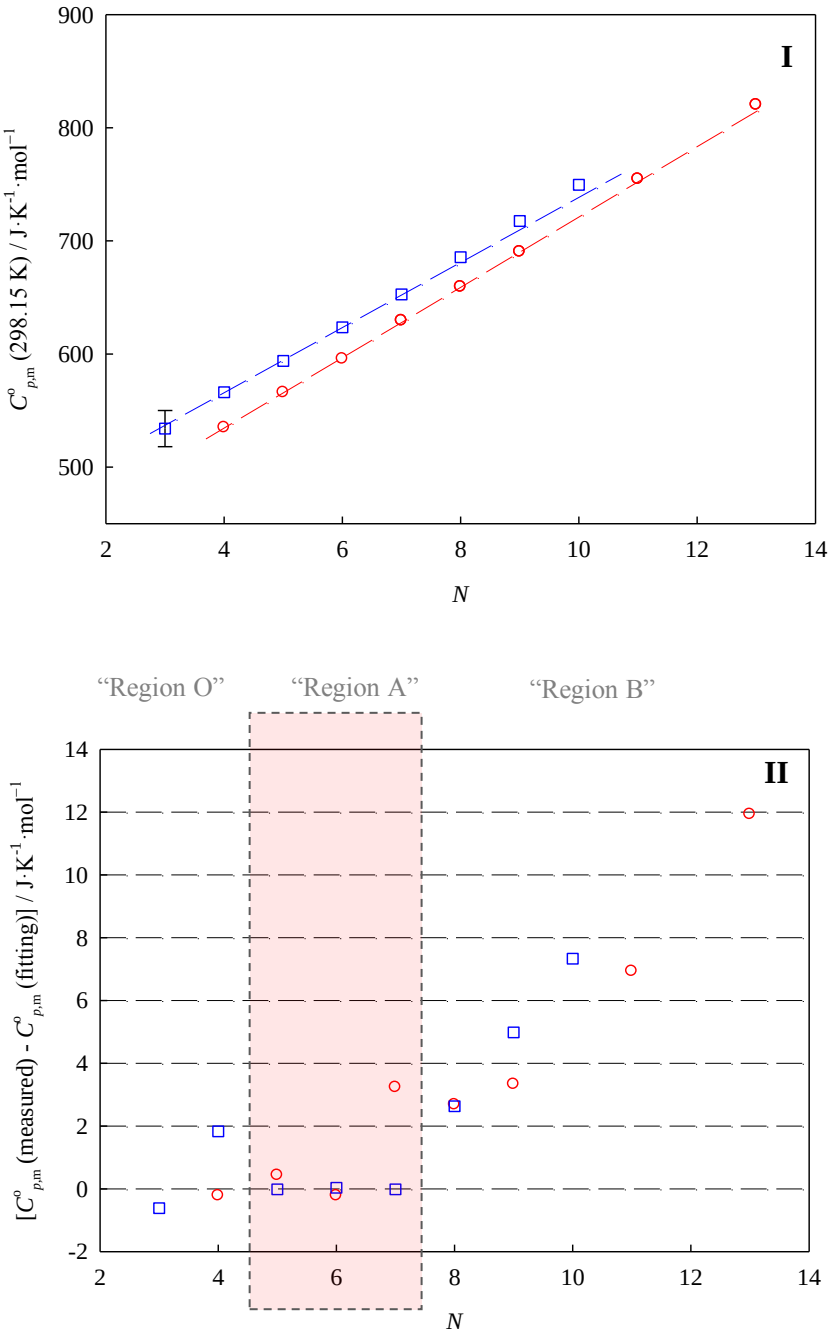

Figure 8. Graphic representation of the molar heat capacities (I), deviation of the $C^{o}_{p,m}$ (fitting "Region A") from the $C^{o}_{p,m}$ (measured), at 298.15 K, as a function of the total number of carbon atoms in the alkyl side chains of the cation, *N*. ○ - $[C_{N-1}C_1im][NTf_2]$[8,29] (N = 3 - 9, 11, 13), "Region A" ($[C_3C_1im][NTf_2]$ - $[C_5C_1im][NTf_2]$); □ - $[^2C_{N-2}{}^1C_2Py][NTf_2]$ (N = 4 - 10); $[^2C_1{}^1C_2Py][NTf_2]$ [7], "Region A" ($[^2C_3{}^1C_2Py]$ $[NTf_2]$ - $[^2C_5{}^1C_2Py]$ $[NTf_2]$).

Figure 9 presents the plots of the specific heat capacity (I) and the volumic heat capacities (II) against the total number of carbon atoms in the alkyl side chains of the cation, *N*, of the ionic liquids.

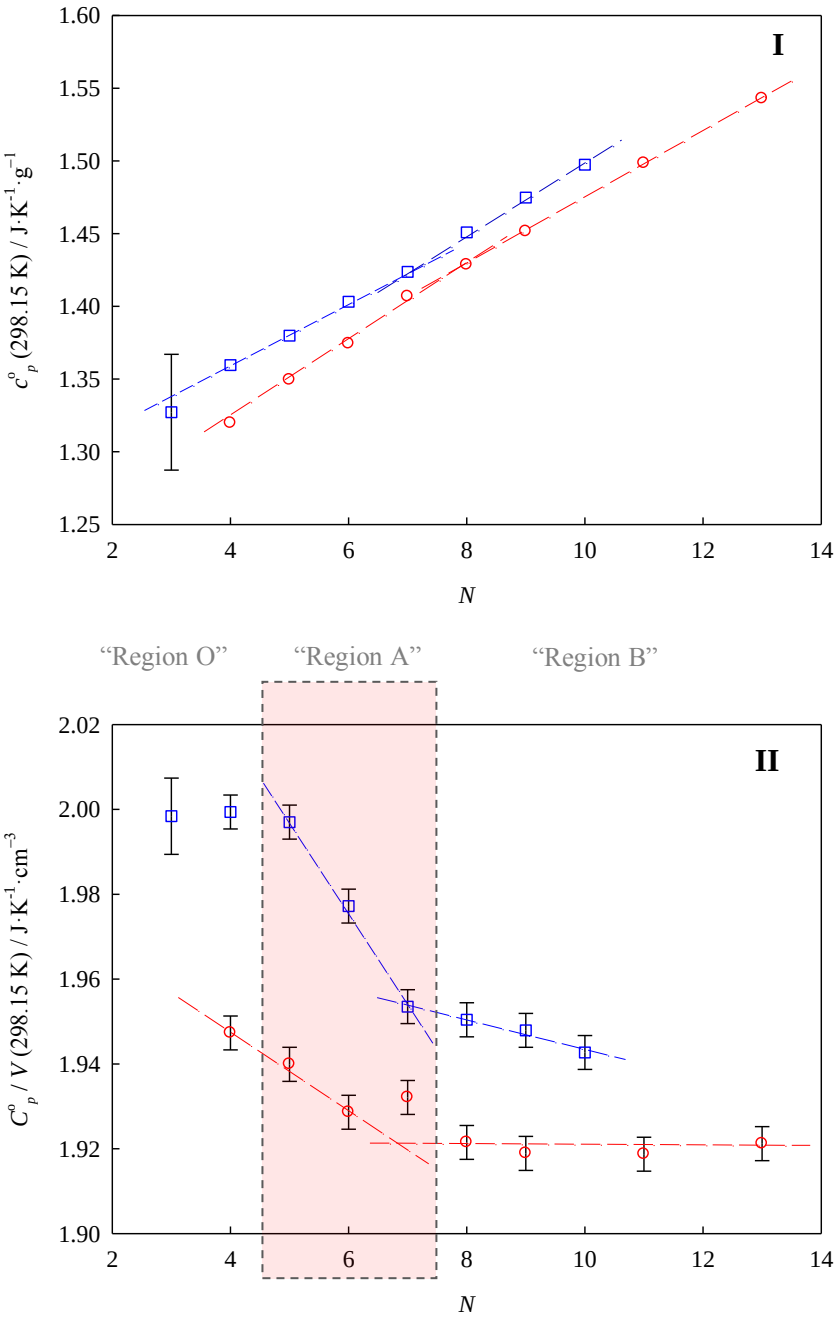

Figure 9. Graphic representation of the specific heat capacities (I) and the volumic heat capacities (II), at 298.15 K, as a function of the total number of carbon atoms in the alkyl side chains of the cation, *N*. ○ - $[C_{N-1}C_1im][NTf_2]$[8,29] (N = 3 - 9, 11, 13); □ - $[^2C_{N-2}{}^1C_2Py][NTf_2]$ (N = 4 - 10); $[^2C_1{}^1C_2Py][NTf_2]$ [7].

A subtle trend shift in the specific heat capacities trend starting from [$^2C_5{}^1C_2Py$][NTf_2] is clearly observed, and is in agreement with the findings evidenced for the viscosity data. There is a gradual increase of the specific heat capacities along the series, related with the increase of the contribution of the methylene group, $-CH_2-$, to the heat capacity of the ionic liquid.

The volumic heat capacities represented in figure 9 (II) show an accentuated decrease in the "Region A" ([$^2C_3{}^1C_2Py$][NTf_2] to [$^2C_5{}^1C_2Py$][NTf_2]), and starting from [$^2C_5{}^1C_2Py$][NTf_2] the decrease of the C_p^o/V values become attenuated in "Region B" ([$^2C_6{}^1C_2Py$][NTf_2] to [$^2C_8{}^1C_2Py$][NTf_2]). Considering the associated uncertainty, the C_p^o/V values for the outlier-region "Region O", [$^2C_1{}^1C_2Py$][NTf_2] and [$^2C_2{}^1C_2Py$][NTf_2], are identical to the C_p^o/V of [$^2C_3{}^1C_2Py$][NTf_2], being considered as an outlier from the homologous series. The strong decrease of the C_p^o/V values from [$^2C_3{}^1C_2Py$][NTf_2] to [$^2C_5{}^1C_2Py$][NTf_2] is mainly due to the decrease of the density of the ionic liquids along the series. From [$^2C_6{}^1C_2Py$][NTf_2] to [$^2C_8{}^1C_2Py$][NTf_2] the C_p^o/V decrease is a result of a balance between the decrease in the density and the increase of the volumic heat capacities per $-CH_2-$ group.

The molar and the specific heat capacities obtained for the pyridinium ionic liquids are slightly higher than the values found for the imidazolium ionic liquids[27], and becomes significantly higher for the volumic heat capacities. Additionally, it is interesting to observe that the trend shift in the volumic heat capacities is more evident for the pyridinium ionic liquids than for the imidazolium ionic liquids, in agreement with the previous results concerning the viscosities.

FINAL REMARKS

The dependence of the heat capacities, at T = 298.15 K, as well as the temperature dependencies of density and viscosity, all as a function of the alkyl chain length in the position 2 of the core 1-ethylpyridinium cation, was explored and compared with the alkylimidazolium based series.

The effect of the cation, size and structure is reflected in the comparative analysis with the $[C_{N-1}C_1im][NTf_2]$ ionic liquid series. For the same number of carbons in the alkyl chain, *N*, the pyridinium ionic liquids present similar densities, lower thermal expansion coefficients, higher viscosities, higher molar, specific and volumic heat capacities. when compared with the $[C_{N-1}C_1im][NTf_2]$ series.

The trend shift in thermophysical properties, found in this work, presents a clear indication that in the pyridinium based ionic liquids the nanostructuration starts at $[^2C_5{}^1C_2Py][NTf_2]$, in quite nice agreement with what was previously observed in the imidazolium ionic liquids series. The observed trend shift in the viscosity and in the heat capacities of the pyridinium ionic liquids is even more pronounced in the pyridinium than in the imidazolium ionic liquids series. This work confirms and is an additional support for the understanding of the trend shift and the relation with the structural organization of the ionic liquids and their particular properties, tuning capability and application potential.

AKNOWLEDGMENTS

Thanks are due to Fundação para a Ciência e Tecnologia (FCT), Lisbon, Portugal and to FEDER for financial support to Centro de Investigação em Química, University of Porto. Ana S.M.C. Rodrigues and Marisa A.A. Rocha acknowledge the financial support from FCT and the European Social Fund (ESF) under the Community Support Framework (CSF) for the award of a Research Grants SFRH/BD/81261/2011 and SFRH/BD/60513/2009, respectively. Miguel Vilas and Emilia Tojo acknowledge the financial support from the University of Vigo (11VIA18) and the Xunta de Galicia (INCITE08PXIB314253PR).

REFERENCES

(1) P. Wasserscheid, T. Welton, Eds.; *Ionic Liquids in Synthesis*, 2nd Ed.; Wiley-VCH: Weinheim, Germany, 2008.

(2) K. Shimizu, M. F. Costa Gomes, A. A. H. Pádua, L. P. N. Rebelo, J. N. Canongia Lopes, *J. Mol. Struct. : THEOCHEM* **2010**, *946*, 70–76.

(3) M. F. C. Gomes, J. N. C. Lopes, A. A. H. Padua, *Top. Curr. Chem.* **2010**, *290*, 161–183.

(4) J. N. Canongia Lopes A. A. H. Padua, *J. Phys. Chem. B* **2006**, *110*, 3330–3335.

(5) M. A. A. Rocha, J. A. P. Coutinho, L. M. N. B. F. Santos, *J. Chem. Phys.* **2013**, 139, 104502.

(6) M. A. A. Rocha, F. M. S. Ribeiro, A. I. M. C. L. Ferreira, J. A. P. Coutinho, L. M. N. B. F. Santos, *J. Mol. Liq.* **2013**, accepted.

(7) M. García-Mardones, I. Bandrés, M. C. López, I. Gascón, C. Lafuente, *J. Solution Chem.* **2012**, *41*, 1836–1852.

(8) M. A. A. Rocha, C. M. S. S. Neves, M. G. Freire, O. Russina, A. Triolo, J. A. P. Coutinho, L. M. N. B. F. Santos, *J. Phys. Chem. B* **2013**, doi: 10.1021/jp406374a.

(9) W. Zheng, A. Mohammed, L. G. Hines, D. Xiao, O. J. Martinez, R. A. Bartsch, S. L. Simon, O. Russina, A. Triolo, E. L. Quitevis, *J. Phys. Chem. B* **2011**, *115*, 6572–6584.

(10) M. G. Freire, A. R. R. Teles, M. A. A. Rocha, B. Schröder, C. M. S. S. Neves, P. J. Carvalho, D. V. Evtuguin, L. M. N. B. F. Santos, J. A. P. Coutinho, *J. Chem. Eng. Data* **2011**, *56*, 4813–4822.

(11) W. Xu, L.-M. Wang, R. A. Nieman, C. A. Angell, *J. Phys. Chem. B* **2003**, *107*, 11749–11756.

(12) M. A. A. Rocha, C. F. R. A. C. Lima, L. R. Gomes, B. Schröder, J. A. P. Coutinho, I. M. Marrucho, J. M. S. S. Esperança, L. P. N. Rebelo, K. Shimizu, J. N. C. Lopes, L. M. N. B. F. Santos, *J. Phys. Chem. B* **2011**, *115*, 10919–10926.

(13) M. A. A. Rocha, J. A. P. Coutinho, L. M. N. B. F. Santos, *J. Phys. Chem. B* **2012**, *116*, 10922–10927.

(14) M. A. A. Rocha, B. Schröder, J. A. P. Coutinho, L. M. N. B. F. Santos, *J. Chem. Thermodyn.* **2013**, Submitted. (Paper V).

(15) J. M. S. S. speran a, J. N. Canongia Lopes, M. Tariq, L. M. N. B. F. Santos, J. W. Magee, L. P. N. Rebelo, *J. Chem. Eng. Data* **2010**, 55, 3–12.

(16) D. H. Zaitsau, G. J. Kabo, A. A. Strechan, Y. U. Paulechka, A. Tschersich, S. P. Verevkin, A. Heintz, *J. Phys. Chem. A* **2006**, *110*, 7303–7306.

(17) A. Deyko, S. G. Hessey, P. Licence, E. A. Chernikova, V. G. Krasovskiy, L. M. Kustov, R. G. Jones, *Phys. Chem. Chem. Phys.* **2012**, *14*, 3181–3193.

(18) A. Deyko,; K. R. J. Lovelock, P. Licence, R. G. Jones, *Phys. Chem. Chem. Phys.* **2011**, *13*, 16841–16850.

(19) K. R. J. Lovelock, A. Deyko, J.-A. Corfield, P. N. Gooden, P. Licence, R. G. Jones, *Chem. Phys. Chem.* **2009**, *10*, 337–340.

(20) E. I. Izgorodina, M. Forsyth, D. R. MacFarlane, *Aust. J. Chem.* **2007**, *60*, 15–20.

(21) J. F. B. Pereira, S. P. M. Ventura, F. A. Silva, S. Shahriari, M. G. Freire, J. A. P. Coutinho, *Sep. Purif. Technol.* **2013**, 113, 83–89.

(22) J. F. B. Pereira, F. Vicente, V. C. Santos-Ebinuma, J. M. Araújo, A. Pessoa, M. G. Freire, J. A. P. Coutinho, *Process Biochem.* **2013**, *48*, 716–722.

(23) H. Passos, M. P. Trindade, T. S. M. Vaz, L. P. Da Costa, M. G. Freire, J. A. P. Coutinho, *Sep. Purif. Technol.* **2013**, *108*, 174–180.

(24) S. Stevanovic, A. Podgorsek, L. Moura, C. C. Santini, A. A. H. Padua, M. F. Costa Gomes, *Int. J. Greenh. Gas Con.* **2013**, *17*, 78–88.

(25) A. Podgoršek, A. S. Pensado, C. C. Santini, M. F. Costa Gomes, A. A. H. Pádua, *J. Phys. Chem. C* **2013**, *117*, 3537–3547.

(26) Y. Deng, P. Besse-Hoggan, M. Sancelme, A.-M. Delort, P. Husson, M. F. C. Gomes, *J. Hazard. Mater.* **2011**, *198*, 165–174.

(27) M. A. A. Rocha, M. Bastos, J. A. P. Coutinho, L. M. N. B. F. Santos, *J. Chem. Thermodyn.* **2012**, *53*, 140–143.

(28) S. M. Urahata, M. C. C. Ribeiro, *J. Chem. Phys.* **2005**, *122*, 024511.

(29) M. Tariq, A. P. Serro, J. L. Mata, B. Saramago, J. M. S. S. Esperança, J. N. Canongia Lopes, L. P. N. Rebelo, *Fluid Phase Equilib.* **2010**, *294*, 131–138.

(30) P. Verdía, E. J. González, B. Rodríguez-Cabo, E. Tojo, *Green Chem.* **2011**, *13*, 2768-2776.

(31) M. Vilas, M. A. A. Rocha, E. Tojo, L. M. N. B. F. Santos, Manuscript (Paper XII).

(32) P. J. Carvalho, T. Regueira, L. M. N. B. F. Santos, J. Fernandez, J. A. P. Coutinho, *J. Chem. Eng. Data* **2010**, *55*, 645–652.

(33) J. Konicek, W. Suurkuusk, I. Wadsö, *Chem. Scr.* **1971**, *1*, 217–220.

(34) J. Suurkuusk, I. Wadsö, *J. Chem. Thermodyn.* **1974**, *6*, 667–679.

(35) L. M. N. B. F. Santos, M. A. A. Rocha, A. S. M. C. Rodrigues, V. Štejfa, M. Fulem, M. Bastos, *J. Chem. Thermodyn.* **2011**, *43*, 1818–1823.

(36) R. Sabbah, A. Xu-Wu, J.S. Chickos, M.L. Planas Leitão, M.V. Roux, L.A. Torres, *Thermochim. Acta* **1999**, *331*, 93–204.

(37) R. D. Chirico, V. Diky, J. W. Magee, M. Frenkel, K. N. Marsh, *Pure Appl. Chem.* **2009**, *81*, 791–828.

(38) M.E. Wieser, M. Berglund, *Pure Appl. Chem.* **2009**, *81*, 2131–2156.

(39) A. M. Fernandes, M. A. A. Rocha, M. G. Freire, I. M. Marrucho, J. A. P. Coutinho, L. M. N. B. F. Santos, *J. Phys. Chem. B* **2011**, *115*, 4033–4041.

(40) Y. Yoshida, O. Baba, G. Saito, *J. Phys. Chem. B* **2007**, *111*, 4742–4749.

CHAPTER 5

Conclusions and Future Perspectives

This chapter summarizes the major conclusions from the research done in this Ph.D. thesis and presents some ideas that can be explored in the future. This thesis was a contribution for the improvement of the research facilities of the group, as well as to the understanding of the big research puzzle that is nowadays the field of ionic liquids.

5.1 Overall Comments and Conclusions

Improvement of Methodologies and Scientific Installations

A part of this Ph.D. thesis was dedicated to contribute to the development and reassembling of methodologies and scientific installations in our laboratories.

A new Knudsen effusion apparatus combined with a quartz crystal microbalance, installation II (KEQCM II) was designed, developed and constructed, and some improvements concerning the Knudsen effusion / QCM methodology for the vapor pressure measurement of ionic liquids were made.

The heat capacities of ionic liquids were measured by a high precision heat capacity drop calorimeter that was reassembled, modernized and tested.

Since the laboratories were not equipped with a suitable drying system for ionic liquids, a small equipment for simultaneous drying of different ionic liquid samples was developed.

Besides having contributed to the development and construction of the new Knudsen effusion apparatus and the drop calorimeter, my main contributions in this part consist of the test and calibration of the apparatus as well as maintaining it working during the period of the Ph.D. thesis.

Volatility Study of Ionic Liquids

Optimization and improvements of the methodology for vapor pressure measurements of ionic liquids were performed. The ionic liquid families considered for the vapor pressures measurements were:

- 1-alkyl-3-methylimidazolium bis(trifluoromethylsulfonyl)imide, $[C_{N-1}C_1im][NTf_2]$
- 1,3- dialkylimidazolium bis(trifluoromethylsulfonyl)imide, $[C_{N/2}C_{N/2}im][NTf_2]$
- 1-alkylpyridinium bis(trifluoromethylsulfonyl)imide, $[C_NPy][NTf_2]$
- 1-ethyl-2-alkylpyridinium bis(trifluoromethylsulfonyl)imide, $[^2C_{N-2}{}^1C_2Py][NTf_2]$

An overview of the volatility results ($\Delta_l^g G_m^o$ (T = 460 K)) obtained for the thirty studied ionic liquids is presented in figure 5.1.

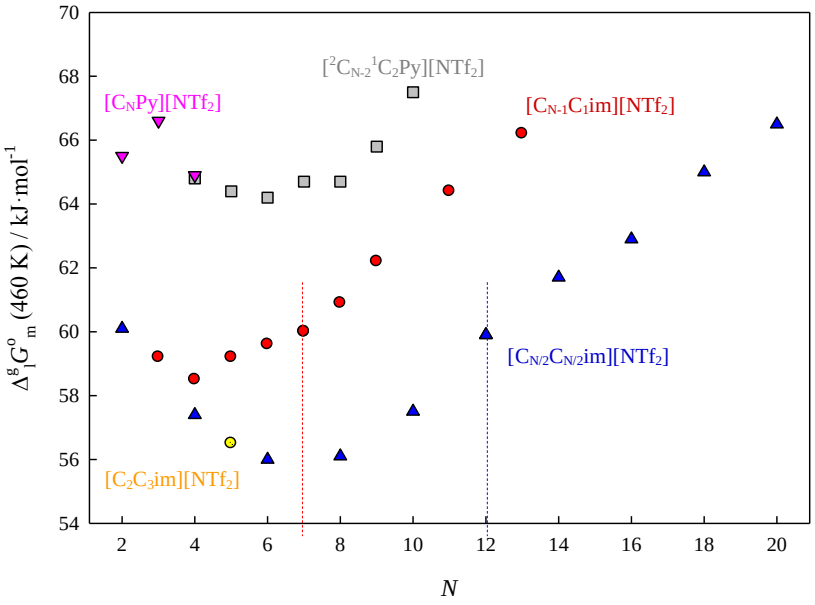

Figure 5.1. Standard (p^o=10^5 Pa) molar Gibbs energy of vaporization, at T = 460K, as a function of the total number of carbons in the alkyl side chains of the cation, *N*. ▲ (blue), [C$_{N/2}$C$_{N/2}$im][NTf$_2$] (N = 2, 4, 6, 8, 10, 12, 14, 16, 18, 20) [1-3]; ● (red), [C$_{N-1}$C$_1$im][NTf$_2$] (N = 3 − 9, 11, 13) [4]; ● (yellow), [C$_2$C$_3$im][NTf$_2$] [2]; ■ (gray), [^{2}C$_{N-2}$^{1}C$_2$Py][NTf$_2$] (N = 4 − 10) [5]; ▼ (pink), [C$_N$Py][NTf$_2$] (N = 2, 3, 4) [6].

The $\Delta_l^g G_m^o$ profile along the growing alkyl side chain presents a non-linear behaviour for the ionic liquids with shorter alkyl chain length, with an initial increase of volatility due to the marked effect of steric hindrance of the alkyl chain, reaching a maximum volatility plateau around propyl (C$_3$). The volatility trend reflects the overlapping of the two main interaction potentials: electrostatic and non-electrostatic, reaching a nearly linear increment of the Gibbs energy of vaporization (volatility decrease) after [C$_3$C$_1$im][NTf$_2$] (N=4), [C$_3$C$_3$im][NTf$_2$] (N=6) and [^{2}C$_3$^{1}C$_2$Py][NTf$_2$] (N=5), indicating that the electrostatic potential reaches a linear decrease, lower than the increment of the non-electrostatic interaction potential per methylene group, −CH$_2$−. Due to an enthalpic and entropic compensation, the nanostructuration of ionic liquids observed in other properties is hardly detected in the Gibbs energy of the vaporization trend.

The graphic representations of the standard molar enthalpies and entropies of vaporization, at T = 460 K, as a function of the total number of carbons in the alkyl side chains of the cation, *N*, are presented in figures 5.2 and 5.3.

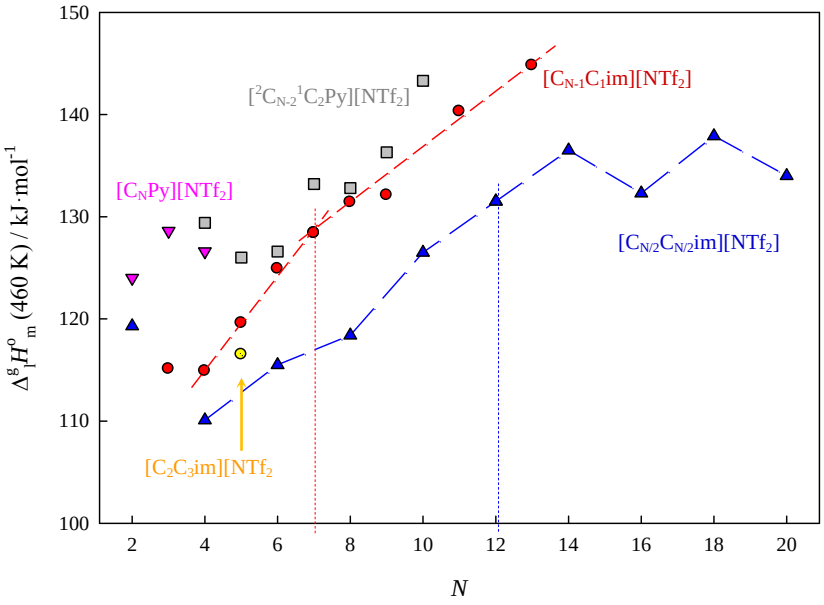

Figure 5.2. Standard (p^o=10^5 Pa) molar enthalpy of vaporization, at T = 460K, as a function of the total number of carbons in the alkyl side chains of the cation, *N*. ▲ (blue), [C$_{N/2}$C$_{N/2}$im][NTf$_2$] (N = 2, 4, 6, 8, 10, 12, 14, 16, 18, 20) [1-3]; ● (red), [C$_{N-1}$C$_1$im][NTf$_2$] (N = 3 − 9, 11, 13) [4]; ● (yellow), [C$_2$C$_3$im][NTf$_2$] [2]; ■ (gray), [^{2}C$_{N-2}$^{1}C$_2$Py][NTf$_2$] (N = 4 − 10) [5]; ▼ (pink), [C$_N$Py][NTf$_2$] (N = 2, 3, 4) [6].

The $\Delta_l^g H_m^o$ profile along the growing alkyl side chain presents also a non-linear behaviour for the ionic liquids, especially visible in the region of the ionic liquids with shorter alkyl chain length. The observed decrease in the enthalpies of vaporization is related with the decrease of the cohesive energy due to the effect of the steric hindrance of the cation's alkyl chain on the electrostatic interactions. The decrease in the enthalpies of vaporization determines the increase of volatility in the ionic liquid series in that region. The general overview of the enthalpies of vaporization, after the first members of the series, could be described as an increase of the enthalpies of vaporization along the alkyl chain length of the cation, being a result of the overlapping of the increase of the non-electrostatic interactions with the decrease of the electrostatic interactions. A trend shift on the $\Delta_l^g H_m^o$ along the growing alkyl side chain lengths of the different cations was found and is related with the onset of nanostructuration / segregation of the ionic liquids.

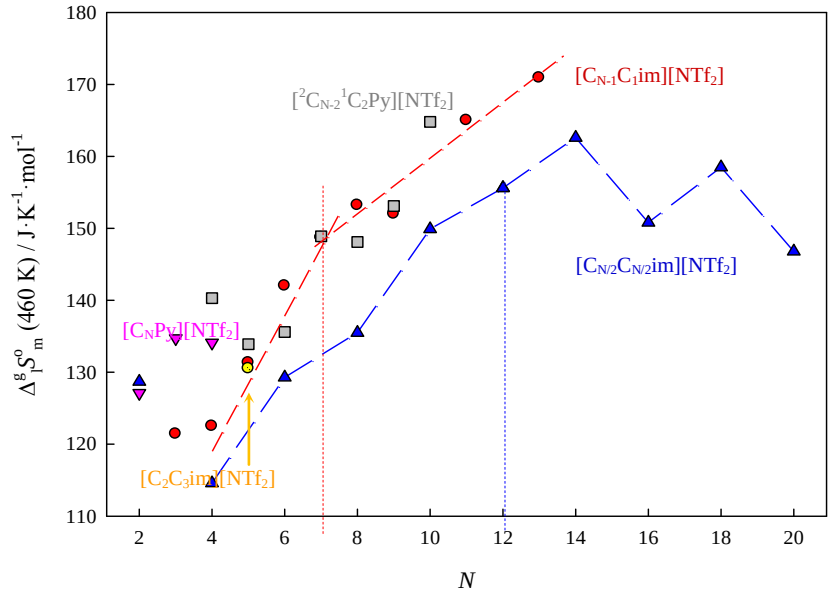

Figure 5.3. Standard (p^o=10^5 Pa) molar entropy of vaporization, at T = 460K, as a function of the total number of carbons in the alkyl side chains of the cation, *N*. ▲ (blue), [$C_{N/2}C_{N/2}$im][NTf_2] (N = 2, 4, 6, 8, 10, 12, 14, 16, 18, 20) [1-3]; ● (red), [$C_{N-1}C_1$im][NTf_2] (N = 3 − 9, 11, 13) [4]; ● (yellow), [C_2C_3im][NTf_2] [2]; ■ (gray), [$^2C_{N-2}{}^1C_2$Py][NTf_2] (N = 4 − 10) [5]; ▼ (pink), [C_NPy][NTf_2] (N = 2, 3, 4) [6].

The $\Delta_l^g S_m^o$ overview along the alkyl side chain presents a non-linear behaviour with a shape similar to the one observed for the enthalpies of vaporization. In the case of [C_1C_1im][NTf_2] and [C_2Py][NTf_2], the entropies of vaporization are in the same range, which is an indication that the bulk organization in the liquid is similar and is mainly ruled by the stronger electrostatic interactions and the more spherical-like shape of the ion pairs in the liquid. After the initial region, an increase of the entropies of vaporization is observed for all the studied ionic liquids series. Some interesting results were obtained for [$C_{N-1}C_1$im][NTf_2] and [$C_{N/2}C_{N/2}$im][NTf_2], where a trend shift along the series in the entropies of vaporization was detected, with a clear decrease of the entropies of vaporization per methylene group, −CH_2−, in agreement with the increase of the alkyl chain dynamics in the liquid phase in the non-polar domains. The symmetric ionic liquids, [$C_{N/2}C_{N/2}$im][NTf_2], show lower entropies of vaporization (with a clear odd-even effect) than the asymmetric ones, [$C_{N-1}C_1$im][NTf_2], indicating a different structural organization in-between the two series.

It is interesting to observe that both asymmetric ionic liquid series, [$C_{N-1}C_1$im][NTf_2] and [$^2C_{N-2}{}^1C_2$Py][NTf_2], present similar entropies of vaporization for the

same total number of carbons on the cation's alkyl chains, which indicates an identical structural organization in the liquid phase.

Heat Capacities of Ionic Liquids

The heat capacities of the ionic liquids under study were measured, at T = 298.15 K, using a high-precision heat capacity drop calorimeter developed by Wadsö [7,8] and reassembled, modernized and tested during this Ph.D. thesis. [9] The ionic liquids families considered for the heat capacity measurements were:

- 1-alkyl-3-methylimidazolium bis(trifluoromethylsulfonyl)imide, $[C_{N-1}C_1im][NTf_2]$
- 1,3- dialkylimidazolium bis(trifluoromethylsulfonyl)imide, $[C_{N/2}C_{N/2}im][NTf_2]$
- 1-alkyl-3-methylimidazolium hexafluorophosphate, $[C_{N-1}C_1im][PF_6]$
- 1-ethyl-2-alkylpyridinium bis(trifluoromethylsulfonyl)imide, $[^2C_{N-2}{}^1C_2Py][NTf_2]$

An overview of the volumic heat capacity results obtained for the studied ionic liquids is presented in figure 5.4.

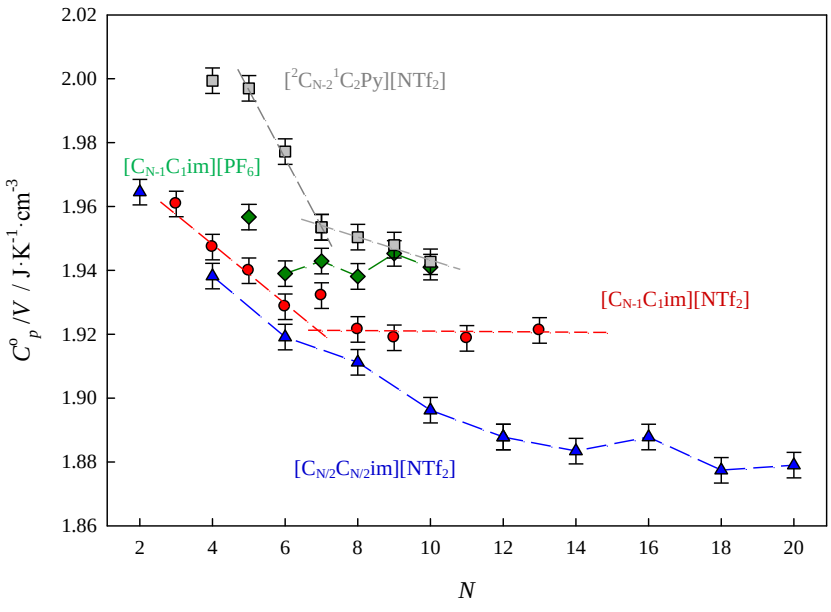

Figure 5.4. Volumic heat capacities as a function of the total number of carbon atoms in the alkyl side chains of the cation, *N*. ▲ (blue), $[C_{N/2}C_{N/2}im][NTf_2]$ (N = 2, 4, 6, 8, 10, 12, 14, 16, 18, 20) [10]; ● (red), $[C_{N-1}C_1im][NTf_2]$ (N = 3 − 9, 11, 13) [11]; ◆ (green), $[C_{N-1}C_1im][PF_6]$ (N = 5 − 10) [12]; ■ (gray), $[C_{N-2}C_2Py][NTf_2]$ (N = 4 − 10) [13].

From the representation of the volumic heat capacities against the total number of carbons in the alkyl side chains of the cation, it is clear that the symmetric imidazolium based ionic liquids, $[C_{N/2}C_{N/2}im][NTf_2]$, have lower heat capacities than the asymmetric series, $[C_{N-1}C_1im][NTf_2]$. In both imidazolium bistriflamide series, the trend shift is found to be around C_6, in agreement with the data obtained for the thermodynamic properties of vaporization. For the case of the $[C_{N-1}C_1im][PF_6]$ ionic liquid series, an interesting odd-even effect was detected in the so-called nanostructuration / segregation region. In the dialkylpyridinium series, $[^2C_{N-2}{}^1C_2Py][NTf_2]$, a clear shift in the trend of the C_p^o / V around $[^2C_5{}^1C_2Py][NTf_2]$ was found, similar to the one observed for the imidazolium bistriflamide series.

Viscosities and Densities of Ionic Liquids

Viscosity and density measurements for the pure ionic liquids were performed at atmospheric pressure in the temperature range from 278.15 to 363.15 K. An overview of the viscosity results obtained for the studied ionic liquids are presented in figure 5.5.

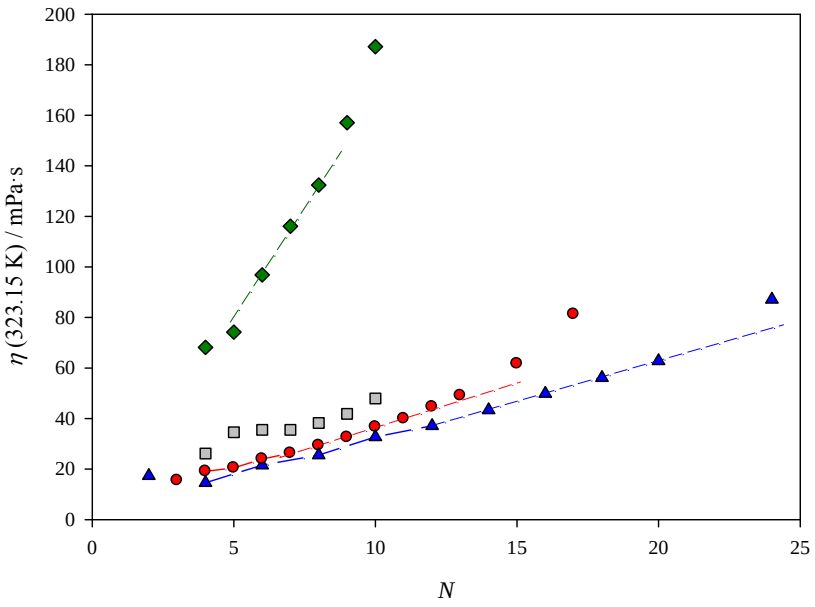

Figure 5.5. Viscosity, at 323.15 K and 0.1MPa, as a function of the total number of carbon atoms in the alkyl side chains of the cation, *N*. ▲ (blue), $[C_{N/2}C_{N/2}im][NTf_2]$ (N = 2, 4, 6, 8, 10, 12, 14, 16, 18, 20) [14]; ● (red), $[C_{N-1}C_1im][NTf_2]$ (N = 3 − 13, 15, 17) [14,15]; ◆ (green), $[C_{N-1}C_1im][PF_6]$ (N = 4 − 10) [16,17]; ■ (gray), $[C_{N-2}C_2Py][NTf_2]$ (N = 4 − 10) [18].

The viscosity of the $[C_{N-1}C_1im][PF_6]$ ionic liquids is significantly higher than the bistriflamide based ionic liquids series, which is a consequence of the highest energy barrier (figure 5.6 (II)) of the hexafluorophosphate based ionic liquids arising from the stronger electrostatic interaction of the cation-$[PF_6]^-$ than the cation-$[NTf_2]^-$. The pre-exponential parameter of the VTF equation depicted in figure 5.6 (I) is significantly smaller for the $[PF_6]^-$ anion, reflecting their sphericity. The nanostucturation in ionic liquids is also reflected in the trend of the viscosity along the alkyl chain series (figure 5.5). The VTF parameters that were obtained from the fitting of the experimental results give some additional insights concerning the nanostructuration. The pre-exponential parameter reaches a constant value around the region where the nanostructuration of the non-polar domains takes place. In this region, there are some indications that the energy barriers present a decrease in their increment per $–CH_2–$, in agreement with the observations on enthalpies of vaporization.

Concerning the density results, it was found that for the same total number of carbon atoms in the alkyl side chains of the cation, *N*, the $[^2C_{N-2}{}^1C_2Py][NTf_2]$ ionic liquids present similar densities when compared with the $[C_{N-1}C_1im][NTf_2]$ ionic liquids. It is interesting to observe that when changing a cation from a five (imidazolium) to a six membered ring (pyridinium), the contribution to the densities is maintained. Above *N* = 6 and for the same total number of carbons in the alkyl chains, the $[C_{N/2}C_{N/2}im][NTf_2]$ ionic liquids seems to present a somewhat lower density than the $[C_{N-1}C_1im][NTf_2]$ family.

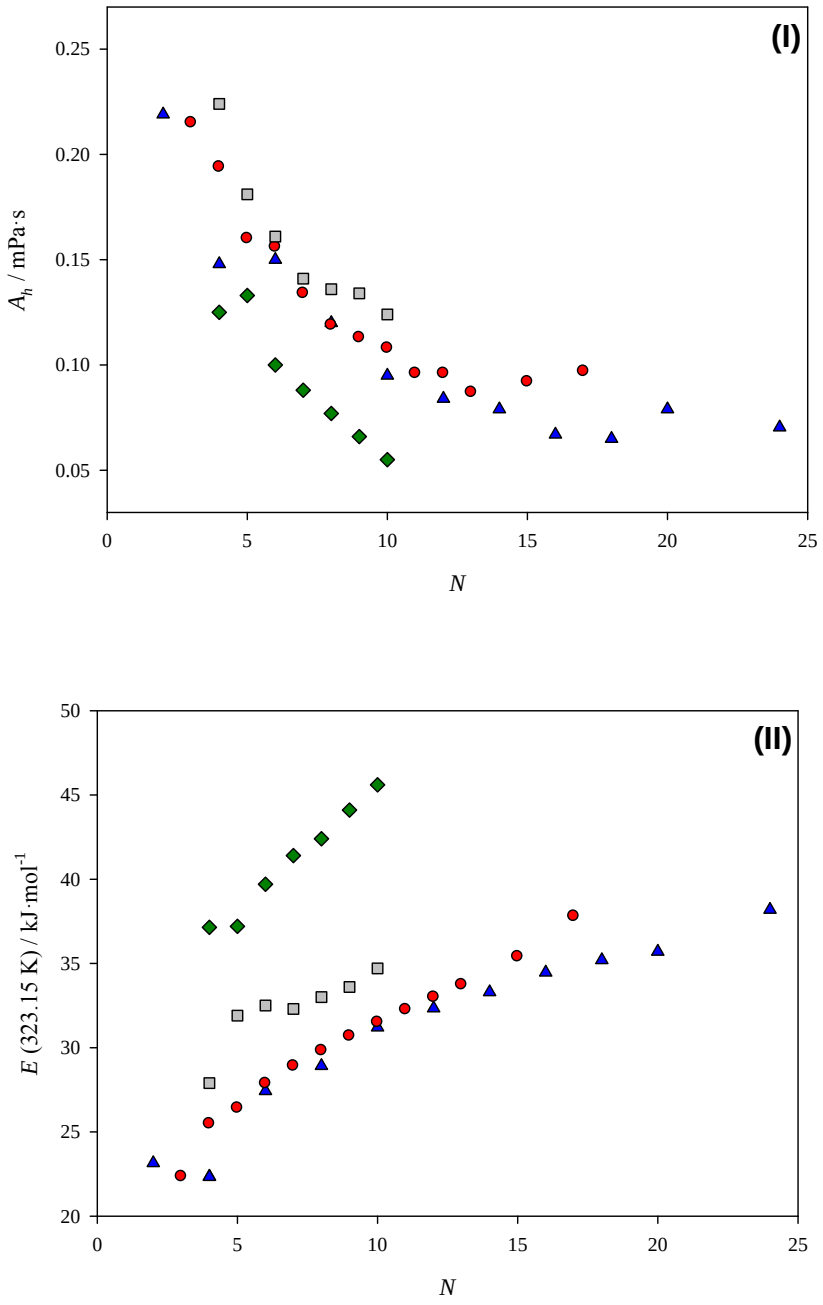

Figure 5.6. Graphic representation of the **(I)** pre-exponential coefficient, A_η, of the VTF equation and **(II)** energy barrier, E, at 323.15 K and 0.1MPa, as a function of the total number of carbon atoms in the alkyl side chains of the cation, *N*. ▲ (blue), $[C_{N/2}C_{N/2}im][NTf_2]$ (N = 2, 4, 6, 8, 10, 12, 14, 16, 18, 20) [14]; ● (red), $[C_{N-1}C_1im][NTf_2]$ (N = 3 − 13, 15, 17) [14,15]; ◆ (green), $[C_{N-1}C_1im][PF_6]$ (N = 4 − 10) [16,17]; ■ (gray), $[C_{N-2}C_2Py][NTf_2]$ (N = 4 − 10) [18].

5.2 Future Perspectives

The present work was a contribution to the molecular understanding of thermodynamics of ionic liquids. The comprehension of the so-called nanostructuration of ionic liquids and the effect on their physicochemical properties is fundamental to their tuning and design to a specific application. There is still an immense work to be done, mainly in the molecular interpretation of the thermodynamic properties of ionic liquids. Future work will include recent families of ionic liquids (e.g., heavily fluorinated ionic liquids). On the experimental side, further work on the studied ionic liquid systems with different techniques will lead to a more profound understanding of cause and effect of nanostructuration. Promising fields are thermophysical property determinations of binary ionic liquid mixtures as well as solvation thermodynamics of aromatic and non-aromatic molecular solvents in ionic liquids.

References

(1) Rocha, M. A. A.; Coutinho, J. A. P.; Santos, L. M. N. B. F., *J. Phys. Chem. B* 116 (**2012**) 10922 - 10927.

(2) Rocha, M. A. A.; Ribeiro, F. M. S.; Schröder, B.; Coutinho, J. A. P.; Santos, L. M. N. B. F., *J. Chem. Thermodyn.* (**2013**) doi: 10.1016/j.jct.2013.09.020

(3) Rocha, M. A. A.; Coutinho, J. A. P.; Santos, L. M. N. B. F., Manuscript (Paper VIII).

(4) Rocha, M. A. A.; Lima, C. F. R. A. C.; Gomes, L. R.; Schröder, B.; Coutinho, J. A. P.; Marrucho, I. M.; Esperança, J. M. S. S.; Rebelo, L. P. N.; Shimizu, K.; Canongia Lopes, J. N., Santos, L. M. N. B. F., *J. Phys. Chem. B* 115 (**2011**) 10919 - 10926.

(5) Vilas, M.; Rocha, M. A. A. ; Tojo, E.; Santos, L. M. N. B. F., Manuscript (Paper XII).

(6) Rocha, M. A. A.; Santos, L. M. N. B. F., *Chem. Phys. Lett.* (**2013**), doi: 10.1016/j.cplett.2013.08.095.

(7) Konicek, J.; Suurkuusk, J.; Wadsö, I., *Chem. Scr.* 1 (**1971**) 217-220.

(8) Suurkuusk, J.; Wadsö, I., *J. Chem. Thermodyn.* 6 (**1974**) 667-679.

(9) Santos, L. M. N. B. F.; Rocha, M. A. A.; Rodrigues, A. S. M. C.; Štejfa, V.; Fulem, M.; Bastos, M., *J. Chem. Thermodyn.* 43 (**2012**) 1818-1823.

(10) Rocha, M. A. A.; Coutinho, J. A. P.; Santos, L. M. N. B. F., *J. Chem. Phys.* 139 (**2013**) 104502.

(11) Rocha, M. A. A.; Bastos, M.; Coutinho, J. A. P.; Santos, L. M. N. B. F., *J. Chem. Thermodyn.* 53 (**2012**) 140–143.

(12) Rocha, M. A. A.; Ribeiro, F. M. S.; Coutinho, J. A. P.; Santos, L. M. N. B. F., Manuscript (Paper X).

(13) Rocha, M. A. A.; Vilas, M.; Rodrigues, A. S. M. C.; Tojo, E.; Santos, L. M. N. B. F., Manuscript (Paper XIII).

(14) Rocha, M. A. A.; Neves, C. M. S. S.; Freire, M. G.; Russina, O.; Triolo, A.; Coutinho, J. A. P.; Santos, L. M. N. B. F., *J. Phys. Chem. B* 117 (**2013**) 10889–10897.

(15) Tariq, M.; Carvalho, P. J.; Coutinho, J. A. P.; Marrucho, I. M.; Lopes, J. N. C.; Rebelo, L. P. N., *Fluid Phase Equilib.* 301 (**2011**) 22–32.

(16) Rocha, M. A. A.; Ribeiro, F. M. S.; Ferreira, A. I. M. C. L.; Coutinho, J. A. P.; Santos, L. M. N. B. F., *J. Mol. Liq.* (**2013**).

(17) Neves, C. M. S. S. M.; Batista, L. S.; Cláudio, A. F. M.; Santos, L. M. N. B. F.; Marrucho, I. M.; Freire, M. G.; Coutinho, J. A. P., *J. Chem. Eng. Data* 55 (**2010**) 5065–5073.

(18) Rocha, M. A. A.; Vilas, M.; Rodrigues, A. S. M. C.; Tojo, E.; Santos, L. M. N. B. F., Manuscript (Paper XIII).